

T H E   J O U R N A L   O F

# PHYSICAL CHEMISTRY

*Volume 73*

JANUARY—APRIL 1969

PAGES 1—1180

FREDERICK T. WALL, *Editor*

MARILYN H. PERRIN, ROBERT G. LINCK, AND ROBERT L. VOLD, *Assistant Editors*

EDITORIAL BOARD

R. BERSOHN  
S. BRUNAUER  
L. F. DAHL  
J. R. FRESCO  
G. J. HILLS  
J. R. HUIZENGA  
M. KASHA

W. J. KAUFMANN  
W. R. KRIGBAUM  
A. KUPPERMANN  
R. A. MARCUS  
W. J. MOORE  
W. A. NOYES, JR.  
B. S. RABINOVITCH

R. E. RICHARDS  
F. S. ROWLAND  
W. G. SCHNEIDER  
R. L. SCOTT  
R. SEIFERT  
S. I. WEISSMAN

CHARLES R. BERTSCH, *Senior Production Editor*

---

JOSEPH H. KUNYEY  
*Director of Business Operations*  
*Director of Publications Research*

RICHARD L. KENYON  
*Director of Publications*

DAVID E. GUSHEE  
*Publication Manager, Journals*

EASTON, PA.  
MACK PRINTING COMPANY  
1969

THE JOURNAL OF  
PHYSICAL CHEMISTRY

---

Volume 73, Number 1 January 1969

The Complexation Reactions of Cobalt(II) and Nickel(II) with Glycylsarcosine . . . . .	Kenneth Kustin and Robert F. Pasternack	1
The Diaphragm Cell Method for the Investigation of Thermal and Self-Thermal Diffusion in Liquid Electrolyte Solutions . . . . .	Andrzej S. Cukrowski	6
Ultraviolet Studies of the Adsorption of $\beta$ -Diketones on Evaporated Metal Films . . . . .	Kosaku Kishi and Shigero Ikeda	15
The Radiation-Induced Isomerization of Stilbene in 2-Propanol and Acetone . . . . .	H. P. Lehmann	20
On the Utility of the Concept of Water Structure in the Rationalization of the Properties of Aqueous Solutions of Proteins and Small Molecules . . . . .	Alfred Holtzer and Marilyn F. Emerson	26
Viscosity of Water at Various Temperatures . . . . .	Lawrence Korson, Walter Drost-Hansen, and Frank J. Millero	34
Kinetics of Rotation around the Aryl-Nitrogen Bond in Some <i>ortho</i> -Substituted Acetanilides . . . . .	T. H. Siddall, III, and W. E. Stewart	40
Cross-Phenomenological Coefficients. XI. Nonlinear Transport Equation . . . . .	R. P. Rastogi, Kehar Singh, and M. L. Srivastava	46
Peroxide Formation in the $\gamma$ Radiolysis of Aerated Aqueous Solutions of Methyl Iodide . . . . .	J. Shankar, K. V. S. Rama Rao, and L. V. Shastri	52
The N-Methylpropionamide-Water System. Densities and Dielectric Constants at 20-40° . . . . .	Thomas B. Hoover	57
On the Concentration Dependence of Transport Coefficients in Multicomponent Mixtures . . . . .	Hansjürgen Schonert	62
An Electron Spin Resonance Investigation of the Anion Radicals 1,4-Dimethylanthrasemiquinone and 1,4,5,8-Tetramethylanthrasemiquinone . . . . .	Richard H. Schlossel, David H. Geske, and Wilson M. Gulick, Jr.	71
Hydrogen Ion Titration and Sodium Ion Activity of Tropomyosin Solutions . . . . .	Shozo Iida and Nobuhisa Imai	75
Apparent Invariance of Activity Coefficients of Calcium Sulfate at Constant Ionic Strength and Temperature in the System $\text{CaSO}_4\text{-Na}_2\text{SO}_4\text{-NaNO}_3\text{-H}_2\text{O}$ to the Critical Temperature of Water. Association Equilibria . . . . .	LeRoy B. Yeatts and William L. Marshall	81
The Effects of Solvent and Temperature on Magnetically Nonequivalent Methylen Protons in Asymmetric Phosphorus Compounds . . . . .	L. S. Frankel, H. Klapper, and J. Cargioli	91
Temperature Dependence of the Electrical and Diffusional Mobilities of $^{22}\text{Na}$ and $^{137}\text{Cs}$ in Molten $\text{LiNO}_3$ , $\text{NaNO}_3$ , and $\text{RbNO}_3$ . . . . .	Jan C. Th. Kwak and J. A. A. Ketelaar	94
Counterion Transference Numbers in Ion-Exchange Membranes . . . . .	N. Lakshminarayanaiah	97
A Nuclear Magnetic Resonance Study of Anisotropic Molecular Rotation in Liquid Chloroform and in Chloroform-Benzene Solution . . . . .	Wesley T. Huntress, Jr.	103
A Comparison of Triethyl- and Trimethylammonium Headgroups in the Adsorption of <i>n</i> -Alkyl Quaternary Ammonium Ions at the Mercury Surface . . . . .	R. J. Meakins, M. G. Stevens, and R. J. Hunter	112
Energetics of the Pyrochlorophyll-Sensitized Photoreduction of Nitro Compounds . . . . .	G. R. Seely	117
The Quenching of Pyrochlorophyll Fluorescence by Nitro Compounds . . . . .	G. R. Seely	125
Relation of the Catalytic Activity of $\text{MgO}$ to Its Electron Energy States . . . . .	C. G. Harkins, W. W. Shang, and T. W. Leland	130
Binary Diffusion Studies with a Wedge Interferometer . . . . .	J. L. Duda, W. L. Sigelko, and J. S. Vrentas	141

# RADIATION CHEMISTRY

## ADVANCES IN CHEMISTRY SERIES NOS. 81 AND 82

Seventy-seven papers and 34 abstracts from the International Conference on Radiation Chemistry at Argonne National Laboratories, chaired by Edwin J. Hart. Includes review and research papers from 12 countries besides U.S., Canada, and England, including 8 from U.S.S.R. and two other East European countries.

**Volume I** groups papers on radiation in aqueous media, radiation of biological systems, dosimetry, and one plenary lecture.

**Volume II** has papers on radiation of gases, of solids, and of organic liquids, plus three plenary lectures.

No. 81 Radiation Chemistry—I  
No. 82 Radiation Chemistry—II

616 pages with index  
558 pages with index  
Each \$16.00

Ordered together \$30.00

Cloth (1968)

Set of L.C. cards free with library orders.

Other books in the ADVANCES IN CHEMISTRY SERIES in physical and colloid chemistry include:

**No. 68 Mössbauer Effect and its Application in Chemistry.** Ten papers that will familiarize chemists with Mössbauer spectroscopy as an analytical tool, for studying chemical bonding, crystal structure, electron density, magnetism, and other properties. Cloth (1967) 178 pages \$8.00

**No. 67 Equilibrium Concepts in Natural Water Systems.** Sixteen papers represent the collaboration of aquatic chemists, analytical chemists, geologists, oceanographers, limnologists, and sanitary engineers, working with simplified models to produce fruitful generalizations and valuable insights into the factors that control the chemistry of natural systems. Cloth (1967) 344 pages \$11.00

**No. 64 Regenerative EMF Cells.** Seventeen papers survey current progress and research on regenerative systems for converting and storing electrical energy. Principal emphasis is on thermally regenerative systems, but chemical and photochemical systems are considered. Cloth (1967) 309 pages \$11.00

**No. 63 Ordered Fluids and Liquid Crystals.** Twenty-two studies on characterization, properties, and occurrence of these phenomena in many substances such as tristearin, p-azoxyanisole, mono-and di-hydric alcohols, phospholipids and polypeptides. Cloth (1967) 332 pages \$11.50

**No. 58 Ion-Molecule Reactions in the Gas Phase.** Eighteen papers survey spectrometric and other methods for producing and studying ion-molecule reactions, such as pulsed sources for studing thermal ions, reactions in flames and electrical discharges. Cloth (1966) 336 pages \$10.50

**No. 54 Advanced Propellant Chemistry.** Primarily directed to the search for new oxidizers; 26 papers survey oxygen-containing oxidizers, fuels and binders, fluorine systems including oxygen difluoride and difluoramines and liquid systems. 290 pages Cloth (1966) \$10.50

**No. 47 Fuel Cell Systems.** Developments in theory, performance, construction, and new systems for the energy converter that is proving itself in military and space uses. 360 pages Cloth (1965) \$10.50

**No. 43 Contact Angle, Wettability, and Adhesion.** Twenty-six papers on theoretical and practical approaches to wettability and adhesion; with summary of the surface chemical studies of W. A. Zisman, the 1963 Kendall Award winner. Cloth (1964) 389 pages \$10.50

**No. 40 Mass Spectral Correlations.** By Fred W. McLafferty. Over 4000 spectral listed by mass/charge ratios of fragment ions with the most probable original structures for each. Paper (1963) 117 pages \$6.00

**No. 33 Solid Surfaces and the Gas-Solid Interface.** Thirty-seven papers from the Kendall Award Symposium honoring Stephen Brunauer. Theory and techniques for studying surface phenomena. Cloth (1961) \$12.00

**No. 31 Critical Solution Temperatures.** By Alfred W. Francis. CST answers the question, "Do two liquids mix?" and is widely used for screening solvents. Over 6000 systems are included, 70% with a hydrocarbon as one component; nearly 1100 non-hydrocarbon solvents are listed. Cloth (1961) 246 pages \$8.00

**No. 29 Physical Properties of Chemical Compounds—III.** By Robert R. Dreisbach. Supplements earlier volumes with properties of 434 aliphatic compounds and 22 miscellaneous compounds and elements. Index to volumes I, II, and III. Cloth (1961) 489 pages \$10.00

**No. 25 Physical Functions of Hydrocolloids.** Papers on natural gums, gelatin pectins and related polysaccharides, and theoretical and functional aspects of hydrocolloids, emulsions, foams, and dispersions. Strong food industry emphasis. Paper (1960) 103 pages \$5.00

**No. 22 Physical Properties of Chemical Compounds—II.** By Robert R. Dreisbach. Properties of 476 alkanes, haloalkanes, alkenes, haloalkenes, diolefins, and alkynes. Cloth (1959) 491 pages \$10.00

**No. 18 Thermodynamic Properties of the Elements.** By D. R. Stull and G. C. Sinke. Tabulated values of heat capacity, heat content, entropy, and free energy function of solid, liquid, and gas states of first 92 elements in range of 298° to 3000°K. Some auxiliary data frequently included. Cloth (1956) \$8.00

**No. 15 Physical Properties of Chemical Compounds.** By Robert R. Dreisbach. Tables of parameters for calculating physical properties of 511 organic cyclic compounds. Cloth (1955) 536 pages \$10.00

All books postpaid in U.S. and Canada; plus 20 cents in PUAS and elsewhere.

**Order from:**      **SPECIAL ISSUES SALES, DEPT.**  
**DEPT. M**  
**AMERICAN CHEMICAL SOCIETY**  
**1155 SIXTEENTH ST., N.W.**  
**WASHINGTON, D.C. 20036**

The Entropies of the Hydrates of Sodium Hydroxide. II. Low-Temperature Heat Capacities and Heats of Fusion of $\text{NaOH} \cdot 2\text{H}_2\text{O}$ and $\text{NaOH} \cdot 3.5\text{H}_2\text{O}$ . . . . .	P. R. Siemens and W. F. Giauque	149
Transport Processes in Hydrogen-Bonding Solvents. II. Conductance of Tetraalkylammonium Salts in 1-Butanol and 1-Pentanol at $25^\circ$ . . . . .	D. Fennell Evans and Philip Gardam	158
Partial Molal Volume of $[\text{Bu}_3\text{N}-(\text{CH}_2)_8-\text{NBu}_3]\text{Br}_2$ , a Large Bolaform Electrolyte, in Water at 10 and $25^\circ$ . . . . .	T. L. Broadwater and D. Fennell Evans	164
A Dimensionless Constant Characteristic of Gases, Equations of State, and Intermolecular Potentials . . . . .	Eugene M. Holleran	167
Thermodynamic Properties of Nonaqueous Solutions. VI. Enthalpies of Solution of Some Tetraalkylammonium Iodides in Water and N,N-Dimethylformamide at $25^\circ$ . . . . .	Om N. Bhatnagar and Cecil M. Criss	174
The Pyrolysis of Biacetyl and the Third-Body Effect on the Combination of Methyl Radicals . . . . .	K. J. Hole and M. F. R. Mulcahy	177
Diffusion in Binary Liquid Mixtures . . . . .	T. Loftin and E. McLaughlin	186
Mass Spectrometric Study of the Reactions of Atomic Oxygen with Ethylene and Formaldehyde . . . . .	John T. Herron and Ralph D. Penzhorn	191
Application of the Potentiostatic Method. Determination of the Rate Constant for the Dissociation of Acetic Acid . . . . .	Ronald R. Schroeder and Irving Shain	197
A Correlation of Molecular Flexibility with Volume and Heat of Mixing of Organic Solutes with Water and a Glycol-Water Mixture . . . . .	K. R. Brower, John Peslak, Jr., and James Elrod	207
Silver and Sodium Ion Transport Numbers into Pyrex from Binary Nitrate Melts . . . . .	A. G. Keenan and W. H. Duewer	212
Electron Spin Resonance Spectroscopy of the 1-Methylphenalenyl and the 1-Phenylphenalenyl Radicals . . . . .	I. C. Lewis and L. S. Singer	215
Estimation of the Bisulfate Ion Dissociation in Solutions of Sulfuric Acid and Sodium Bisulfate . . . . .	Richard E. Lindstrom and Henry E. Wirth	218
Electrolyte-Solvent Interaction. XIX. Solvation by Molecular Picric Acid . . . . .	Alessandro D'Aprano and Raymond M. Fuoss	223
The Rotatory Properties of Molecules Containing Two Peptide Groups: Theory . . . . .	Peter M. Bayley, Egil B. Nielsen, and John A. Schellman	228
The Relation between the Amounts of Chemisorbed and Physisorbed Water on Metal Oxides . . . . .	Tetsuo Morimoto, Mahiko Nagao, and Fujiko Tokuda	243
Liquid Ion-Exchange Membranes with Weakly Ionized Groups. I. A Theoretical Study of Their Steady-State Properties . . . . .	John Sandblom	249
Liquid Ion-Exchange Membranes with Weakly Ionized Groups. II. The Resistance and Electromotive Force of a Thin Membrane . . . . .	John Sandblom	257

#### NOTES

Onsager's Reciprocal Relation. An Examination of Its Application to a Simple Membrane Transport Process . . . . .	E. H. Bresler and R. P. Wendt	264
Nuclear Magnetic Resonance and Thermochemical Studies on the Influence of Urea on Water Structure . . . . .	S. Subramanian, D. Balasubramanian, and J. C. Ahluwalia	266
Isotope Effects in the Diffusion of $^{12}\text{C}$ - and $^{14}\text{C}$ -Substituted Molecules in the Liquid Phase . . . . .	L. B. Eppstein	269
Shereshevsky's Equation and Binary-Solution Surface Tension . . . . .	Donald J. Cotton	270
Calculation of the Wavelength Maxima for Some Triphenylmethane Dye Carbonium Ions . . . . .	Edward O. Holmes, Jr.	273
The Sign of the $^{11}\text{B}-^{19}\text{F}$ Coupling Constant in Boron Trifluoride and Related Compounds . . . . .	S. A. Fieldhouse and I. R. Peat	275
Proton Magnetic Resonance in Octahedral Complexes of Iron(II) and Cobalt(III) with $\alpha,\alpha'$ -Dipyridyl . . . . .	C. R. Kanekar, C. L. Khetrapal, and S. V. Nipankar	276
Temperature Dependence of Reactions of the Hydrated Electron . . . . .	S. R. Logan	277
Mass Spectra of Hydrolyzed Bromine Fluorides . . . . .	Eric N. Sloth, Lawrence Stein, and Clayton W. Williams	278
Relaxation Spectra of Nickel(II)- and Cobalt(II)-Picolinic Acid Complexes . . . . .	A. Kowalak, K. Kustin, and R. F. Pasternack	281
The Photoxidation of <i>t</i> -Butyl Iodide at Low Temperatures . . . . .	Theodore Mill and Roger Stringham	282

## AUTHOR INDEX

- |   |   |   |  |
|---|---|---|--|
| <p>Ahluwalia, J. C., 266<br/>         Balasubramanian, D., 266<br/>         Bayley, P. M., 228<br/>         Bhatnagar, O. N., 174<br/>         Bresler, E. H., 264<br/>         Broadwater, T. L., 164<br/>         Brower, K. R., 207<br/> <br/>         Cargioli, J., 91<br/>         Cotton, D. J., 270<br/>         Criss, C. M., 174<br/>         Cukrowski, A. S., 6<br/> <br/>         D'Aprano, A., 223<br/>         Drost-Hansen, W., 34<br/>         Duda, J. L., 141<br/>         Duewer, W. H., 212<br/> <br/>         Elrod, J., 207<br/>         Emerson, M. F., 26<br/>         Eppstein, L. B., 269<br/>         Evans, D. F., 158, 164</p> | <p>Fieldhouse, S. A., 275<br/>         Frankel, L. S., 91<br/>         Fuoss, R. M., 223<br/> <br/>         Gardam, P., 158<br/>         Geske, D. H., 71<br/>         Giauque, W. F., 149<br/>         Gulick, W. M., Jr., 71<br/> <br/>         Harkins, C. G., 130<br/>         Herron, J. T., 191<br/>         Hole, K. J., 177<br/>         Holleran, E. M., 167<br/>         Holmes, E. O., Jr., 273<br/>         Holtzer, A., 26<br/>         Hoover, T. B., 57<br/>         Hunter, R. J., 112<br/>         Huntress, W. T., Jr., 103<br/> <br/>         Iida, S., 75<br/>         Ikeda, S., 15<br/>         Imai, N., 75<br/> <br/>         Kanekar, C. R., 276</p> | <p>Keenan, A. G., 212<br/>         Ketelaar, J. A. A., 94<br/>         Khetrapal, C. L., 276<br/>         Kishi, K., 15<br/>         Klapper, H., 91<br/>         Korson, L., 34<br/>         Kowalak, A., 281<br/>         Kustin, K., 1, 281<br/>         Kwak, J. C. T., 94<br/> <br/>         Lakshminarayanaiah, N., 97<br/>         Lehmann, H. P., 20<br/>         Leland, T. W., 130<br/>         Lewis, I. C., 215<br/>         Lindstrom, R. E., 218<br/>         Lofin, T., 186<br/>         Logan, S. R., 277<br/> <br/>         Marshall, W. L., 81<br/>         McLaughlin, E., 186<br/>         Meakins, R. J., 112<br/>         Mill, T., 282<br/>         Millero, F. J., 34</p> | <p>Morimoto, T., 243<br/>         Mulcahy, M. F. R., 177<br/>         Nagao, M., 243<br/>         Nielsen, E. B., 228<br/>         Nipankar, S. V., 276<br/>         Pasternack, R. F., 1, 281<br/>         Peat, I. R., 275<br/>         Penzhorn, R. D., 191<br/>         Peslak, J., Jr., 207<br/>         Rao, K. V. S. R., 52<br/>         Rastogi, R. P., 46<br/> <br/>         Sandblom, J., 249, 257<br/>         Schellman, J. A., 228<br/>         Schlossel, R. H., 71<br/>         Schönert, H., 62<br/>         Schroeder, R. R., 197<br/>         Seely, G. R., 117, 125<br/>         Shain, I., 197<br/>         Shang, W. W., 130<br/> <br/>         Shankar, J., 52<br/>         Shastri, L. V., 52<br/>         Siddall, T. H., III, 40<br/>         Siemens, P. R., 149<br/>         Sigelko, W. L., 141<br/>         Singer, L. S., 215<br/>         Singh, K., 46<br/>         Sloth, E. N., 278<br/>         Srivastava, M. L., 46<br/>         Stein, L., 278<br/>         Stevens, M. G., 112<br/>         Stewart, W. E., 40<br/>         Stringham, R., 282<br/>         Subramanian, S., 266<br/> <br/>         Tokuda, F., 243<br/> <br/>         Vrentas, J. S., 141<br/> <br/>         Wendt, R. P., 264<br/>         Williams, C. W., 278<br/>         Wirth, H. E., 218<br/> <br/>         Yeatts, L. B., 81</p> |
|---|---|---|--|

THE JOURNAL OF  
PHYSICAL CHEMISTRY

*Registered in U. S. Patent Office © Copyright, 1969, by the American Chemical Society*

VOLUME 73, NUMBER 1 JANUARY 24, 1969

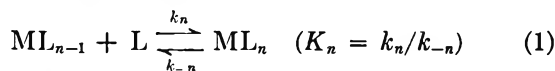
**The Complexation Reactions of Cobalt(II) and Nickel(II)  
with Glycylsarcosine**

by Kenneth Kustin and Robert F. Pasternack<sup>1</sup>

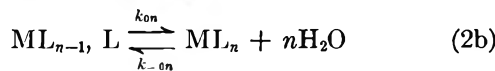
*Department of Chemistry, Brandeis University, Waltham, Massachusetts 02154 (Received September 13, 1968)*

The kinetics of complexation of cobalt(II) and nickel(II) with glycylsarcosine have been studied at 25° and an ionic strength of 0.1 M using the temperature-jump method. Only the glycylsarcosinate anion is an attacking form of this ligand in the pH range investigated. The reactions studied are of the form  $ML_{n-1}^{(3-n)+} + L^- \xrightleftharpoons[k_{-n}]{k_n} ML_n^{(2-n)+}$  with  $n = 1$  or 2 and  $M = Co$  or  $Ni$ . The rate constants for cobalt(II) are  $k_1 = 4.6 \times 10^5 M^{-1} \text{ sec}^{-1}$ ,  $k_{-1} = 75 \text{ sec}^{-1}$ ,  $k_2 = 8.0 \times 10^5 M^{-1} \text{ sec}^{-1}$ , and  $k_{-2} = 300 \text{ sec}^{-1}$ . For nickel, the rate constants are  $k_1 = 2.0 \times 10^3 M^{-1} \text{ sec}^{-1}$ ,  $k_{-1} = 7.2 \times 10^{-2} \text{ sec}^{-1}$ ,  $k_2 = 8.0 \times 10^3 M^{-1} \text{ sec}^{-1}$ , and  $k_{-2} = 1.8 \text{ sec}^{-1}$ . These results have been compared with amino acid and peptide chelating agents having no substituents on the amine or peptide nitrogen. The presence of a methyl group on the peptide nitrogen in glycylsarcosine appears to have no effect on the kinetics of formation of the monosubstituted cobalt complex or nickel complex. The presence of the methyl group plays a role for the cobalt ion by enhancing the rate of the reaction  $CoL^+ + L^-$  (formation of the bis complex) relative to the formation of the monocomplex more so for glycylsarcosine than for other homologous ligands. For nickel(II), the relative rate of enhancement is the same as for homologous ligands.

The application of fast-reaction techniques has led to the conclusion, based upon experimental evidence, that substitution of a ligand into the inner coordination sphere of a metal ion proceeds *via* a general two-step process.<sup>2</sup> The mechanism which has therefore proven consistent with the available experimental data for reactions of the type



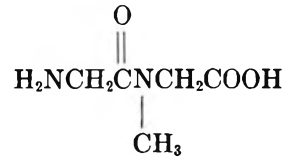
in which  $M$  is a labile metal ion,  $L$  is the incoming ligand (charges have been neglected for the sake of convenience), and  $n = 1, 2, \dots, N$ , where  $N$  is the maximum coordination number, consists of the two steps



Step a is the rapid, essentially diffusion limited dis-

placement of the bulk solvent molecules to form an ion pair,  $ML_{n-1}$ ,  $L$ . This reaction is in equilibrium with respect to the ensuing step and is described by the equilibrium quotient,  $K_{an}$ . Second, and slower, is the substitution of the reactant ligand into the metal ion's inner coordination sphere.

In this study we are reporting on a determination of the rate constants shown in reaction 1 for glycylsarcosine, whose structural formula is shown below. Of



primary interest is the determination of what role, if

(1) Department of Chemistry, Ithaca College, Ithaca, N. Y., 14850.

(2) M. Eigen, *Z. Electrochem.*, **64**, 115 (1960).

any, is played by the methyl group on the peptide nitrogen.

### Experimental Section

Fisher reagent grade nitrate salts of potassium, cobalt, and nickel were used. The glycylsarcosine was purchased from Nutritional Biochemicals Corp. and was used without further purification. The course of the chemical reaction was followed using the pH indicators phenol red and bromothymol blue purchased from Aldrich and Fisher, respectively.

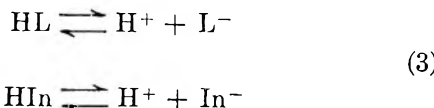
The temperature-jump apparatus, which has been described elsewhere,<sup>3a</sup> was modified to include a Dumont KM 2433 photomultiplier tube. Solutions were always freshly prepared by dissolving weighed amounts of the solid materials in distilled water and adjusting the pH by the dropwise addition of dilute NaOH and/or HNO<sub>3</sub> to  $\pm 0.01$  pH unit. The temperature was  $25 \pm 1^\circ$ .

Test solutions of either metal ion or ligand in the absence of the other showed no discernible relaxation effects. Each relaxation time represents an average of at least three photographic determinations. The relative error for these determinations is  $\pm 10\%$ .

Attempts to verify these results by another technique were made using a stopped-flow apparatus.<sup>3b</sup> Under the conditions of sensitivity that can be achieved with this technique, the cobalt(II)-glycylsarcosine reaction is too rapid to be detected at  $25^\circ$ . Measurements on the nickel(II) system at this temperature were successful, however, and the results of a representative experiment are also given. The relative error in the rate constant thus determined is  $\pm 20\%$ .

### Results

*Temperature-Jump Results.* The reactions under study are metal-ligand complexations in which the ligand is dibasic and exists in solution in at least three forms, H<sub>2</sub>L<sup>+</sup>, HL, and L<sup>-</sup>, differing in their degree of protonation. However, in the pH region investigated, the concentration of H<sub>2</sub>L<sup>+</sup> is so small it need not be considered. Present in the solution, in addition to the reactants and inert electrolyte, is a pH indicator, through which the reaction is monitored. Hence, in deriving the relaxation expressions for metal-ligand complexations, the equilibria



must also be considered.

Protonolytic reactions of the type of reaction 3 are very rapid<sup>4</sup> and can be assumed to reach equilibrium far more quickly than reactions involving metal-containing species. All the pertinent equilibrium constants used in this study are given in Table I. Although the equilibrium contribution of HL is taken into considera-

tion, the reactions studied are of the type shown in eq 1 with  $n = 1$  or 2. A reaction such as



is kinetically distinguishable from reaction 1. Its inclusion in the mechanism would be as a result of the observation of a hydrogen ion dependence.<sup>5</sup> No such dependence is exhibited by this system, indicating that, within experimental error, complexation with HL is kinetically insignificant in the pH range studied.

**Table I:** Stoichiometric Equilibrium Constants at Ionic Strength 0.1 M<sup>a</sup> and 25°

$$\begin{aligned} K_1^{\text{H}} &= [\text{H}^+][\text{L}^-]/[\text{HL}] & = 2.34 \times 10^{-6}^b \\ K_1^{\text{Ni}} &= [\text{NiL}^+]/[\text{Ni}^{2+}][\text{L}^-] & = 3.09 \times 10^{1c} \\ K_2^{\text{Ni}} &= [\text{NiL}_2]/[\text{NiL}^+][\text{L}^-] & = 4.79 \times 10^{3c} \\ K_1^{\text{Co}} &= [\text{CoL}^+]/[\text{Co}^{2+}][\text{L}^-] & = 6.17 \times 10^{3b} \\ K_2^{\text{Co}} &= [\text{CoL}_2]/[\text{CoL}^+][\text{L}^-] & = 2.63 \times 10^{3b} \\ K_{\text{In}_1} &= [\text{H}^+][\text{In}_1^-]/[\text{HIn}_1] & = 7.94 \times 10^{-8d} \\ K_{\text{In}_2} &= [\text{H}^+][\text{In}_2^-]/[\text{HIn}_2] & = 1.26 \times 10^{-8d} \end{aligned}$$

<sup>a</sup> All equilibrium constants were corrected to  $\mu = 0.1 \text{ M}$  using the formula suggested by D. D. Perrin and V. S. Sharma, *J. Chem. Soc.*, 724 (1967). <sup>b</sup> S. P. Datta and B. R. Rabin, *Trans. Faraday Soc.*, **52**, 1117 (1956). <sup>c</sup> R. B. Martin, M. Chamberlin, and J. T. Edsall, *J. Amer. Chem. Soc.*, **82**, 495 (1960). These authors quote a value of  $\log K_3^{\text{Ni}} = 2.1$  but state that it only serves to indicate the presence of a tris complex and is not an evaluation of the strength of the binding. The kinetic results indicate that for nickel(II) as for cobalt(II), tris complexes, if they exist, are a minority species whose presence, over the entire concentration range studied, is in our case experimentally undetectable. <sup>d</sup> I. M. Kolthoff, *J. Phys. Chem.*, **34**, 1466 (1930). HIn<sub>1</sub> is bromothymol blue and HIn<sub>2</sub> is phenol red.

Furthermore, the kinetic data fit the theoretical equations (*vide infra*) without the introduction of a third parameter describing the rate of formation of a tris complex. The thermodynamic data have also been fit best under the assumption of no tris complex. It is therefore concluded that only two complexes are of importance in these studies.

A general treatment for obtaining relaxation time expressions in metal-ligand systems represented by eq 1 has already been given.<sup>6</sup> The reciprocal relaxation times for systems involving two coupled complexation reactions are

$$1/\tau_{+-} = (1/2)[(a_{11} + a_{22}) \pm \sqrt{(a_{11} + a_{22})^2 - 4(a_{11}a_{22} - a_{12}a_{21})}] \quad (5)$$

(3) (a) P. Hurwitz and K. Kustin, *Inorg. Chem.*, **3**, 823 (1964); (b) P. Hurwitz and K. Kustin, *Trans. Faraday Soc.*, **62**, 427 (1966).

(4) M. Eigen, W. Kruse, G. Maass, and L. DeMaeyer, *Progr. Reaction Kinetics*, **2**, 286 (1964).

(5) G. Davies, K. Kustin, and R. F. Pasternack, *Trans. Faraday Soc.*, **64**, 1006 (1968).

(6) G. G. Hammes and J. I. Steinfield, *J. Amer. Chem. Soc.*, **84**, 4639 (1962).

where

$$\begin{aligned} a_{11} &= k_{-1} + k_1 \{ [M]/[(1 + \alpha) + [L]]\} \\ a_{12} &= k_{-1} - k_1 [M]/(1 + \alpha) \\ a_{21} &= k_2 [(L) - [ML]/(1 + \alpha)] \\ a_{22} &= k_{-2} + k_2 \{ [ML]/[(1 + \alpha) + [L]]\} \end{aligned} \quad (6)$$

where

$$\alpha = [H] \left[ K_{In}^H + [L] \frac{K_{In} + [H]}{K_{In} + [H] + [In]} \right]^{-1}$$

The experimental conditions and a summary of the observed relaxation times are shown in Table II. The calculated relaxation times are shown for comparison. Equation 5 was used in these calculations with trial values of the rate constants. The rate constants which best fit the data are given in Table III.

*Stopped-Flow Results.* In a rapid-mixing experiment, one syringe contained the metal ion, the other had the ligand and the indicator. Both syringes contained dissolved  $KNO_3$  and were of such an acidity that the solution in the mixing chamber had the values of ionic strength and pH appropriate to this study.

If the back-reaction of reaction 1 is neglected, the rate law may be written

$$d[NiL]/dt = k_1[Ni][L] \quad (7)$$

Table II: Relaxation Spectra of Cobalt(II)-Glycylsarcosine and Nickel(II)-Glycylsarcosine Solutions

$10^3[\text{glycyl-sarcosine}]_0$ , M	$10^3[\text{Co}^{2+}]_0$ , M	$10^3[\text{H}^+]$ , M	$\tau$ , msec	
			Exptl	Calcd
3.99	2.04	0.447	0.62	0.76
1.78	1.34	5.62	1.3	1.4
1.69	1.15	1.32	1.2	1.2
3.04	1.21	3.55	1.3	1.2
4.96	1.07	5.25	1.3	1.2
2.11	3.19	5.25	0.74	0.68
5.32	3.08	2.51	0.56	0.57
7.57	2.45	35.5	0.70	0.90
4.77	2.10	20.9	0.87	1.1

$10^3[\text{glycyl-sarcosine}]_0$ , M	$10^3[\text{Ni}^{2+}]_0$ , M	$10^3[\text{H}^+]$ , M	$\tau$ , sec	
			Exptl	Calcd
3.93	2.00	3.16	0.083	0.088
1.64	2.41	2.45	0.11	0.094
3.41	3.38	1.62	0.064	0.057
7.22	4.01	1.26	0.051	0.056
1.62	1.79	2.29	0.16	0.11
5.34	2.39	0.871	0.088	0.088
6.93	2.99	3.72	0.056	0.069
1.18	2.99	3.31	0.14	0.11
6.92	1.95	21.4	0.097	0.098
0.545	6.20	0.540	$k_1 = 2 \times 10^3 M^{-1} \text{ sec}^{-1}$ $\text{sec}^{-1a}$	

<sup>a</sup> Stopped-flow experiment.

Table III: Rate Constants at 25° and  $\mu = 0.1$

Metal	n	$k_n$ , $M^{-1} \text{ sec}^{-1}$	$k_{-n}$ , $\text{sec}^{-1}$
$\text{Co}^{2+}$	1	$4.6 \times 10^6$	75
	2	$8.0 \times 10^6$	300
$\text{Ni}^{2+}$	1	$2.0 \times 10^3$	$7.2 \times 10^{-2}$
	2	$8.0 \times 10^3$	1.8

Since the extent of reaction is followed by observing the changes in light transmission through the solution at the absorption maximum of the *basic* form of the coupled acid-base indicator, the working equation is

$$-dA/dt = (k_1 \epsilon l / \gamma) [Ni][L] \quad (8)$$

where  $A$  is the absorbancy,  $\epsilon$  is the extinction coefficient per unit path length ( $M^{-1} \text{ cm}^{-1}$ ),  $l$  is the path length (cm), and

$$\gamma = [( \beta + 1 )( K_{In}^H + [H] ) + \beta [L] ] / [H]$$

where

$$\beta = (K_{In} + [H]) / [In]$$

The oscilloscopes obtained by this method are a display of per cent transmittance vs. time. Consequently, the data were converted to absorbancy and replotted in conformance to the units implied by eq 8. The method of initial slopes was used in order to ensure that neglect of the back-reaction would not introduce an appreciable error. Figure 1 is an example of the graphical evaluation of a stopped-flow experiment. (Experimental conditions are given in the figure caption.) The result of these determinations yields the value  $k_1 = 2.0 \times 10^3 M^{-1} \text{ sec}^{-1}$  ( $\pm 20\%$ ), in good agreement with the temperature-jump experiments.

However, the analysis of the stopped-flow experiment, unlike that of the temperature-jump experiment, is fully independent of the equilibrium constant for metal complex formation. Therefore, the value of the rate constant does not reflect uncertainties in the metal-ligand equilibrium quotient.

### Discussion

Before discussing the glycylsarcosine results, it will be useful to summarize, briefly, the main features of eq 2, the mechanism of fast metal complex substitution reactions. With step (a) rapid and the steady-state approximation applied to the concentration of the ion pair, the observed second-order rate constant is

$$k_n = k_{0n} K_{an} \quad (9)$$

In this case, which may be referred to as normal substitution, the slow step is the expulsion of a water molecule from the metal ion's inner coordination sphere. This process is characterized by  $k_{0n}$ .

Two approaches have been used to determine the

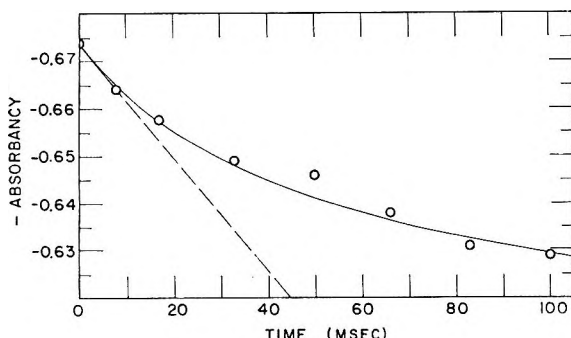


Figure 1. Stopped-flow experiment. Initial concentrations (zero time):  $[Ni^{2+}] = 6.20 \times 10^{-3} M$ ; [glycylsarcosine] =  $5.45 \times 10^{-4} M$ ; [phenol red] =  $1.20 \times 10^{-6} M$ ;  $[H^+] = 5.40 \times 10^{-9} M$ . Absorbancy at zero time is 0.674. Necessary final conditions are  $[H^+] = 8.20 \times 10^{-9} M$  and an absorbancy of 0.573. A smooth curve has been drawn through the experimental points. The dashed line represents the tangent to the curve at zero time. It has a slope of 1.2.

effect of ligand properties on  $k_{0n}$ . In one approach  $K_{an}$  is calculated for a series of ligands of like charge, and the computed rate constant,  $k_{0n}$ , is examined for effects of ligand properties. In another approach, a series of measured second-order rate constants is used to determine empirically a constant value of  $K_{an}$  for ligands of like charge.

For each metal ion, the  $k_{01}$  rate constant has been found to be relatively insensitive to ligand properties.<sup>7</sup> The value of this rate constant is also in reasonably good agreement with the rate constant for the removal of a water molecule from the inner coordination sphere of the fully aquated ion.<sup>8</sup> In a number of special cases the rate of substitution has been observed to fall below the normal value. For chelating agents with relatively unfavorable geometries, (e.g.,  $\beta$ -amino acids) the rate of chelate ring closure is rate determining, and the limiting case of eq 9 no longer applies.<sup>9</sup>

It has also been observed that neutral or positively charged ligands are unreactive. This observation is by no means a general rule but depends upon charge separation. For large zwitterions the positive charges may be so effectively screened that the neutral ligand reacts as though it had unit negative charge.<sup>10</sup> Smaller neutral ligands such as glycine show very little tendency to react.<sup>11</sup> An interesting example of an intermediate case is given by arginine.<sup>12</sup> This amino acid has a positively charged terminal guanidine group which remains charged while the ligand is bound to the metal ion. Nevertheless, the electrostatic repulsion appears only in the association rate constants; the dissociation rate constants remain typical of other amino acids.

The situation regarding the formation of higher order complexes is less certain. For example, the rate constants  $k_{02}$  have been shown to depend upon the nature of previously complexed ligand, owing to its influence on the rate of release of the remaining water molecules

from the inner coordination sphere of the metal ion.<sup>7</sup> Among the ligand characteristics which have been shown to be important in determining this rate are ligand charge<sup>7</sup> and structure.<sup>13</sup>

In order to facilitate the following discussion of the nickel and cobalt results, some pertinent rate constants have been presented in Table IV, to which further reference will be made.

**Cobalt (II).** Previous work has shown that one set of rate constants apply for the reactions of cobalt(II) with the oligoglycines (diglycine, triglycine, and tetraglycine).<sup>14</sup> The values (cf. Table IV) are  $k_1 \sim 3 \times 10^6 M^{-1} sec^{-1}$  and  $k_2 \sim 2 \times 10^6 M^{-1} sec^{-1}$ . For glycylsarcosine,  $k_1 = 5 \times 10^6 M^{-1} sec^{-1}$ , in good agreement with the value obtained for these oligoglycines. All these  $k_1$  rate constants are a factor of 3–5 smaller than the corresponding value for cobalt(II) with glycine. Since the five ligands each carry a formal charge of –1, based on the simple mechanism discussed in the previous section, one could anticipate better agreement among these rate constants. It has been suggested that the final ML complex for the oligopeptides does not involve bonding to the carboxyl oxygen, the site of the negative charge.<sup>15</sup> The ligand is then considered to be attacking the metal ion as if it were a neutral species.<sup>11</sup> However, this approach is not completely satisfactory either since the  $k_1$  values measured are a factor of 2–5 times greater than those normally obtained for cobalt(II) with neutral ligands. We are led to conclude that the complexation reactions follow the normal pattern for cobalt(II) with the oligopeptides including glycylsarcosine and that the methyl group plays no major role in determining this rate but that the simple approach for calculating  $K_{a1}$ , the ion-pair equilibrium constant, is not applicable in this case. Whether this is due to the size of the ligand or the remoteness of the negative site from the positive metal ion cannot be determined from this study alone. It might be mentioned that the value of  $k_1$  for cobalt(II) with the dipeptide L-carnosine in which bonding does occur to the carboxyl group is  $4 \times 10^6 M^{-1} sec^{-1}$ , again in good agreement with the above values. However,

(7) M. Eigen and R. G. Wilkins, "Mechanisms of Inorganic Reactions," Advances in Chemistry Series, No. 49, American Chemical Society, Washington, D. C., 1965.

(8) T. J. Swift and R. E. Connick, *J. Chem. Phys.*, **37**, 307 (1962); **41**, 2553 (1964).

(9) K. Kustin, R. F. Pasternack, and E. Weinstock, *J. Amer. Chem. Soc.*, **88**, 4610 (1966).

(10) K. Kustin and R. F. Pasternack, *ibid.*, **90**, 2805 (1968).

(11) J. Cassatt and R. G. Wilkins, *J. Amer. Chem. Soc.*, **90**, 6045 (1968).

(12) G. Davies, K. Kustin, and R. F. Pasternack, *Int. J. Chem. Kinetics*, in press.

(13) D. W. Margerum and H. M. Rosen, *J. Amer. Chem. Soc.*, **89**, 1088 (1967).

(14) G. Davies, K. Kustin, and R. F. Pasternack, to be submitted for publication.

(15) See p 355, H. C. Freeman, *Advan. Protein Chem.*, **22**, 257 (1967).

Table IV: Selected Complexation Rate Constants for Cobalt(II) and Nickel(II)<sup>a</sup>

Ligand	Charge of attacking form	$k_1$	$k_2$	$k_3$	Ref
Cobalt(II)					
L-Glycine	-1	$1.5 \times 10^6$	$2.0 \times 10^6$	$8.0 \times 10^6$	b
Malonic acid	-1	$7 \times 10^6$			c
$\alpha$ -Alanine	-1	$6.0 \times 10^6$	$8.0 \times 10^6$	$9.0 \times 10^4$	d
Glycylsarcosine	-1	$4.6 \times 10^6$	$8.0 \times 10^6$		e
L-Carnosine	-1	$4.2 \times 10^5$			f
Triglycine	-1	$3.1 \times 10^6$	$1.0 \times 10^6$		b
Tetraglycine	-1	$2.6 \times 10^6$	$2.3 \times 10^6$		b
Glycylglycine	-1	$2.0 \times 10^5$	$1.6 \times 10^5$		b
L-Arginine	0	$1.5 \times 10^5$	$8.7 \times 10^5$	$2.0 \times 10^6$	g
1,10-Phenanthroline	0	$1.4 \times 10^5$			h
Imidazole	0	$1.3 \times 10^6$	$1.1 \times 10^6$		i
Ammonia	0	$9.5 \times 10^4$			j
Nickel(II)					
L-Glycine	-1	$4.1 \times 10^4$	$5.6 \times 10^4$	$4.3 \times 10^4$	b
$\alpha$ -Alanine	-1	$2.0 \times 10^4$	$4.0 \times 10^4$		d
Oxalic acid	-1	$5 \times 10^3$			k
Imidazole	0	$5.0 \times 10^3$	$4.3 \times 10^3$		i
1,10-Phenanthroline	0	$3.9 \times 10^3$			h
Ammonia	0	$3.3 \times 10^3$			j
Glycylglycine	-1	$3.2 \times 10^3$	$9.2 \times 10^3$	$4.0 \times 10^3$	b
Malonic acid	-1	$3.1 \times 10^3$			l
L-Arginine	0	$2.3 \times 10^3$	$2.4 \times 10^4$	$3.5 \times 10^4$	g
Glycylsarcosine	-1	$2.0 \times 10^3$	$8.0 \times 10^3$		e
Tetraglycine	-1	$1.8 \times 10^3$	$4.9 \times 10^3$		b
Triglycine	-1	$1.7 \times 10^3$	$5.5 \times 10^3$		b

<sup>a</sup> All association rate constants have the units  $M^{-1} \text{ sec}^{-1}$ . <sup>b</sup> G. Davies, K. Kustin, and R. F. Pasternack, to be submitted for publication. These values are more recent than those of footnote i. <sup>c</sup> F. P. Cavasino, *Ric. Sci. Rend.*, **A35**, 1120 (1965). <sup>d</sup> K. Kustin, R. F. Pasternack, and E. Weinstock, *J. Amer. Chem. Soc.*, **88**, 4610 (1966). <sup>e</sup> This work. <sup>f</sup> K. Kustin and R. F. Pasternack, *J. Amer. Chem. Soc.*, **90**, 2805 (1968). <sup>g</sup> G. Davies, K. Kustin, and R. F. Pasternack, *Int. J. Chem. Kinetics*, in press. <sup>h</sup> R. H. Holyer, C. D. Hubbard, S. F. A. Kettle, and R. G. Wilkins, *Inorg. Chem.*, **4**, 929 (1965). <sup>i</sup> G. G. Hammes and J. I. Steinfeld, *J. Amer. Chem. Soc.*, **84**, 4639 (1962). <sup>j</sup> D. B. Rorabacher, *Inorg. Chem.*, **5**, 1891 (1966). Rate constant at 20°. <sup>k</sup> G. H. Nancollas and N. Sutin, *ibid.*, **3**, 360 (1964). <sup>l</sup> F. P. Cavasino, *J. Phys. Chem.*, **69**, 4380 (1965).

there is a further complicating feature in this case; a positive center exists in the molecule, albeit far removed from the binding site.

The  $k_2$  value for glycylsarcosine is a factor of 4 greater than that obtained for the oligoglycines. Since the charge and statistical effect (number of remaining waters relative to the total number of sites on the metal) are quite likely the same for all these ligands, it appears that the presence of the methyl group on the peptide nitrogen atom, which serves to increase the electron-pair donating ability of a bound atom, has enhanced the rate of release of a water molecule from the monocomplex to a small though detectable extent.

*Nickel(II)*. As for cobalt(II), the  $k_1$  values for the oligoglycines agree very well with the value obtained for glycylsarcosine ( $k_1 \sim 2 \times 10^3 M^{-1} \text{ sec}^{-1}$ ). Here once again, the methyl group is playing no significant role in determining the rate of the formation of the ML complex. However, when the  $k_1$  value is compared with the appropriate rate constant for glycine, the

factor proves much larger for nickel than for cobalt. For nickel(II)

$$\frac{k_1^{\text{glycine}}}{k_1^{\text{oligopeptides}}} \sim 20$$

Furthermore, whereas the cobalt value for  $k_1$  is larger than that obtained for neutral ligands, the nickel value is comparable with or even a little smaller than that obtained for neutral ligands.

We therefore conclude that normal kinetic chelation behavior is not being exhibited by nickel(II). Since the cobalt(II) chelation showed normal behavior for anionic attack, it is reasonable to assume that carboxylate coordination is important in the finally formed chelate. Applying the same reasoning leads us to conclude that since normal kinetics is not followed for anionic attack in the nickel(II) case, carboxylate bonding is not important here. This conclusion is also supported by the limited number of reported structure determinations for metal-peptide chelates.<sup>15</sup>

In a previous study,<sup>9</sup> it had been shown that a departure from normal kinetics in the reactions of certain bidentate chelating agents could be ascribed to sterically hindered chelate ring closure. The experimental evidence in support of this conclusion was that the effect was exhibited by ions more labile than nickel(II), namely, Co(II) and Mn(II), but not by nickel(II) itself. For the oligoglycines and glycylsarcosine the opposite is true; that is, reaction with cobalt(II) is normal, while that with nickel(II) is inhibited. The grounds for this behavior should therefore be found in the nature of the nickel(II) chelate's structure. Without further experimental evidence, the details of this interaction remain an open question. However, the kinetic evidence leads us to the conclusion that the bonding model is somewhat different for the nickel complexes of these oligopeptides than for the cobalt complexes. It would appear that whereas bonding to the carboxyl oxygen might be of considerable importance in cobalt complexes, it plays a small role in the nickel complexes. From a molecular model of glycylsarcosine we learn that for effective bonding to the carboxyl oxygen the cobalt ion must be associated with

the peptide nitrogen rather than the carbonyl oxygen atom of the dipeptide.

This model is consistent with the observation that the methyl group bound to the peptide nitrogen atom more effectively influences the rate of the formation of the bis complex for cobalt(II) than for nickel(II). The  $k_2$  value for nickel(II) is about the same for the oligoglycines and glycylsarcosine ( $k_2 \sim 7 \times 10^3 M^{-1} \text{ sec}^{-1}$ ), while for cobalt(II) the glycylsarcosine value is significantly larger than the oligoglycine value.

One further bit of kinetic evidence for a difference between the bonding in nickel peptides and cobalt peptides involves the  $k_2/k_1$  ratios. This ratio is greater than unity for nickel(II) and the oligoglycines but less than unity for cobalt(II) and these same ligands. The degree of enhancement ( $k_2/k_1$ ) has been shown to be strongly dependent on the nature of the ligand bonding.<sup>13</sup>

*Acknowledgment.* The authors gratefully acknowledge partial support from the Public Health Service Research Grant GM8893-06 from the National Institute of General Medical Sciences, Public Health Service (K. K.), and from the Petroleum Research Fund for Grant 2982B (R. F. P.)

## The Diaphragm Cell Method for the Investigation of Thermal and Self-Thermal Diffusion in Liquid Electrolyte Solutions<sup>1</sup>

by Andrzej S. Cukrowski<sup>2</sup>

*Institute of Physical Chemistry, Polish Academy of Sciences, Warsaw, Poland*

*Accepted and Transmitted by The Faraday Society (November 6, 1967)*

The diaphragm cell method with a magnetically operated stirring system has been adapted for the time-dependent and the stationary-state measurements of thermal and self-thermal diffusion in liquids. The phenomenological equations derived here describe the rate of change of concentrations. Formulas which allow the calculation of the activation energy from the average for the diaphragm values of diffusion and self-diffusion coefficients in polythermal and isothermal conditions have been given. Experiments with dilute aqueous solutions of NaCl, KCl, <sup>22</sup>NaCl, and <sup>22</sup>Na in KCl have been carried out. Diffusion and self-diffusion coefficients under polythermal conditions, activation energies, the Soret coefficients, and heats of transport are evaluated. The Soret coefficient and the heat of transport of NaCl in extreme dilution have been measured. Comparison with other experimental and theoretical results is given.

### I. Introduction

The method discussed here makes it possible to investigate thermal diffusion as well as self-thermal diffusion, *i.e.*, the transport of a small amount of a labeled tracer ion under polythermal conditions, in liquid electrolyte solutions. Contrary to widely investigated

thermal diffusion,<sup>3</sup> self-thermal diffusion in liquid electrolyte solutions has not been investigated yet.

(1) This work comprises part of the Ph.D. dissertation of A. S. Cukrowski, Institute of Physical Chemistry, Polish Academy of Sciences, Warsaw.

(2) Institute of Basic Technical Problems, Polish Academy of Sciences, Warsaw.

In the theoretical section we present the equations which describe the concentrations as functions of time and which allow us to study a polythermal process at any instant, contrary to the measurements<sup>4,5</sup> performed under stationary conditions.<sup>6</sup>

In the Experimental Section self-thermal diffusion as well as thermal diffusion data are presented.

The apparatus used enabled us to investigate the stationary states of thermal and self-thermal diffusion as well as the rate of attainment of these states. For this reason we could use only those methods in which it is possible to measure the concentration of radioactive ions. That is why the conductometric and optical methods and those methods in which the thermoelectric powers are measured could not be used.<sup>3</sup> The thermogravitational method<sup>3</sup> also is not suitable here because it is not possible to investigate the transport of the radioactive ions in the stationary state of thermal diffusion. Also electrothermal diffusion,<sup>7,8</sup> which is especially convenient for the measurements of thermal diffusion in electrolyte solutions, cannot be applied here to measure the self-thermal diffusion of a radioactive ion in pure water because the voltage needed is too high. The diaphragm cell method seems to be the most suitable for the investigations of thermal and self-thermal diffusion. It has already been applied for thermal diffusion,<sup>4,5</sup> but the laminar layer, which always exists in the vicinity of the diaphragm and directly affects transport processes, has not been reduced in the papers mentioned to such an extent as it has been under isothermal conditions by Stokes.<sup>6,9</sup> That is why we tried to adapt the Stokes method to polythermal conditions.

## II. The Time Dependence of Concentrations during Thermal Diffusion in the Diaphragm Cell Method

The derivations will be limited to thermal diffusion in binary electrolyte solutions. The discussion of the self-thermal diffusion equations, which can be performed in a similar manner, will be given in section IV.

The electrolyte discussed consists of solvent 0 and ions 1 and 2. In the derivations to be given, the scheme of the diaphragm cell method as presented in Figure 1 will be adopted. The apparatus contains two vessels which are separated by means of a porous diaphragm. Let the effective cross section of the diaphragm be  $A$  and the effective average length along the diffusion path be  $l$ . The quantities connected with the lower and upper vessels will be denoted by the subscripts L and U, respectively. We assume that the mixing is sufficient to maintain, in each vessel, constant temperatures  $T_L$  and  $T_U$  and molar concentrations  $c_{i,L}$  and  $c_{i,U}$  ( $i = 0-2$ ). In other words, temperature and concentration gradients exist in the diaphragm only. We assume that the temperature gradient is stationary; i.e.,  $T_L$  and  $T_U$  are constant during the experiment. It means that the relaxation time for the temperature

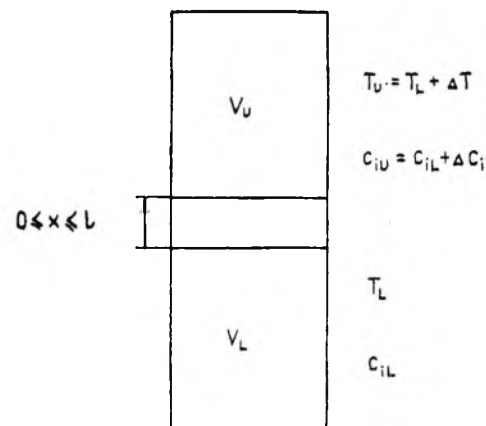


Figure 1. Scheme of the diaphragm cell method.

change is much smaller than for diffusion processes. We want to determine now the concentrations of components in both vessels as a function of time. We shall take into account suitable boundary conditions.

If we assume that the volume of the liquid in porous diaphragm is negligible

$$c_{i,L}V_L + c_{i,U}V_U = c_{i,A}(V_L + V_U) \quad (i = 0-2) \quad (1)$$

where  $c_{i,A}$  denotes the average concentration of  $i$ th component for both vessels. For molar fractions eq 1 can be presented in the form

$$N_{i,L} = \frac{1}{V_L} [N_{i,A}(V_L + V_U) - N_{i,U}V_U'] \quad (i = 0-2) \quad (2)$$

where

$$V_k' = V_k \frac{c_k}{c_A} \quad (k = L \text{ or } U) \quad (3)$$

where  $c$  denotes the sum of the concentrations of the ions and solvent and  $A$  is used for the average quantities for both vessels. From eq 3 we see that for dilute solutions, for which  $c_A = c_L = c_U$ ,  $V_L'$  and  $V_U'$  are equal to  $V_L$  and  $V_U$ , respectively. It is sufficient to discuss the thermal diffusion of one ion only because in binary-electrolyte solutions the two ions move together owing to electroneutrality.<sup>10</sup> Therefore, let us further discuss ion 1 only. We assume, as Robinson and

(3) H. J. V. Tyrrel, "Diffusion and Heat Flow in Liquids," Butterworth & Co., London, 1961.

(4) K. F. Alexander, *Z. Phys. Chem. (Leipzig)*, 197, 233 (1951).

(5) R. L. Saxton, E. L. Dougherty, and H. G. Drickamer, *J. Chem. Phys.*, 22, 1166 (1954).

(6) Such equations under isothermal conditions have been presented in R. A. Robinson and R. H. Stokes, "Electrolyte Solutions," 2nd ed., Butterworth & Co., London, 1959.

(7) B. Baranowski and J. Demichowicz, *Roczn. Chem.*, 27, 494 (1953).

(8) B. Baranowski and J. Demichowicz, *ibid.*, 29, 603 (1955).

(9) R. H. Stokes, *J. Amer. Chem. Soc.*, 72, 763 (1950).

(10) B. Baranowski and A. S. Cukrowski, *Z. Phys. Chem. (Leipzig)*, 228, 292 (1965).

Stokes<sup>6</sup> did, that the ions do not accumulate inside the diaphragm; *i.e.*, the number of ions entering into the diaphragm from one side is equal to the number of ions coming out from the other side. Thus we obtain

$$\begin{aligned}\frac{dc_{1,L}}{dt} &= -J_1(t) \frac{A}{V_L} \\ \frac{dc_{1,U}}{dt} &= J_1(t) \frac{A}{V_U}\end{aligned}\quad (4)$$

where  $J_1(t)$  denotes the flow of ion 1 through the diaphragm at time  $t$ . From eq 4 it follows that

$$\frac{d\Delta N_1}{dt} = \beta' l J(t) \quad (5)$$

where

$$\beta' = \frac{A}{l} \left( \frac{1}{V_L} \frac{dN_{1,L}}{dc_{1,L}} + \frac{1}{V_U} \frac{dN_{1,U}}{dc_{1,U}} \right) \quad (6)$$

which for dilute solutions, after assuming that  $c$  is constant, simplifies to

$$\beta' = \frac{1}{c_A} \beta = \frac{A}{c_A l} \left( \frac{1}{V_L} + \frac{1}{V_U} \right) \quad (7)$$

Now we shall solve eq 5 in such a way as to obtain the formula in which measurable quantities are directly correlated. In the case of a one-dimensional problem, the phenomenological equation can be written as

$$J_1 = -D_1 \frac{\partial N_1}{\partial x} - D_1' N_1 \frac{\partial T}{\partial x} \quad (8)$$

We define the Soret coefficient as

$$S_{T_1} = -\frac{D_1'}{D_1} \quad (9)$$

In order to introduce the measurable quantities into eq 8, we shall define the average quantities for the diaphragm in the following way

$$\overline{J_1(t)} = \frac{1}{\Delta N_1 \Delta T} \int_{N_{1,L}}^{N_{1,L} + \Delta N_1} \int_{T_L}^{T_L + \Delta T} J_1 dN_1 dT \quad (10)$$

In the same way we define  $\overline{D_1(t)}$  and  $\overline{D_1'(t)N_1(t)}$ . In these averages we integrate only with respect to  $N_1$ , because, as it follows from the electroneutrality condition, there exists only one independent molar fraction in the system.<sup>10</sup> We also assume that the gradients of molar fractions and temperatures are independent of the  $x$  coordinate. After integrating eq 8, we get

$$\overline{J_1(t)} = -\overline{D_1(t)} \frac{\Delta N_1}{l} - \overline{D_1(t)N_1(t)} \frac{\Delta T}{l} \quad (11)$$

The molar fraction difference is a continuous, strictly monotonic function of time. Therefore, we can write the inverse function

$$t = t(\Delta N_1) \quad (12)$$

The average quantities defined in eq 10 are functions of time only because they are averaged for the quantities inside the diaphragm which are functions of place and time. Taking this into account and using eq 11, we write eq 5 as

$$\begin{aligned}\int_{(\Delta N_1)_0}^{(\Delta N_1)_t} \frac{d\Delta N_1}{\overline{D_1(\Delta N_1)\Delta N_1} + \overline{D_1'(\Delta N_1)N_1(\Delta N_1)\Delta T}} &= \\ - \int_0^t \beta' dt \quad (13)\end{aligned}$$

This is the general solution of the problem discussed.

Let us introduce some simplifying assumptions, making the integration of eq 13 possible. It will be shown at the end of this section that these approximations are sufficient for dilute aqueous electrolyte solutions. If we neglect the effects of changes of  $\Delta N_1$  on  $D_1$  and  $D_1'$ , we have

$$\overline{D_1(t)} = \overline{D_1(\Delta N_1)} = \overline{D_1} \quad (14)$$

$$\begin{aligned}\overline{D_1'(t)N_1(t)} &= \overline{D_1'(\Delta N_1)N_1(\Delta N_1)} = \\ \overline{D_1'N_1(\Delta N_1)} &= \overline{D_1'} \overline{N_1(\Delta N_1)} \quad (15)\end{aligned}$$

The coefficients  $\overline{D_1}$  and  $\overline{D_1'}$  have been averaged with respect to temperature and they do not depend on molar fraction and time. We assume also that  $V_L'$ ,  $V_U'$ , and  $\beta'$  are constant and do not depend on molar fractions and time. As we can see from eq 3 and 6, it means that we neglect here the effect of change of ionic concentration, of the order of 0.05  $N$ , on the sum of concentrations  $c$ , of the order of 50  $N$ .

Now we will discuss the quantity  $\overline{N_1(\Delta N_1)}$ . From the assumption that grad  $N_1$  is independent of the  $x$  coordinate, it follows that

$$N_1 = N_{1,L} + \frac{x}{l} \Delta N_1 \quad (16)$$

From eq 2 it follows that

$$N_{1,L} = \frac{V_L + V_U}{V_L' + V_U'} N_{1,A} - \frac{V_U'}{V_L' + V_U'} \Delta N_1 \quad (17)$$

After taking into account eq 10 and 15–17, we obtain the average value of the molar fraction in the diaphragm

$$\overline{N_1(\Delta N_1)} = \frac{V_L + V_U}{V_L' + V_U'} N_{1,A} + \frac{V_L' - V_U'}{V_L' + V_U'} \frac{\Delta N_1}{2} \quad (18)$$

If we assume that  $\beta'$  does not depend on  $\Delta N_1$  and take into account eq 13–15 and 18, we obtain

$$\begin{aligned}\int_{(\Delta N_1)_0}^{(\Delta N_1)_t} \frac{d\Delta N_1}{\left( \overline{D_1} + \overline{D_1'} \frac{V_L' - V_U'}{V_L' + V_U'} \frac{\Delta T}{2} \right) \times} &= \beta' t \quad (19) \\ \Delta N_1 + \bar{D}' \frac{V_L + V_U}{V_L' + V_U'} N_{1,A} \Delta T\end{aligned}$$

Equation 20 can be integrated if we take into account that  $\Delta T$  does not depend on  $\Delta N_1$  and assume that  $\bar{D}_1$ ,  $\bar{D}'_1$ ,  $V_L'$ , and  $V_U'$  also do not depend on  $\Delta N_1$ . After integrating we obtain

$$\frac{(\Delta N_1)_t + \gamma}{(\Delta N_1)_0 + \gamma} = \exp[-(1 + \alpha)\bar{D}_1\beta't] \quad (20)$$

where

$$\alpha = \frac{\bar{D}'_1}{\bar{D}_1} \frac{V_L' - V_U'}{V_L' + V_U'} \frac{\Delta T}{2} \quad (21)$$

$$\gamma = \frac{\bar{D}'_1 \frac{V_L + V_U}{V_L' + V_U} N_{1,A} \Delta T}{\bar{D}_1 + \bar{D}'_1 \frac{V_L' - V_U'}{V_L' + V_U} \frac{\Delta T}{2}} \quad (22)$$

For  $t \rightarrow \infty$ , the right side of eq 20 vanishes and  $\gamma$  can be eliminated. Thus we obtain the final equation sought for

$$\ln \frac{(\Delta N_1)_t - (\Delta N_1)_{\infty}}{(\Delta N_1)_0 - (\Delta N_1)_{\infty}} = -(1 + \alpha)\bar{D}_1\beta't \quad (23)$$

If we start from  $(\Delta N_1)_0 = 0$ , according to eq 23 we can compute the time required for obtaining the desired  $(\Delta N_1)_t/(\Delta N_1)_{\infty}$

$$t = \frac{-1}{\bar{D}_1\beta'(1 + \alpha)} \ln \left[ 1 - \frac{(\Delta N_1)_t}{(\Delta N_1)_{\infty}} \right] \quad (24)$$

For practical computations,  $\alpha$  in eq 23 and 24 is very small and can often be neglected. To verify this fact it is sufficient to use  $V_L$  and  $V_U$  instead of  $V_L'$  and  $V_U'$  in eq 21.

In isothermal conditions, eq 23 simplifies to the result obtained by Robinson and Stokes,<sup>6</sup> because then  $\Delta T = 0$  and  $\alpha = 0$ , and, owing to  $(\Delta N_1)_{\infty} = 0$ , it can be written that

$$\ln \frac{(\Delta N_1)_t}{(\Delta N_1)_0} = -\bar{D}_1\beta't \quad (25)$$

In the discussed result<sup>6</sup>  $\bar{D}^c\beta$  instead of  $\bar{D}_1\beta'$  is used, where the diffusion coefficient  $D^c$  is defined in the molar concentration scale<sup>11</sup>

$$J_1 = -D^c \frac{\partial c_1}{\partial x} \quad (26)$$

The product  $\bar{D}^c\beta$  can be used in eq 25 if we take into account that for dilute solutions

$$\bar{D}_1\beta' = \bar{D}^c\beta \quad (27)$$

Let us discuss now the simplifying assumptions 14–16. If we took into account that  $N_1$  was a weakly nonlinear function of  $x$  and if we did not neglect the small concentration dependence of  $D_1$  and  $D'_1$ , it would have an effect on  $\alpha$ , which is negligible, and  $\gamma$ . The role of  $\gamma = (\Delta N_1)_{\infty}$ , as is seen from eq 23, depends on how large  $(\Delta N_1)_{\infty}$  would be in comparison to  $(\Delta N_1)_0$  and

$(\Delta N_1)_t$ . If they are large in comparison to  $(\Delta N_1)_{\infty}$ , the role of  $\gamma$  is not important. It is so in the case of the measurement of the diffusion coefficient under polythermal conditions. In such experiments one uses values of  $(\Delta N_1)_0$  and  $(\Delta N_1)_t$ , considerably larger than  $(\Delta N_1)_{\infty}$ . The role of  $\gamma$  is more important in the thermal diffusion process in which we start from  $(\Delta N_1)_0 = 0$ . However, even if the effect of the discussed simplifications were large, eq 24 could be used as a very convenient one for the evaluation of time which is necessary to obtain the stationary state. This equation would not be fulfilled well if in the denominator of eq 18 higher powers of  $\Delta N_1$  appeared. Generally, the concentration dependence of the quantities which determine the flow through the diaphragm is sufficiently small and for this reason we could use the discussed simplifications 14–16.

### III. The Diffusion Coefficient under Polythermal Conditions

From eq 23 we can obtain the average value of the diffusion coefficient under polythermal conditions  $\bar{D}_1$ . This quantity describes the process we have been mainly interested in, *i.e.*, the rate of attainment of the stationary state.

We shall show here that  $\bar{D}_1$  can also be useful to obtain the activation energy of diffusion process. For this purpose we need to relate  $\bar{D}_1$  with  $D_1$ .

If we neglect the concentration dependence of  $D_1$ , we can write

$$\bar{D}_1 = \frac{1}{\Delta T} \int_{T_L}^{T_L + \Delta T} D_1 \, dT \quad (28)$$

We assume the following temperature dependence of the diffusion coefficient:

$$D_1 = D_{1,0} \exp\left(-\frac{E}{RT}\right) \quad (29)$$

From eq 28 and 29 after integrating we obtain

$$\bar{D}_1 = \frac{D_{1,0}}{\Delta T} \left\{ (T_L + \Delta T) \exp\left[-\frac{E}{R(T_L + \Delta T)}\right] - T_L \exp\left(-\frac{E}{RT_L}\right) + \frac{E}{R} \left\{ -Ei\left(-\frac{E}{RT_L}\right) - \left(-\frac{E}{R(T_L + \Delta T)}\right) \right\} \right\} \quad (30)$$

where  $-Ei(-x)$  is the tabulated function

$$-Ei(-x) = \int_{-\infty}^{-x} \frac{\exp p}{-p} \, dp \quad (31)$$

If we know the value of  $\bar{D}_1$  under polythermal conditions and the isothermal value of the diffusion coefficient

(11) The molar fraction scale has been used here in order to make the derivations clearer; molar fractions, contrary to molar concentrations, do not depend on temperature. Equation 27 makes it possible also to use  $D^c$  in eq 23 and 24.

cient at temperature  $T = D_1(T)$ , we can express the activation energy of diffusion when eq 30 and 31 are taken into account

$$\frac{\bar{D}_1}{D_1(T)} = \frac{\exp \frac{E}{RT}}{\Delta T} \left\{ (T_L + \Delta T) \exp \left[ \frac{-E}{R(T_L + \Delta T)} \right] - T_L \exp \left( \frac{-E}{RT_L} \right) + \frac{E}{R} \left\{ -[-Ei \times \left( \frac{E}{R(T_L + \Delta T)} \right)] - Ei \left( \frac{-E}{RT_L} \right) \right\} \right\} \quad (32)$$

From this equation the activation energy can be obtained by the successive-approximation method. For small  $\Delta T$  we can assume that the average value  $\bar{D}_1$  equals the value of the diffusion coefficient at the average temperature,  $D_1(T_L + \frac{1}{2}\Delta T)$ . Then we get

$$\bar{D}_1 = D_{1,0} \exp \frac{-E}{R(T_L + \frac{1}{2}\Delta T)} \quad (33)$$

and

$$E = \frac{R \ln \frac{D_1}{D_1(T)}}{\frac{1}{T} - \frac{1}{T_L + \frac{1}{2}\Delta T}} \quad (34)$$

This can be treated as the first approximate solution of eq 32.

The derivations presented above could be given in the molar concentration scale. We would have then in eq 29  $D^c$ ,  $D_{1,0}^c$ , and  $E^c$  and such quantities would appear in eq 30, and 32-34.

#### IV. Self-Thermal Diffusion

In the case of self-thermal diffusion, the derivation procedure is much the same as that presented in sections II and III. It is sufficient to introduce here instead of quantities  $D_1$  and  $D_1'$  defined in eq 8, the quantities  $D_{3,12}$  and  $D_{3,12}'$ , defined in the same way for the tracer ion. It is possible to take into account the gradients of temperature and molar fraction of a tracer ion only because cross-effect representing the effect of the gradient of  $N_1$  on the flow of the tracer ion,  $J_3$ , can be neglected.<sup>12</sup> It should be taken into account in the derivations that the average quantities defined in eq 10 and 11 should then be integrated with respect to  $N_3$ . In this way we could obtain for the self-thermal diffusion of the tracer ion such equations as eq 21, 23, 24, 27, 30, 32, 33, and 34, where  $D_{3,12}$ ,  $D_{3,12}'$ ,  $N_3$ , and  $E_3$  instead of  $D_1$ ,  $D_1'$ ,  $N_1$  and  $E$  should be introduced.

The experiments of self-thermal diffusion can be performed if we introduce a small amount of radioactive isotope, 3, to the binary electrolyte in which a stationary temperature difference is maintained. At the beginning of the experiment, the binary-electrolyte solution can

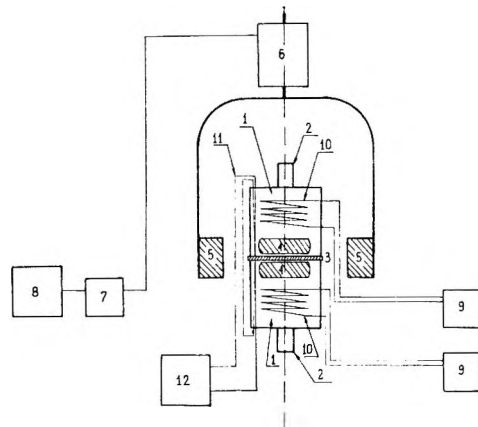


Figure 2. Diagram of the apparatus used. Between two vessels made of Rasotherm glass (1) and locked with corks (2) there is a diaphragm made of porous glass (3). In the vicinity of the diaphragm the magnetic stirrers (4) are placed in both vessels. The magnet (5) is rotated by an electric motor (6) whose speed is controlled by an autotransformer (7) switched on the stabilized voltage source (8). A constant-temperature difference is maintained by means of thermostats (9) which are combined with multiloop coils (10). Temperatures are measured with copper-constantan thermocouples (11) in both vessels in the vicinity of the diaphragm with the accuracy of 0.02° on the compensator (12).

find itself in the initial or stationary state of thermal diffusion. In both cases equations similar to eq 23 can be used. There is only the difference in  $\alpha^*$ . In the first case there will be  $(D_{3,12})_0$  and in the second  $(D_{3,12}')_\infty$ . The subscripts 0 and  $\infty$  denote here the initial and stationary state, respectively.

#### V. Experimental Section

The apparatus, which is an adaptation of the Stokes method<sup>9</sup> to polythermal conditions, is schematically shown in Figure 2.

The measurements were performed as follows. The two vessels were filled with the air-freed hot aqueous solutions of electrolyte, and a few minutes later the magnet was set into motion. After the experiment was finished, the solutions were removed from both vessels and their concentrations were determined.

The concentration of the electrolyte was measured by Zeiss interferometer with an accuracy of about 0.00005 N for 0.02 N solutions. For concentrations higher than 0.05 N the accuracy was not higher than 0.1%, because creeping of the electrolyte in the interferometer made it impossible to obtain a higher accuracy in these ranges. In the Soret coefficient measurements the effect of creeping, which depends on the concentration, could be partly compensated, because in this case the difference of concentrations in both vessels is very small.

The radioactivity was measured with an accuracy

(12) A. S. Cukrowski and B. Baranowski, *Z. Phys. Chem. (Leipzig)*, in press.

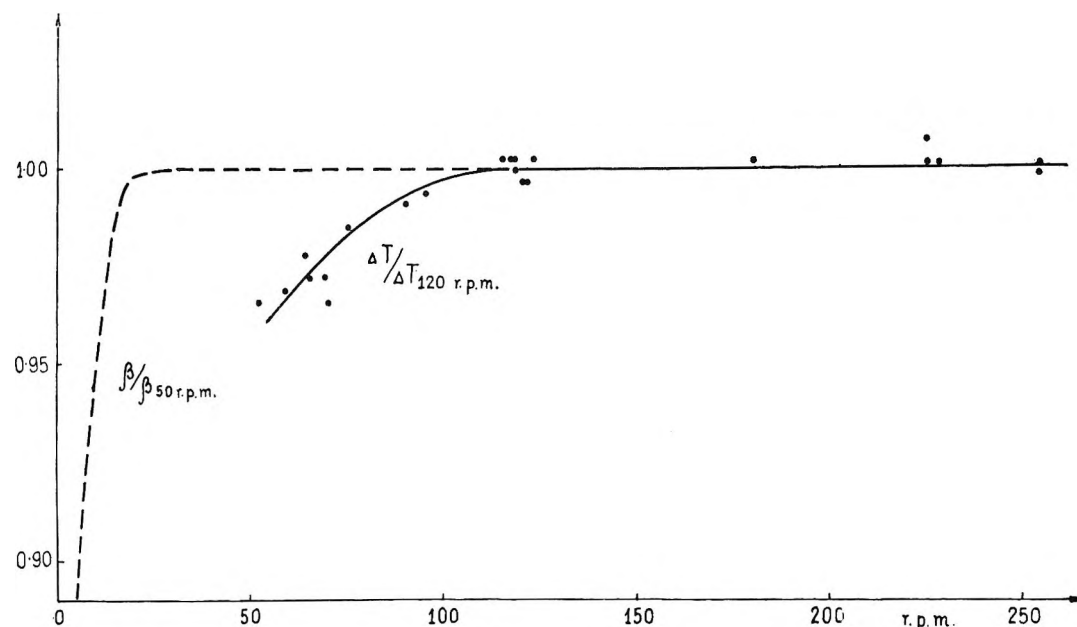


Figure 3. The influence of the stirring rate on the change of the isothermal diffusion cell constant,  $\beta/\beta(50 \text{ rpm})$ ,<sup>9</sup> dashed line, and the temperature difference on the diaphragm,  $\Delta T/\Delta T(120 \text{ rpm})$ , solid line.

0.5% by a Geiger-Müller counter placed in a small vessel filled with the examined solution.

The speed of magnet rotation was 100–120 rpm. For polythermal experiments the rate of stirring has to be higher than for isothermal conditions because there is an additional effect of stirring rate on the temperature difference on the diaphragm. The temperature difference was stable within more than 0.5%. This is shown in Figure 3.

The solution with which we fill the diaphragm must be of a higher temperature than that maintained during the experiment in order to reduce gas desorption during the filling procedure.

## VI. The Rate of Attainment of Stationary States

In order to compute the average value of diffusion coefficient in polythermal conditions, it is sufficient to know the following values: the molar fraction or molar concentration differences in the initial state of the experiments, those after time  $t$ , and those in the stationary state, the time of the experiment, and constants  $\alpha$  and  $\beta$ . The constant  $\alpha$  can be computed if the volumes of both vessels, temperatures, and the Soret coefficient,  $\bar{D}_1'/\bar{D}_1$ , are known. For the computation of  $\alpha$  the simplifying assumption  $V_L' = V_L$  and  $V_U' = V_U$  has been introduced. The constant  $\beta$  can be obtained from the isothermal experiment according to eq 25 and 27. In order to calculate the rate of attainment of stationary states, eq 7, 21, 23, 24, and 27 have been used.

From eq 7 and 24 it follows that if we neglect  $\alpha$ , the time required for obtaining the desired molar fraction difference  $(\Delta N_1)_t$  is proportional to  $(i/A)/[(1/V_L) + (1/V_U)]$ . Thus for the applied cross section of the diaphragm the time of the experiment can be shortened if

we use smaller vessels or if the diaphragm is thinner. Therefore, we used small vessels of about  $20 \text{ cm}^3$  capacity for one volume. Diaphragms of 1-mm thickness made of porous glass of the density of pores G-4 enabled Alexander,<sup>4</sup> in stationary-state investigations in which he did not use the stirrers, to shorten the time of experiment to 12 hr. In our investigations we could not use such thin diaphragms because the convection caused by the intensive stirring exerted an influence on the accuracy of time-dependent measurements and also decreased  $(\Delta N_1)_t$ . For this reason we used in all experiments the diaphragm made of porous glass of density G-4 and thickness of about 2.5 mm which enabled us to obtain after about 50 hr the stationary state with the desired accuracy for different electrolytes. The diaphragm diameter was about 3 cm.

As an illustration of the rate of attainment of stationary state, we present in Figure 4 the value of  $(\Delta N_1)_t/(\Delta N_1)_\infty$  as a function of time.

We used here a 0.1  $N$  aqueous solution of NaCl. Temperatures at the lower and upper vessels were  $T_L = 54.0^\circ$  and  $T_U = 21.95^\circ$ , respectively, and the temperature difference was  $\Delta T = 32.05^\circ$ . The obtained value of the Soret coefficient was  $S_{T_1} = (\Delta N_1)_\infty / N_1 \Delta T = 1.25 \times 10^{-3} \pm 0.03 \times 10^{-3} \text{ }^\circ\text{C}^{-1}$ . We calculated the values of  $(\Delta N_1)_t/(\Delta N_1)_\infty$  as a function of time, using eq 24 and the experimentally determined values of  $S_{T_1}$  and  $\bar{D}^c \beta$ . The values of  $\bar{D}^c \beta$  was  $2.1 \times 10^{-5} \pm 0.1 \times 10^{-5} \text{ sec}^{-1}$ . The value of  $\alpha$  could be neglected because it was only equal to 0.0002.

## VII. The Kinetic Measurements of Thermal and Self-THERMAL DIFFUSION

We measured the average polythermal diffusion co-

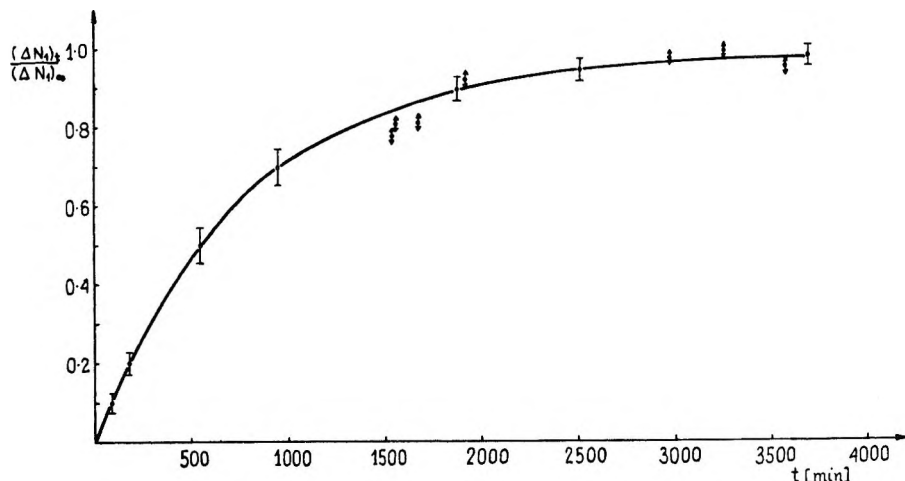


Figure 4. The rate of attainment of the stationary state:  $\diamond$ , experimental results obtained when starting with the initial concentrations equal to both vessels;  $\bullet$ , calculated results obtained from eq 24 based on  $\bar{D}^e \beta$  obtained in the experiments in which the initial concentrations in both vessels were 0 and 0.22  $N$ , respectively.

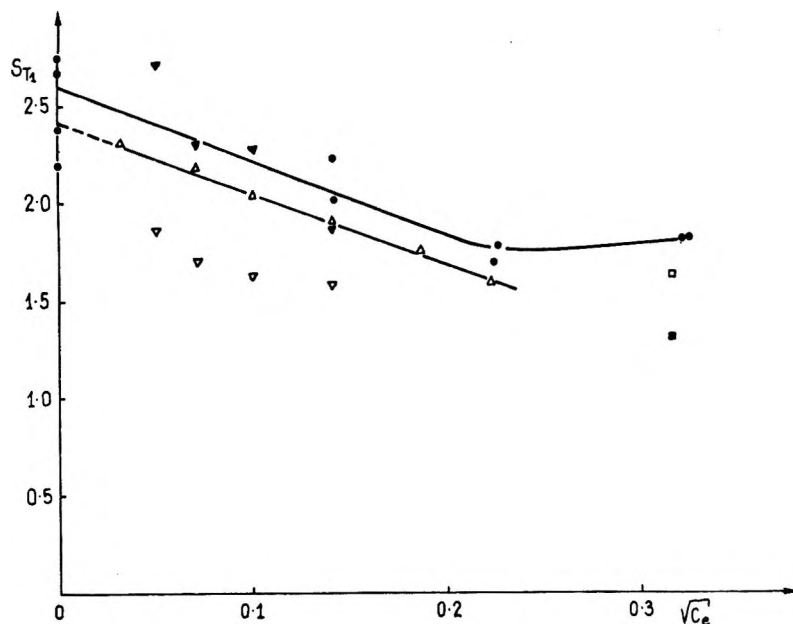


Figure 5. The Soret coefficient of NaCl as a function of the square root of the molar concentration (for the ranges of the concentrations used, we have disregarded the difference between molar concentration and molality, which for the accuracy of the discussed results is negligible):  $\bullet$ , the present work;  $\nabla$ , Agar and Turner (J. N. Agar, and J. C. R. Turner, *Proc. Roy. Soc., A* **255**, 307 (1960), conductometric method,  $T = 25^\circ$ ,  $\Delta T = 9.92^\circ$ , results obtained from the initial-state measurements;  $\nabla$ , the same paper, results obtained from the stationary-state measurements;  $\Delta$ , Snowdon and Turner (P. N. Snowdon, J. C. R. Turner, *Trans. Faraday Soc.*, **56**, 1812 (1960)), conductometric method,  $T = 25.3 \pm 0.1^\circ$ ,  $\Delta T = 10^\circ$ ;  $\square$ , Alexander,<sup>4</sup> diaphragm cell method, convection mixing,  $T_L = 44.3^\circ$ ,  $T_U = 19.6^\circ$ ;  $\blacksquare$ , the same paper,  $T_L = 48.4^\circ$ ,  $T_U = 21.5^\circ$ .

efficients,  $\bar{D}^e$ , for aqueous solutions of KCl (the initial concentrations were 0.2200 and 0.0000  $N$ ) and  $\bar{D}^{*,e}$  for radioactive  $^{22}\text{Na}$  in 0.1  $N$  KCl. The value of  $\bar{D}^e \beta$  obtained here from the measurement of diffusion in aqueous KCl solution at  $25^\circ$  was  $1.855 \times 10^{-5} \pm 0.005 \times 10^{-5}$  sec $^{-1}$ . The isothermal value of  $\bar{D}^e$  for the applied range of concentrations was  $\bar{D}^e = 1.852 \times 10^{-5}$  cm $^2$ /sec. This enabled us to calculate  $\beta = 1.002$  cm $^{-2}$ . The volumes of vessels were  $V_L = 18.9$  cm $^3$  and  $V_U = 19.4$  cm $^3$ . On the basis of eq 12 we computed

$A/i = 9.53$  cm. In these experiments the temperatures were  $T_L = 54.05^\circ$  and  $T_U = 29.0^\circ$ ; thus  $\Delta T = 25.05^\circ$ . The average values of diffusion and self-diffusion coefficients in polythermal conditions are given in Table I besides the isothermal values<sup>6,13</sup> at  $25^\circ$ . From these values, using eq 32 for  $E^c$ , we computed activation energies for diffusion and self-diffusion. Sufficient accuracy was already obtained when using simplified

(13) R. J. Mills, *J. Phys. Chem.*, **61**, 1258 (1957).

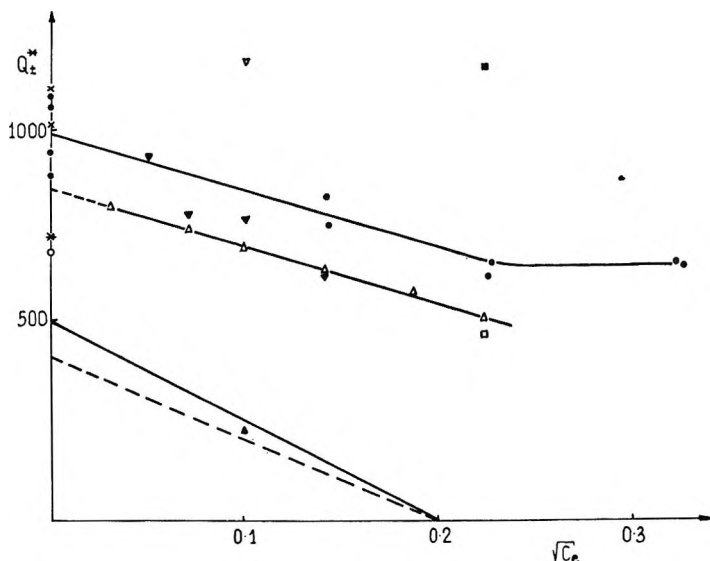


Figure 6. The heat of transport of NaCl as a function of the square root of the molar concentration (see the caption to Figure 5): ●, present work; ▼, Agar and Turner (J. N. Agar and J. C. R. Turner, *Proc. Roy. Soc.*, A255, 307 (1960), conductometric method,  $T = 25^\circ$ ,  $\Delta T = 9.29^\circ$ ; ▽, the same paper,  $T = 34.7^\circ$ ,  $\Delta T = 9.14^\circ$ ; Δ, Snowdon and Turner (P. N. Snowdon and J. C. R. Turner, *Trans. Faraday Soc.*, 56, 1812 (1960)), conductometric method,  $T = 25.3 \pm 0.1^\circ$ ,  $\Delta T = 10^\circ$ ; □, Alexander (K. F. Alexander, *Z. Phys. Chem. (Leipzig)*, 203, 212 (1954)), thermogravitational method,  $T = 25^\circ$  (the value computed by J. N. Agar *Rev. Pure Appl. Chem.*, 8, 1 (1958)); ■, Baranowski, Baranski, and Fulinski (B. Baranowski, S. Baranski, and A. Fulinski, *Roczn. Chem.*, 31, 229 (1957)), electrothermal diffusion method,  $T = 47^\circ$ ; ○, Haase and Hoch (R. Haase and K. Hoch, *Z. Phys. Chem. (Frankfurt am Main)*, 46, 63 (1965)), electrochemical method,  $T = 25^\circ$  (the result obtained from the measurement of the initial and stationary value of thermoelectric force extrapolated to zero concentration); ▲, Butler and Turner (B. D. Butler and J. C. R. Turner, *J. Phys. Chem.*, 69, 3598 (1965)), conductometric method,  $T = 9.35^\circ$ ,  $\Delta T = 9.5^\circ$ ; ×, Helfand and Kirkwood (E. Helfand and J. G. Kirkwood, *J. Chem. Phys.*, 32, 857 (1960)), theoretical results; \*, Agar (J. N. Agar, *Advan. Electrochem. Electrochem. Eng.*, 3, 31 (1963)), theoretical result; —, Helfand and Kirkwood (E. Helfand and J. G. Kirkwood, *J. Chem. Phys.*, 32, 857 (1960)), the theoretical value of the common slope for 1:1 aqueous electrolyte solutions at  $25^\circ$ ; ——, Agar (J. N. Agar, *Advan. Electrochem. Electrochem. Eng.*, 3, 31 (1963)), the theoretical value of the common slope for 1:1 aqueous solutions at  $25^\circ$ .

eq 34. These values as well as the Soret coefficients are also presented in Table I.

Table I

	KCl (0.0–0.22 N)	$^{22}\text{Na}$ in 0.1 N KCl
$\bar{D}^c$ (isothermal), cm <sup>2</sup> /sec	$1.852 \times 10^{-5}$	$1.322 \times 10^{-5}$
$\bar{D}^c$ (polythermal), cm <sup>2</sup> /sec	$2.91 \times 10^{-5} \pm 0.09 \times 10^{-5}$	$2.01 \times 10^{-6} \pm 0.06 \times 10^{-6}$
$E^c$ , cal/mole	$5000 \pm 300$	$4600 \pm 300$
$S_T$ , °C <sup>-1</sup>	$1.32 \times 10^{-3} \pm 0.03 \times 10^{-3}$	$1.2 \times 10^{-3} \pm 0.2 \times 10^{-3}$

### VIII. The Measurements of Stationary States of Thermal and Self-Thermal Diffusion

We have also investigated the concentration dependence of the Soret coefficient and the heat of transport for diluted NaCl aqueous solutions. Using the  $^{22}\text{Na}$  radioactive isotope we were able to determine the Soret coefficient and the heat of transport of the electrolyte for infinite dilution. We verified that for aqueous solutions of  $^{22}\text{NaCl}$  the concentration was 0.0000 N, on the interferometer it was 0.0000 N within an accuracy of

0.00005 N, and when measured by the conductometric method it did not exceed 0.00002 N. The initial radioactivity of radioactive isotope  $^{22}\text{Na}$  was about 0.05 mCi and it was diluted about 1000 times. In these investigations the temperatures were  $T_L = 55.0^\circ$  and  $T_U = 29.1^\circ$ ; thus  $\Delta T = 25.9^\circ$ . For solutions more dilute than 0.05 N the experiments have had to be limited to the measurements of the stationary state only because the diaphragm cell method cannot be used for a study of the rate of attainment of the stationary state in this case.

The results obtained here are presented in Table II. In this table we also present the values of the heat of transport of electrolyte,  $Q^*_{\pm}$ , which we computed from the Soret coefficient data using the equation<sup>3</sup>

$$Q^*_{\pm} = -\gamma RT^2 S_{Ti} \left( 1 + \frac{\partial \ln y_{\pm}}{\partial \ln c_e} \right) \quad (35)$$

where  $\gamma$  denotes the number of ions formed by dissociation,  $R$  is the universal gas constant,  $T$  is the absolute temperature,  $y_{\pm}$  is the activity coefficient of the electrolyte on the molar concentration scale,<sup>14</sup> and  $c_e$  is the molar concentration of the electrolyte.

For NaCl at infinite dilution the average value of

**Table II**

$c_e$	$\sqrt{c_e}$	$10^3 S_{T_1}, ^\circ\text{C}^{-1}$	$Q^* \pm, \text{kcal/mol}$
0.0000	0.0000	-2.74	1.09
0.0000	0.0000	-2.68	1.06
0.0000	0.0000	-2.38	0.95
0.0000	0.0000	-2.20	0.87
0.0200	0.1414	-2.22	0.83
0.0202	0.1422	-2.01	0.76
0.0508	0.2254	-1.69	0.63
0.0513	0.2265	-1.78	0.66
0.1041	0.3226	-1.82	0.66
0.1064	0.3262	-1.81	0.66

$S_{T_1}$  was  $-2.50 \times 10^{-3} \pm 0.26 \times 10^{-3} \text{ }^\circ\text{C}^{-1}$  and the average value of  $Q^* \pm$  was  $1.0 \pm 0.1 \text{ kcal/mol}$ .

Figure 5 shows the Soret coefficient of NaCl as a function of  $\sqrt{c_e}$  from Table II. For comparison we present also in this figure the results obtained with other experimental methods.

The heat of transport of the electrolyte as function of  $\sqrt{c_e}$  from Table II is presented in Figure 6. In this figure we have shown also, for comparison, the results obtained with other experimental methods.

When using the values for the range 0.0000–0.0500  $N$  given in Table II and using the method of the best least-squares quadratic fits we have obtained the value of the slope  $Q^* \pm$  as a function of  $\sqrt{c_e}$  equal to  $-1.5 \pm 0.3$ . We see that the value of this result is smaller than that of the theoretical results in which electrophoretic terms are neglected: Helfand and Kirkwood,<sup>16</sup>

-2.57 (in the concentration ranges used here it would be about 10% higher); and Agar,<sup>16</sup> -2.1. However, it can be seen from Figure 6 that in the experimental result of Snowdon and Turner the slope is similar to that obtained here.

### IX. Conclusions

The method described here is the adaptation of the isothermal diaphragm cell method with the magnetic stirring system to the polythermal conditions. This method enables us to measure diffusion, self-diffusion, thermal diffusion, and self-thermal diffusion. It permits us to measure the stationary state as well as rate of attainment of this stationary state. The possibility of measuring the transport process of a small amount of radioactive ion in binary and also (not investigated here) multicomponent solutions is especially interesting. This method also enables us to measure the Soret coefficients of various ions at infinite dilution. All these possibilities are not obtainable by any other method and that is why this time-consuming tedious method (the time of experiment is about 50 hr) is recommended.

*Acknowledgments.* I wish to express my gratitude to Professor Baranowski for his care of this work and for many useful suggestions and critical comments.

(14) H. S. Harned and B. B. Owen, "The Physical Chemistry of Electrolytic Solutions," 3rd ed., Reinhold Publishing Corp., New York, N. Y., 1958.

(15) E. Helfand and J. G. Kirkwood, *J. Chem. Phys.*, **32**, 857 (1960).

(16) J. N. Agar, *Advan. Electrochem. Electrochem. Eng.*, **3**, 31 (1963).

# Ultraviolet Studies of the Adsorption of $\beta$ -Diketones on Evaporated Metal Films

by Kosaku Kishi and Shigero Ikeda

*Department of Chemistry, Faculty of Science, Osaka University, Toyonaka, Osaka, Japan* (Received January 2, 1968)

Ultraviolet absorption spectra of  $\beta$ -diketones adsorbed on metals such as Ti, V, Cr, Mn, Fe, Co, and Ni give interesting information on the chemical bonding of the species. Acetylacetone and trifluoroacetylacetone adsorbed on the metals give band peaks around 300 m $\mu$  and ethylacetacetate absorbs at 280 m $\mu$ . These bands are assigned to the  $\pi-\pi^*$  transition of the chemisorbed  $\beta$ -diketonate anions. The d<sub>π</sub>-π\* band is observed on several metals. These spectra differ from those of the  $\beta$ -diketonates coordinated to the metal ions and are explained on the basis of the degree of  $\pi$  interaction between the  $\beta$ -diketonate  $\pi$  and metal d<sub>π</sub> orbitals. In the case of Cr, the spectra vary considerably according to the conditions of preparation of the films. The observations are interpreted in terms of the presence of a variety of adsorption sites.

## Introduction

Information about the chemical bonding of a chemisorbed species is quite important in order to aid discussion of the mechanisms of catalytic reactions by metals and other phenomena concerning metal surfaces. Blyholder<sup>1</sup> has attempted to explain the infrared band shifts for CO chemisorbed on a metal by a molecular orbital approach. An adsorbent atom is regarded as the central atom in a complex with the surrounding metal atoms and the chemisorbed molecule as ligands. Bond<sup>2</sup> has tried to describe the states of unsaturated hydrocarbon species adsorbed on a metal by applying Goodenough's proposal<sup>3</sup> for the explanation of both the collective and the localized electrons and for the band structure of the first transition metals.

Ultraviolet and visible studies of the chemisorbed states, however, enable us to get substantial information much more directly about the bonding of the chemisorbed species and about the electronic states of surface metal atoms. The ultraviolet technique, despite its high applicability, has scarcely been used for the investigation of an adsorbed species on a metal. In a preceding paper,<sup>4</sup> we developed an ultraviolet technique for such a system by using evaporated thin metal films, and we obtained the electronic spectra of acetylacetone chemisorbed on iron and nickel. In the following experiments, ultraviolet spectra are reported for acetylacetone (Hacac) and trifluoroacetylacetone (Hfta) adsorbed on Ti, V, Cr, Mn, Fe, Co, and Ni and ethylacetacetate on Fe. The spectra are subsequently compared with those of the corresponding coordination compounds. Acetylacetone and trifluoroacetylacetone are abbreviated below in the present paper as acac<sup>-</sup> and tfa<sup>-</sup>, respectively.

## Experimental Section

The ultraviolet cell used was described in the previous paper.<sup>4</sup> Thin iron foil, nickel wire, and small

metal blocks of the other elements were wound by a thin tungsten filament. After 7 hr of cell evacuation at 10<sup>-5</sup> mm, the filament was preheated electrically for 20 min to remove dissolved species in the filament and the metal. Then the metal was evaporated from the filament onto the quartz cell windows by elevating the temperature. In some cases for the preparation of metal films, the windows were externally cooled by liquid nitrogen. Then  $\beta$ -diketone was introduced into the cell. After exposure of the metal to the  $\beta$ -diketone for a definite time, ultraviolet spectra due to adsorbed species were measured, on condensing the gas by a liquid nitrogen trap.

The spectra were recorded on a Hitachi EPS-2 recording spectrophotometer. A wire gauge was used to reduce the reference transmission because there was a large decrease of transmission in the sample beam due to scattering by the films.

GR grade acetylacetone, trifluoroacetylacetone, and EPR grade ethylacetacetate were obtained from Nakarai Pure Chemicals and were distilled several times in a vacuum. The purities of Ti, V, Cr, Mn, Fe, Co, and Ni were 99.99, 99.8, 99.99, 99.9, 99.99, 99.9, and 99.8%, respectively.

## Results

*The Ultraviolet Spectra of Hacac Adsorbed on the Metals.* The spectra of the adsorbed species on Ti, V, Cr, Mn, Fe, Co, and Ni are shown in Figure 1. For Ti, V, Cr, and Co, the cell windows were cooled externally by liquid nitrogen as the metals were evaporated. On recording each spectrum, Hacac vapor was removed by condensation with a liquid nitrogen trap. The

- (1) G. Blyholder, *J. Phys. Chem.*, **68**, 2772 (1964).
- (2) G. C. Bond, *Discussions Faraday Soc.*, **41**, 200 (1966).
- (3) J. B. Goodenough, *Phys. Rev.*, **120**, 67 (1960).
- (4) K. Kishi, S. Ikeda, and K. Hirota, *J. Phys. Chem.*, **71**, 4384 (1967).

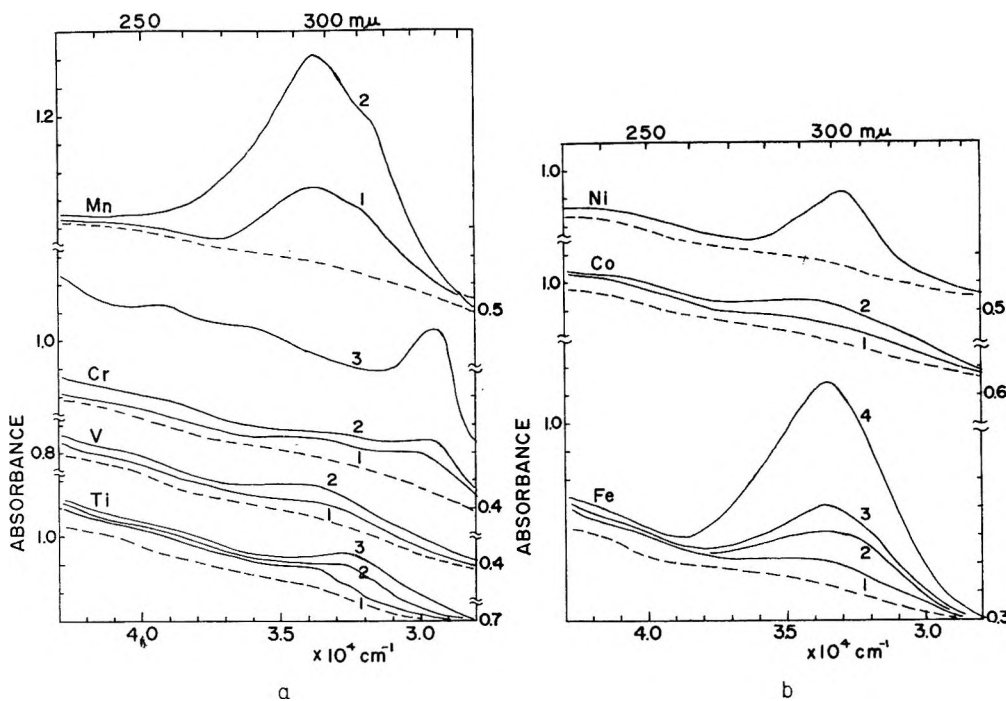


Figure 1. Spectra of acetylacetone adsorbed on the metals as a function of adsorbing time (a): Ti: (1) 0.5 hr, (2) 2 hr, (3) 15 hr; V: (1) 2 hr, (2) 18 hr; Cr: (1) 3 hr, (2) 17 hr, (3) after heating the filament for 20 sec; Mn: (1) 1 min, (2) 3 min, (3) 20 hr; (b) Fe: (1) 10 min, (2) 1 hr, (3) 4 hr, (4) 17 hr; Co: (1) 1 hr, (2) 16 hr; Ni: 20 hr. The dashed line represents the background spectrum of the metal.

exposure time of the films to the vapor (8 mm) were as follows: Ti: (1) 0.5 hr, (2) 2 hr, (3) 15 hr; V: (1) 2 hr, (2) 18 hr; Cr: (1) 3 hr, (2) 17 hr; Mn: (1) 1 min, (2) 3 min, (3) 20 hr; Fe: (1) 10 min, (2) 1 hr, (3) 4 hr, (4) 17 hr; Co: (1) 1 hr, (2) 16 hr; Ni: 20 hr. The intensities of these bands depended largely on the metal used. Case 3 (Cr) was obtained after heating the filament in the vapor for about 20 sec to the temperature at which the filament became slightly red. These band peaks are listed in Table I, with the corresponding ones of the coordination compounds<sup>5</sup> presented for comparison. Two peaks each were observed for Cr and Mn. A considerable band shift was observed for Ti with increasing exposure time.

Table I: Ultraviolet Data for Adsorbed  $\text{acac}^-$  on Metals

Metal	Wave-length, $m\mu$	Adsorbing time	Wavelength ( $\text{M}(\text{acac})_3$ ) in $\text{CHCl}_3$ , <sup>a</sup> $m\mu$
Ti	290	0.5 hr	309
	310	15 hr	
V	296	18 hr	290
Cr	290, 336	17 hr	272, 334
Mn	297, 314	3 min	272, 318
Fe	298	17 hr	273
Co	295	16 hr	257
Ni	303	20 hr	296

<sup>a</sup> Reference 5.

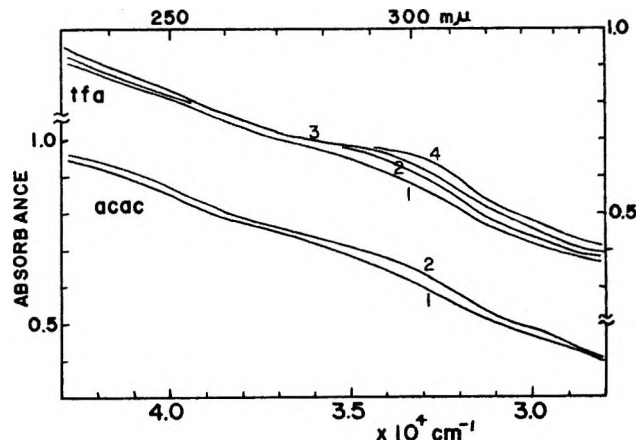


Figure 2. Spectra of adsorbed  $\text{acac}^-$  and  $\text{tfa}^-$  on Cr evaporated without the cell cooling as a function of adsorbing time: acac: (1) 0.5 hr; (2) 3 hr; tfa: (1) 5 min, (2) 30 min, (3) 1 hr, (4) 3 hr.

The relative intensity of the two bands of Cr varied according to the preparation conditions of the film. Figure 2 and the spectra of Cr in Figure 1 show the representative cases of such variation. In the spectra of Figure 1, obtained with the cell cooled by liquid nitrogen during the metal evaporation, the stronger band was observed at 336 m $\mu$  and another at about 290 m $\mu$ . The increase in intensity of the 336-m $\mu$  band was larger than that of the 290-m $\mu$  band. Figure 2 was recorded

(5) D. W. Barnum, *J. Inorg. Nucl. Chem.*, **21**, 221 (1961).

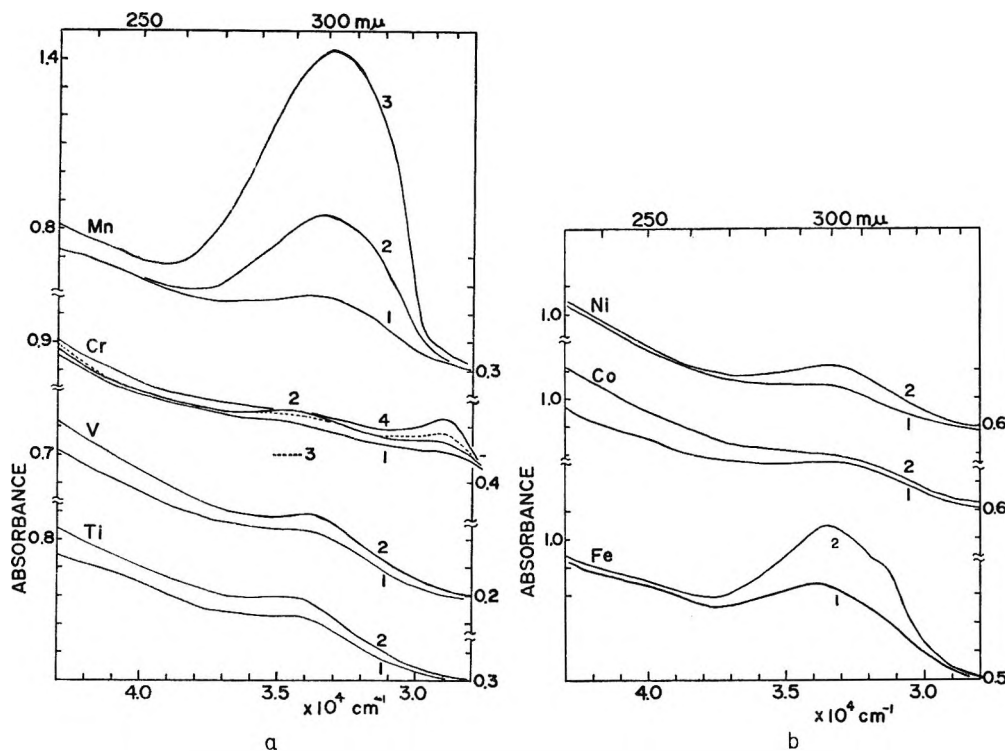


Figure 3. Spectra of trifluoroacetylacetone adsorbed on the metals as a function of adsorbing time: (a) Ti: (1) 2 hr, (2) 18 hr; V: (1) 2 hr, (2) 18 hr; Cr: (1) 5 min, (2) 20 min, (3) 50 min, (4) 18 hr; Mn: (1) 30 sec, (2) 5 min, (3) 30 min; (b) Fe: (1) 10 min, (2) 2 hr; Co: (1) 30 min, (2) 20 hr; Ni: (1) 2 hr, (2) 18 hr.

for the Cr film prepared without cooling the cell windows during evaporation. In case 1, obtained after 0.5 hr of adsorbing time, only the 290-m $\mu$  band was observed. After 3 hr of adsorption, the 290-m $\mu$  band increased slightly in intensity and the weaker 336-m $\mu$  band appeared.

*The Ultraviolet Spectra of Htfa Adsorbed on the Metals.* The spectra due to the adsorbed species are shown in Figure 3. The spectra were recorded in a similar way to that for Hacac. The adsorbing times of Htfa (10 mm) onto the films were as follows: Ti: (1) 2 hr, (2) 18 hr; V: (1) 2 hr, (2) 18 hr; Cr: (1) 5 min, (2) 20 min, (3) 50 min, (4) 18 hr; Mn: (1) 30 sec, (2) 5 min, (3) 30 min; Fe: (1) 10 min, (2) 2 hr; Co: (1) 30 min, (2) 20 hr; Ni: (1) 2 hr, (2) 18 hr. The band positions are listed in Table II. In the cases of Cr and Fe, two bands were observed.

Table II: Ultraviolet Data for Adsorbed tfa<sup>-</sup> on Metals

Metal	Wavelength, m $\mu$	Adsorbing time
Ti	295	18 hr
V	296	18 hr
Cr	293, 345	18 hr
Mn	303	5 min
Fe	298, 320	2 hr
Co	304	20 hr
Ni	303	18 hr

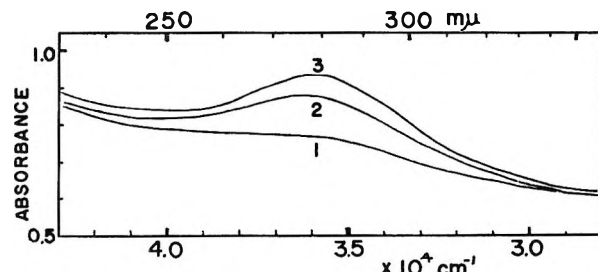


Figure 4. Spectra of ethylacetoacetate adsorbed on iron after exposures of: (1) 30 min, (2) 3 hr, (3) 5 hr.

Figure 2 and Cr in Figure 3 show the effect of the different preparation conditions of the Cr films on the spectra of the adsorbed species. Figure 3 was recorded for the film prepared by cooling the cell windows with liquid nitrogen. Two band peaks exist at 293 and 345 m $\mu$ . The intensity of the 345-m $\mu$  band increased monotonically with adsorption time and grew more rapidly than the 293-m $\mu$  band. However, the latter band increased in intensity at first and then slightly decreased as shown by cases 1-3. Figure 2 was recorded for the Cr film prepared without the cell cooling. Cases 1-4 were obtained after exposing the film to the vapor for 5 min, 30 min, 1 hr, and 3 hr, respectively. Only one band appeared, at about 295 m $\mu$ , and shifted moderately to longer wavelength with increasing adsorbing time. The 345-m $\mu$  band was not detected even after 15 hr of adsorption.

*The Ultraviolet Spectra of Ethylacetoacetate Adsorbed on Iron.* Figure 4 shows the spectra recorded after exposing iron film to ethylacetoacetate (1 mm) for (1) 30 min, (2) 3 hr, and (3) 5 hr. The band maximum exists at 280 m $\mu$ . When Hacac (8 mm) was subsequently introduced into the cell, the 280-m $\mu$  band disappeared and another band was observed at 298 m $\mu$ .

*Reactivity of Oxides.* On iron or manganese surface oxide prepared by exposing the metal film to air for only 5 min, Hacac was adsorbed more rapidly than on an unmodified film. On the other hand, evaporated iron or manganese film was oxidized in air at about 200° for 1.5 hr in an electric furnace. After cooling the film to room temperature and evacuating the cell, it was exposed to Hacac for 20 hr. No adsorbed species, however, was detected on the oxides by the ultraviolet technique.

## Discussion

*Hacac Adsorbed on the Metals.* In the preceding paper,<sup>4</sup> it was reported that the infrared spectra of Hacac adsorbed on iron and nickel corresponded well to those of Fe(acac)<sub>3</sub> and Ni(acac)<sub>2</sub>, respectively, and that the ultraviolet spectra of the species were similar to that of free acac<sup>-</sup> in basic solution which was due to the  $\pi-\pi^*$  transition. Moreover, from these observations, it was concluded that the adsorbed species was acac<sup>-</sup> and that the  $\pi$  interaction was weak between the  $\pi$  orbitals of acac<sup>-</sup> and the d<sub>π</sub> orbitals of iron or nickel as the adsorbent.

In the cases of Ti, V, Cr, Mn, and Co, absorption bands were also observed around 300 m $\mu$  as listed in Table I. The adsorbed species on these metals therefore must be acac<sup>-</sup>. These bands were assigned to the  $\pi-\pi^*$  transition of adsorbed acac<sup>-</sup>.

The strongest  $\pi-\pi^*$  band of metal acetylacetones listed in Table I, however, varies from 309 m $\mu$  of Ti(acac)<sub>3</sub> to 256 m $\mu$  of Co(acac)<sub>3</sub>. In the case of Cr, however, the spectra of both the complex and adsorbed species were quite specific and will be discussed later with that for the tfa-Cr system. Barnum<sup>5</sup> has correlated both the shift to shorter wavelength and the splitting of the  $\pi-\pi^*$  band of the complexes with the increase of metal-ligand  $\pi$  interaction and with the resulting mutual interaction of the ligand orbitals.

These different observations for the adsorbed species and the complexes are expected for the following reasons: (1) the mutual  $\pi$  interaction of acac<sup>-</sup> would not exist when one acac<sup>-</sup> molecule is adsorbed on an adsorbent atom, and (2) the occupation of 3d orbitals is different for the two systems, and also the charge of the adsorbent atom must be smaller than those of metal ions in the complexes. Thus the metal-ligand  $\pi$  interaction is weaker for all of the metals in adsorbed states. In addition, a steric restriction may make it difficult for an adsorbent atom, which forms a chelate ring with

acac<sup>-</sup>, to use the d<sub>π</sub> orbital perpendicular to the ring for the  $\pi$  interaction.

The band shift with increasing exposure time for Ti suggests the weakening of the acac<sup>-</sup> adsorbent  $\pi$  interaction. Since the  $\pi-\pi^*$  band of Ti(acac)<sub>3</sub> was observed at 309 m $\mu$ , the acac<sup>-</sup>-metal  $\pi$  interaction may initially be stronger than that of the complex, so that the metallic character of the adsorbent atom decreases by aging and/or with increasing number of adsorbed species.

As the 318-m $\mu$  band of Mn(acac)<sub>3</sub> has been assigned to d<sub>π</sub>- $\pi^*$  transition<sup>5</sup> and the 314-m $\mu$  band for adsorption on Mn is not found in either acac<sup>-</sup> alone or the metal film itself, the latter band was assigned to the same kind of charge transfer as in the complex.

In the Fe-Hacac system, however, the second band was observed at about 350 m $\mu$ <sup>4</sup> only when the adsorbent-adsorbate was exposed to air, and also the band shift from 298 to 280 m $\mu$  occurred, indicating a strengthening of the acac<sup>-</sup>-Fe  $\pi$  interaction. From the assignment of the 350-m $\mu$  band of Fe(acac)<sub>3</sub>,<sup>5</sup> the 350-m $\mu$  band for adsorption is considered to come from the d<sub>π</sub>- $\pi^*$  transition in the adsorbed state.

*Htfa Adsorbed on the Metals.* For all of the metals investigated, a band was observed near 300 m $\mu$  for the adsorbed species. The free tfa<sup>-</sup> in basic solution gave a single nearly symmetric peak at 294 m $\mu$ , at the same position as that of acac<sup>-</sup>. Therefore, Htfa is also concluded to be adsorbed on metals as the enolate form (tfa<sup>-</sup>), and these bands are assigned to the  $\pi-\pi^*$  transition.

Only a single peak was obtained for Mn, being unlike the two for Hacac. The difference may be explained as follows. The approach of the energy level of the d<sub>π</sub> orbital to that of the  $\pi_3$  orbital of tfa<sup>-</sup>-Mn results in an overlapping of the  $\pi-\pi^*$  and d<sub>π</sub>- $\pi^*$  bands.

However, two peaks were observed for the tfa<sup>-</sup>-Fe system and only one for the acac<sup>-</sup>-Fe. The d<sub>π</sub>- $\pi^*$  band of Fe(tfa)<sub>3</sub> exists at 350 m $\mu$ , at a longer wavelength than the band of the adsorbed tfa<sup>-</sup>. The 320-m $\mu$  band can be considered to be due to the d<sub>π</sub>- $\pi^*$  transition, as in the case of acac<sup>-</sup>-Mn. The variation with different  $\beta$ -diketones, however, is not yet understood.

The large effect of the preparation condition of the film on the relative intensity of the two bands for Cr suggests that these bands originate from different states of adsorbates. The strong band of Cr(acac)<sub>3</sub> is at considerably longer wavelength (334 m $\mu$ ) than that of the other complexes. (The assignment of the band will be described in detail theoretically by Hanazaki, et al.<sup>6</sup>) The 336- and 345-m $\mu$  bands for Hacac and Htfa, respectively, are considered to be due to an adsorbed species electronically similar to the complex and/or the complex adsorbed on the film. By considering that less crystal growth and sintering are expected for

(6) I. Hanazaki, F. Hanazaki, and S. Nagakura, submitted for publication in *J. Chem. Phys.*

the film prepared with cell cooling, such species must be formed when the  $\beta$ -diketones are adsorbed on Cr with a lower number of surrounding metal atoms, as for example at edges and dislocations. However, the film is expected to be sintered seriously when it is prepared without cell cooling, and an adsorbent atom will bond to a much higher number of surrounding metal atoms than that obtained on cooling the cell windows. Therefore, the 290- and the 295- $m\mu$  bands for Hacac and Htfa, respectively, must originate from the species which are formed on such a Cr atom. These species would partly change to the complexlike species with increasing coverage or increasing time. The decrease in intensity of the 293- $m\mu$  band for Htfa-Cr with cell cooling is well described by such a change.

*Reactivity of Oxides.* Kammori, *et al.*,<sup>7</sup> have studied the solvation of metallic iron and iron oxide in  $\beta$ -diketones in order to separate them. In the presence of oxygen, the metal dissolved more easily in the solvent but the oxide would not dissolve. The results of the present study for adsorption are in accord with this. The reactivity of Hacac with the surface oxide prepared by exposure to air for 5 min was quite different from that with the bulk oxide. The fact suggests that the metal-oxygen bonding differs considerably for the two kinds of oxides.

*Role of Conduction Bands for the Adsorption.* The over-all reaction for the formation of  $\text{Fe}(\text{acac})_3$  from iron metal and Hacac is formulated as



The iron atom of the bulk metal with no electric charge must become charged during this reaction. The central iron of  $\text{Fe}(\text{acac})_3$  is trivalent and the d electron occupation is considered to be  $d_{x^2-y^2}^3$ . Moreover, the electrons with collective properties in the bulk metal must change into localized electrons during the solvation. If the solvation is the extreme case of chemisorption, the

adsorption of Hacac would induce a small but similar change in the conduction bands with collective properties, being formed with  $\text{sp}^3$  hybrid orbitals according to Goodenough's model. More generally, the contribution of the conduction bands to chemisorption may have an effect on the electric conductivity of the metal film during adsorption.

*Substitution Reactions on a Metal Surface.* Adsorbed  $\text{acac}^-$  on iron was substituted rapidly by  $\text{HCOO}^-$  on subsequent addition of  $\text{HCOOH}$ , and the adsorbed oxygen was probably displaced by  $\text{acac}^-$  after the introduction of Hacac.<sup>4</sup> The chemisorbed species for the ethylacetacetate-iron system, that giving the 280- $m\mu$  band, was concluded also to be the enolate form by considering that ethylacetacetate is chemically similar to the other  $\beta$ -diketones investigated. The displacement of the 280- $m\mu$  band by the 298- $m\mu$  band after the introduction of Hacac indicates that the chemisorbed ethylacetacetate was substituted by  $\text{acac}^-$  instantly. Without the preadsorption of ethylacetacetate on the surface, it would take several hours, as shown in the adsorption study of Hacac, for the corresponding amount of  $\text{acac}^-$  to be chemisorbed. Such competition and acceleration for adsorption may be useful for describing inhibition, acceleration, and selectivity in catalytic reactions.

#### General Remarks

Although the above discussions of the band position of the  $\pi-\pi^*$  transition considered only the degree of adsorbent metal-adsorbate  $\pi$  interaction, other factors may play an important role in some cases. This research indicates that the comparison of data obtained by this technique with that of coordination compounds will give us much valuable information on both metal adsorbents and adsorbed species.

(7) O. Kammori and I. Taguchi, *Bunsiki Kagaku*, 15, 1223 (1966).

# The Radiation-Induced Isomerization of Stilbene in 2-Propanol and Acetone

by H. P. Lehmann<sup>1</sup>

*Max Planck Institut für Kohlenforschung, Abteilung Strahlenchemie, Mülheim/Ruhr, West Germany*  
(Received March 15, 1968)

The radiation-induced isomerization of stilbene was studied in 2-propanol and acetone. In 2-propanol the precursors of the *trans*-to-*cis* isomerization are shown to be ionic species, while an energy-transfer mechanism is operative in acetone. The *cis*-to-*trans* isomerization in both solvents was found to be catalyzed by radiation-produced intermediates of the solvents, most probably electrons. In mixtures of acetone in 2-propanol the amount of isomerization of *trans*-stilbene indicated that a reaction between acetone triplets and 2-propanol was competing with the energy-transfer process between acetone triplets and *trans*-stilbene.

## Introduction

The radiation-induced isomerization of *trans*-stilbene in benzene and cyclohexane has been shown to proceed through the triplet state of *trans*-stilbene.<sup>2-5</sup> The manner in which the excited state of the stilbene is formed in such solutions is interpreted in different ways by the various groups. Thus it has been shown that in benzene one-third of triplet *trans*-stilbene molecules ( $G \approx 1.7$ ) arise through excitation energy transfer from triplet benzene molecules. The remainder of the stilbene triplets were attributed either to energy transfer from benzene singlets or to reactions of ionic species.<sup>5,6</sup> Hentz, *et al.*,<sup>4</sup> reached somewhat similar conclusions for benzene solutions but in cyclohexane favored an ionic mechanism as the precursor of all the triplet stilbene. In all cases, however, formation of the triplet state of *trans*-stilbene by interaction between radiation-produced intermediates of the solvent and the solute was established.

In the radiation chemistry of alcohols the only evidence obtained for the formation of excited states of solutes in alcoholic solutions has been reported in work on the pulse radiolysis of aromatic compounds in methanol, ethanol, and 2-propanol.<sup>7,8</sup> In both instances a very weak absorption band, which was observed on the pulse radiolysis of anthracene or *p*-terphenyl in 2-propanol<sup>7</sup> and anthracene in ethanol,<sup>8</sup> was attributed to triplet-state absorption. In the  $\gamma$  radiolysis of acetone product formation has been accounted for in terms of the spontaneous decomposition of acetone, possibly in an electronically excited state.<sup>9-13</sup> When solutions of naphthalene, anthracene, and 1,2-benzanthracene in acetone were subjected to pulse radiolysis, absorption peaks were identified as being characteristic of the triplet states of the solutes and were interpreted as having their origin through an energy-transfer process between the solvent and solute.<sup>14</sup>

In this work further evidence was sought for the production of excited states in  $\gamma$ -irradiated 2-propanol and acetone by using *trans*-stilbene as the solute and measuring the *trans*-to-*cis* isomerization. This direc-

tion was used in almost all the experiments, in view of the observed catalytic isomerization of *cis*-stilbene to *trans*-stilbene by ions or radicals produced in the solvent during radiolysis.<sup>4</sup>

## Experimental Section

**Materials.** 2-Propanol (Merck analytical grade) was refluxed for 24 hr over 2,4-dinitrophenylhydrazine and then distilled onto a molecular sieve (Merck 4A) for drying. A further distillation from the molecular sieve was performed just prior to use. Acetone (Merck analytical grade) was dried over a molecular sieve and was distilled before use. *trans*-Stilbene (Merck scintillation grade) was used without further purification (mp 124–125°). *cis*-Stilbene was prepared by the photolysis of a saturated solution of *trans*-stilbene in benzene for 48 hr, using diacetyl as a sensitizer, at wavelengths  $>330$  m $\mu$ . Under these conditions the final equilibrium was 90% *cis*, which was then isolated by elution through an alumina column with benzene. Gas chromatographic analysis showed the final product

- (1) Radiation Laboratory, University of Notre Dame, Notre Dame, Ind. 46556.
- (2) H. P. Lehmann, G. Stein, and E. Fischer, *Chem. Commun.*, 583 (1965).
- (3) R. A. Caldwell, D. G. Whitten, and G. S. Hammond, *J. Amer. Chem. Soc.*, **88**, 2659 (1966).
- (4) R. R. Hentz, D. B. Peterson, S. B. Srivastava, H. F. Barzynski, and M. Burton, *J. Phys. Chem.*, **70**, 2362 (1966).
- (5) E. Fischer, H. P. Lehmann, and G. Stein, *J. Chem. Phys.*, **45**, 3905 (1966).
- (6) G. Stein in "The Chemistry of Excitation and Ionization," G. R. A. Johnson and G. Scholes, Ed., Taylor and Francis Ltd., London, 1967, p 25.
- (7) J. P. Keene, T. J. Kemp, and G. A. Salmon, *Proc. Roy. Soc., A287*, 494 (1965).
- (8) S. Arai and L. M. Dorfman, *J. Chem. Phys.*, **41**, 2190 (1964).
- (9) P. Ausloos and J. F. Paulson, *J. Amer. Chem. Soc.*, **80**, 5117 (1958).
- (10) J. D. Strong and J. G. Burr, *ibid.*, **81**, 775 (1959).
- (11) P. J. Ausloos, *ibid.*, **83**, 1056 (1961).
- (12) R. Barker, *Trans. Faraday Soc.*, **59**, 375 (1963).
- (13) J. Kuchera, *Collect. Czech. Chem. Commun.*, **30**, 3080 (1965).
- (14) S. Arai and L. M. Dorfman, *J. Phys. Chem.*, **69**, 2239 (1965).

to be >99.9% *cis*. Naphthalene was freshly sublimed before use (mp 80°).

*Apparatus and Procedure.* All the experiments were carried out with 10 ml of solution contained in 20 mm o.d. Pyrex glass ampoules. The solutions were degassed, by five to six freeze-thaw cycles on a high-vacuum apparatus, sealed, and irradiated in the Mülheim  $^{60}\text{Co}$   $\gamma$ -ray source.<sup>15</sup> The irradiations were performed in positions in the source giving a dose rate of  $3.85 \times 10^{17} \text{ eV ml}^{-1} \text{ min}^{-1}$  measured using the ferrous sulfate dosimeter, taking  $G(\text{Fe}^{3+}) = 15.6$ . Corrections in the dose rate were made for the different electron densities of the dosimeter, 2-propanol, and acetone. The ampoules and all other glassware in which the solutions were handled were masked with black tape to reduce to the absolute minimum isomerization induced by light. Unirradiated blanks were run with each set of experiments to check such isomerization.

All analyses for the isomerization were made by gas chromatography using an Aerograph Model 1520 instrument. Samples were injected onto a  $1/8$  in.  $\times$  6 ft column, packed with silicone gum rubber on Chromosorb W, 80–100 mesh, operating at 175° with a hydrogen flame detector and using argon as the carrier gas. Under these conditions the *cis*- and *trans*-stilbene had retention times of approximately 6 and 11 min, respectively.

## Results

*2-Propanol Solutions.* *trans*-Stilbene is relatively insoluble in 2-propanol, as compared with benzene, for example, and it was found that a 0.01 *M* solution was almost the limiting solubility at 20°, the temperature at which the irradiations were carried out. Irradiation of *trans*-stilbene in 2-propanol resulted in the formation of small amounts of *cis*-stilbene, while the major effect was the reaction of the stilbene to other products. Table I shows the *G* values for the isomerization as well as for the consumption of 0.01 *M* *trans*-stilbene alone in solution and in the presence of 0.1 and 0.3 *M* naphthalene. It may be seen that the presence of naphthalene enhances the isomerization, while at the same time protecting the *trans*-stilbene from radiation-induced destruction. The *G* values given in Table I are all calculated from linear yield-dose plots for doses up to approximately  $10^{20} \text{ eV ml}^{-1}$ .

*cis*-Stilbene (0.01 *M*) in 2-propanol, on the other hand, shows a different behavior upon irradiation, in that the yield-dose plot for *trans*-stilbene formation is nonlinear for the dose range measured. Figure 1 illustrates this effect, in addition to showing the *cis*-stilbene destruction as a function of dose. The relatively large amount of isomerization at low doses falls off with increasing dose, and hence two values for  $G(\text{cis} \rightarrow \text{trans})$  may be calculated from the yield-dose plot, corresponding to initial and final isomerization yields. These two *G* values are shown in Table I.

**Table I:** Effect of  $\gamma$  Irradiation on Solutions of Stilbene in 2-Propanol

Solutes	$G(\text{isomerization})^a$	$G(\text{consumption})^b$
$10^{-2} \text{ M}$ <i>trans</i> -stilbene	0.03	3.07
$10^{-2} \text{ M}$ <i>trans</i> -stilbene- $10^{-1} \text{ M}$ C <sub>10</sub> H <sub>8</sub>	0.23	2.05
$10^{-2} \text{ M}$ <i>trans</i> -stilbene- $3 \times 10^{-1} \text{ M}$ C <sub>10</sub> H <sub>8</sub>	0.33	1.86
$10^{-2} \text{ M}$ <i>cis</i> -stilbene	0.27 <sup>c</sup>	1.44
	0.02 <sup>d</sup>	

<sup>a</sup> Isomerization yield. <sup>b</sup> Yield of consumption of stilbene.  
<sup>c</sup> Initial yield. <sup>d</sup> Final yield.

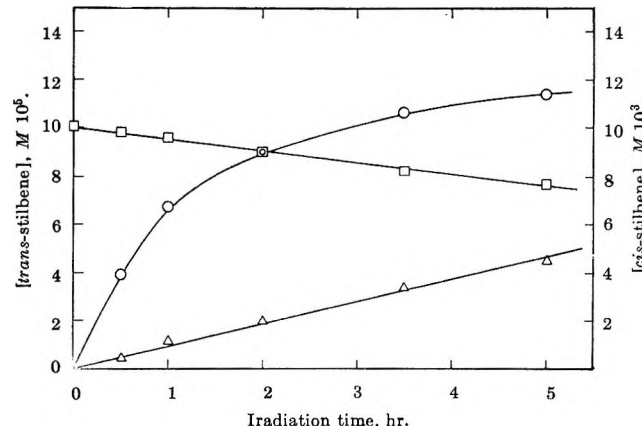


Figure 1. Effect of  $\gamma$  irradiation on  $10^{-2} \text{ M}$  *cis*-stilbene in 2-propanol:  $\square$ , *cis*-stilbene consumption;  $\circ$ , *trans*-stilbene formation;  $\Delta$ , “product” formation (arbitrary units).

Also plotted in Figure 1 are points for a “product” of the radiolysis of stilbene in 2-propanol. This product, which was also observed in irradiated solutions of stilbene in acetone, had a retention time on the gas chromatograph of approximately 1.5 relative to *trans*-stilbene. Some experiments were carried out to try to identify this substance. A 0.05 *M* solution of *cis*-stilbene in 2-propanol was irradiated for a longer period (dose,  $\sim 3 \times 10^{20} \text{ eV ml}^{-1}$ ) in order to form enough product to effect an isolation and identification. The irradiated solution was eluted through an alumina column with benzene, to remove most of the stilbene, followed by chloroform. A final clean separation was brought about by preparative thin-layer chromatography eluting with chloroform. After the chloroform had evaporated off, an nmr spectrum was made on the residue (<50 mg). Examination of the nmr spectrum showed characteristic peaks which allowed the product to be tentatively identified as an addition product of stilbene with the 2-propyl radical.

Very small amounts of phenanthrene were also detected as radiolysis products of the irradiation of both

(15) H. Kronert and G. O. Schenck, *Chem.-Ing.-Tech.*, **35**, 641 (1963).

stilbenes in 2-propanol. This identification was made by comparing the retention time of a peak on the gas chromatograph with the retention time for pure phenanthrene. By a similar comparison technique neither tetraphenylcyclobutane nor diphenylethane was detected as radiolysis products.

*Acetone Solutions.* The radiation-induced isomerization yields for stilbene in acetone are shown in Table II. The  $G$  values for *trans*-to-*cis* isomerization were all calculated from linear yield-dose plots for doses up to  $5 \times 10^{19}$  eV ml $^{-1}$ . For *cis*-to-*trans* isomerization, however, the yield-dose plots were nonlinear over this dose range, and two values for  $G(cis \rightarrow trans)$  are given, corresponding to the initial and final yields. The  $G$  values for stilbene disappearance are given only for dilute solutions, as the changes in the original stilbene in the more concentrated solutions were too small to warrant the determination of  $G(-stilbene)$ .

**Table II:** Effect of  $\gamma$  Irradiation on Solutions of Stilbene in Acetone

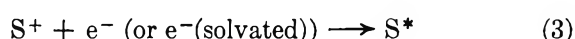
Solute	$G(\text{isomerization})^a$	$G(\text{consumption})^b$
$5 \times 10^{-3} M$ <i>trans</i> -stilbene	0.86	4.1
$10^{-2} M$ <i>trans</i> -stilbene	0.90	4.5
$5 \times 10^{-2} M$ <i>trans</i> -stilbene	0.91	
$10^{-1} M$ <i>trans</i> -stilbene	1.15	
$10^{-2} M$ <i>trans</i> -stilbene- $10^{-2} M$ C <sub>10</sub> H <sub>8</sub>	0.85	4.8
$10^{-2} M$ <i>trans</i> -stilbene- $10^{-1} M$ C <sub>10</sub> H <sub>8</sub>	1.13	4.3
$10^{-2} M$ <i>cis</i> -stilbene	1.05 <sup>c</sup>	2.9
	0.14 <sup>d</sup>	
$5 \times 10^{-2} M$ <i>cis</i> -stilbene	2.5 <sup>c</sup>	
	0.73 <sup>d</sup>	

<sup>a</sup> Isomerization yield. <sup>b</sup> Yield of consumption of stilbene.  
<sup>c</sup> Initial yield. <sup>d</sup> Final yield.

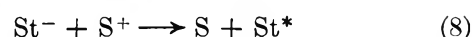
*Mixed Solvents.* Figure 2 illustrates the variation of  $G(trans \rightarrow cis)$  in 0.01  $M$  *trans*-stilbene in 2-propanol-acetone mixtures up to 20 vol % in acetone (corresponding to  $\sim 2.76 M$ ). Also shown is the  $G(\text{isomerization})$  which would be expected on increasing the amount of acetone in 2-propanol based on the value of  $G(trans \rightarrow cis)$  of 0.03 and 0.9 for 0.01  $M$  *trans*-stilbene in 2-propanol and acetone, respectively. It can be seen that the amount of isomerization in such solutions is less than would be expected on the basis of a simple addition of the yields according to the fraction of the two liquids present. As the acetone concentration is increased, the isomerization yield tends toward the expected value.

## Discussion

A general mechanism to account for the action of high-energy radiation on a liquid may be given as



In the presence of *trans*-stilbene the following reactions can also take place



where S denotes a solvent molecule and St, *t*-St, and *c*-St indicate a stilbene, *trans*-stilbene, and *cis*-stilbene molecule, respectively. Products may be atoms, radicals or molecular products.  $S^*$  signifies excited molecules without stipulation whether singlet (s) or triplet (t).

The above reaction scheme is a general mechanism to fit the observations made in the radiation-sensitized isomerization of stilbene in benzene and cyclohexane.<sup>2-5</sup> As has been stated previously, the final short-lived species immediately before isomerization of *trans*-stilbene is generally agreed to be the triplet state of the

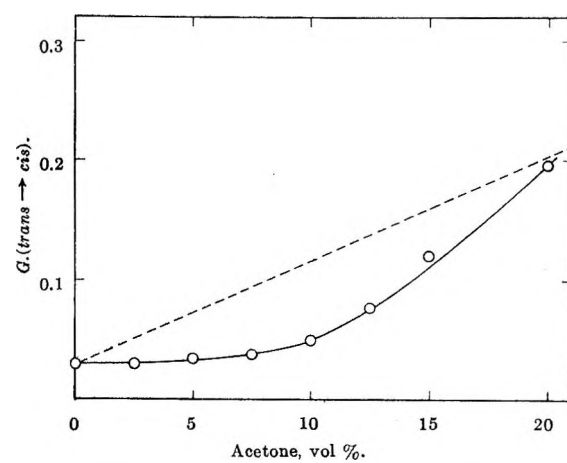


Figure 2. Effect on  $G(trans \rightarrow cis)$  of adding acetone to  $10^{-2} M$  *trans*-stilbene in 2-propanol: —, experimental results; ---, calculated  $G(trans \rightarrow cis)$ . (See the text.)

molecule. It has been shown in the direct and sensitized photoisomerization of stilbene that  $k_{12}/(k_{11} + k_{12}) \approx 0.5$  and  $k_{14}/(k_{13} + k_{14}) \approx 0.27$ ; i.e., a triplet *trans*-stilbene molecule has about the same chance to isomerize as to return to its ground state, whereas for the triplet *cis*-stilbene only about one-fourth are isomerized.<sup>16</sup>

*2-Propanol Solutions.* Reactions 1–6 have been postulated as occurring in the  $\gamma$  radiolysis of 2-propanol, with all the reactions taking place in the spurs so that the only species which are readily reactive to solutes are solvated electrons, H atoms, and radicals.<sup>17,18</sup>

*trans*-Stilbene in irradiated 2-propanol can then react according to 7–12 as well as through proton-transfer reactions with 2-propanol or 2-propanol radical cations<sup>8,19</sup>



where Ar signifies a *trans*-stilbene or a naphthalene molecule. Pulse-radiolysis studies on aromatic compounds in alcohols have given a value for the rate constants for these reactions of  $k_{15} \approx 10^4 M^{-1} \text{ sec}^{-1}$  in 2-propanol and  $k_{16} \approx 2 \times 10^{10} M^{-1} \text{ sec}^{-1}$  in ethanol.<sup>8</sup> If it is assumed that  $k_{15}$  and  $k_{16}$  for *trans*-stilbene and naphthalene in 2-propanol are of the same order as these values, it may be seen that reaction 16 is negligible in comparison to eq 15, owing to the very low concentration of  $\text{ROH}_2^+$  in such irradiated solutions.

$G(\text{trans} \rightarrow \text{cis}) \approx 0.03$  in a 0.01 M *trans*-stilbene solution in 2-propanol indicates the formation of triplet *trans*-stilbene with a yield  $G(t\text{-St}^t) \approx 0.06$ . Concurrent with the isomerization are the alternate reactions of *trans*-stilbene leading to products other than *cis*-stilbene and the results in Table I show that the *trans*-stilbene consumption is always greater than the isomerization. Thus reaction 15, which is probably the major process in the *trans*-stilbene destruction, predominates in these irradiated solutions, although the fact that isomerization does occur shows that reactions 8 and/or 9 also take place.

It has been demonstrated that in dilute solutions of stilbene in benzene the addition of naphthalene to the solutions brings about enhancement of isomerization upon irradiation, owing to the physical properties of triplet naphthalene (*e.g.*, lifetime and excitation energy) relative to those of triplet benzene and triplet stilbene.<sup>2,5</sup> Thus the naphthalene accepts energy from the solvent and passes it on to the solute. The limiting solubility of *trans*-stilbene in 2-propanol did not permit concentrations greater than 0.01 M to be used, and, therefore, naphthalene was added to the solutions to achieve a greater scavenger concentration range by inducing the double energy-transfer effect. The presence of naphthalene in the solutions was found to enhance the isomerization (see Table I), and a value of  $G(t\text{-St}^t) \approx$

0.66 may be calculated in the solutions containing 0.3 M naphthalene. At this concentration, however, there may be some direct excitation of the naphthalene upon irradiation. From the results obtained on the isomerization of *trans*-stilbene in pure naphthalene<sup>5</sup> it is estimated that at this concentration direct excitation can lead to  $G(\text{excited naphthalene}) \approx 0.2$ , showing that the naphthalene is indeed acting as an enhancer for the radiation-induced isomerization in 2-propanol.

The formation of triplet stilbene or triplet naphthalene may be brought about, in dilute solutions either by energy transfer from the solvent, reaction 9, or by an ionic mechanism, reactions 7 and 8.

In considering first the energy-transfer mechanism it is assumed that in these solutions, where the energy level of the donor molecules is higher than that of the acceptor molecules, the energy transfer rate is diffusion controlled with a rate constant  $k \approx 10^{10} M^{-1} \text{ sec}^{-1}$ .

As the rate of decay of naphthalene triplets is very slow (lifetime  $\sim 10^{-4} \text{ sec}^{20}$ ), the radiation-produced naphthalene triplet molecules will undergo quenching by processes involving the *trans*-stilbene or radiation-produced radicals. Under the experimental conditions used, however, the concentration of *trans*-stilbene is considerably in excess of the radical concentration, and there will therefore be complete energy transfer from naphthalene to stilbene.

On the basis of these observations and the  $G$  values for triplet molecules in the absence and presence of 0.1 M naphthalene, the lifetime for an excited 2-propanol molecule can be calculated to be  $< 10^{-10} \text{ sec}$ . This is very short when compared with the lifetimes of other species with which the solutes can react in irradiated 2-propanol, *e.g.*, solvated electrons, which in 2-propanol have a half-life of 5  $\mu\text{sec}$ .<sup>21</sup>

The alternative mode of producing a triplet *trans*-stilbene is through an ionic mechanism. Freeman and Fayadh<sup>22</sup> have calculated that for a solute to compete with geminate recombination of ions within the spurs the following relationship must hold

$$k_{e^- + \text{solute}} [\text{solute}] > 10^{10 \pm 1} \text{ sec}^{-1} \quad (\text{A})$$

On this basis the rate constant for the reaction between stilbene and the electron must be  $10^{11}$  to  $10^{12} M^{-1} \text{ sec}^{-1}$  if the stilbene is to compete with ion recombination within the spurs (reaction 3). This rate constant is much faster than any known for solvated electrons,

(16) S. Malkin and E. Fischer, *J. Phys. Chem.*, **68**, 1153 (1964).

(17) W. V. Sherman, *ibid.*, **70**, 667 (1966).

(18) C. von Sonntag, G. Lang, and D. Schulte Frohlinde in "The Chemistry of Excitation and Ionization," G. R. A. Johnson and G. Scholes, Eds., Taylor and Francis Ltd., London, 1967, p 123.

(19) S. Arai, E. L. Tremba, J. R. Brandon, and L. M. Dorfman, *Can. J. Chem.*, **45**, 1119 (1967).

(20) G. Porter and F. Wilkinson, *Proc. Roy. Soc.*, **A264**, 1 (1961).

(21) I. A. Taub, D. A. Harter, M. C. Sauer, and L. M. Dorfman, *J. Chem. Phys.*, **41**, 979 (1964).

(22) G. R. Freeman and J. M. Fayadh, *ibid.*, **43**, 86 (1965).

and the reaction is therefore unlikely to occur under the prevailing reaction conditions.

The stilbene anion, however, is known to exist.<sup>23</sup> In this work the protection shown to *trans*-stilbene by naphthalene which also reacts with electrons (see Table I) indicates that the *trans*-stilbene anion will be produced in 2-propanol. The possibility therefore exists for the stilbene anion to undergo neutralization with a 2-propanol or 2-propanol radical cation, which has escaped into the bulk of the solution, and thereby form a stilbene excited state. The low isomerization yield indicates that such a reaction is taking place, but only to a small extent.

In the solutions containing naphthalene it is assumed that all the original excitation is of the naphthalene, as it is present in large excess, and the isomerization is brought about through energy transfer to the stilbene. In this case also the short lifetime estimated for the excited 2-propanol will preclude an energy-transfer process between 2-propanol and naphthalene. Naphthalene has been shown to react with solvated electrons in  $\gamma$ -irradiated alcohols.<sup>8, 24, 25</sup> The naphthalene anion can then react through reactions 15 and 16, resulting in the hydrogen adduct free radical or undergo neutralization with the 2-propanol or 2-propanol radical cations leading to the formation of excited molecules of naphthalene. The results obtained in this work, showing that the presence of naphthalene in the *trans*-stilbene solution enhances the isomerization, indicates that some neutralization of the naphthalene anion leading to excitation does take place.

At a naphthalene concentration of 0.3 M it is considered likely that there will be some scavenging of electrons from the spurs if one considers expression A and assumes that  $k_{e(\text{solvated})+C_{10}H_8}$  in 2-propanol is not significantly different from the value in ethanol, ( $k \approx 5 \times 10^9 M^{-1} \text{ sec}^{-1}$ ).<sup>8</sup> Thus in the naphthalene solutions, excitation takes place through naphthalene reacting according to reactions 7 and 8, both in the spurs and in the bulk of the solution, followed by energy transfer to the stilbene.

The radiation-induced *cis*-to-*trans* isomerization in 2-propanol was found to behave in a similar manner to that observed in cyclohexane and benzene.<sup>4, 26</sup> In cyclohexane an anionic chain mechanism was proposed for the isomerization in view of the value for  $G(\text{free electron}) \approx 0.1^{27}$  for that compound. In 2-propanol, where  $G(e^- \text{ (solvated)}) \approx 1$ ,<sup>17, 28</sup>  $G(\text{initial isomerization}) \approx 0.27$  indicates that in this solvent the mechanism does not necessarily involve a chain. It is assumed that the mechanism involves catalysis by electrons as H atoms, which also exist in the irradiated solutions, will probably react preferentially with the 2-propanol in view of the rate constant for this reaction ( $k_{H+2\text{-propanol}} \approx 5 \times 10^7 M^{-1} \text{ sec}^{-1}$ )<sup>29</sup> and the relative amounts of substances present. A cationic mechanism is also discounted in view of the lack of evidence for the

formation of aromatic cations on the radiolysis of aromatic compounds in alcohols.<sup>8, 24, 25</sup>

The nonlinearity of the yield-dose plot (Figure 1) shows that with increasing dose a radiolysis product is being formed which is competing with the *cis*-stilbene for the species which initiates the isomerization reactions. One radiolysis product of 2-propanol is acetone,<sup>18</sup> which is a good electron scavenger and has been used specifically as such in some radiation chemical studies (e.g., ref 30). At the higher doses, therefore, there will be a competition for the solvated electrons and the value of  $G(cis \rightarrow trans) \approx 0.02$  at the higher doses shows almost complete scavenging of electrons by radiolysis products.

*Acetone Solutions.* The  $G$  values for the *trans*-to-*cis* isomerization of solutions of *trans*-stilbene in acetone (Table II) show that there is far more isomerization than in 2-propanol and that at 0.01 M stilbene the triplet-state precursors are nearly all being scavenged, the increase in isomerization with a tenfold increase in solute concentration being relatively small. The addition of naphthalene to the solutions enhanced the isomerization somewhat to a limiting value in 0.1 M solute (stilbene or naphthalene).

In studies on the pulse radiolysis of some aromatic compounds in acetone,<sup>14</sup> the formation of the triplet states of these solutes was accounted for in terms of an energy-transfer mechanism from triplet acetone. The triplet states of the solutes, identified from optical absorption spectra, were found to have a rate constant for formation of  $\approx 5 \times 10^9 M^{-1} \text{ sec}^{-1}$  and a  $G$  value of 1–2, and they were produced by an energy-transfer mechanism from acetone triplets and not by a charge-recombination reaction. By direct comparison the results obtained in this work, i.e.,  $G(trans \rightarrow cis) \approx 1.15$  in 0.1 M solute leading to  $G(t-St^t) \approx 2.3$ , may be accounted for in terms of energy transfer from radiation-produced acetone triplets. The  $G$  value for triplet acetone ( $G = 2.3$ ) is in good agreement with the pulse work considering the different types of radiation used.

Irradiated solutions of *cis*-stilbene in acetone showed similar effects to those observed in 2-propanol. If energy transfer alone were to account for the isomerization, the value of  $G(cis \rightarrow trans)$  should be 0.6–0.7 taking  $G(\text{acetone triplet}) \approx 2.3$ . The initial  $G$  values for the isomerization of *cis*-stilbene in acetone show that here

- (23) F. S. Dainton and G. A. Salmon, *Proc. Roy. Soc.*, **A285**, 319 (1965).
- (24) J. P. Guarino, M. R. Ronayne, and W. H. Hamill, *Radiat. Res.*, **17**, 379 (1962).
- (25) M. R. Ronayne, J. P. Guarino, and W. H. Hamill, *J. Amer. Chem. Soc.*, **84**, 4230 (1962).
- (26) R. R. Hentz, K. Shima, and M. Burton, *J. Phys. Chem.*, **71**, 461 (1967).
- (27) A. O. Allen and A. Hummel, *Discussions Faraday Soc.*, **36**, 95 (1963).
- (28) M. Sauer, S. Arai, and L. M. Dorfman, *J. Chem. Phys.*, **42**, 708 (1965).
- (29) E.g., G. Scholes and M. Simic, *J. Phys. Chem.*, **68**, 1738 (1964).
- (30) J. T. Allan and G. Scholes, *Nature*, **187**, 218 (1960).

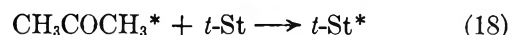
also more than one mechanism must be considered. By analogy to the results obtained in cyclohexane, benzene,<sup>4,26</sup> and 2-propanol, an anionic mechanism may be postulated. Acetone, as already mentioned, is a good electron scavenger, and in view of its excess over *cis*-stilbene it is more likely to react preferentially with the electrons. The isomerization of the *cis*-stilbene will therefore probably depend on a charge-transfer mechanism from the acetone anion to stilbene followed by conversion. A cationic mechanism is ruled out in this instance by the observation that a large amount of *cis*-stilbene (>10%) is required to show the *cis*-stilbene cation when irradiated in acetone at -196°.<sup>31</sup>

In all the irradiations it was found that the isomerization reactions were a relatively small part of the effect of the radiation on the solutes. This indicates that the intermediates produced on irradiating 2-propanol and acetone will react with the stilbenes and this will account for the phenanthrene and other products observed in the irradiated solutions. In this work the effect of stilbene on the radiolysis products of 2-propanol and acetone was not determined, but some effect would be expected in view of the observations in cyclohexane where the yields of products originating from radicals were decreased.<sup>4</sup>

*Mixed Solvents.* The results obtained for the isomerization of *trans*-stilbene in acetone led to the conclusion that perhaps acetone could enhance the isomerization in 2-propanol in a way similar to the effect shown by naphthalene, with the advantage over the latter being that acetone is completely miscible with 2-propanol.

It has been demonstrated in both photochemical<sup>32</sup> and radiation chemical<sup>18</sup> work on solutions of benzophenone in 2-propanol that triplet benzophenone can extract a hydrogen atom from 2-propanol. Strong and Burr<sup>10</sup> observed that in irradiated acetone-2-propanol mixtures the acetone was behaving as an H atom scavenger rather than as an energy acceptor. The results in this work show that both these effects are operative in that the isomerization, rather than being enhanced, is less than the amount to be expected on the basis of the fraction of the two liquids present and the values of *G*(isomerization) in pure acetone and 2-propanol. Thus not only is the acetone not acting as an energy bridge in such solutions but also the acetone triplets, which are formed by the direct action of the radiation on acetone (>0.1 M), are reacting in other ways rather than transferring their energy to the *trans*-stilbene.

The broken line (Figure 2) was, as stated above, an estimate of the amount of isomerization which might be expected on the basis of the fraction of the two liquids present and the values of *G*(isomerization) of 0.01 M *trans*-stilbene in the pure liquids. This is therefore an estimate of the amount of triplet acetone in solution (*G*(triplet acetone) = 2*G*(*cis*)) and is necessarily a lower limit as, by analogy to the naphthalene results, there will be some triplet formation by neutralization of the acetone anions. The results obtained in this work therefore indicate that there is a reaction between acetone triplets and 2-propanol analogous to that observed for benzophenone.<sup>18</sup> The decay of acetone triplets is fairly slow, 10<sup>-6</sup> to 10<sup>-7</sup> sec,<sup>33-35</sup> relative to energy transfer to *trans*-stilbene which is diffusion controlled, and the reactions of the triplet acetone in these solutions may therefore be considered to be a simple competition



Such a competition may be expressed kinetically as

$$\frac{G(cis)'' - G(cis)'}{G(cis)'} = \frac{k_{17}[2\text{-propanol}]}{k_{18}[t\text{-St}]} \quad (B)$$

where *G*(*cis*)'' is the calculated value of the *cis*-stilbene yield and *G*(*cis*)' is the experimental value.

At low acetone concentrations *G*''(*cis*) is considered to be a closer measure of the amount of acetone triplets in solution, as the triplets formed through neutralization will be small, and hence an estimate of  $k_{17} \approx 10^7 \text{ M}^{-1} \text{ sec}^{-1}$  was made from expression B, taking  $k_{18}$  to be  $10^{10} \text{ M}^{-1} \text{ sec}^{-1}$ .

*Acknowledgment.* The author wishes to express his gratitude to Stiftung Volkswagenwerk for the award of a fellowship during the tenure of which this work was carried out. The author also wishes to thank Professor Dr. G. O. Schenck and the staff of the Max Planck Institut für Kohlenforschung, Abteilung Strahlenchemie, for the hospitality extended to him.

(31) T. Shida and W. H. Hamill, *J. Amer. Chem. Soc.*, **88**, 3683 (1966).

(32) A. Becket and G. Porter, *Trans. Faraday Soc.*, **59**, 2038 (1963).

(33) F. Wilkinson and J. T. Dubois, *J. Chem. Phys.*, **39**, 377 (1963).

(34) R. F. Borkman and D. R. Kearns, *J. Amer. Chem. Soc.*, **88**, 3467 (1966).

(35) P. J. Wagner, *ibid.*, **88**, 5672 (1966).

# On the Utility of the Concept of Water Structure in the Rationalization of the Properties of Aqueous Solutions of Proteins and Small Molecules<sup>1</sup>

by Alfred Holtzer and Marilyn F. Emerson

*Department of Chemistry, Washington University, St. Louis, Missouri 63130 (Received March 21, 1968)*

It is demonstrated for several cases chosen from the literature that arguments based upon the concept of water structure are sufficiently ambiguous so that the change, in a given physical property, that accompanies dissolution of a solute in water can always be "explained," whether that change is positive or negative. The number of examples and the range of physical properties discussed are sufficiently great to arouse suspicion that such arguments are almost always equivocal and that, therefore, rationalizations of most experimental data on this basis are devoid of content.

## Introduction

In 1945, Frank and Evans<sup>2</sup> postulated the formation of hydrogen-bonded, quasi-crystalline structures of water molecules around isolated, nonpolar molecules in aqueous solution. This hypothesis, they argued, successfully explains the unusual enthalpy ( $\Delta H \leq 0$ ) and entropy ( $\Delta S < 0$ ) effects associated with the transfer of a nonpolar solute from a hydrocarbon environment (at some low solute mole fraction) to water (at the same low solute mole fraction). They termed these regions of greater crystallinity "icebergs," but emphasized that the structure of these icebergs need not be the same as that in ordinary ice nor the same for all icebergs.

It has been suggested<sup>3</sup> that the volume changes accompanying such solute transfer provide evidence that the icebergs are indeed quite different in structure from ordinary ice. The transfer of nonpolar substances from hydrocarbons to water at 25° is accompanied by a decrease in volume, whereas the formation of ordinary ice from water results in a volume increase.

All these enthalpy, entropy, and volume effects become less extraordinary as the temperature is increased. Thus, at temperatures above 50°, hydrocarbons in water begin to behave more like hydrocarbons in nonpolar solvents. Frank and Evans attributed this to the melting of the icelike structures with increasing temperature.

The particular relevance of the Frank-Evans idea to protein and polypeptide chemistry has been clearly pointed out by Kauzmann.<sup>3</sup> Kauzmann recognized not only that the tendency of nonpolar side chains to adhere to one another in aqueous solution (*i.e.*, the formation of hydrophobic bonds) should be an important factor in the stabilization of particular conformations of polypeptide chains but also that the molecular events in the process could be specified in much more detail by using the Frank-Evans approach. On this basis, he concluded that formation of hydrophobic bonds in proteins is attended by the melting of icebergs

and therefore that these bonds are stabilized by solvent entropy effects, since the transfer of a nonpolar group from water to the (nonpolar) interior of the protein molecule should show  $\Delta G < 0$ , though it is endothermic ( $\Delta H > 0$ ).

As evidence has accumulated that hydrophobic interactions do, indeed, contribute appreciably to the maintenance of the native conformation of a protein molecule,<sup>4-6</sup> interest in the molecular rationalization of these interactions on the basis of solvent structural effects has, of course, also increased.<sup>7</sup> This interest is understandable, since even a rough, strictly qualitative, picture of the molecular events involved would be quite helpful in dealing with a variety of problems of protein chemistry. For example, it would be extremely useful in predicting the influence of a particular additive upon a protein in solution. There is convincing evidence that many protein denaturants owe their action, at least in large part, to hydrophobic effects.<sup>3,8</sup> With an unequivocal picture of the underlying molecular processes, it would be possible to deduce from the physical properties of aqueous solutions of a given additive whether solvent structure has been broken or formed. Knowledge of the effects upon proteins of substances of *known* influence on water structure could then lead to an estimate of the efficacy of the additive as a denaturant and, perhaps in some cases, to a rough idea of what portions of the protein molecule it might affect most.

- (1) This investigation was supported by Research Grant RG-5488 from the Division of General Medical Sciences, Public Health Service.
- (2) H. S. Frank and M. W. Evans, *J. Chem. Phys.*, **13**, 507 (1945).
- (3) W. Kauzmann, *Advan. Protein Chem.*, **14**, 1 (1959).
- (4) C. Tanford, J. D. Hauenstein, and D. B. Rands, *J. Amer. Chem. Soc.*, **77**, 6409 (1955).
- (5) J. C. Kendrew, G. Bodo, H. M. Dintzis, R. G. Parrish, H. Wykoff, and D. C. Phillips, *Nature*, **181**, 662 (1958).
- (6) C. Tanford, *J. Amer. Chem. Soc.*, **84**, 4240 (1962).
- (7) G. Nemethy and H. A. Scheraga, *J. Phys. Chem.*, **66**, 1773 (1962).
- (8) D. F. Waugh, *Advan. Protein Chem.*, **9**, 325 (1954).

This is an obviously desirable goal, and the present tone of the literature suggests that great progress toward its attainment is being made. Recent publications on protein solutions, or on the physical properties of aqueous solutions of small molecules, often contain numerous (usually rather positive) statements about the role of water structure. Unfortunately, the qualitative arguments put forward by different authors often have led to quite contradictory conclusions; indeed, in many cases, even a single given argument is sufficiently indeterminate as to be capable of producing several, contradictory conclusions.

It is our contention that, in fact, the position has been little advanced since the work of Frank and Evans<sup>2</sup> and Kauzmann<sup>3</sup> and that the widespread practice of invoking changes in water structure to rationalize experimental data can only serve to perpetuate the illusion that some real understanding exists. The illusion is soon dispelled when prediction, rather than rationalization, is attempted. It is our view that one cannot, in general, examine the bulk physical properties of an aqueous solution of a nonelectrolyte and determine unambiguously whether the solute is "structure forming" or "structure breaking" (if, indeed, the terms mean anything definite at all). If this is true, then a large number of authors have been led into error. By examining in detail a few rather typical statements from the literature, it will be shown how easy it is to be misled, apparently by the pictorial simplicity of the iceberg model, into drawing an unwarranted conclusion.

The reader, of course, may feel that the particular statements selected are atypical; we urge, therefore, that he search the recent literature for more. Careful examination along the lines suggested below will reveal, we are confident, one or more characteristic errors: (1) the particular physical properties to be interpreted are selected so that a self-consistent physical picture emerges; *i.e.*, "bothersome" facts are ignored, or (2) a given physical property is interpreted sufficiently superficially, usually by improper or arbitrary subtraction of structure-independent factors, so that the answer becomes determinate (but its accuracy indeterminate), or (3) words suggesting quantitation (*e.g.*, "appreciable") are used to describe an effect (in spite of the absence of any proper quantitative evaluation) and then are taken literally.

Before we proceed, a word is in order about those parts of the iceberg idea that we consider acceptable, at least for the sake of argument. In brief, we agree that the correct interpretation of enthalpies and entropies of transfer of simple, nonpolar substances from hydrocarbons to water is that icebergs form, in the Frank-Evans sense, about the nonpolar materials in the aqueous environment. However, it should be emphasized that this is an interpretation of, not a rigorous deduction from, the data. Indeed, the idea only follows from the experimental observations if it is assumed that, in

water, the effects of solvent rearrangement dominate the enthalpies and entropies. There are numerous other molecular contributions, of course, but they are assumed to be less important. It must be recognized, however, that domination of the enthalpy and entropy by a particular interaction does not necessarily mean that it dominates some other, arbitrarily chosen, property. Let us now consider some of the ideas that have emerged from the original proposal.

### The Properties of D<sub>2</sub>O<sup>9</sup>

The interpretation of bulk properties in terms of the "flickering-cluster" concept has led to the inference that D<sub>2</sub>O is more highly structured than H<sub>2</sub>O at the same temperature.<sup>10</sup> No conclusion in the field would appear to be more strongly supported by the facts: the temperature of maximum density, the freezing and boiling point, the enthalpy and entropy of vaporization, and, perhaps most striking of all, the viscosity of D<sub>2</sub>O are all higher than the corresponding values for H<sub>2</sub>O. In some cases, the differences are small (*e.g.*, 4% in the case of the entropy of vaporization), in some large (25% in the case of viscosity), but all are in the direction indicating a greater structure for D<sub>2</sub>O. However, there is always one omission in this context, the dielectric constant.

The omission is startling, because the large dielectric constant of H<sub>2</sub>O is customarily, and very convincingly, cited as evidence for the existence of extensive regions of cooperative structure in this liquid.<sup>11-13</sup> In an electric field, these regions can be polarized (by a mechanism that has not yet been clarified) so that a relatively large dipole moment is induced in the field direction.<sup>14,15</sup> Now let us consider, rather superficially, what should happen to the dielectric constant when D<sub>2</sub>O is substituted for H<sub>2</sub>O. The molecular dipole moments in the gas phase of H<sub>2</sub>O and D<sub>2</sub>O are identical,<sup>16</sup> the electronic polarizability of the D<sub>2</sub>O molecule is a bit greater (by about 5%); and the geometry and spacings of the molecular arrangements in the solid phases are virtually identical. The picture we have, then, is that in each

(9) The authors are grateful to Professor Walter Kauzmann for his counsel; before we had his advice this section was considerably less cogent than the reader finds it. Needless to say, any guilt that remains is our own.

(10) For a summary of the relevant properties of H<sub>2</sub>O and D<sub>2</sub>O, see G. Nemethy and H. A. Scheraga, *J. Chem. Phys.*, **41**, 680 (1964).

(11) W. M. Latimer and W. H. Rodebush, *J. Amer. Chem. Soc.*, **42**, 1419 (1920).

(12) J. Edsall and J. Wyman, "Biophysical Chemistry," Academic Press, New York, N. Y., 1958, Chapter 2.

(13) L. Pauling, "The Nature of the Chemical Bond," Cornell University Press, Ithaca, N. Y., 1960, Chapter 12.

(14) C. P. Smyth, "Dielectric Behavior and Structure," McGraw-Hill Book Co., Inc., New York, N. Y., 1955.

(15) J. L. Kavanau, "Water and Water-Solute Interactions," Holden-Day Inc., San Francisco, Calif., 1964.

(16) For a summary of the relevant properties of H<sub>2</sub>O and D<sub>2</sub>O, see I. Kirshenbaum, "Physical Properties and Analysis of Heavy Water," McGraw-Hill Book Co., Inc., New York, N. Y., 1951, and ref 10.

liquid there are clusters that are identical in geometric arrangement of their constituent molecules; the only difference in the clusters themselves is that the D<sub>2</sub>O clusters contain molecules of slightly greater electronic polarizability, which would give them a higher moment in the applied field and lead to a slightly higher dielectric constant for D<sub>2</sub>O. This effect, however, should be minor—the contribution of electronic distortion to the dielectric constant of water is supposedly small. What is *not* minor is that the conventional interpretation of the other physical properties insists that in D<sub>2</sub>O there be more such clusters or that their average size be greater or both. In either case we would predict that the polarization of these regions, as described above, would lead to a higher dielectric constant for D<sub>2</sub>O.

The experimental result, however, is just the reverse.<sup>17,18</sup> The difference, as in many other properties, is very small, but the dielectric constant of D<sub>2</sub>O is distinctly lower than that of H<sub>2</sub>O over the entire normal liquid range.

Understandably reluctant to give up our earlier, seemingly well-butressed conclusion that D<sub>2</sub>O is the more structured liquid, we simply assume that we cannot perform such a superficial analysis of the dielectric constant and expect to be able to make a valid prediction, even a qualitative one. How, then, can we look at the question?

A clue to the problem of the effect of structure in the liquid is available from measurements of the dielectric constants of D<sub>2</sub>O ice and H<sub>2</sub>O ice.<sup>19</sup> In the solid form, both substances are essentially completely structured. The experimental finding is that heavy ice has a slightly lower (~2%) dielectric constant. The superficial analysis (as in the previous paragraph), when applied to ice, would predict that the two should be the same. The temptation is strong to call 2% "small" and to hail the agreement between theory and experiment as a kind of triumph of superficiality. However, having eschewed the superficial view because of its failure to yield the correct answer for the liquid, we must rather admit that a difference of 2% means that some other structure-independent effect must contribute to the dielectric constant in such a manner as to reduce the D<sub>2</sub>O value relative to H<sub>2</sub>O. What this effect is cannot be specified at present. However, since the dipole moment of the water molecule in the condensed phase can be considerably larger than that of the isolated molecule (by a factor of about 2 in ice<sup>20</sup>) and since this increase may very well be sensitive to effects essentially quantum mechanical in nature, such as the amplitudes of zero point motions, it may account for the difference in the two ices.

In any event, admitting that such a structure-independent effect is present can serve to remove the liquid anomaly. The important factors are the molecular dipole moment in the liquid and the angular correlation between dipoles.<sup>21,22</sup> Since the more structured liquid

(presumably D<sub>2</sub>O) has improved dipole-dipole correlation, its dielectric constant would be increased relative to H<sub>2</sub>O. However, the structure-independent factor described above (be it the condensed-phase value of the dipole moment or whatever) acts in the opposite direction. Thus the assumption that D<sub>2</sub>O has more structure than H<sub>2</sub>O does not lead to a clear prediction of the relative dielectric constants, since it is not known, *a priori*, which effect, the amount of iceberg or the structure-independent factor, dominates. This resort to nonsuperficiality thus neutralizes the dielectric constant "anomaly."

Unfortunately, nonsuperficiality, once invoked, has insidious effects. The gnawing fear grows that perhaps there are opposing effects that contribute to the *other* physical properties of H<sub>2</sub>O and D<sub>2</sub>O, thus precluding any firm, *a priori*, prediction of the relative amounts of clusters in the two liquids.

A closer look at the viscosity, for example, confirms this idea. It is natural that suspicion should first fall on the viscosity. The realization that the dielectric constant changes are rather subtle, on a molecular level, and not susceptible to simple, qualitative arguments immediately directs ones troubled gaze to the viscosity; hydrodynamic problems are notoriously refractory to intuitive analysis.

One might begin by inquiring what the ratio of the viscosities (of H<sub>2</sub>O and D<sub>2</sub>O) would be in the normal course of events, that is, if they were "simple" fluids without specific structure or bothersome intramolecular degrees of freedom. The quantitative theory of viscosity of simple fluids is certainly not at a stage near perfection, but it does seem clear that, ignoring quantum effects, which are probably small for water near room temperature, several factors contribute:<sup>23</sup> (a) differences in the molecular masses, (b) differences in moment of inertia, and (c) differences in intermolecular potential. Since the viscosity varies as the square root of the mass, factor a alone accounts for a difference somewhat over 5% out of the 25% total observed. The second factor (b) is rather more difficult to estimate, but since all three of the principal moments of inertia of D<sub>2</sub>O are about double the corresponding ones for water, an additional 1 or 2% is certainly to be expected.<sup>23</sup> Finally, the effects of differences in inter-

(17) J. Wyman and E. N. Ingalls, *J. Amer. Chem. Soc.*, **60**, 1184 (1938).

(18) G. A. Vidulich, D. F. Evans, and R. L. Kay, *J. Phys. Chem.*, **71**, 656 (1967).

(19) R. P. Auty and R. H. Cole, *J. Chem. Phys.*, **20**, 1309 (1952).

(20) L. Onsager and M. Dupuis in "Electrolytes," B. Pesce, Ed., Pergamon Press Ltd., New York, N. Y., 1962, p 27.

(21) J. G. Kirkwood, *J. Chem. Phys.*, **7**, 911 (1939).

(22) H. Frohlich, "Theory of Dielectrics," 2nd ed., Oxford University Press, London, 1958, p 49.

(23) S. A. Rice, J. P. Boon, and H. T. Davis in "Simple Dense Fluids," H. Frisch and Z. Salsburg, Eds., Academic Press, New York, N. Y., 1968.

molecular potential must be accounted for. Since the Lennard-Jones parameters for D<sub>2</sub>O have not been determined, we must rely on analogy: in the case of CH<sub>4</sub>-CD<sub>4</sub>, this factor augments the viscosity of the isotopic species by another 1% or so.<sup>23</sup> Consequently, considering only factors not related to the specific structure of the liquid, more than one-third of the observed difference can be explained. In fact, the theory is sufficiently inexact<sup>23</sup> that one cannot say for sure that these factors do not account for *all* the difference.

Even if we assume that the remaining ( $\sim 15\%$ ) difference is real, however, it surely is explainable if all hydrogen bonds (not only the nice linear ones found in ice and textbooks) formed by D<sub>2</sub>O are simply slightly stronger than their H<sub>2</sub>O counterparts, *i.e.*, if D<sub>2</sub>O molecules are slightly stickier. This specific interaction is not included in factor c, which was derived only for intermolecular potentials characteristic of simple fluids. In any event, the augmented "stickiness" of D<sub>2</sub>O obviously is not necessarily productive of clusters in the Frank-Wen sense, and the viscosity difference seems clearly explainable without their presence. As far as we know, a continuum model would produce a viscosity increase that is enough to make up the remaining difference between the results of simple fluid theory and experiment, if there is, in reality, such a difference. Indeed, the hydrodynamic effect of Frank-Wen clusters is moot. Their influence on the viscosity would depend not only on their volume fraction but also on their ability to act, in part, as obstacles more or less penetrable by (nonhydrogen bonded) "solvent." One could envision such clusters in D<sub>2</sub>O being more rigid than those in H<sub>2</sub>O, and thus remaining relatively impenetrable, while the H<sub>2</sub>O clusters are hydrodynamically more penetrable by "solvent." It is a well-known result of the theory of viscosity that such partially penetrable obstacles can produce a higher viscosity than impenetrable ones. Thus it is conceivable that an increase in (Frank-Wen-type) structure might *decrease* the viscosity if it is accompanied by a decrease in penetrability of the clusters sufficient to offset their lesser volume concentration.

Thus a superficial consideration of the physical properties of H<sub>2</sub>O and D<sub>2</sub>O leads to satisfactory explanations of all of them in terms of the relative amounts of clusters in the two liquids; all, that is, except the dielectric constant. In order to account for the experimental dielectric properties, a more penetrating analysis has to be made, the result being that an experimental result in either direction can be "explained" but no prediction made. However, when a similar, but still qualitative, analysis of other properties is attempted, the result is often that either experimental result can be rationalized. The existence of more clusters in D<sub>2</sub>O, for example, does not necessarily require a higher viscosity.

We wish to make it perfectly clear that we *believe* that D<sub>2</sub>O is more *structured* than H<sub>2</sub>O, although not necessarily in the Frank-Wen sense. We merely wish to

emphasize that even in this simplest, best established case, qualitative arguments based on the flickering-cluster concept are not unambiguous.

### The Relationship of Icebergs to Ice<sup>9</sup>

As a second example, we might quote an argument that was mentioned above concerning the nature of the icebergs, as revealed by volume changes.<sup>3</sup> This argument on the volume change accompanying transfer of a nonpolar molecule from a hydrocarbon to water (a volume change which is negative) makes the tacit assumption that the formation of the iceberg *dominates* the volume change (as it does the enthalpy and entropy); since the sign of the experimental volume change, and thus the sign of the volume change on iceberg formation, is opposite to that for the formation of (real) ice from liquid water, it is concluded that the icebergs do not have a true icelike structure.

However, a different interpretation is possible. It is often suggested that nonpolar solutes dissolve interstitially in water, at least so far as they are able, *i.e.*, so as to break as few normal water-water hydrogen bonds as possible. If this were the only factor involved, a negative volume change on transfer of the nonpolar molecule from a hydrocarbon to water would result. If, in addition, however, some truly icelike structure formed about the solute in water, this would tend to make the volume change positive. The observed, negative volume change could then result by domination of the former effect over the latter. Since there is at present no way of assessing the relative contributions of these two effects, the argument offered here, while it cannot refute the earlier one, would seem to be of equal force. It is also obvious that the lack of a quantitative measure of these individual effects makes any such argument indeterminate; not even the sign of the volume change follows uniquely from the idea of water structure.

At this point, it is hard to avoid the impression that there is a strong semantic component to the disagreement between the two arguments. Much depends on the interpretation to be placed on the phrase "true icelike structure." If we interpret this very strictly, *i.e.*, if we require that dissolution of a nonpolar molecule in water be precisely like embedding the molecule in a single ice crystal, then the logic of the earlier argument (of ref 3) acquires strength but at the expense of content. It is true that small, nonpolar molecules are not very soluble in ice, which is rich in interstitial spaces. Therefore, such solutes evidently cannot fit into a single ice crystal without displacing some water molecules, an effect which should surely serve to increase the volume, contrary to the observation. Hence, that the iceberg is not a small, *completely undistorted* ice crystal seems indisputable, but, of course, it is rarely thought of in such literal terms anyway. On the other hand, if the strictness of interpretation is relaxed to allow *some* dis-

tortion of the ice structure near the solute particle (a situation covered in the preceding paragraph by the phrase "so far as they are able"), then the argument of the last paragraph acquires relative force and the situation becomes ambiguous.

How much freedom is to be allowed in distorting the structure locally while still calling it truly icelike? Obviously, this is a matter of taste rather than substance. It does, however, emphasize precisely the point we are trying to make, namely, how very difficult it is to use the flickering-cluster model in making even qualitative deductions that are at once nontrivial and unambiguous. The model seems to become less distinct the more closely it is examined.

### Influence of Solutes on Water Structure

Finally, we consider a recent paper that purports to delineate the changes in solvent structure that accompany dissolution of urea in water.<sup>24</sup> It goes without saying that this problem is central to our interest in assessing the efficacy of protein denaturants. Furthermore, the entire paper is devoted to a discussion of this one problem. The result, however, far from being definitive or convincing, provides instead a multitude of examples of the kind of reasoning we are examining.

We do not wish to risk misstating the arguments in question, and we therefore suggest that the reader obtain a copy of the paper and examine each of the statements carefully as we proceed. Briefly stated, the supposition is that hydrocarbons dissolve interstitially in aqueous solution—the more stable the interstices in a particular aqueous solvent, the better solvent it is for hydrocarbons. It is concluded that a urea molecule can enter into the normal clusters of water molecules without distorting them appreciably and that the cluster is (with its interstices) slightly stabilized by its presence, thus accounting for the hydrophobic bond-breaking power of urea. Five physical properties of aqueous urea solutions are cited in support of this contention. Let us examine the argument in each case.

(1) *Solubility.* Since the argument here consists of only two sentences, we can state it in full. "It is a well-known fact that urea has an extremely high solubility in water (about 20 m at 25°). The ease of mixing urea with water means that urea is able to compete with water molecules for the hydrogen bonds." This argument has not been well put. Clearly, the absolute magnitude of the solubility can tell us nothing. Tetramethylurea (a liquid), for example, is miscible in all proportions with water; solid N,N'-dimethylurea ("which, would not be able to enter into cluster formation"<sup>24</sup>), for another, is as soluble as urea. The point is that urea is known to be strongly hydrogen bonded in the solid state. It is thus reasonable to conclude, from its large solubility in water, that a strong, attractive urea-water interaction must exist—strong, that is, compared with the interaction of water with hydrocarbons. This

conclusion, unfortunately, is as irrelevant as it is incontestable, because it contains no information about the nature of the structure formed when a urea molecule interacts with water. Perhaps urea molecules participate in the regular water clusters; perhaps a new type of cluster is formed; perhaps hydrogen bonding, while it exists, is less regular in the solution and there is a net cluster disruption. None of these possibilities is inconsistent with high solubility, which requires only that the net free energy of dissolution be strongly negative, a result that could be achieved by any of the molecular routes described. Since no one knows, or can estimate, the contribution to the free energy of these various molecular events, no one can decide which of the many molecular models is correct. In fact, it may well be that different mechanisms are involved for different solutes. Sucrose is also very soluble in water, yet it has spectacularly less effect on proteins and on the hydrophobic bonds in micelles<sup>25,26</sup> than does urea.

(2) *Heat Capacity.* The infinite-dilution partial molal heat capacity of urea is "very close" to that of pure, solid urea, which, it is argued, "shows that a similar environment exists in the solid state and in aqueous solutions."

The superficiality of this analysis can be seen by considering the following statement, cooked up by ourselves, which uses identical logic and, as the reader can readily verify by consulting ref 24, almost identical wording. "The molal heat capacity of water (which is indicative of the environment of the water molecule in the pure liquid) is of the order of 18 cal/mol deg, which is far from that of the solid (~10 cal/mol deg). This shows that a dissimilar environment exists in the solid state and in the pure liquid. As it is known that in the solid the water molecule is hydrogen bonded, this must not be true in the liquid. Thus, water is an unstructured liquid."

The fallacy is easy to spot: it lies in using a vague word like "dissimilar" and then acting as though it means "completely different from." In the statement from ref 24 the word "similar" is used and then tacitly converted to "exactly the same." Even if the equality of heat capacities were evidence that the environment of a urea molecule is "similar" in the solid and in aqueous solution, we must then ask: "Similar in what respect?" The question, alas, cannot be answered, since it is not possible to take as given a particular molecular arrangement in solution and show just how "similar" it has to be to the solid in order to get heat capacities that agree to the correct degree of approximation. In other words, no one knows how sensitive the heat capacity

(24) M. Abu-Hamdiyyah, *J. Phys. Chem.*, 69, 2720 (1965).

(25) M. F. Emerson, Ph.D. Thesis, Washington University, St. Louis, Mo., 1966.

(26) M. F. Emerson and A. Holtzer, *J. Phys. Chem.*, 71, 3320 (1967).

may be to postulated changes in the structure of the solution.

More important, however, is the possibility that the agreement is fortuitous. We might just as well have suggested, for example, that this argument about the (constant-pressure) heat capacity (temperature derivative of the enthalpy) hold for the enthalpy as well; i.e., one could, with equal justice, argue that if the environments are similar, the enthalpies should be too. In fact, of course, they are quite different, dissolution of urea in water being so spectacularly endothermic that the solvent often freezes when the process is carried out. Closer examination of all the heat capacity data confirms this suspicion; the agreement, in fact, exists only for room temperature. In the same reference cited in ref 24 for these data<sup>27</sup> the reader's attention is explicitly called to the slight variation of the heat capacity of solid urea with temperature compared with the pronounced temperature coefficient of the infinite dilution partial molal heat capacity of urea in water. The difference between the two is only about 15% at 25° (this is apparently the definition in ref 24 of "very close") but becomes about 100% at 2°. The agreement at room temperature is quite obviously fortuitous.

One might add that it is easy to find examples of other compounds for which the two heat capacities happen to agree at room temperature. For sucrose, for example, the agreement is, percentagewise, better than for urea.<sup>28</sup> Yet, a molecule of molecular weight over 300 can scarcely be thought of as able to "enter" clusters of water molecules with "only slight" distortion.

(3) *Viscosity.* The argument here is that an increase (decrease) in viscosity upon addition of solute to water indicates that the solute is structure forming (breaking); urea increases the viscosity of water slightly, confirming the notion of the structure forming tendency of this solute.

This argument is inexplicably superficial; in fact, two of the references given in ref 24 refute it.<sup>29,30</sup> If spherical particles (solute molecules) are inserted into a structureless solvent, the suspension will have a higher viscosity than that of the pure solvent because of the distortion of the solvent flow lines by the solute particles. A quantitative and definitive theory of this effect was first presented by Einstein<sup>31</sup> who found that, at infinite dilution

$$[\eta] = \eta_{sp}/c_h = \frac{\eta - \eta_0}{\eta_0 c} = 2.5v_h \quad (1)$$

where  $\eta$  and  $\eta_0$  are the viscosities of the solution and solvent, respectively,  $c_h$  is the concentration of the hydrodynamic solute particle, i.e., of the spheres (in grams per cubic centimeter of solution); and  $v_h$  is the specific volume of the spheres (in cubic centimeter per gram). Thus a spherical particle, when introduced into a structureless solvent, would increase the viscosity, and such

an increase is therefore not necessarily an indication of any perturbation of solvent structure whatever.

A more sophisticated analysis of the problem has been attempted,<sup>30</sup> but, we believe also without success. In ref 30 deviations of the observed viscosity from Einstein behavior are interpreted in terms of the solvent structural effect; i.e., a value of  $[\eta]/2.5v_h$  that is greater than unity supposedly indicates the formation of solvent structure, and a value less than unity supposedly indicates the disruption of structure. In spite of this refinement, however, analysis of the viscosity cannot yield the required information, as the following discussion will show.

Clearly, several assumptions are involved here. In using the Einstein formulation, it must be assumed that the solute molecule is spherical. Since the solute molecules in question are small and since the theory of the viscosity of ellipsoids demonstrates that the viscosity increment varies rather slowly with axial ratio for near-spheres, this assumption is probably not seriously in error. However, it is now necessary to insert a numerical value for  $v_h$ , the specific volume of the spheres. For this, the reciprocal of the density of the pure solute is used,<sup>30</sup> be it solid or liquid. The second assumption, then, is that a solute particle occupies the same volume in solution as it does when pure; this is, in general, wrong, and one can only hope the effect is not large.

Even accepting the assumptions, however, it can be shown that deviations from Einstein behavior can be caused by factors other than the formation or breakage of (cooperative) solvent structure, and therefore such deviations cannot be interpreted uniquely in terms of changes in such structure. Einstein's theory applies to the kinetic unit in solution, and this may consist of more than just a solute molecule. A less superficial use of the Einstein relation thus might be as follows.

First we must note that if the hydrodynamic particle is solvated, then the quantity  $\eta_{sp}/c_h$  is not experimentally accessible. The analogous quantity that can be measured is, of course,  $\eta_{sp}/c$ , where  $c$  is the mass of dry solute contained in 1 ml of solution. If the kinetic unit is a solvated solute molecule binding  $w$  g of solvent/g of (dry) solute, then

$$c_h = c(1 + w) \quad (2)$$

Furthermore, the specific volume of the kinetic unit is given by

(27) E. J. Cohn and J. T. Edsall, "Proteins, Amino Acids and Peptides as Ions and Dipolar Ions," Reinhold Publishing Corp., New York, N. Y., 1943, p 171.

(28) Reference 27, p 169.

(29) R. W. Gurney, "Ionic Processes in Solution," McGraw-Hill Book Co., Inc., New York, N. Y., 1953, Chapter 9.

(30) J. A. Rupley, *J. Phys. Chem.*, **68**, 2002 (1964).

(31) A. Einstein, *Ann. Phys.*, **19**, 289 (1906); "Investigations on the Theory of Brownian Movement," Dover Publications, Inc., New York, N. Y., 1956.

$$v_h = \frac{v + \frac{w}{\rho_b}}{1 + w} \quad (3)$$

where  $v$  is the volume of 1 g of dry solute particles and  $\rho_b$  is the density of bound solvent. Again, the experimentally accessible quantity is rather  $\bar{v}$ , the increase in volume of solution upon addition of 1 g of dry solute. This quantity is

$$\bar{v} = v + \left( \frac{w}{\rho_b} - \frac{w}{\rho_0} \right) \quad (4)$$

i.e.,  $\bar{v}$  represents the sum of the increase of the volume of solution due to the displacement of solvent by solute particles and the change in solvent volume suffered by bound solvent. Eliminating  $v$  between eq 3 and 4, we find

$$v_h = \frac{\bar{v} + \frac{w}{\rho_0}}{1 + w} \quad (5)$$

Using eq 2 and 5 in eq 1, we obtain

$$[\eta] = \eta_{sp}/c = 2.5 \left( \bar{v} + \frac{w}{\rho_0} \right) \quad (6)$$

Since  $[\eta]$  and  $\bar{v}$  are operational quantities, eq 6 suggests  $[\eta]/2.5\bar{v}$  as the significant quantity, i.e., that  $\bar{v}$  should have been used in ref 30 instead of the reciprocal of the density of pure solute.

Unfortunately, this more complete interpretation is difficult to implement in any practical way that would allow conclusions to be drawn about water structure. Values of  $[\eta]/2.5\bar{v}$  greater than unity could signify deviations from Einstein's equation caused by a net structure formation in the surrounding solvent, since this would lead to an increased *local* solvent viscosity, in violation of one of the Einstein assumptions. However, since eq 6 shows that  $[\eta]/2.5\bar{v}$  is simply  $1 + (w/\bar{v}\rho_0)$ , it could also mean that the solute particle simply carries some solvent with it (i.e., that  $w > 0$ ), a situation quite distinct from the cooperative structure formation considered hitherto. In fact, beyond the solvation layer, cooperative structure might be *broken*, the experimental observation reflecting both effects. The occurrence of a value of  $[\eta]/2.5\bar{v}$  that is greater than unity thus does not have a unique structural interpretation, because of the possibility of solvation—even if we assume the solute particles are spherical in shape.

Since, from a simple solvation viewpoint,  $w < 0$  would seem to be senseless, it might appear that an experimental value of  $[\eta]/2.5\bar{v}$  that is less than unity would be more susceptible to interpretation in terms of solvent structure. Unfortunately, closer examination, as we shall see, does not bear this out.

In deriving Einstein's equation, it must be assumed

that the spheres are "wet," i.e., that the contact layer of solvent moves with the same velocity as the surface of the spheres. For macroscopic bodies immersed in a fluid, this assumption is undeniably correct,<sup>32</sup> but for a single solute molecule surrounded by solvent particles that are comparable with it in dimensions, it is, in general, false. In other words, it seems clear that there could be some "slip" at the surface of contact of the kinetic unit (centered around the solute molecule) and the solvent. Clearly, this would reduce the viscous drag and consequently the coefficient of viscosity would be smaller. For solute molecules that are approximately the same size as the solvent molecules we cannot expect the "no-slip" condition to hold rigorously; so the measured viscosity may be less than that for Einstein spheres, i.e., we might find  $[\eta]/2.5\bar{v} < 1$ .

Indeed, one would expect Einstein's theory to work for colloidal particles, i.e., for spheres much larger than a solvent molecule, but not for anything else. Thus, as before, it is not possible to draw conclusions about water structure from the change in the property in question (in this case the viscosity) as solute is added.

(4) *Dielectric Constant.* The argument in ref 24 is that the molar dielectric increment of urea  $\Delta\epsilon/\Delta c$  is positive (= 2.72) and that this is caused not by the high dipole moment of urea (4.56 D) but by its influence in increasing solvent structure. As evidence for the latter, it is claimed that N,N'-dimethylurea "which would not be able to enter into cluster formation" has a larger dipole moment (4.8 D) than urea and yet a dielectric increment of zero.

In this case, the argument is apparently based on a simple mistake; the wrong value of  $\Delta\epsilon/\Delta c$  seems to have been transcribed. In fact, the source cited in ref 24<sup>33</sup> gives a value of  $\Delta\epsilon/\Delta c = 3$  (not zero) for N,N'-dimethylurea. This value is about the same as that for urea, as is the dipole moment.

When we consider the above data and add to them the fact that N,N-dimethylurea has a dipole moment of 4.7 D and  $\Delta\epsilon/\Delta c \sim 0$  and that both methanol and acetamide (each with a healthy dipole moment and both described in ref 24 (*via* Frank and Wen<sup>34</sup>) as "...able to enter clusters with only slight distortion...") actually *lower* the dielectric constant of water, it is apparent that both the dipole moment and the structural influence of a solute will be important and that, without a way of calculating the first, the second cannot be estimated from the data.

(5) *Ideality of Urea Solutions in Water.* This argument is typical; if the reader will consult it in the original<sup>24</sup> it will be seen that the phrase "nearly ideal"

(32) R. P. Feynman, R. B. Leighton, and M. Sands, "The Feynman Lectures on Physics," Addison-Wesley Publishing Co., Inc., Reading, Mass., 1964, Chapter 41.

(33) J. Wyman, *Chem. Rev.*, 19, 213 (1936).

(34) H. S. Frank and W. Y. Wen, *Discussions Faraday Soc.*, 24, 133 (1957).

is applied to solutions of urea in water and then made to mean "truly ideal" and thus to rule out urea-urea association in solution, thus setting the stage for the thesis that a urea molecule can enter water clusters almost unnoticed. In fact, however, the amount of "nonideality" produced depends on the association constant and may be "large" or "small." Thus, while urea-water solutions are, indeed, more nearly ideal than hydrocarbon-water solutions, they are not nearly "nearly ideal" enough to rule out some urea-urea association. In fact, the thermodynamic properties of these solutions have been interpreted quantitatively in terms of exactly such interactions.<sup>35</sup> The latter interpretation is quite self-consistent, but, of course, so may be many another model. However, the existence of some associative urea-urea interaction, even if it could be proven, would not give any definitive information about the influence of isolated urea molecules or water structure.

Under the circumstances, it is not surprising that when a *prediction* is attempted (that the alkyl-substituted ureas, because of their decreased ability to hydrogen bond with water, will not be able to participate in cluster formation as easily and, in fact, will, themselves, use up the available interstices and thus will not be as effective as urea in breaking hydrophobic bonds<sup>24</sup>), it is precisely opposite to the experimental result.<sup>25,26</sup> Indeed, one would expect such predictions to be right in about 50% of the cases, since the predictions are of the form: "A should affect the system more than B," and the argument leading to the prediction, is, in fact, indeterminate.

It would seem, then, that aqueous solutions are too complex to be interpreted molecularly in the facile manner that has become rather common. It is note-

worthy, however, that we have raised no fundamental difficulties that were not envisioned by Frank and Evans, who stated the following in their comments about icebergs: "It is not implied that the structure is exactly icelike, nor is it necessarily the same in every case when the word iceberg is used."<sup>2</sup> With this to fall back on, however, it is clear that a qualitative explanation can readily be supplied for *any* experimental result simply by postulating a suitable kind of iceberg.<sup>36</sup> Unfortunately, since no experimental methods, except, possibly definitive X-ray or neutron diffraction, can give such specific structural information, the "explanation" cannot be tested by experiment, can lead to no unique prediction, and therefore can convey no more information than was obtained by doing the experiment in the first place. Water is structural, all right, but knowing that doesn't seem to help. The situation would appear to be bad enough without the curiously assured, yet essentially sterile, invocations of water structure that seem to be proliferating so boundlessly in the literature.

*Acknowledgment.* The authors wish to thank Professor Walter Kauzmann of Princeton University for a thoughtful and informative review of the manuscript. We also wish to thank Professor Joseph Kurz of Washington University for several stimulating discussions.

(35) J. A. Schellman, *Compt. Rend. Trav. Lab. Carlsberg Sér Chim.*, **29**, 223 (1955).

(36) "Another thing I must point out is that you cannot prove a vague theory wrong." (R. Feynman, "The Character of Physical Law," The Massachusetts Institute of Technology Press, Cambridge, Mass., 1965, p 158.)

## Viscosity of Water at Various Temperatures

by Lawrence Korson, Walter Drost-Hansen, and Frank J. Millero

*Contribution No. 980 from the Institute of Marine Sciences, University of Miami, Miami, Florida 33149  
(Received April 12, 1968)*

The relative viscosity of water has been measured with high precision in the range from 8 to 70° using a modified Cannon-Ubbelohde suspended-meniscus, dilution viscometer with a semiautomatic, optical viscometer reader. Measurements were made at 1° intervals with a relative precision of about 0.001%. The apparent energy of activation for viscous flow of water was calculated from these data. The result is given by an equation of the form  $\Delta E^\ddagger = A + BT + CT^2 + DT^3 + ET^4$ . The root-mean-square deviation from this expression was 3.7 cal/g-mol (*i.e.*, approximately 0.1% in  $\Delta E^\ddagger$ ). The results obtained did not reveal any abrupt changes, at discrete temperatures, in the observed energy of activation values. The suggestion is offered that some of the thermal anomalies ("kinks") which have been reported in bulk properties of water may have arisen from structural transitions in ordered water structures near interfaces.

### Introduction

Various workers<sup>1-12</sup> have reported the existence of thermal anomalies ("kinks") in the properties of bulk water and bulk aqueous systems. Other workers have specifically denied the existence of such anomalies.<sup>13-16</sup> Recent studies in our laboratory have been concerned with very careful measurements of various properties of water and aqueous solutions to determine if thermal anomalies do or do not exist. In this paper, we describe measurements that have been made on the viscosity of water from 8 to 70°, at 1° intervals. High-precision measurements were made by a semiautomatic method and the approach chosen was specifically designed to answer the question of whether or not evidence exists for thermal anomalies in the flow behavior of water.

A secondary objective of the present study was to provide accurate values for the viscosity of water without aspiring for the ultimate in accuracy, such as expected from a study in a standards laboratory. Numerous workers have carefully measured and compiled data for the viscosity of water at various temperatures.<sup>17-29</sup> The most reliable and thorough study comes from the National Bureau of Standards (from 0 to 60°);<sup>25-27</sup> the results of the present study compare favorably with those obtained at the National Bureau of Standards.

### Experimental Method

**Apparatus.** Cannon-Ubbelohde suspended-meniscus, dilution viscometers were used for all the measurements. The viscometers were modified to allow connections to be made to them by means of ground-glass joints, rather than rubber tubing (to avoid contamination). The viscometer was positioned in a constant-temperature bath (of 5-gal. capacity, see Figure 1). The temperature bath was completely insulated with expanded polystyrene to minimize heat transfer. A small window was cut in the side of the temperature-bath insulation to allow the viscometer efflux bulb to be

observed. The temperature of the bath was controlled to better than  $\pm 0.001^\circ$  using either a Hallikainen Thermotrol or a Bayley precision temperature controller. The bath was equipped with an auxiliary heater

- (1) S. Seely, *Phys. Rev.*, **52**, 662 (1937).
- (2) L. W. Tilton and J. K. Taylor, *J. Res. Natl. Bur. Stand.*, **18**, 205 (1937).
- (3) M. Magat, *J. Phys. (Paris)*, (7), **6**, 179 (1935).
- (4) V. P. Frontas'ev, *Dokl. Akad. Nauk SSSR*, **111**, 1014 (1956).
- (5) V. P. Frontas'ev and L. S. Shraiber, *J. Struct. Chem. (USSR)*, **6**, 493 (1965).
- (6) C. Salama and D. A. I. Goring, *J. Phys. Chem.*, **70**, 3838 (1966).
- (7) M. J. Blandamer, M. F. Fox, and M. C. R. Symons, *Nature*, **214**, 163 (1967).
- (8) W. Drost-Hansen and M. Lavergne, *Naturwissenschaften*, **43**, 511 (1956).
- (9) W. Drost-Hansen, *Ann. N. Y. Acad. Sci.*, **125**, 471 (1965).
- (10) W. Drost-Hansen, "Proceedings of the First International Symposium on Water Desalination," Washington, D.C., 1965, Vol. I, U.S. Government Printing Office, Washington, D.C., 1967, p 382.
- (11) W. Drost-Hansen, Advances in Chemistry Series, No. 67, American Chemical Society, Washington, D. C., 1967, p 70.
- (12) W. Drost-Hansen, *Ind. Eng. Chem.*, **57**, 18 (1965).
- (13) E. W. Rusche and W. B. Good, *J. Chem. Phys.*, **45**, 4667 (1966).
- (14) M. Falk and G. S. Kell, *Science*, **154**, 1013 (1966).
- (15) S. D. Hamann, *Nature*, **215**, 1263 (1967).
- (16) T. F. Young, presented at the Southwest Regional Meeting of the American Chemical Society, Albuquerque, N. M., Nov 1966.
- (17) "International Critical Tables," Vol. V, McGraw-Hill Book Co., Inc., New York, N. Y., 1929, p 10.
- (18) Landolt-Börnstein, "Zahlenwerte und Funktionen," 6th ed., Vol. IV, Springer-Verlag, Berlin, 1955, Part 1, p 613.
- (19) R. A. Robinson and R. H. Stokes, "Electrolyte Solutions," Butterworth and Co. Ltd., London, 1959, p 457.
- (20) J. R. Moszyński, *J. Heat Transfer*, **83**, 111 (1961).
- (21) E. A. Bruges, B. Latto, and A. K. Ray, *Int. J. Heat Mass Transfer*, **9**, 465 (1966).
- (22) E. C. Bingham, National Bureau of Standards Bulletin 14, U. S. Government Printing Office, Washington, D. C., 1918, p 59.
- (23) W. Weber, *Z. Angew. Phys.*, **7**, 96 (1955).
- (24) J. Kestin and J. H. Whitelaw, *J. Eng. Power*, **88**, 82 (1966).
- (25) J. R. Coe and T. B. Godfrey, *J. Appl. Phys.*, **15**, 625 (1944).
- (26) R. C. Hardy and R. L. Cottingham, *J. Res. Natl. Bur. Stand.*, **42**, 573 (1949).

and a cooling coil; thus measurements could be made over an extended temperature range and the bath temperature could be changed rapidly. The temperature of the bath was measured to  $\pm 0.0001^\circ$  with a Hewlett-Packard quartz-crystal thermometer. As stated by the manufacturer, the accuracy is determined by "linearity" and "short-term stability" of the instrument. The absolute linearity, referred to a straight line through 0 and  $100^\circ$ , is better than  $\pm 0.02^\circ$  in this temperature range. The instrument has a short-term stability of better than  $\pm 0.0002^\circ$  (*i.e.*, "reading-to-reading variation at constant probe temperature") and a long-term (30 days) zero drift of less than  $\pm 0.01^\circ$ . The thermometer probes were calibrated periodically in a mixture of shaved ice (frozen from distilled water) and water. It was presumed that the uncertainty of the absolute temperature was  $\pm 0.02^\circ$ . The precision, however, approached  $0.0002\text{--}0.0003^\circ$  in consecutive measurements. The thermometer output was applied directly to a digital-to-analog converter (Hewlett-Packard) and was monitored on a strip-chart recorder. The temperature fluctuations in the thermostat during a run were less than  $\pm 0.0003^\circ$  near ambient and were  $\pm 0.001^\circ$  at the highest and lowest temperatures. We expected the fluctuations within the viscometer to be somewhat smaller.

The flow times were measured with a Rehovoth automatic viscometer reader. The reader consists essentially of a telescope with two photoelectric cells in the focal plane of the objective. The two photoelectric cells were placed so as to coincide approximately with the images of the upper and lower fiducial marks on the viscometer efflux bulb. Two light sources were placed in the bath, behind the viscometer. A Transistor Specialties, Inc. universal counter (Model 361) was connected to the external printer output of the viscometer reader. The counter provides a six-digit readout, allowing times to be recorded to within 1 msec.

The semiautomatic mode of operation of the instrument was simplified by the use of a specially designed clamping-and-positioning device shown in Figure 1. The viscometer was firmly clamped to a 0.5-in. stainless steel rod which was machined to sharp points at both ends. The bottom of the rod was set into a socket which was fixed with epoxy cement to the bottom of the constant-temperature bath. The top of the rod was secured with a clamp which made it easy to position the viscometer vertically. This clamping arrangement permitted the removal of the viscometer from the bath (for cleaning purposes) and its return to the original position. Because of the mode of operation of the automatic viscometer reader, it was imperative that the viscometer be returned to the original position at which the telescope of the viscometer reader was focused. The rigid positioning mechanism further served to eliminate vibrations due to vigorous stirring in the bath.

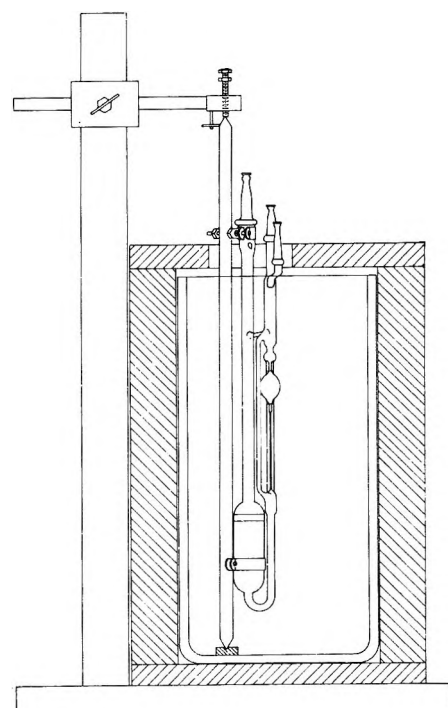


Figure 1. A schematic diagram of the clamping and positioning of the viscometer in an insulated constant-temperature bath.

Exploratory experiments indicated a difference of 0.7% in flow times when the viscometer was at a  $5^\circ$  deflection from the vertical. Since it is important that the effective pressure head be highly reproducible, a leveling device was used to provide vertical alignment of the viscometer at the beginning of each experiment. The leveling device consisted of a brass shaft with a leveling bubble mounted on one end, in a plane perpendicular to the shaft. The shaft was machined to fit into the large fill tube of the viscometer. With this device, it proved possible to ensure great precision in alignment.

*Procedure of Operation.* The water used in the experiments was prepared by the following two methods. Originally, the water was obtained from a Barnstead still and was redistilled in a single-stage, all-glass still. Water for the second group of runs was obtained from a three-stage glass still fed directly by a Barnstead still. The first stage contained a phosphoric acid-permanganate solution, the second stage contained an alkaline-permanganate solution, and the third stage contained only the distillate. As the steam left each boiling flask, it was passed through a superheater, consisting of a baffled glass cylinder, packed firmly with glass wool (first stage) or quartz wool (second and third stages). Each superheater was heated with electric heating tapes

- (27) J. F. Swindells, J. R. Coe, and T. B. Godfrey, *J. Res. Natl. Bur. Stand.*, **48**, 1, (1952).
- (28) P. M. Kampmeyer, *J. Appl. Phys.*, **23**, 99 (1952).
- (29) A. Korosi and B. M. Fabuss, *Anal. Chem.*, **40**, 157 (1968).

and was maintained between 140 and 200°. The final condenser was made of fused quartz. The resistance of the water was measured with a conductivity cell connected in parallel with the still output. The resistivity of the water was about  $2.5 \times 10^6$  ohm cm. No differences in viscosity were observed between runs made with water produced by the two different methods. Subsequent to these measurements, improvements have been made in the operation of the still. Presently, argon is passed through the system during distillation. As a result of this modification,  $(4-6) \times 10^6$ -ohm cm water is now obtained routinely. The organic content (measured with a Beckman GC-5 gas chromatograph) is found to be less than 0.2 ppb.

Before use, the viscometers were thoroughly cleaned with cleaning solution (concentrated  $H_2SO_4$  with  $KMnO_4$ ) and were rinsed with distilled water. Any  $MnO_2$  residue was subsequently removed with  $H_2O_2$  in dilute HCl. The viscometer being used was charged with 10–30 ml of freshly distilled, filtered water and was positioned (as well as leveled) in the constant-temperature bath. The water was filtered immediately before use to remove lint or other particulate matter which might accidentally be introduced in the handling of the water. It was found that filtering was necessary in order to obtain the highest reproducibility in flow times. After thermal equilibrium was reached, the efflux bulb was filled by pressurizing the filling arm of the viscometer. This was accomplished by blowing air through a tube partially filled with Ascarite (to minimize the possible effects of  $CO_2$  being added to the water). The tube was packed with quartz wool confined by a millipore filter and was connected to the inlet tube of the viscometer. After raising the level to the appropriate height, the liquid was permitted to fall (the pressure being the same on both sides of the liquid, namely, atmospheric). The "appropriate height" selected was the center of the upper viscometer bulb. This choice allowed the liquid to reach terminal velocity in the capillary before timing was started. Also, by raising the liquid to the same height for each run, it was possible to minimize uncertainty in drainage. When making a measurement, the meniscus passed the points at which the photoelectric cells were focused, and each cell, in turn, delivered start and stop pulses to the timer.

Flow times for pure water at constant temperature were reproducible to within  $\pm 0.002$ – $0.003$  sec, out of approximately 380 sec at the lowest temperature (8°) and 115 sec at the highest temperature (70°). At room temperature, this corresponds to a relative precision of 0.001%.

## Results and Calculations

Flow times for water were measured over a temperature range from 8 to 70° at 1° intervals. Table I shows a sample log of the data.<sup>30</sup> The temperature values presented in Table I for the individual runs are

the averages of values read every 10 sec during the given run. While any of these temperatures do not likely represent the absolute temperature, it is felt that the differences between consecutive, average temperatures (approximately 1° apart) are highly precise, probably within a few ten-thousandths of 1°.

**Table I:** Sample Viscosity Data Log

Run no.	Time of day	Temp., °C	Flow time, sec	Av. time, sec	Av. temp., °C
2a	13-43	40.0025	180.141		
2b	13-53	40.0024	180.139		
2c	13-58	40.0021	180.141		
2d	14-04	40.0021	180.142	180.141	40.0023
3a	14-24	41.0020	176.922		
3b	14-29	41.0016	176.925		
3c	14-53	41.0016	176.922	176.923	41.0017
4a	15-21	42.0024	173.799		
4b	15-26	42.0026	173.802		
4c	15-31	42.0027	173.802	173.801	42.0026

The flow times, at various temperatures, were used to calculate the apparent (Arrhenius) energy of activation,  $\Delta E^\ddagger$ , for the viscous flow of water defined by

$$\Delta E^\ddagger = R \frac{d \ln \tau}{d(1/T)} \simeq R \frac{d \ln \tau}{\Delta(1/T)} \quad (1)$$

where  $\tau$  is the flow time in seconds,  $R$  is the gas constant, and  $T$  is the absolute temperature. It is assumed that since the measurements were made at 1° intervals that  $\Delta \ln \tau / \Delta(1/T) \simeq d \ln \tau / d(1/T)$ .

In order to facilitate the search for the existence or nonexistence of thermal anomalies, it was reasonable to use essentially a derivative method which promised the greatest precision in evaluating the data. It is for this reason that the data have been presented in terms of the apparent energies of activation.

The calculated, average values of  $\Delta E^\ddagger$  as a function of temperature are shown in Figure 2. Each point represents the average  $\Delta E^\ddagger$  of two or more (as many as five determinations) independent determinations at each temperature. Although the absolute flow times on occasion differed by as much as 0.04% from day to day, the values for the average apparent energy of activation,  $\Delta E^\ddagger$ , did not differ significantly. The average of the maximum spread of the individual values for the energy of activation,  $\Delta E^\ddagger$ , at any given temperature, obtained over a period of 2 years, is approximately 10 cal/mol, corresponding to 0.2% in  $\Delta E^\ddagger$  at low temperatures and 0.3% at high temperatures.

(30) Material supplementary to this article has been deposited as Document No. NAPS-00128 with the ASIS National Auxiliary Publication Service, c/o CCM Information Sciences, Inc., 22 West 34th St., New York, N. Y. 10001. A copy may be secured by citing the document number and by remitting \$1.00 for microfiche or \$3.00 for photocopies. Advance payment is required. Make checks or money orders payable to ASIS-NAPS.

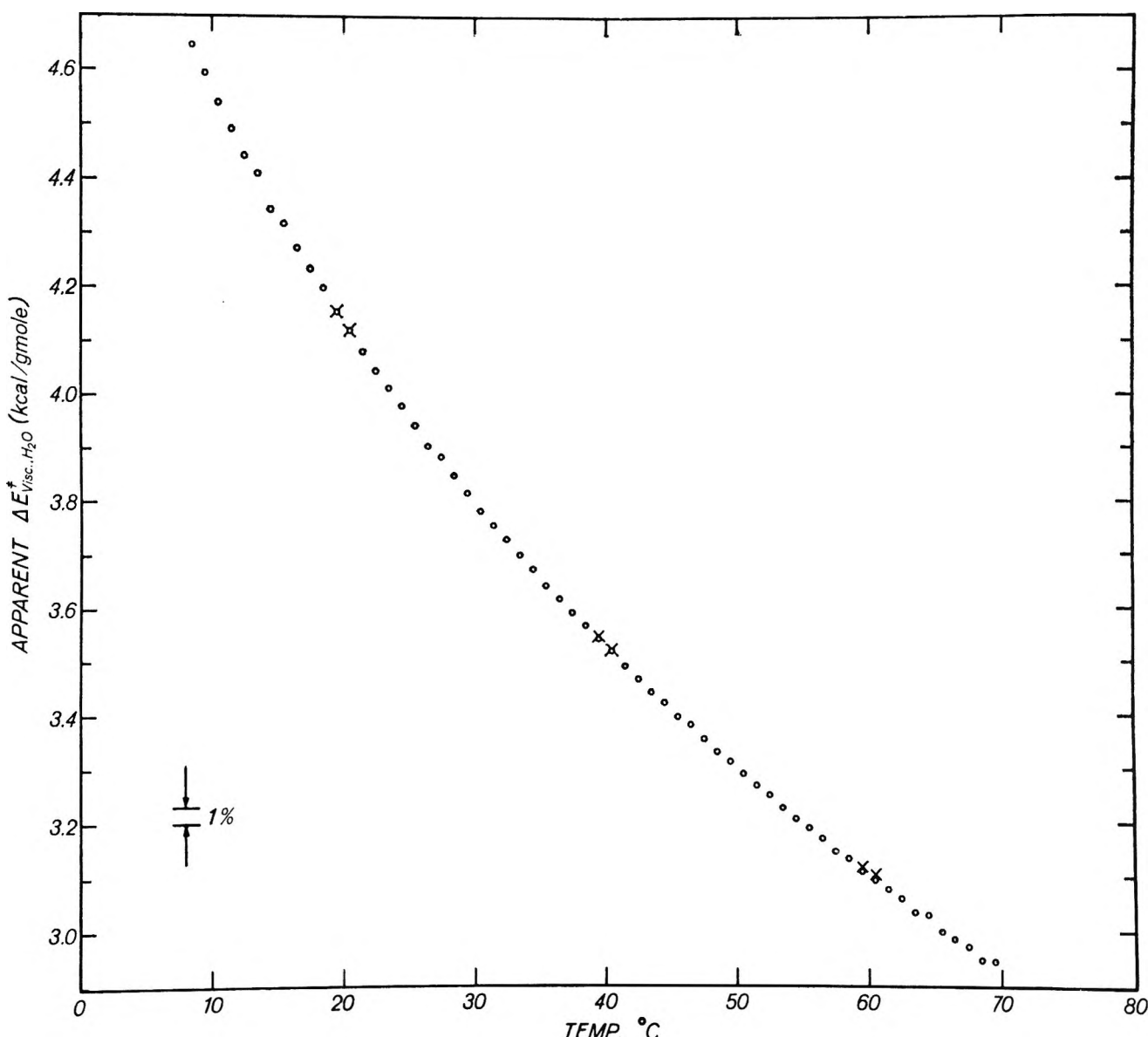


Figure 2. The apparent (Arrhenius) energy of activation,  $\Delta E^\ddagger$ , for the viscous flow of water as a function of the temperature: ○, Cannon-Ubbelohde viscometer No. D619; ×, Cannon-Ubbelohde viscometer No. D618.  $\Delta E^\ddagger = A + BT + CT^2 + DT^3 + ET^4$  ( $\sigma = \pm 0.1\%$ ).

The average  $\Delta E^\ddagger$  values at various temperatures were fit to an equation of the form

$$\Delta E^\ddagger = A + BT + CT^2 + DT^3 + ET^4 \quad (2)$$

where  $A = 4.454967 \times 10^6$ ,  $B = -5.1384039 \times 10^3$ ,  $C = 2.2632508 \times 10^1$ ,  $D = -4.4669185 \times 10^{-2}$ , and  $E = 3.321779 \times 10^{-5}$ . The root-mean-square deviation between the experimental points and those calculated from this equation is 3.7 cal/mol or 0.1% at 30°. This deviation may be caused by an error in the temperature measurement of  $\pm 0.001^\circ$  or an error in flow time of  $\pm 0.003$  sec.

Most of the measurements were made with a single viscometer (Cannon-Ubbelohde dilution type, No. D619, size 50). As a check on these results, a number of measurements were made, at discrete temperatures,

using a second viscometer of the same type (No. D618, size 50). The values for the energies of activation, calculated from these measurements (also shown in Figure 2), agree within 0.15% with the least-squares best fit curve produced by the original data.

Having secured a reliable equation for the apparent energy of activation,  $\Delta E^\ddagger$ , for water as a function of temperature, one can, in principle, integrate this equation, solve for the constant of integration with an "accepted" flow time at one temperature, and calculate the flow times at any other temperature. From eq 1 and 2 one obtains upon integration

$$R \ln \tau = Q + \frac{A}{T} + B \ln T + CT + \frac{D}{2}T^2 + \frac{E}{3}T^3 \quad (3)$$

The constant  $Q$  was evaluated by using the flow times of three independent determinations at  $20^\circ$  ( $\tau = 274.363 \pm 0.002$  sec and  $T = 293.1549 \pm 0.0003$  K). This calculation was made carrying 18 digits. The program was written in FORTRAN and was run on an IBM 1401 computer. The constant of integration  $Q$  was found to be equal to  $-25703.8837$  cal/mol. Using this constant, flow times were then calculated at  $5^\circ$  intervals between  $0$  and  $100^\circ$  from eq 3.

The absolute viscosity of water,  $\eta$ , can be determined from the flow times,  $\tau$  (obtained from eq 3), from the relationship

$$\nu = \frac{\eta}{d^0} = \tau K \left( 1 - \frac{d^a}{d^0} \right) - \frac{L}{\tau^n} \quad (4)$$

where  $\nu$  is the kinematic viscosity,  $d^0$  is the density of water,  $d^a$  is the density of air,<sup>31</sup>  $K$  is the instrument constant,  $L$  is the kinetic energy correction constant, and  $n$  is a constant that depends upon the shape of the capillary of the viscometer.<sup>32,33</sup>  $K$ ,  $L$ , and  $n$  were determined (assuming they are independent of temperature) by using the values for the viscosity,  $\eta$ , of water at six temperatures. The values for the viscosity of water at  $20$ ,  $25$ ,  $30$ ,  $40$ ,  $50$ , and  $60^\circ$  from the National Bureau of Standard<sup>25-27</sup> were used together with the flow times (calculated from eq 3) to determine optimal values for  $K$ ,  $L$ , and  $n$  using a least-squares best fit. The optimal values were found to be  $K = 3.6678 \times 10^{-3}$ ,  $L = 82.1$ , and  $n = 1.95$ . Using these constants and the flow times from eq 3, the viscosities of water at various temperatures have been calculated and are given in Table II. Also included in this table are selected literature values.

Although it has been customary to assume that  $n = 1$  with capillary viscometers, it was proposed by Cannon, et al.,<sup>34</sup> that  $n = 2$ . The value of  $K$  and  $L$  have also been calculated by using only two literature values for the viscosity of  $H_2O^{24-26}$  at  $20$  and  $60^\circ$  and assuming that  $n = 2$ . This choice results in values of  $K = 3.6675 \times 10^{-3}$  and  $L = 104.1$ . The viscosity values obtained by this method are essentially identical with those values secured in the first treatment. As an example, in the latter case, one obtains  $\eta_{45} = 0.59628$  cP, while the other treatment yields  $\eta_{45} = 0.59631$  cP.

The values for the viscosity of water shown in Table II agree very well with the literature values between  $10$  and  $70^\circ$ ; however, at higher and lower temperatures the agreement is less satisfactory. Thus the equation for determining  $\Delta E^\pm$  does not represent the viscous flow of water over the entire temperature range ( $0$ – $100^\circ$ ) but only over the range in which measurements were made. The following equation can be used to obtain the viscosity of  $H_2O$  at temperatures between those listed in Table II

$$\log \frac{\eta_t}{\eta_{20}} = \frac{A(20 - t) - B(t - 20)^2}{t + C} \quad (5)$$

where  $\eta_t$  represents the viscosity of water at any temperature ( $t$ ) between  $10$  and  $70^\circ$ ,  $\eta_{20}$  is the viscosity of water at  $20^\circ$ ,  $A = 1.1709$ ,  $B = 0.001827$ , and  $C = 89.93$ .

### Discussion

The objectives of the present study were to obtain precise values for the viscosity of water as a function of temperature and, in particular, to determine if such data would or would not support the contention that thermal anomalies exist in the viscous flow of water at discrete temperatures. It is believed that the values for the viscosity of water obtained in this study compare favorably with those obtained by previous workers<sup>25-27</sup> and may, in fact, provide more precise data than have been available before (at least as far as the temperature dependence is concerned) in the interval from  $10$  to  $70^\circ$ .

Table II: The Viscosity of Water at Various Temperatures

Temp, °C	Present study	$\eta_{H_2O}$ , cP
0	1.7916	1.7865 <sup>b</sup>
5	1.5192	1.5184, <sup>c</sup> 1.5170 <sup>b</sup>
10	1.3069	1.3061 <sup>b</sup>
15	1.1382	1.1381 <sup>b</sup>
20	1.0020	(1.0020) <sup>d</sup>
25	0.8903	(0.8903) <sup>b,e-g</sup>
30	0.7975	0.7975, <sup>b</sup> (0.7976) <sup>e</sup>
35	0.7195	
40	0.6532	(0.6531), <sup>b,c,e</sup> 0.6526, <sup>f</sup> 0.6527 <sup>g</sup>
45	0.5963	
50	0.5471	(0.5471), <sup>b</sup> 0.5467 <sup>f</sup>
55	0.5042	
60	0.4666	0.4665, <sup>c,g</sup> 0.4668, <sup>b</sup> (0.4666) <sup>f</sup>
65	0.4334	
70	0.4039	0.4045 <sup>g</sup>
75	0.3775	0.3784 <sup>g</sup>
80	0.3538	0.3548, <sup>c</sup> 0.3546 <sup>g</sup>
85	0.3323	
90	0.3128	0.3148, <sup>c</sup> 0.3143 <sup>g</sup>
95	0.2949	0.2976 <sup>c</sup>
100	0.2783	0.2822, <sup>c</sup> 0.2820 <sup>g</sup>

<sup>a</sup> The numbers in parentheses are those used in the present treatment to evaluate the constants  $K$ ,  $L$ , and  $n$  in eq 4. <sup>b</sup> C. S. Crague, unpublished work, quoted in ref 25. <sup>c</sup> From ref 26.

<sup>d</sup> Reference value (1.0020 cP) used to calculate the viscosities at various temperatures from literature relative viscosities (relative to water at  $20^\circ$ ). <sup>e</sup> From ref 25. <sup>f</sup> J. F. Swindells, unpublished work, quoted in ref 25. <sup>g</sup> From ref 29.

(31) The density of air was calculated ("Handbook of Chemistry and Physics," 35th ed, Chemical Rubber Publishing Co., Cleveland, Ohio, 1953) by assuming the air was 100% saturated with water vapor.

(32) W. A. Caw and R. G. Wylie, *Brit. J. Appl. Phys.*, 12, 94 (1961).

(33) J. R. Van Wazer, R. E. Colwell, K. Y. Kim, and J. W. Lyons, "Viscosity and Flow Measurements, a Laboratory Handbook of Rheology," Interscience Division, John Wiley & Sons, Inc., New York, N. Y., 1963.

(34) M. R. Cannon, R. E. Manning, and J. D. Bell, *Anal. Chem.*, 32, 355 (1960).

One of the present authors (Drost-Hansen)<sup>8-12</sup> has reviewed much of the available data suggesting the existence of thermal anomalies ("kinks") in the properties of water and aqueous solutions. Based on the available evidence, it was proposed that thermal anomalies exist in the properties of water and aqueous solutions at a number of discrete temperatures. Several other investigators<sup>3,35-37</sup> have specifically claimed the existence of kinks in the energy of activation for viscous flow of water. The results of the present study suggest no evidence whatever for the reality of such anomalies.

A possible resolution to the conflicting evidence regarding the existence of anomalies in the bulk properties of water has been suggested in a recent note by Drost-Hansen.<sup>38,38a</sup> A review of all the available evidence for thermal anomalies in the properties of water and aqueous solutions suggests that the anomalies may, indeed, be real but possibly owe their existence to specific, interfacial effects. Elsewhere, Drost-Hansen<sup>39</sup> has presented a "three-layer model" of water near interfaces. It is suggested that the water near interfaces (for instance, the glass-water interface) may be structured and the interfacial structures possess definite, thermal stability limits. Thus the thermal anomalies sometimes seen in what has been presumed to be the viscosity of bulk water may be manifestations of spurious effects due to (more or less) abrupt changes in the properties of water near interfaces. However, the question of the existence of thermal anomalies in other bulk properties of water and aqueous solutions should not be dismissed lightly on this basis.

In summary, it is concluded that under conditions where surface interferences are minimized there is no evidence for the existence of thermal anomalies in the

viscous flow of water between 8 and 70°. Earlier data<sup>8-11</sup> have frequently suggested the existence of such anomalies and it is proposed that the cause of these anomalies may be traced to structural transitions in ordered water structures near various interfaces (such as the glass-water as well as the air-water interface). Measurements are in progress in this laboratory to examine the hypothesis that the viscous flow of water near interfaces shows anomalies.

*Acknowledgments.* The authors wish to thank Miss Irene Cooper and Mr. Douglas Oppenheimer for their assistance with the viscosity measurements. The authors also wish to acknowledge the support of the Office of Saline Water for this study.

(35) M. M. Qurashi and A. K. M. Ahsanullah, *Brit. J. Appl. Phys.*, 12, 65 (1961).

(36) E. Forslind, Handlingar, Svenska Forskningsinstitutet För Cement Och Betong Vid Kungl. Tekniska Högskolan I Stockholm, No. 16, Stockholm, 1952.

(37) D. F. Othmer and J. W. Conwell, *Ind. Eng. Chem.*, 37, 1112 (1945).

(38) W. Drost-Hansen, *Chem. Phys. Lett.* in press.

(38a) NOTE ADDED IN PROOF. Since the writing of this paper, additional flow time measurements have been made at 1° intervals to obtain values in the temperature range of 0-25°, thus allowing us to extend the range of apparent energies of activation to include values from 0 to 8°. The data from the recent work have been combined with the data quoted in this paper, and a new set of values has been obtained for the coefficients in eq 2 for the apparent energy of activation. The new values are:  $A = 5.912439 \times 10^6$ ,  $B = -7.0249972 \times 10^3$ ,  $C = 3.1775238 \times 10^1$ ,  $D = -6.4329251 \times 10^{-2}$ , and  $E = 4.9045775 \times 10^{-5}$ . The root-mean-square deviation ( $\Delta E^\pm$  values from 0 to 70°) is 3.3 cal/mol or, again, approximately 0.1% at 30°. The new data do not suggest any anomalous behavior for the viscous flow of water in the lower temperature range and, in particular, no anomaly in the region of maximum density.

(39) Preliminary report: W. Drost-Hansen, *Ind. Eng. Chem.*, 60, 8 (1968).

# Kinetics of Rotation around the Aryl-Nitrogen Bond in Some *ortho*-Substituted Acetanilides<sup>1</sup>

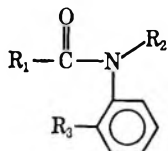
by T. H. Siddall, III, and W. E. Stewart

Savannah River Laboratory, E. I. du Pont de Nemours & Co., Aiken, South Carolina 29801 (Received May 2, 1968)

Kinetic quantities are reported for rotation around the aryl-nitrogen bond for eight *ortho*-substituted anilides of the type  $R_1C(O)N(R_2)(o-R_3)C_6H_5$ . The data are obtained by combining measured reequilibration rates of separated diastereoisomers with pmr signal shape analyses; kinetic quantities cover a range of rates of up to  $10^6$ . Possible activated states are discussed.

## Introduction

There have now been a number of studies of slow rotation around the aryl-nitrogen bond in anilides of the general type<sup>2-4</sup>



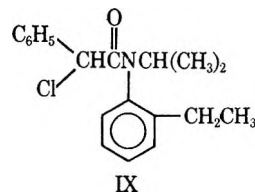
and a limited quantitative study with diortho-substituted anilides.<sup>5</sup> Only ref 3 and 4 have reported quantitative studies with anilides with single *ortho* substitution. Even in these two cases the kinetic data for the rotation were obtained solely by pmr signal shape analysis, and in one of these cases the analysis was approximate. Signal shape analysis can yield reliable results in the most sensitive region of intermediate exchange. However, over any extension, to the range of high and low exchange rates, signal shape analysis is subject to a variety of systematic errors.<sup>6</sup> In other words, the free energy of activation,  $\Delta F^*$ , in the central part of the exchange region may be reliably determined, but the energy of activation,  $E_a$ , and the frequency factor,  $A_0$ , may be much less certain.

This paper reports results that reduce the likely errors in  $E_a$  and  $A_0$ . This work is based on compounds of the general type above, except that  $R_1$  contains an asymmetric carbon atom. We were able to separate nine anilides of this type into substantially pure diastereoisomers (or epimers) as crystalline solids. Reequilibration of the pure isomers was followed by the growth and decay of the appropriate pmr signals.<sup>5,7</sup> In this way rates were determined at lower temperatures. For six of these compounds, rates could be obtained by signal shape analysis<sup>8</sup> at higher temperature. (Only the central part of the exchange region was used.) By combining these two techniques, reequilibration and signal shape analysis, rate measurements were extended over a range of  $10^6$  and a temperature range up

to  $150^\circ$ .<sup>9</sup> The range of these experiments permitted  $E_a$  and  $\log A_0$  to be determined to within 5%.

## Experimental Section

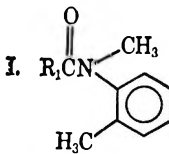
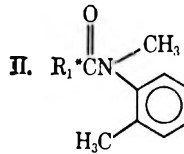
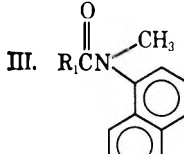
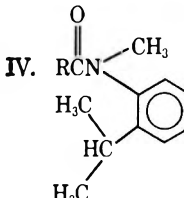
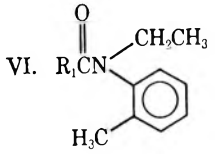
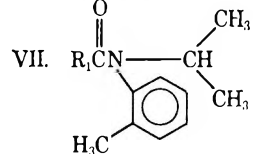
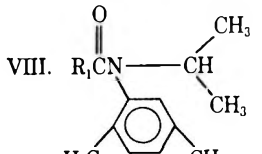
The anilides (listed in Table I and Table II) were synthesized as previously described<sup>2</sup> and were given initial purification by distillation under high vacuum. In most cases, a pure crystalline isomer was easily obtained from such solvents as hexane, methylcyclohexane, or diethyl ether, or mixtures of one of these with methylene chloride or acetone. However, in no case did we isolate both epimers of the same compound. The isomer that was isolated is identified by its pmr signals (see Table III). Compound V was obtained as a pure isomer only after long standing as a two-phase system with hexane at about  $-5^\circ$ . Compounds VII and IX were obtained as one epimer somewhat con-



taminated by the other epimer and in poor yield only after standing for weeks in hexane solution at about

- (1) The information contained in this article was developed during the course of work under Contract AT(07-2)-1 with the U. S. Atomic Energy Commission.
- (2) (a) T. H. Siddall, III, and C. A. Prohaska, *J. Amer. Chem. Soc.*, **88**, 1172 (1966); (b) T. H. Siddall, III, *J. Org. Chem.*, **31**, 3719 (1966).
- (3) B. J. Price, J. A. Eggleston, and I. O. Sutherland, *J. Chem. Soc.*, 922B (1967).
- (4) Y. Shvo, E. C. Taylor, K. Mislow, and M. Raban, *J. Amer. Chem. Soc.*, **89**, 4910 (1967).
- (5) T. H. Siddall, III, *Tetrahedron Lett.*, 4515 (1965).
- (6) A. Allerhand, H. S. Gutowsky, J. Jonas, and R. A. Meinzer, *J. Amer. Chem. Soc.*, **88**, 3185 (1966).
- (7) T. H. Siddall, III, *Inorg. Nucl. Chem. Lett.*, **1**, 155 (1965).
- (8) T. Nakagawa, *Bull. Chem. Soc. Jap.*, **39**, 1006 (1966).
- (9) Such a combination of techniques was first suggested by A. Mannschreck (see A. Mannschreck, A. Mattheus, and G. Rissmann, *J. Mol. Spectrosc.*, **23**, 15 (1967)).

**Table I:** Kinetic Quantities

Compd <sup>a</sup>	$10^{-6}k_{298},^b$ sec <sup>-1</sup>	$\Delta F^{\circ}_{298},^c$ kcal/mol	$E_a,$ kcal/mol	Log $A_0$
I. 	8,000	20.3	19.2	11.9
II. 	13,000	20.1	19.8	12.5
III. 	850	21.7	22.6	13.5
IV. 	300	22.3	22.1	12.7
V. 	5,600	20.5	18.9	11.5
VI. 	1,400	21.3	21.1	12.6
VII. 	1.7	25.4	23.8	11.6
VIII. 	1.8	25.3	23.5	11.4

<sup>a</sup> A 100-mg sample of the compound plus 500  $\mu$ l of  $\text{CHCl}_2\text{CHCl}_2$ .  $R_1 = \text{C}_6\text{H}_5(\text{Cl})\text{HC}-$ , except  $R_1^* = \text{C}_6\text{H}_5(\text{OC(O)CH}_3)\text{HC}-$ . <sup>b</sup> See footnote *a*, Table II.

$-5^\circ$ . Perhaps the rate-limiting step in the isolation of epimers of VII and IX involves asymmetric transformation and is the process of epimerization itself, which

would be very slow ( $k < 10^{-7}$  sec<sup>-1</sup>) below  $0^\circ$  for these compounds. However, VIII, with similar epimerization rate, was obtained as a pure epimer in the same

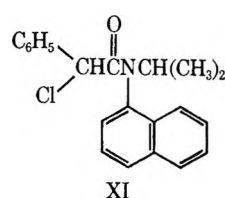
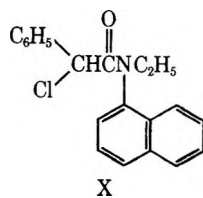
**Table II:** Equilibrium Results<sup>a</sup>

Compd	Equil constant ( <i>K</i> )
I	1.0 (-15°), 0.94 (0°), 0.95 (3°), 1.0 (80°)
II	0.50 (1°), 0.66 (20°), 0.69 (60°), 0.60 (90°)
III	0.81 (7°), 0.81 (24°), 0.77 (30°), 0.90 (90°)
IV	1.8 (22°), 1.6 (60°), 1.6 (80°), 1.7 (105°)
V	1.0 (-5°), 1.0 (5°), 1.1 (90°)
VI	1.0 (-5°), 1.0 (5°), 1.0 (25°), 1.1 (80°), 1.1 (110°)
VII	1.4 (22°), 1.3 (60°), 1.3 (80°), 1.3 (144°)
VIII	1.6 (22°), 1.6 (60°), 1.6 (80°)
IX <sup>b</sup>	2.0 (25°), 2.0 (80°), 1.7 (144°)

<sup>a</sup> For *o*-methyl compounds, *K* is always the ratio of the area of the low-field methyl signal to the area of the high-field methyl signal. For III and IV, *K* is calculated from the ratio of the areas of high-field to low-field signal for the proton  $\alpha$  to the carbonyl group. For IX, *K* is the ratio of the low field to the high field for the  $\alpha$ -proton signal. For close examination of the spectra, we believe this is a consistent comparison of epimers. However, there is no proof of this. The rate data are calculated to be consistent with these assumptions. <sup>b</sup> Values for IX are approximate; signal overlap precludes accurate values.

way with comparative ease, though in unmeasured yield.

Even after months of standing



have given no crystalline products.

In times past,<sup>10</sup> the process of "second-order" asymmetric transformation by crystallization has been of considerable interest. Some of the compounds in Table I may be particularly well suited to a study of this process by nmr spectroscopy. However, we have not explored this possibility.

All experiments were performed in  $\text{CHCl}_2\text{CHCl}_2$  that had been passed through a column of Linde Molecular Sieve shortly before use. This solvent was chosen because of its properties as a solvent, its stability, boiling point, and lack of signals at high field. Samples for signal shape analysis or samples which were kept for any length of time were sealed under vacuum.

All measurements were made with a Varian A-60 spectrometer equipped with the V-6057 variable-temperature accessory. The methyl alcohol and ethylene glycol "thermometers" provided with this accessory were calibrated against a thermocouple. The manufacturer claims a control of  $\pm 2^\circ$ ; our experience supports this. This uncertainty of up to  $2^\circ$  is the controlling error in our experimental work. Almost always, a scatter of  $2^\circ$  is sufficient to account for the scatter of rates on Arrhenius plots of our data. It is this scatter that sets a typical variance of about 5% in determina-

**Table III:** Detailed Rate Data

Compd and comment	Temp; °C	<i>k</i> , sec <sup>-1</sup>
I. The methyl signal at lower field grows in.	-5 <sup>a</sup> +5 <sup>a</sup> 90 <sup>b</sup> 95 <sup>b</sup> 100 <sup>c</sup> 125 <sup>c</sup> 131 <sup>c</sup> 135 <sup>c</sup>	$3.4 \times 10^{-4}$ $7 \times 10^{-4}$ 2.9 4.1 5 17 34 47
II. The methyl signal at higher field grows in.	-14 <sup>a</sup> +1 <sup>a</sup> 131 <sup>c</sup> 135 <sup>c</sup>	$7 \times 10^{-5}$ $5 \times 10^{-4}$ 50 100
III. The $\alpha$ -proton signal at higher field grows in (proton $\alpha$ to carbonyl).	7 <sup>a</sup> 14 <sup>a,d</sup> 25 <sup>a</sup> 104 <sup>b</sup> 106 <sup>b</sup> 109 <sup>b</sup> 111 <sup>a,d</sup> 120 <sup>a,d</sup>	$9 \times 10^{-5}$ $1.9 \times 10^{-4}$ $6 \times 10^{-4}$ 2.9 3.2 5 3.7 6
IV. The $\alpha$ -proton signal at lower field grows in.	23 <sup>a</sup> 33 <sup>a</sup> 42 <sup>a</sup> 135 <sup>b</sup> 145 <sup>b</sup>	$3.2 \times 10^{-4}$ $5 \times 10^{-4}$ $1.9 \times 10^{-3}$ 5 20
V. The methyl signal at lower field grows in.	-5 <sup>a</sup> +5 <sup>a</sup> 90 <sup>b</sup> 95 <sup>b</sup> 101 <sup>b</sup> 132 <sup>c</sup> 135 <sup>c</sup> 137 <sup>c</sup> 141 <sup>c</sup> 150 <sup>c</sup>	$1.5 \times 10^{-4}$ $4.4 \times 10^{-4}$ 2.7 3.1 4.5 20 25 29 35 60
VI. The methyl signal at lower field grows in.	0 <sup>a</sup> 22 <sup>a,e</sup> 22 <sup>a,f</sup> 22 <sup>a,g</sup> 22 <sup>a,h</sup> 100 <sup>b</sup> 110 <sup>b</sup> 114 <sup>b</sup> 119 <sup>b</sup> 131 <sup>c</sup> 140 <sup>c</sup> 144 <sup>c</sup>	$6 \times 10^{-5}$ $1.1 \times 10^{-3}$ $8 \times 10^{-4}$ $8 \times 10^{-4}$ $9 \times 10^{-4}$ 2.5 3.5 4.4 5.5 25 26 35
VII. The methyl signal at higher field grows in.	22 <sup>a</sup> 60 <sup>a</sup> 80 <sup>a</sup>	$1.1 \times 10^{-6}$ $1.0 \times 10^{-4}$ $1.1 \times 10^{-3}$
VIII. The methyl signal at higher field grows in.	22 <sup>a</sup> 60 <sup>a</sup> 80 <sup>a</sup>	$1.2 \times 10^{-6}$ $1.0 \times 10^{-4}$ $9 \times 10^{-4}$

<sup>a</sup> From reequilibration. <sup>b</sup> From signal shape analysis of  $\alpha$ -proton signals. <sup>c</sup> From signal shape analysis of methyl signals.

<sup>d</sup> Second set of experiments. <sup>e</sup> 100 mg/500  $\mu$ l. <sup>f</sup> 25 mg/500  $\mu$ l. <sup>g</sup> 50 mg/500  $\mu$ l. <sup>h</sup> 200 mg/500  $\mu$ l.

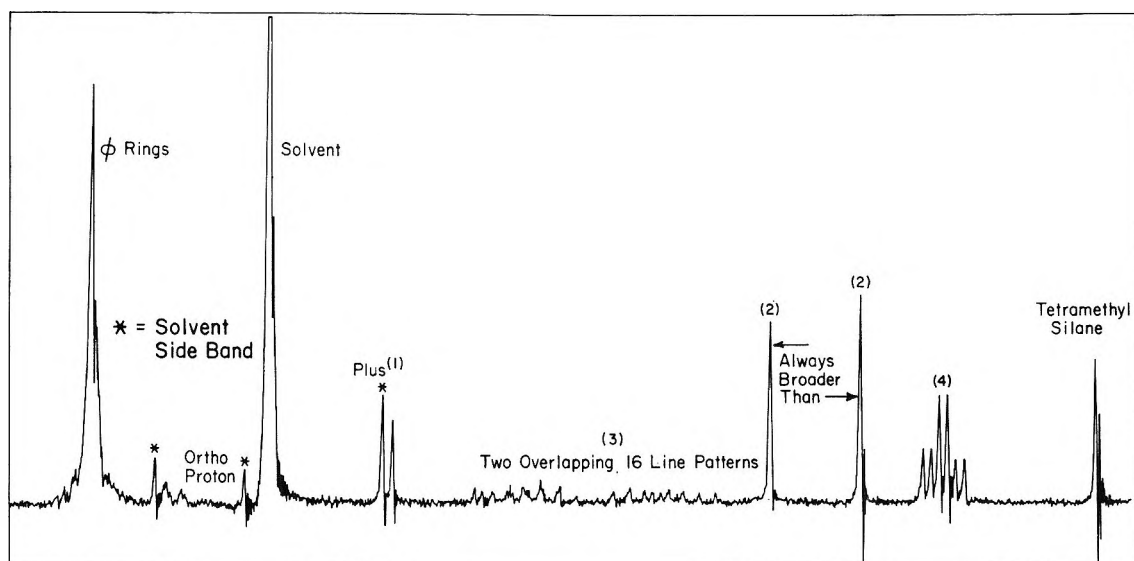
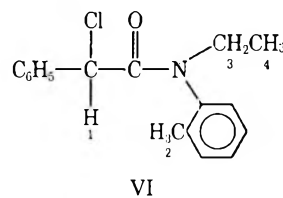


Figure 1. Pmr spectrum of



(100 mg and 500  $\mu$ l. of  $\text{CHCl}_2\text{CHCl}_2$  at 40°).

tions of  $E_a$  and  $\log A_0$ , as estimated from least-squares fits of data to Arrhenius plots. It is interesting to see so many reports in the literature to a much higher precision obtained with the same equipment, but with no indications that any unusual precautions have been taken or modifications made to ensure better temperature control.

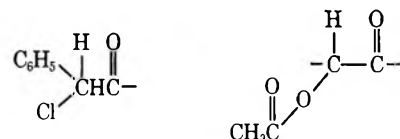
The signal shapes of rate constants were determined by manually matching the theoretical<sup>8</sup> and experimental spectra. At least two of the matching parameters suggested by Nakagawa<sup>8</sup> were used for each match. We preferred manual matching to computer best fit matching. The manual matching is at least as rapid when a number of similar spectra are to be treated. Also as a matter of personal preference, we obtained a better "feel" with respect to obtaining good experimental spectra and making the match to the theoretical spectra.

Aside from the rate constant itself, three other physical parameters enter the signal shape equation. These are signal width at half-signal-height in the absence of exchange ( $w$ ), the chemical shift between sites in the absence of exchange, and the relative isomer (or site) population (see Table II for isomer ratios). We extrapolated these quantities into the region of intermediate exchange from their temperature dependence in the region of slow exchange. In some cases  $w$  was slightly different for the two sites for the ring methyl protons (see Figure 1 where  $w = 1.2$  and  $1.4$  cps). In

these cases, we took the average of the two values. The large chemical shift between ring methyl sites (typically 0.6–0.8 ppm) makes the error caused by this averaging inconsequential. The detailed techniques and calculations for obtaining rate data from reequilibration experiments have already been described.<sup>5,7</sup>

## Results

The kinetic quantities are summarized in Table I. The kinetic results have all been computed for the equilibration with the low-field methyl signal and/or high-field signal from the proton  $\alpha$  to the carbonyl group growing in. Table II is a compilation of equilibrium results. Table III gives the detailed kinetic data. Figure 1 gives the pmr spectrum of VI as an illustration to assist in the discussion below. The *o*-methyl signals were used for monitoring the rates in the reequilibration experiments with I, II, and V-VIII. For I, V, and VI, both the *o*-methyl signals and the signals from the proton  $\alpha$  to the carbonyl group



were used in the signal shape analysis. For II, the

(10) For example, see the review by M. M. Harris, *Progr. Stereochem.*, 2, 157 (1958).

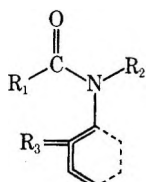
$\alpha$ -proton signals were obscured by the solvent signal. For VII and VIII, the signals are not broadened enough even at the boiling point of the solvent, 146°, to allow signal shape analysis. The reequilibration rates for III and IV were monitored with the  $\alpha$  (to carbonyl)-proton signals as was the signal shape analysis. Compound IX is not listed in the tables. Owing to overlap of signals, a quantitative study could not be made with this compound. However, it was possible to conclude qualitatively that, as expected, the barrier to rotation in IX is even greater than with VII and VIII. Although separate signals sets were generally observable from the N substituents of each epimer of a pair, signal overlap prevented their utility in rate studies.

The standard concentration for the kinetic runs was 100 mg of the compound diluted with 500  $\mu$ l of  $\text{CHCl}_2\text{-CHCl}_2$ . However, the concentration dependence was investigated with VI and found to be nil (see Figure 1). The work at 25, 50, and 200 mg of VI with 500  $\mu$ l of solvent was done at the same time. The work at 100 mg of VI was done several months earlier. The close agreement at 25, 50, and 200 mg reflects the sort of precision obtainable when all the temperature controls are set and left unchanged.

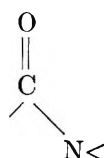
A substituent other than hydrogen on the nitrogen atom of these anilides is apparently required for slow rotation to be detectable by pmr. None of the indicative signal multiplicity could be obtained for  $\text{C}_6\text{H}_5\text{-}(\text{Cl})\text{CHC(O)NHC}_6\text{H}_5$  or  $\text{C}_6\text{H}_5\text{(Cl)}\text{CHC(O)NH(1-C}_{10}\text{-H}_7)$  even with  $\text{C}_6\text{H}_5\text{(Cl)}\text{CHC(O)NH-}o,o'-(\text{CH}_3)_2\text{C}_6\text{H}_3$ . Negative results were obtained at -65° in  $\text{CDCl}_3$ . It might be thought that rotation is rapid because of tunnelling by the proton on nitrogen. However, even when this proton was replaced by deuterium, no evidence of slow rotation could be obtained.

## Discussion

*Indications as to the Activated State.* It is now well established<sup>2b</sup> that the ground state for these molecules is



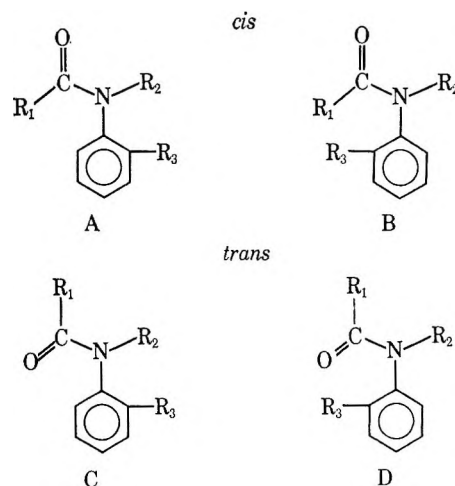
The benzene ring is out of the amide plane, that is, the plane defined by the amide group



Rotational isomerism is possible around the carbonyl-nitrogen (amide) bond. However, the isomer as shown above with the R<sub>2</sub> group *cis* to oxygen is the only

isomer observable by pmr spectroscopy. The *trans* isomer must exist at least 2 or 3 kcal in energy above the *cis* isomer.

There are four possible activated states for rotation around the nitrogen-aryl bond (called simply the aryl bond below), of which A is to be preferred



Of the two *cis* activated states, A must represent the more favorable passing position for steric reasons. Any substituents on R<sub>2</sub> that are in the amide plane can be rotated around the single bond to nitrogen out of the amide plane to allow a conformation favorable to the passing of R<sub>3</sub> through that plane. A similar cooperative rotation that takes R<sub>1</sub> out of the amide plane requires rotation around the amide bond. From analogy with similar compounds,<sup>2b</sup> rotation around the amide bond with its double-bond character must involve not less than 10 kcal. In this sense, R<sub>3</sub> is "smaller" than R<sub>1</sub>C(O)-. A similar argument selects C in preference to D, but not by so wide a margin because the oxygen atom is obviously smaller than R<sub>1</sub>. If the passing of R<sub>3</sub> past R<sub>2</sub> is the ultimate barrier to rotation around the aryl bond, then A is to be preferred over C. This follows plausibly because the *cis* isomer has a thermodynamic preference of at least 2 kcal (though admittedly in the ground state). This analysis is obviously very much simplified and rests on the assumption that cross terms between primary considerations are negligible. It must be regarded as providing a working hypothesis rather than a firm choice between activated states.

There are a number of considerations from Table I that are consistent with the choice of A as the activated state. The difference in rotational barrier between I and V is almost within experimental error, and the difference between I and VI is only about 1 kcal. The benzyl and the methyl groups are almost if not the same "size," and the ethyl group is only a little larger. This could be the case equally whether the passing interaction were R<sub>1</sub>-R<sub>3</sub> or R<sub>2</sub>-R<sub>3</sub>, provided R<sub>2</sub> can be rotated to a minimum size. However, the large increase in barrier with VII and VIII suggests that R<sub>2</sub>-R<sub>3</sub> is the

limiting passing interaction. The 2-propyl group is larger than the other groups in a general sense. Also, there is independent evidence that the preferred angle of the 2-propyl group places its methine proton pointing toward the carbonyl group<sup>11</sup> and its methyl groups in a maximum interfering position. The relatively small barrier for IV as compared with VII and VIII can also be interpreted as corroborating evidence. The optimum conformation of the *o*-2-propyl group is probably also the optimum passing conformation, that is with the methine proton pointed toward nitrogen.

A further test is provided by altering R<sub>1</sub>. If changes in the size of R<sub>1</sub> have little effect, then B tends to be eliminated. Unfortunately no exhaustive comparison can be made at present. R<sub>1</sub> in II is too much like R<sub>1</sub> in I. Preliminary work in this laboratory shows that rotation in (C<sub>6</sub>H<sub>5</sub>)(C<sub>2</sub>H<sub>5</sub>O)P(O)NC<sub>2</sub>H<sub>5</sub>(*o*-CH<sub>3</sub>C<sub>6</sub>H<sub>4</sub>) is almost identical quantitatively with rotation in VI. Published values for CH<sub>3</sub>C(O)N(CH<sub>2</sub>C<sub>6</sub>H<sub>5</sub>)(*o*-CH<sub>3</sub>C<sub>6</sub>H<sub>4</sub>) and C<sub>6</sub>H<sub>5</sub>C(O)N(CH<sub>2</sub>C<sub>6</sub>H<sub>5</sub>)(*o*-CH<sub>3</sub>C<sub>6</sub>H<sub>4</sub>) are E<sub>a</sub> = 18.3 and 17.2 kcal/mol and log A<sub>0</sub> = 12.0 and 12.1;<sup>3</sup> for CH<sub>3</sub>C(O)N(CH<sub>2</sub>C<sub>6</sub>H<sub>5</sub>)(*o*-CH<sub>3</sub>C<sub>6</sub>H<sub>4</sub>)  $\Delta F^*$  = 20.0 kcal/mol at 135° also indicates that the size of R<sub>1</sub> is of lesser consequence. There is, however, a limit to indifference as to R<sub>1</sub>. Rotation seems to be rapid in some formanilides.<sup>2b</sup> The weight of the limited evidence that has to do with R<sub>1</sub> is therefore against B, but more work is required.

*Other Observations as to Size.* Two other observations as to "size" can also be made, but without obvious bearing on the choice of activated state. First, the rigid fused ring of III provides more hindrance to rotation than the methyl group. Also the frequency factor for rotation in III is decidedly higher than for all the other compounds. The data quoted for III were obtained in two separate sets of experiments performed several months apart. The second set of experiments was done after it was seen that III differed from the other compounds. Second, the *m*-methyl group in VIII has no detectable hindering effect whatever. The kinetic runs with VIII could have been taken as good duplicates for runs with VII. It is also interesting to note that at 100°, bromine substitution in the 6 position C<sub>6</sub>H<sub>5</sub>ClCHC(O)N(CH<sub>3</sub>)(1-CH<sub>3</sub>-3,5-Br<sub>2</sub>C<sub>6</sub>H<sub>2</sub>) raises the barrier ( $\Delta F^*$ ) by 10 kcal/mol.<sup>5</sup>

"Normal" vs. "Abnormal" First-Order Reactions. The frequency factors for all these compounds place

rotation around the aryl bond in the category of "normal" first-order reactions. The average of log A<sub>0</sub> = 12.2 ( $\Delta S^*$  = -3 eu). This allows for some constraint of 1 or 2 degrees of internal motion or for a small increase in order in intermolecular interactions in the activated state. It has been observed several times<sup>12-14</sup> that the majority of first-order reactions in the gas phase center around  $\Delta S^* = 0$ . There is growing evidence that this may be the "normal" situation for rotation in amides and possibly other compound types in the liquid state.<sup>3,4,15</sup>

Reports of low-frequency factors for internal motion in amides may deserve close scrutiny. If the low-frequency factor is substantiated, there must be some very unusual activated state such as the triplet state. A high-frequency factor might indicate a high degree of intermolecular order that is lost on activation.

### Equilibrium Results

The equilibrium population ratios of diastereoisomers are of interest.<sup>10</sup> The equilibrium ratios of the anilides in this study are all less than 2, as expected. The temperature effect on the ratio is slight, as was observed in a similar situation.<sup>16</sup> Evidently some crowding is required, in most cases, to produce a ratio different from 1.0 (compare I, V, and VI with III, IV, VII, and VIII). This might be explained on the basis that the various parts of the molecule must be crowded together before the relatively remote asymmetric  $\alpha$ -carbon atom can influence population at the mobile asymmetry center at the aryl bond. However, II stands as a glaring contradiction to any assumption that crowding is the only factor.

(11) T. H. Siddall, III, and W. E. Stewart, *J. Mol. Spectrosc.*, **24**, 290 (1967).

(12) S. Glasstone, K. J. Laidler, and H. Eyring, "The Theory of Rate Processes," McGraw-Hill Book Co., Inc., New York, N. Y., 1941.

(13) V. N. Kondrat'ev, "Kinetics of Gas Reactions," Academy of Sciences, Moscow, 1958.

(14) R. B. Cundall, *Progr. Reaction Kinetics*, **2**, 165 (1964).

(15) See, for example, (a) A. Loewenstein, A. Melera, P. Rigny, and W. Walter, *J. Phys. Chem.*, **68**, 1597 (1964); (b) A. Allerhand and H. S. Gutowsky, *J. Chem. Phys.*, **41**, 2115 (1964); (c) R. C. Neuman, Jr., D. N. Roark, and V. Jonas, *J. Amer. Chem. Soc.*, **89**, 3412 (1967); (d) A. Mannschreck, A. Mattheus, and G. Rissman, *J. Mol. Spectrosc.*, **23**, 15 (1967); (e) K. H. Abramson, P. T. Inglefield, E. Krakower, and L. W. Reeves, *Cin. J. Chem.*, **44**, 1685 (1966); (f) J. P. Chupp and J. F. Olin, *J. Org. Chem.*, **32**, 2297 (1967); (g) G. Isaksson and J. Sandström, *Acta Chem. Scand.*, **21**, 1605 (1967).

(16) T. H. Siddall, III, *J. Phys. Chem.*, **70**, 2050 (1966).

## Cross-Phenomenological Coefficients. XI. Nonlinear Transport Equations

by R. P. Rastogi,<sup>1</sup> Kehar Singh, and M. L. Srivastava

*Department of Chemistry, University of Gorakhpur, Gorakhpur UP, India* (Received May 28, 1968)

An improved technique for the experimental measurement of electroosmotic pressure and streaming potentials involving pressure differences of the order of a few centimeters of pressure has been described. Measurements on electroosmotic velocity and electroosmotic pressure are reported for higher magnitudes of pressure and potential differences,  $\Delta P$  and  $\Delta\phi$ , respectively, for Pyrex-acetone systems. Data on electroosmotic flow  $J_{\Delta P=0}$  obey the equation  $J_{\Delta P=0} = L_{12}(\Delta\phi/T) + \frac{1}{2}L_{122}(\Delta\phi/T)^2$ , whereas the data for net flow  $J_{\text{total}}$  due to both  $\Delta P$  and  $\Delta\phi$  are found to satisfy the nonlinear transport equation  $J = L_{11}(\Delta P/T) + L_{12}(\Delta\phi/T) + L_{112}(\Delta P\Delta\phi/T^2) + \frac{1}{2}L_{122}(\Delta\phi/T)^2 + \frac{1}{2}L_{1112}(\Delta P)^2 \cdot \Delta\phi/T^3 + \frac{1}{2}L_{1122}[\Delta P(\Delta\phi)^2/T^3]$ , where  $L_{11}$ ,  $L_{12}$ ,  $L_{112}$ ,  $L_{122}$ ,  $L_{1112}$ , and  $L_{1122}$  are constants.

### Introduction

Nonlinear transport processes have attracted attention quite recently.<sup>2-5</sup> A clear understanding of these is needed for the study of related phenomena and for the future development of nonlinear thermodynamics of irreversible processes. The thermal transpiration relation for an ideal gas<sup>4</sup> and the kinetic data for a monomolecular reversible reaction<sup>2b</sup> show that the transport equation resulting from the Taylor expansion of the flows expressed as functions of forces adequately describes the processes in the nonlinear range. However, theoretical studies based on the Chapman-Enskog theory of nonuniform gases using a higher approximation to the distribution function show that the second derivatives of gradients and particularly of barycentric velocity would appear in the nonlinear transport equation.<sup>6</sup> It is desirable to conduct experimental studies to examine the point. Unfortunately, the experimental studies in the nonlinear region are very scarce, primarily because such studies are difficult. Useful information has only recently been obtained for electroosmosis.<sup>3</sup>

In the present paper an experimental investigation of electroosmosis for the nonlinear region has been described. Since the nonlinear region is expected to appear when the pressure difference  $\Delta P$  and potential difference  $\Delta\phi$  are high, suitable techniques have been developed for the measurements of electroosmotic pressure and electroosmotic velocity under such conditions. The results have been discussed in the present paper.

### Experimental Section

**Materials.** BDH acetone was refluxed for 3 hr with a small amount of potassium permanganate. It was subsequently distilled and the distillate was kept overnight over  $K_2CO_3$  to remove moisture. The distillate was subjected to fractional distillation twice. The density of the purified sample was 0.7742 g/ml at 35°.

Pyrex sinter (Porosity G-4) was used. Pyrex sinter was treated with hot 1:1 nitric acid and was washed

repeatedly with distilled water to remove traces of nitric acid. Finally, it was dried in an electrically operated oven at 120–140° and was allowed to cool slowly. This treatment is essential in order to avoid fluctuations in the permeability of the glass membrane.

**Apparatus. Measurement of Electroosmotic Flow and Hydrodynamic Flow.** For electroosmotic velocity and ordinary permeability measurements, the experimental setup described by Rastogi and Jha<sup>3</sup> was used. The cross-sectional area of the exit capillary in our case was  $11.11 \times 10^{-2} \text{ cm}^2$ . Potential difference up to 600 V could be applied with an electronically operated power supply. The strength of the current flowing through the system was below 2 mA. The difference of pressure on the two faces of the membrane was measured, to  $\pm 0.001$  cm, with a cathetometer. The volume flux was determined by noting the rate of advancement of the acetone-air interface in the exit capillary. Time could be recorded to  $\pm 0.1$  sec with a stopwatch.  $J_{\text{total}}$  was measured by applying the potential difference and pressure difference simultaneously.

**Measurement of Electroosmotic Pressure.** The procedure employed by Rastogi and Jha can only be used for the measurement of electroosmotic pressure of a small magnitude. Since measurements were needed for  $\Delta P$  of the order of 20 cm of pressure, a new apparatus, shown in Figure 1, was designed. The Pyrex glass sinter (M) partitions a glass tube 30 cm long into two compartments A and B. S and S' are the two coiled platinum electrodes. Tubes C and D were filled with mercury. G and H are the two glass tubes connected to the two half-cells A and B. Portion abcde

(1) Visiting Professor, Department of Chemistry, Indiana University, Bloomington, Ind.

(2) (a) R. P. Rastogi and R. C. Srivastava, *Physica*, **25**, 391 (1959); (b) R. P. Rastogi, R. C. Srivastava, and K. Singh, *Trans. Faraday Soc.*, **61**, 854 (1965).

(3) R. P. Rastogi and K. M. Jha, *ibid.*, **62**, 585 (1966).

(4) R. P. Rastogi and K. Singh, *ibid.*, **63**, 2917 (1967).

(5) H. J. M. Hanley and Steele, *ibid.*, **59**, 2661 (1963).

(6) R. P. Rastogi and B. P. Misra, unpublished results.

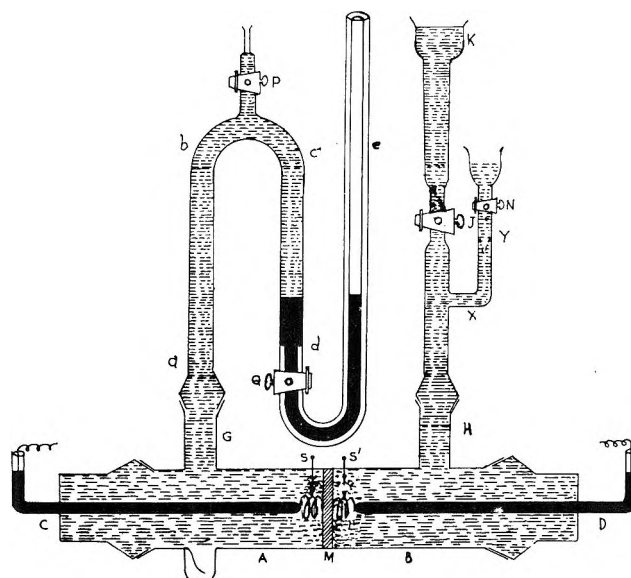


Figure 1. The apparatus for the measurement of electroosmotic pressure and streaming potential: A, B, half-cells; C, D, glass tubing containing mercury; M, glass membrane; G, H, glass tubes; P, Q, J, N, stopcocks; K, reservoir; S, S', coiled platinum electrode.

having stopcocks P and Q could be attached to G with the help of a standard ground-glass joint. Mercury is partly filled in capillary tube e. Portion YXK is attached to H by a ground-glass joint.

The cell was washed repeatedly with deaerated acetone. Air contained in the pores of the membrane was removed by passing acetone a number of times through it with a suction pump. Cell GCABDH was then filled with acetone. Part of limb cde was filled with purified mercury. This was attached to G. Limb YXK having a bent tube XY was then attached to H. Limb KJH was filled with acetone by adjusting the stopcocks J and N. Part abc was filled with acetone by opening stopcocks J, P, and Q and keeping stopcock N closed. All the air could be removed with the help of stockcock P. When limb abc was completely filled with acetone, stopcock P was closed. The potential difference across the electrodes was applied with the help of a regulated dc power supply. The resulting pressure difference was determined by noting the level of the mercury in limbs d and e. This was done with the help of a cathetometer. The necessary correction due to changes in the level of acetone in reservoir K was also made. The apparatus was kept in an air thermostat maintained at  $35 \pm 0.1^\circ$ . The electroosmotic pressure difference was measured for various potential differences.

*Measurement of Streaming Potential.* The above apparatus could also be used for the measurements of streaming potential. Mercury was adjusted to a desired level in e, so that  $\Delta P$  could correspond to difference in mercury level in d and e. Stopcock Q was closed before attaching limb abcde to the cell. Acetone was filled in the cell as already described. The elec-

trodes were then connected to a Cambridge Lindemann electrometer. The pressure difference was noted. Stopcock Q was then gently opened, and the instantaneous deflection of the electrometer needle was recorded. Different magnitudes of pressure differences were applied, and the corresponding values of streaming potentials were determined in a similar manner.

The technique described above for the measurement of the electroosmotic pressure difference and the streaming potential is better than the methods reported earlier<sup>3</sup> in the following respects.

(a) The time required for the attainment of steady state is considerably smaller. The time rarely exceeds 5 min, whereas the earlier method took 1–2 hr.

(b) The conductivity of acetone remains practically unaltered during the measurements.

(c) The electroosmotic pressure and streaming potential can be measured for much higher magnitudes of forces.

## Results

The results are plotted in Figures 2–4. Results of the measurements of  $J_{\text{total}}$  are given in Tables I and II.

Table I:  $J_{\text{total}}$  for Fixed  $\Delta\phi$  for Membrane I ( $\Delta\phi = 400 \text{ V}, 35 \pm 0.1^\circ$ )

$\Delta P$ , cm. of acetone	$10^3 J_{\Delta\phi = 0}$ , $\text{cm}^3 \text{ sec}^{-1}$	$10^3 J_{\text{total}}$ , $\text{cm}^3 \text{ sec}^{-1}$
51.31	37.00	73.03
58.31	44.25	79.42
70.31	52.25	86.88
82.01	60.47	97.13
93.31	69.09	109.82

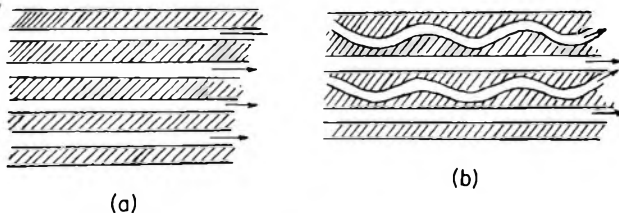
Table II:  $J_{\text{total}}$  for Fixed  $\Delta P$  for Membrane I ( $\Delta P = 93.31 \text{ cm}$  of acetone,  $35 \pm 0.1^\circ$ )

$\Delta\phi$ , V	$10^3 J_{\Delta P = 0}$ , $\text{cm}^3 \text{ sec}^{-1}$	$10^3 J_{\text{total}}$ , $\text{cm}^3 \text{ sec}^{-1}$
100	11.16	76.43
200	24.25	87.16
300	38.93	100.84
400	51.50	113.87
500	66.50	131.39
600	78.93	146.75

## Discussion

*Membrane Characteristics.* The first-order coefficients  $L_{ik}$  depend upon the structural factor  $G$  in addition to intensive parameters. Pyrex sinter is a composite membrane<sup>7</sup> consisting of a parallel array of elements (which may be schematically represented as follows) and not a series array

(7) O. Kedam and A. Katchalsky, *Trans. Faraday Soc.*, 59, 1931 (1963).



This was confirmed experimentally since  $L_{11}$  remains the same even when the direction of forces is inverted. The arrangement b would be more near to reality, since the individual capillaries would have a different geometry. The net flow  $J$  would be the sum of the corresponding flows  $j_i$  through various capillaries given by

$$J = \sum a_i j_i \quad (1)$$

where  $a_i = A_i / \sum A_i$  ( $A_i$  is the area of cross section of the  $i$ th capillary). The cross section can be circular, elliptical, or of any other shape. The cross-phenomenological coefficients  $L_{ik}$  and  $L_{ijk}$  would be related to individual  $l_{ik}$  by the relations

$$\begin{aligned} L_{ik} &= \sum a_i l_{ik} \\ L_{ijk} &= \sum a_i l_{ijk} \end{aligned} \quad (2)$$

where  $l_{ik}$  would depend on the length of the capillary and the pore geometry. Hence these would be different for different capillaries in the Pyrex sinter. Table III shows how  $L_{11}$  depends upon pore geometry.

Table III

Type of pore	$L_{11}$	
Circular pore <sup>a</sup>	$\pi a^4 / 8\eta l$	$a$ is the radius of the pore; $\eta$ is the viscosity; and $l$ is the length of the pore
Elliptical pore <sup>a</sup>	$[\pi a^3 b^3 / (a^2 + b^2)](1/\eta l)$	$a$ and $b$ are the semi-major and semi-minor axes, respectively; $\eta$ is the viscosity; and $l$ is the length of the pore
Equilateral pore <sup>a</sup>	$(27a^4 / 20\sqrt{3})(1/\eta l)$	$a$ is the side of the equilateral triangle; $\eta$ is the viscosity; and $l$ is the length of the pore

<sup>a</sup> A. S. Ramsay, "A Treatise on Hydromechanics, Part II Hydrodynamics," G. Bell and Sons, Ltd., London, 1957.

The average pore size of the sinter was estimated by the method suggested by Rastogi, Kehar Singh, and Shri Nath Singh.<sup>8</sup> It can be shown that

$$r = \sqrt{2\xi D(L_{11}/\pi L_{12})} \quad (3)$$

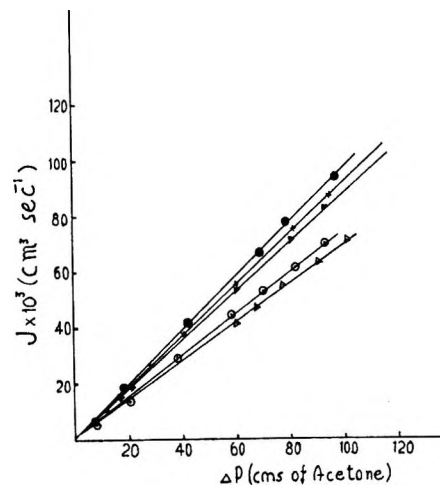


Figure 2. The dependence of volume flow,  $J$ , on pressure difference,  $\Delta P$ :  $\circ$ , membrane I;  $\bullet$ , membrane II;  $\triangle$ , membrane III;  $\times$ , membrane IV;  $\blacktriangle$ , membrane V.

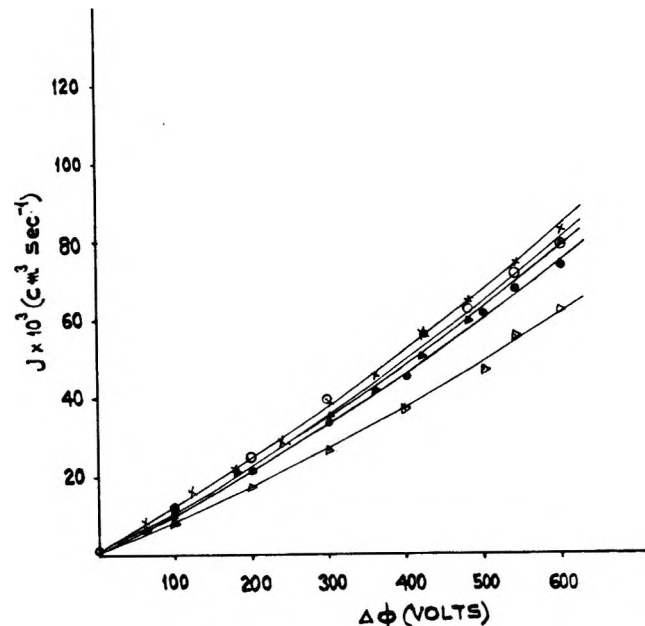


Figure 3. The dependence of volume flow,  $J$ , on potential difference,  $\Delta\phi$ :  $\circ$ , membrane I;  $\bullet$ , membrane II;  $\triangle$ , membrane III;  $\times$ , membrane IV;  $\blacktriangle$ , membrane V.

where  $\xi$  is the  $\xi$  potential at the Pyrex-acetone interface and  $D$  is the dielectric constant. Using the value<sup>9</sup> of  $\xi = 0.07$  and the values of  $L_{11}$  and  $L_{12}$  estimated in this investigation,  $r$  could be estimated for each membrane. Knowing the thickness of the membranes,  $n$ , the number of capillaries could be determined. The membrane parameters are given in Table IV. The thickness of the membrane was 0.3 cm. The pore size is greater than the thickness of the electrical double layer.

*Nonlinear Transport Processes.* For Markoffian sys-

(8) R. P. Rastogi, K. Singh, and S. N. Singh, *Ind. J. Chem.*, in press.

(9) R. P. Rastogi and B. M. Misra, *Trans. Faraday Soc.*, **63**, 2926 (1967).

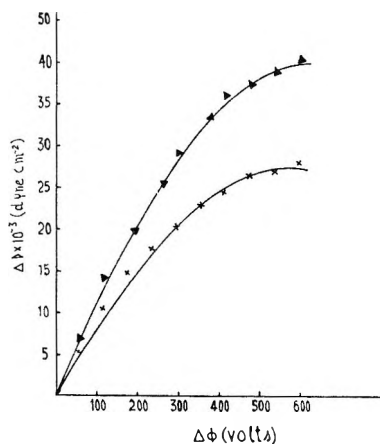


Figure 4. The dependence of the electroosmotic pressure,  $\Delta P$ , on potential difference,  $\Delta\phi$ :  $\times$ , membrane IV;  $\blacktriangle$ , membrane V.

Table IV: Membrane Parameters

Membrane	$10^{17}$ (pore radii), cm	$10^{-6} n$
I	3.0	3.9
II	3.7	2.0
III	3.6	1.6
IV	3.2	3.2
V	3.4	2.4

tems, the fluxes at a given instant depend only on the value of affinity at that instant. On the other hand, for a non-Markoffian system, the fluxes may depend on the values of the affinities at previous times as well as at that instant. For example, a pure resistor is a Markoffian system, whereas a circuit with capacitance and inductance is non-Markoffian. It has been pointed out recently<sup>4</sup> that for a Markoffian system the flux  $J$  can be written as function of forces  $X_1, X_2, \dots$ , and the structural factor  $G$ , *viz.*

$$J = f(X_1, X_2, \dots; G) \quad (4)$$

When the structure factor  $G$  is kept constant, we can write for a system where only two forces  $X_1$  and  $X_2$  operate

$$\begin{aligned} J = L_{11}X_1 + L_{12}X_2 + 1/2L_{111}X_1^2 + L_{112}X_1X_2 + \\ 1/2L_{122}X_2^2 + 1/6L_{1111}X_1^3 + 1/2L_{1112}X_1^2X_2 + \\ 1/2L_{1122}X_1X_2^2 + 1/6L_{1222}X_2^3 + \dots \quad (5) \end{aligned}$$

where  $L_{ij}$  and  $L_{ijk}$ , etc., are the phenomenological coefficients. It has been shown that equations of type of eq 5 are valid in the case of chemical reactions<sup>2b</sup> and thermoosmosis of ideal gases.<sup>4</sup>

In electroosmotic experiments, the mass flux  $J$  would depend on the pressure gradient  $\Delta P$  and the potential gradient  $\Delta\phi$  only, since the pore geometry would remain unchanged. It may be noted that normally viscous flow occurs in the pores and hence radial-velocity

gradients are present. In the equation for entropy production terms containing the product of the viscous-pressure tensor and the gradient of barycentric velocity along with the product of the axial vector and the mean angular velocity of the constituent particles would appear.<sup>10</sup>

Bearman and Kirkwood have shown that linear phenomenological relations are obtained when the viscosity term can be neglected.<sup>11</sup> Hence, one may expect that nonlinear terms would arise on account of the velocity gradient. However, as pointed out by Mikulecky and Caplan,<sup>12</sup> the measured flows are average flows over the plane of the membrane. Using an averaging procedure, they have shown that the local dissipation function just corresponds to that for mechanical equilibrium (when the gradient of pressure and velocity are both zero). Hence it follows that we would still get linear phenomenological equations in the changed circumstances. Bearman<sup>13</sup> has examined recently the practical importance of inertial and viscous terms in the phenomenological equations deduced from the statistical-mechanical theory. He finds that in the case of diffusion such terms are negligible. However, it is questionable whether such terms still remain negligible when higher order coefficients are taken into account. As a first approximation, it appears that eq 5 may correctly describe electroosmosis in the nonlinear range.

We shall now examine the experimental data in order to ascertain the extent to which it satisfies eq 5 where  $J$  is the mass flow and  $X_1 = \Delta P/T$  and  $X_2 = \Delta\phi/T$ .

Equation 5 can be written for mass flow  $J$  and the electric current  $I$  in the following manner

$$\begin{aligned} J = L_{11}\frac{\Delta P}{T} + L_{12}\frac{\Delta\phi}{T} + 1/2L_{111}\left(\frac{\Delta P}{T}\right)^2 + \\ L_{112}\frac{\Delta P\Delta\phi}{T^2} + 1/2L_{122}\left(\frac{\Delta\phi}{T}\right)^2 + \\ 1/6L_{1111}\left(\frac{\Delta P}{T}\right)^3 + 1/2L_{1112}\frac{(\Delta P)^2\Delta\phi}{T^3} + \\ 1/2L_{1122}\frac{\Delta P(\Delta\phi)^2}{T^3} + 1/6L_{1222}\left(\frac{\Delta\phi}{T}\right)^3 - \dots \quad (6) \end{aligned}$$

$$\begin{aligned} I = L_{21}\frac{\Delta P}{T} + L_{22}\frac{\Delta\phi}{T} + 1/2L_{211}\left(\frac{\Delta P}{T}\right)^2 + \\ L_{212}\frac{\Delta P\Delta\phi}{T^2} + 1/2L_{222}\left(\frac{\Delta\phi}{T}\right)^2 + \\ 1/2L_{2112}\frac{\Delta P(\Delta\phi)^2}{T^3} + 1/6L_{2111}\left(\frac{\Delta P}{T}\right)^3 + \\ 1/2L_{2112}\frac{(\Delta P)^2\Delta\phi}{T^3} + 1/6L_{2222}\left(\frac{\Delta\phi}{T}\right)^3 + \dots \quad (7) \end{aligned}$$

(10) S. R. de Groot and P. Mazur, "Non-equilibrium Thermodynamics," North-Holland Publishing Co., Amsterdam, 1962.

(11) R. J. Bearman and J. G. Kirkwood, *J. Chem. Phys.*, **28**, 136 (1958).

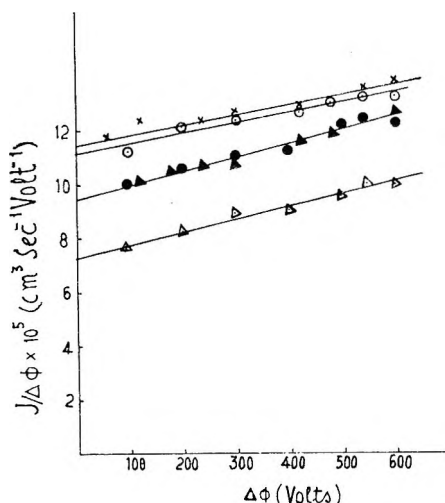


Figure 5. The estimation of  $L_{12}$  and  $L_{122}$  using eq 9:  $\circ$ , membrane I;  $\bullet$ , membrane II;  $\Delta$ , membrane III;  $\times$ , membrane IV;  $\blacktriangle$ , membrane V.

when the third-order terms are retained. The experimental data for  $J_{\Delta\phi=0}$ ,  $J_{\Delta P=0}$ ,  $J_{\text{total}}$ ,  $(\Delta P/\Delta\phi)_{J=0}$ , and  $(\Delta\phi/\Delta P)_{J=0}$  have been obtained in the present investigation. With these five types of independent data, it should be possible to get the desired information about nonlinear transport equations.

When  $\Delta\phi = 0$ , we have

$$J_{\Delta\phi=0} = L_{11} \frac{\Delta P}{T} + \frac{1}{2} L_{111} \left( \frac{\Delta P}{T} \right)^2 + \frac{1}{6} L_{1111} \left( \frac{\Delta P}{T} \right)^3 + \dots \quad (8)$$

The experimental results for hydrodynamic flow  $J$  are plotted in Figure 2 against the pressure gradient  $\Delta P$ . Straight lines are obtained, showing that  $L_{11} = 0$  and  $L_{111} = 0$ . This is expected, since Poiseuille's law has a much greater range of validity. It should be noted that the curve does not pass through the origin. Flow occurs even when  $\Delta P = 0$ . This is due to capillary-active forces at the acetone-air interface in the capillary where the rate of movement of the meniscus is observed. This behavior was also observed by Rastogi and Jha.<sup>3</sup> Necessary corrections for this residual flow have been made in subsequent analysis wherever needed. From the slope  $L_{11}$  was estimated.

When  $\Delta P = 0$ , the electroosmotic velocity is given by

$$J_{\Delta P=0} = L_{12} \frac{\Delta\phi}{T} + \frac{1}{2} L_{122} \left( \frac{\Delta\phi}{T} \right)^2 + \frac{1}{6} L_{1222} \left( \frac{\Delta\phi}{T} \right)^3 + \dots \quad (9)$$

In Figure 5,  $J_{\Delta P=0}/\Delta\phi$  has been plotted against  $\Delta\phi$ . A straight line is obtained showing thereby that  $L_{1222} = 0$ .  $L_{12}$  and  $L_{122}$  could be estimated from the intercept

and slope of the curve. The thermodynamic consistency of  $L_{12}$  was checked by the estimation of  $L_{21}$  from streaming-potential measurements using the procedure of Rastogi and Jha.<sup>3</sup>

Equation 6 can be written as

$$J_{\text{total}} - (J_{\Delta P=0} + J_{\Delta\phi=0}) = L_{112} \frac{\Delta P \Delta\phi}{T^2} + \frac{1}{2} L_{1112} \frac{(\Delta P)^2 \Delta\phi}{T^3} + \frac{1}{2} L_{1122} \frac{\Delta P (\Delta\phi)^2}{T^3} + \dots \quad (10)$$

Equation 10 can be used for the interpretation of experimental results, since the measurements of  $J_{\text{total}}$  have been made for (i) different magnitudes of  $\Delta\phi$ , keeping  $\Delta P$  constant, and (ii) different magnitudes of  $\Delta P$ , keeping  $\Delta\phi$  constant. A rearrangement of eq 10 yields

$$\frac{J_{\text{total}} - (J_{\Delta P=0} + J_{\Delta\phi=0})}{\Delta P \Delta\phi} = \frac{L_{112}}{T^2} + \frac{1}{2} \frac{L_{1112}}{T^3} \Delta P + \frac{1}{2} \frac{L_{1122}}{T^3} \Delta\phi + \dots \quad (11)$$

When the left-hand side of eq 11 is plotted against  $\Delta P$ , keeping  $\Delta\phi$  fixed, a straight line is obtained as indicated in Figure 6. The intercept gives  $(L_{112}/T^2) + \frac{1}{2} L_{1112}(\Delta P/T^3)$  and the slope gives  $\frac{1}{2} L_{1122}/T^3$ . Similarly, on plotting the left-hand side of eq 11 against  $\Delta\phi$  when  $\Delta P$  is fixed, a straight line is obtained (Figure 7). Here again the intercept gives  $(L_{112}/T^2) + \frac{1}{2} L_{1112}(\Delta P/T^3)$  and the slope yields  $\frac{1}{2} L_{1122}/T^3$ . From these the values of  $L_{112}$  could be obtained. The phenomenological coefficients are given in Table V for five membranes.

In order to ascertain further the validity of nonlinear transport equations of the type of eq 6, we shall examine another set of data involving measurements on (i) sol-

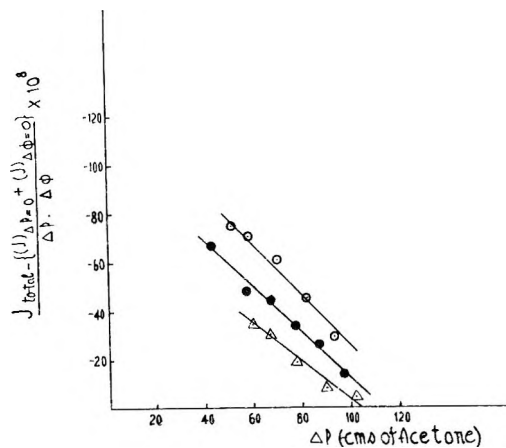


Figure 6. The estimation of  $L_{112}$  and  $L_{122}$  using eq 11:  $\circ$ , membrane I;  $\bullet$ , membrane II;  $\Delta$ , membrane III.

(12) D. C. Mikulecky and S. R. Caplan, *J. Phys. Chem.*, **70**, 3049 (1966).

(13) R. J. Bearman, *J. Chem. Phys.*, **31**, 751 (1959).

**Table V:** Phenomenological Coefficients<sup>a</sup>

Membrane	$10^6(L_{11}/T)$ , cm <sup>6</sup> dyn sec <sup>-1</sup>	$10^4(L_{12}/T)$ , cm <sup>6</sup> sec <sup>-1</sup>	$10^4(L_{21}/T)$ , cm <sup>6</sup> sec <sup>-1</sup>	$10^8(L_{122}/T^2)$ , cm <sup>8</sup> sec <sup>-1</sup>	$10^{10}(L_{112}/T^2)$ , cm <sup>10</sup> sec <sup>-1</sup>	$10^4(L_{1112}/T^3)$ , cm <sup>7</sup> sec <sup>-1</sup>	$10^{-2}(L_{1112}/T^3)$ , cm <sup>5</sup> sec <sup>-1</sup>
I	0.96	1.13	1.10	6.60	-20.2 <sup>c</sup>	3.64	2.12
II	1.27	0.94	0.92	10.6	-19.1 <sup>c</sup>	3.26	2.28
III	0.92	0.72	0.70	9.60	-17.7 <sup>c</sup>	2.80	3.00
IV	1.10	1.07	1.03	10.7	-13.1	0.70	6.68
V	1.06	0.97	0.98	12.0	-12.1	1.40	9.96

<sup>a</sup> For membranes I-III, values of phenomenological coefficients are calculated from  $J_{\text{total}}$  measurements, and for membranes IV and V, values of phenomenological coefficients are calculated from electroosmotic pressure difference measurements. <sup>b</sup> Estimated from streaming potential measurements. <sup>c</sup> Mean values of  $L_{112}/T^2$  obtained from Figures 6 and 7.

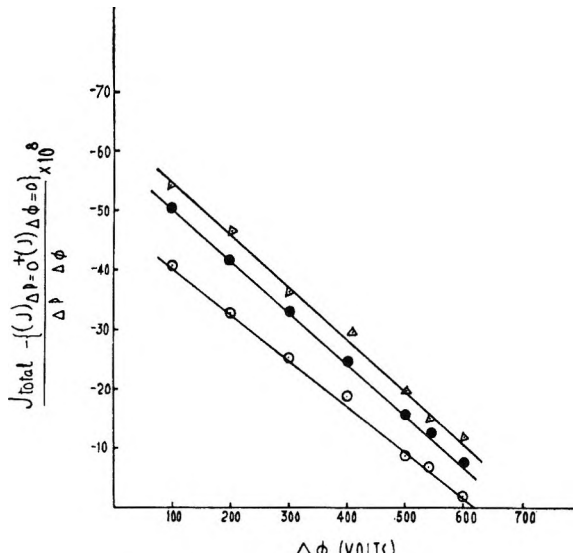


Figure 7. The estimation of  $L_{1122}$  and  $L_{112}$  using eq 11:  
 ○, membrane I; ●, membrane II; △, membrane III.

vodynamic flow, (ii) electroosmotic flow, and (iii) electroosmotic pressure.

$L_{11}$ ,  $L_{12}$ , and  $L_{122}$  were estimated from solvodynamic flow and electroosmotic flow in the usual manner. The other three coefficients  $L_{112}$ ,  $L_{1112}$ , and  $L_{1122}$  were obtained from electroosmotic pressure data by solving a set of simultaneous equations when the appropriate values of coefficients were substituted into eq 6 when  $J = 0$ . Values of  $(\Delta P)_{J=0}$  calculated by using these sets of coefficients are compared with experimentally measured values of electroosmotic pressure for a definite value of  $\Delta\phi$  in Table VI.

The theoretical values of  $(\Delta P)_{J=0}$  retaining first-order terms, second-order terms, and third-order terms have been given for the sake of comparison. Table VI further confirms that third-order terms are necessary to describe the experimental data reported in this article. Thus it follows that the experimental data are in agreement with eq 6. However, it would be interesting to examine whether the data can also be satisfied with a similar transport equation having higher order derivatives of pressure and potential.

Table VI

Mem- brane	$\Delta\phi,$ V	Exptl	$10^{-3}(\Delta P)_{J=0}$ , dyn cm $^{-2}$		
			Theor		
			First order <sup>a</sup>	Second order <sup>a</sup>	Third order <sup>a</sup>
IV	100	8.5	10	8	9
	200	15.5	19	13	16
	300	20.5	29	16	21
	400	24.5	39	20	24
	500	26.5	49	22	26
	600	28.0	58	25	28
V	100	11.5	9	10	11
	200	21.5	17	26	21
	300	29.5	26	47	31
	400	35.5	35	81	37
	500	39.0	46	135	39
	600	40.5	52	234	41

<sup>a</sup> Calculated using eq 6 and retaining terms up to the stated order.

The most important point is to ascertain whether  $\partial^2 P / \partial x^2$  and  $\partial^2 \phi / \partial x^2$  have finite values in the present case. We consider the gradient along the  $x$  axis only for the sake of simplicity. Experimental data for solvodynamic flow when  $\Delta\phi = 0$  show that the terms containing higher derivatives of pressure are not significant. However, this does not necessarily prove that  $\partial^2 P / \partial x^2$  is zero. If the radii of the capillaries in the Pyrex sinter are uniform, then it can be shown from Bernoulli's principle that the pressure gradient would be uniform along the capillaries and the velocity of the fluid would be the same all along the tube. In fact inside the capillary  $\partial P / \partial x = \text{constant}$ , whereas the pressure difference at the ends of the capillary is  $\Delta P$ . This is true for the potential also. Hence, in all likelihood  $\partial^2 P / \partial x^2$  and  $\partial^2 \phi / \partial x^2$  would be zero in the present case.

*Acknowledgment.* The authors wish to thank the Indian Council of Scientific and Industrial Research for the award of a Junior Research Fellowship to M. L. S. This work forms part of the program of the CSIR Research Unit.

# Peroxide Formation in the $\gamma$ Radiolysis of Aerated Aqueous Solutions of Methyl Iodide

by J. Shankar, K. V. S. Rama Rao, and L. V. Shastri

*Chemistry Division, Bhabha Atomic Research Centre, Trombay, Bombay, India* (Received May 23, 1968)

In the  $\gamma$  radiolysis of aerated aqueous solutions of  $\text{CH}_3\text{I}$ , with added KI, the major products formed are hydrogen peroxide, iodine, and methyl hydroperoxide. The initial  $G$  values of these products are compatible with the known yields of the primary species ( $e_{\text{aq}}^-$ , H, and OH) from water. Addition of iodine greatly reduces the yield of methyl hydroperoxide and that of methanol enhances the hydrogen peroxide yield. A sequence of reactions has been proposed in order to explain the effects of variation in the concentrations of the solutes, pH, and dose rate upon the product yields. It is shown that (i) the capture of  $e_{\text{aq}}^-$  by  $\text{CH}_3\text{I}$  is dissociative (*i.e.*,  $\text{CH}_3\text{I} + e_{\text{aq}}^- \rightarrow \text{CH}_3 + \text{I}^-$ ) ruling out any reaction of the anion  $\text{CH}_3\text{I}^-$  itself (*e.g.*,  $\text{CH}_3\text{I}^- + \text{H}^+ \rightarrow \text{CH}_4 + \text{I}^-$ ), and (ii) the methyl hydroperoxide is formed by the reaction of  $\text{CH}_3\text{O}_2$  radicals with iodide ions or  $\text{I}_2^-$  radical ions, more likely the latter. Relative rate constants determined in neutral solutions are  $k_{e_{\text{aq}}^- \cdot \text{H} + \text{CH}_3\text{I}} / k_{e_{\text{aq}}^- \cdot \text{H} + \text{O}_2} = 0.4$  and  $k_{\text{OH} + \text{CH}_3\text{OH}} / k_{\text{OH} + \text{CH}_3\text{I}} = 0.65$ .

## Introduction

Recent pulse radiolysis work<sup>1</sup> has shown that methyl iodide and other alkyl halides react efficiently with solvated electrons from water. The resulting anion  $\text{RX}^-$  is believed to have a short lifetime and dissociates to give the corresponding alkyl radical and the halide ion.<sup>2</sup> Johnson and Simic,<sup>3</sup> however, have suggested that in the vapor-phase radiolysis of water and methyl bromide  $\text{CH}_3\text{Br}^-$  is sufficiently stabilized to participate in a chemical reaction. In this paper we present our results on the peroxide formation from aqueous solutions of methyl iodide which can be explained by a dissociative capture of electrons by the latter.

## Experimental Section

Methyl iodide obtained from Distillation Products Inc. was purified by repeated shaking with an aqueous solution of potassium iodide followed by several washings with triply distilled water obtained by redistilling the laboratory distilled water with acidic potassium dichromate and then with alkaline potassium permanganate in an all-Pyrex apparatus. Only freshly prepared triply distilled water was used. All other chemicals used in this work were BDH Analar grade.

Hydrogen peroxide, iodine, and the alkyl hydroperoxide yields were estimated by reacting an aliquot with 0.1  $M$  potassium iodide solution containing ammonium molybdate and measuring  $\text{I}_3^-$  absorption at 352  $\mu\text{m}$  according to Ghormley's method.<sup>4</sup> The initial optical density measured on a Beckman DU spectrophotometer within 40 sec after mixing the reagents gave the total amount of iodine and hydrogen peroxide, after correcting for any small contribution from the alkyl-hydroperoxide reaction with iodide ion during this time. The latter reaction was slow and required nearly 2 hr for completion. The difference between

the final and the corrected initial optical densities gave an estimate of the organic hydroperoxide.<sup>5</sup> Hydrogen peroxide yield was separately estimated by first extracting iodine with carbon tetrachloride soon after irradiation. For methyl iodide solutions, the amount of the organic peroxide as determined was the same both with and without carbon tetrachloride extraction.

There was a lapse of about 40 min after irradiation before the solutions could be analyzed for iodine and the peroxides. Control experiments showed a negligible reaction between 10<sup>-2</sup>  $M$  KI and the peroxides during this time.

Methyl hydroperoxide was prepared from dimethyl sulfate according to the method described by Hanst and Calvert.<sup>6</sup> A 0.05  $M$  stock solution was obtained by shaking the ether extract containing the hydroperoxide with water. The acidity was adjusted with sulfuric acid and the pH was measured in the presence of air.

All the irradiations were done in a Gamma Cell 200, a 3.7-kCi cobalt-60 source. Using a Fricke dosimeter the dose rate was established as  $3.27 \times 10^{20}$  eV l.  $^{-1}$  min $^{-1}$ . The dose actually absorbed by the samples was evaluated by correcting for electron density differences.

## Results

Hydrogen peroxide, iodine, and methyl hydroperox-

- (1) A. Szutka, J. K. Thomas, S. Gordon, and E. J. Hart, *J. Phys. Chem.*, **69**, 289 (1965).
- (2) J. K. Thomas, *ibid.*, **71**, 1919 (1967).
- (3) G. R. A. Johnson and M. Simic, *ibid.*, **71**, 2775 (1967).
- (4) A. O. Allen, C. J. Hochanadel, J. A. Ghormley, and T. W. Davis, *ibid.*, **56**, 575 (1952).
- (5) K. V. S. Rama Rao, K. Srinivasan, and L. V. Shastri, *Proc. AEET Symp. Nucl. Radiat. Chem., India*, 109 (1966).
- (6) P. L. Hanst and J. G. Calvert, *J. Phys. Chem.*, **63**, 71 (1959).

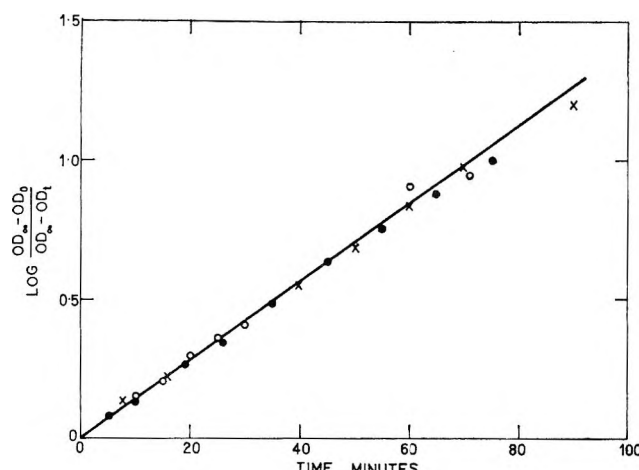


Figure 1. Rate of oxidation of iodide in Ghormley's reagent at room temperature: X, synthetic  $\text{CH}_3\text{OOH}$ ; O, irradiated solution of  $\text{CH}_3\text{I}$  ( $0.1 \text{ M}$ ) and  $\text{KI}$  ( $5 \times 10^{-3} \text{ M}$ ); ●, irradiated solution of  $\text{CH}_3\text{I}$  ( $0.1 \text{ M}$ ) (no  $\text{KI}$  added).

ide were found to be the major products in the radiolysis of aerated aqueous solutions of methyl iodide. Formaldehyde was also detected, but it could not be estimated accurately by the chromotropic acid colorimetric method<sup>7</sup> under our experimental conditions, i.e., in the presence of iodine, the iodide ion, and the organic peroxide. The identity of the organic peroxide has been established by comparing its rate of oxidation of iodide ion (Ghormley's reagent) with that of a solution of methyl hydroperoxide prepared from dimethyl sulfate. Figure 1 shows that the organic peroxides formed in the radiolysis of methyl iodide solutions, both in the presence and in absence of added potassium iodide, have a rate identical with the methyl hydroperoxide prepared in the laboratory. The pseudo-first-order rate constant is  $3.16 \times 10^{-2} \text{ min}^{-1}$  at room temperature ( $25^\circ$ ).

Table I summarizes the initial values of  $G(\text{H}_2\text{O}_2)$ ,  $G(\text{I}_2)$ , and  $G(\text{CH}_3\text{OOH})$  at various concentrations of methyl iodide and iodide ion.  $G(\text{I}_2)$  and  $G(\text{CH}_3\text{OOH})$  increase with increasing concentration of methyl iodide. The hydroperoxide yield reaches a limiting value at  $\text{CH}_3\text{I} \geq 0.004 \text{ M}$ , where all solvated electrons essentially react with this solute. A 100-fold variation in iodide ion concentration does not seem to affect this limiting yield. There is also no discernible effect of dose rate on the initial yields (Table II). Increasing dose, however, decreases the  $G$  values as can be noted from Figure 2.

In one experiment (Table I) an aqueous solution containing  $0.1 \text{ M}$  methyl iodide and  $0.001 \text{ M}$  potassium iodide was saturated with iodine and was irradiated. The total iodine concentration ( $\text{I}_2 + \text{I}_3^-$ ) in this solution was  $1.80 \times 10^{-3} \text{ M}$ . Under these conditions the hydroperoxide yield was greatly reduced. Addition of an OH radical scavenger,  $0.1 \text{ M}$  methanol, decreased the iodine yield but increased the hydrogen peroxide yield (Table I).

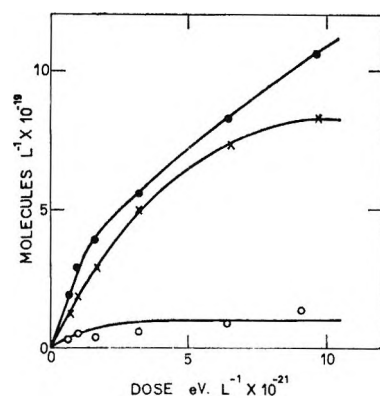


Figure 2. Yields of  $\text{I}_2$ ,  $\text{CH}_3\text{OOH}$ , and  $\text{H}_2\text{O}_2$  from aerated neutral solutions of  $\text{CH}_3\text{I}$  ( $0.1 \text{ M}$ ) and  $\text{KI}$  ( $10^{-2} \text{ M}$ ): ●,  $\text{I}_2$ ; X,  $\text{CH}_3\text{OOH}$ ; ○,  $\text{H}_2\text{O}_2$ .

Table I: Yields of  $\text{H}_2\text{O}_2$ ,  $\text{I}_2$ , and  $\text{CH}_3\text{OOH}$  from Aerated Solutions ( $[\text{O}_2] = 2.4 \times 10^{-4} \text{ M}$ ; Dose,  $9.8 \times 10^{20} \text{ eV l.}^{-1}$ ; pH  $\sim 6$ )

Composition, M		$G(\text{H}_2\text{O}_2)$	$G(\text{I}_2)$	$G(\text{CH}_3\text{OOH})$
$[\text{CH}_3\text{I}]$	$[\text{KI}]$			
$10^{-4}$	$10^{-3}$	0.70	0.05	0.10
$5 \times 10^{-4}$	0	0.70	0.28	0.80
$5 \times 10^{-4}$	$10^{-3}$	0.60	0.60	0.80
$10^{-3}$	$10^{-3}$	0.65	1.10	1.15
$1.5 \times 10^{-3}$	$10^{-3}$	0.40	1.35	1.70
$4 \times 10^{-3}$	$10^{-3}$	0.40	1.70	2.05
$10^{-2}$	$10^{-4}$			
$10^{-2}$	$10^{-3}$	$0.35 \pm 0.1$	$1.75 \mp 0.1$	2.10
$10^{-1}$	0	0.75	2.05	2.00
$10^{-1}$	$10^{-4}$			
$10^{-1}$	$10^{-3}$	$0.5 \pm 0.1$	$2.9 \mp 0.1$	2.10
$10^{-1}$	$10^{-2}$			
$10^{-1}^a$	$10^{-3}$	...	...	0.23
$10^{-1}^b$	0	1.10	1.45	1.80

<sup>a</sup> Saturated with iodine; i.e.,  $[\text{I}_2] = 1.3 \times 10^{-3} \text{ M}$ ,  $[\text{I}_3^-] = 5 \times 10^{-4} \text{ M}$ , and  $[\text{I}^-] = 5 \times 10^{-4} \text{ M}$ . <sup>b</sup> Contains  $0.1 \text{ M}$  MeOH.

Table II: Effect of Dose Rate on the Yields of  $\text{H}_2\text{O}_2$ ,  $\text{I}_2$ , and  $\text{CH}_3\text{OOH}$  from Aerated Solutions ( $[\text{CH}_3\text{I}] = 0.1 \text{ M}$ ,  $[\text{KI}] = 10^{-2} \text{ M}$ , pH 5)

Dose rate, eV l.⁻¹ min⁻¹	$G(\text{H}_2\text{O}_2)$ + $\text{I}_2$	$G(\text{CH}_3\text{OOH})$
$6.72 \times 10^{19}$	3.6	2.0
$1.31 \times 10^{20}$	3.5	2.06
$1.74 \times 10^{20}$	3.4	2.03
$3.22 \times 10^{20}$	3.6	2.06
$9.26 \times 10^{20}$	3.4	2.0

Following the suggestion<sup>3</sup> of Johnson and Simic that methane resulted from charge neutralization ( $\text{CH}_3\text{Br}^- + \text{H}_3\text{O}^+ \rightarrow \text{CH}_4 + \text{Br} + \text{H}_2\text{O}$ ) in the vapor-phase radiolysis of methyl bromide and water at  $140^\circ$ , we investigated whether any similar reaction would occur with

(7) C. E. Bricker and H. R. Johnson, *Ind. Eng. Chem. Anal. Ed.*, 17, 400 (1945).

$\text{CH}_3\text{I}^-$  in liquid water radiolysis. The experimental conditions are given in Table III. Since  $G(\text{CH}_3\text{I}^-) =$

**Table III:** Yields from Daeaerated Solutions of  $\text{CH}_3\text{I}^a$  (Dose,  $(1.5\text{--}4.5) \times 10^{21}$  eV l.  $^{-1}$ )

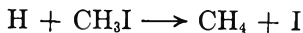
$[\text{CH}_3\text{I}]_t$ $M$	pH	$G(\text{H}_2)$	$G(\text{CH}_4)$
0.1 <sup>b</sup>	5	0.3	0
0.1	2	0.3	0
0.1	1.4	0.3	0
$10^{-3}$	6.5	0.5	0
$10^{-3}$	2	0.5	0
$10^{-3}$	1.3	0.45	0

<sup>a</sup> The volume of the sample irradiated was 25 ml. <sup>b</sup>  $G(\text{I}_2) = 0.17$  and  $G(\text{H}_2\text{O}_2) = 0.3$  at a dose of  $4.5 \times 10^{21}$  eV l.  $^{-1}$ .

$G_{e_{aq}} - [1 + (k_{\text{H}^+ + e_{aq}} - [\text{H}^+]/k_2[\text{CH}_3\text{I}])]$ ,  $G(\text{CH}_3\text{I}^-) = 1.8$  for  $0.1 M$   $\text{CH}_3\text{I}$  (pH 1.4). This value has been obtained from kinetic data available in literature.<sup>8</sup> It will be somewhat lower (1.3) based on our value of  $k_2$  (see the Discussion). However, it does not make any difference, since no methane could be detected although the pH was varied from 5 to 1.4. The fraction of  $\text{CH}_3\text{I}^-$  giving methane at any pH would be

$$\frac{1}{1 + \frac{k_d}{k_{\text{H}^+ + \text{CH}_3\text{I}^-} - [\text{H}^+]}}$$

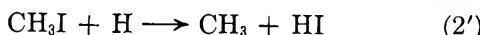
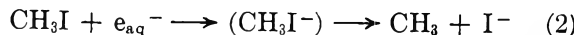
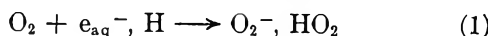
where  $k_d$  is the rate constant for the dissociation of  $\text{CH}_3\text{I}^-$  to  $\text{CH}_3$  and  $\text{I}^-$ . Experimentally,  $G(\text{CH}_4)$  may be taken as  $<0.01$ , since this was the lower limit for detection of methane by gas chromatography (flame ionization detector). Hence  $k_{\text{CH}_3\text{I}^- + \text{H}^+} < 10^6 M^{-1} \text{ sec}^{-1}$ , taking  $k_d > 1.25 \times 10^7 \text{ sec}^{-1}$ . The fact that no methane was obtained even in solutions which were  $10^{-3} M$  in  $\text{CH}_3\text{I}$  at pH 1.3 shows that the reaction



is unimportant. These two facts are also corroborated by the constancy of  $G(\text{CH}_3\text{OOH})$  over the pH range 5–1 (Table IV).

## Discussion

It is observed that  $G(\text{CH}_3\text{OOH})$  decreases with decreasing  $\text{CH}_3\text{I}$  concentration. This results from the competition between  $\text{CH}_3\text{I}$  and oxygen for solvated electrons and H atoms according to the reactions

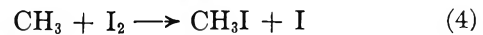


The transient  $\text{CH}_3\text{I}^-$  ion formed in reaction 2 can be expected to dissociate to the  $\text{CH}_3$  radical and  $\text{I}^-$  within a short time as explained below. Pulse radiolysis of

**Table IV:** Effect of pH on the Yields of  $\text{H}_2\text{O}_2$ ,  $\text{I}_2$ , and  $\text{CH}_3\text{OOH}$  from Aerated Solutions (Dose,  $9.81 \times 10^{20}$  eV l.  $^{-1}$ )

System	pH	$G(\text{H}_2\text{O}_2 + \text{I}_2)$	$G(\text{H}_2\text{O}_2)$	$G(\text{I}_2)$	$G(\text{organic peroxide})$
$[\text{CH}_3\text{I}] = 0.1 M$ , $[\text{KI}] = 10^{-2} M$	5	3.5	...	...	2.05
	3.1	3.4	...	...	2.10
	2.7	3.6	...	...	2.10
	1.4	3.8	...	...	2.05
$[\text{CH}_3\text{I}] = 5 \times 10^{-4} M$ , $[\text{KI}] = 10^{-3} M$	1	3.8	...	...	2.10
	6	...	0.60	0.60	0.80
	2.3	...	0.85	1.40	0.85
	6	2.30	...	...	1.20
$\text{C}_6\text{H}_{11}\text{I}$ (satd), $[\text{KI}] = 10^{-3} M$	2	3.78	...	...	1.77
	6	...	0.60	...	2.0
$[\text{Br}^-] = 10^{-3} M$					

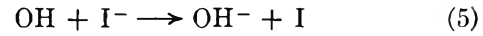
aqueous methyl iodide solutions<sup>2</sup> has indicated that the lifetime of  $\text{CH}_3\text{I}^-$  is less than 80 nsec, which was the response time of the apparatus. The intermediate participation of methyl and methylperoxy radicals in aerated solutions is indicated by the ultimate formation of methyl hydroperoxide and its suppression in the presence of iodine (Table I). Iodine is an efficient radical scavenger and can effectively remove methyl radicals even in the presence of oxygen



At  $[\text{I}_2 + \text{I}_3^-] = 1.8 \times 10^{-3} M$  and  $[\text{CH}_3\text{I}] = 0.1 M$ ,  $G(\text{CH}_3\text{OOH}) = 0.23$ . Taking  $k_{\text{I}_2 + e_{aq}^-} = 5.1 \times 10^{10} M^{-1} \text{ sec}^{-1}$  and  $k_2 = 1.65 \times 10^{10} M^{-1} \text{ sec}^{-1}$  it can be calculated that  $k_4/k_3 \approx 1.6$ , which is close to the value of 1.3 reported in the literature for  $\text{CH}_3$  radical reactions.<sup>2</sup> The work of Hamill and coworkers<sup>10</sup> on the radiolysis of 3-methylpentane glasses containing alkyl iodides has also indicated such a dissociative electron attachment.

## Formation of Methyl Hydroperoxide

The fate of the methylperoxy radicals largely depends upon the presence of other species. Most of our solutions contained added iodide ions which efficiently react with OH radicals giving  $\text{I}_2^-$  radical ions<sup>11</sup>



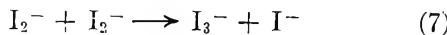
(8) M. Anbar and P. Neta, *Int. J. Appl. Radiat. Isotopes*, **18**, 493 (1967).

(9) J. K. Thomas, S. Gordon, and E. J. Hart, *J. Phys. Chem.*, **68**, 1524 (1964).

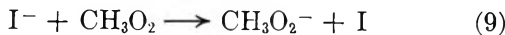
(10) D. W. Skelly, R. G. Hayes, and W. H. Hamill, *J. Chem. Phys.*, **43**, 2795 (1965).

(11) J. K. Thomas, *Trans. Faraday Soc.*, **61**, 702 (1965).

$I_2^-$  ions normally disproportionate in the absence of any other reacting species<sup>12, 13</sup>



We propose that either  $I^-$  or  $I_2^-$  reduces methylperoxy radicals giving hydroperoxide and iodine



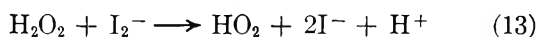
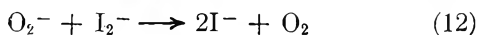
The remaining  $CH_3O_2$  radicals might disproportionate to give formaldehyde and methanol<sup>14</sup>



It is difficult to distinguish and say whether  $CH_3OOH$  arises from the reaction of  $CH_3O_2$  with  $I_2^-$  (reaction 8) or with  $I^-$  ions (reaction 9), since both reactions would give the same  $G(I_2)$ . Also reaction 9 shows that the disproportionation of  $CH_3O_2$  radicals can be suppressed if sufficient  $I^-$  is initially added. However, even with a 100-fold variation in KI from  $10^{-4}$  to  $10^{-2} M$  (Table I), 0.1 M  $CH_3I$  solutions give the same  $G(CH_3OOH)$ , which is significantly less than the total yield of H atoms and  $e_{aq}^-$  ( $G = 3.2$ ) that would have reacted with  $CH_3I$ . A competition between reactions 9 and 10 should also be sensitive to dose rate, which we have not observed (Table II). Any effect due to dose rate may not, however, be substantial when radical-radical reactions are competing, e.g., reactions 8 and 10. Thus we can conclude that  $I_2^- + CH_3O_2 \rightarrow I_2 + CH_3O_2^-$  is the reaction responsible for the peroxide formation.

A reaction sequence such as the above requires that  $\frac{1}{2}G_{OH} < G(I_2) \geq G(CH_3OOH)$ . This is supported by our iodine yields from 0.1 M methyl iodide solutions (Table I).

At lower methyl iodide concentrations the reaction  $O_2 + e_{aq}^- \rightarrow O_2^-$  becomes prominent and the resulting  $O_2^-$  competes for  $I_2^-$  as well as for  $CH_3O_2$  radicals



Reaction 11 has been suggested by Weiss<sup>15</sup> in his work on aqueous solutions of methane and oxygen, and in our own laboratory we have made detailed kinetic evaluation of alkylperoxy radical reactions with  $O_2^-$ .<sup>16</sup> Reaction 12 is responsible for low iodine yields at low concentrations of methyl iodide (Table I). Reaction 13 seems to be responsible for the slight reduction of  $G(H_2O_2)$  in the presence of KI.

### Material Balance and Competition for Reducing Radicals

Considering reactions 1–13 (except reaction 4) as responsible for the various products, we can derive an expression for material balance. Reactions 5 and 8 or 9

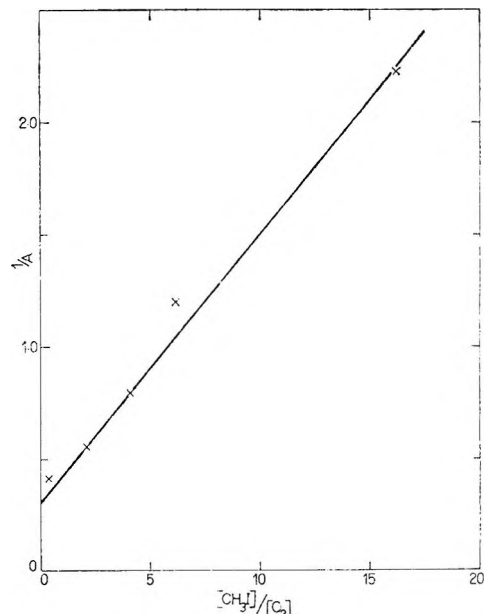
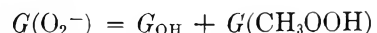
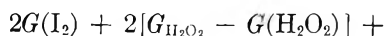
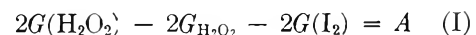


Figure 3. Plot of  $1/G(O_2^-)$  (from eq I) vs.  $[CH_3I]/[O_2]$ .

give rise to iodine, while reactions 12 and 13 destroy iodine. Then we can write, for iodine atoms



The second and third terms on the left-hand side of the above equation account for the I atoms initially formed but subsequently converted to  $I^-$  (reactions 12 and 13). The right-hand side of the equation represents the total number of iodine atoms that have ever been formed (reactions 5 and 9). It is easily verified that any contribution due to  $O_2^- + CH_3O_2 \rightarrow CH_3O_2^- + O_2$  does not alter the relation. Rearranging the equation we can get



Since at pH 6

$$G(O_2^-) = \frac{G_{e_{aq}^-}}{1 + k_2[CH_3I]/k_1[O_2]} +$$

$$\frac{G_H}{1 + k_2'[CH_3I]/k_1'[O_2]}$$

and assuming that  $k_2/k_1 \approx k_2'/k_1'$ , a plot of  $[CH_3I]/$

(12) M. Anbar, D. Meyerstein, and P. Neta, *J. Phys. Chem.*, **68**, 2967 (1964).

(13) T. Sawai, Y. Shinozaki, and G. Meshitsuka, *Bull. Chem. Soc. Jap.*, **39**, 951 (1966).

(14) (a) J. H. Raley, L. M. Porter, F. F. Rust, and W. E. Vaughan, *J. Amer. Chem. Soc.*, **73**, 15 (1951); (b) D. F. Dever and J. G. Calvert, *ibid.*, **84**, 1362 (1962).

(15) G. R. A. Johnson and J. Weiss, *Chem. Ind.*, 13, 358 (1955).

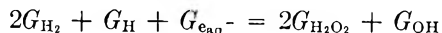
(16) L. V. Shastri, K. Srinivasan, and K. V. S. Rama Rao, *Proc. AEET Symp. Nucl. Radiat. Chem., India*, 43 (1967).

$[O_2]$  vs.  $1/A$  should give a straight line with an intercept of  $1/(G_{e_{aq}} + G_H)$ . Taking  $G_{OH} = 2.4$  and  $G_{H_2O_2} = 0.7$  at pH 6, the values of  $G(O_2^-)$  have been calculated and are summarized in Table V and are plotted in Figure 3. From the plot it is calculated that  $k_2/k_1 = 0.4$  and  $G_{e_{aq}} + G_H = 3.2$ . This is in agreement with other estimates of  $G_{e_{aq}} = 2.6$  and  $G_H = 0.6$ .<sup>17</sup> Our plot does not distinguish H and  $e_{aq}$ , since either of them may have comparable reactivity with  $CH_3I$  or oxygen. From measurement of absolute rate constants, by pulse radiolysis,  $k_2/k_1$  appears to be 0.8.<sup>8</sup> The discrepancy between this and our value is not due to any increased solubility of oxygen in methyl iodide solutions which was verified experimentally.

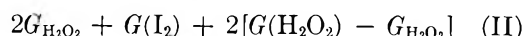
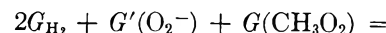
**Table V:**  $G(O_2^-)$  and  $G(CH_3O_2)$  According to Eq I and II, Respectively, Calculated for the Data in Table I for Solutions Containing  $CH_3I$  and KI

$[CH_3I]/[O_2]$	$G(O_2^-)$ (A)	$G(CH_3O_2)$ (B)	$A + B$
0.416	2.4	0.6	3.0
2.06	1.8	1.2	3.0
4.1	1.25	1.75	3.0
6.2	0.8	2.2	3.0
16.5	0.45	2.55	3.0

Let us consider whether all  $CH_3O_2$  radicals that have been formed give only  $CH_3OOH$ . The material balance equation for primary yields in radiolysis of water is given by



Since the reducing radicals give  $O_2^-$  and  $CH_3O_2$ , and OH radicals give iodine atoms, we can write from reactions 8 and 11-13



where  $G_{H_2O_2} = 0.7$ ,  $G_{H_2} = 0.4$ , and  $G'(O_2^-) = G(CH_3OOH) - G(I_2)$ .

For example, for  $10^{-4} M$   $CH_3I$  solutions, analysis gives  $G(CH_3OOH) = 0.1$ ,  $G(I_2) = 0.05$ , and  $G(H_2O_2) = 0.7$  (Table I). One can verify according to eq II that  $0.8 + 0.05 + G(CH_3OO) = 2 \times 0.7 + 0.05$  or  $G(CH_3O_2) = 0.6$ , while only one-tenth of these  $CH_3O_2$  react to give  $CH_3OOH$ . Similar calculations for other data yield  $G(CH_3O_2)$  values at other concentrations of  $CH_3I$ . These are also given in Table V. It may be noted that  $G(CH_3O_2) + G(O_2^-) = 3.0$ , which is about equal to the total reducing radicals in the radiolysis of water.

### Radiolysis in the Absence of Potassium Iodide

It is interesting to note that  $0.1 M$   $CH_3I$  solutions without potassium iodide still give about the same  $G(CH_3OOH)$  as those containing KI (Table I). Methyl

iodide undergoes hydrolysis in aqueous solutions, and the presence of  $I^-$  is unavoidable even in freshly prepared solutions. We have estimated that for  $[CH_3I] = 0.1 M$  the concentration of iodide ion arising by virtue of hydrolysis would be about  $10^{-5} M$  in 1 hr.  $I_2^-$  could arise from the reaction sequence



The I atom from reaction 14 could either be the  $(ICH_3I)$  complex observed by Thomas or the  $(IH_2O)$  complex proposed by him.<sup>2</sup> Although in that work  $I_2^-$  has not been observed in the absence of potassium iodide, our much lower dose rate of  $3.27 \times 10^{20} eV l^{-1} min^{-1}$  as compared with his dose rate of  $\approx 10^{19} eV l^{-1} \mu sec^{-1}$  would certainly favor the reaction of  $(ICH_3I)$  with  $I^-$  ( $\approx 10^{-5} M$ ), existing in solution because of hydrolysis. At the very high intensities of pulse radiolysis a second-order disproportionation ( $k = 3 \times 10^9 M^{-1} sec^{-1}$ ) takes precedence. At low concentrations of  $I^-$ , formed on hydrolysis, it is reasonable to assume an equilibrium between I atoms and  $I^-$  ions. While reaction 8 utilizes  $I_2^-$ , disturbing this equilibrium, I atoms destroy  $CH_3O_2$  radicals to some extent, e.g.



The net effect of reactions 8, 10, and 15 would be a decrease in  $G(I_2)$ , which has actually been observed for solutions of methyl iodide alone (Table I). An iodide ion concentration in excess of  $10^{-4} M$  seems adequate to suppress I atoms and to promote reactions 7, 8, and 10.

Addition of  $0.1 M$  methanol increases  $G(H_2O_2)$  but decreases  $G(I_2)$  and  $G(CH_3OOH)$  (Table I). The small decrease in organic peroxide may not warrant any great efficiency of methanol for reaction with  $CH_3$  radicals, since  $k_{CH_3+O_2}/k_{CH_3+CH_3OH} = 2 \times 10^7$ .<sup>2</sup> However, methanol could compete with  $CH_3I$  for OH radicals, decreasing the I atoms or  $I_2^-$  yield. The resulting  $CH_2OH$  radicals give  $HO_2$  radicals and formaldehyde in the presence of oxygen.<sup>18</sup> While some  $HO_2$  radicals undergo reaction 11 to give the organic peroxide, the rest of them would disproportionate giving additional  $H_2O_2$ . If reaction 14 followed by reaction 8 is responsible for  $G(I_2) = 1.45$ , then  $k_{OH+CH_3OH}/k_{OH+CH_3I} = 0.65$  for  $G_{OH} = 2.4$ .

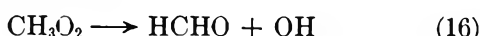
### Reasons for High $I_2$ Yields

The value of  $G(I_2) = 2.9$  for solutions of  $0.1 M$   $CH_3I$  and added  $I^-$  (Table I) is inconsistent with the primary yields of water decomposition, viz.,  $G_{e_{aq}} = 2.6$ ,  $G_H = 0.6$ , and  $G_{OH} = 2.4$ , which should give a maximum of  $G(I_2) = 2.3$ . A unimolecular dissociation of  $CH_3O_2$  radicals not undergoing reaction 8 to give formaldehyde

(17) E. M. Fielden and E. J. Hart, *Radiat. Res.*, 32, 564 (1967).

(18) E. J. Hart, J. K. Thomas, and S. Gordon, *Radiat. Res. Suppl.*, 4, 74 (1964).

and OH radicals could explain the additional iodine. In other words, step 10 should be replaced by reaction 16, as suggested by Bates and Spence.<sup>19</sup> Such a re-



action has also been suggested by Norrish in his extensive work on the autoxidation of methane at high temperatures<sup>20</sup> and in the flash photolysis of methyl iodide at 140°.<sup>21</sup> However, other workers<sup>22</sup> have concluded that the dissociation of  $\text{CH}_3\text{O}_2$  radicals according to reaction 16 is insignificant up to 50°. The absence of additional iodine at  $[\text{CH}_3\text{I}] = 0.01 M$  (Table I) also indicates that reaction 16 may not be important in solution at room temperature. The significant point, however, is the fact that while  $\text{CH}_3\text{O}_2$  radicals preferentially dissociate or disproportionate in the gas phase, their main reaction in solution in the presence of reactive anions is the formation of hydroperoxide. It would be interesting to study the chemistry of  $\text{CH}_3\text{O}_2$  radicals in solution when no anions likely to react with them are formed. Photolysis of methyl iodide solutions in organic solvents has given ample evidence for the formation of methyl radicals and iodine atoms.<sup>23</sup>

However, this work has not been done in the presence of oxygen.

It is quite possible that some scavenging of spur-electrons at high methyl iodide concentration is responsible for the additional iodine observed. For degassed solutions of 0.1 M  $\text{CH}_3\text{I}$  we found that  $G(\text{H}_2) = 0.3$ .

In conclusion, we have considered the possible reactions of  $\text{CH}_3\text{O}_2$  and  $\text{I}_2^-$  radicals and have proposed a mechanism consistent with our results. A kinetic evaluation of the reactions of the intermediates is quite complex. Direct observation of the transient-species spectra by the pulse radiolysis technique would be more convenient for determining the kinetics.

(19) J. R. Bates and R. Spence, *J. Amer. Chem. Soc.*, **53**, 1689 (1931).

(20) R. G. W. Norrish, *Discussions Faraday Soc.*, **10**, 269 (1951).

(21) J. F. McKellar and R. G. W. Norrish, *Proc. Roy. Soc., A263*, 51 (1961).

(22) (a) J. A. Gray, *J. Chem. Soc.*, 3150 (1952); (b) W. J. Blaedel, R. A. Ogg, and A. A. Leighton, *J. Amer. Chem. Soc.*, **64**, 2499 (1942).

(23) R. F. Pottie, W. H. Hamill, and R. R. Williams, Jr., *ibid.*, **80**, 4224 (1958).

## The N-Methylpropionamide-Water System. Densities and

### Dielectric Constants at 20-40°<sup>1</sup>

by Thomas B. Hoover

National Bureau of Standards, Washington, D. C. 20234 (Received May 24, 1968)

Densities and dielectric constants of the N-methylpropionamide (NMP)-water system were measured at 20, 30, and 40°. The curve of excess molar volume of the system vs. mole fraction of water was essentially independent of temperature and had a minimum of  $-1.32 \text{ cm}^3$  at 0.6 mol fraction water. The molar volume of transfer of NMP from the pure liquid to a dilute solution in water had a minimum of  $-6.0 \text{ cm}^3$  at 0.9 mol fraction of water. The dielectric data for the system were analyzed in terms of correlation factors calculated on the basis that the square of the gas-phase moment and the high-frequency dielectric constant for the mixture were linear functions of the mole fractions of the components. The structural properties of the system are discussed with respect to the corresponding data for the mixtures of water with N-methylacetamide, ethanol, or acetic acid. NMP and water each exert a strong effect on the structure of the other.

### Introduction

The N-monosubstituted amides are of interest for their remarkably high dielectric constants, a property which has been attributed to extensive chainwise association through hydrogen bonding.<sup>2</sup> Furthermore, the miscibility of these compounds with water and several nonpolar organic liquids permits the preparation of mixed solvents covering an extremely wide

range of dielectric constants. N-Methylpropionamide (NMP)-water mixtures have been employed in this

(1) Presented in part at the 154th National Meeting of the American Chemical Society, Chicago, Ill., Sept 1967.

(2) (a) S. J. Bass, W. I. Nathan, R. M. Meighan, and R. H. Cole, *J. Phys. Chem.*, **68**, 509 (1964); (b) R.-Y. Lin and W. Dannhauser, *ibid.*, **67**, 1805 (1963); (c) S. Mizushima, T. Simanouti, S. Nagakura, K. Kuratani, M. Tsuboi, H. Baba, and O. Fujioka, *J. Amer. Chem. Soc.*, **72**, 3490 (1950).

laboratory in an investigation of solvent effects on the kinetics of the hydrolysis of acetal.<sup>3</sup> The dielectric constant measurements obtained for that study have recently been extended and supplemented by density determinations.

The structural properties of the mixed system NMP-water are of interest since each component is highly structured through hydrogen bonding, but in different ways. Many of the unique properties of water are determined by its three-dimensional network of bonding,<sup>4</sup> while NMP exhibits remarkably long chains of linear associations.<sup>2a</sup> Density and dielectric constant measurements were expected to shed some light on the configuration of the mixtures. Hovermale, Sears, and Plucknett<sup>5</sup> have used these properties to study the structure of binary mixtures of N-methylacetamide (NMA) with water and aliphatic alcohols and have interpreted the associations in terms of the apparent Debye polarizations of the mixtures.

## Experimental Section

The preparation and purification of NMP have been described.<sup>6</sup> The material was reclaimed by repeated fractional distillations after having been used for conductivity measurements and had a specific conductance of  $1.16 \times 10^{-7} \text{ ohm}^{-1} \text{ cm}^{-1}$  ( $30^\circ$ ) ( $n^{25}\text{D} = 1.4350$  and  $\text{fp} = -30.9^\circ$ ). Gas chromatography on a Carbowax 20M liquid phase showed 0.11% water and no propionic acid, while Karl Fischer titration of a 100-cm<sup>3</sup> sample showed less than 0.01% water.

Density measurements were made in a bicapillary pycnometer of approximately 20 cm<sup>3</sup> capacity. The pycnometer was calibrated with distilled water at each temperature. The standard error of the calibration was 0.01%. Densities of the three most dilute solutions of NMP in water were also measured in each of three 50-cm<sup>3</sup> single-capillary pycnometers at  $30^\circ$ . The standard deviations of the densities of each of these solutions were less than 0.01%.

Dielectric constants were measured at audiofrequencies by the substitution method with a Jones-Dike conductivity bridge (Leeds and Northrup No. 4666). The bridge had, in series with the X arm, a 14-ohm coil used to balance the resistance of the slide-wire fine-adjustment circuit of the S arm. This coil was shorted so that only the lead resistance (less than 0.02 ohm) was in series with the reference capacitor. The inequality of the distributed capacitances of the ratio arms was adjusted to less than 2 pF. A calibrated General Radio Type 722-H capacitor and a fixed 1000-ohm shunt were connected in parallel across the unknown (X) arm. The shunt ensured that no changes in the bridge setting above the 100-ohm decade would have to be made as the cell was inserted or removed from the circuit. The difference between the bridge coil capacitances for the two settings under these circumstances was assumed to change the balance condi-

tion by less than 5 pF. All of the solutions having dielectric constants greater than 90 actually required adjustment only of the 10-ohm and lower decades. The maximum specific conductance of the solutions was  $8.8 \times 10^{-6} \text{ ohm}^{-1} \text{ cm}^{-1}$  (0.884 mol fraction of water at  $40^\circ$ ).

A two-terminal borosilicate glass cell with concentric, cylindrical platinum electrodes was used. The dielectric constant,  $\epsilon$ , was calculated from the observed capacitance,  $C$ , in picofarads, by the equation

$$\epsilon = (C - a)/b \quad (1)$$

The constants  $a$  and  $b$  and their standard errors were obtained by fitting the equivalent form

$$C = a + b\epsilon \quad (2)$$

to the five data points for nitrobenzene ( $35^\circ$ ), water ( $20^\circ$ ), and NMP ( $20$ ,  $30$ , and  $40^\circ$ ). The reference values of these standards were obtained with an absolute (three-terminal) cell and a General Radio Type 1615-A capacitance bridge. The constants of eq 2 and their standard errors were  $a = 2.7 \pm 0.9$  and  $b = 8.149 \pm 0.007$ . The precision of the calibration supports the assumption that variations in the bridge coil intercapacitances were not a serious source of error.

Measurements were made at 1, 2, 4, 8, and 16 kHz. The variation of the measured capacitance over the experimental frequency range was greatest for the water-rich mixtures but did not exceed 1%. The extrapolated capacitance did not differ from the value measured at 8 kHz by more than 0.2% and the uncertainty in the correction for polarization is probably not greater than 0.2%. The indicated precision of the cell calibration was 0.1%, and errors in the calibration of the reference capacitor or in temperature control were less than this. The over-all uncertainty is  $\pm 1\%$  based on a standard error of 0.2% and an allowance of  $\pm 0.5\%$  for bias.

The density and dielectric constant values for pure NMP were obtained as a part of a more extensive characterization program,<sup>7</sup> based on several additional samples of NMP. The densities obtained with the pycnometer of the present study were within  $\pm 0.02\%$  of the pooled results obtained with three quartz single-capillary pycnometers and two dilatometers. Since NMP was used as a calibrating fluid for the dielectric cell, values of  $\epsilon$  obtained with the three-terminal cell are reported in Table I. The dielectric constants reported

- (3) R. K. Wolford and R. G. Bates, *J. Phys. Chem.*, **66**, 1496 (1962).
- (4) (a) J. D. Bernal and R. H. Fowler, *J. Chem. Phys.*, **1**, 515 (1933);  
(b) L. Pauling in "Hydrogen Bonding," D. Hadzi, Ed., Pergamon Press Ltd., London, 1959, p 1.
- (5) R. A. Hovermale, P. G. Sears, and M. K. Plucknett, *J. Chem. Eng. Data*, **8**, 490 (1963).
- (6) T. B. Hoover, *J. Phys. Chem.*, **68**, 876 (1964).
- (7) C. G. Malmberg and T. B. Hoover, unpublished results.

**Table I:** Dielectric Constants and Densities of N-Methylpropionamide-Water Mixtures

$x_2$ , mol fraction of H <sub>2</sub> O	20°		30°		40°	
	$\epsilon$	$\rho_t$ g/cm <sup>3</sup>	$\epsilon$	$\rho_t$ g/cm <sup>3</sup>	$\epsilon$	$\rho_t$ g/cm <sup>3</sup>
0	185.3	0.93449	166.7	0.92647	150.6	0.91847
0.0174	178	0.9355	161	0.9275	146	0.9194
0.0435	171	0.9364	155	0.9286	141	0.9205
0.0880		0.9388		0.9309		0.9229
0.2779		0.9501		0.9421		0.9341
0.3541	111	0.9553	103	0.9473	96	0.9393
0.4909	97	0.9665	91	0.9586	86	0.9503
0.7571	85	0.9912	81	0.9834	77	0.9752
0.8842	83	0.9992	79	0.9929	76	0.9860
0.9283				0.99325		
0.9513				0.99331		
0.9846				0.99360		
1.0000	80.10	0.99820	76.55	0.99565	73.15	0.99222

here for pure NMP are 9% higher than those of ref 2a<sup>8</sup> and 1.5% higher at 30° than those of Leader and Gormley.<sup>9</sup> The temperature variation of  $\epsilon$  is in good agreement with ref 2a but is significantly greater than that of ref 9.

Solutions were made by weight, with buoyancy corrections, and both the NMP and the solutions were stored and transferred under argon. The concentrations (given in mole fraction of water), densities, and dielectric constants are listed in Table I.

### Volumetric Behavior

The volumetric behavior of the system NMP-water is shown as the excess molar volume,  $V^E$ , in Figure 1. This quantity, values of which at 30° are plotted, is nearly independent of temperature over the range of observations. For comparison, the corresponding data for the systems water-NMA, water-acetic acid, and water-ethanol are included. These examples were intended to represent a wide variation of possible organic solute-water interactions through hydrogen bonding, but within a small range of molar volumes. They include the next homolog of NMP, the strongly dimerized acetic acid, and the (presumably) more waterlike ethanol. The phenomenon of contraction (negative  $V^E$ ) when a hydrogen-bonding liquid is added to water is quite general, but apparently only the poly(ethylene glycol) ethers<sup>10</sup> show a greater negative excess volume than NMP. Such a contraction is frequently interpreted<sup>11</sup> in terms of the two-structure model for water.<sup>12</sup> On the basis of the density functions used by Némethy and Scheraga,<sup>13</sup> a shift in the equilibrium between low-density structured "icebergs" and more dense "monomer" water by the addition of NMP cannot account for the minimum  $V^E$  for this system.

In the predominantly aqueous range of compositions it is helpful to consider the apparent volume change on transferring 1 mol of the organic component from the pure liquid to a dilute solution in water. In Figure 2 this change,  $\Delta V_2$ , is shown for four polar solutes

$$\Delta V_2 = \Phi_2 - \bar{V}_2 = V^E/x_2 \quad (3)$$

where  $\bar{V}_2$  is the molar volume of the pure organic component and  $\Phi_2$  is its apparent molar volume in the solution at mole fraction  $x_2$ . Both amides, like ethanol, show a pronounced minimum in  $\Delta V_2$  near 0.1 mol fraction. The interpretation of this behavior in the case of

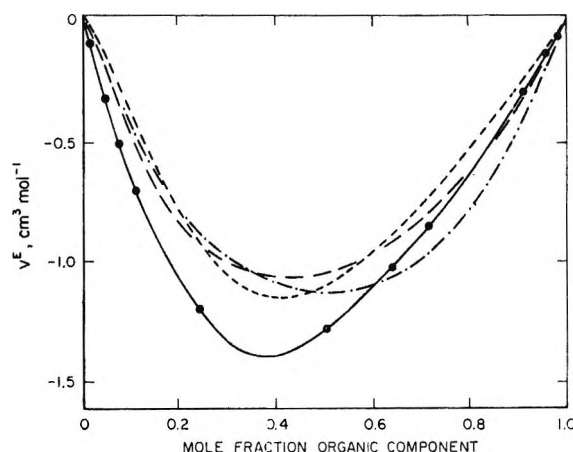


Figure 1. Excess molar volume at 30°: ●, NMP, this work; — · —, NMA;<sup>6</sup> — — —, ethanol; - · - · -, acetic acid.

(8) The low result seems to have been almost completely accounted for by adventitious water in the sample (R. H. Cole, private communication).

(9) G. R. Leader and J. F. Gormley, *J. Amer. Chem. Soc.*, **73**, 5731 (1951).

(10) W. J. Wallace, C. S. Shephard, and C. Underwood, *J. Chem. Eng. Data*, **13**, 11 (1968).

(11) F. Franks and D. J. G. Ives, *Quart. Rev.*, **20**, 1 (1965).

(12) (a) H. S. Frank and W-Y. Wen, *Discussions Faraday Soc.*, **24**, 133 (1957); (b) A thorough and recent review of theories of water structure is given by W. Drost-Hansen, "Equilibrium Concepts in Natural Water Systems," *Advances in Chemistry Series*, No. 67, American Chemical Society, Washington, D. C., 1967.

(13) G. Némethy and H. A. Scheraga, *J. Chem. Phys.*, **36**, 3401 (1962). If the addition of a small amount of NMP converted all the water to the dense form, the maximum contraction would be 1.325 cm<sup>3</sup>/mol at 30°. At 60 mol % water the calculated contraction is  $0.6 \times 1.325 = 0.795$  cm<sup>3</sup>/mol, while the experimental value is 1.32 cm<sup>3</sup>/mol.

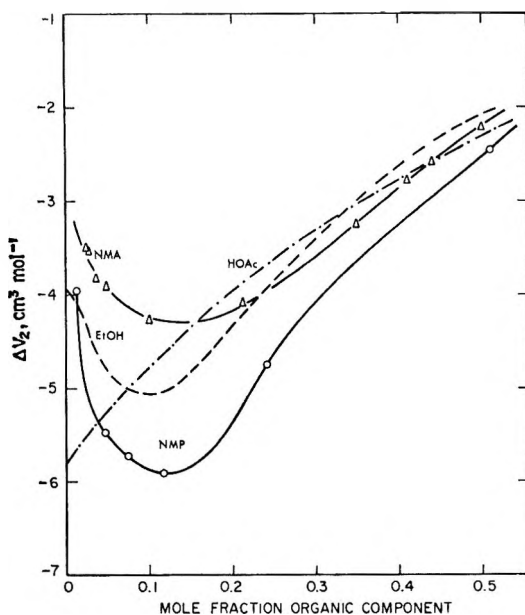


Figure 2. Molar volume of transfer from organic liquid to aqueous solution at 30°; O, NMP, this work; Δ, NMA;<sup>6</sup> — — —, ethanol; - - -, acetic acid.

the alcohols has been discussed by Franks and Ives.<sup>11</sup> The minimum in  $\Delta V_2$  results from competing effects on water due to the polar and nonpolar ends of the organic molecule. The hydroxyl end of the alcohol is structure breaking while the hydrocarbon end reinforces a low-density structure in the water. A similar interpretation probably applies as well to the amides. The apparent molar volume of transfer for acetic acid is characteristic of solutes, such as dioxane, having strong specific interactions with water, and reaches its extreme value in the infinitely dilute solution.

That the minimum in  $\Delta V_2$  for ethanol and both amides occurs at a finite concentration indicates a cooperative effect among the organic molecules. The contraction on adding the solute is greater when some is already present in the solution, within rather narrow limits. Although it is tempting to consider that self-association of the solute through hydrogen bonding may be reducing the structure-breaking effects of the polar groups upon water, the association constant of NMA in aqueous solution<sup>14</sup> rules out such an explanation. At mole fractions less than 0.5, NMA is almost completely unassociated. A more satisfying interpretation lies in the cooperative, specific participation of the solute molecules with water to form a clathrate type of structure.<sup>11</sup> As Franks and Ives<sup>11</sup> are careful to point out, it is not clear what structure is stabilized, since crystalline clathrate hydrates of these solutes are not known but evidently the organic molecules help to form or to stabilize "holes" in the water structure. These holes are able to accommodate, at least partially, the solute molecules with a consequent economy of volume. On this basis, the maximum structural

stabilization occurs at the concentrations corresponding to the minimum in the  $\Delta V_2$  curves. These concentrations, representing 6–9 mol of water/mol of organic solute, are consistent with the stoichiometry of known clathrate hydrates.<sup>15</sup>

In the concentration range where the curves of  $\Delta V_2$  for NMA and NMP are nearly parallel, the vertical displacement is a measure of the chain length, or  $-\text{CH}_2-$ , effect.<sup>13</sup> The size of this effect is considerably smaller than the average value of  $-1.2 \text{ cm}^3/\text{CH}_2-$  found by Friedman and Scheraga<sup>16</sup> from measurements on a series of normal alcohols but is closer to the values found when the  $-\text{CH}_2-$  was introduced between the hydroxyl groups of glycols.<sup>17</sup>

### Dielectric Behavior

The dielectric constants of NMP–water mixtures are portrayed in Figure 3 in terms of a deviation function,  $\Delta\epsilon$ , representing the deviation from an ideal volume mixture relation.

$$\Delta\epsilon = \epsilon_{12} - \varphi_1\epsilon_1 - \varphi_2\epsilon_2 \quad (4)$$

where  $\varphi_1$  and  $\varphi_2$  are the volume fractions of the components based on the densities of the pure liquids. It has been found that the dielectric constants of many polar mixtures can be represented as linear functions of the volume fraction,<sup>18</sup> and the alcohol–water mixtures show only moderate positive deviations from this relation.<sup>11</sup> Comparison on a volume fraction basis largely compensates for the "dipole-dilution" effect discussed by Franks and Ives.<sup>11</sup> The very large negative deviations shown in Figure 3 for the NMP system, then, are clear evidence of changes in the degree of alignment of dipoles with changing composition. In the alcohol

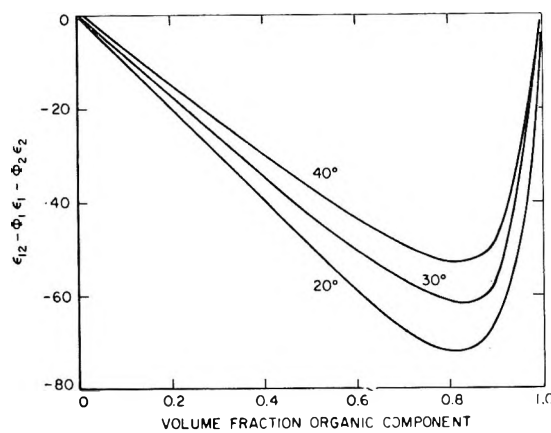


Figure 3. Dielectric constant deviations (NMP–water).

(14) I. M. Klotz and J. S. Franzen, *J. Amer. Chem. Soc.*, **84**, 3461 (1962).

(15) D. N. Glew, *J. Phys. Chem.*, **66**, 605 (1962).

(16) M. E. Friedman and H. A. Scheraga, *ibid.*, **69**, 3795 (1965).

(17) K. Nakanishi, N. Kato, and M. Maruyama, *ibid.*, **71**, 814 (1967).

(18) D. Decroocq and J. C. Jungers, *Compt. Rend.*, **252**, 1454 (1961).

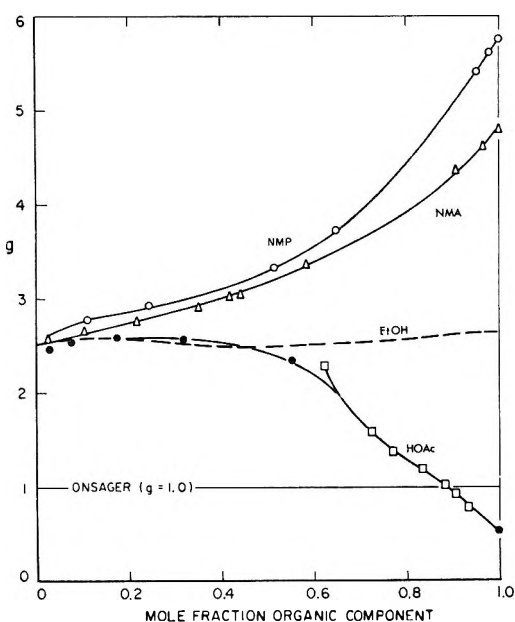


Figure 4. Correlation parameters: O, NMP (30°), this work; Δ, NMA (30°);<sup>5</sup> — — —, ethanol (25°) (J. H. Hall and H. O. Phillips, *West Va. Univ. Bull., Eng. Expt. Sta. Research Bull.*, **26**, 26 (1954)); ●, acetic acid (25°);<sup>25</sup> □, acetic acid (25°).<sup>24</sup>

systems the nearest analog is in the small dip shown by *t*-butyl alcohol containing 15 mol % water.<sup>19</sup> The water-N-butylacetamide system investigated by Reynaud<sup>20</sup> is qualitatively similar to water-NMP and the sharp decrease in  $\epsilon$  as small amounts of water were added to the amide was ascribed to the breaking of amide-amide hydrogen bonds by the water.

The degree of orientation of dipoles in pure liquids is indicated by the Kirkwood correlation parameter,  $g$ , but there is no simple theoretical treatment that is valid for mixtures of polar molecules. (See Figure 4.) The variation of  $g$  with composition was estimated by an adaptation of the equation given by Cole<sup>21</sup> (eq 5), where  $\mu$  is the permanent dipole moment,  $N/V$  is

$$\frac{4\pi N \mu^2}{9kTV} = \frac{(\epsilon_0 - \epsilon_\infty)(2\epsilon_0 + \epsilon_\infty)}{\epsilon_0(\epsilon_\infty + 2)^2} \quad (5)$$

the number density (molecules per cubic centimeter), and  $\epsilon_0$  and  $\epsilon_\infty$  are the low- and high-frequency dielectric constant limits, respectively. In the mixtures it was assumed that the appropriate values of  $\mu^2$  and  $\epsilon_\infty$  in eq 5 are linear functions of the mole fractions of the components. Gas-phase values were used for  $\mu$ ,<sup>22</sup> and  $\epsilon_\infty$  for water and acetic acid components were taken as 10% greater than the square of the refractive index;<sup>23</sup> the values of  $\epsilon_\infty$  used for the other components were the following: ethanol, 2.20;<sup>23</sup> NMA, 2.51,<sup>2a</sup> and NMP, 2.54.<sup>2a</sup>

On the basis of the empirical  $g$  factors, the two amides resemble each other, differing mainly in the extent of as-

sociation in the pure liquids, but differ sharply from ethanol and acetic acid. As the concentration of the organic component increases, the water structure is broken down and there is less cooperative interspecies association. Above 50 mol % amide the dielectric properties of the solution are dominated by the amide. The near constancy of  $g$  for mixtures of ethanol and water has been pointed out before.<sup>11</sup> The acetic acid-water system is difficult experimentally because of the high conductances encountered. Campbell and Gieskes<sup>24</sup> were not able to carry their measurements of the dielectric constant above 45 mol % water. Borovikov and Fialkov,<sup>25</sup> using a resonance technique, reported values for the entire composition range. Their results suggest that acetic acid is very similar to ethanol in the essentially aqueous region. At more than 90 mol % acetic acid,  $g$  becomes less than 1, as a result of the antiparallel coordination of the dimers.<sup>26</sup>

### Conclusions

With respect to the volumetric behavior in dilute solutions in water, NMP resembles its homolog, NMA, qualitatively but shows more pronounced effects. At less than 0.1 mol fraction of NMP there is evidence for very strong reinforcement of the water structure around the organic molecules, leading to a deep minimum in  $\Delta V_2$ . At higher concentrations the greater structure-making influence of NMP relative to NMA follows, at least qualitatively, the predictions based on the greater length of the hydrocarbon moiety.

The dielectric data reveal a much closer resemblance between the two amides than between any other pair of the organic solutes. The two sets of evidence, density and dielectric constant, show quite clearly that NMP and water each have a strong effect on the structure of the other. In the primarily aqueous solutions this effect is shown by increased density, while in the organic-rich solutions it is revealed by a sharp decrease in the dielectric constant.

*Acknowledgment.* The author is indebted to Professor H. S. Frank for his comments and general suggestions concerning the interpretation of these results.

- (19) A. C. Brown and D. J. G. Ives, *J. Chem. Soc.*, 1608 (1962).
- (20) R. Reynaud, *Compt. Rend., Ser. C*, **266**, 489 (1968).
- (21) R. H. Cole, *J. Chem. Phys.*, **27**, 33 (1957).
- (22) R. D. Nelson, Jr., D. R. Lide, Jr., and A. A. Maryott, "Selected Values of Electric Dipole Moments for Molecules in the Gas Phase," National Bureau of Standards Report NSRDS-NBS1C, U. S. Department of Commerce, Washington, D. C., Sept 1967.
- (23) W. Dannhauser and L. W. Bahe, *J. Chem. Phys.*, **40**, 3058 (1964).
- (24) A. N. Campbell and J. M. T. M. Gieskes, *Can. J. Chem.*, **42**, 1379 (1964).
- (25) Yu. Ya. Borovikov and Yu. Ya. Fialkov, *Elektrokhimiya*, **1**, 1106 (1965).
- (26) C. P. Smyth and H. E. Rogers, *J. Amer. Chem. Soc.*, **52**, 1824 (1930).

# On the Concentration Dependence of Transport Coefficients in Multicomponent Mixtures

by Hansjürgen Schönert<sup>1</sup>

*Department of Chemistry, Georgetown University, Washington, D. C. 20007 (Received May 27, 1968)*

It is shown that the transport coefficients of thermodynamics of irreversible processes can be expanded into a Taylor series with respect to the concentrations. The general behavior of the leading terms is evaluated. Friction coefficients are discussed. This may be used to show some conclusions as to the transport properties of multicomponent solutions in which one or more components have vanishingly small concentrations. Some examples are given.

## Introduction

In two previous publications<sup>2</sup> we have shown how the phenomenological equations of thermodynamics of irreversible processes can be rearranged so as to contain only conventional transport coefficients (*i.e.*, transport numbers, diffusion coefficients, and sedimentation coefficients) and how these equations can be transformed so as to apply to the laboratory reference frame. In order to describe a system of  $n$  neutral and ionic constituents in a solvent,  $\frac{1}{2}n(n + 1)$  conventional transport coefficients are required. The corresponding expressions, eq A2 and A5 (symbols and equations indicated with A refer to those of ref 2), contain the same number of phenomenological coefficients  $a_{ik}$ , *viz.*, one gross mobility for each of the  $n$  constituents plus  $\frac{1}{2}n(n - 1)$  diffusion coefficients for the neutral and ionic constituents, the latter combined so as to form electroneutral combinations.

Although all possible transport processes are in principle included, these equations have only limited applicability in view of the difficult and time-consuming measurements required for the experimental determinations of  $\frac{1}{2}n(n + 1)$  coefficients. Also, the integration of the system of coupled partial differential equations, interrelated by the continuity equations, is feasible only in simple cases. Then the question arises whether, in those cases where only an approximate insight into the phenomena is required, rules can be established for the determination of the order of magnitude of coefficients and their concentration dependence so as to simplify the system of equations while retaining the essential predictions of the theory.

A general statistical-kinetic theory of transport processes in multicomponent systems has not yet been developed to the extent that coefficients can be calculated from it. In order to establish the above-mentioned rules one has to rely on experimental results and on certain principles of continuity which will be deduced in the first section of this paper. In the second section subsequent rules for the concentration depen-

dence of the phenomenological coefficients will be given. A better foundation for these will be provided in the case of solutions with two solutes. In the third part the transformation into friction coefficients will be discussed.

In the literature<sup>3-9</sup> (no claim of completeness is made) similar discussions can be found for special systems, but to our knowledge no systematic and coherent treatment has been given as yet; hence this paper.

## Limiting Laws and Continuity Conditions for Conventional Transport Coefficients

As has already been explained elsewhere,<sup>2</sup> one can describe the transport phenomena in terms of diffusion fluxes and generalized forces either for the species or for the neutral and ionic constituents. These two descriptions always differ when the solution contains more species than constituents, *i.e.*, when there are dissociation or association equilibria between various species. Since we must distinguish below between these cases, we will indicate solution components with the indices I, II, ... and solution species with 1, 2, .... In order not to load the equations with too many indices, we will restrict the treatment to two components in solutions. The components may be either nonelectrolytes or neutral combinations of electrolytes. Extension to solutions with more than two components

(1) Institut für Physikalische Chemie, Technische Hochschule, Aachen, Germany.

(2) H. Schönert, *Z. Phys. Chem.* (Frankfurt), **54**, 245 (1967); Part II: **57**, 164 (1968); see also D. G. Miller, *J. Phys. Chem.*, **71**, 616, 3588 (1967).

(3) R. Schlögl, "Stofftransport durch Membranen," Steinkopff, Darmstadt, Germany, 1964, p 50.

(4) K. S. Spiegler, *Trans. Faraday Soc.*, **54**, 1408 (1958).

(5) A. Klemm, *Z. Naturforsch.*, **8a**, 397 (1953); **17a**, 805 (1962).

(6) R. W. Laity, *J. Chem. Phys.*, **30**, 682 (1959); *J. Phys. Chem.*, **63**, 80 (1959); **67**, 671 (1963).

(7) J. Rastas, *Acta Polytech. Scand.*, **50** (1966).

(8) O. Kedem and A. Katchalsky, *J. Gen. Physiol.*, **45**, 143 (1961).

(9) D. G. Miller, *J. Phys. Chem.*, **71**, 616 (1967).

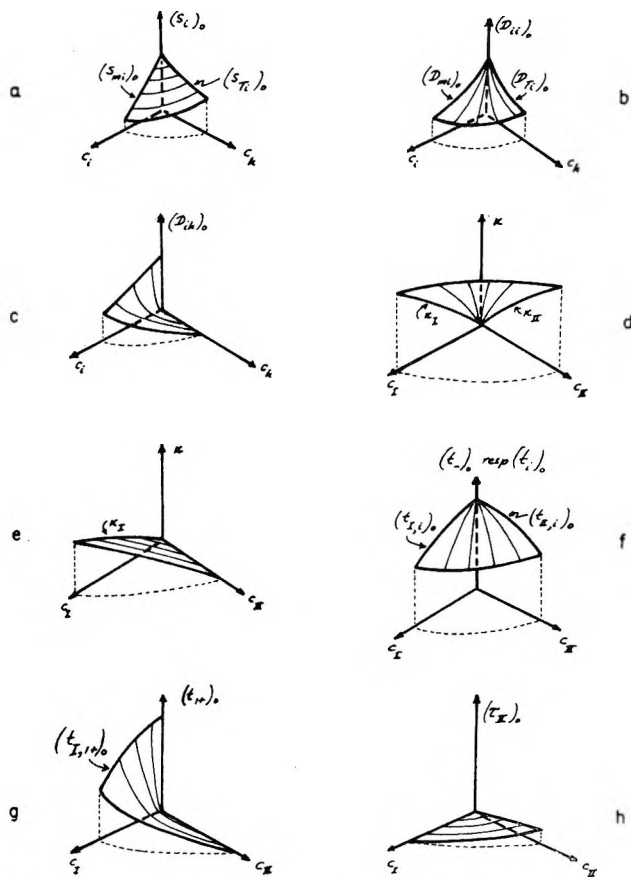


Figure 1. Several coefficients as functions of two concentrations: (a) sedimentation coefficient  $(s_i)_0$ ; (b) main diffusion coefficient  $(D_{ii})_0$ ; (c) cross-term diffusion coefficient  $(D_{ik})_0$ ; (d) specific electrical conductivity ( $\kappa$ ), case a (see the text); (e) specific conductance ( $\kappa$ ), case b (see the text); (f) transference number of common anion  $(t_{-})_0$ , case a, or of any ion in case b; (g) transference number  $(t_{i+})_0$  of cation  $i+$  in case a; (h) reduced transference number  $(\tau_{II})_0$  of nonelectrolyte II.

neither presents fundamental problems nor yields essentially new aspects.

The empirical rules and continuity conditions given below refer to measurable, conventional transport coefficients. They refer therefore to components and not to species. The discussion will follow this order: sedimentation coefficients, diffusion coefficients, specific conductivity, and transport numbers. To illustrate the rules, the above quantities are depicted schematically in Figure 1.

If we assume that the components of the solution sediment in a field of gravitation with a finite velocity (relative to that of the solvent) other than zero over the total range of concentrations,  $c_I$  and  $c_{II}$ , then it follows from the definitions of sedimentation coefficients  $(s_i)_0$  via

$$(s_i)_0 \vec{v} = (\vec{v}_i - \vec{v}_0) \quad (i = I \text{ or } II) \quad (1)$$

that the coefficients  $(s_i)_0$  in general are neither zero nor infinitely large. They follow therefore the concentra-

tion dependence indicated in Figure 1, with the limiting values

$$\lim_{c_k \rightarrow 0} (s_i)_0 = (s_{m,i})_0 \quad (k \neq i = I \text{ or } II) \quad (2)$$

$$\lim_{c_i \rightarrow 0} (s_i)_0 = (s_{T,i})_0 \quad (i = I \text{ or } II) \quad (3)$$

where the indices m and T denote mutual and tracer and were selected by analogy to the notation of diffusion coefficients proposed by Dunlop.<sup>10</sup>  $(s_{m,i})_0$  is the sedimentation coefficient in the binary system of solvent and component  $i$  and depends only on  $c_i$ , while  $(s_{T,i})_0$  is the  $c_k$  dependent value in the system containing solvent and component  $k$ .  $(s_{T,i})_0$  describes, for example, the sedimentation of biopolymers present in low concentration in buffered solutions, and, combined with eq 4-6 and some thermodynamic relations, it yields the limiting values of the Svedberg equation in multicomponent systems.<sup>11-16</sup>

For the diffusion coefficients we have the limiting laws

$$\lim_{c_i \rightarrow 0} (D_{ik})_0 = 0 \quad (k \neq i = I \text{ or } II) \quad (4)$$

$$\lim_{c_i \rightarrow 0} (D_{kk})_0 = (D_{mk})_0 \quad (5)$$

$$\lim_{c_k \rightarrow 0} (D_{tk})_0 = (D_{Tk})_0 \quad (6)$$

The relations expressed by eq 4 can be deduced from the condition of conservation of mass in diffusion. Equations 5 and 6 imply continuity conditions.

The above laws are known and have been reported and discussed in several places,<sup>10-20</sup> especially with respect to their meaning for tracer diffusion<sup>7,10,15,20</sup> and for the applicability of the Svedberg equation in multicomponent systems.<sup>11-16</sup> There  $(D_{mk})_0$ , the mutual diffusion coefficient, is the  $c_k$ -dependent diffusion coefficient in the binary system of solvent and solute  $k$ , whereas  $(D_{Tk})_0$  depends on  $c_i$  and describes the tracer diffusion of component  $k$  in the system containing solvent and component  $i$ .

In the discussion of the limiting behavior of the spe-

- (10) P. J. Dunlop, *J. Phys. Chem.*, **69**, 1693 (1965).
- (11) L. Peller, *J. Chem. Phys.*, **29**, 415 (1958).
- (12) H. Schönert, *J. Phys. Chem.*, **64**, 733 (1960).
- (13) R. L. Baldwin, *J. Amer. Chem. Soc.*, **80**, 496 (1958).
- (14) R. Haase and H. Schönert, *Z. Elektrochem., Ber. Bunsenges. Phys. Chem.*, **64**, 1155 (1960).
- (15) L.-O. Sundelöf, *Ark. Kemi*, **20**, 369 (1963).
- (16) G. J. Hooymans, R. Haase, S. Ljungren, and P. J. Mijnlieff in "Ultracentrifugal Analysis," J. W. Williams, Ed., Academic Press, New York, N. Y., 1963.
- (17) P. J. Dunlop, *J. Phys. Chem.*, **61**, 994 (1957).
- (18) I. J. O'Donnell and L. J. Gosting in "The Structure of Electrolytic Solutions," W. J. Hamer, Ed., John Wiley & Sons, Inc., New York, N. Y., 1959.
- (19) L. A. Woolf, D. G. Miller, and L. J. Gosting, *J. Amer. Chem. Soc.*, **84**, 317 (1962).
- (20) P. J. Dunlop, *J. Phys. Chem.*, **68**, 26 (1964).

specific conductance,  $\kappa$ , and of the transport numbers,  $(t_i)_0$ , one should distinguish between two cases: (a) the case of two electrolytic solutes and (b) the case of component I being an electrolyte and component II being a nonelectrolyte.

(a) The specific conductance is different from zero over the whole concentration range (except for  $c_I = c_{II} = 0$ ), and therefore one can write

$$\lim_{c_k \rightarrow 0} \kappa = \kappa_i \quad (k \neq i = \text{I or II}) \quad (7)$$

Consequently the specific conductance  $\kappa_i$  in a binary system consisting of solvent and electrolyte  $i$  is a function only of  $c_i$ .

(b) In the binary mixture of solvent and nonelectrolyte II, the conductivity vanishes

$$\lim_{c_I \rightarrow 0} \kappa = 0 \quad (8)$$

Moreover we have, as before

$$\lim_{c_{II} \rightarrow 0} \kappa = \kappa_I \quad (9)$$

Equations 7–9 appear to be trivial. However, they must be satisfied as limiting cases of a more general formulation, and for this reason they have been given here.

For the transport numbers in case a we have the following. When the electrolytes I and II dissociate into the ionic species  $1+$ ,  $1-$ ,  $2+$ , and  $2-$  with common anion ( $1- = 2- = -$ ), then (denoting stoichiometric numbers with  $\nu_i$ )

$$\begin{aligned} (t_{1+})_0 \vec{I} &= z_{1+}\nu_{1+}c_I F(\vec{v}_{1+} - \vec{v}_0) \\ (t_{2+})_0 \vec{I} &= z_{2+}\nu_{2+}c_{II} F(\vec{v}_{2+} - \vec{v}_0) \\ (t_-)_0 \vec{I} &= z_- (\nu_{1-c_I} + \nu_{2-c_{II}}) F(\vec{v}_- - \vec{v}_0) \end{aligned}$$

and since the electrical current is unequal to zero except for  $c_I = c_{II} = 0$ , the following relations must be satisfied

$$\begin{aligned} \lim_{c_I \rightarrow 0} (t_{1+})_0 &= 0 \\ \lim_{c_{II} \rightarrow 0} (t_{2+})_0 &= 0 \end{aligned} \quad (10)$$

with the continuity conditions

$$\begin{aligned} \lim_{c_{II} \rightarrow 0} (t_{1+})_0 &= (t_{I,1+})_0 \\ \lim_{c_I \rightarrow 0} (t_{2+})_0 &= (t_{II,2+})_0 \\ \lim_{c_I \rightarrow 0} (t_-)_0 &= (t_{I,-})_0 \end{aligned} \quad (11)$$

The limiting values  $(t_{ik})_0$  of binary systems depend only on  $c_i$ . Equations for the concentration dependence of transport numbers which are more general than eq 10 and 11 have already been formulated, proven,<sup>21,22</sup> and

used as the basis of further conclusions.<sup>9</sup> In case b the electrolyte I dissociates into a cationic ( $i = 1+$ ) and an anionic ( $i = 1-$ ) constituent, the transport numbers of which are finite and in general unequal to zero over the whole concentration range. Hence continuity requires that the extrapolated value for vanishingly small concentration of the nonelectrolyte  $(t_{I,i})_0$ , must be equal to that in a binary mixture of solvent and electrolyte and consequently depends on  $c_I$  only. The reduced transport number  $(\tau_{II})_0$  of the neutral component II must satisfy the condition

$$\lim_{c_{II} \rightarrow 0} (\tau_{II})_0 = 0 \quad (12)$$

since according to eq A3 and A9

$$(\tau_{II})_0 \vec{I} = F c_{II} (\vec{v}_{II} - \vec{v}_0)$$

whereas the electrical current density remains finite for vanishing  $c_{II}$ .

### Concentration Dependence of the Phenomenological Coefficients $a_{ik}$

In order for the above-mentioned limiting laws to hold, the transport coefficients  $a_{ik}$  introduced into the phenomenological equations of thermodynamics of irreversible processes must also follow certain limiting laws. From the continuity of  $(s_i)_0$ ,  $(D_{ik})_0$ , etc., it follows that the transport coefficients must also be continuous functions of the concentrations. It is therefore easiest to try to expand them in a power series in the concentrations, whereby, as we will show, the limiting laws always determine the first term of the power series. This is the distinguishing and only general conclusion which can be drawn from eq 1–12. The situation in this case is analogous to that in the expansion of logarithms of activity coefficients in power series in the concentrations:<sup>23,24</sup> the first term of the power series is determined by the limiting laws, e.g., those of Raoult, Henry, van't Hoff, Debye-Hückel, etc. The usefulness of these considerations lies in their possible generalizations.

At this point one has the choice of using in the expansions the concentrations of either the species or the components. In principle both formulations can be used, because the concentrations of the species are coupled to those of the components through the equilibrium conditions and the conservation of mass. In this work we will expand the coefficients  $a_{ik}$  of the species in terms of the concentrations  $c_i$  of the species, since this is better adapted to the actual kinetic conditions in solution and also makes for a better description of anomalous be-

(21) D. A. McInnes, *J. Amer. Chem. Soc.*, **47**, 1922 (1925).

(22) P. Van Rysselberghe, *ibid.*, **55**, 990 (1933).

(23) R. Haase, "Thermodynamik der Mischphasen," Springer-Verlag, Heidelberg, 1956.

(24) G. Scatchard and S. S. Prentiss, *J. Amer. Chem. Soc.*, **56**, 1486, 2314, 2330 (1934).

havior caused by dissociation and/or association equilibria. (In thermodynamics<sup>23</sup> a similar procedure is followed, where one assumes, as a first approximation, that in very dilute solutions the activity coefficients of all species in solution are equal to 1 and then tries to explain deviations from ideal behavior *via* plausible assumptions regarding dissociation and association.) Examples of similar procedures are, for example, the attempts to allow for anomalous diffusion *via* incomplete dissociation<sup>25-28</sup> or for anomalous electrophoretic and sedimentation profiles *via* coupled fast chemical reactions.<sup>29-32</sup>

When we denote the species in solution with the indices  $i$ ,  $k$  and  $\alpha, \beta, \dots, \mu$ , respectively, then the following series expansions result for  $a_{ik}$  in solutions containing nonelectrolytes as a consequence of the above-enumerated limiting laws and continuity conditions

$$a_{ii} = a_{ii}^{(0)}c_i(1 + a_{ii}^{(1)}c_\alpha^m c_\beta^n \dots c_\mu^p + \dots) \quad (13a)$$

$$a_{ik} = a_{ik}^{(0)}c_i c_k(1 + a_{ik}^{(1)}c_\alpha^m c_\beta^n \dots c_\mu^p + \dots) \quad (i \neq k; m + n + \dots + p > 0) \quad (13b)$$

where  $i$  and  $k$  denote nonelectrolytic species and where the expansion is in terms of concentrations of all species. The series should be continued with increasing order of the concentrations. The coefficients  $a_{ik}^{(0)}$ ,  $a_{ik}^{(1)}$ , etc. depend only on temperature and pressure and satisfy the Onsager reciprocity relations

$$a_{ik}^{(j)} = a_{ki}^{(j)}$$

Without further discussion of the meaning of the separate terms, we will show with a few detailed examples that for eq 2-6 the first term of the above series expansion is always necessary and that the higher terms are sufficient.

The simplest example is a system consisting of a solvent and two nonelectrolytic components I and II and not containing any other species. Then the phenomenological equations for the diffusion fluxes ( $\vec{J}_i$ )<sub>0</sub> and ( $\vec{J}_{II}$ )<sub>0</sub> and for the generalized forces  $\vec{Y}_I$  and  $\vec{Y}_{II}$  result in<sup>2,33</sup>

$$(\vec{J}_i)_0 = \sum_{k=1}^{II} a_{ik} \vec{Y}_k \quad (i = I \text{ or } II) \quad (14)$$

and, in view of eq 1, we obtain the expressions for the sedimentation coefficients ( $s_i$ )<sub>0</sub>

$$(s_i)_0 = \frac{1}{c_i} [a_{i,I}(M_I - \rho V_I) + a_{i,II}(M_{II} - \rho V_{II})] \quad (i = I \text{ or } II) \quad (15)$$

In order that conditions 2 and 3 are satisfied, the following conditions pertain to a series expansion of  $a_{ik}$ .

(1) The first terms in  $a_{ii}$  must be proportional to  $c_i$ .

(2) The first terms in  $a_{I,II}$  and  $a_{II,I}$  must be proportional to  $c_I$  and  $c_{II}$ , respectively, and, in view of the

Onsager reciprocity relations, must be proportional to  $c_I c_{II}$ .

(3) The higher terms in  $a_{I,i}$  and  $a_{II,i}$  must contain at least  $c_I$  and  $c_{II}$ , respectively, or higher powers  $c_I^m$  or  $c_{II}^m$ , respectively, where  $m > 1$ .

Thus the general form of eq 13a and b and their first terms are given explicitly. The limiting behavior of diffusion coefficients then follows automatically, *viz.*<sup>33</sup>

$$(D_{ik})_0 = \sum_{j=1}^{II} a_{ij} \left( \frac{\partial \mu_j}{\partial c_k} \right)_{T,P} \quad (16)$$

where the chemical potential  $\mu_j$  is given by

$$\mu_j = \mu_j^0 + RT \ln c_j y_j \quad (j = I \text{ or } II) \quad (17)$$

with a series expansion for the logarithms of the activity coefficients<sup>23,24</sup>

$$\ln y_j = \sum_{n=0}^{\infty} \sum_{m=0}^{\infty} \alpha_{jn,m} c_I^n c_{II}^m \quad (n + m \geq 1) \quad (18)$$

By combining eq 13a, 13b, 16, 17, and 18, it follows that

$$(D_{I,I})_0 = a_{I,I}^{(0)} c_I (1 + \dots) \times \frac{RT}{c_I} \left( 1 + \sum_{n=1}^{\infty} \sum_{m=0}^{\infty} \alpha_{In,m} n c_I^n c_{II}^m \right) + a_{I,II}^{(0)} c_I c_{II} (1 + \dots) \times RT \left( \sum_{n=1}^{\infty} \sum_{m=0}^{\infty} \alpha_{II,n,m} n c_I^{n-1} c_{II}^m \right) \quad (19a)$$

$$(D_{I,II})_0 = a_{I,I}^{(0)} c_I (1 + \dots) \times RT \left( \sum_{n=0}^{\infty} \sum_{m=1}^{\infty} \alpha_{In,m} c_I^n m c_{II}^{m-1} \right) + a_{I,II}^{(0)} c_I c_{II} (1 + \dots) \times RT \left( \frac{1}{c_{II}} + \sum_{n=0}^{\infty} \sum_{m=1}^{\infty} \alpha_{II,n,m} c_I^n m c_{II}^m \right) \quad (19b)$$

from which eq 4-6 follow immediately. Analogous derivations apply for  $(D_{II,II})_0$  and  $(D_{II,I})_0$ . The first terms of eq 19b and of the appropriate series expansion for  $(D_{II,I})_0$  agree with the relations found empirically by Ellerton and Dunlop.<sup>34</sup>

(25) H. S. Harned and R. M. Hudson, *J. Amer. Chem. Soc.*, **73**, 3781, 5880 (1951).

(26) J. M. Creeth and R. H. Stokes, *J. Phys. Chem.*, **64**, 946 (1960).

(27) W. H. Stockmayer, *J. Chem. Phys.*, **33**, 1291 (1960).

(28) C. W. Garland, S. Tong, and W. H. Stockmayer, *J. Phys. Chem.*, **69**, 1718, 2469 (1965).

(29) R. A. Alberty and E. L. King, *J. Amer. Chem. Soc.*, **73**, 517 (1951).

(30) G. A. Gilbert and R. C. Ll. Jenkins, *Nature*, **177**, 853 (1956).

(31) G. A. Gilbert, *Discussions Faraday Soc.*, **13**, 195 (1953); **20**, 68 (1955).

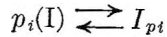
(32) L. W. Nichol, J. L. Bethune, G. Kegeles, and E. L. Hess in "The Proteins," 2nd ed., H. Neurath, Ed., Academic Press, New York N. Y., 1964, Chapter 9.

(33) R. Haase, "Thermodynamik der irreversiblen Prozesse," Steinkopff, Darmstadt, Germany, 1962; J. Meixner and H. G. Reik, "Handbuch der Physik," Vol. III/2, Springer-Verlag, Heidelberg, 1959.

(34) H. D. Ellerton and P. J. Dunlop, *J. Phys. Chem.*, **71**, 1291 (1967).

The conditions become more complicated when the components I and II give rise to more than two species, when, for example, component I associates with itself to form I, I<sub>2</sub>, I<sub>3</sub>... (as with nonionic soaps) or with component II to form associates of the type (I, II), (I<sub>2</sub>, II), (I, II<sub>2</sub>), etc. (as, for example, with donor-acceptor complexes). These associates must then be considered as kinetic entities in the solution, and it is understandable that one obtains a better description when the above-mentioned phenomena are accounted for by relating the coefficients  $a_{ik}$  with species rather than components.

As to the first example given, the association equilibria can be written as



$$(p_1 = 1, p_2 = 2, \dots, p_i = i, \dots, p_n = n)$$

The phenomenological equations for the species  $i = 1, 2, \dots, n$  and  $i = \text{II}$  then become

$$(\vec{J}_i)_0 = \sum_{k=1}^n a_{ik} \vec{Y}_k + a_{i,\text{II}} \vec{Y}_{\text{II}} \quad (i = 1, 2, \dots, n, \text{II})$$

The stoichiometric (*i.e.*, measurable) diffusion flux  $(\vec{J}_i)_0$  of component I can be calculated as

$$(J_i)_0 = \sum_{i=1}^n p_i (\vec{J}_i)_0 = \sum_{i=1}^n \sum_{k=1}^n p_i a_{ik} \vec{Y}_k + \sum_{i=1}^n p_i a_{i,\text{II}} \vec{Y}_{\text{II}}$$

It follows from the association equilibrium that the following relations must exist between the generalized forces of species and those of components

$$\vec{Y}_k = p_k \vec{Y}_1 \quad (k = 1, 2, \dots, n)$$

so that finally

$$(\vec{J}_i)_0 = \sum_{i=1}^n \sum_{k=1}^n p_i p_k a_{ik} \vec{Y}_1 + \sum_{k=1}^n p_k a_{i,\text{II}} \vec{Y}_{\text{II}}$$

Likewise it follows that

$$(\vec{J}_{\text{II}})_0 = \sum_{k=1}^n a_{\text{II},k} \vec{Y}_k + a_{\text{II},\text{II}} \vec{Y}_{\text{II}} = \sum_{k=1}^n a_{\text{II},k} p_k \vec{Y}_1 + a_{\text{II},\text{II}} \vec{Y}_{\text{II}}$$

The stoichiometric coefficients  $a_{ik}$  therefore have the values

$$a_{\text{I},\text{I}} = \sum_{i=1}^n \sum_{k=1}^n p_i p_k a_{ik}$$

$$a_{\text{I},\text{II}} = a_{\text{II},\text{I}} = \sum_{i=1}^n p_i a_{i,\text{II}}$$

They obey the Onsager reciprocity relations and with eq 13a and b fulfill the limiting conditions for conventional transport coefficients  $(s_i)_0$  and  $(D_{ik})_0$ . The latter can be shown to follow from the above scheme by considering the equilibrium conditions and also by realizing that all dissociations must become complete and all associations will disappear in the limiting case.

Similar considerations can be invoked when one has equilibria different from the above-mentioned example of polymerization. In all cases the limiting laws 2-6 are followed when relations 13a and b hold.

Next we will investigate the situation in a multicomponent electrolytic solution, for which eq 13b must be modified,<sup>7</sup> as well as eq 18, since now the logarithms of the activity coefficients must be expressed by a series expansion with fractional powers<sup>23,24,35</sup> in accordance with the Debye-Hückel treatment. The form of the series expansion for  $a_{ik}$  is indicated by the theory of transport phenomena of Onsager, *et al.*<sup>36,37</sup> (compare also Rastas<sup>7</sup>, Miller<sup>9</sup>, and Haase and Richter<sup>38</sup>)

$$a_{ik} = a_{ik}^{(0)} c_i c_k \frac{1}{\sqrt{\Gamma}} (1 + \dots) \quad (i \neq k) \quad (20)$$

where  $i$  and  $k$  now denote charged particles, and the ionic strength,  $\Gamma$ , is given by

$$\Gamma = \frac{1}{2} \sum_i z_i^2 c_i \quad (21)$$

Eq 13a, describing the diagonal terms  $a_{ii}$ , remains valid.

As an application we will take the system described earlier<sup>2</sup> in which the electrolyte I forms the species  $(1+)_{p_i}$   $(1-)_{q_i}$  ( $i = 1, 2, \dots, n - 1$ ) while electrolyte II with net formula  $(2+)_{\nu_2+} (2-)_{\nu_2-}$  completely dissociates into its ionic constituents  $2+$  (index  $i = n$ ) and  $2-$  ( $2-$  is identical with anion  $1-$  with the index  $i = n - 1$ ; *i.e.*, both electrolytes have a common anionic constituent). It then follows from eq A35 and following that

$$A_{1,1} = \sum_{i=1}^{n-1} \sum_{k=1}^{n-1} p_i p_k B_{ik} / \nu_{1+\nu_2+} \\ A_{1,\text{II}} = \sum_{i=1}^{n-1} p_i B_{in} / \nu_{1+\nu_2+} \\ A_{\text{II},\text{II}} = B_{nn} / \nu_{2+\nu_2+} \quad (22)$$

where

$$B_{ik} = \frac{\sum_{r=1}^n \sum_{s=1}^n z_r z_s (a_{rs} a_{ik} - a_{ir} a_{ks})}{\sum_{r=1}^n \sum_{s=1}^n z_r z_s a_{rs}} \quad (23)$$

and

$$(s_i)_0 = \frac{1}{c_i} [A_{i1}(M_1 - \rho V_1) + A_{i2}(M_{\text{II}} - \rho V_{\text{II}})] \quad (i = \text{I or II}) \quad (24)$$

(35) H. S. Harned and B. B. Owen, "The Physical Chemistry of Electrolyte Solutions," Reinhold Publishing Corp., New York, N. Y., 1958; R. A. Robinson and R. H. Stokes, "Electrolyte Solutions," Butterworth and Co. Ltd., London, 1959.

(36) L. Onsager and R. M. Fuoss, *J. Phys. Chem.*, **36**, 2689 (1932).

(37) L. Onsager and S. K. Kim, *ibid.*, **61**, 215 (1957).

(38) R. Haase and J. Richter, *Z. Naturforsch.*, **22a**, 1761 (1967).

$$(D_{ik})_0 = \left[ A_{iI} \left( \frac{\partial \mu_I}{\partial c_k} \right) + A_{iII} \left( \frac{\partial \mu_{II}}{\partial c_k} \right) \right] \quad (i \text{ or } k = I \text{ or } II) \quad (25)$$

Investigation of the limiting equation for the sedimentation coefficients  $(s_I)_0$  (eq 2) yields among others the expression

$$\lim_{c_{II} \rightarrow 0} \frac{1}{c_I} A_{I,II} (M_{II} - \rho V_{II}) = \lim_{c_{II} \rightarrow 0} \frac{1}{c_I} \sum_{i=1}^{n-1} p_i B_{in} / \nu_{1+\nu_{2+}} (M_{II} - \rho V_{II}) \quad (26)$$

with (compare eq 23)

$$B_{in} = \frac{\sum_{r=1}^n \sum_{s=1}^n z_r z_s (a_{rs} a_{in} - a_{ir} a_{ns})}{\sum_{r=1}^n \sum_{s=1}^n z_r z_s a_{rs}} \quad (27)$$

It is clear that all terms in the numerator of eq 26 contain the index  $n$ , whereas *not* all in the denominator do, so that the limiting value of eq 26 is zero (*cf.*, eq 20 and  $c_n = \nu_{2-} c_{II}$ ). Likewise in eq 23 all the terms with index  $n$  vanish in the limiting case, resulting in

$$\lim_{c_{II} \rightarrow 0} (s_I)_0 = \frac{1}{c_I} (M_I - \rho V_I) \sum_{i=1}^{n-1} \sum_{k=1}^{n-1} p_i p_k B_{ik} / \nu_{1+\nu_{2+}}$$

with

$$B_{ik} = \frac{\sum_{i=1}^{n-1} \sum_{k=1}^{n-1} z_r z_s (a_{rs} a_{ik} - a_{ir} a_{ks})}{\sum_{i=1}^{n-1} \sum_{k=1}^{n-1} z_r z_s a_{rs}} \quad (28)$$

Note that this expression is equal to  $(s_{mI})_0$ , *i.e.*, to that for the sedimentation coefficients of a binary system, as follows from comparison with eq A34.

The limiting behavior of the diffusion coefficients, eq 23, can be determined from similar considerations in conjunction with a few well-known expressions for the chemical potentials  $\mu_i$

$$\mu_i = \mu_i^0 + RT \ln (\nu_{i+} c_I)^{\nu_{i+}} (\nu_{1-} c_I + \nu_{2-} c_{II})^{\nu_{i-}} y_i^{\nu_i} \quad (29)$$

$$\ln y_i = Az_{i+} z_{i-} \sqrt{\Gamma} + \dots \quad (i = I \text{ or } II) \quad (30)$$

Here  $A$  is the constant of the Debye-Hückel limiting law,<sup>35</sup> and  $\nu_i = \nu_{i+} + \nu_{i-}$ . In view of the definition of the ionic strength, eq 21, the limiting conditions for the chemical potentials<sup>15,23</sup> follow as

$$\begin{aligned} \lim_{c_{II} \rightarrow 0} c_{II} \left( \frac{\partial \mu_{II}}{\partial c_I} \right)_{T,P} &= 0 \\ \lim_{c_I \rightarrow 0} c_I \left( \frac{\partial \mu_I}{\partial c_{II}} \right)_{T,P} &= 0 \\ \lim_{c_I \rightarrow 0} c_I \left( \frac{\partial \mu_{II}}{\partial c_{II}} \right)_{T,P} &= 0 \end{aligned} \quad (31)$$

of which the last two can also be written for species  $i = 1, 2, \dots, n-2$

$$\begin{aligned} \lim_{c_i \rightarrow 0} c_i \left( \frac{\partial \mu_I}{\partial c_{II}} \right)_{T,P} &= \lim_{c_I \rightarrow 0} c_I \left( \frac{\partial \mu_I}{\partial c_{II}} \right)_{T,P} = 0 \\ \lim_{c_i \rightarrow 0} c_i \left( \frac{\partial \mu_{II}}{\partial c_{II}} \right)_{T,P} &= \lim_{c_I \rightarrow 0} c_I \left( \frac{\partial \mu_{II}}{\partial c_{II}} \right)_{T,P} = 0 \\ (i = 1, 2, \dots, n-2) \end{aligned} \quad (32)$$

These species are those which electrolytes I and II do not have in common, so that  $c_i \rightarrow 0$  can also be written as  $c_I \rightarrow 0$ . On the other hand,  $A_{I,II}$  is at least proportional to  $c_n = \nu_{2-} c_{II}$  via the terms  $B_{in}$ , as was discussed in conjunction with eq 27. Therefore, eq 31 yields

$$\lim_{c_{II} \rightarrow 0} A_{I,II} \left( \frac{\partial \mu_{II}}{\partial c_I} \right)_{T,P} = 0$$

and also, according to eq 25

$$\lim_{c_{II} \rightarrow 0} (D_{I,I})_0 = A_{I,I} \left( \frac{\partial \mu_I}{\partial c_I} \right)_{T,P} = (D_{mI})_0$$

where all terms with  $i$  or  $k = n$  cancel, as was the case with the sedimentation coefficients in eq 28, and where  $(D_{mI})_0$  denotes the diffusion coefficient which describes the binary system eq A34. To prove the limiting behavior of  $(D_{I,II})_0$  one must consider that all species  $i = 1, 2, \dots, n-2$  vanish for  $c_i \rightarrow 0$ , whereas the concentration of the common anion  $i = n-1$  does not vanish. However, for this common anion the formula for species  $(1+)_{p_i} (1-)_{q_i}$  results in the value  $p_{n-1} = 0$ , so that eq 22 becomes

$$\begin{aligned} A_{I,I} &= \sum_{i=1}^{n-2} \sum_{k=1}^{n-2} p_i p_k B_{ik} / \nu_{1+\nu_{1+}} \\ A_{I,II} &= \sum_{i=1}^{n-2} p_i B_{in} / \nu_{1+\nu_{2+}} \end{aligned}$$

In view of eq 13a, 20, and both  $A_{I,I}$  and  $A_{I,II}$  contain at least one factor  $c_i$  ( $i = 1, 2, \dots, n-2$ ), so that combination with eq 32 yields

$$\begin{aligned} \lim_{c_I \rightarrow 0} A_{I,I} \left( \frac{\partial \mu_I}{\partial c_{II}} \right)_{T,P} &= 0 \\ \lim_{c_I \rightarrow 0} A_{I,II} \left( \frac{\partial \mu_{II}}{\partial c_{II}} \right)_{T,P} &= 0 \end{aligned}$$

and consequently eq 25 results in

$$\lim_{c_I \rightarrow 0} (D_{I,II})_0 = 0$$

The limiting conditions for the specific conductance  $\kappa$ , eq 7, and for the transport numbers  $t_i$ , eq 10 and 11, can easily be shown to be correct by combining eq 13a and 20 with the relations eq A10 and A12 expressing  $\kappa$  and  $t_i$  as functions of  $a_{ik}$

$$\kappa = \sum_{i=1}^n \sum_{k=1}^n z_i z_k a_{ik} F^2$$

$$\frac{\langle t_i \rangle_0}{z_i} = \frac{\sum_{k=1}^n z_k a_{ik}}{\kappa / F^2}$$

According to the preceding discussion we have, e.g.

$$\lim_{c_{II} \rightarrow 0} \kappa = \lim_{c_{II} \rightarrow 0} \sum_{i=1}^n \sum_{k=1}^n z_i z_k a_{ik} F^2 = \sum_{i=1}^{n-1} \sum_{k=1}^{n-1} z_i z_k a_{ik} F^2 = \kappa_I$$

$$\lim_{c_I \rightarrow 0} \kappa = \lim_{c_I \rightarrow 0} \sum_{i=1}^n \sum_{k=1}^n z_i z_k a_{ik} F^2 = \sum_{i=n-1}^n \sum_{k=n-1}^n z_i z_k a_{ik} F^2 = \kappa_{II}$$

and corresponding expressions can be derived for the transport numbers.

After the above treatment of solutions containing either two nonelectrolytes or two electrolytes, we will now investigate those which contain one electrolyte and one nonelectrolyte.

In this case eq 13a applies to the diagonal matrix elements  $a_{ii}$ ; eq 13b applies for either two neutral species or for one neutral and one charged species; and eq 20 applies for two electrically charged species. The limiting laws for the sedimentation and diffusion coefficients follow according to the scheme discussed before, and the only new and interesting relation, eq 12, follows immediately from eq A12

$$(\tau_{II})_0 = \frac{\sum_k z_k a_{IIk}}{\kappa / F^2} = \frac{\sum_k z_k a_{IIk}^{(0)} c_{II} c_k (1 + \dots)}{\kappa / F^2}$$

Summarizing, it can be concluded that the eq 13a, 13b, and 20 in terms of phenomenological coefficients  $a_{ik}$  describe systems with two solutes, which may be either electrolytes or nonelectrolytes, and include dissociation and association equilibria. Although the above constitute only a few examples of a general multicomponent system with arbitrary high-speed chemical reactions, one may consider these equations as sufficiently general and proven. It should be emphasized that always the first term in the series expansions is not only sufficient but also necessary. Before drawing further conclusions from them we will show in the next section that the above equations are also compatible with the concept of friction coefficients as introduced by various authors.

### Transformation into Friction Coefficients

In this paper all considerations have been based on a system of equations

$$(\vec{J}_i)_0 = \sum_{k=1}^n a_{ik} \vec{X}_k \quad (i = 1, 2, \dots, n) \quad (33)$$

The diffusion fluxes

$$(\vec{J}_i)_0 = c_i (\vec{v}_i - \vec{v}_0) \quad (34)$$

are taken with respect to the velocity  $v_0$  of the solvent.

Consequently the diffusion flux  $(\vec{J}_0)_0$  of the solvent is zero, and the summation over the forces includes solute species only. This type of description is advantageous when the solvent is present in large excess, as in dilute solutions. Accordingly we have developed the coefficients  $a_{ik}$  around the point  $c_i = 0$  ( $i = 1, 2, \dots$ ), i.e., around the point where all components or species exhibit infinite dilution. This clearly shows that the relations for the coefficients  $a_{ik}$  cannot be retained upon a change in the choice of the reference velocity but that they must be transformed together with the diffusion fluxes. The system of eq 33 and 34 does not constitute the only possibility for describing transport phenomena. Apart from the choice of a reference velocity different from  $\vec{v}_0$ , as often suggested by the experiment,<sup>33</sup> one can also use, for example, the inverse system

$$\vec{X}_i = \sum_{k=1}^n r_{ik} (\vec{J}_k)_0 \quad (35)$$

with the generalized friction coefficients  $r_{ik}$

$$r_{ik} = \frac{|a_{mn}|_{ik}}{|a_{mn}|} \quad (36)$$

Here  $|a_{mn}|$  denotes the determinant formed from the elements  $a_{mn}$ , and  $|a_{mn}|_{ik}$  the subdeterminant pertinent to element  $a_{ik}$ .

This transformation of the system of eq 33 is permissible because in a solution containing  $n$  solute components there are precisely  $n$  mutually independent diffusion fluxes and generalized forces.

Onsager and Kim<sup>37</sup> reported the results of their theory for multicomponent mixtures in the form of eq 36 (the movement of ions is computed relative to that of the solvent). When one adopts eq 13a and 20 for the coefficients  $a_{ik}$ , then one can calculate the terms  $r_{ik}$  for very dilute solutions by expanding the determinants  $|a_{mn}|$  and  $|a_{mn}|_{ik}$  and retaining only terms with the lowest power of  $c_m$  and  $c_n$

$$r_{ii} = \frac{1}{a_{ii}^{(0)} c_i} (1 + \dots) \quad (37)$$

$$r_{ik} = -\frac{a_{ik}^{(0)}}{a_{ii}^{(0)} a_{kk}^{(0)} \sqrt{\Gamma}} (1 + \dots) \quad (i \neq k)$$

This is compatible with the equations of Onsager and Kim; the friction coefficients  $r_{ii}$  are to a first approximation proportional to  $1/c_i$ , whereas the off-diagonal terms  $r_{ik}$ , which are related to electrophoretic and relaxation effects, are proportional to  $1/\sqrt{\Gamma}$ . The coefficients  $a_{ik}^{(0)}$  depend, in a complicated way, on the ionic equivalent conductances at infinite dilution and on the ionic valencies, and they must be calculated separately for every case. This has been done, for example, in the approximate calculation<sup>39</sup> of diffusion

coefficients  $(D_{ik})_0$ . Equation 35 can be transformed further into

$$\vec{X}_i = \sum_{k=1}^n r_{ik} c_k (\vec{v}_k - \vec{v}_i) + \sum_{k=1}^n r_{ik} c_k (\vec{v}_i - \vec{v}_0)$$

With the introduction of a friction coefficient  $r_{i0}$  between species  $i$  and solvent 0, defined by

$$r_{i0} c_0 = - \sum_{k=1}^n r_{ik} c_k \quad (38)$$

One thus obtains

$$\vec{X}_i = - \sum_{k=0}^n r_{ik} c_k (\vec{v}_i - \vec{v}_k) \quad (39)$$

In this or a similar form the phenomenological equations have been proposed by Lamm,<sup>40,41</sup> Onsager,<sup>42</sup> Klemm,<sup>5</sup> and Laity<sup>6</sup> and have been investigated further and applied to special cases by other authors.<sup>4,8,20,43,44</sup> The following advantages have been emphasized especially.

(a) Friction coefficients  $r_{ik}$  are independent of the choice of reference velocity. The coefficients  $r_{i0}$  describing the friction between solvent and solute species  $i$  should be approximately constant in dilute solutions, as well as the coefficients  $r_{ik}$  between two uncharged species  $i$  and  $k$ , whereas  $r_{ik}$  for two electrically charged species  $i$  and  $k$  tends to infinity upon increasing dilution. This concentration dependence, however, is more suspected than strictly proved.

(b) In concentrated solutions as well as in molten salts, in membranes and in ion exchangers, the friction coefficients retain their simple meanings (and are most often implicitly considered to be constant), whereas the coefficients  $a_{ik}$  become complicated functions of all kinds of interactions.

However, one can always transform the conductivity coefficients  $a_{ik}$  into the friction coefficients  $r_{ik}$  and vice versa by taking the diffusion fluxes in eq 33 with respect to the velocity  $\vec{v}_k$  of any component  $k$ . As such one can select, for example, the velocity of the solvent (eq 34), or, in molten salts, the velocity of an arbitrarily selected ionic constituent,<sup>5,45</sup> or, in membranes, the velocity of the membrane frame.<sup>46</sup> Since one thus obtains only  $n$  independent fluxes and forces in a mixture of  $n + 1$  components, it is a matter of convention or efficiency whether one uses the coefficients  $a_{ik}$  or  $r_{ik}$ . At any rate, eq 13a, 13b, and 20 are compatible with the above-mentioned characteristics of  $r_{ik}$ ; since eq 33 and 34 only contain relative velocities, the coefficients  $a_{ik}$  also depend only on relative velocities.

In dilute solutions of neutral components we have for the coefficients  $r_{ik}$ , instead of eq 37

$$r_{it} = \frac{1}{a_{ii}^{(0)} c_i} (1 + \dots) \quad (40)$$

$$r_{ik} = - \frac{a_{ik}^{(0)}}{a_{ii}^{(0)} a_{kk}^{(0)}} (1 + \dots) \quad (i \neq k)$$

as we can deduce by expanding the determinants (eq 36) using eq 13a and b. For both electrically charged and uncharged species it follows to the same approximation that

$$r_{i0} c_0 \approx -r_{ii} c_i = -\frac{1}{a_{ii}^{(0)}} \quad (41)$$

$$\vec{X}_i \approx \frac{1}{a_{ii}^{(0)}} (\vec{v}_i - \vec{v}_0) + \sum_{k=1}^n \frac{a_{ik}^{(0)} c_k}{a_{ii}^{(0)} a_{kk}^{(0)}} (\vec{v}_i - \vec{v}_k)$$

Equations 37, 40, and 41 express the suspected qualities of  $r_{ik}$  for dilute solutions where  $c_0$  is approximately constant. Whether the coefficients  $r_{ik}$  also possess these qualities in concentrated solutions is questionable anyway, as is indicated by the calculation of diffusion measurements, in aqueous solutions of amino acids.<sup>47</sup>

### Final Considerations

Since eq 13a, 13b, and 20 have been derived from the limiting behavior of conventional transport coefficients, conclusions can only be drawn within the above limits. When a solution is very dilute with respect to all components, one can consequently neglect all coupling coefficients  $a_{ik}$  when  $i \neq k$  and obtain

$$(\vec{J}_i)_0 = c_i (\vec{v}_i - \vec{v}_0) = a_{ii}^{(0)} c_i \vec{X}_i \quad (42)$$

from which one can see that the coefficients  $a_{ii}^{(0)}$  have the meaning of a mobility at infinite dilution.

For nonelectrolytes this approximation is equivalent to Fick's law for diffusion and to the Svedberg sedimentation equation; for electrolytes eq 42 is equal to the Nernst–Planck equations and in case of a suitable choice of reference velocity they constitute the generalization of the Nernst–Planck equations in ion exchangers.<sup>3</sup> They do not give any new results not already known and are only listed here for the sake of completeness and in order to show that the general relations (eq 13a, 13b, and 20) lead to the well-known transport equations of dilute ideal solutions.

Since  $a_{ii}^{(0)}$  finds an interpretation via eq 42, eq 13b and c for  $a_{ik}$  with  $i \neq k$  may be considered as being reasonable; these off-diagonal coupling coefficients describe the exchange of momentum between species  $i$  and  $k$  and are therefore proportional to the product  $c_i c_k$ . The far-reaching coulombic forces introduce the

- (39) H. Schönert, *Z. Phys. Chem. (Frankfurt)*, **51**, 196 (1966).
- (40) O. Lamm, *J. Phys. Chem.*, **61**, 948 (1957).
- (41) O. Lamm, *Acta Chem. Scand.*, **8**, 1120 (1954); **11**, 362 (1957).
- (42) L. Onsager, *Ann. N. Y. Acad. Sci.*, **46**, 241 (1945).
- (43) S. Ljungren, *Trans. Roy. Inst. Technol. Stockholm* **172** (1961).
- (44) A. J. Staverman, Ch. A. Kruissink, and D. T. F. Pals, *Trans. Faraday Soc.*, **61**, 2805 (1965).
- (45) H. Schönert and C. Sinistri, *Z. Elektrochem.*, **66**, 413 (1962).
- (46) D. C. Mikulecky and S. R. Caplan, *J. Phys. Chem.*, **70**, 3049 (1966).
- (47) H. D. Ellerton, G. Reinfelds, D. E. Mulcahy, and P. J. Dunlop, *ibid.*, **68**, 403 (1964).

additional factor  $1/\sqrt{\Gamma}$ . If this interpretation is taken as meaningful, it is likely that the coefficients  $a_{ik}^{(0)}$  decrease in the following order: ions, dipolar species, and nonpolar species. They would also be expected to decrease with decreasing size of the species. Finally, we want to draw some conclusions to demonstrate the usefulness of the above considerations.

First we look at the limiting behavior of the reduced transport number  $(\tau_{II})_0$  of a nonelectrolyte component II in a solution of solvent and electrolyte I, which describes the transport of component II with respect to the solvent under the influence of an electric field.<sup>48-51</sup> The electrolyte I dissociates into  $\nu_1$  cations 1 and  $\nu_2$  anions 2 with valencies  $z_1$  and  $z_2$  and concentrations  $c_1 = \nu_1 c_I$  and  $c_2 = \nu_2 c_I$ , respectively. Then we find from eq A12 that

$$(\tau_{II})_0 = \frac{z_1 a_{II,1} + z_2 a_{II,2}}{z_1^2 a_{II} + 2z_1 z_2 a_{12} + z_2^2 a_{22}}$$

Introducing eq 13a, 13b, and 20, one gets

$$\lim_{c_I \rightarrow 0} (\tau_{II})_0 = \frac{(\nu_1 z_1 a_{II,1}^{(0)} + \nu_2 z_2 a_{II,2}^{(0)}) c_{II}}{\nu_1 z_1^2 a_{II}^{(0)} + \nu_2 z_2^2 a_{22}^{(0)}}$$

This means that, in a solvent mixture, one of the non-electrolytes (here designated II) is transported with respect to the other nonelectrolyte even in the case of infinite dilution of the electrolyte. The determination of transference numbers of electrolytes in solvent mixtures<sup>35</sup> therefore should be reassessed in view of this finding.

The second example concerns the limiting behavior of an ionic species in a supporting electrolyte II. The concentration,  $c_I$ , of electrolyte I is vanishingly small. In order to simplify the equations, electrolyte I is assumed to be completely dissociated. Therefore, we have three ionic species, 1-3 (for example,  $\text{Na}^+$ ,  $\text{K}^+$ , and  $\text{Cl}^-$ , with components I and II equal to  $\text{NaCl}$  and  $\text{KCl}$ , respectively) and the summation in eq 22-28 is from  $n = 1-3$  with  $p_1 = 1$ ,  $q_1 = 0$  and  $p_2 = 0$ ,  $q_2 = 1$ . The tracer species is species 1.

Taking eq 3, 4, and 6 into account, the general transport expression (eq A44) reduces to

$$(J_1)_0 = \frac{(t_1)_0}{z_1} \frac{\vec{I}}{F} - \nu_{1+}(D_{T,I,I})_0 \text{grad } c_I + \nu_{1+}(S_{T,I,I})_0 c_I g$$

This is the starting equation for the phenomenological treatment of the tracer diffusion, polarography in supporting electrolytes, and diffusion-sedimentation behavior of biopolymers in supporting electrolytes. Here we only want to look at the relationship between mobility and tracer diffusion. We have, according to eq A11, 13a, and 20

$$(u_1)_0 = \frac{1}{c_I} \sum_{k=1}^3 z_k a_{ik} F = \\ F a_{II}^{(0)} z_1 \left( 1 + \frac{a_{12}^{(0)} z_2 c_2}{a_{II}^{(0)} z_1 \sqrt{\Gamma}} + \frac{a_{13}^{(0)} z_3 c_3}{a_{II}^{(0)} z_1 \sqrt{\Gamma}} \right)$$

Furthermore, using eq 23-30, together with eq 13a and 20, we find that

$$(D_{T,I,I})_0 = a_{II}^{(0)} R T$$

So we have finally

$$\frac{RT}{F} \frac{(u_1)_0}{z_1} = (D_{T,I,I})_0 \left( 1 + \frac{a_{12}^{(0)} z_2 c_2}{a_{II}^{(0)} z_1 \sqrt{\Gamma}} + \frac{a_{13}^{(0)} z_3 c_3}{a_{II}^{(0)} z_1 \sqrt{\Gamma}} \right)$$

and therefore the Nernst-Einstein relationship between mobility and diffusion coefficient is only approximately valid. The same conclusion can be drawn as to the relation between the mobility and the sedimentation coefficient.

As the last example we consider the sedimentation of two polyelectrolytes, I and II, in a supporting buffer solution. Neglecting to a first approximation the effect of the buffer ions (primary and secondary charge effect) and fixing our attention on the mutual influence of the two polymers, we may consider the system as consisting of a solvent and two nonelectrolytes. With eqs 13a, b, and 15, we have

$$(s_I)_0 = a_{I,I}^{(0)} (M_I - \rho V_I) \times \\ \left[ 1 + \frac{a_{I,II}^{(0)} c_{II} (M_{II} - \rho V_{II})}{a_{I,I}^{(0)} (M_I - \rho V_I)} \right]$$

This means that  $(s_I)_0$  is a function of  $c_{II}$  and likewise  $(s_{II})_0$  is a function of  $c_I$ . This mutual influence in sedimentation behavior does only vanish for  $c_I, c_{II} \rightarrow 0$ . This fact is in accord with the observation and interpretation of the Johnston-Ogston effect,<sup>52</sup> which is especially pronounced for two polyelectrolytes because of the high charge and the great size of these molecules.

*Acknowledgments.* The author wishes to thank Dr. R. de Levie for the translation of the manuscript, Professor Dr. R. Haase (Aachen) for his valuable advice and guidance, Professor L. C. W. Baker for his invitation to visit the Chemistry Department of Georgetown University, and the Deutsche Forschungsgemeinschaft for financial support.

(48) G. Scatchard in "Proteins, Amino Acids and Peptides," E. J. Cohn and J. T. Edsall, Ed., Reinhold Publishing Corp., New York, N. Y., 1943, p 39.

(49) L. G. Longsworth, *J. Amer. Chem. Soc.*, **69**, 1288 (1947).

(50) D. G. Miller, *Amer. J. Phys.*, **24**, 595 (1956).

(51) M. Spiro, *J. Inorg. Nucl. Chem.*, **25**, 903 (1963).

(52) J. P. Johnston and A. G. Ogston, *Trans. Faraday Soc.*, **42**, 789 (1946).

## An Electron Spin Resonance Investigation of the Anion Radicals

### 1,4-Dimethylanthrasemiquinone and 1,4,5,8-Tetramethylanthrasemiquinone<sup>1</sup>

by Richard H. Schlossel, David H. Geske,<sup>2a</sup> and Wilson M. Gulick, Jr.<sup>2b</sup>

Department of Chemistry, Cornell University, Ithaca, New York 14850 (Received May 29, 1968)

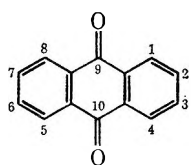
Electron spin resonance spectra have been observed for the radical anions 1,4,5,8-tetramethylanthrasemiquinone and 1,4-dimethylanthrasemiquinone. For the former radical in dimethoxyethane solution we find 12 equivalent methyl protons with  $a_H = 0.329$  G and 4 ring protons with  $a_H = 1.153$  G. Assignments for spectra of both radicals indicate that the methyl groups are freely rotating on the time scale of the esr experiment. This finding is in contrast to a previous report in which rotation of methyl groups in the 1 position of several anthrasemiquinone anions was reported to be so strongly hindered that the protons were no longer magnetically equivalent.

#### Introduction

The chemical literature is replete with studies of semiquinone radicals,<sup>3</sup> including several papers concerning anthrasemiquinones.<sup>4</sup> Interest in the two radicals discussed here, however, was generated by a recent report by Elofson and coworkers<sup>5</sup> in which it was asserted that the rotation of methyl groups in the 1 position of several anthrasemiquinone anions was sufficiently hindered that the methyl protons were magnetically nonequivalent and exhibited different esr hyperfine coupling constants. This assertion was made for radicals in 2-propanol solution at room temperature.

We found it remarkable that the rotation of such methyl groups should be so completely hindered, since, to our knowledge, in the host of radicals studied by esr in solution at room temperatures, no similar assertions have previously been possible.<sup>6</sup> In fact, on the basis of part of the work presented here, these assertions have already been questioned.<sup>7</sup> We report here esr data for the 1,4,5,8-tetramethylanthrasemiquinone anion and a reexamination of the esr spectrum of one of the radicals reported<sup>5</sup> to exhibit nonequivalent methyl protons, 1,4-dimethylanthrasemiquinone anion.

We shall employ throughout the standard numbering scheme given below.



#### Experimental Section

**Materials.** Solvents and reagents were commercially available and were purified by established literature methods prior to use. Tetrabutylammonium perchlorate (Southwestern Analytical Chemicals), or the tetraethyl salt (Distillation Products Industries), was

employed as the supporting electrolyte in electrochemical procedures at a concentration of 0.1 M.

1,4,5,8-Tetramethylanthraquinone (TMAQ) and 1,4-dimethylanthraquinone (DMAQ) were synthesized by modifications<sup>8</sup> of the procedures described by Alder and Kuth.<sup>9</sup> Final purification of both compounds was effected via vacuum sublimation. Satisfactory elemental analyses and exact agreement with literature<sup>9</sup> melting points were obtained for both quinones.

**Electrochemistry.** Polarography was carried out using the Oak Ridge National Laboratory three-electrode polarograph described previously.<sup>10</sup> Polarographic data were obtained in acetonitrile using tetraethylammonium perchlorate supporting electrolyte.

Radicals for esr measurements were produced by total electrolytic reduction of TMAQ and DMAQ in 1,2-dimethoxyethane (DME) solution to yield the corresponding semiquinone anions (TMAQ<sup>-</sup> and DMAQ<sup>-</sup>). A vacuum electrolysis cell similar to that described by Bolton and Fraenkel<sup>11</sup> was employed.

(1) Abstracted from the Ph.D. thesis of R. H. Schlossel, Cornell University, 1968.

(2) (a) Deceased, Dec 4, 1967; (b) author to whom correspondence should be addressed at the Florida State University, Tallahassee, Fla., 32306.

(3) W. M. Gulick, Jr., and D. H. Geske, *J. Amer. Chem. Soc.*, **88**, 4119 (1966), and references cited therein.

(4) See, for example, G. Vincow and G. K. Fraenkel, *J. Chem. Phys.*, **34**, 1333 (1961).

(5) R. M. Elofson, K. F. Schulz, B. E. Galbraith, and R. Newton, *Can. J. Chem.* **43**, 1553 (1965).

(6) Different coupling constants for the protons of a methyl group were observed for the propyl radical in propane solution in the temperature range -145 to -180°C (R. W. Fessenden and R. H. Schuler, *J. Chem. Phys.*, **39**, 2147 (1963)).

(7) D. H. Geske, *Progr. Phys. Org. Chem.*, **4**, 188 (1967).

(8) The authors thank Professor M. J. Goldstein for helpful suggestions with the syntheses.

(9) K. Alder and R. Kuth, *Angew. Chem.*, **609**, 32, 35 (1957).

(10) K. Kuwata and D. H. Geske, *J. Amer. Chem. Soc.*, **86**, 2101 (1964).

(11) J. R. Bolton and G. K. Fraenkel, *J. Chem. Phys.*, **40**, 3307 (1964).

**Table I:** Results

Radical	Position	Calcd <sup>a</sup> spin density ( $\rho_c^\pi$ )	Hyperfine splittings, G		No. of equiv spins of $I = 1/2$
			Calcd <sup>b</sup> ( $a$ )	Exptl <sup>c</sup> ( $ a $ )	
DMAQ <sup>-</sup> (ethanol), line width of 0.045 G	1	0.02191	0.767	0.837	6
	2	0.03939	-1.064	1.193	2
	5	0.02071	-0.559	0.433	2
	6	0.03738	-1.009	0.931	2
DMAQ <sup>-</sup> (DME), line width of 0.035 G	1	0.01143	0.400	0.512	6
	2	0.04167	-1.125	1.179	2
	5	0.01054	-0.285	0.210	2
	6	0.04035	-1.089	0.902	2
TMAQ <sup>-</sup> (DME), line width of 0.055 G	1	0.01142	0.400	0.329	12
	2	0.04161	-1.123	1.153	4
Anthrasemiquinone (DME)	1	0.01055	-0.285	0.271 <sup>d</sup>	4
	2	0.04041	-1.091	0.974 <sup>d</sup>	4
Anthrasemiquinone (ethanol-water)	1	...	...	0.550 <sup>d</sup>	4
	2	...	...	0.962 <sup>d</sup>	4

<sup>a</sup> Calculated using molecular orbital parameters from M. R. Das and G. K. Fraenkel, *J. Chem. Phys.*, **42**, 1350 (1965), and methyl group parameters from C. A. Coulson and V. A. Crawford, *J. Chem. Soc.*, 2052 (1953). Spin densities given include the approximate configuration interaction method of McLachlan (A. D. McLachlan, *Mol. Phys.*, **3**, 233 (1960)). <sup>b</sup> Calculated via  $a_H = -27 \rho_c^\pi$  and  $a_{H(CH_3)} = 35 \rho_c^\pi$ . <sup>c</sup> Uncertainty estimated at the 1% level. <sup>d</sup> Data from M. R. Das and G. K. Fraenkel, *J. Chem. Phys.*, **42**, 1350 (1965).

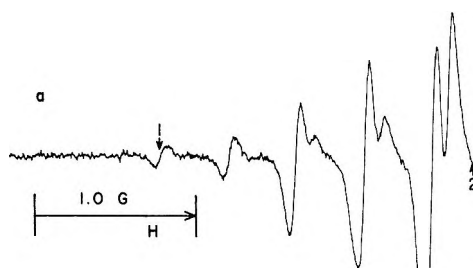
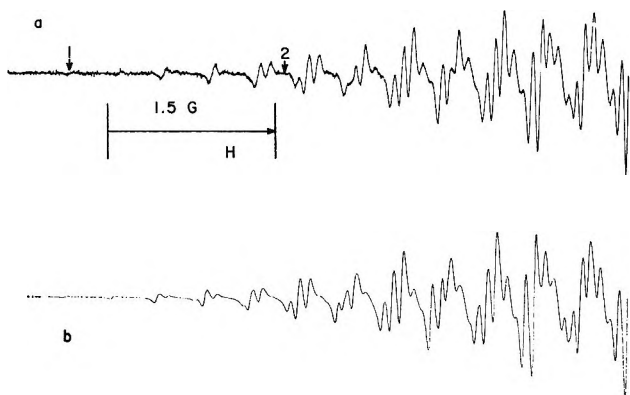


Figure 1. (a) Low-field half of the esr spectrum of 1,4-dimethylanthraquinone anion in absolute ethanol (small numbered arrows indicate points of correspondence in Figures 1a and 2a); (b) computed spectrum based on the assignment and line width given in Table I.

Samples prepared in this way were stable at room temperature for several weeks. DMAQ was also reduced electrolytically in absolute ethanol using a cell designed in these laboratories and described elsewhere.<sup>12</sup>

**Esr Spectra.** The Varian X-band 100-kHz spectrometer system employed has been described previously<sup>10</sup> as has the method of magnetic field calibration.<sup>3</sup> The Varian V-4547 variable-temperature accessory was used to obtain spectra below room temperature. Simulations of esr spectra were computed using a modification of the program devised by Stone and Maki<sup>13</sup> executed on a Control Data Corp. 1604 computer.

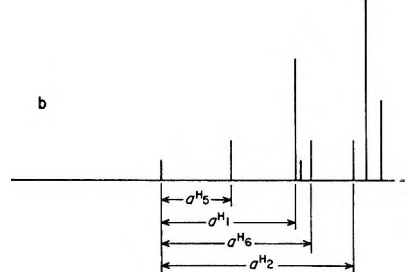


Figure 2. (a) Esr spectrum of 1,4-dimethylanthraquinone anion in absolute ethanol, low-field end line region (see Figure 1a for position relative to the rest of the spectrum); (b) reconstruction of this portion of the spectrum based on the assignment given in Table I.

## Results

Esr results are summarized in Table I. All spectra

(12) W. M. Gulick, Jr., W. E. Geiger, Jr., and D. H. Geske, *J. Amer. Chem. Soc.*, **90**, 4218 (1968).

(13) E. W. Stone and A. H. Maki, *J. Chem. Phys.*, **38**, 1999 (1963).

**Table II:** Polarographic Results in Acetonitrile

	1st reduction wave			2nd reduction wave		
	$-E_{1/2}^a$	$-[E_{3/4} - E_{1/4}]^b$	$I^c$	$-E_{1/2}^a$	$-[E_{3/4} - E_{1/4}]^b$	$I^c$
DMAQ	1.082	55	4.3	1.569	52	3.8
TMAQ	1.272	49	3.2	1.727	70	3.1
Anthraquinone <sup>d</sup>	0.94	...	1.5	1.45	...	1.5
Nitrobenzene <sup>e</sup>	1.147	56	4.1	...	...	...

<sup>a</sup> Volts *vs.* aqueous saturated calomel electrode. <sup>b</sup> Millivolts; for a reversible electron transfer  $-56/n$  mV is predicted (J. Tomes, *Coll. Czech. Chem. Commun.*, **9**, 1281 (1937)). <sup>c</sup>  $I = i_d/Cm^{2/3}t^{1/6}$ . <sup>d</sup> Data from M. E. Peover, *J. Chem. Soc.*, 4540 (1962). <sup>e</sup> Data from D. H. Geske and A. H. Maki, *J. Amer. Chem. Soc.*, **82**, 2671 (1960).

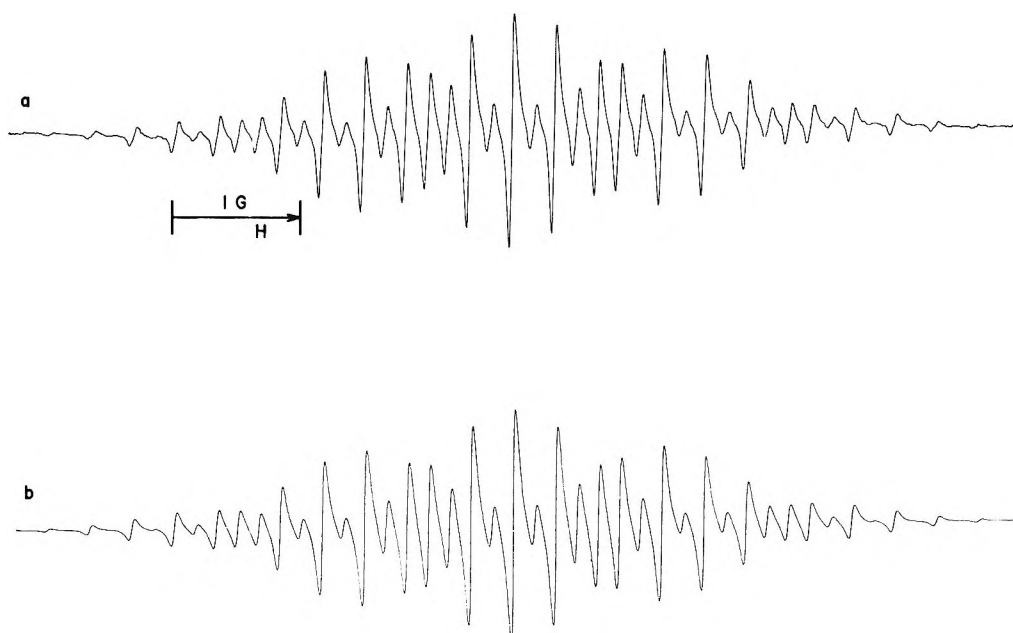


Figure 3. (a) ESR spectrum of 1,4,5,8-tetramethylantraquinone anion in 1,2-dimethoxyethane; (b) computed spectrum based on the assignment and line width given in Table I.

obtained were assignable *only* on the basis of magnetic equivalence of all methyl protons.<sup>14</sup> Figure 1 compares the ESR spectrum of DMAQ<sup>-</sup> in absolute ethanol at 25° with a computed spectrum based on the coupling constants and line width indicated in Table I. In Figure 2 a detailed assignment of the end line region of this spectrum is shown. Comparable agreement between experimental and computed spectra was obtained for DMAQ<sup>-</sup> in DME. In Figure 3 the experimental spectrum of TMAQ<sup>-</sup> in DME at 25° is compared with a spectrum computed using the parameters given in Table I. Magnetic equivalence of the methyl protons in TMAQ<sup>-</sup> is retained at lower temperatures. At -50° in DME the spectrum is readily assigned to 12 methyl protons with  $a_H = 0.353$  G, 4 ring protons with  $a_H = 1.153$  G, and a line width of 0.087 G. Electrochemical results are given in Table II.

## Discussion

Careful examination of the spectra presented here, particularly the end line regions, convinces us that the

assignments given are correct. Particular attention was paid to eliminating alternative assignments in which one proton from each methyl group had a coupling constant significantly smaller than the other two protons. Such alternative assignments proved completely unacceptable for TMAQ<sup>-</sup> and exceedingly unlikely for DMAQ<sup>-</sup> in either solvent.

When possible, assignments of coupling constants to specific molecular positions have been made from the numbers of equivalent protons involved as deduced from the ESR splitting patterns. The ambiguities remaining for DMAQ<sup>-</sup> were resolved with the aid of molecular orbital calculations and by comparison of the effect of changing the solvent medium with the solvent effect reported<sup>15</sup> for anthrasemiquinone.

The previous assignment given for DMAQ<sup>-</sup> in 2-propanol<sup>6</sup> is six pairs of equivalent protons with coupling

(14) A detailed discussion of these assignments and consideration of alternative assignments can be found in the Ph.D. thesis of R. H. Schlossel, Cornell University, 1968.

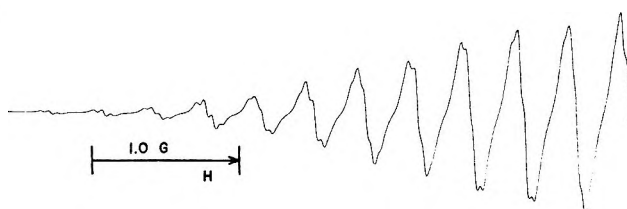


Figure 4. Computed esr spectrum of 1,4-dimethylanthraquinone anion in 2-propanol based on the assignment of Elofson, *et al.*,<sup>5</sup> and assuming a line width of 0.035 G (see the text).

constants as follows: ring protons:  $a_H = 0.68$ ,  $a_H = 0.64$  and  $a_H = 0.33$ , and methyl protons:  $a_H = 0.99$ ,  $a_H = 0.96$  all  $a_H = 0.05$  (all values in gauss). Although we were unable to obtain esr spectra of either radical in 2-propanol, we feel that the ethanol system is sufficiently similar to permit reasonable comparison. The previous report<sup>5</sup> gave no indication of the experimental line width; however, for the sake of comparison a computed spectrum based upon the coupling constants given above and a very narrow line width, 0.035 G, is given in Figure 4. This computed spectrum appears to be better resolved than the previous<sup>5</sup> experimental spectrum of DMAQ<sup>-</sup>, yet it is not certain that *unambiguous* assignment of even this spectrum is possible.

It is clear that the previous assignment is wholly incompatible with the experimental results given here. Thus, barring the unlikely circumstance of some unique medium effect of basic 2-propanol, we are compelled to reject as untenable the assertion of blocked rotation of 1-methyl groups in anthrasemiquinone radicals. We conclude just the opposite, that down to at least

$-50^\circ$  the rotation of methyl groups in these radicals is rapid with respect to any geometrically induced difference in hyperfine frequency.

Since the esr spectra of methylated anthrasemiquinones were previously<sup>5</sup> assigned by a computerized numerical analysis,<sup>16</sup> we wish to emphasize the cautions with which one must approach any type of mathematical analysis which attempts to analyze and reproduce observed data. First, given a sufficient number of adjustable parameters, it is possible to reproduce any set of data. Second, the confidence one may put in the conclusions drawn from any such analysis procedure must depend on the accuracy and detail of the *data* which are being approximated. The implications for computer analysis of esr spectra follow in a straightforward manner.

*Acknowledgment.* The authors gratefully acknowledge support for this research from the National Science Foundation under Grant GP-4906, as well as through Grant GP-1687 for partial support for purchase of the esr spectrometer.

(15) M. R. Das and G. K. Fraenkel, *J. Chem. Phys.*, **42**, 1350 (1965). The experimental proton splittings from this reference for anthrasemiquinone in basic ethanol-water are in turn taken from G. Vincow and G. K. Fraenkel, *J. Chem. Phys.*, **34**, 1333 (1961). In a personal communication, Dr. M. R. Das assures us that substantially identical proton splittings were observed when anthrasemiquinone was generated by electroreduction in neutral absolute ethanol. Thus the differences between splittings observed in DME and ethanol represent a true solvent effect rather than a pH or gegenion effect.

(16) R. Newton, K. F. Schulz, and R. M. Elofson, *Can. J. Chem.*, **44**, 752 (1966).

# Hydrogen Ion Titration and Sodium Ion Activity of Tropomyosin Solutions

by Shozo Iida and Nobuhisa Imai

Department of Physics, Faculty of Science, Nagoya University, Chikusa-ku, Nagoya, Japan (Received June 4, 1968)

Potentiometric titrations and Na<sup>+</sup> ion activity measurements in tropomyosin solutions were carried out over a wide range of pH by using an improved hydrogen electrode and a Na<sup>+</sup>-sensitive glass electrode. The experimental results were analyzed by the theories of rodlike polyelectrolyte, since both tropomyosin monomer and its fibrous polymers, whose transformation is reversibly controlled by salt concentration, are highly charged and rodlike. The titration data indicated the normal titration behavior of the main ionizable groups in high and low salt concentrations. The agreement of the experimental and theoretical values of Linderstrøm-Lang parameter  $w$  was satisfactory in acidic and neutral pH's. A further analysis of  $w_{\text{exptl}}$  in the polymer state supported side-overlapping polymerization. The Henderson-Hasselbach relation was useful for the analysis of carboxyl regions, and these plots showed abnormal pH changes in the isolectric precipitation regions. The small values of  $w_{\text{exptl}}$  at high pH were interpreted to be due to the medium penetration into protein resulting from unfolding. The additivity rule for counterion activity was perfectly established at high and neutral pH's, and a thermodynamic relationship between pH and counterion activity derived from the additivity rule was also experimentally confirmed.

## Introduction

Tropomyosin, one of the muscle proteins, characteristically polymerizes into fibrous form at low ionic strength and depolymerizes reversibly at high salt concentration.<sup>1</sup> Tropomyosin is a rodlike protein with a length<sup>2</sup> of 400 Å and has a great number of ionizable groups and a high helical content (nearly 100%) at acidic and neutral pH's.<sup>3,4</sup> The degree of polymerization is remarkably affected by pH, showing two maxima at pH 6.5 and 8.5,<sup>5</sup> which suggests the strong connection of ionizable groups to the polymerization process. Both polymer and monomer states are stable enough for accurate thermodynamic observations.

Tropomyosin is thus a very interesting protein for electrochemical investigations as a rodlike polyelectrolyte. It is especially worthwhile to examine whether or not the behaviors of hydrogen and counterions can be explained by the polyelectrolyte theories.

In this study, accurate hydrogen ion titrations are carried out over a wide range of pH in cases of both high and low salt concentrations, and Na<sup>+</sup> ion activity measurements are carefully done at various NaCl concentrations and pH's. These data are analyzed by the polyelectrolyte theories. It can be concluded from these results that the behavior of hydrogen ions can be elucidated by these theories and that the ionization constants of the main groups of tropomyosin are not abnormal (*i.e.*, no appreciable buried groups are present in tropomyosin). It is also found that the additivity rule for counterions, which is an important rule in usual polyelectrolytes,<sup>6,7</sup> is satisfactorily applicable to the tropomyosin solutions.

In our titration experiments, a hydrogen electrode is preferably used to avoid the asymmetry potential which is inevitable in glass electrodes and causes a considerable error in the titrations at high and low pH's.

Since the usual hydrogen electrodes with platinum black are not available in weakly buffered, neutral solutions because of the error due to the release of acidic substances occluded in the electrode, the Hammett-type hydrogen electrode,<sup>8,9</sup> which is free from this error, is employed in our experiments. On the basis of our pH measurements, the Hammett electrode is found to perform well in the titrations of very dilute tropomyosin solutions.

## Experimental Section

**Materials.** Tropomyosin was prepared according to the procedure of Bailey<sup>1</sup> or Tsao<sup>10</sup> with slight modification. After actin was extracted in water from acetone-dried muscle by Mommaerts' method,<sup>11</sup> the insoluble residue was washed three times with ethanol and then twice with ether, prior to drying in air overnight. Tropomyosin was extracted at room temperature from this ether-dried muscle in 1 M KCl over a 10-hr period. Isoelectric precipitate of tropomyosin, made by lowering the pH of the solution to 4.8 with HCl, was gathered and again dispersed in 1 M KCl by bringing the pH to 7 with KOH. Next, 70% aqueous ammonium sulfate

- (1) K. Bailey, *Biochem. J.*, **43**, 271 (1948).
- (2) T. C. Tsao, K. Bailey, and C. S. Adavi, *ibid.*, **49**, 27 (1951).
- (3) C. E. Bodwell, D. R. Kominz, and B. J. Dunleavy, *Biochem. Biophys. Acta*, **21**, 210 (1963).
- (4) C. Cohen and A. G. Szent-Györgyi, *J. Amer. Chem. Soc.*, **79**, 248 (1957).
- (5) S. Iida and T. Ooi, *Arch. Biochem. Biophys.*, **121**, 526 (1967).
- (6) Z. Alexaderowicz, *J. Polym. Sci.*, **56**, 9 (1962).
- (7) G. S. Manning and B. H. Zimm, *J. Chem. Phys.*, **43**, 4250 (1966).
- (8) L. P. Hammett, *J. Amer. Chem. Soc.*, **46**, 7 (1924).
- (9) H. T. Beans and L. P. Hammett, *ibid.*, **47**, 1215 (1925).
- (10) T. C. Tsao and K. Bailey, *Biochem. Biophys. Acta*, **11**, 102 (1953).
- (11) W. F. H. M. Mommaerts, *J. Biol. Chem.*, **198**, 445 (1952).

was added to the solution, and the resulting impure precipitate was removed by centrifugation. Solid ammonium sulfate was then added to the supernatant to 60% saturation, and the resulting precipitate of tropomyosin was gathered and dialized against pure water. The above treatment was repeated three times. After the dialysis the absence of sulfate ion was confirmed with  $\text{BaCl}_2$ .

For sodium activity measurements,  $\text{NH}_4^+$  ions in solution were completely exchanged by  $\text{Na}^+$  ions by repeated additions of excess  $\text{NaCl}$  to the solution and dialysis against deionized water.

The concentration of tropomyosin was obtained by uv spectroscopy at  $277 \text{ m}\mu$  where the value of  $\text{OD}_{277}^{1\%}$  was 2.82.

The KOH and NaOH solutions used in the titrations were freshly prepared before each titration. In the case of KOH, the grains of KOH were carefully washed and dissolved immediately into  $\text{CO}_2$ -free water. In the case of NaOH,  $\text{CO}_2$ -free solutions were directly obtained from the supernatant phase of a saturated NaOH solution.

The alkali concentrations were determined by titration with a standard HCl whose acidity had accurately been obtained conductometrically by consulting MacInnes's table. The determination of relative alkali concentrations with respect to HCl solution was required to be highly accurate.

## Methods

**Titration.** The pH measurements were performed with a KCl-saturated calomel and hydrogen electrode assembly described in the next section.

Hydrogen gas was produced by electrolysis of 20% NaOH solution and was purified by bubbling through a series of three pyrogallol-NaOH solutions. The fresh hydrogen gas covered the solution and was never bubbled through the solution. The total volume of each solution in the cell (made of Pyrex) was 20 ml. Each solution was agitated by a magnetic stirrer prior to measurement. The stirrer was stopped during each reading.

Before initiation of a titration, each of the solutions was incubated for several hours with stirring to establish hydrogen equilibrium and to assure complete removal of  $\text{CO}_2$  gas from the solution, the cell being tightly sealed from air. After the incubation, pH response of the hydrogen electrode followed by a drop of alkali or acid from a micropipet was generally very fast, and a quick reading was possible for salt solutions at high or low pH range. At neutral pH range of protein solutions or even simple salt solutions, however, the response was not fast, and this retardation was similarly observed in the case of fresh glass electrodes. Each reading during a titration was made after the complete establishment of equilibrium.

The cell was immersed in an isothermal bath ( $25 \pm$

$0.05^\circ$ ) composed of a 1 M aqueous KCl solution which was very effective in avoiding noise even when high-impedance electrodes, such as sodium electrodes, were used. The pH readings were made with a potentiometer combined with a galvanometer as a sensitive detector which detected a deviation of  $\text{pH } 2 \times 10^{-4}$  unit on 1 mm of its mirror scale. A laboratory-made amplifier whose input impedance was more than  $10^{11}$  ohms was set before the potentiometer (Shimadzu Type PD) and was used for both hydrogen and glass electrodes.

The hydrogen ion titration was carried out by successive additions of KOH or HCl from a microburet (Metrohm E 374) which had a total capacity of 1 ml and a fine-scale division of  $10^{-3}$  ml.

A solvent blank, to be subtracted from the curves of protein solutions, was experimentally obtained in the following way. Experimental curves of pH vs.  $\log C_{\text{H}}$  (or  $C_{\text{OH}}$ ) were first made for simple KCl solutions of which concentrations were the same as the protein solutions. ( $C_{\text{H}}$  is the concentration of hydrogen ions.) Each of these curves could be expressed graphically by several continuous straight lines with slightly different gradients over a wide range of  $C_{\text{H}}$ , so that the experimental relationship between pH and alkali concentration needed to bring the simple salt solution to that pH could be given. From these formulas, any salt-blank value corresponding to one pH of the protein solution could be computed with great accuracy. In this procedure, the activity coefficient of hydrogen ions in protein solution was assumed to be the same as the simple salt solutions at the same pH.

The pH measurements were performed for salt solutions prior to the titration of protein, and this procedure was very useful not only as a check of the electrodes but also a reconfirmation of the previously determined alkali concentrations.

**Hydrogen Electrode.** A gold plate ( $1 \times 1 \text{ cm}$ ; thickness, 0.1 mm) which was connected with a glass-sealed gold wire (1 mm in diameter) was first washed in fused NaOH in a nickel furnace (30 ml) for 1 hr to expel the acidic substances occluded in the gold plate. Next, brighten platinum was deposited on the gold plate by electrolysis in 3%  $\text{NaPtCl}_4$  solution at pH 9-10 for a few minutes with a current density of  $20 \text{ mA/cm}^2$ . Then the electrode was washed in distilled hot water for 10 min before use. This electrode (Hammett's electrode<sup>8,9</sup>) has no bad effect resulting from the release of acidic substances occluded in the electrode and is usable for weakly buffered solutions or very dilute protein solutions (as low as 0.01% concentration).

**Sodium Electrode.** A Horiba No. 1012  $\text{Na}^+$  electrode was employed for sodium ion activity measurement. This electrode could detect sodium ion activity  $10^{-5}$  mol with negligible error at pH more than 7. The electrode was cleaned after each series of experiments and refreshed occasionally by 8% HF solution (for 1

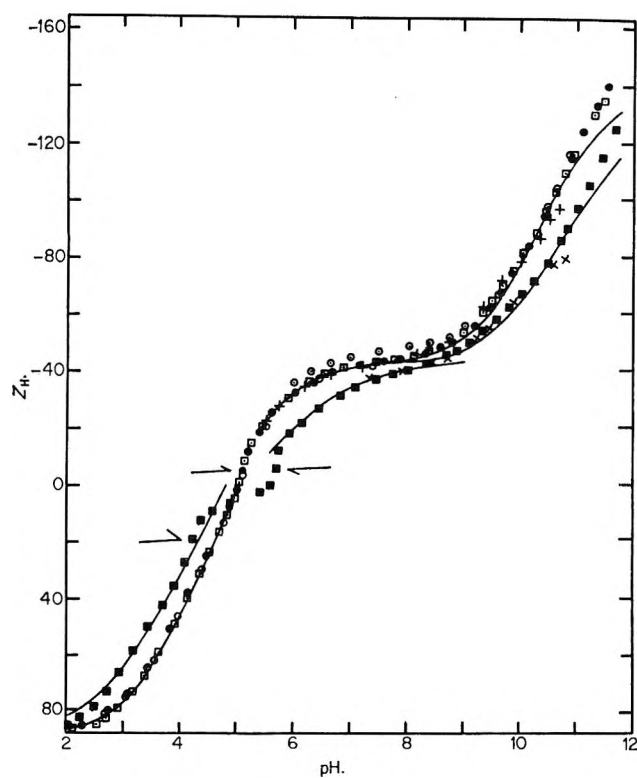


Figure 1. Hydrogen ion titration curves of tropomyosin in 1 M KCl and 0.01 M KCl at 25°: 1 M KCl: +, 0.006 mg/ml; □, 5 mg/ml; ●, 2 mg/ml; ○, O, back-titration; 0.01 M KCl: ■, 2 mg/ml; ×, 0.006 mg/ml. Arrows indicate precipitation regions.

min) and concentrated NaOH. The asymmetry potential which always accompanied glass electrodes was calibrated before each experiment using a set of standard NaCl solutions.<sup>12</sup>

*Calomel Electrode.* The calomel electrode was kept immersed in saturated KCl in a glass vessel (50 ml) in the isothermal bath, and a KCl liquid-junction tube from the vessel was joined to a glass tube having a pin hole at its end which contacted the measured solution. The pin hole on the glass tube was carefully made such that leakage of KCl was as small as possible within a negligible diffusion potential.

## Results

Figure 1 shows the whole aspect of the hydrogen ion titration of tropomyosin between pH 2 and 12 at KCl concentrations 0.01 and 1.0 M. The backward titrations are done for 1.0 M KCl. The ordinate,  $Z_H$ , represents the algebraic sum of H<sup>+</sup> ions bound to and released from a protein molecule. If no specific binding of coexistent salt ions is postulated, the value of  $Z_H$  is equal to the number of net charges of a protein. The solid lines are the theoretical curves, as described later.

The titrations originate from neutral pH to high pH (up to 12) or to low pH (down to 2). As seen in Figure 1, the backward titration curves coincide almost perfectly with the forward titration curves. A slight dif-

ference, however, is observed in the neutral region between the backward titration from high pH and its original forward titration. This is theoretically due to partial alkali denaturation.

In Figure 1, the titration curves for different protein concentrations are also shown for the case of 1.0 M KCl. The coincidence of these curves, including the case of a very dilute protein concentration, demonstrates the high accuracy of our pH measurements.

The isoelectric precipitation region in 1.0 M KCl is between pH 5.3 and about 3.0, the lower limit of which is very indefinite, while the precipitation region in 0.01 M KCl is clearly definite between pH 5.8 and 4.2. The precipitation points are indicated by arrows in the figure. Even in the precipitation regions, the titration curves are reproducible and the pH readings are very stable.

The pH is generally expressed with degree of ionization,  $\alpha_i$ , and intrinsic ionization constant,  $K_0^i$ , of group  $i$  by the relation

$$\text{pH} = \text{p}K_0^i + \log \frac{\alpha_i}{1 - \alpha_i} + 0.868wZ \quad (1)$$

$$Z = \sum_i n_i \alpha_i \quad (2)$$

where  $wZ$  is the free energy change (divided by  $kT$ ) due to electrostatic interaction and  $n_i$  is the number of ionizable groups,  $i$ , with a positive sign for basic groups and a negative sign for acidic groups. According to Linderstrøm-Lang,  $w$  is independent of the protein net charge  $Z$  on the basis of the Debye-Hückel approximation and is dependent on molecular dimension and ionic strength. The point  $Z = 0$  can be obtained on a titration curve by finding the point such that the amount of acid needed to bring the solution at the  $Z = 0$  point to the flat region of the titration curve at sufficiently low pH is equal to the total number of basic groups. The total number of basic groups is calculated to be 87 on the basis of the amino acid analysis.

In Figure 2,  $\text{pH} - \log [\alpha_c/(1 - \alpha_c)]$  is plotted for carboxyl groups as a function of  $Z_H$  in low and neutral pH ranges. The degree of ionization of carboxyl groups,  $\alpha_c$ , is calculated from the amount of added alkali without calibrating imidadol groups, the total number of which is negligibly small in comparison with carboxyl groups (see Table I).

As seen in Figure 2, there seem to be two transition-like  $w$  changes in 0.01 M KCl and one change in 1.0 M KCl in the precipitation regions. The appearance of only the one change in 1.0 M KCl is probably related to the unclear cutoff precipitation on the low pH side.

By approximating the curves in Figure 2 by several straight lines (shown by the solid lines), the values of  $w$  are calculated from the corresponding slopes and the intrinsic  $pK$ 's of carboxyl groups are obtained by extrap-

(12) N. Imai and H. Eisenberg, *J. Chem., Phys.*, **44**, 130 (1966).

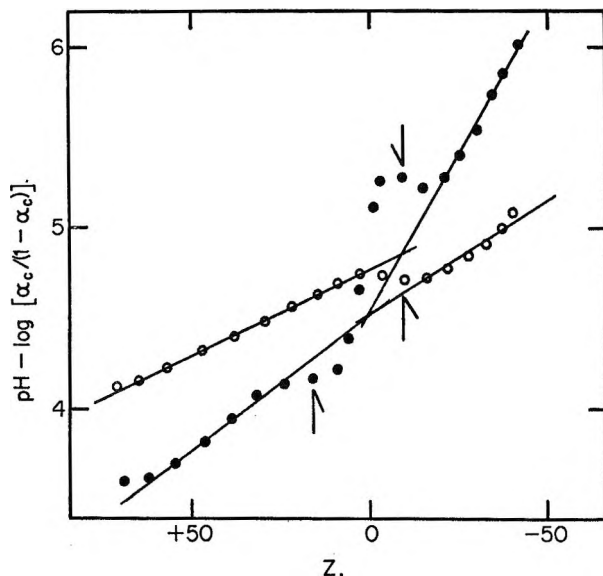


Figure 2. Logarithmic plots for the dissociation of carboxyl groups at ionic strength 0.01 (●) and 1 M KCl (○). Arrows indicate the precipitation regions.

Table I: Parameters Used for the Calculation of Theoretical Titration Curves

Group	No.	pK <sub>int</sub>
Carboxyl	128	4.6, 4.78*
Imidazole	3	(7.0) <sup>b</sup>
Sulphydryl	3	(9.0) <sup>b</sup>
ε-Amino	60	9.9
Phenolic	8	(10.4) <sup>c</sup>
Guanidyl	23	11.6

\* Value in precipitation region in 1 M KCl. <sup>b</sup> Assumed values. <sup>c</sup> Value by S. Lowey.

olating these straight lines to  $Z = 0$ . The solid curves in Figure 1 are the theoretical curves based on these  $w$ 's. In the alkali region, however, these  $w$ 's are not available because of the unfolding of tropomyosin, as has been reported.<sup>13</sup> Therefore, pK's of guanidyl and ε-amino groups and  $w$ 's are suitably chosen so as to make the calculation curves fit the experimental curves in the alkali region. By this procedure, the results of the amino acid analysis<sup>14</sup> and the spectroscopical pK value of phenol group in tropomyosin<sup>13</sup> are applied, and the pK values of imidazol and sulphydryl groups, whose total numbers are very small, are suitably assumed. Molecular weight of tropomyosin is taken to be  $5.4 \times 10^4$ .<sup>2,15</sup> The intrinsic pK's and  $w$ 's thus obtained are summarized in Tables I and II.

The theoretical values of  $w$  listed in Table II are calculated by the Hill relation valid for rodlike macromolecules<sup>16</sup>

$$w = \frac{e_0^2}{DkTL} \frac{K_0(\kappa a)}{\kappa a K_1(\kappa a)} + \ln \frac{a}{R} \quad (3)$$

Table II: Experimental and Theoretical Values of  $w$

Region	0.01 M KCl		1 M KCl	
	$w_{\text{exptl}}$	$w_{\text{theor}}$	$w_{\text{exptl}}$	$w_{\text{theor}}$
Acidic	0.018		0.00815	
Neutral	0.040		0.008	
Alkali	0.0090		0.0030	

where  $e_0$ ,  $D$ , and  $\kappa$  denote elementary charge, dielectric constant of solvent, and Debye-Hückel parameter, respectively; and  $L$ ,  $R$ , and  $a$  are the length, radius, and impenetrable radius (for small ions) of the protein rod, respectively. The functions  $K_0(x)$  and  $K_1(x)$  represent modified Bessel functions. Equation 3 should be applicable for both rodlike tropomyosin monomer and its fibrous polymer. In the case of the polymer,  $L$  in eq 3 should be the length per monomer if  $Z$  is taken as number of net charges per monomer. Putting into the equation  $a = 9 \text{ \AA}$ ,  $R = 8 \text{ \AA}$ , and  $L = 400 \text{ \AA}$ , which are reasonable values for tropomyosin monomer, we have the theoretical value of  $w$  in 1 M KCl. If the end-to-end association of monomers is assumed for the polymer,  $w$  in neutral 0.01 M KCl can also be calculated using the same numerical dimensional values. These theoretical values of  $w$  are listed in Table II. The above rigid, rodlike model is not suitable for the calculation of  $w$  in alkali region because of the unfolding of tropomyosin, so that a medium-penetrable rod model is necessarily applied. This analysis will be discussed in the next section.

As observed in Figure 2, the plots are not completely expressed by the combinations of straight lines. It has been experimentally known in synthetic polyelectrolyte solutions that the following Henderson-Hasselbach equation is more applicable for pH- $\alpha$  relation and is more effective in recognizing the conformational transition<sup>17</sup>

$$\text{pH} = m \log [\alpha / (1 - \alpha)] + \text{p}K_1 \quad (4)$$

where  $K_1$  and  $m$  are practically constants independent of  $\alpha$ . Equation 4 is equivalent to the relation

$$1 - \alpha = \frac{K_2 a_H^{1/m}}{1 + K_2 a_H^{1/m}} \quad (5)$$

where  $K_2$  is a constant and  $a_H$  is the  $\text{H}^+$  ion activity in solution. In polymethacrylic acid solutions, the values of  $m$  and  $K_1$  suddenly change at a certain critical  $\alpha$ , where the conformational change of polyion takes place.<sup>17</sup> In Figure 3 the Henderson-Hasselbach plots of tropomyosin in the ionizing region of carboxyl groups

(13) S. Lowey, *J. Biol. Chem.*, **240**, 2421 (1965).

(14) D. R. Komintz, A. Hough, P. Symonds, and K. Laki, *Arch. Biochem. Biophys.*, **50**, 148 (1954).

(15) T. Ooi, K. Mihashi, and H. Kobayashi, *ibid.*, **98**, 1 (1962).

(16) T. L. Hill, *ibid.*, **57**, 229 (1955).

(17) J. C. Leyte and M. Mandel, *J. Polym. Sci.*, **2**, 1879 (1964).

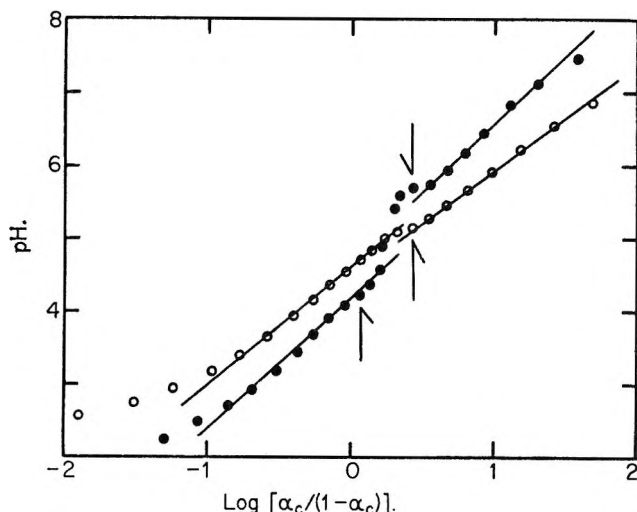


Figure 3. Henderson-Hasselback plots of carboxyl groups. The symbols are the same as in Figure 2.

are shown. Obviously the plots are composed of several straight lines for both cases of salt condition. This fact more clearly demonstrates the transition-like phenomena in the neighborhood of the isoelectric precipitation regions.

According to the counterion activity, the following relation, the so-called "additivity rule," has been experimentally and theoretically proven

$$a_p = \gamma_s C_s + \gamma_p C_p \quad (6)$$

where  $a_p$  is the counterion activity in the polyelectrolyte solution with added salt concentration  $C_s$ , and  $\gamma_s$  and  $\gamma_p$  denote the activity coefficients of counterions in a simple salt solution having a concentration  $C_s$  and in a salt-free polyelectrolyte solution with a net-charge concentration  $C_p$ , respectively. Equation 6 has been one of the most important rules in highly charged polyion systems. This rule implies that the number of counterions in the ion-condensed phase in the vicinity of a polyion is not affected by the addition of salt; i.e., the effective polyion charge is kept constant against added salt concentration. The salt effect is the alteration of electric potential in the vicinity of polyions to keep the additivity rule. In Figure 4, the observed values of  $a_p - \gamma_s C_s$  for Na<sup>+</sup> ions in tropomyosin solutions are plotted against added NaCl concentration,  $C_s$ . As observed in the figure, the establishment of the additivity rule is perfect in the region of the present NaCl concentrations. In these NaCl concentration ranges, tropomyosin maintains the polymer form at neutral pH's and is in the dispersed state at pH 10.

In Figure 5, Na<sup>+</sup> ion activity in a salt-free solution is plotted against added NaOH concentration, with the pH change during this process indicated by the broken line. An appreciable breaking point is observed in the figure, and this point appears just at the pH where the association of  $\epsilon$ -amino groups start. This fact

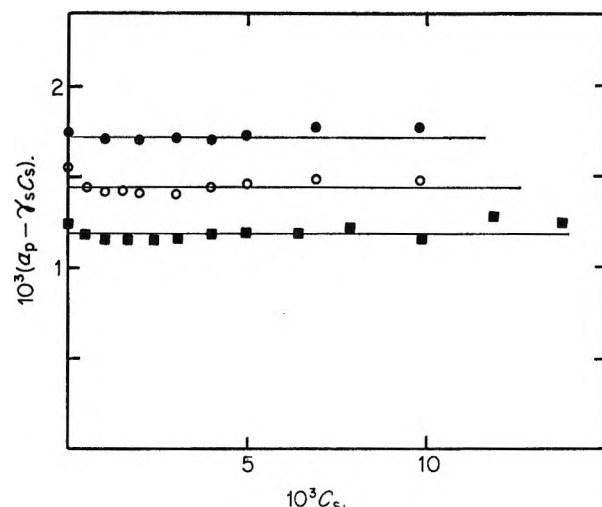


Figure 4. Sodium ion activity *vs.* added NaCl concentration at three pH's in tropomyosin solutions: ●, pH 9.98; ○, pH 8.14; ■, pH 7.06. The ordinate represents the difference between sodium ion activity in tropomyosin and in simple salt solution at the same salt concentration.

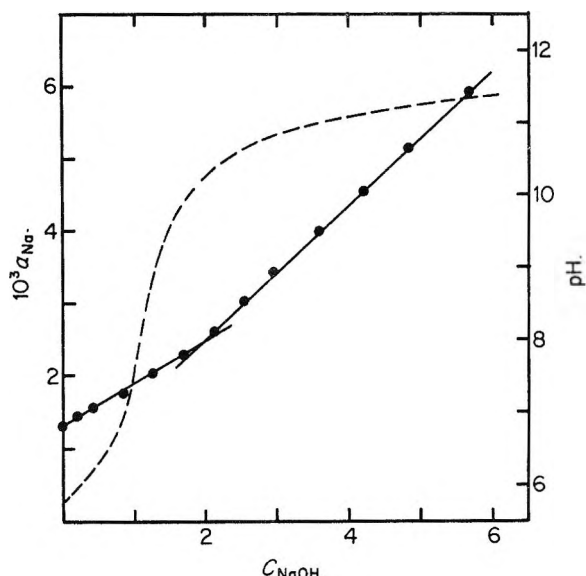


Figure 5. Activity change of sodium ion resulting from addition of NaOH. The dashed line shows the corresponding pH change.

suggests that the two different processes of increasing negative charges of tropomyosin give the different binding characters for Na<sup>+</sup> ions.

### Discussions

As seen in Figure 2,  $w_{\text{exptl}}$  (experimental value of  $w$ ) at acidic pH is almost the same as  $w_{\text{exptl}}$  at neutral pH in the case of 1 M KCl. This is reasonable in view of the fact that unfolding of tropomyosin is not likely at acidic pH. The unlikelihood of the conformational change at acidic pH has been shown by the data of optical rotatory dispersion, in which the same helical contents are observed at both acidic and neutral

pH's.<sup>13,18</sup> The disagreement of the values of  $w_{\text{exptl}}$  between neutral and acidic pH's observed in the case of 0.01 M KCl is attributed to the side-overlapping polymerization in the neutral region, which has been concluded from the light-scattering experiments.<sup>15</sup> According to their result, the increase of polymer length for addition of one monomer to a polymer corresponds to 35% of monomer length in the side-overlapping polymerization. This means that  $L$ , length per monomer, should be 140 Å (= 400 Å × 0.35) in neutral pH instead of the 400 Å found in acidic pH. This value of  $L$  gives a  $w$  which is three times larger than the  $w$  in neutral pH. Our data show the ratio  $w_{\text{neutral}}/w_{\text{acid}} = 2.2$ , which corresponds to 50% side overlapping using the assumption of uniform charge distribution on the protein. Although we cannot discuss in detail the degree of the overlapping from the titration data, the large value of  $w_{\text{exptl}}$  in neutral 0.01 M KCl may be interpreted at least qualitatively by this polymer structure. The theoretical values of  $w$  in Table II show fairly good agreement with the experimental values, at least in order of magnitude.

At alkali pH, the values of  $W_{\text{exptl}}$  are small in both salt concentrations. This is attributed to the unfolding of protein due to the charge repulsion between ionized acidic groups. If we suppose that the medium becomes able to penetrate into the protein as a result of swelling at alkali pH, the following expression of  $w$ , derived for a medium-penetrable rod model, would be applicable

$$w = \frac{2e_0^2}{DkTL(\kappa R)^2} \times \left( 1 - \frac{K_1(\kappa R)}{K_1(\kappa R)I_0(\kappa R) + K_0(\kappa R)I_1(\kappa R)} \right) \quad (7)$$

This relation is obtained from the electric potential at the center of the rod, and the potential is derived under the assumptions of uniform charge distribution of groups inside the rod and the Debye-Hückel linear approximation. From this equation, the values of  $R$  which give the experimental  $w$ 's at alkali pH (0.009 for 1 M KCl and 0.003 for 0.01 M KCl) are calculated by using the previous value of  $L$  (= 400 Å). These calculated values of  $R$  are 10 Å for 1 M KCl and 46 Å for 0.01 M KCl. This fact suggests the considerable expansion of protein in low ionic strength. The small increase of  $R$  in 1 M KCl is due to the strong depression of electric potential by salt ions inside protein, principally dominant in concentrated salt in the medium-penetrable model. By referring to the viscosity data which have demonstrated the sharp depolymerization with respect to pH's greater than 8.5 in 0.01 M KCl,<sup>5</sup> we may conclude that the unfolding is accompanied

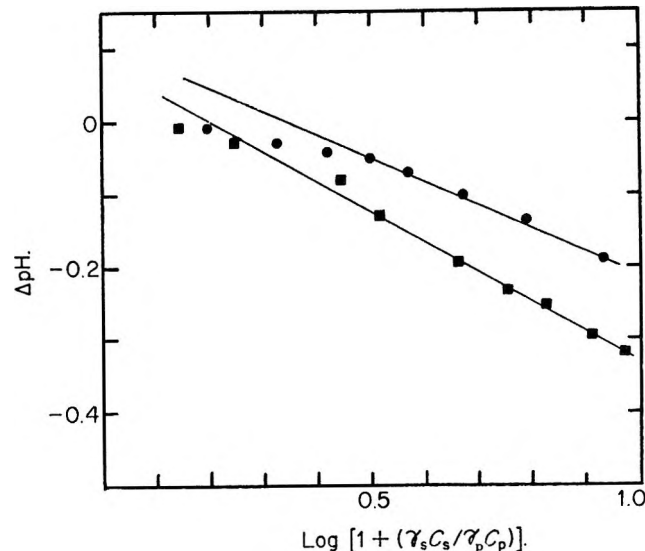


Figure 6. pH change resulting from addition of NaCl to tropomyosin at two initial pH's: ●, pH 9.98; ■, 7.06.

by the depolymerization. This conclusion agrees with the results of the optical rotatory dispersion.<sup>13</sup>

As shown in Figure 4, the additivity rule is satisfied in tropomyosin solutions. The validity of this rule can be experimentally confirmed by testing the applicability of the following equation between pH and added salt concentration

$$\Delta \text{pH} = \text{pH}(C_s) - \text{pH}(0) = \left( \frac{\partial}{\gamma_s \partial C_p} (\gamma_p C_p) - 1 \right) \log \left( 1 + \frac{\gamma_s C_s}{\gamma_p C_p} \right) \quad (8)$$

where pH(0) denotes the value of pH at  $C_s = 0$  and  $\Delta \text{pH}$  is deviation of pH at salt concentration  $C_s$  from pH(0). This equation has been thermodynamically derived on the basis of the additivity rule.<sup>19</sup> By using the values of  $\gamma_p C_p$  obtained from Figure 4, the values of pH experimentally observed can be plotted against  $\log [1 + (\gamma_s C_s / \gamma_p C_p)]$  as shown in Figure 6. These plots are almost straight and this result again demonstrates the applicability of the additivity rule in tropomyosin solutions. (The change of  $\gamma_s$  in eq 8 is practically insignificant.) Under the further assumption of constant  $\gamma_p$  against  $C_p$ , which has been nearly satisfied experimentally in usual polyelectrolytes, the values of  $\gamma_p$  are calculated to be about 0.52 for pH 7 and 0.61 for pH 10.

*Acknowledgments.* We wish to express our thanks to Professor F. Oosawa and the members of Polymer Laboratory in Department of Physics, Nagoya University, who gave us their valuable suggestions.

(18) C. E. Bodwell, D. R. Komins, and B. J. Duntley, *Biochem. Biophys. Res. Commun.*, 21, 210 (1965).

(19) F. Oosawa, *Biopolymers*, 6, 135 (1968).

# Apparent Invariance of Activity Coefficients of Calcium Sulfate at Constant Ionic Strength and Temperature in the System CaSO<sub>4</sub>-Na<sub>2</sub>SO<sub>4</sub>-NaNO<sub>3</sub>-H<sub>2</sub>O to the Critical Temperature of Water. Association Equilibria<sup>1,2</sup>

by LeRoy B. Yeatts and William L. Marshall

*Reactor Chemistry Division, Oak Ridge National Laboratory, Oak Ridge, Tennessee 37830 (Received June 7, 1968)*

To obtain and interpret activity coefficient behavior over wide ranges of temperature and concentration, measurements were made of the solubility of calcium sulfate in mixed aqueous solutions of sodium nitrate and sodium sulfate at ionic strengths ( $I$ ) from 0.25 to 6  $m$  and at temperatures from 0 to 350°. With the assumption of ion association, the activity coefficients of the neutral molecule (CaSO<sub>4</sub><sup>0</sup>) and of the ions were found to remain constant, at all temperatures, as the molality of sodium sulfate was varied widely at constant  $I$ . When  $I$  was varied, the logarithms of the activity coefficients of CaSO<sub>4</sub><sup>0</sup> appeared to be linear functions of  $I^{1/2}$  rather than of  $I$  as is usually considered for neutral molecules. The logarithms of the mean ionic activity coefficients adhered well to an extended Debye-Hückel expression over the ranges of temperature and ionic strength. From the interpretation given, the equilibrium constants and thermodynamic functions were obtained for the formation of the neutral molecule and for the dissociation equilibria.

## Introduction

The question of the existence of ion association for particular electrolytes in aqueous solutions is still debated.<sup>3</sup> For example, association constants for several 1-1 electrolytes, KNO<sub>3</sub>, AgNO<sub>3</sub>, and TlCl, in water solution at 25° are estimated from conductance measurements to be 0.58, 0.51, and 3.1, respectively,<sup>3</sup> indicating an appreciable fraction of ion pairs at finite concentrations. Yet 1-1 salts in general are usually considered to be very strongly or completely ionized at 25° and Debye-Hückel theory used to predict their thermodynamic behavior. Furthermore, in treating the behavior of activity coefficients in mixed-electrolyte solutions, usually the change in formal (stoichiometric) activity coefficients is related to a change in composition of mixed electrolytes at constant ionic strength.<sup>4</sup> With this approach the potential existence of ion pairs, a physically significant entity, is concealed in the formal coefficient. It was therefore the purpose of this study to make solubility measurements of a suitable salt, calcium sulfate, in a mixed-electrolyte system over a wide range of temperature to determine whether an assumption of ion association might account for the major change in formal activity coefficient with change in composition of mixed electrolytes. This finding would provide further support for ion association and also additional clues to the general behavior of electrolyte solutions over wide ranges of temperature and ionic strength.

The extent of association of calcium sulfate in water at 25° was calculated by Money and Davies<sup>5</sup> from the

conductivity data of both MacGregory<sup>6</sup> and Harkins and Paine.<sup>7</sup> They obtained a value for the dissociation constant of 10<sup>-2.28</sup>, assuming first that the conductivity of a completely ionized 2-2 electrolyte is given by an extended form of Onsager's equation and, second, that all deviations from this extended equation are due to ion association. An electrode for measuring calcium ion activity was used with saturated CaSO<sub>4</sub> solutions by Nakayama and Rasnick<sup>8</sup> to determine a dissociation constant of 10<sup>-2.27</sup> at 25°. The activity coefficient of the undissociated CaSO<sub>4</sub> was required for the calculation of  $K_d$  and was assumed to be unity. Bell and

(1) The research was sponsored jointly by the U. S. Atomic Energy Commission and the Office of Saline Water, U. S. Department of the Interior, and was performed at the Oak Ridge National Laboratory under contract with Union Carbide Corp. Presented before the Division of Physical Chemistry at the 153rd National Meeting of the American Chemical Society, Miami Beach, Fla., April 1967.

(2) Paper No. XXI in a series, "Aqueous Systems at High Temperature." Preceding papers: W. L. Marshall, *J. Phys. Chem.*, 71, 3584 (1967); W. L. Marshall and R. Slusher, *J. Chem. Eng. Data*, 13, 83 (1968).

(3) R. A. Robinson and R. H. Stokes, "Electrolyte Solutions," 2nd ed., revised, Prentice-Hall, Inc., Englewood Cliffs, N. J., 1965, pp 392-431.

(4) See ref 3, pp 432-455.

(5) R. W. Money and C. W. Davies, *Trans. Faraday Soc.*, 28, 609 (1932).

(6) A. C. MacGregory, "Lancolt-Börnstein Physikalisch-Chemische Tabellen," Vol. II, J. Springer Publ., Berlin, 1923, p 1081; *Ann. Phys. Chem.*, 51, 126 (1894).

(7) W. D. Harkins and H. M. Paine, *J. Amer. Chem. Soc.*, 41, 1155 (1919).

(8) F. S. Nakayama and B. A. Rasnick, *Anal. Chem.*, 39, 1022 (1967).

George<sup>9</sup> in 1953 estimated the dissociation constants at 0, 25, and 40° to be  $10^{-2.22}$ ,  $10^{-2.31}$ , and  $10^{-2.39}$ , respectively. These values were obtained indirectly from measurements of the solubility of calcium iodate in potassium sulfate solutions, with the assumption that all deviations from the Davies equation could be attributed to incomplete ionization and again that the activity coefficients of uncharged ion pairs are equal to unity. Recently, estimates of the dissociation constants for  $\text{CaSO}_4$  were extended to 200° by solubility measurements at this laboratory.<sup>10</sup> These approximate values ranged from  $10^{-1.9 \pm 0.4}$  at 0° to  $10^{-3.5 \pm 0.6}$  at 200° and could account for the small deviations from an extended Debye-Hückel expression. The use of theoretical equations by Helgeson<sup>11</sup> for the dissociation reaction at 25° gives values for thermodynamic quantities which are in reasonable agreement with those of Bell and George.<sup>9</sup>

Some of the basic concepts that were applied in this present study are indicated in papers by Ramette<sup>12</sup> and Meites, Pode, and Thomas.<sup>13</sup> The present measurements were made generally in the four-component, mixed-electrolyte system  $\text{CaSO}_4\text{-Na}_2\text{SO}_4\text{-NaNO}_3\text{-H}_2\text{O}$  at constant ionic strengths of 0.25, 0.5, 1, 2, and 6 at temperatures of 0.5, 25, 150, 250, and 350°. Sodium sulfate was used to vary the sulfate ion concentration and sodium nitrate was added to adjust the ionic strength of the solutions to the desired constant value. Several studies<sup>14</sup> between 25 and 100° have been made in the past of the solubilities of  $\text{CaSO}_4\cdot 2\text{H}_2\text{O}$  in the presence of soluble sulfates, but no effort was made to maintain constant ionic strength.

## Experimental Section

Stock solutions of 6 M  $\text{NaNO}_3$  and 1 M  $\text{Na}_2\text{SO}_4$  were prepared from weighed quantities of dried reagent grade chemicals and demineralized water. These solutions were diluted quantitatively to the desired concentration for each experiment. Reagent grade  $\text{CaSO}_4\cdot 2\text{H}_2\text{O}$  was suspended in boiling demineralized water, was stirred constantly for about 1 hr to remove soluble impurities, and then was filtered. The recovered material was treated again in this manner and the final product was dried near 100°. An excess of this solid was equilibrated with aqueous solutions of  $\text{NaNO}_3$ ,  $\text{Na}_2\text{SO}_4$ , or mixtures of the two at constant ionic strength for a given experiment. Polyethylene bottles were the containing vessels for the  $0.5 \pm 0.1$  and  $25.0 \pm 0.1^\circ$  experiments; these with their contents were rocked in a constant-temperature water bath for 18–22 hr before sampling. Pressure vessels made from a titanium alloy contained the mixtures for the experiments at  $150 \pm 1$ ,  $250 \pm 1$ , and  $350 \pm 1^\circ$ . The equilibration times before sampling were generally 65 hr at 150°, followed by additional 20-hr periods at both 250 and 350°. A longer equilibration time was used at 150° to assure complete conversion of  $\text{CaSO}_4\cdot 2\text{H}_2\text{O}$ , the

solid added, to  $\text{CaSO}_4$ , the stable solid at the high temperature. The volume of starting materials was sufficient to permit sampling at all three temperatures before reloading of the vessels was required. Solutions at each temperature were filtered through porous Teflon disks,<sup>15</sup> during sample withdrawal, at the temperature of the experiment. The total calcium concentration of each solution sample was determined from a semimicro potentiometric titration with standard EDTA solution. The density and the total weight of solids per unit volume of each solution were determined after equilibration. The former was used to convert molarity to molality and the latter served as a means of checking the prior dilution of standard solutions.

More detailed descriptions of the experimental equipment and procedures have been presented previously.<sup>10, 15–17</sup>

## Results and Discussion

**General.** Our results for the solubility of  $\text{CaSO}_4\cdot 2\text{H}_2\text{O}$  in water are  $0.0132 \pm 0.0002$  m (average deviation) at 0.5° and  $0.0154 \pm 0.0001$  m (average deviation) at 25°, in agreement with previously determined values.<sup>10</sup> The experimentally determined molal solubilities of  $\text{CaSO}_4$  or its dihydrate in aqueous  $\text{Na}_2\text{SO}_4\text{-NaNO}_3$  solutions from 0.5 to 350° are presented in Table I. A plot of the solubilities of  $\text{CaSO}_4\cdot 2\text{H}_2\text{O}$  in aqueous  $\text{NaNO}_3$  solutions at 25° against the molality of  $\text{NaNO}_3$  provides a smooth curve with previous data.<sup>18</sup> The recent solubility measurements in  $\text{NaNO}_3$  at 300° by Templeton and Rodgers<sup>19</sup> are in reasonable agreement with our results at ionic strengths of 0.5 and 1, but at  $I = 2$ , their result is about 25% higher than would be anticipated from a plot of solubility vs. temperature using our data. Comparisons of the solubilities of the dihydrate in the presence of  $\text{NaNO}_3$  (Table I) show that the solubility at 0.5° is less than at 25° up to an ionic strength near 1, at which point the

- (9) R. P. Bell and J. H. B. George, *Trans. Faraday Soc.*, **49**, 619 (1953).
- (10) W. L. Marshall and R. Slusher, *J. Phys. Chem.*, **70**, 4015 (1966).
- (11) H. C. Helgeson, *ibid.*, **71**, 3121 (1967).
- (12) R. W. Ramette, *J. Chem. Educ.*, **43**, 299 (1966).
- (13) L. Meites, J. S. F. Pode, and H. C. Thomas, *ibid.*, **43**, 667 (1966).
- (14) J. M. Bell and W. C. Tabor, *J. Phys. Chem.*, **11**, 637 (1907); A. E. Hill, *J. Amer. Chem. Soc.*, **56**, 1071 (1934); A. E. Hill and N. S. Yanick, *ibid.*, **57**, 645 (1935); A. E. Hill and J. H. Wills, *ibid.*, **60**, 1647 (1938); A. N. Campbell and N. S. Yanick, *Trans. Faraday Soc.*, **28**, 657 (1932).
- (15) W. L. Marshall and E. V. Jones, *J. Phys. Chem.*, **70**, 4028 (1966).
- (16) L. B. Yeatts and W. L. Marshall, *ibid.*, **71**, 2641 (1967).
- (17) J. S. Gill and W. L. Marshall, *Rev. Sci. Instrum.*, **32**, 1060 (1961).
- (18) A. Seidell and J. G. Smith, *J. Phys. Chem.*, **8**, 493 (1904).
- (19) C. C. Templeton and J. C. Rodgers, *J. Chem. Eng. Data*, **12**, 536 (1967).

**Table I:** The Molal Solubilities of  $\text{CaSO}_4 \cdot 2\text{H}_2\text{O}$  and  $\text{CaSO}_4$  in  $\text{Na}_2\text{SO}_4\text{-NaNO}_3\text{-H}_2\text{O}$  Solutions from 0.5 to 350°

$\text{CaSO}_4 \cdot 2\text{H}_2\text{O}^a$	$\text{Na}_2\text{SO}_4$	$\text{NaNO}_3$	$I = 0.504 \pm 0.005$			0.00365	0.0512	0.92	0.00753	0.0479	5.71
(m)	(m)	(m)	0.0350	0	0.386	0.00250	0.102	0.77	0.00637	0.0595	5.58
$T = 0.5^\circ\text{C}$			0.0344	0	0.376	0.00242	0.102	0.77	0.00466	0.0955	5.58
$I^b = 0.229 \pm 0.006$			0.0302	0.0103	0.376				0.00434	0.107	5.52
			0.0261	0.0204	0.356				0.00370	0.140	5.33
			0.0233	0.0305	0.335	0.0185	0	2.12	0.00326	0.179	5.33
0.0226	0	0.151	0.0210	0.0408	0.324	0.0174	0.00213	2.11			
0.0232	0	0.150	0.0186	0.0509	0.294	0.0154	0.00640	2.11			
0.0205	0.00506	0.140	0.0157	0.0712	0.254	0.0130	0.0128	2.11			
0.0196	0.00760	0.140	0.0135	0.0913	0.192	0.0106	0.0213	2.11			
0.0184	0.0101	0.131	0.0105	0.163	0	0.00716	0.0426	2.05			
0.0164	0.0152	0.120	0.0104	0.163	0	0.00449	0.0854	1.90			
0.0151	0.0202	0.121				0.00355	0.143	1.76			
0.0113	0.0404	0.081									
0.00997	0.0506	0.051									
0.00922	0.0607	0.040	0.0474	0	0.876		$I = 5.80 \pm 0.05$		0.000403	0	0.263
0.00841	0.0707	0	0.0283	0.0515	0.771	0.0275	0	5.67	0.000345	0.000110	0.260
0.00813	0.0708	0	0.0203	0.103	0.667	0.0246	0.00595	5.66	0.000291	0.000218	0.258
			0.0159	0.154	0.512	0.0222	0.0118	5.66	0.000140	0.000767	0.231
			0.0136	0.204	0.356	0.0182	0.0238	5.67	0.000132	0.000850	0.255
			0.0123	0.255	0.203	0.0130	0.0475	5.67	0.000124	0.000898	0.266
$I = 0.503 \pm 0.006$											
0.0326	0	0.386	0.0114	0.334	0	0.00816	0.0947	5.53	0.000671	0.00157	0.261
0.0278	0.0103	0.376				0.00803	0.106	5.47	0.000534	0.00175	0.229
0.0239	0.0204	0.356				0.00623	0.142	5.42	0.000512	0.00225	0.255
0.0205	0.0305	0.335				0.00580	0.177	5.28	0.000477	0.00216	0.243
0.0186	0.0408	0.324	0.0638	0	1.92	0.00465	0.291	4.88	0.000245	0.0116	0.240
0.0162	0.0509	0.294	0.0431	0.0534	1.86				0.000233	0.00526	0.244
0.0136	0.0712	0.254	0.0375	0.0745	1.81				0.000138	0.0283	0.200
0.0115	0.0913	0.192	0.0312	0.106	1.70						
0.00853	0.161	0	0.0226	0.174	1.48						
			0.0177	0.255	1.22	0.00133	0	0.240			
			0.0137	0.506	0.51	0.00133	0	0.236	0.000852	0	0.513
$I = 1.02 \pm 0.03$						0.000880	0.00100	0.233	0.000738	0.000323	0.551
0.0469	0	0.880				0.000588	0.00254	0.237	0.000550	0.000644	0.553
0.0276	0.0517	0.773	0.0805	0	5.75	0.000373	0.00501	0.232			
0.0193	0.103	0.670	0.0651	0.0361	5.76	0.000265	0.0109	0.228	0.000377	0.00110	0.523
0.0148	0.154	0.512	0.0568	0.0602	5.62				0.000168	0.00338	0.567
0.0121	0.204	0.356	0.0441	0.108	5.56				0.000104	0.00580	0.549
0.0107	0.255	0.203	0.0329	0.179	5.35	0.00218	0	0.479	0.0000784	0.0108	0.519
			0.0240	0.297	4.97	0.00174	0.00101	0.478			
$I = 2.14 \pm 0.06$			0.0171	0.580	4.05	0.00123	0.00260	0.487			
0.0678	0	1.92				0.00830	0.00505	0.479			
0.0461	0.0534	1.86				0.000355	0.0253	0.428	0.00120	0.00166	1.11
0.0402	0.0747	1.81				0.000325	0.0517	0.361	0.000885	0.00272	1.08
0.0333	0.106	1.70	$\text{CaSO}_4^a$	$\text{Na}_2\text{SO}_4$	$\text{NaNO}_3$				0.000847	0.00333	1.11
0.0240	0.174	1.48							0.000574	0.00542	1.08
0.0187	0.255	1.22							0.000505	0.00865	1.16
									0.000460	0.0105	1.08
$I = 6.02 \pm 0.08$						0.00394	0.000531	1.07	0.000282	0.0175	1.14
0.0858	0	5.78	0.00619	0	0.228	0.00339	0.00154	1.03	0.000238	0.0475	1.13
0.0696	0.0362	5.78	0.00567	0.00995	0.229	0.00314	0.00258	1.03	0.000232	0.0278	1.00
0.0599	0.0600	5.62	0.00427	0.00494	0.229	0.00287	0.00310	1.04	0.000191	0.0558	0.95
0.0469	0.108	5.56	0.00309	0.00963	0.202	0.00239	0.00514	1.02			
0.0363	0.180	5.38	0.00188	0.0246	0.178	0.00177	0.00779	1.04			
0.0263	0.297	4.97	0.00144	0.0485	0.097	0.00155	0.0103	1.03			
0.0176	0.583	4.07				0.00111	0.0156	1.02	0.00447	0.00113	2.28
						0.000682	0.0258	0.97	0.00380	0.00280	2.26
$T = 25^\circ\text{C}$			0.00860	0	0.474	0.000531	0.0514	0.92	0.00291	0.00564	2.27
			0.00842	0.000986	0.473	0.000450	0.102	0.77	0.00201	0.0112	2.25
			0.00650	0.00499	0.471				0.00101	0.0279	2.26
$I = 0.232 \pm 0.006$			0.00508	0.00992	0.455						
0.0257	0	0.151	0.00292	0.0249	0.422	0.00732	0.00107	2.15			
0.0254	0	0.151	0.00199	0.0482	0.336	0.00668	0.00266	2.14	0.0194	0	5.95
0.0232	0.00506	0.141				0.00572	0.00534	2.15	0.0166	0.00618	5.93
0.0208	0.0101	0.131				0.00409	0.0107	2.16	0.0143	0.0125	5.96
0.0207	0.0101	0.131				0.00224	0.0266	2.10	0.0108	0.0246	5.88
0.0177	0.0202	0.121	0.0127	0	1.03	0.00147	0.0533	2.04	0.00906	0.0383	6.12
0.0175	0.0202	0.121	0.0123	0.000510	1.03				0.00760	0.0502	5.99
0.0138	0.0404	0.081	0.0117	0.00153	1.02				0.00626	0.0622	5.83
0.0134	0.0404	0.081	0.0112	0.00305	1.02				0.00496	0.101	5.90
0.0122	0.0506	0.051	0.00918	0.00765	1.03	0.0196	0	5.71	0.00453	0.113	5.84
0.0119	0.0506	0.051	0.00698	0.0153	1.00	0.0170	0.00598	5.71	0.00402	0.151	5.77
0.0104	0.0707	0	0.00562	0.0257	0.96	0.0146	0.0120	5.71	0.00291	0.0279	3.97
0.0102	0.0707	0	0.00407	0.0406	0.97	0.0111	0.0239	5.69	0.00269	0.0568	

<sup>a</sup> Saturating solid phase (molalities expressed as  $\text{CaSO}_4$ ). <sup>b</sup>  $I$  is the ionic strength (molal units). <sup>c</sup> Only data below the dashed line were used to obtain values for  $Q_u$  and  $Q_{isp}$ .

reverse is true as the ionic strength increases to 6. The solubilities of  $\text{CaSO}_4 \cdot 2\text{H}_2\text{O}$  at 0.5 and 25° are approximately 1.8 and 1.6 times greater, respectively, in 6 m  $\text{NaNO}_3$  solutions than in  $\text{NaCl}$  solutions of the same molality;<sup>10</sup> the same trend is true of anhydrous  $\text{CaSO}_4$  at 150°<sup>20</sup> and at 250 and 300°.<sup>19</sup> This behavior was observed also for the solubilities of  $\text{Ca}(\text{OH})_2$  in aqueous  $\text{NaNO}_3$  and  $\text{NaCl}$  solutions at 0.5 and 25°.<sup>16</sup>

**Equilibria.** When aqueous solutions are saturated with calcium sulfate, it was assumed that equilibrium is reached with neutral molecules or ion pairs



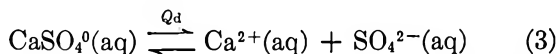
which can be expressed by<sup>21</sup>

$$Q_u = [\text{CaSO}_4^0] \text{ (molal units)} \quad (2)$$

The neutral species is considered to undergo partial dissociation

(20) W. L. Marshall, R. Slusher, and E. V. Jones, *J. Chem. Eng. Data*, **9**, 187 (1964).

(21) In the instances where  $\text{CaSO}_4 \cdot 2\text{H}_2\text{O}$  is the saturating solid, it is conventional to write the corresponding equilibrium expression as  $Q'_u = [\text{CaSO}_4^0][\text{H}_2\text{O}]^2$ . Since in this study molal units are used and we have not considered the reaction of solvent with solute species, the molality of water has a constant 55.51 value in all these solutions. Therefore, the constant term,  $[\text{H}_2\text{O}]^2$ , for convenience was not included in our  $Q_u$  values at 0.5 and 25°. Similarly, our expression for  $K_u$ , when the solid is the dihydrate, does not include



for which the equilibrium quotient expression is

$$Q_d = [\text{Ca}^{2+}][\text{SO}_4^{2-}]/[\text{CaSO}_4^0] \text{ (molal units)} \quad (4)$$

The ionic solubility product quotient is then defined as

$$Q_{isp} = [\text{Ca}^{2+}][\text{SO}_4^{2-}] = Q_d Q_u \quad (5)$$

With these assumptions the molal solubility of calcium sulfate,  $s$ , at constant temperature and ionic strength is given by

$$s = [\text{CaSO}_4^0] + [\text{Ca}^{2+}] \quad (6)$$

Since  $[\text{CaSO}_4^0] = Q_u$  and  $[\text{Ca}^{2+}] = Q_{isp}/[\text{SO}_4^{2-}]$ , then

$$s = Q_u + (Q_{isp}/[\text{SO}_4^{2-}]) \quad (7)$$

The total calcium sulfate and the sodium sulfate molalities are found experimentally. The molality of  $\text{SO}_4^{2-}$  ions is determined in the following manner

$$[\text{SO}_4^{2-}] = (\text{total sulfate}) -$$

$$[\text{CaSO}_4^0] = [\text{SO}_4]_{\text{total}} - Q_u \quad (8)$$

where

$$[\text{SO}_4]_{\text{total}} = s + [\text{Na}_2\text{SO}_4] \quad (9)$$

A more useful form initially of eq 7 is

$$s = Q_u + [Q_{isp}/([\text{SO}_4]_{\text{total}} - Q_u)] \quad (10)$$

indicating that successive approximations of the value for  $Q_u$  are necessary to establish the molality of  $\text{SO}_4^{2-}$  ion. The ionic strength is defined throughout this paper as

$$I \text{ (molal units)} =$$

$$m_{\text{NaNO}_3} + 3m_{\text{Na}_2\text{SO}_4} + 4(s - m_{\text{CaSO}_4^0}) \quad (11)$$

Implicit in these arguments are the complete ionization of  $\text{NaNO}_3$  and  $\text{Na}_2\text{SO}_4$  at all ionic strengths and invariant or nearly invariant activity coefficients at constant ionic strength. If these assumptions are correct, a plot of  $s$  vs.  $1/[\text{SO}_4^{2-}]$ , at constant temperature and ionic strength, should produce a straight line, according to eq 7, with a slope equal to  $Q_{isp}$  (or  $Q_d Q_u$ ) and an intercept equal to  $Q_u$  (or  $[\text{CaSO}_4^0]$ ).

The data in Table I were treated by a method of nonlinear least squares<sup>22</sup> to produce values of  $Q_{isp}$ ,  $Q_u$ , and  $Q_d$ ; these are expressed as logarithms and are presented in Table II. The results for 25, 250, and 350° are plotted according to eq 7 in Figures 1-3 and show the general linear behavior observed at all five temperatures. (The open and filled circles in the figures are used only to distinguish between data at different ionic strengths.) The data at 0.5 and 150° with the corresponding values of  $Q_u$  from Table II also provide straight lines. All plots show a similar ionic strength effect on solubility at constant temperature. In Figures 1-3 a dashed curve was drawn to indicate

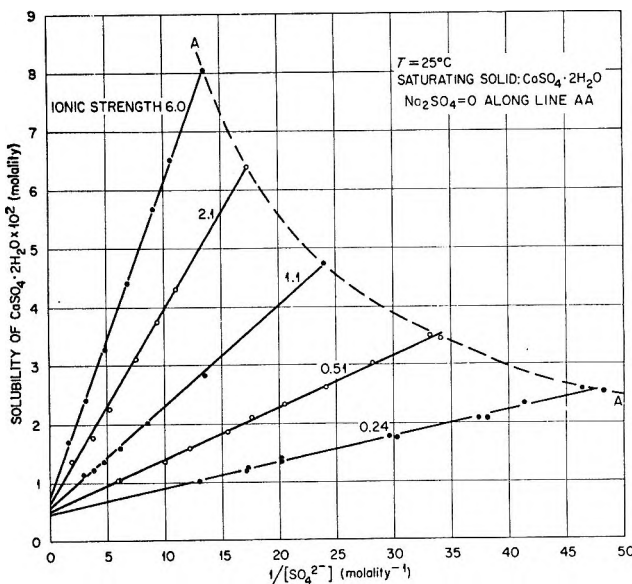


Figure 1. The solubility of  $\text{CaSO}_4 \cdot 2\text{H}_2\text{O}$  in  $\text{Na}_2\text{SO}_4\text{-NaNO}_3\text{-H}_2\text{O}$  at 25° and several constant ionic strengths.

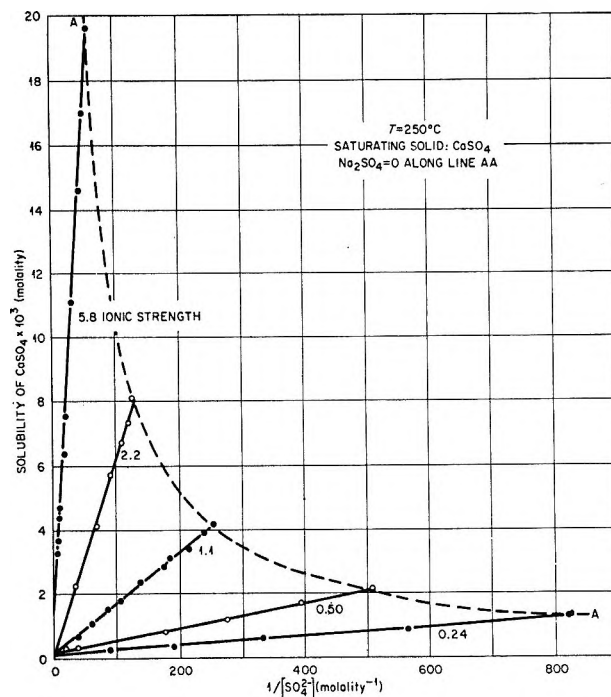


Figure 2. The solubility of  $\text{CaSO}_4$  in  $\text{Na}_2\text{SO}_4\text{-NaNO}_3\text{-H}_2\text{O}$  at 250° and several constant ionic strengths.

$a_{\text{H}_2\text{O}}^2$ , which in molal units would still equal (55.51)<sup>2</sup>. An allowance for a variation in the activity of water over the range of electrolyte compositions at constant  $I$  was unnecessary to describe the system within the precision of the measurements. The authors also consider it misleading to mix units in an equilibrium constant expression, as is frequently done, by multiplying the activity of water on the *mole fraction* scale together with the molality of  $\text{CaSO}_4^0$  and its activity coefficient. These remarks apply also to our considerations of  $Q_{isp}$  and  $K_{isp}$  for  $\text{CaSO}_4 \cdot 2\text{H}_2\text{O}$ .

(22) M. H. Lietzke, U. S. Atomic Energy Commission Report ORNL-3529, Oak Ridge National Laboratory, Oak Ridge, Tenn., April 1962.

solubility in  $\text{NaNO}_3\text{-H}_2\text{O}$  as a function of  $I$ , again at constant temperature; there is no added  $\text{Na}_2\text{SO}_4$  in these solutions so that it represents the three-component system  $\text{CaSO}_4\text{-NaNO}_3\text{-H}_2\text{O}$ . Similar experimental conditions prevailed at the other temperatures (see Table I). The data at 0.5 and 25° contain some results at zero molality of  $\text{NaNO}_3$  or results for the system  $\text{CaSO}_4\text{-Na}_2\text{SO}_4\text{-H}_2\text{O}$ .

**Table II:** Experimentally Obtained Equilibrium Quotients at Several Ionic Strengths from 0.5 to 350°

Temp. <sup>a</sup> °C	$I$	$-\log Q_{isp}$	$-\log Q_u$	$-\log Q_d$
0.5	0.229	3.416	2.49	0.93
	0.503	3.063	2.52	0.54
	1.02	2.726	2.47	0.26
	2.14	2.376	2.56 (2.37) <sup>b</sup>	0.01
	6.02	2.210	2.17	0.04
25	0.236	3.365	2.33	1.03
	0.504	3.055	2.30	0.76
	1.01	2.765	2.24	0.52
	2.10	2.478	2.22	0.26
	6.00	2.269	2.14 (2.04) <sup>b</sup>	0.23
150	0.250	4.540	3.10	1.44
	0.506	4.195	3.19	1.00
	1.07	3.891	2.92	0.97
	2.19	3.537	2.88	0.66
	5.82	3.196	2.66	0.54
250	0.244	5.836	3.95	1.89
	0.498	5.417	3.68 (3.87) <sup>b</sup>	1.55
	1.06	4.802	3.71	1.09
	2.21	4.248	3.47	0.78
	5.82	3.473	2.89	0.58
350	0.263	7.086	4.91	2.18
	0.542	6.291	4.62	1.67
	1.14	5.567	3.80 (4.24) <sup>b</sup>	1.33
	2.30	4.643	3.65	0.99
	6.08	3.521	2.69	0.83

<sup>a</sup> The saturating solid is  $\text{CaSO}_4\cdot 2\text{H}_2\text{O}$  at 0.5 and 25° and  $\text{CaSO}_4$  at 150–350°. <sup>b</sup> The value obtained from the plot of  $\log Q_u$  vs.  $I^{1/2}$  (Figure 5).

The only deviations from the linear relationship, within the precision of the measurements, are found at 350° for the lower ionic strengths of 0.26 and 0.54 (see Figure 3). Without additional information, it is difficult to account for these deviations, although they may be related to significant hydrolysis of  $\text{Ca}^{2+}$  at the highest temperature. The fact that eq 7 applies to the experimental data substantiates the assumption of constant activity coefficients at constant ionic strength with varying  $\text{Na}_2\text{SO}_4/\text{NaNO}_3$  ratio. This is more readily apparent by writing eq 7 in the equivalent form

$$s = (K_u / \gamma_{\text{CaSO}_4^0}) + [K_{isp} / ([\text{SO}_4^{2-}] \gamma_{\text{Ca}^{2+}} \gamma_{\text{SO}_4^{2-}})] \quad (12)$$

where  $K_u$  and  $K_{isp}$  are the equilibrium constants (or equilibrium quotients at  $I = 0$  expressed by eq 2 and 5,

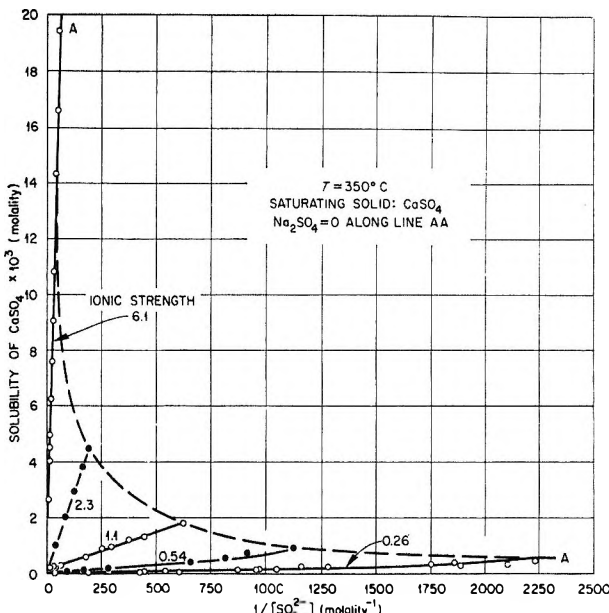


Figure 3. The solubility of  $\text{CaSO}_4$  in  $\text{Na}_2\text{SO}_4\text{-NaNO}_3\text{-H}_2\text{O}$  at 350° and several constant ionic strengths.

respectively) and  $\gamma_{\text{CaSO}_4^0}$ ,  $\gamma_{\text{Ca}^{2+}}$ , and  $\gamma_{\text{SO}_4^{2-}}$  are the activity coefficients for the corresponding species in solution. The above description, however, does not explain differences in solubility of  $\text{CaSO}_4$  in other 1-1 and mixed-electrolyte solutions at very high, constant ionic strengths, as our recent unpublished results show. Some additional interpretation therefore is still needed to account fully for the general solubility behavior under these conditions.

The description of the data by eq 7, within experimental error, constitutes a valid argument against the formation of significant amounts of either  $\text{CaNO}_3^+$  or  $\text{NaSO}_4^-$ . If both of these ion pairs form, the solubility of calcium sulfate,  $s$ , would no longer be given by eq 10 but would be given by the equation

$$s = [\text{CaSO}_4^0] + [\text{Ca}^{2+}] + [\text{CaNO}_3^+] = Q_{ut} \frac{Q_{isp}}{[\text{SO}_4^{2-}]_{\text{total}} - Q_u - [\text{NaSO}_4^-]} + [\text{CaNO}_3^+] \quad (13)$$

where  $[\text{SO}_4^{2-}] = [\text{SO}_4]_{\text{total}} - Q_u - [\text{NaSO}_4^-]$ . If it is assumed that no  $\text{NaSO}_4^-$  forms when the concentration of added  $\text{Na}_2\text{SO}_4$  is low, eq 13 indicates that an upward curvature of the lines (Figures 1-3) is expected, resulting from the formation of increasingly higher concentrations of  $\text{CaNO}_3^+$  as the  $\text{NO}_3^-$  concentration increases. If  $\text{CaNO}_3^+$  does not form at the lower concentrations of  $\text{NaNO}_3$ , then an upward curvature of the lines should appear as the concentration of added  $\text{Na}_2\text{SO}_4$  increases, opposite to the previous case, resulting from the increased solubility of  $\text{CaSO}_4$  due to the formation of increasingly greater amounts of  $\text{NaSO}_4^-$ . If both ion pairs,  $\text{CaNO}_3^+$  and  $\text{NaSO}_4^-$ , form in conjunction with  $\text{CaSO}_4^0$ , then the last two terms in eq 13 must change with mixed-electrolyte composition

such that a straight line with slope  $Q_{isp}$  is still obtained. This is necessary to satisfy the results of the plots in Figures 1-3. While it is true that  $\text{CaNO}_3^+$  and  $\text{NaSO}_4^-$  may play a significant role only where the molalities of  $\text{Ca}^{2+}$ ,  $\text{Na}^+$ ,  $\text{NO}_3^-$ , and  $\text{SO}_4^{2-}$  are highest, the stringent condition placed on eq 13 for linearity must be met at all five experimental temperatures. We suggest that linearity under these conditions is highly improbable and prefer to present the simpler model which satisfactorily describes the experimental results. (Within experimental uncertainty, lower limits of 1350 and 14,000 for the dissociation quotients of  $\text{CaNO}_3^+$  and  $\text{NaSO}_4^-$ , respectively, were calculated at  $I = 6$  and at  $25^\circ$ .)

Both the slope ( $Q_{isp}$ ) and the intercept ( $Q_u$  or  $[\text{CaSO}_4^0]$ ) of the lines are seen to increase with an increase in ionic strength at constant temperature (see Figure 1), following the same general relationship as does the solubility. The ratio slope/intercept, which is the dissociation quotient,  $Q_d$ , and is independent of the extent of hydration of the solid phase, also increases with an increase in  $I$  at constant temperature. The fraction of  $\text{CaSO}_4$  in the form of ion pairs,  $Q_u/s$ , in aqueous  $\text{NaNO}_3$  (no added  $\text{Na}_2\text{SO}_4$ ) at constant  $I$  increases slightly in going from 0.5 to  $25^\circ$  where the solid phase is  $\text{CaSO}_4 \cdot 2\text{H}_2\text{O}$ . Where  $\text{CaSO}_4$  is the saturating solid ( $100$ - $350^\circ$ ), this fraction decreases gradually with increasing temperature. At constant temperature, the degree of association decreases as the ionic strength increases up to about  $I = 3$ , from which point it remains essentially constant. The fraction associated decreases from approximately 0.14 to 0.07 at  $0.5^\circ$ , 0.18 to 0.10 at  $25^\circ$ , 0.12 to 0.07 at  $150^\circ$ , and 0.09 to 0.05 at  $250^\circ$ , at  $I = 0.25$  and 3-6, respectively. Only two data points are available at  $350^\circ$  with no added  $\text{Na}_2\text{SO}_4$ ; therefore, no range is reported. Comparable results<sup>19</sup> for  $\text{CaSO}_4$  dissociation at  $250^\circ$  have been found in the system  $\text{CaSO}_4\text{-NaCl-H}_2\text{O}$ .

*Thermodynamic Considerations.* (a) *Solid-Neutral Species Equilibrium.* A relationship between the logarithm of the activity coefficient for the neutral species and the ionic strength, at constant temperature, was obtained by starting arbitrarily with an equation analogous to the Debye-Hückel expression

$$\log \gamma_{\text{CaSO}_4} = -S^* I^{1/2} / (1 + A_u I^{1/2}) \quad (14)$$

where  $S^*$  and  $A_u$  are constants. In terms of the equilibrium involved (eq 1), the form is

$$\log Q_u = \log K_u + [S^* I^{1/2} / (1 + A_u I^{1/2})] \quad (15)$$

The unsmoothed results for  $Q_u$  and  $I$  were treated by the method of least squares to obtain simultaneously values for  $K_u$ ,  $S^*$ , and  $A_u$ . The values for  $A_u$  varied randomly with temperature. Therefore, the average value, within the standard error, of 0 over all temperatures was adopted. Equation 15 was then reduced to eq 16

$$\log Q_u = \log K_u + S^* I^n \quad (16)$$

the least-squares process was repeated, and the values for  $K_u$ ,  $S^*$ , and the exponent  $n$  were computed. The average value over all temperatures for  $n$  was 0.5. The results for  $S^*$  are plotted in Figure 4 as a function of temperature to obtain smoothed values. Finally,  $\log K_u$  was calculated with eq 16 by the method of least squares from the raw values for  $\log Q_u$  at each ionic strength, using  $n = 0.5$  and smoothed  $S^*$  values. (The values for  $Q_u$  from the solubility measurements at  $0.5^\circ$  and  $I = 2.14$ , at  $25^\circ$  and  $I = 6.00$ , at  $250^\circ$  and  $I = 0.498$ , and at  $350^\circ$  and  $I = 1.14$  were not used in these calculations, since they were inconsistent randomly with the other results.) The results are shown in Figure 5, where  $\log Q_u$  is plotted as a function of  $I^{1/2}$ . The intercept and the slope of the line for each temperature correspond to the calculated values of  $\log K_u$  and  $S^*$ , respectively. The activity coefficients for the neutral species  $\text{CaSO}_4^0$  are equal to  $K_u/Q_u$ . This ratio decreases sharply with increasing ionic strength at all temperatures and especially at the higher temperatures. Hence, the experimental results show a pronounced ionic strength effect upon the activity coefficient of the ion pair  $\text{CaSO}_4^0$ . In many instances where measurements are lacking, activity coefficients of neutral species are arbitrarily set equal to unity,<sup>8-10</sup> or their logarithms are allowed to vary linearly with ionic strength, with a calculation or estimate of the slope.

Theoretical equations have been derived by Scatchard and Kirkwood,<sup>23</sup> Kirkwood,<sup>24</sup> and Bateman,<sup>25</sup> *et al.*, which predict the logarithm of the activity coefficient for a neutral species or a dipolar ion, *in the limit*,

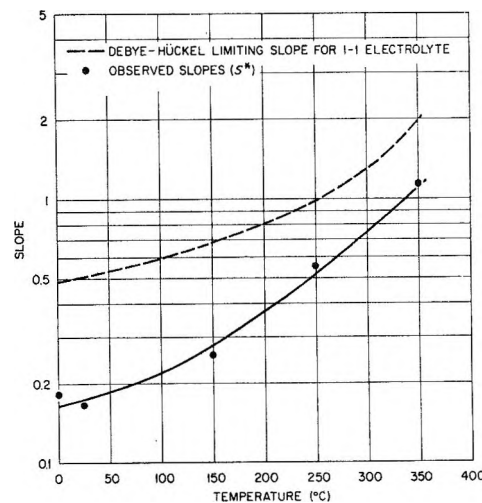


Figure 4. The comparison to  $350^\circ$  between the limiting slopes for a 1-1 electrolyte and the observed slopes for associated  $\text{CaSO}_4$ .

(23) G. Scatchard and J. G. Kirkwood, *Physik. Z.*, **33**, 297 (1932).

(24) J. G. Kirkwood, *Chem. Rev.*, **24**, 233 (1939).

(25) L. C. Bateman, *et al.*, *J. Chem. Soc.*, 979 (1940).

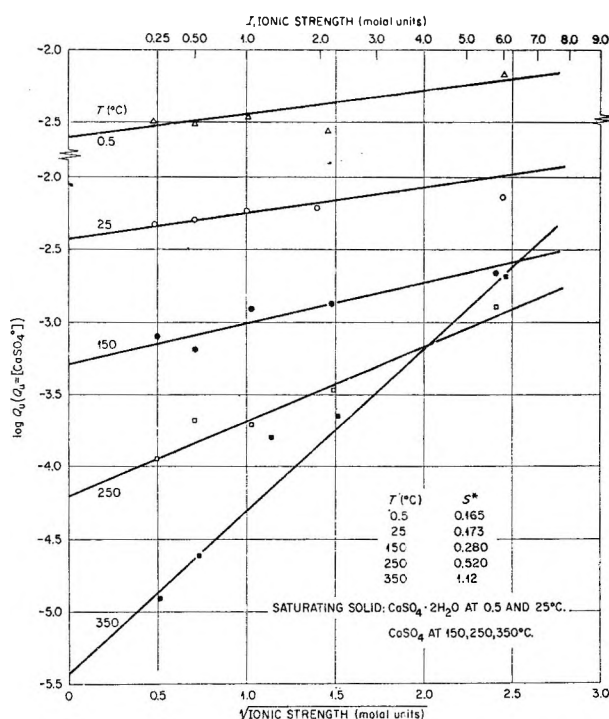


Figure 5. The relationship between the ionic strength and the molality of associated  $\text{CaSO}_4$  from 0.5 to 350°.

to have a dependence on the ionic strength to the first power. The measurements of Cohn<sup>26</sup> and his coworkers on amino acids, proteins, and peptides, along with the considerations of Randall and Failey<sup>27</sup> on the solubility of  $\text{H}_2$ ,  $\text{O}_2$ ,  $\text{N}_2$ ,  $\text{N}_2\text{O}$ ,  $\text{CO}_2$ ,  $\text{H}_2\text{S}$ ,  $\text{NH}_3$ ,  $\text{C}_2\text{H}_2$ , and  $\text{I}_2$  in salt solutions, confirm the form of the limiting law, with the initial term linear in the ionic strength. Above an ionic strength of 0.05–0.1, a polynomial expression is required to relate this dependence. The treatment of our data, given above, establishes empirically, within experimental error, a square-root dependence over a wide range of ionic strength and temperature. A fit to a polynomial expression of equal accuracy was not made since it would require the use of more numerous coefficients. Other investigators<sup>28,29</sup> find that their results for log (solubility) or log (activity) are best described by  $I^{1/2}$  at still lower ionic strengths.

The ion pair  $\text{CaSO}_4^0$  can be pictured as an unsymmetrical molecule with a dipole moment such that the limiting slope of  $\log \gamma_{\text{CaSO}_4^0}$  changes with temperature, in a qualitative manner, as does the Debye-Hückel limiting slope for a 1-1 electrolyte (see Figure 4). Figure 6 shows that the limiting slope for the neutral species  $\text{CaSO}_4^0$  (molar units) varies with  $1/(DT)^2$ . The theoretical considerations of neutral molecules by Kirkwood<sup>24</sup> and Bateman, *et al.*,<sup>25</sup> agree with this observation. In contrast, the limiting slope for ions varies with  $1/(DT)^{1/2}$  (Figure 6).

In order to calculate the values for the various thermodynamic functions describing the solubility equilibrium for anhydrous  $\text{CaSO}_4$  (see eq 1), the assumption

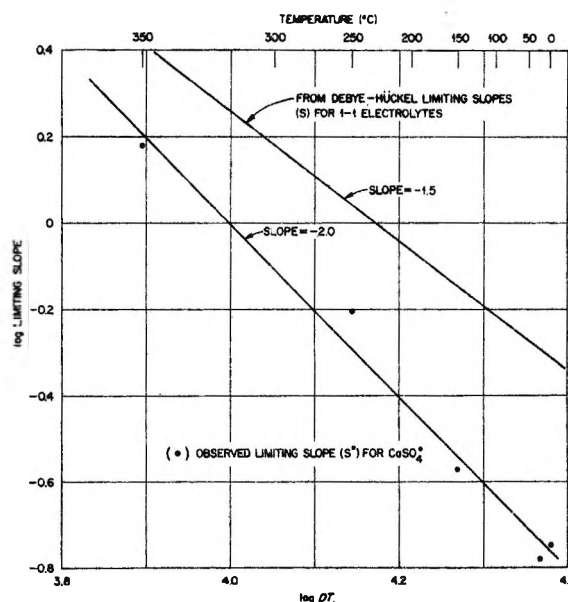


Figure 6. The dependence of the limiting slope for  $\text{CaSO}_4^0$  upon the product of the dielectric constant and temperature (°K).

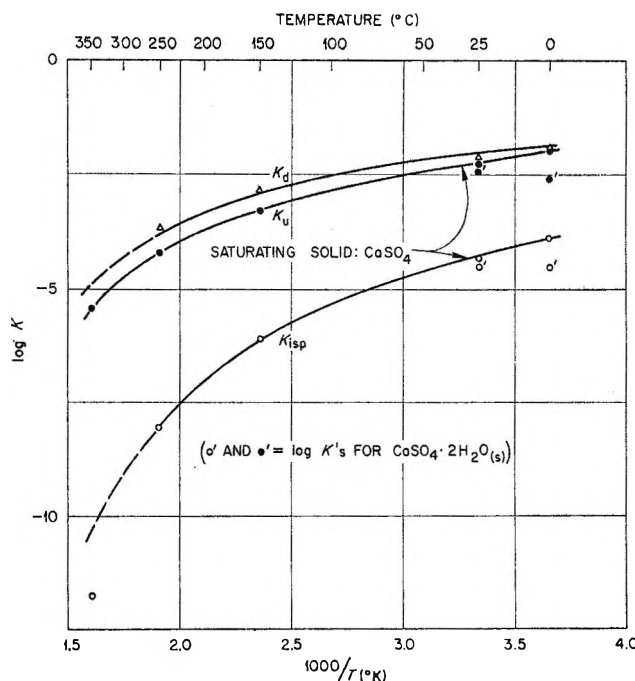


Figure 7. The equilibrium constants for  $\text{CaSO}_4$  from 0.5 to 350°.

was made that the change in standard molal heat capacity,  $\Delta C_p^{\circ}$ , is a linear function of temperature.

(26) E. J. Cohn, *Chem. Rev.*, **19**, 241 (1936); E. J. Cohn, *et al.*, *J. Amer. Chem. Soc.*, **58**, 2365 (1936); E. J. Cohn and J. T. Edsall, "Proteins, Amino Acids, and Peptides," Reinhold Publishing Corp., New York, N. Y., 1943, pp 236–303.

(27) M. Randall and C. F. Failey, *Chem. Rev.*, **4**, 271, 285 (1927).

(28) N. R. Joseph, *J. Biol. Chem.*, **116**, 353 (1936).

(29) A. H. Palmer, *ibid.*, **104**, 359 (1932).

**Table III:** Thermodynamic Functions for the Equilibrium  $\text{CaSO}_4(\text{s})^a \rightleftharpoons \text{CaSO}_4(\text{aq})$ 

Temp, °C	$K_u, m$	$\Delta G^\circ,$ kcal mol <sup>-1</sup>	$\Delta H^\circ,$ kcal mol <sup>-1</sup>	$\Delta S^\circ,$ cal mol <sup>-1</sup> deg <sup>-1</sup>	$\Delta C_p^\circ,$ cal mol <sup>-1</sup> deg <sup>-1</sup>
0	$1.08 \times 10^{-2}$	2.46	-4.05	-23.8	8.88
25	$5.85 \times 10^{-3}$	3.05	-3.95	-23.5	-0.37
50	$3.47 \times 10^{-3}$	3.64	-4.07	-23.9	-9.63
100	$1.37 \times 10^{-3}$	4.89	-5.02	-26.5	-28.1
150	$5.42 \times 10^{-4}$	6.32	-6.89	-31.2	-46.7
200	$1.94 \times 10^{-4}$	8.03	-9.68	-37.4	-65.2
250	$6.10 \times 10^{-5}$	10.1	-13.4	-44.9	-83.7
300	$1.65 \times 10^{-5}$	12.5	-18.0	-53.3	-102
350	$3.84 \times 10^{-6}$	15.4	-23.6	-62.7	-121

<sup>a</sup> The solid phase is anhydrous  $\text{CaSO}_4$ ; when  $\text{CaSO}_4 \cdot 2\text{H}_2\text{O}$  is the solid phase,  $K_u = 2.49 \times 10^{-3}$  and  $3.83 \times 10^{-3}$  at 0 and 25°, respectively. <sup>b</sup>  $\Delta C_p^\circ$  as a linear function of temperature.

With the temperature in degrees Kelvin, this leads to

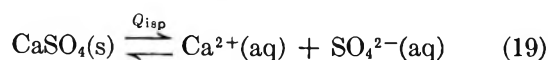
$$\log K_u = -142.051 + 55.3676 \log T + (4435.6/T) - 0.0404600T \quad (17)$$

which defines the curve in Figure 7, where  $\log K_u$  is plotted against the reciprocal of the absolute temperature. Estimates were made of  $K_u$  at 0.5 and 25° for anhydrous  $\text{CaSO}_4$  from the experimentally determined values of  $K_u$  for the dihydrate by noting the relative difference in  $K_{sp}^\circ$ 's which were obtained previously at this laboratory<sup>10,20</sup> for the two solids. The curve was determined by the method of nonlinear least squares mentioned earlier and describes the results well from 0.5 to 350°. Use of the van't Hoff expression with eq 17 relates the standard enthalpy change to the temperature (°K) by

$$\Delta H^\circ (\text{cal mol}^{-1}) = -20290 + 110.01T - 0.185104T^2 \quad (18)$$

The results for  $K_u$  and  $\Delta H^\circ$  were used to calculate  $\Delta G^\circ$  and  $\Delta S^\circ$  for the reaction from the usual thermodynamic equations. All calculated values are listed in Table III. There is no apparent explanation for the shallow maxima through which the values for  $\Delta H^\circ$  and  $\Delta S^\circ$  pass near 25°. Considering the change in heat capacity to be independent of temperature eliminated the maxima but created a greater variance of fit between data and curve.

(b) *Solid-Ion Equilibrium.* The net equilibrium for the dissolution of  $\text{CaSO}_4$  to form ions is



which can be expressed by

$$K_{isp} = Q_{isp} \gamma_\pm^2 \quad (20)$$

where  $\gamma_\pm$  is the mean ionic activity coefficient. Upon using an extended form of the Debye-Hückel expres-

sion for the mean ionic activity coefficient, this equation converts to

$$\log Q_{isp} = \log K_{isp} + [8SI^{1/2}/(1 + A_{isp}I^{1/2})] \quad (21)$$

where  $S$  is the limiting Debye-Hückel slope in molal units for a 1-1 electrolyte (0.4875, 0.5080, 0.6899, 0.9848, and 1.984 at 0.5, 25, 150, 250, and 350°, respectively),  $I$  is the ionic strength in molal units, and  $A_{isp}$  is a constant varying only with temperature. The experimental values for  $\log Q_{isp}$  and  $I$  reported in Table II, along with the theoretical slope ( $S$ ), were used in eq 21 to obtain preliminary values of  $\log K_{isp}$  and  $A_{isp}$  at each temperature by the method of least squares. The calculated values for  $A_{isp}$  were smoothed with respect to temperature, and a revised value of  $\log K_{isp}$  then was calculated. In Figure 8,  $\log Q_{isp}$  is plotted against  $I^{1/2}/(1 + A_{isp}I^{1/2})$  and straight lines result over the range of ionic strength from 0.25 to 6 at 0.5, 25, and 150°. At 250 and 350° there are deviations from the straight-line relationship above ionic strengths 1.5–2. The smoothed values of  $A_{isp}$  are presented in the figure; the intercept of the line for each temperature is equal to  $\log K_{isp}$ , the ionic solubility product constant for that temperature. The logarithm of the ionic activity coefficient at a given ionic strength and a particular temperature is given by  $1/2(\log K_{isp} - \log Q_{isp})$ .

In Figure 7 the variation of  $\log K_{isp}$  for anhydrous  $\text{CaSO}_4$  is plotted vs.  $1/(T/\text{°K})$ . Again, the experimentally derived values for  $K_{isp}$  at 0.5 and 25° were for the saturating solid  $\text{CaSO}_4 \cdot 2\text{H}_2\text{O}$ . Therefore, estimates of  $K_{isp}$  for  $\text{CaSO}_4$  at these temperatures were made by the method described above for obtaining the corresponding  $K_u$ 's. In addition, the apparently low calculated result at 350° was not included in the computation of the curve representing the best least-squares fit of the data. The analogous discrepancy occurred at 350° in the determination of  $K_{sp}^\circ$  for  $\text{Ca}(\text{OH})_2$ , so that now there is reason to suspect that the solubilities of these compounds are decreasing more sharply than expected as the temperature rises from 300° to the critical temperature of water, 374°.

**Table IV:** Thermodynamic Functions for the Net Equilibrium  $\text{CaSO}_4(s) \rightleftharpoons \text{Ca}^{2+}(aq) + \text{SO}_4^{2-}(aq)$ 

Temp, °C	$K_{isp}$ , m <sup>2</sup>	$\Delta G^\circ$ , kcal mol <sup>-1</sup>	$\Delta H^\circ$ , kcal mol <sup>-1</sup>	$\Delta S^\circ$ , cal mol <sup>-1</sup> deg <sup>-1</sup>	$\Delta C_p$ , <sup>c</sup> cal mol <sup>-1</sup> deg <sup>-1</sup>
0	$1.24 \times 10^{-4}$	4.88	-5.05	-36.4	-23.8
25	$5.41 \times 10^{-5}$	5.82	-5.80	-39.0	-35.7
50	$2.38 \times 10^{-6}$	6.83	-6.84	-42.3	-47.6
100	$4.35 \times 10^{-7}$	9.15	-9.82	-50.8	-71.5
150	$6.72 \times 10^{-8}$	12.0	-14.0	-61.3	-95.3
200	$8.48 \times 10^{-9}$	15.3	-19.3	-73.2	-119
250	$8.69 \times 10^{-10}$	19.3	-25.9	-86.4	-143
300	$7.27 \times 10^{-10}$	24.0	-33.6	-101	-167
350	$5.04 \times 10^{-11}$	29.4	-42.6	-115	-191

<sup>a</sup> The solid phase is anhydrous  $\text{CaSO}_4$ ; when  $\text{CaSO}_4 \cdot 2\text{H}_2\text{O}$  is the solid phase,  $K_{isp} = 2.87 \times 10^{-5}$  and  $3.03 \times 10^{-5}$  at 0 and 25°, respectively. <sup>b</sup>  $\Delta C_p^\circ$  as a linear function of temperature. <sup>c</sup>  $K_{isp} = 1.88 \times 10^{-12}$  from the experimental data at 350° (see the text).

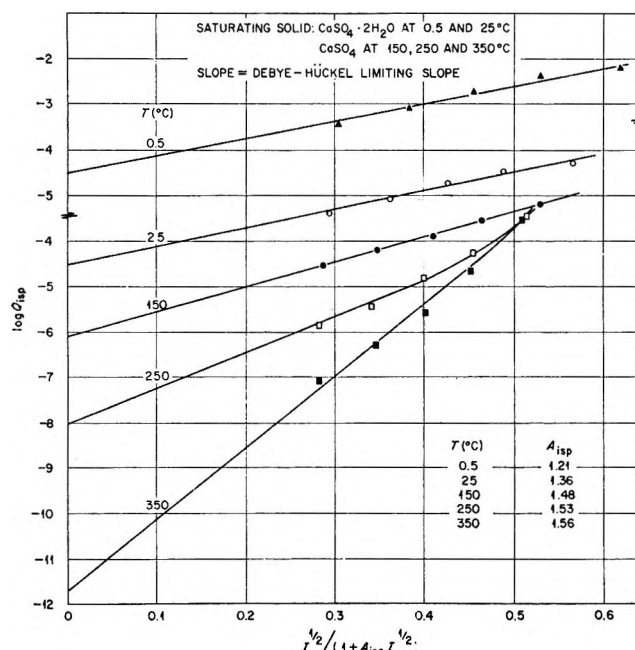


Figure 8. The variation of the ionic solubility product for  $\text{CaSO}_4$  with the ionic strength function from 0.5 to 350°.

The values for the thermodynamic functions of this equilibrium when anhydrous  $\text{CaSO}_4$  is the solid phase were determined, again assuming that  $\Delta C_p^\circ$  is a linear function of temperature. Hence

$$\log K_{isp} = -133.207 + 53.5472 \log T + (3569.6/T) - 0.0520925T \quad (22)$$

and the standard enthalpy change-temperature correlation is given by

$$\Delta H^\circ \text{ (cal mol}^{-1}\text{)} = -16,331 + 106.39T - 0.238323T^2 \quad (23)$$

Calculated values for the thermodynamic functions at several temperatures are given in Table IV. Again, it was found that considering  $\Delta C_p^\circ$  for the reaction as a constant independent of temperature was not satis-

factory. The mean heat capacities ( $\overline{\Delta C_p}^\circ$ ) for the reaction at 25, 25–100, 25–150, and 25–200° from this investigation are -36, -54, -66, and -88 cal deg<sup>-1</sup> mol<sup>-1</sup>, respectively. Corresponding values for  $\overline{\Delta C_p}^\circ$  of -85, -74, -70, and -74 cal deg<sup>-1</sup> mol<sup>-1</sup> were calculated from Criss and Cobble's<sup>30</sup> average ionic heat capacities along with Kelley's<sup>31</sup> expression for the heat capacity of solid anhydrous  $\text{CaSO}_4$ . The latter values remain essentially constant with rising temperature, and a relatively good agreement with our results exists at the higher temperatures.

(c) *Dissociation Equilibrium.* The equilibrium quotients for the dissociation of the neutral molecule into ions (eq 3) were obtained from eq 5. The experimental, unsmoothed results in Table II for  $\log Q_{isp}$  and  $\log Q_u$  were used, with the exception of four values for  $\log Q_u$  that were taken from the straight lines in Figure 5. To evaluate  $K_d$  at each temperature from the experimental information, the following identities were applied

$$\log Q_d = \log Q_{isp} - \log Q_u = \log K_{isp} + [8SI^{1/2}/(1 + A_{isp}I^{1/2})] - \log K_u - S*I^{1/2} \quad (24)$$

leading to

$$\log Q_d + S*I^{1/2} = \log K_d + [8SI^{1/2}/(1 + A_{isp}I^{1/2})] \quad (25)$$

The function  $\log Q_d + S*I^{1/2}$  is plotted against  $I^{1/2}/(1 + A_{isp}I^{1/2})$  in Figure 9. The linear relationship using the theoretical limiting slope ( $S$ ) is seen to hold well except at 250°, where the dashed curve shows the deviation from linearity. This curvature may be due to experimental error, since both the 150 and 350° results lie reasonably close to the lines calculated by the method of least squares. However, the intercept value,  $\log K_d$ ,

(30) C. M. Criss and J. W. Cobble, *J. Amer. Chem. Soc.*, 86, 5390 (1964).

(31) K. K. Kelley, U. S. Bureau of Mines Bulletin 584, U. S. Government Printing Office, Washington, D. C., 1960, p 46.

**Table V:** Thermodynamic Functions for the Dissociation Equilibrium  $\text{CaSO}_4^0(\text{aq}) \rightleftharpoons \text{Ca}^{2+}(\text{aq}) + \text{SO}_4^{2-}(\text{aq})$ 

Temp, °C	$K_d, m$	$\Delta G^\circ,$ kcal mol <sup>-1</sup>	$\Delta H^\circ,$ kcal mol <sup>-1</sup>	$\Delta S^\circ,$ cal mol <sup>-1</sup> deg <sup>-1</sup>	$\Delta C_p^\circ, a$ cal mol <sup>-1</sup> deg <sup>-1</sup>
0	$1.17 \times 10^{-3}$	2.41	-1.11	-12.9	-31.1
25	$9.29 \times 10^{-3}$	2.77	-1.93	-15.8	-34.0
50	$6.83 \times 10^{-3}$	3.20	-2.81	-18.6	-36.9
100	$3.13 \times 10^{-3}$	4.27	-4.80	-24.3	-42.6
150	$1.23 \times 10^{-3}$	5.63	-7.07	-30.0	-48.4
200	$4.35 \times 10^{-4}$	7.28	-9.63	-35.7	-54.1
250	$1.42 \times 10^{-4}$	9.21	-12.5	-41.5	-59.9
300	$4.40 \times 10^{-5}$	11.4	-15.6	-47.2	-65.6
350	$1.30 \times 10^{-5}$	13.9	-19.0	-52.9	-71.4

<sup>a</sup>  $\Delta C_p^\circ$  as a linear function of temperature.

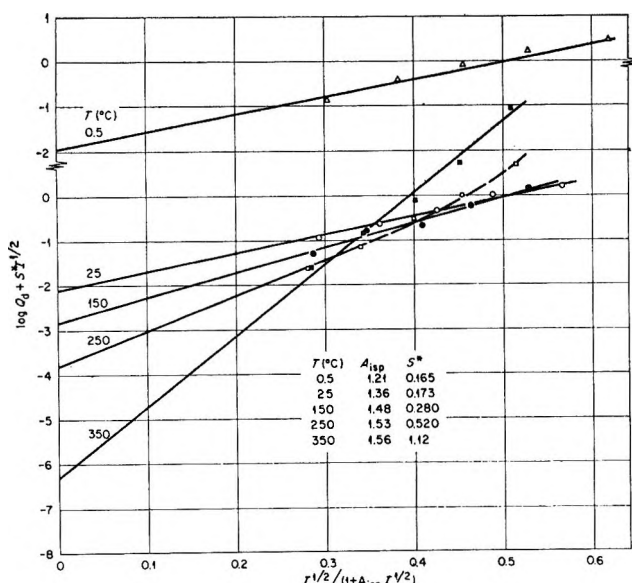


Figure 9. The relationship between the dissociation quotient for  $\text{CaSO}_4$  and the ionic strength from 0.5 to 350°.

at 250° does not appear to be especially erroneous, since on Figure 7 it falls close to the smooth curve with the results at lower temperatures, and this curve has a logical symmetry with the other curves shown. Extrapolation above 250° is used in Figure 7 for the same reason given earlier for the  $\log K_{isp}$  curve, since the two are related.

With  $\Delta C_p^\circ$  as a linear function of temperature, the dependence of the equilibrium constant for eq 3 upon temperature is

$$\log K_d = 3.53483 + 0.180124 \log T - (674.13/T) - 0.0125832T \quad (26)$$

independent both of the presence or form of solid  $\text{CaSO}_4$  (hydrate or anhydrous). Calculated values for  $pK_d$  at 0, 25, and 40° are 1.93, 2.03, and 2.11, respectively, which are 0.28 pK unit less at each temperature than those estimated by Bell and George.<sup>9</sup> The 25° value of Money and Davies<sup>5</sup> is 2.28 and that of Nakayama and Rasnick<sup>8</sup> is 2.27 for  $pK_d$ . In all three of these cases where  $pK_d = 2.29 \pm 0.02$  at 25°, it was assumed that the activity coefficient for the neutral  $\text{CaSO}_4^0$  species was unity. The relationship

$$K_d = Q_d \gamma_{\text{Ca}^{2+}} \gamma_{\text{SO}_4^{2-}} / \gamma_{\text{CaSO}_4^0} \quad (27)$$

with the fact that we find  $\gamma_{\text{CaSO}_4^0}$  decreasing sharply from unity with increasing  $I$  indicates one reason for the earlier values of  $K_d$  being smaller and the values for  $pK_d$  being larger than is the actual case. The present determination of values for  $\gamma_{\text{CaSO}_4^0}$  should have produced a more reliable value for  $K_d$ . Within the limits of the stated precision, estimates of this constant made previously at this laboratory<sup>10</sup> at 0, 25, 100, and 200° agree with the present ones. The standard enthalpy change is given by

$$\Delta H^\circ (\text{cal mol}^{-1}) =$$

$$3084 + 0.360T - 0.057568T^2 \quad (28)$$

Calculated values for  $\Delta H^\circ$ ,  $\Delta G^\circ$ , and  $\Delta S^\circ$  at several temperatures are given in Table V. Bell and George reported values at 25° for  $\Delta G^\circ$ ,  $\Delta H^\circ$ , and  $\Delta S^\circ$  of  $3.15 \pm 0.03$  kcal mol<sup>-1</sup>,  $-1.65 \pm 0.20$  kcal mol<sup>-1</sup>, and  $-16.1 \pm 0.8$  cal deg<sup>-1</sup> mol<sup>-1</sup>, respectively. At temperatures above 100°, there is reasonably good agreement between our results for  $\log K_d$  and the extrapolated ones by Helgeson.<sup>11</sup>

# The Effects of Solvent and Temperature on Magnetically Nonequivalent

## Methylene Protons in Asymmetric Phosphorus Compounds

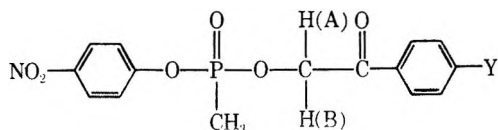
by L. S. Frankel, H. Klapper, and J. Cargioli

*Physical Chemistry Department, Chemical Research Laboratory, Edgewood Arsenal, Maryland 21010  
(Received June 17, 1968)*

The high-resolution nmr spectra of compounds of type  $p\text{-NO}_2\text{C}_6\text{H}_4\text{O})\text{P}(\text{O})(\text{CH}_3)(\text{OCH}_2\text{COC}_6\text{H}_4-p\text{-Y}$  where Y is H, Cl, CH<sub>3</sub>, NO<sub>2</sub>, and OCH<sub>3</sub> have been studied as a function of solvent and temperature. Solvents with high dielectric constants (DMSO-d<sub>6</sub>) give equivalent methylene protons while solvents of low dielectric constants (CDCl<sub>3</sub>) give magnetically nonequivalent methylene protons. When magnetic nonequivalence is observed, the methylene protons form the AB part of an ABX spin system where X is the phosphorus nucleus. A two-conformer model is used to fit the observed temperature dependence. The activation energy obtained is comparable to the temperature dependence of the dielectric constant of the medium.

Many nmr studies have been reported on the effect of asymmetric carbon centers in causing magnetic non-equivalence in nearby methylene<sup>1-3</sup> or methyl<sup>3-5</sup> protons. Nonequivalent methyl groups<sup>6-9</sup> in organophosphorus compounds, with an asymmetric phosphorus atom, have also been published. However, there are few examples of nonequivalent methylene protons due to an asymmetric phosphorus atom.<sup>7,10</sup> The number of experimental nmr parameters which will manifest the effect of an asymmetric phosphorus atom will, in general, be greater than in an asymmetric carbon atom because of additional coupling with the phosphorus. The origin of the nonequivalence is strictly due to symmetry effects which may be further augmented by the effect of conformational preference.

We have studied the effect of solvent and temperature on the spectra of the methylene protons, H(A) and H(B), in compounds of the type



where Y is H, Cl, CH<sub>3</sub>, NO<sub>2</sub>, or OCH<sub>3</sub>.<sup>11</sup>

Spectra were obtained on a Varian HA-100 nmr spectrometer. When required, supplementary spectra were obtained on a Varian A-60 nmr spectrometer. All the compounds to be reported are solids. Their spectra were recorded as dilute solutions (50 mg/ml of solvent) containing less than 5 vol % tetramethylsilane (TMS).

The methylene resonances form the AB part of an ABX spin system where X is the phosphorus atom. The two quartets of the AB portion can be unambiguously assigned by comparing the intensities of the satellites. The coupling constants  $J_{AX}$  and  $J_{BX}$  may be of like or unlike sign. The value of the chemical shift depends on the relative sign choice of  $J_{AX}$  and  $J_{BX}$

through the term  $D_{\pm}$ .<sup>12</sup> If one picks a relative sign convention for  $J_{AX}$  and  $J_{BX}$  and compares a 60- and 100-Mc spectra, the sign choice must predict the correct field-strength dependence of the chemical shift. For the systems we report  $J_{AX}$  and  $J_{BX}$  have the same relative sign, although the absolute value of the sign is not obtained. Further support for this conclusion is obtained from Table I. The magnitude of the coupling constants obtained,  $8 < J_{HX} < 15$ , is within the expected range.<sup>5,13</sup> Assignment of different signs would lead to one unusually large value for  $J_{HX}$ .

From the detailed analysis of the AB part of the ABX spectrum, one obtains three different manifestations (four experimental parameters) of the nonequivalence of the methylene protons. These parameters are listed

- (1) P. R. Shafer, D. R. Davis, M. Vogel, K. Nagarajan, and J. D. Roberts, *Proc. Nat. Acad. Sci. U. S.*, **47**, 49 (1961).
- (2) G. M. Whitesides, F. Kaplin, K. Nagarajan, and J. D. Roberts, *ibid.*, **48**, 1113 (1962).
- (3) G. M. Whitesides, D. Holtz, and J. D. Roberts, *J. Amer. Chem. Soc.*, **86**, 2628 (1964).
- (4) W. G. Betrude, *ibid.*, **87**, 4023 (1965).
- (5) K. D. Berlin, D. H. Burpo, and R. V. Pagilagan, *Chem. Commun.*, **20**, 1060 (1967).
- (6) T. H. Siddal, III, and C. A. Prohaska, *J. Amer. Chem. Soc.*, **84**, 2502, 3467 (1962).
- (7) D. G. Rowsell, *J. Mol. Spectrosc.*, **23**, 32 (1967).
- (8) A. P. Lane, D. A. Morton-Blake, and P. S. Payne, *J. Chem. Soc., A*, 1492 (1967).
- (9) R. Kent and W. Sim, *Chem. Commun.*, **4**, 191 (1968).
- (10) T. H. Siddal, III, *J. Phys. Chem.*, **70**, 2249 (1966).
- (11) These compounds were characterized by C. Lieske, Medical Research Laboratories, Edgewood Arsenal, Md. 21010. One compound, Y = H, is described in C. N. Lieske, E. G. Miller, Jr., J. J. Zeger, and G. M. Steinberg, *J. Amer. Chem. Soc.*, **88**, 188 (1966). The nmr spectra of all the compounds were in consonance with their proposed structure.
- (12) For a definition of this term, see J. A. Pople, W. G. Schneider, and H. J. Bernstein, "High-Resolution Nuclear Magnetic Resonance," McGraw-Hill Book Co., Inc., New York, N. Y., 1959, p 133.
- (13) J. W. Emsley, J. Feeney, and L. H. Sutcliffe, "High Resolution Nuclear Magnetic Resonance Spectroscopy," Vol. 2, Pergamon Press Ltd., London, 1966, Table 12.62.

**Table I:** Summary of Results

$\gamma$	Solvent	$\epsilon^a$	$\langle J_{AB} \rangle$ ( $\pm 0.2$ ), cps	$\langle \nu_A - \nu_B \rangle$ ( $\pm 0.005$ ), ppm	$\langle J_{AX} \rangle^b$ , cps	$\langle J_{BX} \rangle^b$ , cps	$\langle J_{AX} + J_{BX} \rangle$ ( $\pm 0.2$ ), cps	$J_{P-CH_3}$ ( $\pm 0.15$ ), cps	$\delta_{P-CH_3}^c$ ( $\pm 0.5$ ), cps	$\Delta\nu$ ( $\pm 0.1$ ), cps
H	$CDCl_3$	5.05	16.9	0.166	15.0	9.6	24.5	18.2	117.7	0.55
	$CD_3I$	7.0	16.7	0.155	15.8	9.4	25.4	18.2	115.0	0.50
	$CD_3COCD_3$	21.4	17.3	0.068	$15.0 \pm 1.2$	$9.0 \pm 1.2$	24.0	<i>f</i>	<i>f</i>	0.30
	$CD_3NO_2$	37.5	17.4	0.076	$14.0 \pm 1.2$	$9.3 \pm 1.2$	23.3	18.2	114.8	0.45
	$DMSO-d_6$	48.9		<0.015	$11.8 \pm 0.2$	<i>d</i>	23.6 <sup>e</sup>	18.2	116.0	0.40
Cl	$CDCl_3$		16.7	0.175	14.8	9.5	24.2	18.2	117.5	0.40
	$DMSO-d_6$			<0.015	$11.8 \pm 0.2$	<i>d</i>	23.6 <sup>e</sup>	18.0	115.0	0.75
$CH_3$	$CDCl_3$		16.7	0.158	15.0	9.4	23.4	18.2	117.5	0.75
	$DMSO-d_6$			<0.015	$11.8 \pm 0.2$	<i>d</i>	23.6 <sup>e</sup>	18.0	115.0	0.80
$NO_2$	$CDCl_3$		17.0	0.185	14.6	9.7	24.3	18.3	119.0	0.60
	$DMSO-d_6$			<0.015	$11.3 \pm 0.2$	<i>d</i>	22.6 <sup>e</sup>	18.1	116.0	0.50
$OCH_3$	$CDCl_3$		16.5	0.160	15.0	9.5	24.6	18.3	118.0	0.45
	$DMSO-d_6$			<0.015	$11.8 \pm 0.2$	<i>d</i>	23.6 <sup>e</sup>	18.2	115.0	0.65
<i>g</i>	$CDCl_3$		16.8	0.083	11.0	11.0	22.0	18.3	110.0	0.90
	$DMSO-d_6$			<0.015	10.8	<i>d</i>	21.6 <sup>e</sup>	18.2	105.0	0.50

<sup>a</sup>  $\epsilon$  is the solvent dielectric constants for protonated solvents. <sup>b</sup> The maximum error in  $J_{AX}$  is  $\pm 0.4$  cps or is specified. <sup>c</sup> Chemical shift from TMS at 60 Mcps. <sup>d</sup> Since the methylene protons appear to be equivalent, only a single  $J_{HX}$  is obtained. <sup>e</sup> For  $DMSO-d_6$  solutions these values were obtained by doubling  $J_{AX}$ . <sup>f</sup> Cannot be determined due to proton impurities in the deuterated solvent.

<sup>g</sup> The solute is  $(C_6H_5COCH_2)_2P(O)CH_3$ .

in columns 4–7 of Table I. They are: (1) proton coupling between nonequivalent methylene protons,  $\langle J_{AB} \rangle$ ; (2) a chemical shift difference between methylene protons,  $\langle \nu_A - \nu_B \rangle$ ; and (3) heteronuclear proton phosphorus coupling constants which are different for each proton,  $J_{AX} \neq J_{BX}$ .

For all previously reported systems at room temperature, the methylene protons undergo rapid intramolecular rotation with respect to the nmr time frame. The experimental parameters one observes are averages over all conformers.<sup>14</sup>

$$\begin{aligned} \langle \nu_A - \nu_B \rangle &= \sum_i X_i (\nu_{A,i} - \nu_{B,i}) \\ (1) \quad \langle J_k \rangle &= \sum_i X_i J_{k,i} \end{aligned}$$

where  $X_i$  is the mole fraction of a particular conformer and the sum is over all conformers. It has been previously pointed out that chemical shift differences are usually of questionable use because individual conformer frequencies are generally expected to be both temperature and solvent dependent to a much greater degree than the  $J_{k,i}$  coupling constants.<sup>15</sup> Indirect support for this is obtained by studying the  $P-CH_3$  coupling constant and chemical shift as a function of the solvent (Table I) and the temperature dependence of  $J_{P-CH_3}$  (Table II).

There are gross differences in behavior for all compounds in Table I in the solvents  $CDCl_3$  and dimethyl- $d_6$  sulfoxide ( $DMSO-d_6$ ). In  $DMSO-d_6$  the methylene protons appear as a well-resolved doublet. The single coupling constant obtained in  $DMSO-d_6$  is comparable

**Table II:** Summary of Variable-Temperature Results for  $Y = H$  in  $CDCl_3$ 

Temp, °C	$J_{P-CH_3}$ , cps	$\langle J_{AB} \rangle$ , cps	$\langle J_{AX} + J_{BX} \rangle$ , cps	$\langle J_{AX} \rangle$ , cps	$\langle J_{BX} \rangle$ , cps	$\langle \nu_A - \nu_B \rangle$ , ppm
58	18.2	16.7	24.3	14.6	9.8	0.159
30	18.2	16.9	24.5	15.0	9.6	0.166
0	18.2	16.9	24.8	15.5	9.3	0.164
-27	18.2	17.1	25.0	16.1	8.9	0.167
-42	18.2	17.1	25.2	16.5	8.7	0.163
-62	18.2	17.2	25.6	16.8	8.8	0.157

with the mean coupling of  $J_{AX}$  and  $J_{BX}$  in  $CDCl_3$ . The last column of Table I gives the line width,  $\Delta\nu$ , of the methylene protons. For all cases,  $\Delta\nu$  is comparable in  $CDCl_3$  and  $DMSO-d_6$ .

Assuming  $\nu_{k,i}$  and  $J_{k,i}$  are constant for the same compound in different solvents, the extent of conformer preference may be examined by three different criteria,  $\langle \nu_A - \nu_B \rangle$ ,  $\langle J_{AB} \rangle$ , and  $\langle J_{AX} + J_{BX} \rangle$ . Since the errors in  $J_{AX}$  and  $J_{BX}$  can be large while the errors in their sum are small, only the latter quantity is considered. For  $Y = H$ , Table I gives the following orders: for  $\langle \nu_A - \nu_B \rangle$ ,  $CDCl_3 \approx CD_3I > CD_3COCD_3 \approx CD_3NO_2$ ; for  $\langle J_{AB} \rangle$ ,  $CD_3I \approx CHCl_3 > CD_3COCD \approx CD_3NO_2$ ; and for  $\langle J_{AX} + J_{BX} \rangle$ ,  $CD_3I > CDCl_3 > CD_3COCD_3 > CD_3NO_2$ . In the above ordering the results of the variable-temperature study (Table II)

(14) J. A. Pople, *Mol. Phys.*, 1, 1 (1958).

(15) H. S. Gutowsky, G. G. Belford, and P. E. McMahon, *J. Chem. Phys.*, 36, 3353 (1962).

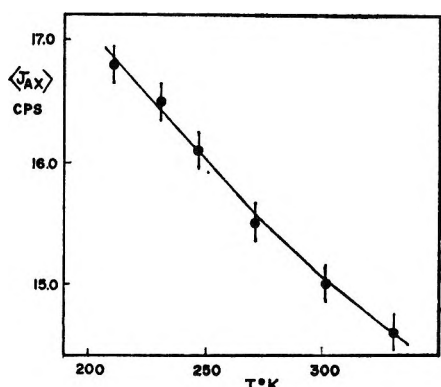


Figure 1. The temperature dependence of  $\langle J_{AX} \rangle$  for  $Y = H$  in  $CDCl_3$ . The solid line calculated from eq 2 is the best fit to the experimental results.

have been employed in the sense that the larger values of  $\langle J_{AB} \rangle$  and  $\langle J_{AX} - J_{BX} \rangle$  have been associated with the case of greater conformer preference. Although the variable-temperature study does not give a definitive result for  $\langle \nu_A - \nu_B \rangle$ , the fact that the larger values of  $\langle \nu_A - \nu_B \rangle$  corresponds to the case of greater conformer preference is suggested based on a comparison with the coupling constants. It is important to realize that in general it is incorrect to associate the larger chemical shifts and coupling constants with a greater degree of conformer preference. This fact follows from eq 1.

It seems reasonable that the variation in  $\langle J_{AB} \rangle$  in different solvents is smaller than  $\langle J_{AX} + J_{BX} \rangle$ , since one expects the former to show smaller changes in each conformer than does the latter. The greater the variation in the  $J_{k,i}$  coupling constants, the greater the total observed variation. Similar solvent effects have been observed in symmetry-restricted carbon analogs.<sup>16-18</sup> The degree of conformer preference appears to follow an approximate inverse dependence with the dielectric constant of the solvent. This is in agreement with an electrostatic model, in that a repulsion energy depends on the inverse of the dielectric constant where a relation between the macroscopic and microscopic dielectric constant is assumed. The lower the dielectric constant, the greater the repulsion energy and hence the greater the conformer preference.<sup>18</sup>

To determine the extent of conformational preference,  $Y = H$  in  $CDCl_3$  was examined as a function of temperature, and the results are summarized in Table II. The approach outlined by Gutowsky, Belford, and McMahon<sup>16</sup> gives, for the simplest possible model (two conformers)

$$\langle J_k \rangle = \frac{J_{k,1}e^{-\Delta E/RT} + J_{k,2}}{e^{-\Delta E/RT} + 1} \quad (2)$$

where  $J_{k,1}$  and  $J_{k,2}$  are the coupling constants in each conformer and  $\Delta E$  is the energy difference between conformers. The data were handled in the following manner. A value of  $\Delta E$  is assumed. This results in a set of equations, one for each temperature, of the form

$$\langle J_k \rangle = AJ_{k,1} + BJ_{k,2}$$

Standard least-squares methods were used to evaluate  $J_{k,1}$  and  $J_{k,2}$ . The value of  $\Delta E$  is then varied until the best fit to eq 2 is obtained. The best fit for  $\langle J_{AX} \rangle$  gives  $\Delta E = 850 \pm 50$  cal,  $J_{AX,1} = -3.5$  cps, and  $J_{AX,2} = 19.5$  cps (Figure 1). The value of  $\Delta E$  obtained is comparable with those reported for ethane derivatives.<sup>15</sup>

The fact that  $\langle J_{BX} \rangle$  increases with temperature while  $\langle J_{AX} \rangle$  shows the opposite dependence is because the coupling constant of one conformer has the opposite sign. The variation of the macroscopic dielectric constant for  $CDCl_3$  (assumed to be the same as  $CHCl_3$ ) with temperature can be fit with a simple exponential with a value of  $\Delta E_\epsilon = 550$  cal.<sup>19</sup> Therefore, a major contribution to  $\Delta E$  can be attributed to the variation of  $\Delta E_\epsilon$ . The total variation of  $\langle \nu_A - \nu_B \rangle$ ,  $\langle J_{BX} \rangle$ , and  $\langle J_{AB} \rangle$  in Table II appears too small to warrant further analysis.

Although the phosphorus is not asymmetric in the last compound in Table I, symmetry restrictions give rise to nonequivalent methylene protons.<sup>20,21</sup> It is interesting to note that in the spectra of this compound  $J_{AX} = J_{BX}$ . Therefore, by one criterion,  $\langle \nu_A - \nu_B \rangle$ , the methylene protons would be classified nonequivalent and by another, equivalent. As with the other compounds in Table I, in  $DMSO-d_6$  the spectra appear to give equivalent methylene protons. This large solvent dependence may be the reason that nonequivalence was not always observed in compounds of this symmetry class.<sup>22</sup>

- (16) R. V. Moen and W. H. Mueller, *J. Org. Chem.*, **31**, 1971 (1966).
- (17) G. M. Whitesides, J. J. Grocki, D. Holtz, H. Steinberg, and J. D. Roberts, *J. Amer. Chem. Soc.*, **87**, 1058 (1965).
- (18) E. I. Snyder, *ibid.*, **85**, 2624 (1963).
- (19) "Handbook of Chemistry and Physics," 46th ed, The Chemical Rubber Co., Cleveland, Ohio, 1965.
- (20) H. Finegold, *J. Amer. Chem. Soc.*, **82**, 2641 (1960).
- (21) J. S. Waugh and F. A. Cotton, *J. Phys. Chem.*, **65**, 562 (1961).
- (22) Footnote 13 of ref 20.

# Temperature Dependence of the Electrical and Diffusional Mobilities of $^{22}\text{Na}$ and $^{137}\text{Cs}$ in Molten $\text{LiNO}_3$ , $\text{NaNO}_3$ , and $\text{RbNO}_3$

by Jan C. Th. Kwak and J. A. A. Ketelaar

Laboratory for Electrochemistry, The University of Amsterdam, Amsterdam, The Netherlands (Received June 19, 1968)

The diffusion coefficients and ionic mobilities of  $^{22}\text{Na}$  and  $^{137}\text{Cs}$  in molten  $\text{LiNO}_3$ ,  $\text{NaNO}_3$ , and  $\text{CsNO}_3$  are measured by a paper electrophoresis method in the temperature range of about  $300\text{--}400^\circ$ . The values of the Arrhenius coefficients and of the preexponential factors are given. The Nernst-Einstein relation between mobility and diffusion coefficient is discussed.

Measurements of the diffusion coefficients and ionic mobilities of alkali tracer ions in pure molten alkali nitrates at  $450^\circ$  were performed in our laboratory by a method of paper chromatography and paper electrophoresis using a strip of paper impregnated with the molten solvent salt.<sup>1-3</sup> Formerly glass-fiber paper and a glass plate as a support were used, but now the paper consisted of quartz fibers and an alumina plate was used as a support. With these materials exchange of tracer ions, especially of sodium ions, was eliminated. Nevertheless, still 1–2% inactive salt of the tracer ion was added in general to the solvent melt, in order to decrease further the danger of absorption by the quartz fibers. The activity of  $^{22}\text{Na}$  and  $^{137}\text{Cs}$  that could be detected in the fibers and the support after the experiment was negligible.<sup>4</sup>

For the interpretation of the results in terms of ionic size and mass and ionic interference it seemed useful to study also the influence of the nature of solute and solvent ions on the temperature dependence of diffusion coefficients and ionic mobilities. In this paper we report diffusion coefficient and ionic mobility measurements for  $^{22}\text{Na}$  and  $^{137}\text{Cs}$  ions in  $\text{LiNO}_3$  ( $270\text{--}400^\circ$ ),  $\text{NaNO}_3$  ( $310\text{--}450^\circ$ ), and  $\text{RbNO}_3$  ( $320\text{--}450^\circ$ ).  $^{22}\text{Na}$  and  $^{137}\text{Cs}$  were chosen because they are very different in size and mass. The choice of  $\text{LiNO}_3$ ,  $\text{NaNO}_3$ , and  $\text{RbNO}_3$  as solvents was made in order that the measurements could be performed in the same temperature range.

## Results

The diffusion coefficients and ionic mobilities are represented within 2–3% as well by a linear temperature dependence as by an Arrhenius equation. We chose to use the latter method, because it has become usual to discuss the temperature dependence of transport parameters in terms of Arrhenius coefficients,  $\Delta H^*$ , resulting from the equations

$$D = D_\infty \exp(-\Delta H_D^*/RT);$$

$$u = u_\infty \exp(-\Delta H_u^*/RT)$$

where  $\Delta H^*$  is calculated in kilocalories per mole and is often interpreted as an activation enthalpy.

In Figure 1 our measurements of the diffusion coefficient of  $^{22}\text{Na}$  in  $\text{NaNO}_3$  are compared with the results of other investigations.<sup>5-8</sup> It is seen that the agreement is reasonable, indicating that the method used gives reliable results for the diffusion coefficient. In the previous investigations<sup>2,3</sup> too high values for  $D(^{22}\text{Na})$  in  $\text{NaNO}_3$  were found, probably due to experimental conditions.  $\text{NaNO}_3$  does not wet the glass plate used as support in these investigations. This causes a rim of

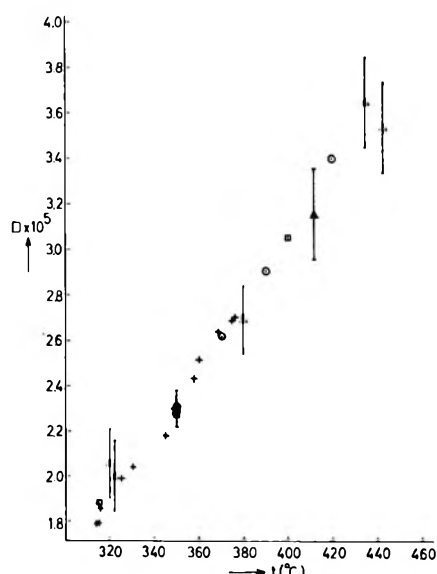
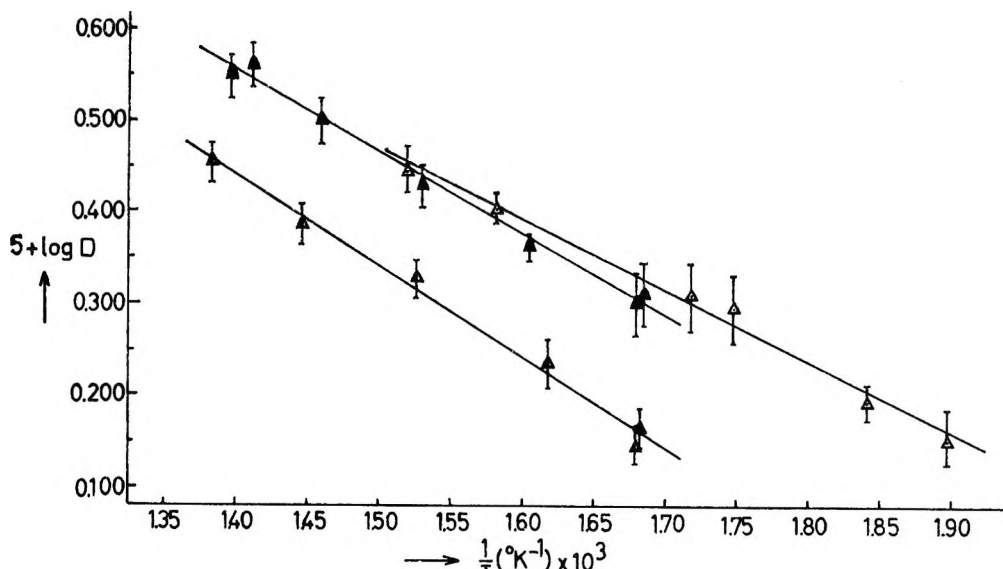
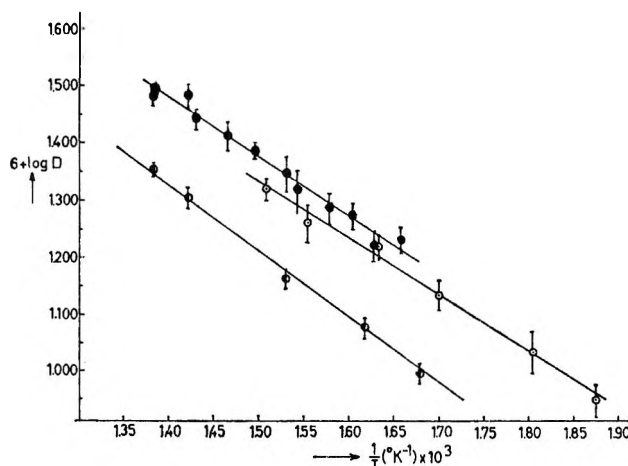


Figure 1. Diffusion coefficients  $D$  ( $\text{cm}^2 \text{ sec}^{-1}$ ) of  $^{22}\text{Na}$  in  $\text{NaNO}_3$ : +, ref 5; O, ref 6; □, ref 7; ▲, ref 8; Δ, this work (errors indicated).

- (1) J. A. A. Ketelaar and E. P. Honig, *J. Phys. Chem.*, **68**, 1695 (1964).
- (2) E. P. Honig and J. A. A. Ketelaar, *Trans. Faraday Soc.*, **62**, 190 (1966).
- (3) J. A. A. Ketelaar and J. C. Th. Kwak, *J. Phys. Chem.*, **71**, 1149 (1967).
- (4) J. C. Th. Kwak, Ph.D. Thesis, University of Amsterdam, 1967.

Figure 2. Diffusion coefficients  $D$  ( $\text{cm}^2 \text{ sec}^{-1}$ ) of  $^{22}\text{Na}$  in:  $\Delta$ , LiNO<sub>3</sub>;  $\blacktriangle$ , NaNO<sub>3</sub>;  $\Delta$ , RbNO<sub>3</sub>.Figure 3. Diffusion coefficients  $D$  ( $\text{cm}^2 \text{ sec}^{-1}$ ) of  $^{137}\text{Cs}$  in:  $\circ$ , LiNO<sub>3</sub>;  $\bullet$ , NaNO<sub>3</sub>;  $\circ$ , RbNO<sub>3</sub>.**Table I:** Arrhenius Coefficients  $\Delta H^*$  (kcal/mol) and Preexponential Constants  $u_\infty$  ( $\text{cm}^2 \text{ V}^{-1} \text{ sec}^{-1}$ ) and  $D_\infty$  ( $\text{cm}^2 \text{ sec}^{-1}$ ) for Electrical Migration and Diffusion of  $^{22}\text{Na}$  and  $^{137}\text{Cs}$  in LiNO<sub>3</sub>, NaNO<sub>3</sub>, and RbNO<sub>3</sub>

	LiNO <sub>3</sub> (265–400°)	NaNO <sub>3</sub> (320–450°)	RbNO <sub>3</sub> (320–450°)
$^{22}\text{Na}$			
$\Delta H_D^*$	$3.55 \pm 0.20$	$4.06 \pm 0.24$	$4.56 \pm 0.24$
$10^4 D_\infty$	$4.3 \pm 0.6$	$6.3 \pm 1.0$	$6.9 \pm 1.2$
$\Delta H_u^*$	$3.53 \pm 0.18$	$2.36 \pm 0.10$	$3.25 \pm 0.30$
$10^8 u_\infty$	$8.2 \pm 1.3$	$2.6 \pm 0.3$	$2.3 \pm 0.5$
$^{137}\text{Cs}$			
$\Delta H_D^*$	$4.54 \pm 0.25$	$4.74 \pm 0.24$	$5.47 \pm 0.40$
$10^4 D_\infty$	$6.6 \pm 1.4$	$8.5 \pm 1.6$	$10.2 \pm 2.0$
$\Delta H_u^*$	$3.44 \pm 0.16$	$2.81 \pm 0.18$	$3.28 \pm 0.26$
$10^8 u_\infty$	$5.4 \pm 0.7$	$2.9 \pm 0.4$	$2.3 \pm 0.4$

free salt at the sides of the paper strip, where turbulence can easily occur. This rim is not present with an alumina support. We find  $D(^{22}\text{Na}) = 3.73 \pm 0.10$  at 450°, resulting in a Nernst-Einstein parameter  $RTu/FD$  of  $0.84 \pm 0.04$  at that temperature.

Figures 2–5 show the  $\log D$  and  $\log u$  vs.  $1/T$  plots for  $^{22}\text{Na}$  and  $^{137}\text{Cs}$  in LiNO<sub>3</sub>, NaNO<sub>3</sub>, and RbNO<sub>3</sub>. Within the standard deviation no curvature could be found in the temperature region investigated. The full lines are calculated with a least-squares method. The coefficients  $D_\infty$ ,  $\Delta H_D^*$ ,  $u_\infty$ , and  $\Delta H_u^*$  are given in Table I. The standard deviations in  $u$  and  $D$  vary between 1.5 and 2% for the different cases. Our results agree reasonably well with other investigations. We find for  $\Delta H_D^*(^{22}\text{Na})$  in LiNO<sub>3</sub>  $3.55 \pm 0.20$ , compared with  $4.4 \pm 0.6$  reported by Lantelme.<sup>7</sup> In NaNO<sub>3</sub> our value for  $\Delta H_D^*(^{22}\text{Na})$  (320–450°) is  $4.06 \pm 0.24$ , compared with  $4.97 \pm 0.08$  (310–380°),<sup>5</sup>  $5.0 \pm 0.7$  (320–400°),<sup>7</sup> and

$4.30 \pm 0.30$  (350–420°).<sup>6</sup> Our value for  $\Delta H_D^*(^{137}\text{Cs})$  in NaNO<sub>3</sub> is  $4.74 \pm 0.24$ , compared with  $4.69 \pm 0.21$ .<sup>7</sup> Although our temperature dependence in this case is identical with the value of Nagarajan and Bockris,<sup>6</sup> our absolute values of  $D(^{137}\text{Cs})$  in NaNO<sub>3</sub> are about 15% lower than the values reported in their work. For the ionic mobilities only comparison with the work of Lantelme<sup>7</sup> can be made. We find  $\Delta H_u^*(^{22}\text{Na})$  in LiNO<sub>3</sub> to be  $3.53 \pm 0.18$  and in NaNO<sub>3</sub>  $2.36 \pm 0.10$ . The corresponding values of Lantelme are, respectively,  $3.9 \pm 0.6$  and  $2.7 \pm 0.4$ . All  $\Delta H^*$  values are expressed in kilocalories per mole.

(5) A. S. Dworkin, R. B. Escue, and E. R. van Artsdalen, *J. Phys. Chem.*, **64**, 872 (1960).(6) M. K. Nagarajan and J. O'M. Bockris, *ibid.*, **70**, 1854 (1966).

(7) F. Lantelme, Ph.D. Thesis, Paris, 1965.

(8) C. A. Angell and J. W. Tomlinson, *Discussions Faraday Soc.*, **32**, 237 (1961).

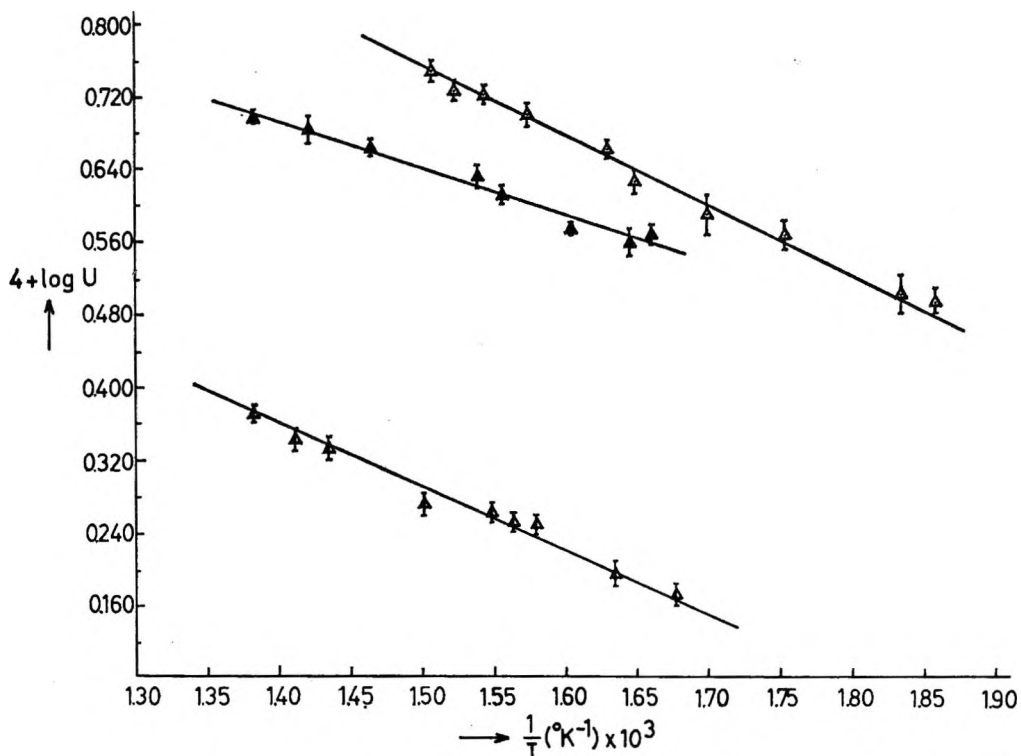


Figure 4. Ionic mobilities  $u$  ( $\text{cm}^2 \text{V}^{-1} \text{sec}^{-1}$ ) of  $^{22}\text{Na}$  in:  $\Delta \text{LiNO}_3$ ;  $\blacktriangle \text{NaNO}_3$ ;  $\Delta \text{RbNO}_3$ .

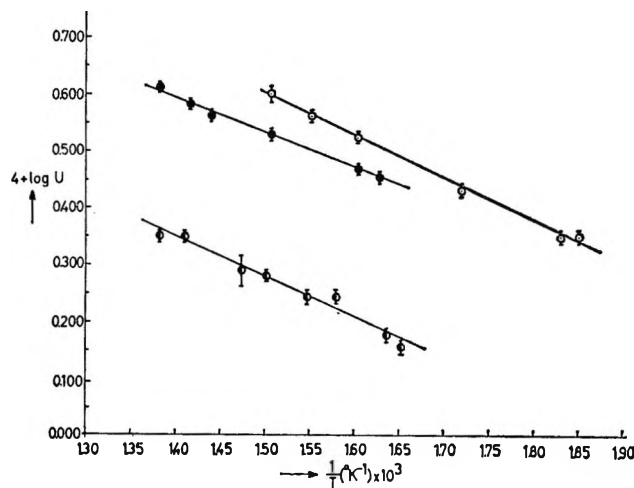


Figure 5. Ionic mobilities  $u$  ( $\text{cm}^2 \text{V}^{-1} \text{sec}^{-1}$ ) of  $^{137}\text{Cs}$  in:  $\text{O} \text{LiNO}_3$ ;  $\bullet \text{NaNO}_3$ ;  $\text{O} \text{RbNO}_3$ .

## Discussion

As can be seen from Table I and from literature data, the trends in the Arrhenius coefficients are different for electrical and diffusional transport. In all three salts studied  $\Delta H_D^*(^{22}\text{Na}) < \Delta H_D^*(^{137}\text{Cs}) < \Delta H_D^*(\text{NO}_3^-)$ ,<sup>5</sup> which is clearly a size effect.  $\Delta H_D^*(^{22}\text{Na})$  and  $\Delta H_D^*(^{137}\text{Cs})$  increase with increasing solvent cation radius; the value of  $\Delta H_D^*(^{137}\text{Cs})$  is largest in  $\text{CsNO}_3$  ( $6.47 \pm 0.32^6$  or  $5.61 \pm 0.27^5$ ). However,  $\Delta H_u^*(^{22}\text{Na})$  and  $\Delta H_u^*(^{137}\text{Cs})$  are about equal in the three solvents studied;  $\text{NaNO}_3$  is hardly a significant

exception. Also in mixtures of  $\text{LiNO}_3$  with  $\text{Ca}(\text{NO}_3)_2$ <sup>9</sup> and  $\text{CdCl}_2$  with alkali chlorides,<sup>10</sup> it was observed that the values of  $\Delta H_u^*$  of the cations are equal within experimental error. This difference in temperature dependence of diffusion coefficients and ionic mobilities is the cause of a different temperature dependence of the Nernst-Einstein parameter  $\alpha = RTu/FD$  in the different cases. When  $\Delta H_D^* - \Delta H_u^* < RT$ , is  $d\alpha/dT > 0$  and when  $\Delta H_D^* - \Delta H_u^* > RT$  is  $d\alpha/dT < 0$ . In  $\text{LiNO}_3$  the Nernst-Einstein parameter of both  $^{22}\text{Na}$  and  $^{137}\text{Cs}$  becomes larger than unity at higher temperatures. This is of course related to the differences in  $u$  and  $D$  when comparing  $\text{LiNO}_3$  with  $\text{NaNO}_3$ . As can be seen from the figures, the diffusion coefficient of  $^{137}\text{Cs}$ , and at higher temperatures also that of  $^{22}\text{Na}$ , is smaller in  $\text{LiNO}_3$  than in  $\text{NaNO}_3$ . Also the fluidity of  $\text{NaNO}_3$  is larger than that of  $\text{LiNO}_3$ .<sup>11</sup> However, the ionic mobilities of both  $^{137}\text{Cs}$  and  $^{22}\text{Na}$  are both appreciably higher in  $\text{LiNO}_3$  than in  $\text{NaNO}_3$ .

In our opinion this different behavior of  $u$  and  $D$  is due to an influence on the ionic mobilities of  $^{137}\text{Cs}$  and  $^{22}\text{Na}$  in  $\text{LiNO}_3$  from a smaller drag effect on the cations from the anions than in the other solvents, caused by a polarization of the  $\text{NO}_3^-$  ion by the small  $\text{Li}^+$  ion.

(9) J. C. Th. Kwak, J. A. A. Ketelaar, and A. J. H. Boerboom, unpublished data.

(10) J. C. Th. Kwak and J. A. A. Ketelaar, submitted for publication in *Electrochim. Acta*.

(11) I. G. Murgulescu and S. Zuca, *Electrochim. Acta*, 11, 1383 (1966).

This polarization causes a decreased interaction of the larger tracer ions with the  $\text{NO}_3^-$  ion.<sup>12,13</sup> It is clear that this effect especially influences the ionic mobility, resulting in a high Nernst-Einstein parameter.

*Acknowledgments.* The authors wish to thank Mr. J. Roele for technical assistance. The present investiga-

tions have been carried out under the auspices of the Netherlands Foundation for Chemical Research (SON) and with financial aid from the Netherlands Organization for the Advancement of Pure Research (ZWO).

(12) C. T. Moynihan and R. W. Laity, *J. Phys. Chem.*, **68**, 3312 (1964).

(13) F. Lantelme and M. Chemla, *Electrochim. Acta*, **10**, 663 (1965).

## Counterion Transference Numbers in Ion-Exchange Membranes

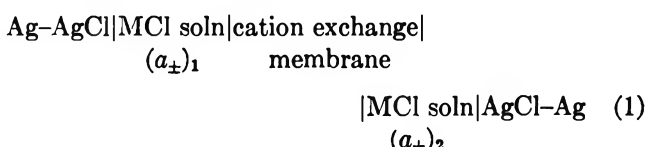
by N. Lakshminarayanaiah

Department of Pharmacology, University of Pennsylvania, Philadelphia, Pennsylvania 19104 (Received June 20, 1968)

Transference numbers of counterions in ion-exchange membranes have been determined by both emf and Hittorf's methods. In general, the transference number derived from the emf data,  $\bar{l}_{+(app)}$ , is lower than the value derived by the Hittorf method,  $\bar{l}_+$ , for any given external electrolyte concentration. This difference is attributed to transport of water occurring across the membrane. The theoretical relationship between these parameters has been derived by Oda and Yawataya. This derivation contains some minor errors which have been clarified in this presentation. The transport number and other relevant data obtained for a cross-linked phenolsulfonate membrane have been used to check the relationship between  $\bar{l}_+$  and  $\bar{l}_{+(app)}$ .

### Introduction

The efficiency with which a membrane transports selectively any particular ionic species is usually inferred by measuring the transference number of the species in the membrane. Two methods are normally used to measure the transport number.<sup>1,2</sup> They are the emf method<sup>3,4</sup> and the Hittorf method.<sup>4</sup> In the emf method, the potential  $E$  arising across the membrane when it separates electrolyte solutions of concentration  $C_1$  and  $C_2$  is measured. If reversible electrodes without forming any liquid junctions are used in membrane cell of the type



the transport number is evaluated from the equation<sup>4-6</sup>

$$E = 2\bar{l}_{+(app)} \frac{RT}{F} \ln [(a_{\pm})_2 / (a_{\pm})_1] \quad (2)$$

where  $(a_{\pm})_2$  and  $(a_{\pm})_1$  are the mean activities of the two solutions, and  $R$ ,  $T$ , and  $F$  have their usual significance. The transport number so derived has been called the apparent transport number  $\bar{l}_{+(app)}$ , because in this type of measurement no correction has been applied for the transport of water occurring across the membrane,

but if very dilute solutions are used,  $\bar{l}_{+(app)}$  will be very close to the true value  $\bar{l}_+$ . In the Hittorf method, a known quantity of electricity is passed through the membrane cell containing an electrolyte solution of known concentration on either side of the membrane. By estimating the concentration change brought about in the two chambers, the true transport number  $\bar{l}_+$  is determined. Here again, how true the value of  $\bar{l}_+$  is depends on the procedure employed in the estimation which may be carried out either volumetrically or gravimetrically. In the volumetric method, correction for water transport must be introduced to get the true value, whereas in the gravimetric method, true value is obtained provided other factors like concentration polarization and electrolyte back-diffusion which have been considered in detail elsewhere<sup>7</sup> are properly controlled.

- (1) J. R. Wilson, Ed., "Demineralization by Electrodialysis," Butterworth and Co., Ltd., London, 1960, p 203.
- (2) Y. Oda and T. Yawataya, *Bull. Chem. Soc. Jap.*, **29**, 673 (1956).
- (3) C. A. Kumins and A. London, *J. Polymer Sci.*, **46**, 395 (1960).
- (4) N. W. Rosenberg, J. H. B. George, and W. D. Potter, *J. Electrochem. Soc.*, **104**, 111 (1957).
- (5) T. M. Ellison and H. G. Spencer, *J. Polymer Sci.*, **B1**, 707 (1963).
- (6) D. K. Hale and D. J. McCauley, *Trans. Faraday Soc.*, **57**, 135 (1961).
- (7) N. Lakshminarayanaiah and V. Subrahmanyam, *J. Polymer Sci.*, **A2**, 4491 (1964).

Two treatments exist in the literature relating  $\bar{t}_+$  to  $\bar{t}_{+(app)}$ . Treatment 1<sup>6,8</sup> consists in equating eq 2 to an integrated form of the equation

$$E = -(2RT/F) \int_I^{II} (\bar{t}_+ - 10^{-3}m_{\pm}M\bar{t}_w) d \ln a_{\pm} \quad (3)$$

where  $m_{\pm}$  is the mean molality of the external solution,  $M$  is the molecular weight of the solvent, and  $\bar{t}_w$  is the transport number of water. Equation 3, which describes the potential of membrane cell of type 1 taking water and co-ion transport into account, has been derived by applying the methods of both quasi<sup>9,10</sup> and irreversible thermodynamics.<sup>10,11</sup> It cannot be integrated without a knowledge of how  $\bar{t}_+$  and  $\bar{t}_w$  vary with the external electrolyte concentration. However, a less accurate approach is to integrate eq 3 within very narrow limits between  $(a_{\pm})_2$  and  $(a_{\pm})_1$  assuming mean values for  $\bar{t}_+$  and  $\bar{t}_w$ . Thus eq 3 becomes

$$E = -2RT/(F)[\bar{t}_+ - 0.018m_{\pm}\bar{t}_w] \ln \frac{(a_{\pm})_1}{(a_{\pm})_2} \quad (4)$$

Equating eq 2 and 4 gives

$$\bar{t}_+ = \bar{t}_{+(app)} + 0.018m_{\pm}\bar{t}_w \quad (5)$$

Treatment 2 has been given by Oda and Yawataya.<sup>2</sup> In its development, some minor errors have crept in and made the development a little inconsistent, although the final result remains correct. A clarified treatment essentially equivalent to that of Oda and Yawataya and relevant data to check the final result and also eq 5 are presented in this paper.

### Theoretical Section

An ion-exchange membrane of fixed charge density  $\bar{X}$  (equiv  $\text{cm}^{-3}$  of swollen membrane) in equilibrium with an electrolyte solution contains  $\bar{X}(1 + \bar{s})$  equiv of counterions and  $\bar{X}\bar{s}$  equiv of co-ions where  $\bar{s}$  is the equivalents of co-ions per equivalent of fixed group present in the membrane due to Donnan uptake of the electrolyte, the latter being negligible in dilute solution.

When an electric field is applied, ions and water move and this movement is phenomenologically called electroosmosis. In a membrane in which interactions between different membrane components, *viz.* counterion, co-ion, water, and membrane matrix, are absent, one may assume that the fixed water in the membrane is negligible and that all mobile water moves with the same velocity and in the same direction as the counterion. As a result, counterions move faster and co-ions move slower than they would otherwise if water stood still. Consequently, the mobilities ( $\bar{U}$ 's), velocity under unit potential gradient,  $\text{cm}^2 \text{ sec}^{-1} \text{ V}^{-1}$ ) of counterions and co-ions in a cation-exchange membrane may be written as<sup>12,13</sup>

$$\bar{U}_+' = \bar{U}_+ + \bar{U}_w \quad (6)$$

$$\bar{U}_-' = \bar{U}_- - \bar{U}_w \quad (7)$$

where +, -, and w stand for cation, anion, and water, respectively.  $\bar{U}_+'$  and  $\bar{U}_-$  are the increased and decreased mobilities due to transport of water.

Due to water transport, the specific conductance of the membrane is increased. If  $\bar{k}'$  is its specific conductance, then

$$\bar{k}' = F[\bar{X}(1 + \bar{s})\bar{U}_+' + \bar{s}\bar{X}\bar{U}_-'] \quad (8)$$

Substituting from eq 6 and 7, eq 8 becomes

$$\bar{k}' = F\bar{X}[(1 + \bar{s})\bar{U}_+ + \bar{s}\bar{U}_- + \bar{U}_w] \quad (9)$$

If water transport is absent, the conductance of the membrane  $\bar{k}$  is given by

$$\bar{k} = F\bar{X}[(1 + \bar{s})\bar{U}_+ + \bar{s}\bar{U}_-] \quad (10)$$

The increase in conductance due to water transport is therefore given by

$$\bar{k}' - \bar{k} = F\bar{X}\bar{U}_w \quad (11)$$

True and apparent transport numbers by definition are given by

$$\bar{t}_+ = \frac{(1 + \bar{s})\bar{U}_+'}{(1 + \bar{s})\bar{U}_+ + \bar{s}\bar{U}_-} \quad (12)$$

$$\bar{t}_{+(app)} = \frac{(1 + \bar{s})\bar{U}_+}{(1 + \bar{s})\bar{U}_+ + \bar{s}\bar{U}_-} \quad (13)$$

It has been shown by Oda and Yawataya<sup>2</sup> from the above equations that

$$\bar{t}_+ - \bar{t}_{+(app)} = [\bar{t}_{-(app)} + \bar{s}] \frac{(\bar{k}' - \bar{k})}{\bar{k}'} \quad (14)$$

Substituting eq 11 in eq 14 gives

$$\bar{t}_+ - \bar{t}_{+(app)} = [\bar{t}_{-(app)} + \bar{s}] \left[ \frac{F\bar{X}\bar{U}_w}{\bar{k}'} \right] \quad (15)$$

When unit potential gradient is applied to a membrane, water present in its pores moves with a velocity of  $\bar{U}_w \text{ cm/sec}$  and the volume of water (ml) flowing per second is given by  $\beta_E$  and is equal to  $(\bar{U}_w a)$  where  $a$  is the pore area of the membrane, but  $\beta$ , the volume of water flowing per coulomb, is given by

$$\beta = V/i \quad (16)$$

where  $V$  is ml/sec of solvent flowing and  $i$  is the current in amperes. However,  $i = (\bar{k}_i a)$  per unit potential gradient and  $\bar{k}_i$  is the specific conductance of the pore

(8) V. Subrahmanyam and N. Lakshminarayanaiah, *J. Sci. Ind. Res. (India)*, B21, 229 (1962).

(9) G. Scatchard, *J. Amer. Chem. Soc.*, 75, 2883 (1953).

(10) G. J. Hills, P. W. M. Jacobs, and N. Lakshminarayanaiah, *Proc. Roy. Soc. (London)*, A262, 246 (1961).

(11) J. W. Lorimer, E. I. Boterenbrood, and J. J. Hermans, *Discussions Faraday Soc.*, 21, 141 (1956).

(12) A. Despic and G. J. Hills, *Discussions Faraday Soc.*, 21, 121 (1956).

(13) Reference 1, p 105.

liquid of an infinitely swollen membrane ( $\bar{k}_i$  is really a modified membrane conductance). Consequently, it follows that

$$\beta_E = \bar{U}_w a = \beta \bar{k}_i a \quad (17)$$

Equation 17 differs from eq 13 of Oda and Yawataya,<sup>2</sup> who wrote it as  $\beta_E = u_s S = \beta k'$ . This is dimensionally incorrect as the pore area  $S$  has been omitted from the term  $\beta k'$ . In view of this, the error present in the step, i.e., equating  $(A/S) = A_s$ , where  $A$  is the fixed charge in equiv  $\text{cm}^{-3}$  of membrane and  $S$  is pore area in  $\text{cm}^2$  and  $A_s$  is fixed charge in equiv  $\text{cm}^{-3}$  of pore solution, leading to their eq 14 follows.

Substitution of eq 17 in eq 15 gives

$$\bar{l}_+ = \bar{l}_{+(app)} + [\bar{l}_{-(app)} + \bar{s}] \frac{F \bar{X} \beta \bar{k}_i}{\bar{k}'} \quad (18)$$

but  $\bar{k}'$  may be equated to  $Q_w \bar{k}_i$  where  $Q_w$  is the volume fraction of water in the membrane. As a result, eq 18 becomes

$$\bar{l}_+ = \bar{l}_{+(app)} + [\bar{l}_{-(app)} + \bar{s}] F \bar{X}_v \beta \quad (19)$$

where  $\bar{X}_v = (\bar{X}/Q_w)$ , equivalents of fixed groups per unit volume of interstitial water, and is identical with  $A_s$  of eq 14 of Oda and Yawataya.<sup>2</sup>

Since the method we have used to measure  $\bar{l}_w$  which is equal to  $(F\beta/18)$  depends on following volume changes in the anode and cathode chambers, the observed volume changes, which measure only solution flow, have been corrected for both salt transport and electrode reactions [see ref 7] to give values for water flow only. In view of this, in the above derivation only water flow is indicated.

The number of moles of water per equivalent of ion-exchange site,  $\bar{W}_e$ , is given by  $1/(18\bar{X}_v)$ . Making the substitutions for  $F\beta$  and  $\bar{X}_v$  and remembering that  $\bar{l}_{+(app)} + \bar{l}_{-(app)} = 1$ , eq 19 assumes the form in which it is expressed by Arnold and Swift,<sup>14</sup> that is

$$\bar{l}_+ = (\bar{l}_w/\bar{W}_e)(1 + \bar{s}) + \bar{l}_{+(app)} \left[ 1 - \frac{\bar{l}_w}{\bar{W}_e} \right] \quad (20)$$

The differences in the relationships between  $\bar{l}_+$  and  $\bar{l}_{+(app)}$  expressed by eq 5 and 20 should be noted. The former expresses it in terms of  $\bar{l}_w$  and the electrolyte concentration with which the membrane is in contact, whereas the latter expresses it in terms of  $\bar{l}_w$ , water, and free salt contents of the membrane.

## Experimental Section

Sodium chloride (AR grade), recrystallized from conductivity water and dried at 200°, was used in the preparation of standard solutions.

Cross-linked phenolsulfonic acid membranes were used in this study. Their preparation and subsequent treatment, determinations of their capacity, and salt and water contents were according to the methods described elsewhere.<sup>7</sup> Membrane potentials and transport

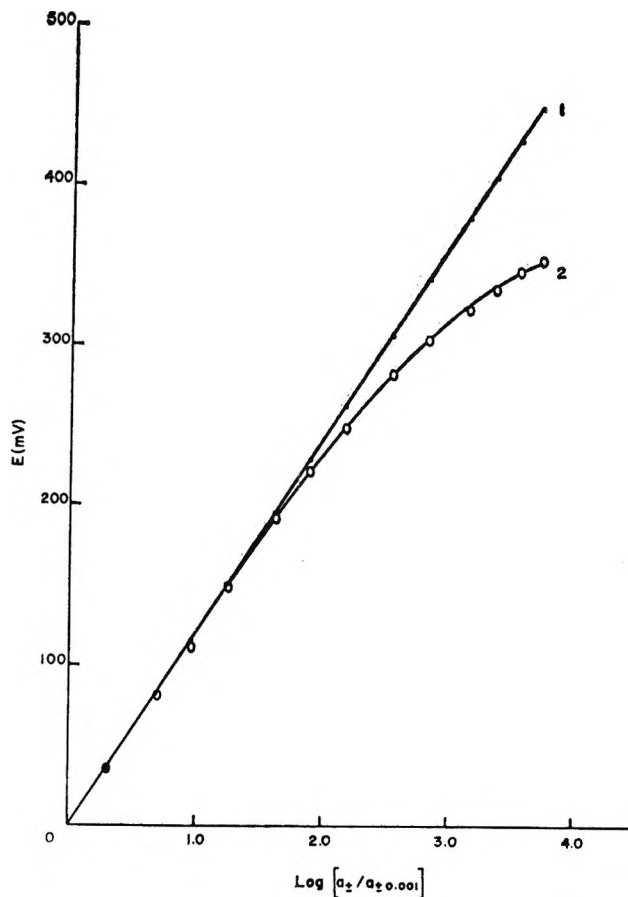


Figure 1. Electrical potential  $E$  arising across phenolsulfonate membrane plotted as a function of  $\log (a_\pm)/(a_{\pm 0.001})$ . Straight line 1 represents the maximum theoretical Nernst potential. Curve 2 represents the algebraic sum of the potentials arising when the ratio of  $C_2$  and  $C_1$  is maintained at about 2 or 3.

numbers  $\bar{l}_+$  and  $\bar{l}_w$  were determined at 25° using half-cells and procedures described in our earlier publications.<sup>7,15,16</sup>

## Results and Discussion

The emf of a membrane cell of type 1 was measured keeping the ratio  $C_2/C_1$  low, either at 2 or 3 in the concentration range 0.001–5.0 N. The potentials measured for the different concentration steps were added and plotted against  $\log (a_\pm/a_{\pm 0.001})$  where  $a_\pm$  was the mean activity of the solution of higher concentration. This plot is shown in Figure 1 (curve 2) along with straight line 1 which represents the maximum theoretical potential calculated according to the Nernst equation

$$E_{\max} = \frac{2RT}{F} \ln \frac{(a_\pm)_2}{(a_\pm)_1} \quad (21)$$

(14) R. Arnold and D. A. Swift, *Aust. J. Chem.*, **20**, 2575 (1967).

(15) G. J. Hills, P. W. M. Jacobs, and N. Lakshminarayanaiah, *Proc. Roy. Soc.*, **A262**, 257 (1961).

(16) N. Lakshminarayanaiah and V. Subrahmanyam, *J. Phys. Chem.*, **72**, 1253 (1968).

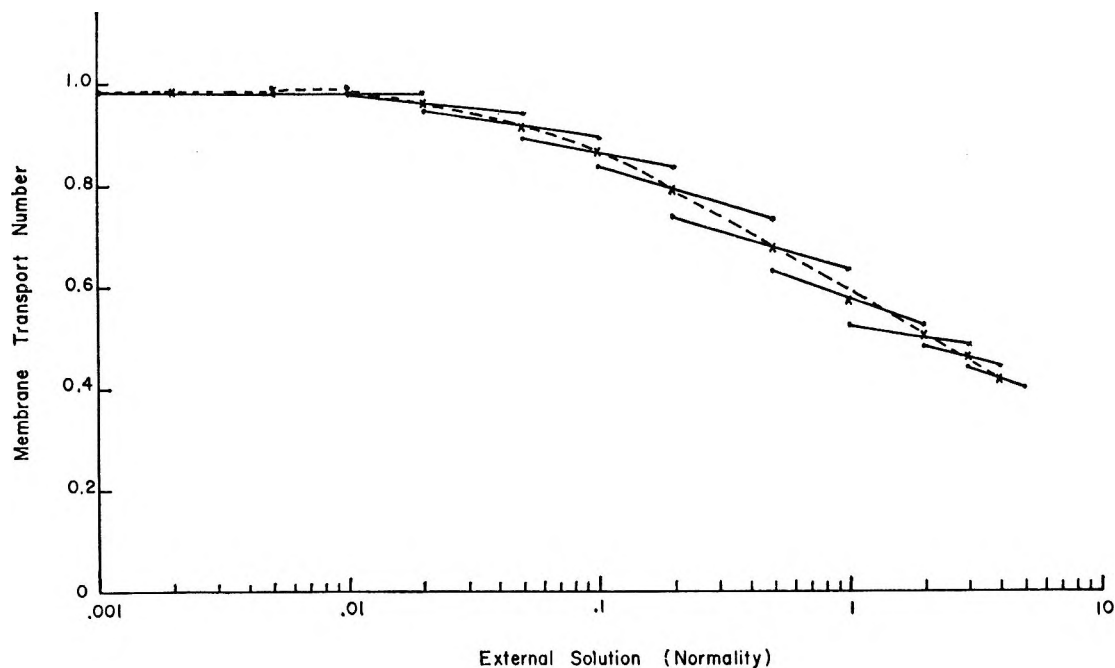


Figure 2. Membrane transport number  $\bar{l}_{+(app)}$  plotted against concentration  $C$ . Values of  $\bar{l}_{+(app)}$  represented by two dots connected by a line are evaluated from eq 2 and 21 by substituting activity values for  $C_2$  and  $C_1$ . The first dot (●—●) on the low concentration side is evaluated from  $C_2$  and  $C_1$  and referred to the concentration  $C_2$  which is less than  $C_1$ . The second dot (—●) connecting the first is evaluated by holding  $C_1$  constant and changing the value of  $C_2$ .  $\bar{l}_{+(app)}$  value is referred to the concentration  $C_2$  which is now greater than  $C_1$ . The value of  $\bar{l}_{+(app)}$  corresponding to concentration  $C_1$  is obtained by interpolation and is shown by a cross (●—X—●). The broken line (----) connecting the crosses represents the variation of  $\bar{l}_{+(app)}$  obtained by interpolation as a function of the external concentration.

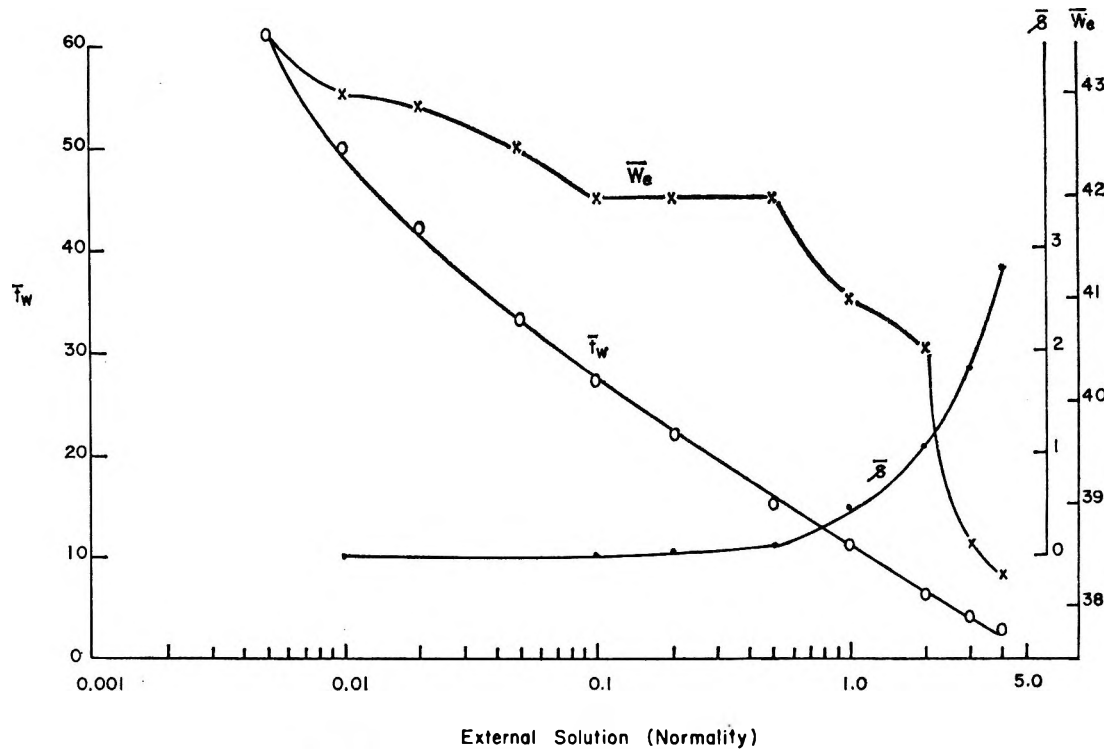


Figure 3. Membrane parameters  $\bar{l}_w$ ,  $\bar{v}_e$ , and  $\bar{s}$  plotted as functions of external concentration.

Thus from eq 2 and 21,  $\bar{l}_{+(app)}$  may be calculated. This value cannot be related in any straightforward

way to the specific concentration of the electrolyte solution used in the measurement of  $E$ . It is usually re-

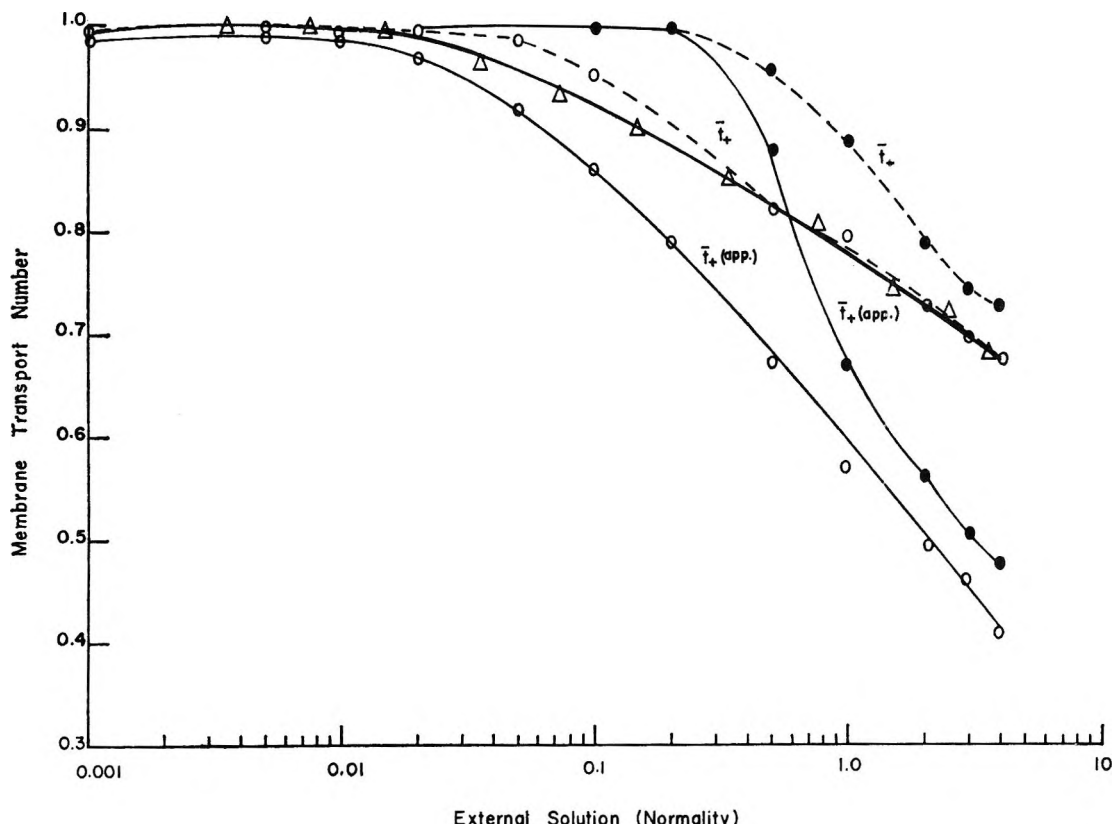


Figure 4. Membrane transport numbers described as functions of external electrolyte concentration. —○—,  $\bar{l}_{+(app)}$  derived by interpolation is plotted against concentration  $C_1$ . —●—,  $\bar{l}_{+(app)}$  derived (eq 23) by using constant transport number value of 0.4 for Na ion referred to aqueous NaCl solution. Solid line (—) refers to observed values of  $\bar{l}_+$ . ---○--- refers to values of  $\bar{l}_+$  calculated (eq 20) using  $\bar{l}_{+(app)}$  values represented by —○—. - - - ● - - - refers to values of  $\bar{l}_+$  calculated (eq 20) using  $\bar{l}_{+(app)}$  values represented by —●—. Δ refers to values of  $\bar{l}_+$  calculated (eq 5) using  $\bar{l}_{+(app)}$  values derived directly from membrane potential measurements using eq 2 and 21 and referred to the mean concentration ( $C_1 + C_2$ )/2.

lated to the mean concentration, *i.e.*  $(C_2 + C_1)/2$ , of the two solutions  $C_2$  and  $C_1$  used in the measurement.<sup>6,8</sup>

Another way the value of  $\bar{l}_{+(app)}$  is related to a specific concentration of the external solution is by the interpolation method described by Oda and Yawataya.<sup>2</sup> This consists in measuring  $E$  using two solutions  $C_1$  and  $C_2$  in membrane cell 1. In the first measurement of membrane potential, solution 2 is so chosen that  $C_2$  is less than  $C_1$  and in the second measurement  $C_1$  is kept constant and  $C_2$  is so chosen that it is now greater than  $C_1$ . Each of the two values of  $\bar{l}_{+(app)}$  calculated from the two potential measurements is now referred to that particular concentration of  $C_2$  used in the experiment and plotted as shown in Figure 2. The value of  $\bar{l}_{+(app)}$  pertaining to the concentration  $C_1$  which is kept constant in the two experiments is obtained by interpolation of the two  $\bar{l}_{+(app)}$  values already derived and plotted. This is represented in Figure 2 by the broken line connecting the  $\bar{l}_{+(app)}$  values so derived. The values of  $\bar{l}_{+(app)}$  derived by this method and those obtained as functions of a mean concentration (values not given) agreed very well according to expectation.

In Figure 3 are given the measured values for the membrane parameters  $\bar{l}_w$ ,  $\bar{W}_e$ , and  $\bar{s}$  as functions of the normality of the external solutions. These values and the corresponding values of  $\bar{l}_{+(app)}$  have been used in eq 20 to calculate values for  $\bar{l}_+$  which are shown in Figure 4 along with the measured values of  $\bar{l}_+$ . Both the measured and the calculated values of  $\bar{l}_+$  show satisfactory agreement over the whole concentration range except for two calculated values (at 0.1 and 0.05 N) which are slightly higher than the observed values. This slight deviation is not considered serious because of the fact that at the two concentrations (0.1 and 0.05 N) membranes belonging to a different batch of preparation had to be used for the estimation of both membrane salt and water contents. The salt content values for these membranes were found to be slightly higher than the values obtained for the other membranes which were used to collect all of the data pertaining to  $\bar{l}_+$ ,  $\bar{l}_w$ , and most of the data related to  $\bar{s}$  and  $\bar{W}_e$ . The water contents of all the membranes belonging to different batches, however, were about equal.

The  $\bar{l}_{+(app)}$  values related to external mean concentration have been used by Subrahmanyam and Lakshmin-

arayanaiah<sup>8</sup> to check eq 5. They found good agreement between calculated and observed  $\bar{t}_+$  values in the case of dilute solutions, but in the case of concentrated solutions, the agreement was unsatisfactory and the calculated values were higher than the observed values. However, in this study the calculated values using eq 5 gave satisfactory agreement with the observed values of  $\bar{t}_+$  over the whole concentration range (see Figure 4). Similar agreement was also noted by Hale and McCauley,<sup>6</sup> who, however, worked at only one concentration (1.0 N NaCl solution) but used a number of differently cross-linked membranes. The results of this study show that eq 5 and 20 generate similar values for  $\bar{t}_+$  and so the two equations may be considered equivalent. This equivalence leads to the relationship

$$\begin{aligned} m_{\pm} &= \frac{55.56}{\bar{W}_e} [1 + \bar{s} - \bar{t}_{+(app)}] \\ m_{\pm} &= \bar{X}_m [\bar{s} + \bar{t}_{-(app)}] \end{aligned} \quad (22)$$

where  $\bar{X}_m$  is the number of equivalents of fixed groups associated with 1000 g of interstitial water.

Provided counterion and co-ion molalities of the membrane phase are measured as functions of external solution molality, eq 22 may be used to estimate  $\bar{t}_{-(app)}$  without measuring membrane potentials. Thus from eq 20,  $\bar{t}_+$  may be calculated if  $\bar{t}_w$  is measured or *vice versa*.

Equation 22 suggests that factors like membrane crosslinking, hydration, etc., which determine ionic mobilities in the membrane phase and thus govern the values for  $\bar{t}_{+(app)}$ , also determine the extent of swelling and electrolyte absorption. These properties are dependent on the nature of the ion. It should therefore be remembered that eq 22 derived in this study using NaCl solutions is based on equivalence of data and thus lacks a sound theoretical basis. It is an approximate equation and should be tested using other electrolyte solutions before its validity is accepted. Studies

in this direction using different ions and membrane systems are in progress.

A different approach to eq 20 has been made by Arnold and Swift,<sup>14</sup> who assumed the following relationships to be true

$$\frac{\bar{U}_+}{\bar{U}_-} = \frac{U_+}{U_-}; \quad t_+ = \frac{U_+}{U_+ + U_-}$$

where the unbarred terms refer to the solution phase. Substitution of these relations into eq 13 gives

$$\bar{t}_{+(app)} = \frac{t_+ (1 + \bar{s})}{t_+ + \bar{s}} \quad (23)$$

$\bar{t}_{+(app)}$  values evaluated according to eq 23 using a value of 0.4 for  $t_+$  of Na ion and  $\bar{s}$  values of Figure 3 are also shown in Figure 4. These values and the corresponding values of  $\bar{t}_+$  calculated from eq 20 (also shown in Figure 4) are all higher than the values derived from the emf data. Similar calculations using even a value of 0.3 for  $t_+$  of Na ion gave values for  $\bar{t}_+$  which were higher than the observed values. In contrast, Arnold and Swift<sup>14</sup> observed good agreement between  $\bar{t}_+$  values observed and those calculated according to eq 23 and 20 for a number of cation-exchange membranes in contact with H<sub>2</sub>SO<sub>4</sub> solutions. The membranes even in 5 N H<sub>2</sub>SO<sub>4</sub> solution when there was considerable Donnan uptake of electrolyte as shown by the values of  $\bar{s}$  showed high permselectivity ( $\bar{t}_+ = 1$ ). This is quite unusual in that the sulfate ions are somehow immobilized and do not seem to interfere with the cation permselectivity of the membranes. In the present study no such unusual situation exists and the chloride ions do reduce the permselectivity of the membrane as revealed by its value of about 0.3 ( $\bar{t}_+ = 0.57$ ) observed in 5 N NaCl solution.

*Acknowledgment.* The work was supported in part by U. S. Public Health Service Grant No. NB-03321.

# A Nuclear Magnetic Resonance Study of Anisotropic Molecular Rotation in Liquid Chloroform and in Chloroform-Benzene Solution<sup>1</sup>

by Wesley T. Huntress, Jr.<sup>2</sup>

Department of Chemistry, Stanford University, Stanford, California 94305 (Received June 27, 1968)

The nuclear spin relaxation times of the deuteron and chlorine-35 in the symmetric-top molecules  $\text{CDCl}_3$  and  $\text{CHCl}_3$  and in two equimolar mixtures  $\text{CDCl}_3\text{-C}_6\text{H}_6$  and  $\text{CHCl}_3\text{-C}_6\text{D}_6$  have been measured as a function of temperature. The reorientation of the molecules in these liquids is shown to be anisotropic. A rotational diffusion equation is assumed for the motion, and the rotational diffusion constants  $D_{||}$  and  $D_{\perp}$  are calculated from the relaxation times of chloroform in the neat liquid and for the chloroform and benzene in the mixtures. The change in the reorientation of chloroform molecules between neat and benzene solution is interpreted in terms of the formation of a complex between chloroform and benzene.

## I. Introduction

Within the limit that a molecule in a liquid reorients in random steps of small angular displacement, the rotational motion may be described by a rotational diffusion equation that is isomorphous to the Schrödinger equation for the free rigid rotor, and the reorientation can be described as rotations about the three principal axes of a diffusion tensor fixed in the molecule analogous to the moment-of-inertia tensor for a free molecule.<sup>3</sup> The frequency of the rotation about any one of the principal diffusion axes is proportional to the component of the diffusion tensor for reorientation about that axis. This particular description has been used extensively for molecular reorientation in liquids, but nearly all applications of the model have assumed isotropic reorientation in which the motion is characterized by a single diffusion constant. Emphasis has usually been placed on the comparison of an experimentally determined isotropic diffusion constant with that calculated hydrodynamically from the viscosity of the liquid. These comparisons have proven to be poor, owing to the inappropriateness of the hydrodynamic assumption for small molecules, and this approach may obscure the most interesting aspect of the problem. The full rotational diffusion tensor gives much more information about the rotational motion of a molecule in a liquid, and recent work has shown that the reorientation of nonspherical and nonlinear molecules in liquids must in general be regarded as anisotropic.<sup>4</sup>

Nmr spectroscopy provides a convenient probe for the study of molecular reorientation, since the nuclear spin relaxation time is dependent on the details of the molecular motion. From an experimental point of view, magnetic nuclei which relax via the quadrupolar mechanism appear the best suited for the study of molecular reorientation.<sup>5</sup> In this paper, the nuclear spin relaxation times of the deuteron and chlorine-35 in neat

deuteriochloroform, chloroform, and mixtures of chloroform and deuteriochloroform with benzene and benzene- $d_6$  are reported. The full rotational diffusion tensors for the molecules, both in neat and benzene solution, are calculated from the relaxation times, and the motion is shown to be anisotropic. The difference in the motion of the chloroform molecules in neat and in benzene solution is interpreted in terms of the formation of a complex between the chloroform and benzene molecules in solution. The applicability of the diffusion equation to the rotational motion of the molecules in liquid chloroform is discussed in section VI.

## II. Theoretical Section

Nuclei of spin  $I > 1/2$  that possess a quadrupole moment relax by the interaction of the nuclear electric quadrupole moment with the molecular electric field gradient at the nucleus. The quadrupole moment of the nucleus is oriented in a space-fixed direction due to the polarization of the magnetic nuclei by the external magnetic field. The field gradient at the nucleus due to the electrons in the bond fluctuates in orientation due to the molecular rotational motion, imparting a time dependence to the quadrupole Hamiltonian that gives rise to the spin relaxation. For covalently bonded quadrupolar nuclei, the electric field gradient at the nucleus is usually quite large, and the quadrupolar interaction can become two or three orders of magnitude larger than any other interaction. Hence, relaxation mechanisms other than the quadrupolar interaction do not contribute significantly to the relaxation time

(1) Submitted in partial fulfillment for the degree of Doctor of Philosophy, Stanford University.

(2) National Institutes of Health Predoctoral Fellow, 1966-1968; Jet Propulsion Laboratory, Pasadena, Calif.

(3) L. D. Favro, *Phys. Rev.*, **119**, 53 (1960); F. Perrin, *J. Phys. Radium*, **5**, 497 (1934); **7**, 1 (1936).

(4) T. T. Bopp, *J. Chem. Phys.*, **47**, 3621 (1967).

(5) W. T. Huntress, *ibid.*, **48**, 3524 (1968).

and may be ignored. This greatly simplifies the expressions for the relaxation time. In addition, the quadrupolar mechanism does not depend on relative translation between molecules in the liquid, and the complication of accounting for relative translation in the expression for the relaxation time is neatly avoided.

The equation for the relaxation time of a quadrupolar nucleus in the case of an axially symmetric field gradient and in the limit of extreme narrowing is<sup>5,6</sup>

$$\frac{1}{T_1} = \left( \frac{3}{80} \right) \left[ \frac{2I+3}{I^2(2I+1)} \right] (e^2 Q q)^2 J^{(2)}(0) \quad (1)$$

where  $I$  is the nuclear spin,  $Q$  is the quadrupole moment of the nucleus, and  $q$  is the field gradient at the nucleus. The quantity  $e^2 Q q$  is the quadrupole coupling constant.  $J^{(2)}(0)$  is the spectral density of the rotational motion at zero frequency, given by the Fourier transform at zero frequency of the correlation function for the molecular reorientation

$$J^{(2)}(0) = \int_{-\infty}^{\infty} \Phi^{(2)}(t) dt \quad (2)$$

and where the correlation function is given by

$$\Phi^{(2)}(t) = \langle \frac{1}{2}[3 \cos^2 \Omega(0) - 1] \times \frac{1}{2}[3 \cos^2 \Omega(t) - 1] \rangle \quad (3)$$

where  $\Omega(t)$  is the angle between the external magnetic field and the direction of the field gradient in the molecule. The braces denote an ensemble average. The first term within the brackets is the tensor projection (hence the superscript 2) of the molecular field gradient onto the space-fixed axis system at some arbitrarily specified initial time  $t = 0$ , and the second term is the tensor projection at some later time  $t$ . In order to calculate the correlation function rigorously, the molecular dynamics must be known. This calculation from first principles is at present intractable, but if it is assumed that the reorientation is characterized by a random walk over small angular displacements, the equation of motion is given by a rotational diffusion equation, which for a symmetric-top molecule is

$$\frac{\partial}{\partial t} P(\Omega, t) = -[D_{||} L_z^2 + D_{\perp} (L_x^2 + L_y^2)] P(\Omega, t) \quad (4)$$

The quantity  $P(\Omega, t)$  is the probability density that the top will be oriented at  $\Omega$  at the time  $t$ , and  $L_i$  is the angular momentum operator about the  $i$ th axis.  $D_{||}$  is the rotational diffusion constant for reorientation about the  $z$  axis, or symmetry axis, and  $D_{\perp}$  is the rotational diffusion constant for reorientation about an axis perpendicular to the symmetry axis. The diffusion constants are statistical parameters for the motion and are functions of the average interactions of the molecule with its environment in the liquid. The solutions to the diffusion equation (eq 4) are exponentially decaying and give for the correlation function (eq 3)<sup>5</sup>

$$\Phi^{(2)}(t) = \sum_{i=0}^2 c_i e^{-t/(\tau_0)_i} \quad (5)$$

$c_0 = (1/4)(3 \cos^3 \theta - 1)^2$  and  $(\tau_0)_0 = (6D_{\perp})^{-1}$ ;  $c_1 = 3 \sin^2 \theta \cos^2 \theta$  and  $(\tau_0)_1 = (5D_{\perp} + D_{||})^{-1}$ ; and  $c_2 = 3/4 \sin^4 \theta$  and  $(\tau_0)_2 = (2D_{\perp} + 4D_{||})^{-1}$  and  $\theta$  is the angle between the symmetry axis of the molecule and the direction of the field gradient. The times  $(\tau_0)_i$  are the angular correlation times for the symmetric top.

Deuteriochloroform is a symmetric-top molecule with the chlorines at an angle of  $110^\circ 55'$  from the symmetry axis along the C-D bond<sup>7</sup> (see Figure 1). Both chlorine-35 and the deuteron are quadrupolar nuclei with spins  $I = 3/2$  and  $I = 1$ , respectively. Assuming that the diffusion equation is an appropriate equation of motion for deuteriochloroform in the liquid, the equations for the relaxation time of the deuteron and chlorine-35 are, respectively

$$\left( \frac{1}{T_1} \right)_D = \frac{(e^2 Q q)^2 D}{16D_{\perp}} \quad (6)$$

$$\left( \frac{1}{T_1} \right)_{Cl} = \frac{(e^2 Q q)^2 c_1}{60D_{\perp}} \left\{ 1 + \frac{3(D_{\perp} - D_{||})}{5D_{\perp} + D_{||}} \times \sin^2 \theta \left[ 1 + \frac{3(D_{\perp} - D_{||})}{2(D_{\perp} + 2D_{||})} \sin^2 \theta \right] \right\} \quad (7)$$

where  $\theta = 110^\circ 55'$ . Since the bonds in deuteriochloroform are all single bonds, it has been assumed that the field gradients are cylindrically symmetric about the C-Cl and C-D bond axes and are oriented along the bond direction.

Since the deuteron lies on the symmetry axis of the molecule, rotation of the molecule about the symmetry axis does not reorient the field gradient. The relaxation time of the deuteron is therefore independent of the  $C_3$  rotation of deuteriochloroform and depends only upon the reorientation about an axis perpendicular to

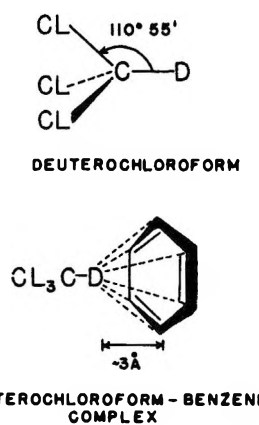


Figure 1.

(6) H. Shimizu, *J. Chem. Phys.*, **40**, 754 (1964).

(7) P. N. Wolfe, *ibid.*, **25**, 976 (1956).

the symmetry axis, or  $D_{\perp}$ . However, both motions of the molecule are effective in reorienting the field gradient at the chlorines, and the relaxation time of the chlorines depends on both  $D_{\perp}$  and  $D_{\parallel}$ . The constant  $D_{\perp}$  can be determined directly from the relaxation time of the deuteron in deuteriochloroform, and  $D_{\parallel}$  can be calculated from  $D_{\perp}$  and the relaxation time of chlorine-35 providing that the quadrupole coupling constants for  $^2\text{D}$  and  $^{35}\text{Cl}$  in deuteriochloroform are known.

### III. The Chloroform-Benzene Complex

The relaxation times of the chlorines and deuteron in deuteriochloroform were measured both in neat solution and in 1:1 equimolar solution in benzene. Chloroform forms a weak complex with benzene.<sup>8,9</sup> Convincing evidence has been given to show that the complex formed is 1:1 in chloroform and benzene.<sup>8,9</sup> The chloroform proton in  $\text{CHCl}_3-\text{C}_6\text{H}_6$  mixtures exhibits a large anomalous upfield shift, indicating that the proton lies above the plane of the benzene ring and very nearly over the center of the ring.<sup>9</sup> The distance of the chloroform proton from the plane of the ring, 3 Å, calculated from this chemical shift<sup>9</sup> indicates that the most probable structure for the complex is one in which the chloroform symmetry axis is perpendicular to the plane of the benzene ring with the chloroform proton (or deuteron) oriented toward the ring (see Figure 1). Therefore, the complex is also a symmetric-top molecule.

Two solutions containing various isotopically substituted chloroform and benzene were studied: an equimolar mixture of  $\text{CDCl}_3$  and  $\text{C}_6\text{H}_6$  (I) and an equimolar mixture of  $\text{CHCl}_3$  and  $\text{C}_6\text{D}_6$  (II). From I the relaxation time of the deuteron gives  $D_{\perp}$  for the complex. Assuming that the substitution of deuterons for protons does not alter the rotational motion significantly, the value of  $D_{\perp}$  is the same for both I and II. The  $\text{C}_6$  motion of benzene in the complex,  $D_{\parallel}(\text{C}_6)$ , can therefore be calculated from the relaxation times of the deuterons in II given the value of  $D_{\perp}$  calculated from the relaxation times of the deuteron in I. The  $\text{C}_6$  motion of the benzene in the complex may or may not be the same as the  $\text{C}_3$  motion of the chloroform in the complex,  $D_{\parallel}(\text{C}_3)$ . This latter motion may be calculated from the relaxation time of chlorine-35 in either I or II and the value of  $D_{\perp}$ .

Not all of the chloroform molecules in the equimolar solutions are complexed with benzene. In order to obtain the relaxation times for the nuclei in the pure complex, the fraction of chloroform complexed must be determined. Since only one chloroform proton resonance line is observed in the proton high-resolution nmr spectrum of II, the exchange of chloroform between the complex and bulk solution must be faster than the difference between the Larmor frequencies of the chloroform proton in the complex and in bulk solution. In

this fast-exchange limit the observed relaxation time is given by

$$\left(\frac{1}{T_1}\right)_{\text{obsd}} = f \left(\frac{1}{T_1}\right)_{\text{complex}} + (1 - f) \left(\frac{1}{T_1}\right)_{\text{bulk}} \quad (8)$$

where  $f$  is the fraction of complexed chloroform. It is assumed that the relaxation time of the nucleus in the bulk solution is equal to the relaxation time of the nucleus in neat solution. It is possible to calculate  $f$  for the equimolar solutions from the chemical shift of the chloroform proton in II. In the fast-exchange limit, the observed chemical shift of this proton is given by a similar expression

$$\begin{aligned} \delta_{\text{obsd}} &= f \delta_{\text{complex}} + (1 - f) \delta_{\text{free}} \\ &= f \Delta + \delta_{\text{free}} \end{aligned} \quad (9)$$

where  $\Delta = \delta_{\text{complex}} - \delta_{\text{free}}$  and the chemical shifts,  $\delta$ , are solution chemical shifts ( $\delta_{\text{solution}} = \delta_{\text{gas}} - \sigma_{\text{solvent}}$ ). The quantity  $\sigma_{\text{solvent}}$  is the shielding due to solvent effects ( $\sigma_{\text{solvent}} = \sigma_A + \sigma_B + \sigma_W + \sigma_E$ ).

The shielding constant  $\sigma_B$  is the shielding due to bulk susceptibility. This effect is eliminated by using an internal reference from which to measure the relative chemical shift. The bulk susceptibility affects the internal reference and solute molecules equally and disappears from the problem. The shielding constant  $\sigma_E$  arises from the effect of neighboring polarized solvent molecules on polar solute molecules and is negligible for chloroform in benzene.<sup>10</sup> The contribution  $\sigma_A$  is due to the magnetic anisotropy of the solvent and should be the same for molecules of approximately the same shape. The internal reference used was tetramethylsilane (TMS). It is assumed that TMS and chloroform are close enough in general shape that  $\sigma_A$  is the same for both. The contribution  $\sigma_W$  is due to van der Waals forces between solvent and solute. Since chloroform demonstrates a small self-association,<sup>9</sup> this effect must be taken into account. The additional chemical shift introduced by chloroform self-association is designated by  $\delta_W(f, T)$  since the amount of self-association depends on the temperature and concentration of chloroform. Equation 9 for the observed solution chemical shift becomes

$$\delta_{\text{obsd}}(T) = f \Delta + \delta_{\text{free}} + \delta_W(f, T) \quad (10)$$

The quantity  $\Delta$  is independent of temperature, since an internal reference was used, and can be obtained by dilution measurements. At low concentrations of chloroform in benzene the contribution of  $\delta_W$  is negligible, and a plot of the observed chemical shift vs. concentra-

(8) M. Tamres, *J. Amer. Chem. Soc.*, **74**, 3375 (1952).

(9) C. W. Reeves and W. G. Schneider, *Can. J. Chem.*, **35**, 251 (1957).

(10) C. J. Creswell and A. L. Allred, *J. Phys. Chem.*, **66**, 1469 (1962).

tion of chloroform yields  $\Delta$  from the slope at infinite dilution and the shift at infinite dilution.<sup>11</sup> Chemical shift studies of chloroform in benzene solution with cyclohexane as an internal reference have shown  $\Delta$  to be independent of temperature.<sup>10</sup> If the observed chemical shift in solution is referred to the value in free chloroform at the same temperature, eq 10 becomes

$$\Delta_{\text{obsd}}(T) = f\Delta + \delta_w(f, T) \quad (11)$$

where  $\Delta_{\text{obsd}} = \delta_{\text{obsd}} - \delta_{\text{free}}$ .

The self-association of chloroform results in a small downfield shift of the chloroform proton indicative of the usual type of hydrogen bonding.<sup>9</sup> This is in contrast to the abnormal large upfield shift for the chloroform proton in the aromatic complex. The chemical shift due to the self-association of chloroform is approximately linear in chloroform concentration,<sup>9</sup> so that for the equimolar solutions I and II

$$\delta_w(f, T) \simeq \frac{1}{2}(1 - f)\delta_w^0(T) \quad (12)$$

and eq 11 becomes

$$\Delta_{\text{obsd}}(T) = f[\Delta - \frac{1}{2}\delta_w^0(T)] + \frac{1}{2}\delta_w^0(T) \quad (13)$$

and  $f$  can be found from

$$f = \left[ \frac{\Delta_{\text{obsd}}(T) - \frac{1}{2}\delta_w^0(T)}{\Delta - \frac{1}{2}\delta_w^0(T)} \right] \quad (14)$$

The value of  $\Delta$  is given by various authors from dilution studies as 1.36,<sup>9</sup> 1.56,<sup>10</sup> and 1.61 ppm,<sup>12</sup> and perhaps as high as 1.91 ppm.<sup>10</sup> In view of such scatter, a value of  $\Delta = 1.5$  is taken as a reasonable and convenient choice. The number  $\Delta_{\text{obsd}}(T)$  was obtained as a function of temperature by measuring the chemical shift of the proton in solution II with 1% added TMS as a reference on a Varian A-60 nmr spectrometer.<sup>13</sup> This shift was referred to the chemical shift measured in the same way for neat chloroform also containing 1% TMS as an internal reference. The number  $\delta_w^0(T)$  was found by calibrating the measured neat chloroform chemical shift from TMS with the value 0.3 ppm at 25°.<sup>9</sup> The results are given in Figure 2. The small temperature dependence of  $\delta_w^0$  is indicative of the self-association of chloroform. The fraction of chloroform complexed in these solutions calculated from this data is given in Figure 3 for the several values of  $\Delta$  obtained from the literature.

#### IV. Relaxation Time Measurements

**A. Chlorine-35.** Chlorine-35 line widths in covalent compounds are on the order of several kilocycles owing to the large quadrupole moment of chlorine-35 and the consequent large quadrupolar interaction. For such lines, a wide-line spectrometer built largely from Varian DP-60 equipment was used, employing a Varian 12-in. nmr high-resolution electromagnet and power supply, a Varian V-4311 radiofrequency unit and probe operating at 4.33 Mc, and a Varian V-4280A precession

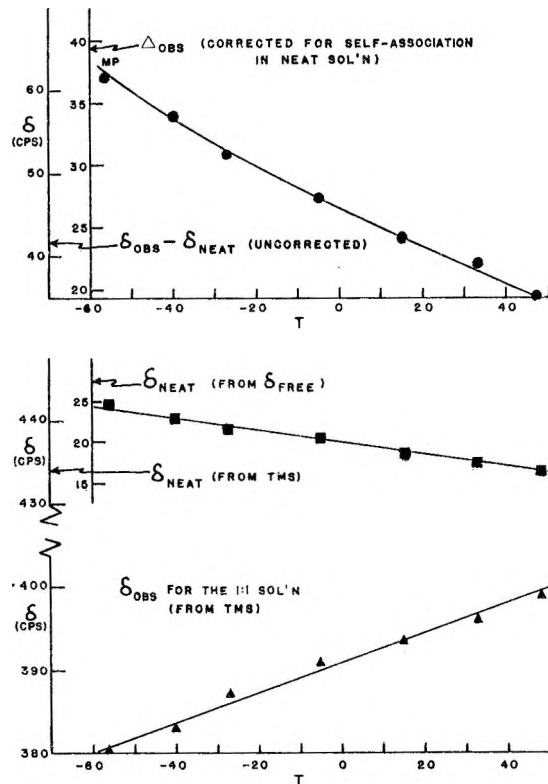


Figure 2. Chemical shift data for the chloroform proton in benzene-*d*<sub>6</sub> and in neat solution.

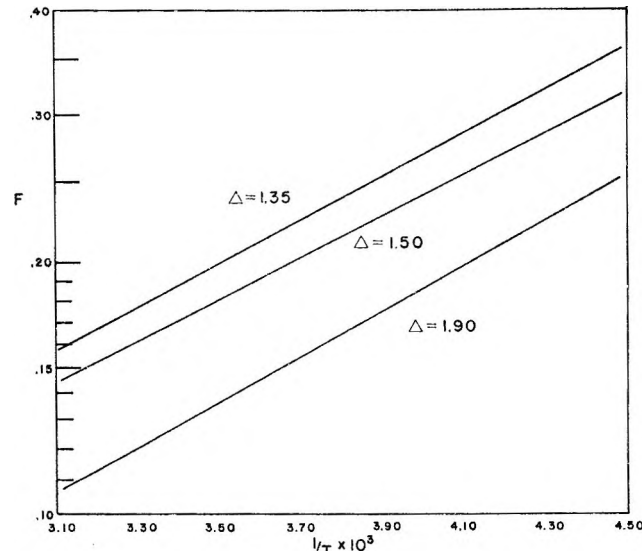


Figure 3. Fraction of chloroform complexed in benzene solution as a function of temperature and for the various literature values of  $\Delta$ .

field-sweep unit. In order to detect lines as broad as several kilocycles, the signal was field modulated to

(11) P. J. Berkeley, Jr., and M. W. Hanna, *J. Phys. Chem.*, **67**, 846 (1963).

(12) P. D. Groves, P. J. Huck, and J. Homer, *Chem. Ind. (London)*, 915 (1967).

(13) The author wishes to acknowledge the assistance of Yoko Kanazawa of the Nmr Laboratories of Stanford University for measuring the proton chemical shifts in these solutions.

obtain a derivative spectrum and phase detected with a PAR JB-4 phase-sensitive detector. The modulation voltage was obtained from the internal-reference oscillator of the phase-sensitive detector through a General Radio 1206B audioamplifier for fine voltage control to the Helmholtz coils in the probe. A Dynakit Mark III audioamplifier was used to match the output impedance of the audioamplifier to the 22-ohm input impedance of the Helmholtz coils. The output of the phase-sensitive detector was recorded on a Bausch & Lomb VOM5 recorder.

The relaxation time  $T_2$  is related to the peak-peak separation  $\Delta\nu_{pp}$  in the derivative spectrum by

$$T_2 = \frac{1}{\sqrt{3}\pi\Delta\nu_{pp}} \quad (15)$$

In order to calculate  $\Delta\nu_{pp}$  from the derivative spectrum, the chart paper was calibrated by recording the side bands produced by modulating the narrow chloride anion signal in a saturated aqueous solution of sodium chloride at a frequency  $\omega_M \gg T_2^{-1}$ . At ambient probe temperature the  $\text{Cl}^-$  line width is 18 cps. A modulation frequency of 1 kcps was employed, producing two first-order side bands symmetrically displaced about the center band separated by 2 kc.

Equation 15 for the relaxation time is valid only with the following limits: (1)  $\gamma H_1 \ll T_2^{-1}$ , (2)  $\omega_M \ll T_2^{-1}$ , and (3)  $\gamma H_M \ll T_2^{-1}$ . For chlorine-35 in deuteriochloroform, the value of  $T_2$  is 20–40  $\mu\text{sec}$  depending on the temperature, or  $T_2^{-1} = (25-50) \times 10^3 \text{ sec}^{-1}$ . The maximum power available from the radiofrequency unit and probe was determined to be  $\gamma_{\text{Cl}}H_1 = 3.3 \times 10^3 \text{ sec}^{-1}$ , and the modulation frequency employed was  $377 \text{ sec}^{-1}$ . Thus the first two conditions were well satisfied. Unfortunately, since chlorine-35 signals in deuteriochloroform are broad and relatively weak, large modulation amplitudes were required to observe them. At values of the modulation voltage where  $\gamma H_M \ll T_2^{-1}$ , the signal-to-noise ratio is unsatisfactory. In order to determine the natural relaxation time, the line widths were measured as a function of modulation voltage for  $\gamma H_M = (3-14) \times 10^3 \text{ sec}^{-1}$  and extrapolated to zero modulation amplitude.

The relaxation times  $T_2$  of chlorine-35 calculated from the measured line width by this method are given in Figure 4 for  $\text{CDCl}_3$ ,  $\text{CHCl}_3$ , solution I, and solution II. The relaxation time measurements as a function of temperature were made with a variable-temperature probe designed by Wallach.<sup>14</sup> Probe temperatures were obtained from  $-35$  to  $50^\circ$  with a stability of  $\pm 10^\circ$ . The chloroform- $d_1$  (99 atom % D) and benzene- $d_6$  (99 atom % D) were obtained from Merck Sharp and Dohme Co. of Montreal and were used without further purification.

The maximum deviation of the experimental relaxation times from the least-squares line in Figure 4 is  $\pm 7.5\%$ . The chlorine-35 relaxation time appears to be

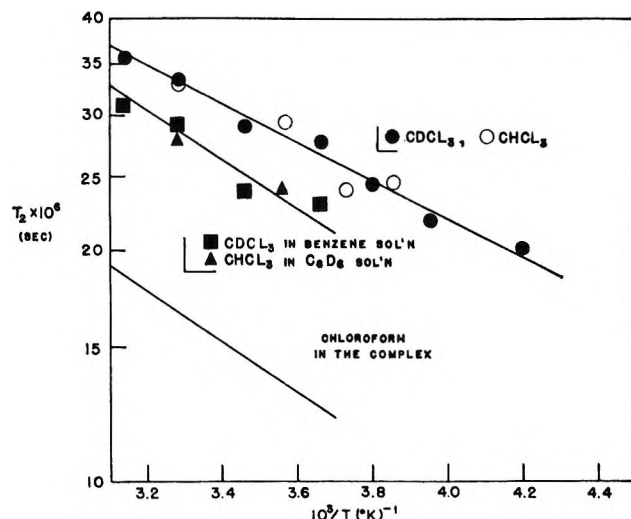


Figure 4. Chlorine-35 relaxation times.

the same in deuterated or undeuterated samples within experimental error, indicating that there is little or no isotope effect in the molecular reorientation by substitution of deuterons for protons. The relaxation times are shorter for the chloroform in benzene solution. Therefore, chlorine-35 line widths are broader and the rotational motion of the molecule has become slower in benzene solution. This is taken as evidence for the formation of the complex in benzene solution.

Also given in Figure 4 are the chlorine-35 relaxation times of  $\text{CDCl}_3$  and  $\text{CHCl}_3$  in the pure benzene complex calculated from the fraction of chloroform complexed in solutions I and II. The maximum error for the relaxation times in the pure complex is  $\pm 20\%$  from the line in Figure 4. This error is largely due to the spread in the literature values for  $\Delta$ .

The plot of  $\ln T_2$  vs.  $1/T$  in Figure 4 appears linear over the temperature range studied. The temperature dependence is therefore described by the equation

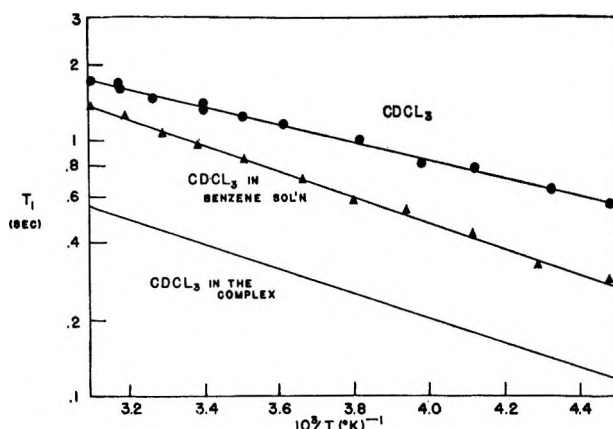
$$T_2 = T_2^0 e^{-E_a/RT} \quad (16)$$

which is characteristic of a thermally activated rate process for the molecular reorientation, with an activation energy given by  $E_a$ . The activation energies for the rotation calculated from the slope of the plots in Figure 4 are  $E_a = 1.2 \pm 0.1 \text{ kcal/mol}$  for neat  $\text{CDCl}_3$  and  $E_a = 2.1 \pm 0.1 \text{ kcal/mol}$  for complexed chloroform.

*B. Deuterium.* The longitudinal relaxation time  $T_1$  of the deuterons was measured with a Magnion ELH-15 spin-echo spectrometer operating at 4.3 Mc, with  $H_1 \approx 11 \text{ G}$ , by using the standard  $180^\circ-90^\circ$  pulse sequence. A temperature probe designed by Bopp<sup>15</sup> was used to obtain the relaxation times as a function of temperature. The samples were prepared on a vacuum line using freeze-pump-thaw cycles to remove dis-

(14) D. Wallach, Ph.D. Thesis, Harvard University, 1968.

(15) T. T. Bopp, Ph.D. Thesis, Harvard University, 1967.

Figure 5. Deuteron relaxation times in  $\text{CDCl}_3$ .

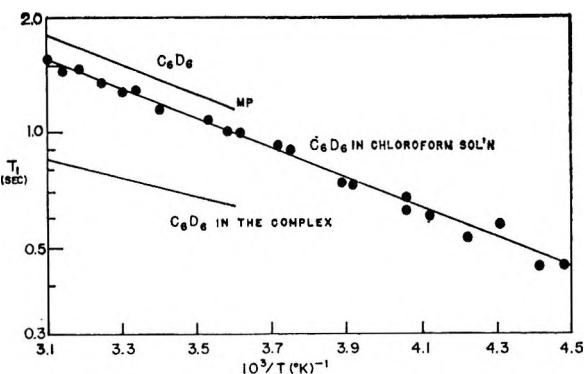
solved gases. The degassed samples were then vacuum distilled into 12-mm diameter sample ampoules which were sealed under vacuum.

The relaxation times  $T_1$  of the deuterons measured by this spin-echo technique as a function of temperature are given in Figure 5 for neat  $\text{CDCl}_3$  and solution I. Also given are the deuteron relaxation times in the pure  $\text{CDCl}_3\text{-C}_6\text{H}_6$  complex calculated from the fraction of chloroform complexed in solution I. The maximum deviation in the relaxation times from the least-squares line in Figure 5 is  $\pm 5\%$ . The maximum deviation in the calculated relaxation times for the complex is  $\pm 15\%$ . The relaxation times are shorter in benzene solution in agreement with the chlorine-35 results. The temperature dependence, given by the slope of  $\ln T_1$  vs.  $1/T$ , is characteristic of activation energies equivalent to  $1.6 \pm 0.1$  kcal/mol for  $\text{CDCl}_3$  and  $2.2 \pm 0.1$  kcal/mol for complexed  $\text{CDCl}_3$ . These values are significantly different than the values calculated from the chlorine-35 data ( $E_a(\text{neat}) = 1.2 \pm 0.1$  kcal/mol and  $E_a(\text{complex}) = 2.1 \pm 0.1$  kcal/mol) and provide direct evidence that the reorientation is anisotropic for both neat  $\text{CDCl}_3$  and the benzene complex.

The measured relaxation times of the deuterons in the equimolar mixture of  $\text{CHCl}_3$  in benzene- $d_6$  (solution II) are given in Figure 6 as a function of temperature. The deuteron relaxation times in neat  $\text{C}_6\text{D}_6$  in Figure 6 were measured elsewhere.<sup>16</sup> Again the relaxation times are longer in neat solution, indicating that the motion of benzene in chloroform solution is slower than in neat solution. The relaxation times of the deuterons in II are also longer than in I. The relaxation time in I is directly proportional to  $D_{\perp}$  in the complex, whereas the relaxation time in II is dependent on both modes of motion. The longer relaxation time in II therefore indicates that the motion about the  $\text{C}_6$  symmetry axis of the benzene in the complex is faster than the tumbling motion of the complex.

## V. Results

In order to calculate the rotational diffusion con-

Figure 6. Deuteron relaxation times in  $\text{C}_6\text{D}_6$ .

stants from the relaxation times for  $\text{CDCl}_3$ , the quadrupole coupling constants are required. The quadrupole coupling constants of chlorine-35 have been measured for a large number of compounds by both nuclear quadrupole resonance in solids and by microwave spectroscopy in gases. The solid-phase value for chlorine-35 in chloroform is  $(e^2Qq)_{\text{Cl}} = 77.0$  Mcps.<sup>17</sup> This is the value extrapolated to  $0^\circ\text{K}$  where torsional motions of the molecule in the lattice which average out part of the coupling constant are not present. The gas-phase value is  $(e^2Qq)_{\text{Cl}} = 80.4$  Mcps.<sup>7</sup> The coupling constant in the solid is lower than the gas-phase value by a factor of  $3.5\%$ , owing to crystal field or other effects. The value for the liquid is presumably somewhere between the values for the solid and gas. Since the value of the coupling constant must be squared in the expression for the relaxation time, the uncertainty in the value of the chlorine-35 coupling constant contributes a maximum error of  $\pm 3.5\%$  in the results if an intermediate value of  $(e^2Qq)_{\text{Cl}} = 79$  Mc is chosen for the liquid. This compares with a maximum error of  $\pm 7.5\%$  for the relaxation times of chlorine-35.

The coupling constants for deuterons are not well known owing to the small value of the deuteron quadrupole moment. No deuteron nqr results have been published and only a few deuteron coupling constants have been measured by microwave spectroscopy. These are given in Table I, along with some values measured by nmr in oriented liquid crystals. No value for deuteriochloroform has been measured. Using the compounds in Table I as model compounds, the coupling constants range over 150–225 kcps. A value of  $(e^2Qq)_D = 170$  kcps is chosen as a reasonable value for  $\text{CDCl}_3$ , since this value of the coupling constant, together with the measured values for the deuteron relaxation times in neat  $\text{CDCl}_3$ , gives results which agree with independent measurements of the motion  $D_{\perp}$  obtained by dielectric relaxation.

The rotational diffusion constants calculated from the chlorine-35 and deuteron relaxation times and quadru-

(16) D. E. Woessner, *J. Chem. Phys.*, **40**, 2341 (1964).

(17) H. S. Gutowsky and D. W. McCall, *ibid.*, **32**, 548 (1963).

**Table I:** Quadrupole Coupling Constants for Deuterium Bonded to Carbon

Compd	$e^2Qq$ , kcps	Method <sup>a</sup>	Foot-note
DC≡N	150	Mw	b
DC≡CCl	175 ± 20	Mw	c
	225 ± 18	Mw	d
DC≡CCH <sub>3</sub>	208 ± 10	Mw	d
DC≡CF	212 ± 10	Mw	d
DHC=O	170 ± 2.0	Mw	e
D <sub>2</sub> C=O	171 ± 3	Mw	f
C <sub>6</sub> D <sub>6</sub>	193 ± 2.6	Nmr	g
C <sub>6</sub> D <sub>12</sub>	174 ± 2	Nmr	g
CD <sub>3</sub> C <sub>6</sub> H <sub>5</sub>	165	Nmr	g

<sup>a</sup> Mw is microwave spectroscopy. <sup>b</sup> R. G. White, *Phys. Rev.*, **94**, 789A (1954). <sup>c</sup> R. G. White, *J. Chem. Phys.*, **23**, 253 (1954). <sup>d</sup> V. W. Weiss and W. H. Flygare, *ibid.*, **45**, 8 (1966). <sup>e</sup> P. Thaddeus, L. C. Krisher, and J. H. N. Loubsen, *ibid.*, **40**, 257 (1964). <sup>f</sup> W. H. Flygare, *ibid.*, **41**, 206 (1966). <sup>g</sup> J. C. Rowell, W. D. Phillips, L. R. Melby, and M. Panar, *ibid.*, **43**, 3442 (1965).

pole coupling constants are given in Figure 7 for neat CDCl<sub>3</sub> and the chloroform-benzene complex. The results for neat chloroform indicate that the reorientation is anisotropic and that  $D_{||} > D_{\perp}$  over the entire liquid range. Representative data and calculations for deuteriochloroform at 20° are given in Table II. Since

**Table II:** Rotational Data and Calculations for Deuteriochloroform at 20°

	$T_1$ , sec	$79 \times 10^{-6}$ (‰Cl)    1.35 (D)
	$31 \times 10^{-6}$ (‰Cl)    1.35 (D)	
	$e^2Qq$ , Mc	
( $\tau_0$ ) <sub>  </sub> , sec	$79 \times 10^{-6}$ (‰Cl)    0.17 (D)	
( $\tau_0$ ) <sub>⊥</sub> , sec		
( $\tau_0$ ) <sub>  </sub> , sec		
$I_{  }$ , amu Å <sup>2</sup>	$0.96 \times 10^{11}$	
$I_{\perp}$ , amu Å <sup>2</sup>	$1.8 \times 10^{11}$	
( $\tau_1$ ) <sub>  </sub> , sec	$1.8 \times 10^{-12}$	
( $\tau_1$ ) <sub>⊥</sub> , sec	$0.92 \times 10^{-12}$	
$I_{  }$ , amu Å <sup>2</sup>	159	
$I_{\perp}$ , amu Å <sup>2</sup>	300	
( $\tau_1$ ) <sub>  </sub> , sec	$0.81 \times 10^{-12}$	
( $\tau_1$ ) <sub>⊥</sub> , sec	$1.10 \times 10^{-12}$	

$I_{||} = 1.89I_{\perp}$ , deuteriochloroform in the gas phase tumbles about twice as fast about a perpendicular axis as it rotates about the C<sub>3</sub> axis. In the liquid, however,  $D_{\perp} = 0.53D_{||}$  (at 20°) so that the motion about the symmetry axis is faster by a factor of about 2 than the motion about a perpendicular axis. With respect to the gas-phase motion then, the tumbling motion of the molecule in the liquid is more hindered than the C<sub>3</sub> motion, presumably due to closer packing and self-association through hydrogen bonding along the C<sub>3</sub> axis. That molecular association through hydrogen bonding may be at least partially responsible for the relatively large hindrance of the perpendicular motion

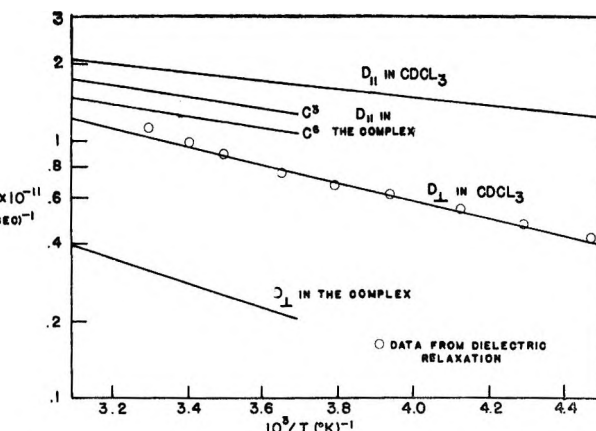


Figure 7. Calculated rotational diffusion constants for chloroform and the chloroform-benzene complex.

is suggested by the evidence from the chemical shift measurements that chloroform is somewhat self-associated in the liquid.

As the temperature is lowered, the values for both  $D_{\perp}$  and  $D_{||}$  become smaller, indicating that the motion becomes slower. The temperature dependences are not the same for both motions. The tumbling motion has a stronger temperature dependence, which may be due to increasing self-association at lower temperatures. If, as for the relaxation times, the temperature dependence is described by an activation energy, the values for the activation energy,  $E_a$ , extracted from the Arrhenius plot of Figure 7 are  $E_a^{\perp} = 1.6 \pm 0.1$  kcal/mol and  $E_a^{||} = 0.7 \pm 0.1$  kcal/mol. The relaxation time of the deuteron directly reflects the temperature dependence of  $D_{\perp}$  and has the same activation energy. The relaxation time of the chlorines depends on both  $D_{\perp}$  and  $D_{||}$  and therefore has an activation energy ( $E_a = 1.2 \pm 0.1$  kcal/mol) intermediate to  $E_a^{\perp}$  and  $E_a^{||}$ .

The results for  $D_{\perp}$  in neat deuteriochloroform are compared in Figure 7 with results obtained from dielectric relaxation in chloroform.<sup>18</sup> The dipole moment in chloroform is directed along the symmetry axis so that the dielectric relaxation time depends only on  $D_{\perp}$ . The dielectric data in Figure 7 have been corrected by a factor

$$\tau_{\text{dielectric}} = \left( \frac{3\epsilon_0}{2\epsilon_0 + \epsilon_{\infty}} \right) \tau_0 \quad (17)$$

where  $\epsilon_0$  and  $\epsilon_{\infty}$  are the dielectric constants of chloroform at zero and infinite frequency, respectively. This factor is introduced to correct for the fact that the macroscopic correlation time associated with the macroscopic polarization measured by dielectric relaxation is somewhat different than the microscopic molecular correlation time.<sup>19,20</sup>

(18) S. Mallikarjun and N. E. Hill, *Trans. Faraday Soc.*, **61**, 1389 (1965).

(19) S. H. Glarum, *J. Chem. Phys.*, **33**, 1371 (1960).

(20) R. H. Cole, *ibid.*, **42**, 637 (1965).

From Figure 7 it can be seen that if a value of 170 kc is chosen for the value of the deuteron quadrupole coupling constant, the dielectric and nuclear magnetic relaxation results agree almost perfectly. The correction to the dielectric data amounts to approximately 20%. From the uncertainty in the exactness of relaxation (eq 17) for the correction factor, the coupling constant may have values from 155 to 170 kc. From the error in the measured relaxation times and the quadrupole coupling constants for chlorine-35 and the deuteron in deuteriochloroform, the maximum error in the calculated diffusion constants amounts to  $D_{\perp}$ ,  $\pm 20\%$  and  $D_{||}$ ,  $\pm 60\%$ . The difference in the error limits is due partially to the nonlinearity of eq 7 in the diffusion constants.

The diffusion constants for the chloroform-benzene complex are also given in Figure 7 for comparison with neat chloroform. The  $C_3$  motion of the chloroform in the complex,  $D_{||}(C_3)$ , has slowed somewhat by a factor of approximately 1.3, or within experimental error in difference from the neat chloroform value. In contrast, the tumbling motion,  $D_{\perp}$ , is slowed considerably, by as much as a factor of 4. This is consistent with the complexing occurring along the symmetry axis of the chloroform and perpendicular to the plane of the benzene ring. The temperature dependence for the motions in the complex becomes stronger, corresponding to increases in the activation energies of 0.7-0.9 kcal/mol for the  $C_3$  motion and of 1.6-2.2 kcal/mol for the tumbling motion.

The results for the  $C_6$  motion of the benzene,  $D_{||}(C_6)$ , in the complex are also given in Figure 7. Since the deuterons in benzene are at an angle of  $90^\circ$  from the symmetry axis, the equation for the relaxation time of these deuterons becomes

$$\frac{1}{T_1} = \frac{(e^2 Q q)^2}{32 D_{\perp}} (5D_{\perp} + D_{||}) \quad (18)$$

The value of  $D_{\perp}$  for the complex is that calculated from the deuteron relaxation time in the  $CDCl_3-C_6H_6$  complex. The value of  $D_{||}(C_6)$  can be calculated using this value for  $D_{\perp}$ , a quadrupole coupling constant for perdeuteriobenzene of 190 kcps from Table I, the relaxation time of perdeuteriobenzene in both the neat liquid and solution II, and the fraction of benzene complexed in solution II. The results show that within experimental error the values of  $D_{||}(C_6)$  and  $D_{||}(C_3)$  are essentially the same at all temperatures. Therefore, the benzene ring and chloroform tetrahedron more than likely do not slip relative to each other in the complex.

The  $C_3$  motion of the chloroform is relatively unaffected on complexing with benzene. If the assumption is made that in a like manner the  $C_6$  motion of the benzene is unaffected on complexing with chloroform, the value of  $D_{||}(C_6)$  is the same for complexed benzene and for benzene in neat solution. The difference be-

tween the relaxation time of benzene in neat and chloroform solution is then ascribed to the change in  $D_{\perp}$  on complexing. The value of  $D_{\perp}$  in neat benzene can be calculated from eq 18 given  $D_{||}(C_6)$  and the relaxation times and quadrupole coupling constant of the deuterons in neat perdeuteriobenzene. The results are given in Table III and indicate that within experimental error the motion in benzene can be considered isotropic and described by a single rotational diffusion constant.

**Table III:** Rotational Diffusion Constants for Benzene- $d_6$

$T,$ $^{\circ}\text{C}$	$10^{-11} D_{\perp}$ ( $\pm 0.5$ ), $\text{sec}^{-1}$	$10^{-11} D_{  }$ ( $\pm 1.0$ ), $\text{sec}^{-1}$
10	1.2	1.3
30	1.3	1.4
50	1.4	1.5

The experimental error in these values and others for the diffusion constants in the complex are comparable with those for neat deuteriochloroform with an additional estimated error of about  $\pm 15\%$  introduced due to the errors in the chemical shift measurements.

## VI. Discussion

The nmr relaxation time is dependent only upon the area under the correlation function (see eq 2), and in order to calculate the correlation function (eq 3) it was necessary to assume a model for the molecular dynamics. The functional form of the correlation function, and consequently the details of the molecular dynamics, cannot be determined by the nmr experiment. The applicability of the assumed diffusion equation to the motion in chloroform can, however, be determined by comparison of the angular correlation time calculated from the experimental diffusion constant,  $(\tau_0)_i = (6D_i)^{-1}$ , with the mean free period of rotation (in radians/sec) for the free rotor,  $(\tau_f)_i = (I/kT)^{1/2}$ . If the time it takes for a molecule in the liquid to rotate through 1 radian about the  $i$ th axis,  $(\tau_0)_i$ , is very much shorter than the time it takes the free molecule in the gas phase to rotate through 1 radian,  $(\tau_f)_i$ , then the motion is most likely diffusional in nature

$$\chi_i = \left( \frac{\tau_0}{\tau_f} \right)_i \gg 1 \quad (19)$$

Applying this criterion to the data in Table II,  $\chi_{\perp} = 2.2$  and  $\chi_{||} = 0.9$  at  $T = 20^\circ$ . Over the temperature range of the measurements,  $\chi_{\perp}$  ranges between the value of 2 at high temperatures and the value of 5 at low temperatures, and  $\chi_{||} \approx 1$  at all temperatures. Inertial contributions to the motion are therefore probably important in chloroform and to the  $C_3$  motion in particular. However, the qualitative interpretation that the  $C_3$

motion is faster than the tumbling motion is still valid.

Unlike the nmr experiment, infrared and Raman band shapes are directly related to the functional form of the rotational correlation function. The band shape is determined by the rotational structure superimposed on the vibrational levels. In a liquid, the rotational line structure disappears, giving a single line the shape of which is given by the rotational spectral density. In principle, the exact form of the rotational correlation function can be calculated from the band shape<sup>21-24</sup>

$$\Phi^{(1)}(t) = \int_{-\infty}^{\infty} \sigma(\omega) e^{i\omega t} d\omega \quad (20)$$

where  $\sigma(\omega)$  is the normalized band shape  $\sigma(\omega) = I(\omega)/\int I(\omega) d\omega$ . The correlation function in eq 20 is a vector correlation function ( $\Phi^{(1)}(t) = \langle \cos \Omega(0) \cos \Omega(t) \rangle$ ). There are problems associated with the infrared and Raman experiments involving the overlap of underlying bands, the assignment of transitions, the determination of transition moments and polarizability tensors for asymmetric molecules, and the frequency shifts that obscure the pure rotational envelope. Nevertheless, if such difficulties can be overcome, a model for the reorientation such as the diffusion equation is not required, and the exact time dependence of the correlation function can be obtained.

Chloroform has two types of bands in the infrared spectrum: parallel bands in which the transition dipole is parallel to the symmetry axis and perpendicular bands in which the transition dipole is perpendicular to the symmetry axis. The parallel bands will yield the correlation function for the perpendicular or tumbling motion since for these transitions  $\Delta K = 0$ . The perpendicular bands will contain information about both modes of motion. If the motion is diffusional, then the correlation functions become

$$\Phi_{||}^{(1)}(t) = e^{-2D_{\perp}t} \quad (21)$$

$$\Phi_{\perp}^{(1)}(t) = e^{-(D_{\perp} + D_{||})t} \quad (22)$$

for the parallel and perpendicular bands, respectively. The band shapes given by the Fourier transform of the functions (eq 21 and 22) are therefore Lorentzian. If inertial contributions are important, the band shapes are non-Lorentzian and the experimental correlation functions will not be exponential. The form of the correlation functions and the appearance of the infrared band shapes for motion in the inertial limit, the diffusion limit, and in intermediate cases are given in ref 22 and 23.

The infrared spectrum of chloroform at the C-H stretch A<sub>1</sub> parallel band ( $\nu_1 = 3020 \text{ cm}^{-1}$ ) and the bending mode E perpendicular band ( $\nu_4 = 1213 \text{ cm}^{-1}$ ) have been reported as a function of temperature.<sup>25</sup> The appearance of the band shapes is Lorentzian, but correlation functions calculated from the Fourier transform of the band shapes are not exactly exponential and indicate that inertial contributions are important at short times  $t < \tau_f$  but that the behavior is exponential at long times  $t > \tau_f$ .

*Acknowledgments.* The author wishes to acknowledge the assistance and encouragement of Professor John D. Baldeschwieler, and helpful discussions with Dan Wallach and T. T. Bopp. The support of the National Science Foundation under Grant GP-4924x and a National Institutes of Health Predoctoral Fellowship to the author are gratefully acknowledged.

- (21) R. G. Gordon, *J. Chem. Phys.*, **43**, 1307 (1965).
- (22) R. G. Gordon, *ibid.*, **42**, 3658 (1965).
- (23) H. Shimizu, *Bull. Chem. Soc. Jap.*, **39**, 2385 (1966).
- (24) H. Shimizu, *J. Chem. Phys.*, **43**, 2453 (1965).
- (25) M. P. Lisitsa and Yu P. Tsystichenko, *Opt. Spectrosk.*, **9**, 229 (1960).

# A Comparison of Triethyl- and Trimethylammonium Headgroups in the Adsorption of *n*-Alkyl Quaternary Ammonium Ions at the Mercury Surface

by R. J. Meakins,<sup>1a</sup> M. G. Stevens,<sup>1b</sup> and R. J. Hunter<sup>1b</sup>

*Division of Applied Physics, National Standards Laboratory, CSIRO, Sydney, Australia* (Received July 3, 1968)

A series of *n*-alkyltriethylammonium compounds with *n*-alkyl chains between 4 and 16 carbon atoms has been prepared and submitted to electrocapillary and differential capacitance measurements at a dropping mercury electrode in 1 *N* potassium chloride. The results indicate that these are more strongly adsorbed than the corresponding compounds with trimethylammonium headgroups. The ratios of the differential capacitances for the two types of compound, calculated from the thicknesses of the adsorbed layers, are in good agreement with the experimental values.

## Introduction

Previous papers described interfacial tension and differential capacitance measurements of a dropping mercury electrode with *n*-alkyltrimethylammonium ions in 1 *N* sulfuric acid<sup>2a</sup> and 1 *N* potassium chloride.<sup>2b</sup> From the concentration dependence of the interfacial tension it was calculated that at favorable potentials and concentrations the compounds with the longest alkyl chains give adsorbed layers in which the quaternary ammonium ions are almost close packed. The large displacement of the electrocapillary maximum toward anodic potentials in each case indicated that the quaternary ammonium ions are adsorbed with the positively charged headgroups toward the mercury surface. This is in contrast to the aliphatic dipolar compounds, which are probably adsorbed with the polar group in the electrolyte.<sup>3</sup>

The adsorbed layer caused a large decrease in the differential capacitance, considered to be due mainly to hindrance of the approach of hydrated cations from the solution toward the metal surface. Other authors, working with adsorbed layers of long-chain aliphatic alcohols, have assumed either complete penetration<sup>4</sup> or complete exclusion<sup>5</sup> of hydrated ions.

It seemed likely that the hindering effect of the adsorbed layer would be increased by increasing the size of the headgroup, and this should therefore lead to a further reduction in the differential capacitance. A series of *n*-alkyltriethylammonium compounds was therefore prepared and submitted to electrocapillary and differential capacitance measurements at a dropping mercury electrode in 1 *N* potassium chloride. The present paper compares the results for these compounds with the corresponding compounds with trimethylammonium headgroups.

## Experimental Section

The apparatus was similar to that used in previous work,<sup>2a,b</sup> except that the counterelectrode was a platinum gauze cylinder of about 70 cm<sup>2</sup>. An automatic phase-sensitive device<sup>7</sup> was used to determine the time interval from the birth of the mercury drop to bridge balance and also the total drop lifetime from which the interfacial tension was calculated. All measurements were made at a frequency of 1.57 kHz.

For the preparation of the *n*-alkyl quaternary ammonium compounds the *n*-alkyl bromides of highest available commercial purity were first distilled through a short column packed with stainless steel gauze cylinders, and the purity was checked by vapor-phase chromatography and mass spectrometry.

The method of preparation of the *n*-alkyltrimethylammonium bromides was similar to that previously described.<sup>8</sup>

To obtain the *n*-alkyltriethylammonium bromides, the appropriate *n*-alkyl bromide was mixed with excess triethylamine in nitrobenzene solvent and the mixture was heated under reflux for 1 hr. Dry ether was then added gradually, with shaking, to give a deposit of fine

(1) (a) Division of Applied Physics, National Standards Laboratory, CSIRO, Sydney, Australia; (b) Department of Physical Chemistry, University of Sydney, Sydney, Australia.

(2) (a) R. J. Meakins, *J. Appl. Chem.*, **15**, 416 (1965); (b) R. J. Meakins, *ibid.*, **17**, 157 (1967).

(3) J. O'M. Bockris, M. A. V. Devanathan, and K. Muller, *Proc. Roy. Soc. A274*, 55 (1963).

(4) M. A. V. Devanathan, *ibid.*, **A267**, 256 (1962).

(5) A. N. Frumkin and B. B. Damaskin, "Modern Aspects of Electrochemistry," J. O'M. Bockris and B. E. Conway, Ed., Butterworth and Co. Ltd., London, 1964, p 149.

(6) R. J. Meakins, *Australasian Corrosion Eng.*, **11**, 5 (1967).

(7) J. B. Hayter, *J. Electroanal. Chem.*, in press.

(8) R. J. Meakins, *J. Appl. Chem.*, **13**, 339 (1963).

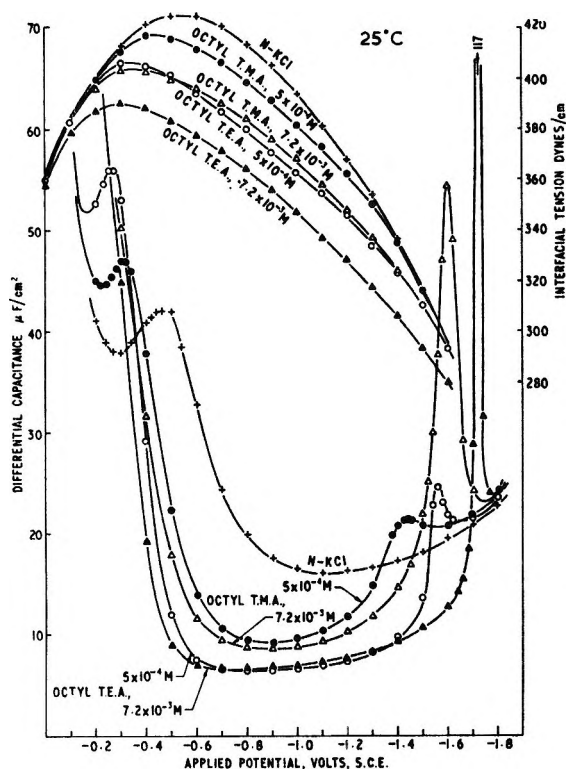


Figure 1. Electrocapillary and differential capacitance curves for a dropping mercury electrode in 1 N KCl containing *n*-octyl quaternary ammonium chlorides. Comparison of the trimethylammonium and triethylammonium headgroups.

crystals. These were filtered off under dry conditions, washed several times with dry ether, and then warmed repeatedly in a vacuum desiccator to remove the last traces of nitrobenzene. Alternatively, the crystals were extracted with dry ether for about 10 hr in a Soxhlet apparatus.

The *n*-alkyl quaternary ammonium bromides were converted to the corresponding chlorides by shaking in alcohol with two separate quantities of freshly prepared silver chloride. After filtration and evaporation of the solvent, the products were recrystallized from dry acetone-ether. The chlorides were more difficult to crystallize than the bromides.

The compounds with the shorter alkyl chains, particularly the chlorides, are deliquescent and were therefore stored in desiccators over silica gel or phosphorus pentoxide.

### Results and Discussion

Figure 1 shows a comparison of the behavior of the triethylammonium and trimethylammonium headgroups in the *n*-octyl quaternary ammonium compounds. The chlorides were used for these measurements because the more strongly adsorbed bromide ion would tend to mask the anodic desorption peaks, particularly at the higher concentrations.

In measurements with the longer chain compounds, the anion is less significant, since smaller concentrations

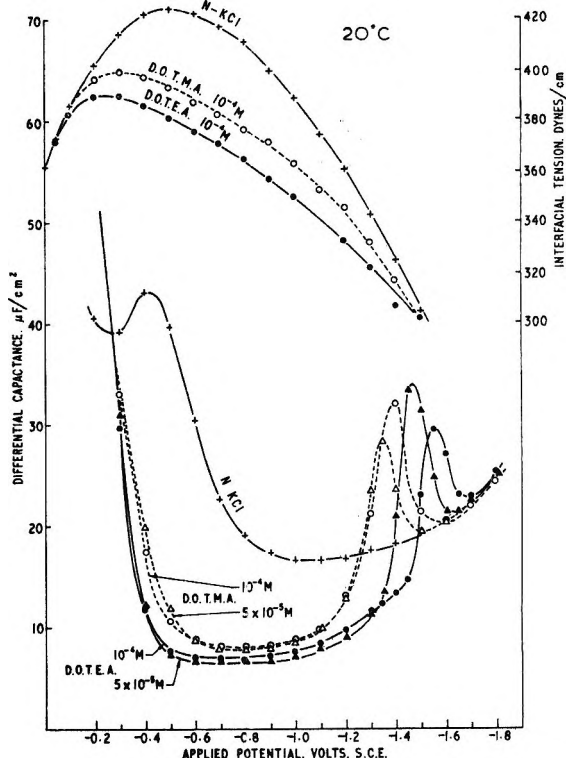


Figure 2. Comparison of electrocapillary properties of *n*-dodecyltrimethylammonium and *n*-dodecyltriethylammonium bromides in 1 N KCl.

are required to give saturated adsorbed monolayers. Some results for the *n*-dodecyltrimethylammonium and *n*-dodecyltriethylammonium bromides are shown in Figure 2.

In all of these results the compounds with the triethylammonium headgroup give the smaller values of the cathodic interfacial tension, indicating that they are more strongly adsorbed than the corresponding *n*-alkyltrimethylammonium compounds. This conclusion is supported by the wider separation between the anodic and cathodic desorption regions in the differential capacitance curves, indicating greater persistence at the mercury surface against the competition of other ions and water molecules.

The latter point was investigated further by studying the behavior of each of the quaternary ammonium compounds at several different concentrations. The results for *n*-hexyltriethylammonium chloride are illustrated in Figure 3. With increasing concentration the anodic and cathodic desorption peaks are both displaced so as to move further apart, but the displacement of the cathodic peak is always larger. This is presumably because at cathodic potentials the quaternary ammonium ions are competing merely with electrostatically attracted potassium ions, whereas on the anodic side they compete with the "specifically adsorbed" chloride ions.

The electrocapillary maxima (ecm) for these solutions were obtained from the corresponding interfacial

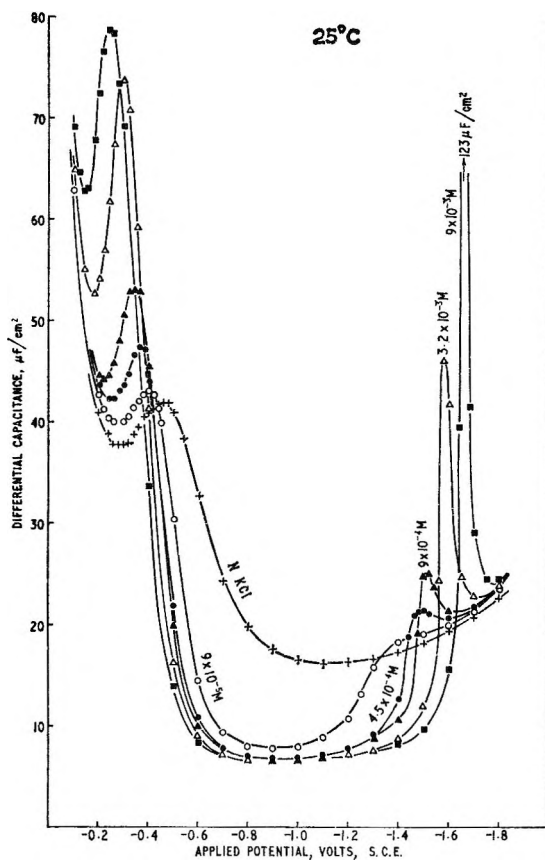


Figure 3. Differential capacitance curves for various concentrations of *n*-hexyltriethylammonium chloride in 1 *N* KCl.

tension curves by computation from isotension potentials. This method was first suggested by Grahame<sup>9</sup> but has not been widely used because of the extensive calculations involved. It is accurate to about 1 mV and involves only the assumption that equal drop times at two different applied potentials correspond to equal values of the interfacial tension.

The results obtained by this method are shown in Table I, together with the observed desorption potentials and also the desorption potentials relative to the electrocapillary maxima.

Similar tables were prepared for each of the compounds investigated, and the values were then used to obtain the relationship between the cathodic desorption potential and the logarithm of the concentration. The results are shown in Figure 4. In each case the relationship is linear, which is in agreement with the results for many dipolar compounds.<sup>10</sup> The gradients are approximately equal for alkyl chains up to eight carbon atoms, but there is a sharp increase for the C<sub>12</sub> and C<sub>14</sub> compounds, with C<sub>10</sub> intermediate. The increase in slope for the longer alkyl chains may be due to the presence of a bimolecular layer of adsorbed ions.<sup>2,11</sup>

If the results for corresponding *n*-alkyltriethylammonium and *n*-alkyltrimethylammonium compounds are compared, it is seen that at any particular con-

**Table I:** Desorption Potentials Relative to the Ecm for Various Concentrations of *n*-Hexyltriethylammonium Chloride, C<sub>6</sub>H<sub>13</sub>N(C<sub>2</sub>H<sub>5</sub>)<sub>3</sub>Cl, at a Dropping Mercury Electrode in 1 *N* KCl

Concn, M	Ecm (sec), V	Desorption potential (sec), V		Desorption potential (relative to ecm), V	
		Anodic	Cathodic	Anodic	Cathodic
0	-0.51	---	---	---	---
8.9 × 10 <sup>-5</sup>	-0.45	-0.38	-1.36	+0.07	-0.91
4.5 × 10 <sup>-4</sup>	-0.41	-0.34	-1.45	+0.07	-1.04
8.9 × 10 <sup>-4</sup>	-0.38	-0.32	-1.47	+0.06	-1.09
3.2 × 10 <sup>-3</sup>	-0.34	-0.28	-1.54	+0.06	-1.20
6.4 × 10 <sup>-3</sup>	-0.31	-0.24	-1.60	+0.07	-1.29
8.9 × 10 <sup>-3</sup>	-0.32	-0.23	-1.62	+0.09	-1.30

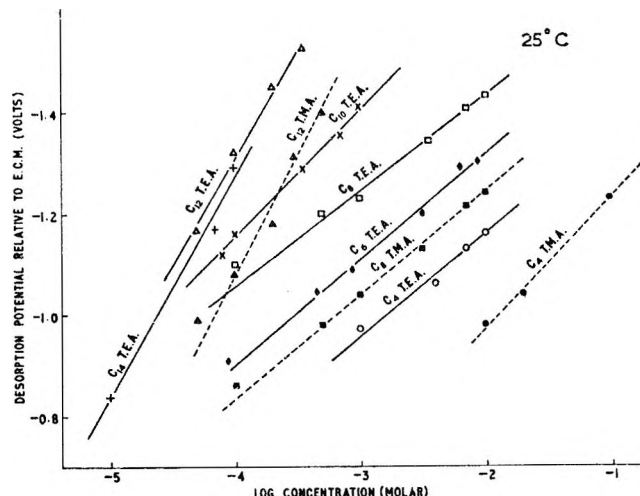


Figure 4. Concentration dependence of the cathodic desorption potentials for *n*-alkyltrimethylammonium and *n*-alkyltriethylammonium chlorides at a dropping mercury electrode in 1 *N* KCl.

centration the former persist at the mercury surface to higher negative potentials. This supports the above conclusion that the *n*-alkyltriethylammonium ions are the more strongly adsorbed.

The main factors leading to this stronger adsorption would be: (a) the larger bulk of nonpolar material in the head group which would favor expulsion from the aqueous phase; and (b) the stronger van der Waals forces of cohesion between the triethylammonium headgroups. Other factors favoring or opposing adsorption, *e.g.*, the van der Waals attraction between the alkyl chains, the mutual repulsion between the positive charges of the headgroups, and the competition by other ions and water molecules for the mercury surface, would be similar for both types of compound at any particular surface concentration and potential.

(9) D. C. Grahame, R. P. Larsen, and M. A. Poth, *J. Amer. Chem. Soc.*, **76**, 4819 (1954).

(10) W. Lorenz and F. Möckel, *Z. Elektrochem.*, **60**, 507 (1956).

(11) J. T. Davies and E. K. Rideal, "Interfacial Phenomena," Academic Press, New York, N. Y., 1961, p 437.

A further point from Figure 3 is that the heights of the desorption peaks for the *n*-hexyltriethylammonium ions increase with increasing concentration. This was also observed with the C<sub>4</sub> and C<sub>8</sub> compounds. From the work of Frumkin and Damaskos<sup>5</sup> it appears that the relationship between the peak height and the logarithm of the concentration should be linear, but in the present work this is approached only in the compounds with the shorter alkyl chains at the highest measured concentrations. At lower concentrations, particularly with the longer chain compounds, the adsorption-desorption process is not able to keep in step with the applied measuring frequency, and hence the true value of the peak capacitance is not obtained. In agreement with this explanation it was found that some measurements with the *n*-octyl compound at a lower frequency gave higher desorption peaks.

For further discussion of these results it is useful to determine the maximum surface concentrations of the various *n*-alkyl quaternary ammonium ions. These were calculated, as previously described,<sup>2a</sup> from the dependence of the interfacial tension,  $\gamma$ , on the bulk concentration,  $c$ , using the Gibbs adsorption equation. The appropriate experimental relationships between  $\gamma$  and log  $c$  are shown in Figure 5, the applied potentials being chosen as those giving the maximum values of the differential capacitance of each compound. The chlorides were used in all cases except *n*-dodecyltrimethylammonium, which was added as the bromide.

The surface concentrations calculated from these results are shown in Table II, together with the derived values of the surface areas per adsorbed ion and the excess surface charges due to the adsorbed layers.

The values for the *n*-alkyltrimethylammonium com-

**Table II:** Maximum Surface Concentrations of *n*-Alkyl Quaternary Ammonium Ions with Trimethylammonium and Triethylammonium Headgroups

<i>n</i> -Alkyl quaternary ammonium ion	No. of carbon atoms in <i>n</i> -alkyl chain	Max. surface concn of the adsorbed ion, mol/cm <sup>2</sup> $\times 10^{-10}$	Surface area per adsorbed ion, Å <sup>2</sup>	Excess surface charge, μC/cm <sup>2</sup>
<b>Trimethylammonium</b>				
<i>n</i> -Butyl-	4	1.70	98	16
<i>n</i> -Octyl	8	2.29	73	22
<i>n</i> -Dodecyl-	12	2.95	57	28
<i>n</i> -Tetradecyl-	14	5.63	30	54
<b>Triethylammonium</b>				
<i>n</i> -Butyl-	4	2.46	68	24
<i>n</i> -Hexyl-	6	2.29	73	22
<i>n</i> -Octyl-	8	2.39	70	23
<i>n</i> -Decyl-	10	2.46	68	24
<i>n</i> -Dodecyl-	12	3.08	54	30
<i>n</i> -Tetradecyl-	14	4.22	39	41

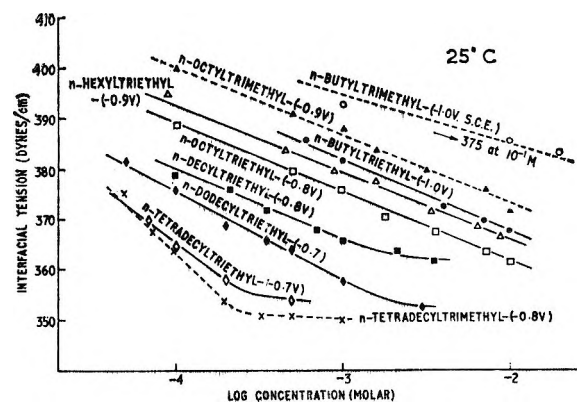


Figure 5. Concentration dependence of the interfacial tension at a dyne in 1 N KCl containing various *n*-alkyltrimethylammonium and *n*-alkyltriethylammonium chlorides. The applied potentials quoted are those giving the minimum differential capacitance.

pounds are similar to those previously obtained with the bromides in 1 N sulfuric acid.<sup>2a</sup> In that work it was pointed out that the surface area required by the trimethylammonium headgroup is about 40 Å<sup>2</sup>, which is double the space required by the extended *n*-alkyl chain. From the surface areas shown in Table II it is evident that the adsorbed ions of the *n*-butyl-, *n*-octyl-, and *n*-dodecyltrimethylammonium compounds are somewhat less than close packed. The C<sub>14</sub> compound, on the other hand, has only 30 Å<sup>2</sup>/adsorbed ion, suggesting the presence of at least a partial bimolecular layer.

From scale molecular models of the triethylammonium headgroup it is found that its surface projection can be approximately represented by an equilateral triangle with a side of about 12 Å, giving a minimum possible surface area of 62 Å<sup>2</sup>. The experimental values in Table II for the compounds with alkyl chains between four and ten carbon atoms are between 68 and 73 Å<sup>2</sup>, indicating that the headgroups are almost close packed. The lower values for the C<sub>12</sub> and C<sub>14</sub> compounds suggest the presence of partial bimolecular layers.

It is interesting now to compare the smallest values of the minimum differential capacitance for compounds with the two types of headgroup. These results are given in Table III, together with the corresponding concentrations and potentials.

In each case the minimum differential capacitance for the triethylammonium compound is smaller than for the trimethylammonium compound. This applies even where the surface concentrations are approximately equal, as, for example, with the C<sub>8</sub> and C<sub>12</sub> compounds (see Table II).

In considering a possible structure for the electrical double layer with adsorbed quaternary ammonium ions it seems unlikely that the hydrophobic alkyl chains would extend outward into the electrolyte. They would most likely be bent over and packed together to

**Table III:** Smallest Values of the Minimum Differential Capacitance for a Dropping Mercury Electrode in 1 N KCl Containing *n*-Alkyltrimethylammonium and *n*-Alkyltriethylammonium Ions

<i>n</i> -Alkyl quaternary ammonium ion	Anion of compd used	Min differential capacitance, $\mu\text{F}/\text{cm}$	Bulk concn giving min differential capacitance, $M$	Applied potential giving min differential capacitance (sce), V
Nil, <i>i.e.</i> , 1 N KCl solution		16.2		-1.10
Trimethylammonium				
<i>n</i> -Butyl-	Chloride	10.6	$1 \times 10^{-1}$	-1.00
<i>n</i> -Octyl-	Chloride	8.6	$1 \times 10^{-2}$	-0.90
<i>n</i> -Dodecyl-	Bromide	7.7	$5 \times 10^{-5}$	-0.80
<i>n</i> -Tetradecyl-	Chloride	7.8	$1 \times 10^{-4}$	-0.75
<i>n</i> -Hexadecyl-	Bromide	7.9	$1 \times 10^{-4}$	-0.75
	Bromide	7.4	$1.5 \times 10^{-4}$	-0.75
Triethylammonium				
<i>n</i> -Butyl-	Chloride	6.9	$1 \times 10^{-2}$	-1.05
<i>n</i> -Hexyl-	Chloride	6.6	$9 \times 10^{-4}$	-0.95
<i>n</i> -Octyl-	Chloride	6.3	$5 \times 10^{-4}$	-0.85
<i>n</i> -Decyl-	Chloride	6.2	$8 \times 10^{-5}$	-0.80
<i>n</i> -Dodecyl-	Chloride	0.5	$5 \times 10^{-5}$	-0.75
<i>n</i> -Tetradecyl-	Bromide	6.5	$5 \times 10^{-5}$	-0.75
<i>n</i> -Hexadecyl-	Chloride	6.7	$7 \times 10^{-5}$	-0.75
	Bromide	6.3	$6 \times 10^{-5}$	-0.80

form a hydrocarbon layer above the headgroups, thus excluding water and also satisfying the van der Waals forces of attraction between the chains. The excess positive charge due to the quaternary ammonium ions would be balanced by chloride counterions, which, if dehydrated, could fit into spaces near the headgroups without having much effect on the thickness of the layer.

The scale molecular models indicate that the thickness of the layer would be about 6.9 Å for the *n*-alkyltrimethylammonium ions and about 8.8 Å for the *n*-alkyltriethylammonium ions. A calculation from molar volumes and densities gives somewhat smaller thicknesses, but the ratio is approximately the same. At these thicknesses the packing is almost perfect for an alkyl chain of ten carbon atoms. With shorter chains there would be some indentations and with longer chains there would be an excess of hydrocarbon, leading probably to a slight thickening of the layer. Figure 6 shows the proposed model of the electrical double-layer "capacitor," with *n*-decyltriethylammonium chloride as the "dielectric," with the metal surface as one "plate," and with the other "plate" consisting of the line through the centers of closest approach of the hydrated potassium ions.

Assuming that the relative permittivities are similar for both types of compound, the ratios of the capacitances should be equal to the inverse of the ratios of the total thicknesses; *i.e.*,  $C_{\text{TMA}}/C_{\text{TEA}} = 12.9/11.0 = 1.17$ , where  $C_{\text{TMA}}$  and  $C_{\text{TEA}}$  are the capacitances of the

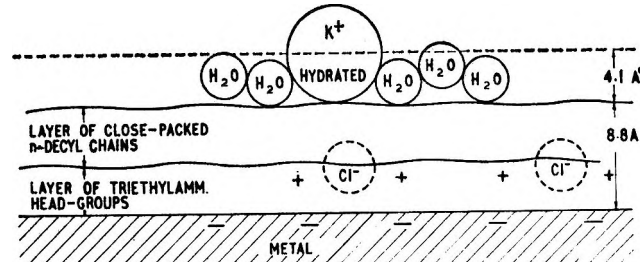


Figure 6. Electrical double layer with specifically adsorbed *n*-decyltriethylammonium ions.

*n*-alkyltrimethylammonium and the *n*-alkyltriethylammonium compounds, respectively.

Under the conditions where the model applies, the capacitance due to the adsorbed layer will be approximately equal to the measured values of the minimum differential capacitance shown in Table III. The

**Table IV**

No. of carbon atoms in the <i>n</i> -alkyl chain	$(C_{\text{TMA}})_{\text{min}}/(C_{\text{TEA}})_{\text{min}}$
4	1.54
8	1.37
12	1.18
14	1.16
16	1.17

ratios from these experimental values are given in Table IV.

The larger values for the compounds of shorter chain length are probably due to imperfect packing in the *n*-alkyltrimethylammonium layer, leaving gaps which would be occupied mainly by water molecules, leading to an enhancement of the effective relative permittivity. With the longer chain compounds the agreement between the theoretical and experimental ratios is quite good.

## Conclusions

In measurements with a dropping mercury electrode in 1 N potassium chloride it is found that *n*-alkyltrimethylammonium ions are adsorbed more strongly than the corresponding *n*-alkyltrimethylammonium ions. The ratios of the minimum values of the capacitances for the two types of compound are in good agreement with the values calculated from the expected thicknesses of the adsorbed layers if it is assumed that the relative permittivities are similar in each case.

# Energetics of the Pyrochlorophyll-Sensitized Photoreduction of Nitro Compounds

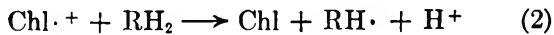
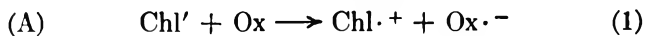
by G. R. Seely

*Contribution No. 324 from the Charles F. Kettering Research Laboratory, Yellow Springs, Ohio 45387  
(Received July 8, 1968)*

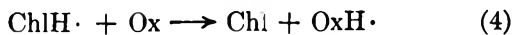
Comparison of the quantum yields of pyrochlorophyll-sensitized photoreduction of substituted nitrobenzenes by hydrazobenzene in ethanol-pyridine solution with the polarographic quarter-wave reduction potentials of the nitro compounds leads to the conclusion that an electron can be transferred from triplet-excited pyrochlorophyll to the nitro compound without input of additional activation energy, if the potential of the nitro compound is greater than -0.80 V (sce) in aqueous ethanol-pyridine. The liquid-junction potential between water and the aqueous ethanol-pyridine mixture used for polarography is estimated to be  $0.05 \pm 0.02$  V from the polarography of complexes of cadmium with pyridine, 2,2'-bipyridyl, and *o*-phenanthroline. With the correction, it is estimated that triplet-excited chlorophyll can reduce oxidants exothermically if their oxidation-reduction potentials are greater than  $-0.60 \pm 0.035$  V (nhe) in water, a value compatible with the reported reducing properties of illuminated chloroplasts. Pyrochlorophyll also sensitizes the reduction of low-potential nitro compounds by ascorbic acid, by a mechanism involving reduction of triplet-excited pyrochlorophyll by ascorbic acid.

## Introduction

We have recently discussed the sensitization by chlorophyll and its derivatives of photochemical oxidation-reduction reactions by two general mechanisms: (A) eq 1 and 2, in which triplet-excited chlorophyll (Chl')



reacts with an oxidant (Ox), and (B) eq 3 and 4, in which it reacts with the reductant ( $\text{RH}_2$ ).<sup>1,2</sup> The experimental conditions under which reactions by these mechanisms could be distinguished were described.



We also noted a correlation between the mechanism

assigned to a sensitized reaction and the polarographic half-wave reduction potential of the oxidant, in that mechanism A was operative if  $E_{1/2}$  was greater than -0.6 V (sce)<sup>3</sup> but not if  $E_{1/2}$  was less than -0.9 V. It was possible to reduce oxidants with  $E_{1/2} < -0.9$  V by mechanism B. Between -0.6 and -0.9 V there was little experimental information available on which to assign a mechanism.

There are grounds for believing that the primary photoreactions of photosynthesis are oxidations of chlorophyll like eq 1, both in system I<sup>4</sup> where pyridine nucleo-

(1) G. R. Seely, *J. Phys. Chem.*, **69**, 2779 (1965).

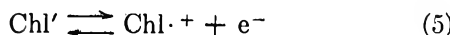
(2) G. R. Seely in "The Chlorophylls," L. P. Vernon and G. R. Seely, Ed., Academic Press, New York, N. Y., 1966, pp 552-554.

(3) Sce, saturated calomel electrode; nhe, normal hydrogen electrode.

(4) Photosynthetic pigment systems I and II as defined by L. N. M. Duysens and J. Amesz, *Biochim. Biophys. Acta*, **64**, 243 (1962).

tide is reduced<sup>5,6</sup> and in system II where water is oxidized.<sup>7,8</sup> It is, therefore, of importance to the understanding of photosynthesis to determine with which oxidants photoexcited chlorophyll can react. Illuminated spinach chloroplasts can reduce ferredoxin ( $E_0 = -0.43$  (nhe))<sup>3,9</sup> and a quaternary bipyridyl salt with  $E_{1/2} = -0.52$  (nhe) or  $-0.76$  (sce),<sup>10</sup> which is in the middle of the potential range in which we have had no information *in vitro*.

We have now examined the photosensitized reduction of a series of substituted nitrobenzenes under experimental conditions where only mechanism A is operative. We have further tested the relationship<sup>1</sup> between the quantum yield of photoreduction and polarographic reduction potential with these nitro compounds, one of the objects being to compare the potential of reaction 5,



the half-cell reaction, with physiologically generated potentials. This should be possible, because reaction 1 would not be expected to occur readily if the potential for reduction of the nitro compound is lower than that for reaction 5. The polarographic reduction potentials of substituted nitrobenzenes cover the previously unexplored range of  $-0.6$  to  $-0.9$  V (sce).

Nitro compounds have been seldom used as oxidants in chlorophyll-sensitized reductions. However, Gurevich observed the sensitized photoreduction of *o*- and *p*-dinitrobenzenes<sup>11</sup> and more recently Hertogs and Wessels studied the photoreduction of 2,4-dinitrophenol, sensitized by chlorophyll in detergent micelles.<sup>12</sup> Chernyuk and Dilung found that nitro compounds stabilized Chl $\cdot$  in frozen media,<sup>13</sup> under conditions which may or may not have involved direct interaction of excited chlorophyll with the nitro compounds.

At the concentration of nitro compound used in the present work, the extent to which the fluorescence of the sensitizer is quenched is so small that only reaction of the triplet state of the sensitizer, Chl', can account for the quantum yields of photoreduction of many of the nitro compounds. In the following paper<sup>14</sup> the photosensitizing activity of the singlet state (Chl\*) is compared with that of the triplet state by examining reactions in a range of nitro compound concentration in which quenching of fluorescence is significant.

## Materials and Methods

The photochemical system consisted of pyrochlorophyll ( $10^{-5}$  M) as the sensitizer, hydrazobenzene ( $3.8 \times 10^{-3}$  M) as the reductant, and a substituted nitrobenzene ( $5 \times 10^{-4}$  M) as the oxidant in 7:3 absolute ethanol-pyridine. The lack of detectable photoreduction of pyrochlorophyll by hydrazobenzene in the absence of an oxidant was evidence of the effective suppression of mechanism B.<sup>1</sup>

Pyrochlorophyll (10-decarbomethoxychlorophyll a) was used as sensitizer instead of chlorophyll, because it

is much more stable in air and because its photochemistry is almost indistinguishable from that of chlorophyll. We felt that for this study it was particularly important to ensure the absence of small, undetected amounts of allomerized chlorophyll derivatives. The preparation of pyrochlorophyll has been described.<sup>15</sup> A few reductions were made with chlorophyll as the sensitizer to test the validity of the substitution.

Nitro compounds were recrystallized until their melting points were satisfactory; hydrazobenzene was recrystallized from methanol-water at least three times or until colorless. Other materials were used as received. At the initial nitro concentration, the fluorescence of pyrochlorophyll was at most 1-2% quenched.<sup>14</sup>

The sensitized reduction of nitro compounds, with hydrazobenzene and ascorbic acid as reductants, was first examined qualitatively on a Cary Model 14 spectrophotometer with a compartment modified to permit scanning the spectrum while the reaction was in progress. After the reaction the solvent was removed, and the residue was chromatographed on Gelman Type SG thin layers, with heptane + 1% butanol. The chromatograms were sprayed with trisodium pentacyanoamino-ferrate or *p*-dimethylaminobenzaldehyde. In most cases, the development of violet or yellow spots on the test samples, and not on the dark control, indicated the presence of amine or hydroxylamine reduction products of the nitro compounds.

In quantitative work, spectral absorbances were determined with a Beckman DU spectrophotometer at intervals during the reaction, and the light absorbed was measured with a calibrated Eppley thermopile. Pyrochlorophyll was excited with light from a projector lamp focused through a 670-nm interference filter. Since most of the nitro compounds and their reduction products do not absorb visible light appreciably, the reaction was followed by the rise of the azobenzene band, which at 470 nm has a molar absorptivity of  $355 M^{-1} \text{ cm}^{-1}$ . Quantum yields are therefore reported as moles of azobenzene produced per einstein of light absorbed by pyrochlorophyll. Approximately 2 mol of azobenzene was produced per mole of nitro compound reduced. With light absorption rates in the neighbor-

- (5) B. Kok, *Biochim. Biophys. Acta*, **48**, 527 (1961).
- (6) H. T. Witt, A. Müller, and B. Rumberg, *Nature*, **192**, 967 (1961).
- (7) J. Weikard, A. Müller, and H. T. Witt, *Z. Naturforsch.*, **18b**, 139 (1963).
- (8) J. Ames, *Biochim. Biophys. Acta*, **79**, 257 (1964).
- (9) K. Tagawa and D. I. Arnon, *Nature*, **195**, 537 (1962).
- (10) C. C. Black, *Biochim. Biophys. Acta*, **120**, 332 (1966).
- (11) A. A. Gurevich, *Dokl. Akad. Nauk SSSR*, **59**, 937 (1948).
- (12) M. Hertogs and J. S. C. Wessels, *Biochim. Biophys. Acta*, **109**, 610 (1965).
- (13) I. N. Chernyuk and I. I. Dilung, *Dokl. Akad. Nauk SSSR*, **165**, 1350 (1965); *Proc. Acad. Sci. USSR, Phys. Chem. Sect.*, **165**, 920 (1965).
- (14) G. R. Seely, *J. Phys. Chem.*, **73**, 125 (1969).
- (15) G. R. Seely, *ibid.*, **71**, 2091 (1967).

hood of  $5 \times 10^{-6}$  einstein l.<sup>-1</sup> sec<sup>-1</sup>, the reduction of *p*-dinitrobenzene was complete in 10 min, and the reduction of *p*-nitroaniline was barely detectable after 4 hr.

The solution was flushed with N<sub>2</sub> (Matheson purified grade) for at least 15 min before irradiation. Under these conditions a residue of O<sub>2</sub> remained, which was rapidly consumed by photosensitized oxidation of hydrazobenzene. Because of this side reaction we omitted the first 50-sec irradiation period from the extrapolation to the initial quantum yield. A few runs were repeated with the residual O<sub>2</sub> more effectively eliminated by passing the N<sub>2</sub> stream through a wash bottle containing methyl viologen, dissolved in ethylene glycol monomethyl ether and reduced with iron.

The solvent mixture was chosen with regard for its use in sensitized photoreactions by mechanism B with ascorbic acid as the reductant.<sup>16</sup> Solutions to test photoreduction of nitro compounds according to mechanism B contained *n*-butylamine (0.14 M) in addition to ascorbic acid ( $4 \times 10^{-3}$  M). This, like other amines, prevents the accumulation of reduced chlorophyll (ChlH<sub>2</sub>) by catalyzing its dark reoxidation by dehydroascorbic acid.<sup>17</sup>

*Polarography.* It would have been desirable to polarograph the nitro compounds in exactly the same solvent mixture as was used for photochemical reduction. However, distinct and reproducible waves were not obtained unless at least 10% water was added to the 7:3 ethanol-pyridine mixture, apparently because of crystallization of KCl at the junction with the aqueous see. As the value of  $E_{1/2}$  (see below) for nitrobenzene was the same with 20% water as with 10% water, it is not likely that the presence of 10% water would invalidate the comparison with photochemical results.

Solutions for polarography contained 10<sup>-3</sup> M nitro compound, 10<sup>-1</sup> M LiClO<sub>4</sub>, and 0.01% polyvinylpyrrolidone as the maximum suppressor. They were flushed for 15 min with prepurified N<sub>2</sub>. Measurements were made with an undamped Sargent Model XXI polarograph. The liquid-junction potential was estimated by polarography of Cd complexes as described later. Potentials were not corrected for the *iR* drop of the cell, because polarography of the Cd complexes showed this to be less than 0.01 V.<sup>18,19</sup>

## Results and Discussion

*Polarography.* In our solvent mixture as in other protic solvents, most nitro compounds are reduced polarographically in an irreversible four-electron wave to the phenylhydroxylamine.<sup>20</sup> The steps of the reduction have recently been investigated in some detail. In protic and aprotic solvents, the first step is reversible transfer of an electron to the nitro compound, to form a free-radical ion.<sup>21-26</sup> In protic solvents the ion is neutralized, and the radical disproportionates to give the

hydrated nitroso species RN(OH)<sub>2</sub>. Dehydration of the latter is followed by rapid reduction to the hydroxylamine.<sup>25,26</sup> Only the first step is reversible; the other steps are not fully reversible or are slow. In particular, the dehydration of RN(OH)<sub>2</sub> to RNO may be slow.<sup>26</sup> The polarographic wave corresponding to the first step is well separated from succeeding waves in aprotic solvents but not in protic ones.<sup>21,22,27</sup>

For a few of the more easily reduced nitrobenzenes and nitronaphthalenes (compounds I, II, XIV, and XVII of Table I), the polarographic wave in ethanol-pyridine approaches a shape corresponding to a reversible one-electron reaction. For most of the others, there is a change to more gradual slope or even an inflection near the middle of the wave, giving it the appearance of two two-electron waves coalesced, the first more nearly reversible than the second.<sup>28</sup>

The half-wave potential,  $E_{1/2}$ , which has theoretical significance for reversible waves, has no such significance for irreversible ones. In the case of the nitro compounds, the half-wave potential for the whole

- (16) G. R. Seely and A. Folkmanis, *J. Amer. Chem. Soc.*, **86**, 2763 (1964).
- (17) A. A. Krasnovskii and E. V. Pakshina, *Dokl. Akad. Nauk SSSR*, **120**, 581 (1958).
- (18) We tried at first to include a "buffer" in the solution, such as dimethylbenzylamine-*p*-toluenesulfonic acid, which has about the same pH (ca. 8.5) in water as that which pyridine would establish by hydrolysis. However, the polarograms of nitro compounds in the presence of a "buffer" showed a prewave, about 0.2 V in advance of the normal wave in unbuffered solution, the magnitude of which increased with the concentration of the acid component of the buffer. The presence of any acid (e.g. acetic, *p*-nitrobenzoic) was sufficient to produce the prewave; dimethylbenzylamine was unnecessary. The prewave was also seen in acidified water-ethanol mixtures. At 10<sup>-2</sup> M toluenesulfonic acid the prewave only was present and had almost the same diffusion current as the normal wave. The position of the normal wave was unaffected by acid concentration, but its magnitude was reduced by that of the prewave. This phenomenon has been explicitly noted and examined by Jannakoudakis and Wildenau,<sup>19</sup> who related it to the consequences of rapid protonation of the reduced nitro radical ion. We noted, however, that the current-voltage trace for each Hg drop had a peculiar "blunt" characteristic, showing that the prewave current reached a maximum well before the drop reached maximum size, and then diminished slightly. On the grounds that the phenomenon probably involved adsorption of a reduced nitro species to the drop, we thought it best to run the polarograms in unbuffered solution.
- (19) D. Jannakoudakis and A. Wildenau, *Z. Naturforsch.*, **22b**, 118, 603 (1967).
- (20) I. M. Kolthoff and J. J. Lingane, "Polarography," 2nd ed., Vol. II, Interscience Publishers, New York, N. Y., 1952, pp 748-764.
- (21) A. H. Maki and D. H. Geske, *J. Amer. Chem. Soc.*, **83**, 1852 (1961).
- (22) W. Kemula and R. Sioda, *Bull. Acad. Pol. Sci., Ser. Chim.*, **10**, 107 (1962).
- (23) L. Holleck and B. Kastening, *Rev. Polarogr. (Kyoto)*, **11**, 129 (1963).
- (24) B. Kastening, *Electrochim. Acta*, **9**, 241 (1964).
- (25) R. Koopmann and H. Gerischer, *Ber. Bunsenges. Phys. Chem.*, **70**, 127 (1966).
- (26) K.-D. Asmus, A. Wigger, and A. Henglein, *ibid.*, **70**, 862 (1966).
- (27) M. Fields, C. Valle, Jr., and M. Kane, *J. Amer. Chem. Soc.*, **71**, 421 (1949).
- (28) The wave shapes are similar to certain of those derived by T. Berzins and P. Delahay, *ibid.*, **75**, 5716 (1953), for two consecutive irreversible electrochemical steps.

**Table I:** Data for the Polarographic Reduction of Nitro Compounds in 63:27:10 Ethanol-Pyridine-Water and for their Pyrochlorophyll-Sensitized Photoreduction by Hydrazobenzene in 70:30 Ethanol-Pyridine

No.	Compd	$-E_{1/4}^a$ V	$-E_{1/2}^b$ V	$E_{1/4}^c - E_{1/4}^d$ V	I	$\phi_0^e$	$[\text{Azo}] / [\text{nitro}]$
I	p-Dinitrobenzene	0.458	0.480 1.58 <sup>c</sup>	0.043	4.8 13.85	0.37	2.21
II	p-Nitrobenzaldehyde	0.626	0.652 1.64	0.044	6.5 2.8	0.21	1.82
III	p-Nitrobenzonitrile	0.640	0.700	0.185	7.7	0.175	2.00
IV	m-Dinitrobenzene	0.661 <sup>d</sup>	0.692	...	16.15	0.135	1.89
V	Methyl p-nitrobenzoate	0.694	0.740	0.125	8.7	0.150	2.06
VI	m-Nitrobenzonitrile	0.735	0.815	0.153	7.6	0.100	2.18
VII	p-Nitrobenzenesulfonamide	0.743	0.826	0.198	6.0	0.150	2.02
VIII	m-Nitrobenzaldehyde	0.788	0.830 1.59	0.093	7.25 3.9	0.070	1.85
IX	p-Nitrobenzoate <sup>e</sup>	0.790	0.950	0.213	5.3	0.120	1.65
X	m-Nitroacetophenone	0.795	0.843	0.112	7.8	0.040	1.73
XI	p-Fluoronitrobenzene	0.810	0.840 1.230	0.059	2.0 4.8	0.0100	f
XII	Methyl m-nitrobenzoate	0.811	0.870	0.139	6.6	0.054	1.95
XIII	p-Nitrochlorobenzene	0.822	0.920	0.180	8.2	0.065	1.30
XIV	1-Nitronaphthalene	0.825	0.855	0.068	6.7	...	...
XV	p-Nitrobiphenyl	0.835	0.891	0.127	4.3	0.032	f
XVI	m-Nitroanisole	0.856	0.899	0.114	8.5	0.0175	f
XVII	5-Nitro-1-naphthylamine	0.862	0.890	0.064	7.7	...	...
XVIII	Nitrobenzene	0.881	0.937	0.149	9.2	0.0135	f
XIX	m-Nitrotoluene	0.895	0.960	0.145	8.6	0.0040	f
XX	m-Nitroaniline	0.906	0.942	0.092	7.7	...	...
XXI	m-Nitrodimethylaniline	0.908	0.937	0.100	6.85	...	...
XXII	p-Nitroacetanilide	0.924	1.009	0.197	6.4	0.006	f
XXIII	p-Nitrotoluene	0.930	1.048	0.218	9.2	0.0041	f
XXIV	p-Nitroanisole	0.957	1.035	0.252	8.25	0.0026	f
XXV	o-Nitroaniline	1.012	1.078	0.150	7.85	...	...
XXVI	p-Nitrophenylhydrazine	1.029	1.094	0.191	8.3	...	...
XXVII	2-Methyl-1-nitronaphthalene	1.034	1.141	0.213	8.15	...	...
XXVIII	p-Nitrodimethylaniline	1.035	1.085	0.151	9.55	...	...
XXIX	p-Nitroaniline	1.037	1.090	0.145	10.15	0.0003	f

<sup>a</sup> Polarographic data listed are the quarter-wave reduction potential  $E_{1/4}$  and the half-wave reduction potential  $E_{1/2}$ , vs. sce, the difference  $E_{1/4} - E_{1/2}$  as a measure of departure from reversibility, and the diffusion-current constant  $I = i_D / cm^2 \cdot t^{1/2}$ . In the last, the diffusion current,  $i_D$ , is expressed in microamperes and the concentration,  $c$ , of the nitro compound was 1 mM. For compounds XIV, XVII, XXV, and XXVII, the drop time,  $t$ , was 5.33 sec and the mercury flow rate,  $m$ , was 1.049 mg/sec. For the other compounds, the drop time was about 3 sec, and  $m$  was 2.462 or 2.25 sec. <sup>b</sup> Photoreduction data listed are the initial quantum yield,  $\phi_0$ , expressed as moles of azobenzene formed per einstein of light absorbed by pyrochlorophyll, and the ratio [azo]/[nitro] of the final azobenzene concentration to the initial nitro concentration (ca.  $5 \times 10^{-4} M$ ). <sup>c</sup> Second waves, when observed, are listed by  $E_{1/2}$  and  $I$  only. <sup>d</sup> The polarogram consists of two overlapping, four-electron waves (cf. diffusion-current constant), the first corresponding to the reduction of IV and the second, probably, to the reduction of m-nitrophenylhydroxylamine. As only the first is germane, the potentials listed are the one-eighth wave potential and the quarter-wave potential. <sup>e</sup> p-Nitrobenzoic acid in the presence of 0.01 M dimethylbenzylamine to ensure complete ionization. <sup>f</sup> The reaction was not allowed to go to completion.

four-electron wave did not seem a particularly appropriate estimate of the potential of the reversible first step. We chose instead the quarter-wave potential,  $E_{1/4}$ , as the potential of reference for the wave. With many of the nitro compounds,  $E_{1/4}$  is near the half-wave potential of the first of the two apparently coalesced two-electron waves.

Polarographic data for the nitro compounds are listed in Table I, in the order of descending  $E_{1/4}$ . The value of  $E_{1/2}$  is listed for comparison with  $E_{1/4}$ , and  $E_{1/4} - E_{1/2}$  as an indication of wave breadth, or departure from reversibility (the value of  $E_{1/4} - E_{1/2} = 0.056$  V for a reversible one-electron wave). Most

values for the diffusion-current constant,  $I$ , lie between 6 and 9 for the nitro compounds. In comparison, the diffusion-current constant for the two-electron wave of 2,5-dimethylbenzoquinone was 4.9. There is an approximate inverse dependence of  $I$  on the square root of the molecular weight, as expected for a diffusion-controlled current. High values of  $I$  for the compounds V, XXVIII, and XXIX (compare with XII, XXI, and XX) relative to their molecular weights suggest that more than four electrons are consumed in their polarographic reduction. The diffusion-current constant for p-dinitrobenzene (I) is low for a four-electron reduction of a compound of its molecular weight, but it would be

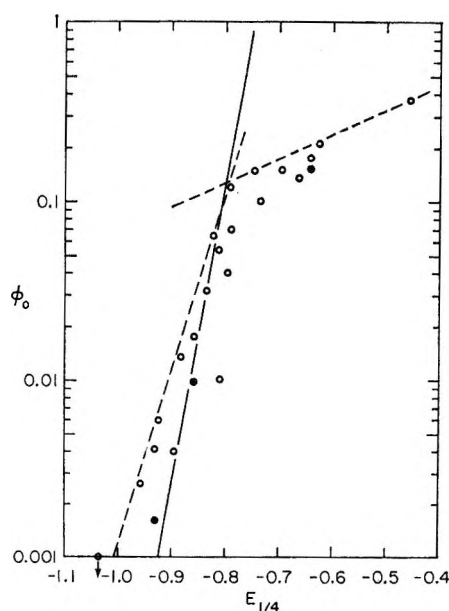


Figure 1. Initial quantum yields ( $\phi_0$ ) of sensitized photoreductions of nitro compounds plotted against their polarographic quarter-wave reduction potentials,  $E_{1/4}$  (see Table I): O, pyrochlorophyll as the sensitizer, hydrazobenzene as the reductant in 7:3 ethanol-pyridine at 24°, trace of residual oxygen present (dashed lines approximate upper bound of these points; the solid line has slope of 0.059 expected for a thermally activated one-electron reaction); ●, same, but oxygen undetectable.<sup>14</sup>

about right if the diffusing species is a charge-transfer complex with pyridine.<sup>29</sup>

*Photoreduction with Hydrazobenzene.* Initial quantum yields for the pyrochlorophyll-sensitized reduction of a series of nitro compounds are listed in Table I and are plotted against  $E_{1/4}$  in Figure 1. There is an evident correlation between these two quantities. For the more rapid photoreductions, which were followed to completion, the ratio of the final azobenzene concentration to the initial nitro concentration is also listed in Table I. This ratio, which is usually rather close to 2, corresponds to a predominantly four-electron reduction of the nitro group, just as in polarographic reduction.

Initial quantum yields trend toward larger values with increasing  $E_{1/4}$ , but with a distinct change in slope near -0.8 V (sce) on the logarithmic plot of Figure 1. If the yields are plotted against  $E_{1/2}$ , a similar but somewhat looser correlation is obtained.

The dashed lines in Figure 1 are the linear approximations of the upper bounds of quantum yields above and below their intersection at -0.80 V. We interpret these data to mean that the oxidation of Chl' by a nitro compound is exothermic, if the potential of the latter is above -0.80 V, and the continued increase of quantum yield with potential merely reflects the increasing efficiency of the follow-up reactions to the primary photochemical steps. If the potential is below -0.80 V, the oxidation of Chl' is endothermic, and the more rapid

change of quantum yield with potential reflects the need for thermal activation.

This interpretation is supported by the dependence of quantum yield on the concentration of the nitro compound. If the reaction of eq 1 is exothermic, its rate should be determined by the collision frequency, and the quantum yield should be nearly independent of nitro concentration at the level used. If the reaction is endothermic, its rate should be limited by the requirement of activation energy, and the quantum yield should vary linearly with nitro concentration. It was observed that if  $E_{1/4} > -0.78$  V, the quantum yield was fairly constant until about 80% of the nitro compound was reduced. If  $E_{1/4} < -0.82$  V, the quantum yield usually decreased rather rapidly as the nitro compound was reduced, and it was not feasible to carry these reductions through to completion. If  $E_{1/4}$  was in the range  $-0.80 \pm 0.02$  V, the quantum yield was roughly proportional to the concentration of the nitro compound remaining.<sup>30</sup>

Although inefficiency of follow-up reactions is probably responsible for much of the retardation of reduction of nitro compounds with  $E_{1/4} < -0.82$ , data presented in the following paper<sup>14</sup> show directly that the initial quantum yields for reduction of *p*-nitrotoluene and *m*-nitroanisole are proportional to the initial concentrations of these compounds in the neighborhood of  $5 \times 10^{-4} M$ , whereas that for *p*-nitrobenzonitrile is not.

The solid line in Figure 1 is drawn with a slope of 0.059 expected of a thermally activated one-electron reaction. Initial quantum yields for nitro compounds with  $E_{1/4} < -0.80$  are consistently greater than those predicted by the line. At least three reasons might be advanced for this. First, reaction of singlet-excited pyrochlorophyll might account for quantum yields of the order of  $10^{-3}$ . Second, mechanism B might not be completely suppressed, though there is no direct evidence for this. Third, oxidation of hydrazobenzene to azobenzene by remaining traces of oxygen might falsely enhance the apparent initial quantum yield of photoreduction of nitro compound. In a control experiment

(29) Conspicuous by their absence in Table I are the nitrophenols. In the polarogram of *p*-nitrophenol, as in that of *p*-fluoronitrobenzene, a small reversible wave ( $E^{1/2} = -0.87$  V and  $I = 1.4$ ) was followed by a larger irreversible wave ( $E^{1/2} = -1.31$  V and  $I = 4.8$ ). Although *p*-nitrophenol exists partially in the ionized form in ethanol-pyridine, the polarogram was almost unchanged by the addition of dimethylbenzylamine or acid, which according to the spectrum drove the nitrophenol into its ionized and neutral forms, respectively. A slow photoreduction of *p*-nitrophenol was sensitized by pyrochlorophyll, but it was impossible, without detailed kinetic data, to tell whether the ionized form, the un-ionized form, or both were reactive. Furthermore, there was spectral evidence for a complex between *p*-nitrophenol and hydrazobenzene and for the photo-reaction of an unknown kind with pyrochlorophyll when ascorbic acid was the reductant. Because neither the polarographic data nor the photochemical data admitted of a simple interpretation, nitrophenols were omitted from the tabulation.

(30) *p*-Fluoronitrobenzene provides an exception to this statement, as its quantum yield dropped off rather quickly. The polarogram suggests that the reduced nitro radical may be particularly resistant to disproportionation or further reduction.

**Table II:** Pyrochlorophyll-Sensitized Photoreduction of Nitro Compounds by Ascorbic Acid ( $4 \times 10^{-3} M$ ) in 70:30 Ethanol-Pyridine with 0.14 M *n*-Butylamine

No.	Compd	$10^4[\text{nitro}], M$	$\lambda, \text{nm}$	$10^{-3}\epsilon, M^{-1}$	$10^{-3}\phi_0$	$-E_{1/4}, \text{V}$
...	(Pyrochlorophyll) <sup>b</sup>	0.084	667	70	2.0	...
XIV	1-Nitronaphthalene	1.0	350	3.5	c	0.825
XI	5-Nitro-1-naphthylamine	2.0	420	2.2	2.2	0.862
XXI	<i>m</i> -Nitrodimethylaniline	2.0	408	1.13	d	0.908
...	<i>p</i> -Nitrophenol	0.5	404	21.28	1.41 <sup>e</sup>	0.91 <sup>f</sup>
XXIV	<i>p</i> -Nitroanisole	2.0	325	2.68	1.76	0.964
XXV	<i>o</i> -Nitroaniline	0.5	415	3.03	2.05	1.012
XXVI	<i>p</i> -Nitrophenylhydrazine	0.5	386	15.7	0.80	1.029
XXVIII	<i>p</i> -Nitrodimethylaniline	0.5	391	10.12	4.8	1.035
XXIX	<i>p</i> -Nitroaniline	0.5	378	16.0	1.11	1.037

<sup>a</sup> Data tabulated are the wavelength ( $\lambda$ ) at which reduction of the nitro compound was followed, its molar absorptivity ( $\epsilon$ ) at that wavelength, the initial quantum yield ( $\phi_0$ ) expressed as moles of nitro compound reduced per einstein of light absorbed by pyrochlorophyll, and the quarter-wave reduction potential of the nitro compound. <sup>b</sup> Control in the absence of a nitro compound and *n*-butylamine. <sup>c</sup> No clear spectral evidence for reduction. <sup>d</sup> Spectral changes indicated that a reaction occurred, but absorption by products at the measuring wavelength prevented determination of quantum yield. <sup>e</sup> A reversible and an irreversible reaction of pyrochlorophyll were noted. <sup>f</sup> Half-wave potential of first wave ( $I = 1.4$ ) of *p*-nitrophenol in the presence of 0.01 M dimethylbenzylamine.

with  $O_2$  (0.2 atm), hydrazobenzene was photooxidized by pyrochlorophyll with a quantum yield of 0.225.

The third possibility appears to be responsible, because when  $O_2$  was more efficiently removed by passage through the reduced viologen solution, the initial quantum yields for *p*-nitrotoluene and *m*-nitroanisole were reduced by a factor of about 2 (solid circles of Figure 1).

*Photosensitization with Chlorophyll.* We have used polarographic potentials measured in 10% aqueous ethanol-pyridine to estimate a value of  $-0.80$  V for the oxidation potential of pyrochlorophyll in anhydrous ethanol-pyridine. As a check on the validity of this estimate for chlorophyll, a series of photosensitized reductions were run with chlorophyll as the sensitizer and certain of the nitro compounds as oxidants in 63:27:10 ethanol-pyridine-water. The photoreduction of chlorophyll in the absence of an oxidant is not completely suppressed in the presence of this much water and proceeds with an initial quantum yield of about  $10^{-4}$ .

Results of this series are plotted in Figure 2. The quantum yields are uniformly higher than in Figure 1, perhaps because the follow-up reactions are more efficient in the presence of water. As with pyrochlorophyll, there appears to be a break in the trend of quantum yields in the vicinity of  $-0.8$  V, but the quantum yield during a run was found not to be so strongly dependent on nitro concentration as it was with pyrochlorophyll in the anhydrous solvent. It seems likely that mechanism B is at least partly responsible for the relatively high yields for the nitro compounds of low potential, and if that is so, the results do not contradict the estimate of  $-0.80$  V (sce) for the oxidation potential for triplet-excited chlorophyll in ethanol-pyridine.

*Photoreduction with Ascorbic Acid.* It was noted in qualitative experiments that those nitro compounds

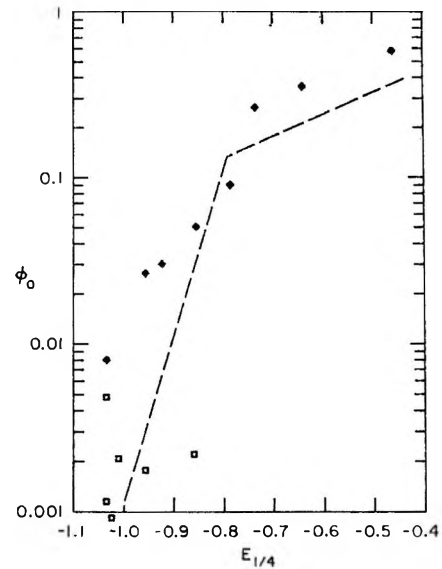


Figure 2. Initial quantum yields ( $\phi_0$ ) of sensitized photoreductions of nitro compounds *vs.* their polarographic quarter-wave reduction potentials ( $E_{1/4}$ ): ●, chlorophyll as the sensitizer, hydrazobenzene as the reductant in 63:27:10 ethanol-pyridine-water (mechanism B not completely suppressed); □, pyrochlorophyll as the sensitizer, ascorbic acid as the reductant in 7:3 ethanol-pyridine (cf. Table II). The dashed lines are the upper bounds of the quantum yields in Figure 1.

which were reduced rapidly with hydrazobenzene were reduced equally rapidly with ascorbic acid. This is in accord with our previous experience with mechanism A.<sup>1,31</sup>

Those nitro compounds which are difficult to reduce with hydrazobenzene by mechanism A should nevertheless be reducible with ascorbic acid by mechanism B.

(31) G. R. Seely, *J. Phys. Chem.*, **69**, 821 (1965).

Since azobenzene is absent, these reactions must be followed by direct observation of the fall of the absorption band of the nitro compound. The experimental conditions and results of some reductions with ascorbic acid are set out in Table II and the initial quantum yields are plotted as open squares in Figure 2.

In all cases but one there was distinct evidence of photoreduction, even for the lowest potential nitro compounds. Although the initial quantum yields were in the same range as those found with hydrazobenzene, the following points should be considered in comparing the two series. (1) The quantum yields plotted in the ascorbic acid series are for the disappearance of the nitro compound; in the hydrazobenzene series they are for the appearance of azobenzene and are therefore probably twice as large. (2) The initial concentration of the nitro compound ranged from 0.4 to 0.1 times that in the hydrazobenzene runs, the quantum yields for which are dependent on the nitro concentration. (3) The quantum yields are in the same range as that for the reduction of pyrochlorophyll by ascorbic acid in the absence of nitro compound. (4) The quantum yield was more nearly constant during runs with ascorbic acid than it was with hydrazobenzene, and the reductions more nearly approached completion. (5) Finally, there is no evident trend of quantum yield with respect to  $E_{1/2}$ . These considerations support the assignment of mechanism B as the dominant mechanism for these reductions.

It is not possible to establish the low-potential limit for sensitized reductions by mechanism B with these nitro compounds. However, it must lie below -1.05 V (sce) in ethanol-pyridine.

*Liquid-Junction Potential.* The potentials in Table I are for polarographic reduction waves in ethanol-pyridine, measured against a saturated aqueous calomel electrode. Included therein is an unknown liquid-junction potential between ethanol-pyridine and saturated KCl, which must be subtracted if the true potential is to be obtained.

The recent resurgence of interest in liquid-junction potentials is related to the opinion that they may not always be as small as previously thought.<sup>32-35</sup> It is recognized that there is no thermodynamically rigorous way to determine these potentials; however, attempts to estimate them have used complexes of metals with ligands which partially shield the metal ion from the solvent. The influence of solvent environment on oxidation and reduction of the metal is thereby minimized, and variations of the measured potentials are presumed to reflect changes in the junction potentials.

Complexes which are stable and soluble and are reversibly oxidized or reduced in a useful potential range for polarography are not plentiful. To estimate the liquid-junction potential between ethanol-pyridine and water, we chose the Cd complexes with pyridine, 2,2'-bipyridyl, and *o*-phenanthroline, which have been stud-

**Table III:** Polarographic Reduction of Cd Complexes of Pyridine, 2,2'-Bipyridyl, and *o*-Phenanthroline in Water and 63:27:10 Ethanol-Pyridine-Water

[Cd], mM	[Ligand], M	Solvent <sup>a</sup>	-E <sub>1/2</sub> , V	I <sup>b</sup>	n <sup>c</sup>
1.0	...	W	0.584	3.63	1.48
Pyridine					
0.2	2.0	W	0.660	2.37	1.95
1.0	1.0	W	0.646	2.49	2.14
1.0	2.0	W	0.660	2.38	1.95
1.0	4.0	W	0.673	1.88	1.91
2.0	2.0	W	0.660	2.43	1.95
5.0	2.0	W	0.676	2.51	1.74
0.5	3.4	EPW	0.639	2.31	1.86
1.0	3.4	EPW	0.641	2.10	1.37
1.0	3.4	EPW	0.639	2.12	1.58
1.0	3.4	EPW	0.640	2.35	1.86
2.0	3.4	EPW	0.651	2.03	1.43
2.0	3.4	EPW	0.659	1.91	1.34
5.0	3.4	EPW	0.657	1.92	1.32
2,2'-Bipyridyl					
0.1	0.01	EWB	0.698	2.49	2.18
0.2	0.01	EWB	0.712	2.46	1.98
0.5	0.01	EWB	0.710	2.53	1.96
0.5	0.01	EWB	0.701	2.44	1.94
0.5	0.01	EWB	0.734	2.42	1.18
0.5	0.01	EW	0.700	2.44	1.84
0.5	0.02	EWB	0.728	2.34	1.92
0.5	0.02	EW	0.724	2.47	1.76
0.5	0.04	EWB	0.755	2.48	1.91
0.5	0.04	EW	0.748	2.50	2.01
1.0	0.01	EWB	0.698	2.60	1.67
1.0	0.01	EWB	0.698	2.50	1.67
1.0	0.01	EWB	0.700	2.41	1.67
0.2	0.01	EPW	0.697	2.53	d
0.5	0.01	EPW	0.664	2.22	d
0.5	0.02	EPW	0.655	2.31	1.86
0.5	0.04	EPW	0.695	2.66	1.18
1.0	0.01	EPW	0.670	2.21	d
<i>o</i> -Phenanthroline					
0.5	0.005	EWB	0.797	2.08	1.71
0.5	0.005	EWB	0.810	2.23	1.89
0.5	0.01	EWB	0.830	2.32	1.48
0.5	0.005	EPW	0.755	2.12	1.59
0.5	0.04	EPW	0.798	1.96	1.60

<sup>a</sup> W, water; EW, 90% water-10% ethanol, to ensure sufficient solubility of the ligand; EWB, 90% water-10% ethanol with buffer (pH 8.5) of 0.02 M dimethylbenzylamine and 0.007 M HClO<sub>4</sub>; EPW, 63% ethanol-27% pyridine-10% water. <sup>b</sup> I =  $i_D/[Cd]^{2/3}t^{1/2}$ , where  $i_D$  is the diffusion current in microamperes, [Cd] is expressed in mmoles per liter,  $m$  and  $t$  were 1.046 mg/sec, and 5.72 sec/drop in EW and 1.049 mg/sec and 5.33 sec/drop in EPW. <sup>c</sup> The number of electrons transferred at the electrode ( $n = 0.059 \times \Delta[\log \{i_D/i\} - 1]/\Delta E$ ). <sup>d</sup> Plot of  $\log \{i_D/i\} - 1$  vs.  $E$  curved throughout.

(32) H.-M. Koepf, H. Wendt, and H. Strehlow, *Z. Elektrochem.* **64**, 483 (1960).

(33) I. V. Nelson and R. T. Iwamoto, *Anal. Chem.*, **35**, 867 (1963); F. Farha, Jr., and R. T. Iwamoto, *ibid.*, **38**, 143 (1966).

(34) I. M. Kolthoff and F. G. Thomas, *J. Phys. Chem.*, **69**, 3049 (1965).

(35) J. F. Coetzee and J. J. Campion, *J. Amer. Chem. Soc.*, **89**, 2513, 2517 (1967).

ied by Douglas, *et al.*,<sup>36</sup> and appear to satisfy the requirements moderately well. They are reduced at the dropping Hg electrode to Cd amalgam, with release of the ligand. Their half-wave potentials are not affected by pH in weakly basic solution but are affected by ligand concentration. It was expected that the use of complexes of similar bond type but of different stability would serve as a check on the reliability of the results. For the probable compositions of these complexes, see Douglas, *et al.*<sup>36</sup>

Polarographic data are recorded in Table III. In water, and water with 10% ethanol, reduction of all three complexes was reversible and required  $n = 2$  electrons, as judged by the linearity and slope of plots of  $\log [(i_D/i) - 1]$  vs.  $E$  and by the value of the diffusion-current constant. In aqueous ethanol-pyridine (EPW), none of the waves were strictly reversible throughout, but in most cases plots of  $\log [(i_D/i) - 1]$  vs.  $E$  were sufficiently linear over the first half of the wave, permitting the evaluation of  $n$ . For these also the slope corresponded approximately to a two-electron reduction. Our results in water were generally in good agreement with those by Douglas, *et al.*<sup>36</sup>

Half-wave potentials for the complexes with pyridine, 2,2'-bipyridyl, and *o*-phenanthroline were lower in water than in EPW by about 0.03, 0.07, and 0.05 V, respectively. Therefore, we estimate a value of  $0.05 \pm 0.02$  V for the water-EPW junction potential.

To convert the estimate of  $-0.80$  V (sce) for the Chl'-Chl<sup>+</sup> couple to the hydrogen scale, it is necessary

to add the potential of the sce ( $0.244$  V) and subtract the liquid-junction potential. The result is about  $-0.60$  V (nhe). Estimation of the probable error in this result is somewhat difficult because the main sources of error are more likely systematic than random. The estimate of  $-0.80$  V (sce) (Figure 1) is probably correct within  $\pm 0.02$  V. The use of  $E_{1/2}$  to estimate the potential of the first reversible step in the reduction of nitro compounds is also probably correct within  $\pm 0.02$  V. These, combined with the probable error in the liquid-junction potential, give a final estimate of  $-0.60 \pm 0.035$  V (nhe) for the Chl'-Chl<sup>+</sup> couple.

This value is compatible with Black's observation that bipyridyl salts with  $E_{1/2} > -0.52$  V are reduced by illuminated chloroplasts,<sup>10</sup> especially when it is considered that the oxidants probably do not react with Chl' directly but with some substance reduced by it. On the basis of the present data, we cannot, of course, exclude the participation of singlet chlorophyll or mechanism B in photosynthesis, but we can conclude that the action of triplet chlorophyll by mechanism A is sufficient to account for observed physiological potentials.

*Acknowledgments.* This research was supported in part by National Science Foundation Grant No. GB-5098. The expert technical assistance of Mr. Thomas Meyer is appreciated.

(36) B. E. Douglas, H. A. Laitinen, and J. C. Bailar, Jr., *J. Amer. Chem. Soc.*, **72**, 2484 (1950).

# The Quenching of Pyrochlorophyll Fluorescence by Nitro Compounds

by G. R. Seely

*Contribution No. 325 from the Charles F. Kettering Research Laboratory, Yellow Springs, Ohio 45387  
(Received July 8, 1968)*

We have examined the quenching of pyrochlorophyll fluorescence by a series of substituted nitrobenzenes in ethanol-pyridine solution and the effect of fluorescence quenching on the quantum yield of sensitized photoreduction of three of the nitro compounds by hydrazobenzene. All nitro compounds examined are at least moderately good quenchers of fluorescence. There is a good correlation between the Stern-Volmer quenching constants and the polarographic quarter-wave reduction potentials of the nitro compounds. The variation of quantum yield of photoreduction with concentration of nitro compound is interpreted as evidence of electron transfer in the quenching process, as proposed by Dilung and Chernyuk. However, the efficiency of photoreduction sensitized by the singlet excited state of pyrochlorophyll is less than that sensitized by the triplet excited state. This can be explained as a consequence of the spin multiplicity of the radical-ion pair created by the electron transfer.

## Introduction

In the preceding paper, the ability of pyrochlorophyll in its triplet excited state to sensitize the photoreduction of aromatic nitro compounds was correlated with the reducibility of the latter as evaluated by the polarographic quarter-wave potential.<sup>1</sup> The intent of that work was to obtain quantitative information which might help in understanding the energetics of the photochemical steps of photosynthesis. Since it is quite possible that the singlet excited state of chlorophyll is the one that is photochemically active in nature, it is desirable to have quantitative information on its reactivity also.

The investigation of the reactivity of the excited singlet state of a pigment molecule is not always simple or straightforward. If the triplet excited state also takes part in the reaction under study, any reaction of the singlet state is superimposed on the often much larger reaction of the triplet state. Because the lifetime of the singlet is very short, the other reagent must be present in such large concentration (*ca.*  $10^{-2} M$ ) that even sluggish reactions of the triplet state become important.

An obvious approach to the problem of reactivity of singlet excited pyrochlorophyll with nitro compounds (by which is implied its ability to transfer an electron) is through study of the quenching of fluorescence. Electron transfer as a mechanism of fluorescence quenching has been under consideration for some time.<sup>2,3</sup> Recently a more detailed mechanism has been proposed, involving the reversible formation of a charge-transfer complex between the photoexcited molecule and the quencher,<sup>4-6</sup> which may degrade by electron transfer to produce an ion pair<sup>4,7</sup> or by intersystem crossing to the triplet state of the fluorescer.<sup>8,9</sup> An alternative quenching mechanism is through intersystem crossing enhanced by the presence of a heavy atom in or near the fluorescing molecule.<sup>10,11</sup> In the case of

chlorophyll, the charge-transfer mechanism is supported by the greater quenching efficacy of oxidants than of reductants.<sup>12</sup> However, to understand the photochemistry of the singlet excited state, we must know whether the charge-transfer complex (which may have only a transitory existence) decays by electron transfer, intersystem crossing, or internal conversion.

The work to be reported consists of two parts: (1) comparison of Stern-Volmer quenching constants for a series of nitro compounds with their polarographic quarter-wave potentials, to determine if there is a potential below which quenching effectively ceases, and (2) measurement of the quantum yield of photoreduction as a function of nitro compound concentration for a few selected compounds. It will be concluded that the evidence favors electron transfer as the mechanism for quenching.

## Experimental Section

The materials were the same as those in the preceding paper. The polarographic and photochemical procedure are also described there. However, the nitrogen with which the solutions for photoreduction

- (1) G. R. Seely, *J. Phys. Chem.*, **73**, 117 (1969).
- (2) J. Weiss and H. Fischgold, *Z. Phys. Chem.*, **B32**, 135 (1936).
- (3) G. K. Rollefson and R. W. Stoughton, *J. Amer. Chem. Soc.*, **63**, 1517 (1941).
- (4) H. Leonhardt and A. Weller, *Ber. Bunsenges. Phys. Chem.*, **67**, 791 (1963).
- (5) T. Miwa and M. Koizumi, *Bull. Chem. Soc. Jap.*, **38**, 529 (1965).
- (6) W. R. Ware and H. P. Richter, *J. Chem. Phys.*, **48**, 1595 (1968).
- (7) W. C. Needler, *ibid.*, **42**, 2972 (1965).
- (8) G. H. Schenk and N. Radke, *Anal. Chem.*, **37**, 910 (1965).
- (9) P. J. McCartin, *J. Amer. Chem. Soc.*, **85**, 2021 (1963).
- (10) M. Kash, *J. Chem. Phys.*, **20**, 71 (1952).
- (11) T. Medinger and F. Wilkinson, *Trans. Faraday Soc.*, **61**, 620 (1965).
- (12) R. Livingston and C.-L. Ke, *J. Amer. Chem. Soc.*, **72**, 909 (1950).

were flushed was passed through reduced methyl viologen solutions to remove the last vestige of oxygen.

Fluorescence was excited with the 6438-Å line of an Osram Cd lamp, isolated by a Baird-Atomic 640-nm interference filter. Fluorescence was detected by an EMI 9558B photomultiplier, after passage through a Corning 2030 red filter, at an angle of 45° from incidence normal to the front face of the sample cuvette (5 mm thick). The output of the photomultiplier was measured by a Keithley 610B electrometer with a 10<sup>6</sup>-ohm input resistance. The relative sensitivity of the photomultiplier to light of different wavelengths was determined by the quantum-counter method with rhodamine B to 600 nm<sup>13</sup> and was extended to 700 nm with methylene blue.<sup>14</sup>

The fluorescence of pyrochlorophyll is strongly reabsorbed, even in dilute solution, and correction must be made for this and the consequent secondary fluorescence if an accurate measure of quenching is to be obtained. Details of this correction will be published later; with it, the electrometer reading  $M_f$  is given by the equation

$$M_f = \frac{CI_0S_f(1 - 10^{-\rho})(1 - R)\phi_f}{4n_f\sqrt{2n_f^2 - 1}(1 - \phi_f R)} \quad (1)$$

The instrument constant  $C$ , which takes into account the solid angle about the cuvette intercepted by the photomultiplier and reflection losses, was evaluated<sup>15</sup> from the intensity,  $M_s$ , of light scattered from a solution of colloidal silica (Ludox, a gift from the E. I. du Pont de Nemours and Co.)

$$M_s = \frac{3CI_0S_s(1 - 10^{-\tau_s})(1 + \cos^2 \theta_s)}{16n_s\sqrt{2n_s^2 - 1}} \quad (2)$$

In these equations  $I_0$  is the intensity of the exciting light;  $S_f$  and  $S_s$  are the relative quantum sensitivities of the photomultiplier to fluorescent and scattered incident light, respectively;  $\tau_s$  is the turbidity of the scattering solution; and  $\rho$  is the absorbance of the pyrochlorophyll solution at 644 nm. The expressions containing the refractive indices  $n_f$  and  $n_s$  of the fluorescence and scattering solutions, respectively, correct for refraction according to Gilmore, *et al.*<sup>16</sup> The angle of scattering,  $\theta_s$ , satisfies the law of sines ( $\sin 45^\circ / \sin \theta_s = n_s$ ). The quantum yield of fluorescence ( $\phi_f$ ) and the fraction of fluorescent light reabsorbed ( $R$ ) were determined from plots of the apparent quantum yield of fluorescence against pyrochlorophyll concentration, in the absence of quencher. The value of  $\phi_f$  was 0.423 for pyrochlorophyll in 7:3 ethanol-pyridine at 24°.

Fluorescence intensity was measured first in the absence of quencher, then after successive additions of solid nitro compound. As the concentration of pyrochlorophyll changed little during the series, the variation in  $R$  was inappreciable. After each addition, the solution was flushed with N<sub>2</sub> (Matheson Co. prepurified

grade) to eliminate quenching by O<sub>2</sub>. The intensity of exciting light, which usually decreased 2–4% during a series, was monitored with a reference cuvette containing pyrochlorophyll solution without quencher.

## Results

*Fluorescence Quenching.* All nitro compounds examined were at least moderately good quenchers. Plots of eq 3, the Stern-Volmer equation, were accu-

$$\phi_f/\phi_Q = 1 + K[Q] \quad (3)$$

rately linear, at least up to quencher concentrations sufficient to reduce the fluorescence intensity by half. In eq 3,  $\phi_f$  and  $\phi_Q$  are the quantum yields of fluorescence in the absence and in the presence, respectively, of a nitro compound having the concentration of [Q]. In some cases the plots deviated from linearity at large [Q], as was noted also by Livingston and Ke,<sup>12</sup> perhaps indicating a contribution from static quenching.

Stern-Volmer constants,  $K$ , and indications of the ranges of nitro concentration and quenching covered are listed in Table I. Values of  $K$  for nitrobenzene, *m*-dinitrobenzene, and *p*-dinitrobenzene generally agree with previously reported values for chlorophyll if allowance is made for differences in the solvent.<sup>12,17,18</sup>

There is an unexpectedly good correlation between the Stern-Volmer constants and the polarographic quarter-wave potentials,  $E_{1/4}$  (Figure 1), which we have adopted as the measure of reducibility of nitro compounds.<sup>1</sup> Indeed, the quarter-wave potential determines  $K$  within a factor of about 2. The points in Figure 1 appear to have a well-defined upper bound, approximated there by a curve which will be discussed later. There is no distinct break in the trend of the points in this plot, as there was in the plot of quantum yields in Figure 1 of the preceding paper.<sup>1</sup> The value of  $E_{1/4}$  below which  $K$  falls rapidly to zero is not apparent from the logarithmic plot; however, on a linear plot of  $K$  vs.  $E_{1/4}$ ,  $K$  extrapolates to zero at approximately –1.08 V.

(13) W. H. Melhuish, *N. Z. J. Sci. Tech.*, **37.2B**, 142 (1955).

(14) Methylene blue appears not to have been previously used as a quantum-counter substance. An  $8.3 \times 10^{-4} M$  solution in ethylene glycol was irradiated with incandescent lamp light through interference filters covering the range 550–700 nm. Fluorescent light at a 45° angle from the front face of the cuvette was admitted to the photomultiplier through a Corning 2600 filter, which blocked the more strongly reabsorbed part of the fluorescence. These measurements were compared with direct measurements of light scattered from a solution of filtered Ludox of known turbidity, under the same conditions of excitation. The calibration with methylene blue was then matched to that with rhodamine B in the region of overlapping data (550–600 nm). We believe that the photomultiplier calibration thus extended to 700 nm is sufficiently accurate for our purposes; however, we have not tested the suitability of methylene blue as a quantum counter dye over an extended wavelength range.

(15) G. Weber and F. W. J. Teale, *Trans. Faraday Soc.*, **53**, 646 (1957).

(16) E. H. Gilmore, G. E. Gibson, and D. S. McClure, *J. Chem. Phys.*, **23**, 399 (1955).

(17) V. B. Evstigneev, V. A. Gavrilova, and A. A. Krasnovskii, *Dokl. Akad. Nauk SSSR*, **74**, 315 (1950).

(18) I. I. Dilung and I. N. Chernyuk, *ibid.*, **140**, 162 (1961); *Zh. Fiz. Khim.*, **37**, 1100 (1963).

**Table I:** Stern-Volmer Constants ( $K$ ) and Other Data on the Quenching of Fluorescence of Pyrochlorophyll by Nitro Compounds in 7:3 Ethanol-Pyridine at 24°

Compd	$-E_{1/4}^a$ V	$10^2 [Q]_{\max}^b$ M	$(\phi_Q/\phi_f)_{\min}$	$K$ , $M^{-1}$
p-Dinitrobenzene	0.458	2.04	0.342	86
p-Nitrobenzaldehyde	0.626	8.57	0.263	32.7
p-Nitrobenzonitrile	0.640	2.89	0.393	50.0
m-Dinitrobenzene	0.661	2.52	0.394	61.7
Methyl p-nitrobenzoate	0.694	3.16	0.392	47.2
m-Nitrobenzonitrile	0.735	3.28	0.420	42.9
p-Nitrobenzenesulfon- amide	0.743	3.54	0.503	28.7
m-Nitrobenzaldehyde	0.788	6.62	0.387	22.3
p-Nitrobenzoate	0.790	6.02	0.446	23.1
m-Nitroacetophenone	0.795	3.50	0.470	30.4
Methyl m-nitrobenzoate	0.811	3.48	0.448	33.2
p-Nitrochlorobenzene	0.822	5.11	0.372	31.1
p-Nitrobiphenyl	0.835	4.05	0.457	29.3
m-Nitroanisole	0.856	5.62	0.465	21.2
Nitrobenzene	0.881	8.00	0.367	22.0
m-Nitrotoluene	0.895	6.00	0.468	20.8
m-Nitroaniline	0.906	14.04	0.453	9.0
m-Nitrodimethylaniline	0.908	7.20	0.499	14.8
p-Nitroacetanilide	0.924	7.44	0.498	13.4
p-Nitrotoluene	0.930	6.41	0.492	16.7
p-Nitroanisole	0.957	10.29	0.469	10.9
p-Nitrophenylhydrazine	1.029	19.60	0.508	4.9
p-Nitrodimethylaniline	1.035	6.04	0.761	6.2
p-Nitroaniline	1.037	32.23	0.554	2.74

<sup>a</sup> Polarographic quarter-wave potential from Table I of preceding article.<sup>1</sup> <sup>b</sup> An indication of the range over which data were taken is given by the maximum value of the concentration of nitro compound used and the extent of reduction of fluorescence ( $\phi_Q/\phi_f$ )<sub>min</sub> at that concentration.

The theoretical maximum value of the Stern-Volmer quenching constant is the product of the actual lifetime,  $\tau$ , of the excited state and the diffusion-limited bimolecular rate constant  $k_Q^{\max}$ , calculated according to Osborne and Porter<sup>19</sup> by eq 4 in which  $R$  is the gas con-

$$k_Q^{\max} = 8RT/2000\eta \quad (4)$$

stant,  $T$  is the absolute temperature, and  $\eta$  is the absolute viscosity. From the measured value of the kinematic viscosity (0.918 cSt), the estimated density (0.846 g/ml), the natural lifetime of pyrochlorophyll fluorescence ( $1.5 \times 10^{-8}$  sec),<sup>20</sup> and the quantum yield (8.423), the maximum value of  $K$  at 25° is 81  $M^{-1}$ , in good agreement with the observed value of 86  $M^{-1}$  for *p*-dinitrobenzene. The lower values for other nitro compounds imply that the fraction of collisions that are effective in quenching the fluorescence is closely correlated with the reducibility of the nitro compound.

There is no influence of the position of a substituent (*meta* or *para*) on the value of the quenching constant, apart from that expressed through the quarter-wave potential.<sup>21</sup>

**Effect of Quenching on Photoreduction.** Correlation of the ability of a nitro compound to quench fluorescence

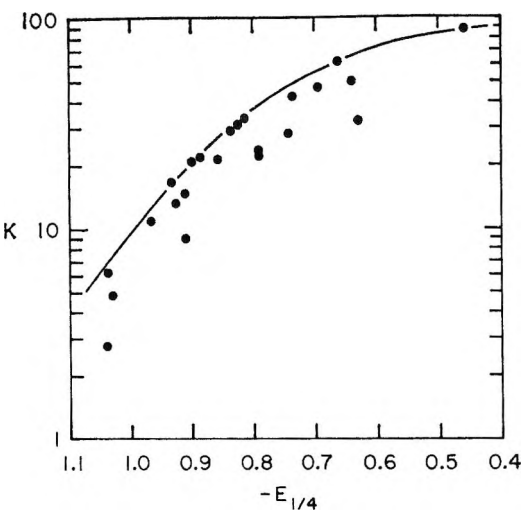
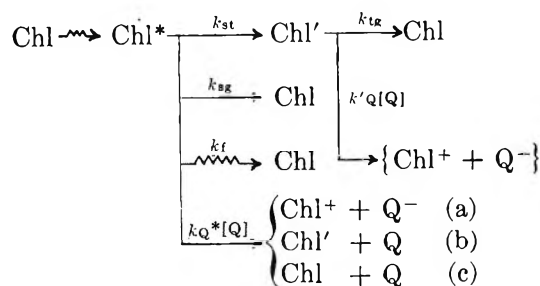


Figure 1. The plot of Stern-Volmer constants,  $K$ , for the quenching of pyrochlorophyll fluorescence in 7:3 ethanol-pyridine by substituted nitrobenzenes against their polarographic quarter-wave reduction potentials,  $E_{1/4}$  (data of Table I).

with its ability to be reduced does not necessarily mean that electron transfer actually occurs during the quenching process. A similar correlation might be expected with the stability of a transitory charge-transfer complex, which might then decay in a number of ways. The alternatives which we consider more probable for the mechanism of quenching are: (a) electron transfer from the singlet excited chlorophyll to the quencher, (b) induced intersystem crossing to the triplet excited state of the sensitizer, and (c) induced internal conversion to the ground state. The relevant processes are summarized and their rate constants defined in the diagram below, where wavy arrows indicate absorption or emission of light.



The quantum yield of fluorescence is given by

$$\phi_Q = k_f / (k_{st} + k_{sg} + k_f + k_Q^*[Q]) \quad (5)$$

or with the introduction of the singlet-state lifetime  $\tau = (k_{st} + k_{sg} + k_f)^{-1}$ , by the equation

(19) A. D. Osborne and G. Porter, *Proc. Roy. Soc., A284*, 9 (1965).

(20) E. Rabinowitch, *J. Phys. Chem.*, 61, 870 (1957).

(21) Those derivatives which have relatively low values of  $K$  (e.g., aldehydes and amines) also happen to be those which are good receivers for hydrogen-bond formation with ethanol of the solvent. We offer no explanation for this observation.

$$\phi_Q = \tau k_f / (1 + \tau k_Q^* [Q]) = \phi_f / (1 + K[Q]) \quad (6)$$

The products of quenching by alternative a are Chl<sup>+</sup> and Q<sup>-</sup>, and the quantum yield  $\phi = \phi_a$  for photosensitized reduction in the presence of hydrazobenzene is given by eq 7, in which  $\beta^*$  and  $\beta'$  are the numbers of molecules of azobenzene produced for each electron transferred from Chl\* and Chl' to the nitro compound.

$$\phi_a = \tau(\phi_Q/\phi_f)[\beta^*k_Q^*[Q] + \beta'k_{st}k_Q'[Q]/(k_{tg} + k_Q'[Q])] \quad (7)$$

Similarly, with alternatives b and c, the quantum yields  $\phi = \phi_b$  and  $\phi_c$  are given, respectively, by

$$\phi_b = \tau(\phi_Q/\phi_f)\beta'k_Q'[Q](k_{st} + k_Q^*[Q])/[(k_{tg} + k_Q'[Q])] \quad (8)$$

$$\phi_c = \tau(\phi_Q/\phi_f)\beta'k_{st}k_Q'[Q]/(k_{tg} + k_Q'[Q]) \quad (9)$$

If the triplet-state reaction is saturated, i.e., if  $k_Q'[Q] \gg k_{tg}$ , then according to mechanism b the quantum yield must increase as [Q] increases, and according to mechanism c the quantum yield must decrease in the ratio  $\phi_Q/\phi_f$ , but according to mechanism a the quantum yield increases only if  $\beta^* > \beta'k_{st}\tau$ . A plot of  $\phi (\phi_f/\phi_Q)$  against [Q] is linear in all three cases, with an intercept  $\tau\beta'k_{st}$  and slopes  $K\beta^*$  (a),  $K\beta'$  (b), and 0 (c).

The effect of concentration on the quantum yield of photosensitized reduction was tested with three nitro compounds: *p*-nitrobenzonitrile, which is easily reduced, and two compounds much harder to reduce yet moderately good quenchers, *m*-nitroanisole and *p*-nitrotoluene. Initial quantum yields for photoreduction of these compounds by hydrazobenzene, sensitized by pyrochlorophyll, are plotted against the initial concentration of nitro compound in Figures 2–4. For all three compounds, once the reaction of the triplet-state pyrochlorophyll is saturated, the quantum yield either remains nearly constant or declines somewhat as fluorescence is quenched.

This result is consistent with quenching mechanism a, but not with mechanisms b or c. Plots of  $\phi (\phi_f/\phi_Q)$  approach linearity at the higher quencher concentrations. Interpreted by mechanism a, the slopes of these plots together with the known values of the Stern–Volmer constants yield the values 0.074, 0.030, and 0.015 for  $\beta^*$  for *p*-nitrobenzonitrile, *m*-nitroanisole, and *p*-nitrotoluene. From the intercepts, the corresponding values of  $\tau\beta'k_{st}$  are 0.172, 0.036, and 0.030. Since  $\tau k_{st} < 1 - \phi_f = 0.577$ ,  $\beta' > 0.30$ , 0.062, and 0.052 for the three compounds. Finally, the values of  $\beta^*/\beta'$  are less than but proportional to 0.25, 0.48, and 0.29.

These results could also be explained as a fortuitous combination of mechanisms b and c. This would require that the apportionment of quenching between mechanisms b and c be similar for three nitro compounds of quite different reducibility. It seems simpler to assume that electron transfer is the dominant quench-

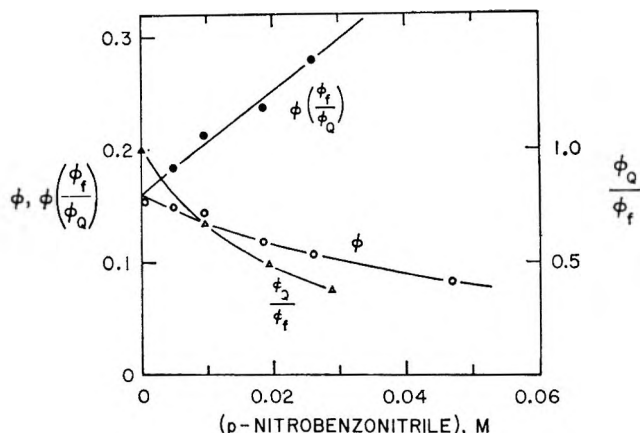


Figure 2. The quantum yield,  $\phi$ , for the pyrochlorophyll-sensitized photoreduction of *p*-nitrobenzonitrile by hydrazobenzene ( $3.7 \times 10^{-3} M$ ) in 7:3 ethanol–pyridine solution, the relative fluorescence yield  $\phi_Q/\phi_f$ , and their quotient as functions of *p*-nitrobenzonitrile concentration.

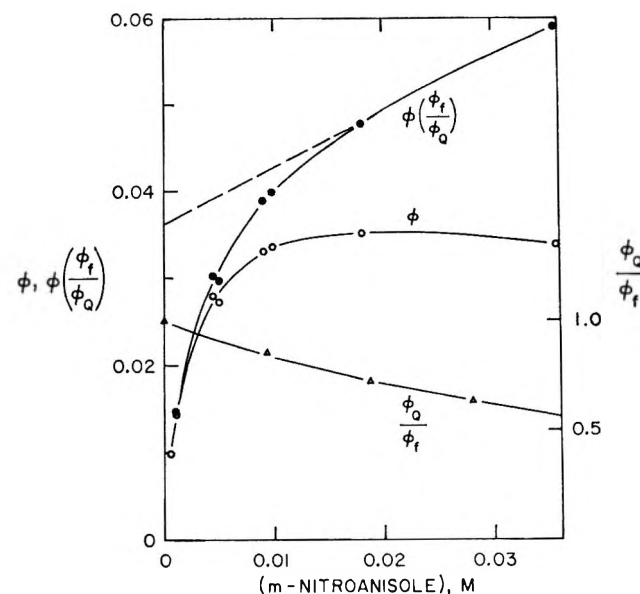


Figure 3. The quantum yield  $\phi$  for the pyrochlorophyll-sensitized photoreduction of *m*-nitroanisole by hydrazobenzene in 7:3 ethanol–pyridine solution, the relative fluorescence yield  $\phi_Q/\phi_f$ , and their quotient as functions of *m*-nitroanisole concentration.

ing mechanism, but that the photochemical efficiency ( $\beta^*$ ) of this reaction is less than that ( $\beta'$ ) from the triplet state.

## Discussion

The trend of the points in Figure 1 indicates that some factor other than an activation energy is limiting the probability of quenching upon an encounter of the singlet-excited pyrochlorophyll molecule with a molecule of nitro compound. The bounding curve shown in the figure has the form of eq 10, in which the parameters have the values  $K_{\max} = 100 M^{-1}$ ,  $E_0 = -0.74 V$ ,

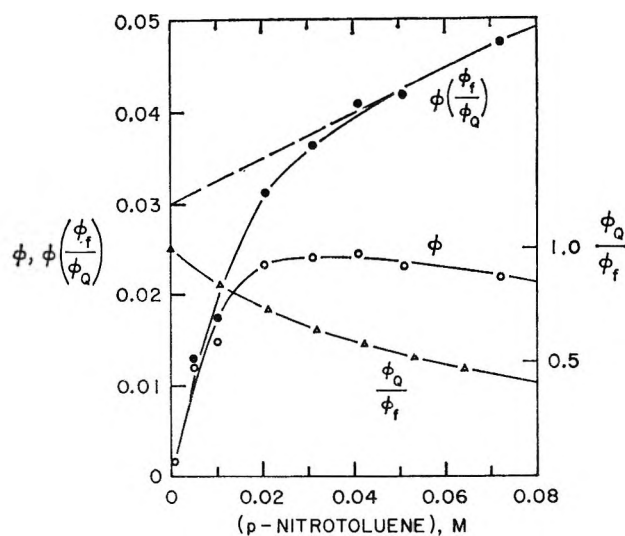


Figure 4. The quantum yield  $\phi$  for the pyrochlorophyll-sensitized photoreduction of *p*-nitrotoluene by hydrazobenzene in 7:3 ethanol-pyridine solution, the relative fluorescence yield  $\phi_Q/\phi_f$ , and their quotient as functions of *p*-nitrotoluene concentration.

and  $\sigma = 0.20$  V, with uncertainties of about 5, 5, and 10%, respectively.

$$K(E_{1/2})/K_{\max} = (1/\sigma\sqrt{2\pi}) \int_{E_0}^{\infty} e^{-(E-E_{1/2})^2/2\sigma^2} dE \quad (10)$$

Equation 10 follows if it is supposed that the fluorescer and the quencher together must have at least as much energy as the pair of ions that would be formed, for quenching by electron transfer to occur. The energy possessed by the fluorescer-quencher pair in the solvent environment is assumed to be normally distributed. The minimum energy required for quenching, and the most probable energy of the pair, are assumed to be linearly related to the potentials  $E_0$  and  $E_{1/2}$ , respectively. The value of  $\sigma$  corresponds to an energy of 4.6 kcal, which is considerably larger than  $RT$  at 25°.

Quenching by electron transfer in this case involves creation of an ion pair in a dielectric medium. At equilibrium, the ion pair would be considerably stabilized by polarization of the dielectric. However, equilibrium does not exist at the instant of electron transfer, and the orientations of the nearby solvent molecules may be regarded as randomly distributed with respect to the virtual ion pair. The distribution of energies of interaction of the ion pair with randomly oriented solvent molecules would be of the right order of magnitude to account for the value of  $\sigma$  in eq 10.

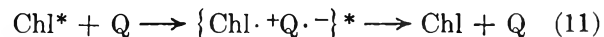
Another way of accounting for the energy distribution would be to assume that electron transfer may take place only on collision at certain mutual orientations. The number of such orientations would then be nor-

mally distributed about  $E_c$ . Still another way might relate the rate of electron transfer to the stability of the postulated intermediate charge-transfer complex,<sup>4</sup> though the basis for the normal distribution is not so evident.

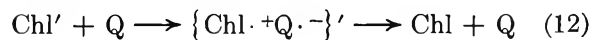
None of these explanations can be established from present data. The reported dependence of the quenching constants for nitrobenzene and *m*-dinitrobenzene on solvent suggests the first.<sup>17</sup>

The electron-transfer mechanism for quenching of fluorescence of chlorophyll and its derivatives was proposed because the ability of a compound to quench was correlated with its ability to oxidize.<sup>18</sup> The stimulating effect of certain amines on the quenching of chlorophyll fluorescence by nitro compounds has also been offered as evidence.<sup>22</sup> The effect of fluorescence quenching on the quantum yield for sensitized reduction of nitro compounds is also best interpreted, in our opinion, as evidence for the electron-transfer mechanism.

The discovery that the efficiency of photoreduction sensitized by singlet-excited pyrochlorophyll was less than that sensitized by triplet-excited chlorophyll ( $\beta^* < \beta$ ) was most unexpected. There is, however, a simple explanation for this, based on the magnetic properties of the excited states. Electron transfer from the excited singlet state produces a radical-ion pair nominally in a singlet state; back-transfer to the ground state is spin allowed (eq 11). The radical-ion pair produced by electron transfer from the triplet



state remains nominally in a triplet state, and back-transfer to the singlet ground state is spin forbidden (eq 12). There is a greater probability that the



latter ion pair will dissociate into free ions, which may then undergo the follow-up reactions of photoreduction.

The participation of the singlet excited state of chlorophyll in the primary acts of photosynthesis is, of course, neither proved nor disproved by the present results. However, since reaction of the singlet state is less efficient than reaction of the triplet state, whether through failure or reversal of electron transfer, there is not the advantage of efficiency which might have been expected from its higher energy.

*Acknowledgments.* This research was supported in part by the National Science Foundation under Grant No. GB-5098. The able technical assistance of Mr. Thomas Meyer is also appreciated.

(22) I. N. Chernyuk and I. I. Dilung, *Dokl. Akad. Nauk SSSR*, **156**, 149 (1964).

## Relation of the Catalytic Activity of MgO to Its Electron Energy States

by C. G. Harkins, W. W. Shang, and T. W. Leland

*Department of Chemical Engineering, Rice University, Houston, Texas 77001 (Received July 17, 1968)*

Catalytic activity of magnesium oxide powder for the hydrogen-deuterium exchange reaction has been studied as a function of surface irradiation with controlled frequencies of ultraviolet radiation from a monochromator. A succession of ultraviolet energies from 3 to 7 eV was applied to the surface and the relative enhancement of the first-order rate constant produced at saturation for each frequency was plotted against the ultraviolet energy. The relative enhancement of the rate constant shows well-defined peaks at 5.7, 4.9, and 4.0 eV. By comparison with work of other investigators on optical absorption, photoconductivity, and epr studies on MgO irradiated with ultraviolet, it is possible to state quantitatively the energy of the electronic transitions affecting the catalyst and, in some cases, to identify the physical nature of the excitation. This technique constitutes reaction rate spectroscopy and should be useful in studying electronic factors in other insulator and semiconductor catalytic surfaces.

### I. Introduction

*Electronic Factors in Catalysis.* The importance of electronic factors in metallic and semiconductor catalysts has traditionally been studied by alloying or impurity-doping techniques. Detailed discussions of the experimental procedures and theoretical ideas are given by Bond<sup>1</sup> and Vol'kenshtein.<sup>2</sup> The role of electronic factors in semiconductor and insulator catalysts can also be studied effectively by exposing a catalyst surface to photon irradiation at frequencies corresponding to transitions between specific electron states in the surface region. In insulators and semiconductors these transitions usually lie in the visible and ultraviolet range (1–7 eV). The photons in this energy range are energetic enough to shift electrons and holes but not to displace atoms. Consequently, surface areas and total ionic vacancy concentrations do not change upon irradiation, and the variation of catalytic activity with electronic energy transitions may be determined on a single sample.

This paper presents several techniques using ultraviolet irradiation to obtain new information on the electronic excitations which influence catalysis. These techniques may be summarized as follows.

1. Ultraviolet irradiation is used at a series of frequencies, determining the maximum rate enhancement at each frequency. With annealing between each exposure to remove the radiation-induced enhancement, the relative change in rate constant may be plotted against the incident frequency to provide a reaction rate spectrum. This furnishes a graphic representation of the energy transitions most important to the catalytic action.

2. Irradiation at one fixed frequency is used as a sensitizing pretreatment followed without annealing by exposure to a second frequency. The relative increase in rate constants by this two-frequency irradiation is compared with the increase which occurs when the

initial sensitizing irradiation is omitted. Such a comparison can give information on the necessity for preliminary excitation steps which must occur before a catalytically important excitation can take place.

3. The effect of irradiation on the exchange rate of a single isotopic reactant with either natural or artificially induced surface impurities is studied. Irradiation-induced exchange at concentrations which must be measured mass spectrometrically can give important evidence concerning the nature of active sites on the surface.

Magnesium oxide is, in many ways, ideal for studies of this nature. It is a wide band gap insulator in which electron energy states above the valence band are sparsely populated. Consequently, a large percentage change in the concentration of electrons occupying the higher energy states can be induced by exposure to relatively low irradiation intensities. It also effectively catalyzes the relatively simple H<sub>2</sub>-D<sub>2</sub> exchange reaction which is convenient for study. It is important also that for magnesium oxide there exists an extensive literature regarding photoconductivity,<sup>3–5</sup> intrinsic optical absorption bands,<sup>6–9</sup> impurity optical absorption bands,<sup>4,10–15</sup> and esr studies.<sup>16–20</sup> This information,

- (1) G. C. Bond, "Catalysis by Metals," Academic Press, New York, N. Y., 1964.
- (2) F. F. Vol'kenshtein, "The Electronic Theory of Catalysis on Semiconductors," The Macmillan Co., New York, N. Y., 1963.
- (3) H. R. Day, *Phys. Rev.*, **91**, 822 (1953).
- (4) W. T. Peria, *ibid.*, **112**, 423 (1958).
- (5) E. Yamaka, *ibid.*, **96**, 293 (1954).
- (6) P. D. Johnson, *ibid.*, **94**, 845 (1954).
- (7) J. R. Nelson, *ibid.*, **99**, 1902 (1955).
- (8) M. L. Cohen, P. J. Lin, D. M. Roessler, and W. C. Walker, *ibid.*, **155**, 992 (1967).
- (9) D. M. Roessler and W. C. Walker, *ibid.*, **159**, 733 (1967).
- (10) F. P. Clarke, *Phil. Mag.*, **2**, 607 (1957).
- (11) R. W. Soshea, A. J. Dekker, and J. P. Sturtz, *J. Phys. Chem. Solids*, **5**, 23 (1958).
- (12) W. Low and M. Weger, *Phys. Rev.*, **118**, 1130 (1960).

combined with observations of the catalytic effect of irradiating at specific ultraviolet energies, can furnish some knowledge of the specific nature of the electronic transitions important in catalysis in addition to an indication of their magnitude.

Significant information is also obtained by extending the irradiation studies to include doped magnesium oxide, such as the work on cation-doped samples by Shang<sup>21</sup> and doping with adsorbed water by Tagawa.<sup>22</sup> These techniques should be important in studying other insulator and semiconductor catalysts.

*The Hydrogen-Deuterium Exchange on MgO.* The catalytic activity of magnesium oxide for the hydrogen-deuterium exchange and the effect of ultraviolet radiation on this system have been discussed previously by Lunsford and Leland.<sup>23,24</sup> The results of that study and the present work show clearly that two distinct mechanisms are involved in the exchange. Catalytic activity by one mechanism (mechanism I) is the result entirely of what is referred to in this paper as "strong" heat treatment which consists of preheating under vacuum for 2 hr at 500° or higher. Mechanism I activity is not influenced in any way by ultraviolet radiation.

A second mechanism (mechanism II) is initiated by a procedure defined here as "moderate" heat treatment. This involves heating under vacuum for about 2 hr at temperatures around 300°. The activity of catalysts with this pretreatment is enhanced by ultraviolet radiation, in some cases to activities greater than produced by mechanism I. Such ultraviolet enhancement in mechanism II catalysts is reversible in that it can be entirely removed by gentle annealing under vacuum at temperatures below 300° and then restored by repeated irradiation. The ultraviolet sensitivity is strongly dependent on both the temperature and time of the pretreatment under vacuum. The degree of enhancement exhibits a maximum as the time is varied at a fixed temperature. An Arrhenius plot<sup>23</sup> of the ultraviolet-enhanced rate constant shows that only the preexponential factor is affected by the irradiation while the activation energy is not changed. The strong preheating which initiates the mechanism I activity, however, produces a large decrease in the activation energy.

Catalysts which receive no prior vacuum heat treatment show no catalytic activity at all. Lunsford,<sup>23</sup> Hindin and Weller,<sup>25</sup> and Tagawa<sup>22</sup> showed that the principal effect of the vacuum preheating is the removal of adsorbed water. Tagawa has shown that adsorbed water is definitely a poison for mechanism I, yet is required for mechanism II. The work of Tagawa showed that the effect of the ultraviolet irradiation in mechanism II is definitely not one of merely removing water from the surface. At high surface concentrations of adsorbed water, both mechanisms are poisoned completely.

The initial model<sup>23</sup> of active magnesium oxide con-

sidered the energy levels of impurity iron in the magnesium oxide matrix and implied that iron doping of the catalyst might affect the activity. The original work of Lunsford<sup>23</sup> also indicated the possibility that all electronic transitions in MgO were not of catalytic importance. Mercury arc irradiation at 3660 Å (3.39 eV) was not as effective as 2537-Å (4.9-eV) light in activating the catalyst. Later work by Lunsford,<sup>16</sup> using epr spectroscopy, correlated the photoactivation of the MgO catalyst with the photoconduction due to V<sub>1</sub> centers. A cutoff wavelength of about 3100 Å (4.0 eV) was proposed for the formation of the V<sub>1</sub> center and the photoproduced active site.

## II. Experimental Section

The principal MgO catalyst used in the present research was Lot No. 27130 of Baker Analyzed reagent grade powder with a BET surface area of 16 m<sup>2</sup>/g. Spectrochemical analysis indicated an impurity level of 110 ppm of cations of the first transition series, with iron constituting 30 ppm of this amount. The catalyst doped with iron and other cations prepared by Shang<sup>21</sup> also used the same MgO powder as starting material.

An equimolar hydrogen-deuterium reactant mixture was prepared from prepurified hydrogen (Matheson) and deuterium (Liquid Carbonic). The components were further purified by diffusion through an Englehard HPD-0-50 palladium thimble before preparation and storage of the reactant mixture. Blank runs preceding each kinetic measurement indicated a maximum initial HD concentration less than 0.5%. Deuterium alone, purified by diffusion, was also stored for surface exchange studies.

Catalyst pretreatment and activity testing were carried out in a standard glass vacuum system, pumped by a trapped mercury diffusion pump maintaining background pressures in the 10<sup>-6</sup> to 10<sup>-7</sup> torr range as indicated by an ionization gauge.

The eventual batch reactor for catalyst study con-

- (13) J. Y. Wong, *Phys. Rev.*, **168**, 337 (1968).
- (14) W. M. Armstrong, A. C. D. Chaklader, and D. G. Evans, *Trans. Brit. Ceram. Soc.*, **61**, 246 (1962).
- (15) G. H. Reiling and E. B. Hensley, *Phys. Rev.*, **112**, 1106 (1958).
- (16) J. H. Lunsford, *J. Phys. Chem.*, **68**, 2312 (1964).
- (17) J. E. Wertz, P. Auzins, J. H. E. Griffiths, and J. W. Orton, *Trans. Faraday Soc.*, **28**, 136 (1959).
- (18) J. E. Wertz, P. Auzins, J. H. E. Griffiths, and J. W. Orton, *ibid.*, **26**, 66 (1958).
- (19) J. E. Wertz, J. W. Orton, and P. Auzins, *J. Appl. Phys.*, **33**, 322 (1962).
- (20) R. L. Nelson, A. J. Tench, and B. J. Harmsworth, *Trans. Faraday Soc.*, **63**, 1427 (1967).
- (21) W. W. Shang, Ph.D. Thesis, Rice University, Houston, Texas, 1968.
- (22) H. Tagawa and T. W. Leland, to be submitted for publication.
- (23) J. Lunsford, Ph.D. Thesis, Rice University, Houston, Texas, 1961.
- (24) J. H. Lunsford and T. W. Leland, *J. Phys. Chem.*, **66**, 2591 (1962).
- (25) S. G. Hindin and S. Weller, *Advan. Catal.*, **9**, 70 (1957).

sisted of a quartz-to-Pyrex graded seal, 1 in. in diameter and about 3 in. long. Sealed to the bottom quartz end was a Supersil II window of 4.5-cm<sup>2</sup> area for transmission of ultraviolet light. The Pyrex end was mated to the vacuum system with a 24/25 high vacuum seal taper joint sealed with an oversize silicone-rubber O ring and Apiezon W wax. This latter arrangement obviated a heated greased joint in the system.

Catalysts were activated after weighing out approximately  $\frac{1}{8}$  g of MgO powder and distributing it evenly over the Supersil window at a depth of approximately 1 mm. An aluminum-block electric furnace, controlled to  $\pm 0.2^\circ$ , heated the catalyst chamber for the appropriate time-temperature-pressure regulated pretreatment cycles. For uv-sensitivity studies, the activation defined here as moderate preheating was carried out at  $292.5^\circ$  and  $5 \times 10^{-6}$  torr of pressure for 3 hr. Annealing cycles between runs were at  $290.5\text{--}291.5^\circ$  for a minimum of 0.5 hr.

For kinetic measurements, a hydrogen-deuterium sample, drawn from storage bulbs through a protective nitrogen-cooled trap, was expanded into the evacuated catalyst chamber. After suitable contact time, the mixture was expanded into a sampling system and analyzed gas chromatographically on an Fe-doped alumina column described by Moore and Ward.<sup>26</sup> The column was operated at liquid nitrogen temperatures with helium as a carrier gas. Isotopic species at the very low concentrations resulting from surface hydrogen exchange with pure D<sub>2</sub> were measured on a CEC 21-104 mass spectrometer.

The principal radiation selector was a Bausch & Lomb grating-type high-intensity monochromator continuously tunable over the 1800-4000-Å range with a band pass of 96 Å. Two light sources, the Bausch & Lomb HP-100 and SP-200 high-pressure mercury arcs, provided a uv continuum for the monochromator.

Intensity control of the monochromator output at a given frequency and band pass was provided by insertion of calibrated wire screens between the light source and the monochromator collective lens. Optical density of these screens, recorded on a Cary uv spectrophotometer, was frequency independent over the range 2000-3500 Å.

Alternate sources for irradiation at 2537 and at 3660 Å were low-pressure mercury arc lamps (Mineralite) manufactured by Ultraviolet Products Industries.

Mineralite lamps were placed directly below the reactor window. Convenient and reproducible location of the catalyst sample near the monochromator exit slit was facilitated by use of an aluminum front surface mirror which reflected the monochromator beam upward through the reactor window supporting the catalyst.

### III. Results

*Photocatalytic Frequency Dependence.* Figure 1 shows

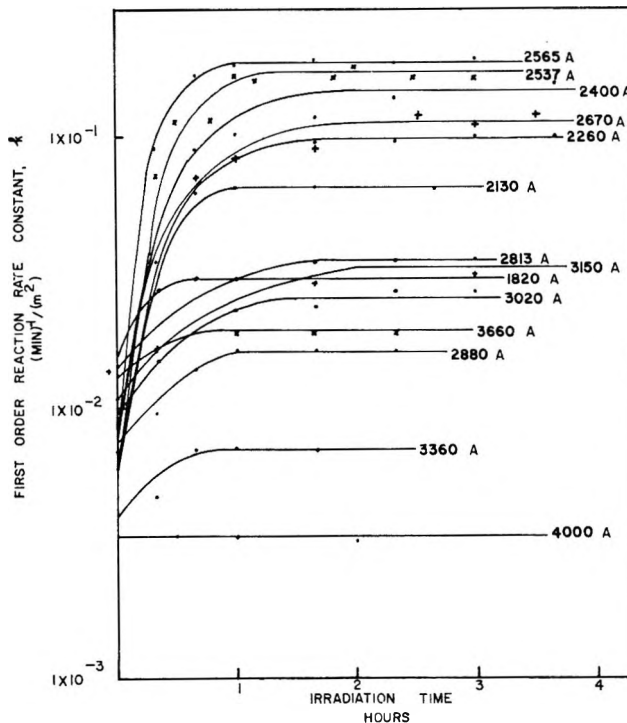


Figure 1. The effect of irradiation at varying frequencies on MgO when the reaction is measured at  $22\text{--}23^\circ$ .

a plot of the first-order reaction rate constant,  $k$ , for HD production as a function of irradiation time and radiation wavelength. This rate constant is obtained from the chromatographic data and contact time by the equations

$$k = -\frac{\ln [1 - (1 + 2K_{eq}^{-1/2})x_{HD}]}{t(1 + 2K_{eq}^{-1/2})} \quad (1)$$

$$k_{25^\circ} = -\left(\frac{0.4735}{t}\right) \ln (1 - 2.112x_{HD})$$

derived and used previously.<sup>23,27</sup> The data of Figure 1 show that the photoenhanced activity of the catalyst rises rapidly and saturates. This behavior is consistent with that reported previously by Lunsford<sup>23,24</sup> for similar samples.

*Intensity Effects.* An experimental complication inherent in the ultraviolet sources is the intensity variation with the frequency of their output. Assurance that the various saturation activity values of Figure 1 reflect entirely a dependence on frequency rather than a secondary dependence on the source intensity required a series of variable-intensity experiments. Results of such experiments at four different wavelengths are shown in Figure 2, where the pertinent time-saturation data from Figure 1, obtained using the Bausch & Lomb HP-100 lamp, are shown on the left.

(26) W. R. Moore and H. R. Ward, *J. Amer. Chem. Soc.*, **80**, 2909 (1958).

(27) W. Fulkerson and T. W. Leland, *J. Catal.*, **2**, 87 (1963).

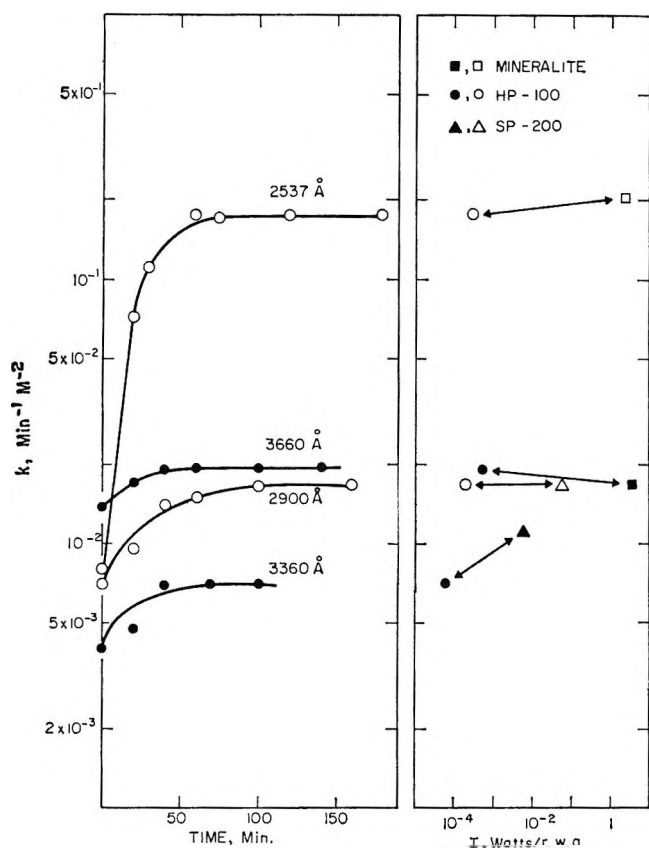


Figure 2. The reaction rate as a function of time and intensity.

These saturation values are replotted as a function of intensity on the right-hand graph of Figure 2, with saturation values obtained using more intense light sources. At 3360 Å, the wavelength of lowest intensity ( $0.8 \times 10^{-4}$  W/reactor window area) used with the Bausch & Lomb HP-100 light source, there is an apparent direct intensity effect. For the other wavelengths, 2537, 2900, and 3660 Å, where all intensities are above an apparent threshold of about  $10^{-4}$  W/reactor window area, there is no appreciable intensity effect within the limits of experimental error. Since all other data shown in Figure 1 were obtained at illumination intensities above this threshold, the catalytic saturation activity is a function only of the frequency of the incident light and is not a function of its intensity.

The time-saturating behavior of these chemical reaction rate measurements is analogous to the results of Day,<sup>3</sup> Clarke,<sup>10</sup> and Dekker<sup>11</sup> for the more physical parameters of photoconductivity and radiation-induced optical absorption, which also showed a dependence only on the frequency and not on the intensity of the incident radiation. Such behavior can be partially understood by considering a two-state model of electron excitation by photons of a constant energy  $E$ . The rate of excitation of electrons from a lower donor state to an upper trapping state is given by the equation

$$\frac{dN^*}{dt} = \sigma_E(N_0 - N^*)I - \lambda_T N^* \quad (2)$$

where  $I$  is the irradiation intensity, photons/sec cm<sup>2</sup>;  $N_0$  is the initial concentration of donors before irradiation, number/cm<sup>3</sup>;  $N^*$  is the concentration of traps containing an excited electron after irradiation time  $t$ , number/cm<sup>3</sup>;  $\sigma_E$  is the apparent cross section for electron excitation by photons of energy  $E$ , cm<sup>2</sup>; and  $\lambda_T$  is the total decay constant for return of an excited electron to its original donor state at temperature  $T$ . Ultraviolet irradiation alters only the preexponential factor of rate constant and not the apparent activation energy for the reaction;<sup>23,24</sup> therefore, it is assumed that the rate constant before radiation,  $k_0$ , is proportional to  $X_0$ , the concentration of active sites on the unirradiated sample, and that the rate constant after irradiation,  $k_t$ , is proportional to the sum of  $X_0$  plus the irradiation-induced active sites equivalent in concentration to  $N^*$ . These assumptions are expressed in the equations

$$k_0 \propto X_0 \quad (3)$$

$$k_t \propto (X_0 + N^*) \quad (4)$$

At steady-state saturation, denoted by subscript s, the derivative in eq 2 is zero and the equation may be solved directly for  $N^*_s$ . Substituting this value into eq 4 and combining with eq 3 gives

$$\frac{k_s - k_0}{k_0} = \frac{N_0}{X_0} \left[ \frac{I}{I + (\lambda_T / \sigma_E)} \right] \quad (5)$$

Equation 5 indicates that the relative enhancement of the rate constant becomes independent of the intensity under two conditions: whenever  $I$  becomes large or the ratio  $\lambda_T / \sigma_E$  becomes small. Both conditions are satisfied by nearly all the data of Figure 1. For these data the intensity  $I$  is above the measured threshold intensity ( $10^{-4}$  W/reactor window area) and the decay constant  $\lambda_T$  is very small at the reaction temperature (23°), as demonstrated by the retention of photoenhancement for several hours after irradiation is ceased.

*Reaction Rate Spectrum.* The relative enhancement of the rate constant,  $(k_s - k_0)/k_0$ , defined by eq 5, may be calculated from the data of Figure 1 and plotted as a function of the irradiation wavelength. The resultant reaction rate spectrum is shown in Figure 3. The spectrum indicates peaks of photocatalytic response at approximately 5.7, 4.9, and 4.0 eV. The position of such peaks on the wavelength axis is a quantitative measure of the excitation energies effective in producing photo-generated active centers. The intensities of these peaks are a semiquantitative indication of the equilibrium concentration of photogenerated centers,  $N^*_s$ , produced at a given irradiation-reaction temperature after the moderate preheating under vacuum.

*Iron-Doping Effects.* A series of MgO samples, doped by coprecipitation and ignition to levels of 50, 80, and 100 ppm of Fe and activated at moderate conditions, showed both an initial activity and a photosensitivity to irradiation at 4.9 eV.

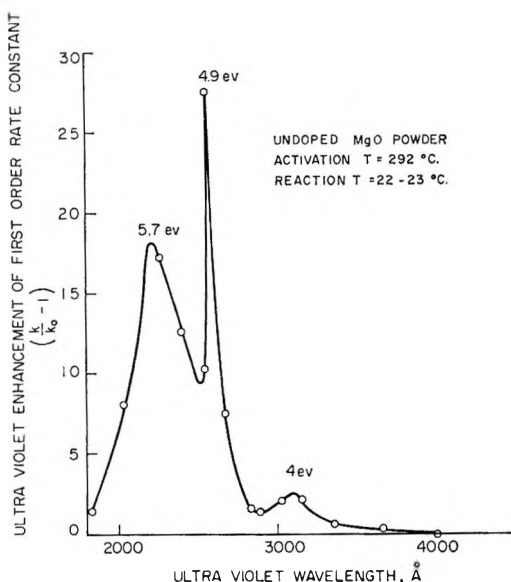


Figure 3. Reaction rate spectrum for  $H_2$ - $D_2$  exchange on  $MgO$ .

Two results are noted.

1. Relative photoenhancements,  $(k_s - k_0)/k_0$ , for the doped catalysts fell in the range 1.2–5.4, with an average of 3.3. These values are almost one order of magnitude lower than the photoresponse of the original sample.

2. No clear trend in specific activity ( $\text{min}^{-1} \text{m}^{-2}$ ) of the series could be related to the Fe concentration. These results indicate that an iron impurity alone is not the active center for catalysis.

*Experimental Evidence for a Hydrogen-Containing Active Site.* Evidence for an ultraviolet-sensitive hydrogen-containing site which takes part in the exchange reaction is given by the data shown in Figure 4. These data were obtained by placing pure deuterium in contact with a new catalyst sample not previously exposed to hydrogen, allowing exchange with the hydrogen species remaining on the catalyst from residual water not removed by moderate thermal activation. Gas-phase samples were taken periodically and analyzed by mass spectrometer for HD enrichment. After these measurements, the reactor was evacuated and the catalyst sample was irradiated under vacuum for 31 min with 4.9-eV light. On completion of this irradiation, a second  $D_2$  sample was introduced to exchange with any residual surface hydrogen. The second exchange, involving a photoactivated hydrogen-containing species, was faster than the original thermally activated exchange in the presence of a potentially larger hydrogen reservoir.

#### IV. Discussion

The analysis of the catalytic behavior of magnesium oxide powder is based upon the current knowledge of its total solid-state electronic structure. This is partially summarized in the band diagram of Figure 5 and is described in detail as follows.

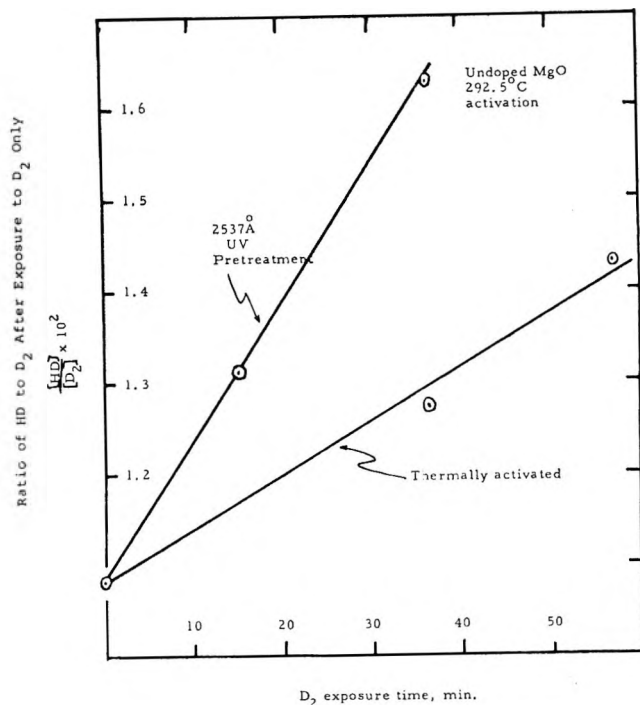


Figure 4. Hydrogen sites on a fresh catalyst surface.

*Band Structure of  $MgO$ .* 1. *Forbidden Band.* The minimum reported value for the forbidden band width in  $MgO$  is 7.4 eV.<sup>6</sup> Day<sup>3</sup> suggested a range of 10–15 eV and Nelson<sup>7</sup> proposed the value to be nearer 10 eV. Optical measurements at such energies are challenging even in simple cases, and the common existence in insulators of exciton states<sup>28</sup> further complicates the determination of the band edge absorption in  $MgO$ . The identification by Cohen<sup>8</sup> and colleagues of the 7.4–7.6-eV absorption as a temperature-dependent first exciton transition lying below the conduction band suggests that values above 8 eV are reasonable. Rössler and Walker<sup>9</sup> indicated that the optical absorption near 10.8 eV is higher exciton structure, but the fundamental width of 10.5 eV used by Sosha, Dekker, and Sturtz<sup>11</sup> appears to be a good average value and is again used in Figure 5 as the reference frame in which the combined work of many authors on electron transitions between various impurities and traps lying within the forbidden band has been placed.

2. *Substitutional Impurities in Magnesium Oxide.* Pure  $MgO$  should be transparent at photon energies below the first exciton level. However, the first row transition metals have ionic radii quite similar to that of the  $Mg^{2+}$  ion and may easily substitute for it in the lattice, producing point-defect energy levels lying in the forbidden band.

The possibility of multiple valence states for these transition metals results in several energy levels being associated with each metal impurity. Electron shifting

(28) C. Kittel, "Introduction to Solid State Physics," 3rd ed, John Wiley & Sons, Inc., New York, N. Y., 1966, p 543.

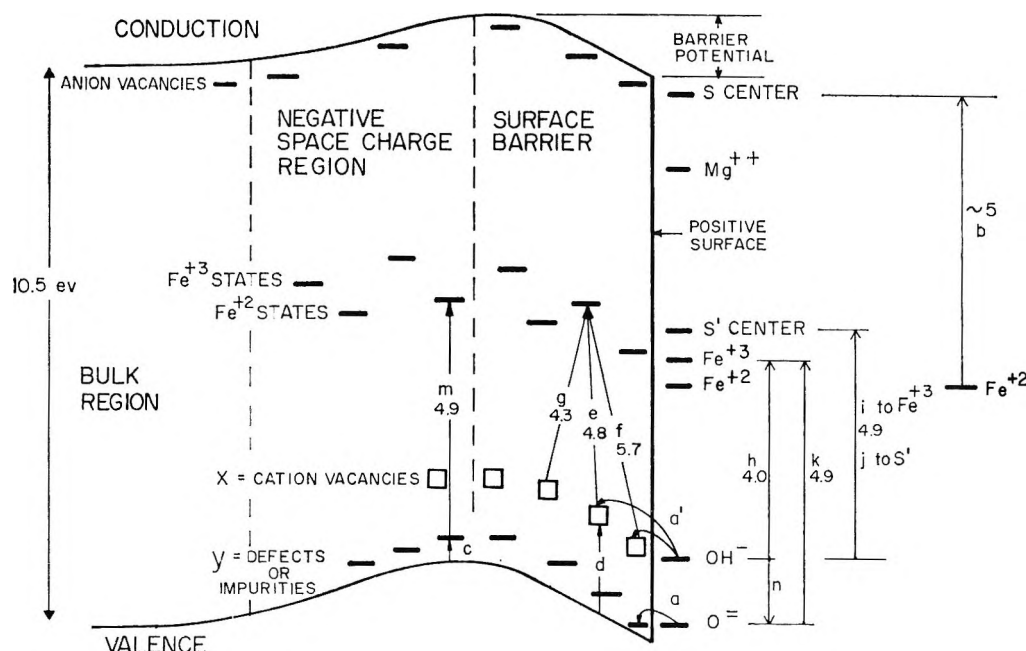


Figure 5. Surface region transitions in MgO.

and valence state change of impurity metal ions, whether induced by optical or by chemical methods, will cause complex changes in the optical and photoconductivity spectra that appear at energies lower than that of the band gap. The fact that magnesium oxide is also photocatalytically responsive to irradiation energies much below the forbidden band width implies at least an indirect effect of impurity ions in the magnesium oxide matrix.

*3. Electron Effects of Iron Impurities.* Of the substitutional impurities in MgO having a known effect on the solid-state electronic transitions, iron is one of the most prevalent and important. While the direct participation of iron alone in the catalytic activity is eliminated by the iron-doping results of this study, some of the electronic transitions associated with iron impurities have energies coinciding with those of the reaction rate spectrum of Figure 3, suggesting an indirect relationship to the catalysis.

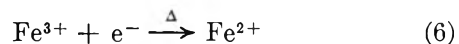
Other impurities may have similar energy transitions and may later be included with iron, but iron impurities are the best understood in the sense of relating specific electron transitions to specific optical transitions, and this relationship is valuable in understanding the observed catalytic effects.

Iron in at least three valence states has been identified by several authors. Figure 5 includes the midband  $\text{Fe}^{3+}$  and  $\text{Fe}^{2+}$  states, as suggested in the band design of Peria,<sup>29</sup> but not the high-energy  $\text{Fe}^+$  which probably lies within 2 eV of the conduction band and is normally empty. Hansler and Segelken<sup>30</sup> suggested that the  $\text{Fe}^{3+}$  state lies 5.8 eV above the valence band and  $\text{Fe}^{2+}$  lies 6.9 eV below the conduction band.

$\text{Fe}^{2+}$  should be the prevalent state on the basis of

charge considerations, but all valence states exist in a complex equilibrium which may be shifted by three forms of treatment: (1) alteration of the lattice environment near the impurity atom by severe heat treatment or heavy particle irradiation, (2) chemical treatment consisting of heating in an oxidizing or reducing atmosphere, and (3) irradiation with uv or X-ray photons.

Much of the basic information about the equilibrium of these states is due to the work of Wertz and his colleagues<sup>17-19</sup> using esr spectroscopy. Wertz<sup>18</sup> indicated that high-temperature vacuum heating ( $1200^\circ$ ) favors the shift



along with the loss of molecular oxygen from the crystal. Samples subjected to this treatment and exposed to 5.0-eV ultraviolet radiation showed an increase in  $\text{Fe}^{3+}$ , *i.e.*, a photoreversal of eq 6. Peria<sup>4</sup> correlated this uv effect with transition b in Figure 5, which represents promotion of an electron from  $\text{Fe}^{2+}$  into a trap lying close to the conduction band and conversion of the  $\text{Fe}^{2+}$  to  $\text{Fe}^{3+}$  then produces a large n-type conductivity increase which is observed experimentally.

Wertz also observed the  $\text{Fe}^+$  state which was predicted by Peria and also trapped holes following 4.9-eV irradiation of severely preheated samples.  $\text{Fe}^+$  formation is given by the equation

(29) W. T. Peria and W. D. McNeil, Wright Air Development Command Technical Report 57-760 Wright Air Force Base, Ohio, August 1958, pp 38-79.

(30) R. L. Hansler and W. G. Segelken, *J. Phys. Chem. Solids*, **13**, 124 (1960).



and is represented on the band diagram by transition m.

Further physical confirmation of the  $\text{Fe}^{2+}$  and  $\text{Fe}^{3+}$  states and the response of their equilibrium concentrations to high-temperature heat treatment in a chemically active atmosphere may be obtained from infrared spectroscopy.  $\text{Fe}^{2+}$  absorbs in the far-infrared<sup>13</sup> at  $105\text{ cm}^{-1}$  and the near-infrared<sup>12</sup> at  $10,000\text{ cm}^{-1}$ . The  $105\text{-cm}^{-1}$  line associated with  $\text{Fe}^{2+}$  decays on heat treatment in molecular oxygen and reappears upon heat treatment in molecular hydrogen.<sup>13</sup> The reverse behavior is confirmed for the  $\text{Fe}^{3+}$  infrared absorption bands.<sup>12</sup>

For samples which had been vacuum preheated at much lower temperatures at conditions close to the photosensitive catalyst activation of this study, Lunsford<sup>16</sup> found a different behavior in the  $\text{Fe}^{2+}$ - $\text{Fe}^{3+}$  shift. Irradiation at uv energies above 4.0 eV caused a decrease in  $\text{Fe}^{3+}$  concentration. In agreement with Lunsford, Wertz also found that 5.0-eV irradiation of a crystal which had not received heat treatment also produced a decrease in  $\text{Fe}^{3+}$ . This reversal in uv response is undoubtedly related to the finding of Lunsford<sup>23</sup> that vacuum heating at lower temperatures removes primarily water and not molecular oxygen. Consequently, an entirely different environment for the ion impurities exists in the moderately heat-treated samples.

The important effects of ultraviolet irradiation on iron in  $\text{MgO}$  in which  $\text{Fe}^{3+}$  has not been shifted entirely to  $\text{Fe}^{2+}$  by strong heat treatment are shown as transitions e, f, g. These transitions were postulated by Peria<sup>4</sup> from uv-absorption results. The absorption spectrum of a wide variety of  $\text{MgO}$  crystals, not severely heat treated, all show well-defined peaks at 5.7 and 4.3 eV. These two peaks disappear completely in samples which have been severely vacuum heat treated and always maintain the same intensity ratio, indicating that they are both associated with the same impurity. Soshea, Dekker, and Sturtz<sup>11</sup> have resolved these two peaks into three, with a third peak at 4.8 eV. All these transitions, shown as e, f, g in Figure 5, convert  $\text{Fe}^{3+}$  to  $\text{Fe}^{2+}$  on electron promotion and therefore can explain the decrease in  $\text{Fe}^{3+}$  observed by Lunsford following uv irradiation in this energy range on moderately heat treated  $\text{MgO}$  samples. The actual  $\text{Fe}^{2+}$ : $\text{Fe}^{3+}$  ratio which remains after irradiation at energies between 4.0 and 5.0 eV is thus the result of an equilibrium between  $\text{Fe}^{3+}$  removal by transitions e, f, g and its production by transition b and other processes. Whether this equilibrium favors  $\text{Fe}^{3+}$  or  $\text{Fe}^{2+}$  after irradiation depends on the initial iron concentration and its environment in the lattice.

The levels designated X and Y on the band diagram represent impurities, cation vacancies, or other defects which can donate to the iron impurities, by transitions such as e, f, g and m, leaving a trapped hole behind.

These trapped holes then explain the low-energy p-type photoconductivity occurring at irradiation by energies less than 2.0 eV, as observed by Day<sup>3</sup> in moderately heat treated magnesium oxide. This p-type photoconductivity is produced by transitions such as c and d. These are broad energy transitions distributed around 1.2 and 2.1 eV, respectively, which promote an electron to the low-lying X and Y states, leaving a transient hole in the valence band for photoconductivity. The broadness of the c and d transition bands indicates a rather wide distribution of the low-lying X and Y point defects.

*4. Intrinsic Defects and Surface States in Magnesium Oxide.* *a. Intrinsic Bulk Defects.* Bulk  $\text{MgO}$  will closely approach stoichiometry, yet a crystal in thermal equilibrium possesses disorder in the form of Schottky defects which consist of anion and cation vacancies in the bulk and surface phases of the crystal. Each type of intrinsic defect will have a corresponding point-defect energy level with the cation vacancy levels lying just above the valence band as hole traps and the anion vacancies lying just below the conduction band serving as electron traps.

The cation vacancy levels serve two main functions in the crystal. The first is stabilization and charge compensation for +3 valence state impurity ions. Such charge compensation by cation vacancies in magnesium oxide has been confirmed by the esr studies of Wertz, Auzins, and Orton.<sup>19</sup> Armstrong, Chaklader, and Evans<sup>14</sup> assigned optical absorption bands at 5.75 and 4.40 eV to this vacancy-stabilized  $\text{Fe}^{3+}$  state. Availability of such charge compensation centers in the crystal will facilitate a shift of the equilibrium in eq 6 to the left and is a specific example of the dependence of the  $\text{Fe}^{3+}$ - $\text{Fe}^{2+}$  equilibrium upon the lattice environment as influenced by its previous thermal history. The second primary function of the cation vacancies is their efficiency in serving as hole traps. The compound center resulting from a hole trapped at a cation vacancy is called a  $V_1$  center. The epr work of Lunsford,<sup>16</sup> correlating  $V_1$  center formation with catalyst activity, showed that its formation occurred at energies close to that of transition e at 4.8 eV. Summation of energy in the band diagrams allows placement of the cation vacancy level about 1.0 eV above the valence band, corresponding to transition c and the identification of the X state as a cation vacancy band.

*b. Intrinsic Surface Defects.* The sum of all cation defects in the crystal must equal the sum of all anion defects in the crystal in order to maintain total electrical neutrality; however, this does not preclude defect concentration gradients between the bulk and surface phases. Such gradients will occur because the free energy of formation of a bulk cation vacancy, surface cation vacancy, bulk anion vacancy, and surface anion vacancy are all different. One would expect the surface layer to be more depleted in the ion with the higher

escaping tendency relative to that in the bulk. In MgO this is the surface O<sup>2-</sup> ion and O<sup>2-</sup> vacancies are the most common surface defects. To preserve over-all charge neutrality, the excess anion vacancies at the surface must be compensated by a bulk excess of cation vacancies. The resulting concentration gradient is a dipolar space charge layer, illustrated in the band diagram of Figure 5 by the downward bending of bands and energy levels near the surface. Such behavior in MgO has been well described by Nelson, Tench, and Harmsworth<sup>20</sup> by analogy to the theory of Kliewer and Koehler<sup>31</sup> for alkali halide crystals.

The creation of oxygen vacancies at the surface undoubtedly accompanies the oxygen removal observed by Wertz on vacuum heating at 1200°. However, formation of these vacancies by oxygen removal from the surface may also be brought about at much lower temperatures. For example, Lunsford and Jayne<sup>32</sup> detected states associated with surface oxygen vacancies induced by vacuum degassing at 800°. From the studies by Winter<sup>33</sup> on the isotopic exchange reaction between oxygen-18 and surface oxygen on MgO, it can be estimated that oxygen removal from the surface probably begins on vacuum heating at temperatures as low as 500°.

This surface oxygen removal promotes the valence shift shown in eq 6 for Fe<sup>3+</sup> impurities, located near the surface. These Fe<sup>3+</sup> impurities will be favored either directly or indirectly to receive electrons left behind when O<sup>2-</sup> is removed as O<sub>2</sub>. These O<sup>2-</sup> vacancies can also serve as surface traps for electrons and the resulting surface anion vacancy with a trapped electron is denoted as an S center. The formation and stability of S-center surface states has been discussed by Nelson, *et al.*,<sup>20</sup> along with the compound S' center in which a surface cation-anion vacancy pair has trapped an electron. Their approximate location is shown in Figure 5. The S center is the surface termination of the anion vacancy band. The S' center is more stable due to the charge compensation of vacancy pairing.

Another type of intrinsic surface energy state, occurring at energies ordinarily in the forbidden band, is due to the lower coordination number and Madelung constant of any ion on the surface, the energy level shift being due to the abrupt change in electrostatic symmetry at the surface. A detailed discussion of these states, arising from termination of the bulk solid phase, has been given by Mark<sup>34</sup> and Levine.<sup>35</sup> Essentially one electron trap is formed for each species of surface cation and one hole trap is formed for each species of surface anion. Thus MgO would have one hole trap for the O<sup>2-</sup> anion and one electron trap for the Mg<sup>2+</sup> surface cation. Assuming about a 60% ionic character for MgO, the intrinsic electron states associated with these surface ions would be located at approximately 1.75 eV below the conduction band and above the valence band. In this calculation, using the MgO

parameters and the procedure of Levine and Mark,<sup>35</sup> we have assumed that the (100), (110), (211), and (210) surface faces are present in equal amounts on the powdered oxide and no allowance was made for other impurities or defects in the surface region. In the presence of cation excesses and oxygen vacancies on the positively charged MgO surface, these results can only establish an upper limit for the levels, but as a rough estimate of the effect of the nature of the surface, the O<sup>2-</sup> surface state is drawn in Figure 5 at about 1.0 eV above the valence band and the Mg<sup>2+</sup> surface state at 2.5 eV below the conduction band.

c. *Impurity Surface States of Magnesium Oxide.* Since the moderately heat treated MgO catalysts have a partially hydrated surface, it was assumed that the surface must also contain OH<sup>-</sup> anions. The surface OH<sup>-</sup> has been placed about 1.0 eV above the O<sup>2-</sup> level in Figure 5. Its placement at a higher energy is based on the principle that the hydrated surface phase is analogous to Mg(OH)<sub>2</sub>. Surfaces of this MX<sub>2</sub> type are not generally treated by Mark and Levine other than to indicate that crystals having faces not analogous to the cation-anion checkerboard surface of MgO incur lateral electrostatic repulsions in the surface layer and have higher energy than MX crystals.

The bulk impurity ion states extend to the surface with their energy levels also altered by the space charge region. Just as the Mg<sup>2+</sup> cations are more stable than O<sup>2-</sup> ions on the surface, the impurity cations may tend to concentrate there and contribute to the positive nature of the surface. Nelson, *et al.*, have pointed out that these excess impurity cations at the surface can also serve as surface traps for electrons, the electrons being provided either by ultraviolet irradiation or by oxygen desorption.

*Relation of the Energy Band Structure of MgO and Catalytic Activity.* Following the derivation of the composite band structure diagram of Figure 5, it is now necessary to correlate the catalytic activity both previously and presently observed on magnesium oxide with its electronic structure. Particular attention is given toward interpreting the reaction rate spectrum of Figure 3.

1. *Mechanism II, the Photosensitive Case.* Figure 5 primarily represents a catalyst activated by moderate heat treatment which undergoes the mechanism II reaction. Nelson, Tench, and Harmsworth<sup>20</sup> have discussed the conditions favorable to O<sup>2-</sup> adsorbed on the surface. It is highly probable that this species is removed by vacuum heating at 300° or is taken into the lattice as O<sup>2-</sup> at surface anion vacancies. Under the

(31) K. L. Kliewer and J. S. Koehler, *Phys. Rev.*, **A140**, 1226 (1965).

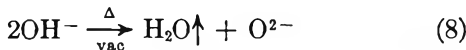
(32) J. H. Lunsford and J. P. Jayne, *J. Phys. Chem.*, **69**, 3183 (1965).

(33) E. R. S. Winter, *Advan. Catal.*, **10**, 196 (1958).

(34) P. Mark, *RCA Rev.*, **26**, 461 (1965).

(35) J. D. Levine and P. Mark, *Phys. Rev.*, **144**, 751 (1966).

moderate activation conditions, all of the physically adsorbed water will have been removed and much of the chemisorbed water will be removed by the reaction



Some chemisorbed water remains to supply the OH<sup>-</sup> ions on the surface shown in Figure 5. That this OH<sup>-</sup> state, or a very similar hydrogen-containing site, is involved in the photocatalysis is indicated by the results shown in Figure 4. Surface oxygen desorption and the creation of extra surface anion vacancies does not begin until the catalyst has been preheated around 500°. For the moderately preheated catalysts, which are kept well below this temperature, a thermal electron source is not available to reduce the number of Fe<sup>3+</sup> states or Y<sup>3+</sup> states originally present in the unactivated sample and the shift to Fe<sup>2+</sup> in eq 6 has not occurred. The trivalent states remain available as trapping centers for any photogenerated electrons, either those generated in the bulk by transitions g, e, and f etc., or by transitions from the low-lying surface impurity states. Transitions to surface states can also occur. The S' center would serve as a surface electron trapping state. A transition such as j, the photopromotion of an electron from a surface OH<sup>-</sup> site into an S' center site, would be totally a surface phenomenon.

Given this catalyst condition, it is possible to make a plausible identification of the energy transitions responsible for activity enhancement. If one modifies the traditional picture of an active site for the reaction, it is possible to identify electronic configurations which perform this type of function.

Fortunately, some sites and some energy transitions may be ruled out completely or assigned secondary roles. This list includes V<sub>1</sub> centers, surface cation impurities, S centers, and S' centers as active sites and transition b as an unlikely site generator.

As pointed out by Lunsford, the V<sub>1</sub> center cannot, by its nature, be a surface defect, yet it may be located near the surface and influence the surface electronic environment. V<sub>1</sub> center concentration follows the catalytic activity, yet the results of this work add evidence to the case for an indirect role, since a definite peak in the catalytic activity spectrum at 4.0 eV occurs at uv energies inadequate to induce a V<sub>1</sub> center. Lunsford had also found that V<sub>1</sub> centers, formed in mechanism II catalysts, were not affected by hydrogen gas, yet in samples prepared by the strong preheating used with the mechanism I catalyst, the V<sub>1</sub> center signal is quickly destroyed by hydrogen. This is in inverse relation to the uv sensitivity of these catalysts.

Surface cation impurities, specifically iron, were discussed and eliminated as a primary site on the basis of the doping experiments of this work. For the doped samples both the initial reaction rate and the ultraviolet photosensitivity were significantly less. In view of the

tendency for such impurities to concentrate at the surface, it does not seem likely that any of them has a direct role as an active site.

S centers are eliminated on the basis of the studies of Nelson, Tench, and Harmsworth<sup>20</sup> who found that H<sub>2</sub> in the gas phase does not seem to affect these centers at all. Furthermore, the S-center esr signal decays to zero in 5 hr at 20°, whereas the observed uv-enhanced activity is much more stable at this temperature. At room temperature, Lunsford and Leland<sup>23,24</sup> found only 20% decrease in the first-order rate constant in a period of 16 hr after irradiation was ceased.

S' centers are more stable and probably have the required lifetime, but in view of their similarity to the S centers, it is assumed that they have no direct interaction with either hydrogen or deuterium. The number of cation vacancy-anion vacancy pairs available to form the S' center should be quite low in the moderately preheated catalyst.

Transition b has been eliminated from direct catalytic importance in mechanism II because the catalyst doped with the Fe<sup>3+</sup> increasing concentrations of iron impurities show decreasing sensitivity to 5-eV ultraviolet radiation.

As a further argument, none of these sites or transitions include or involve the required hydrogen-containing site which is observed experimentally.

Having discarded several sites and transitions from direct catalytic involvement, it is possible to select others which are consistent with the data of this work and previous work in this laboratory. In view of the close parallel between mechanism II activity and uv-induced p-type photoconductivity observed by Lunsford and Leland,<sup>23,24</sup> there is a close relationship between the concentration of holes at the surface and the catalysis. In view of the great sensitivity of mechanism II to absorbed water and the existence of the hydrogen-containing site activated by photons, it is postulated that the photoenhanced activity is associated with a hole trapped at the OH<sup>-</sup> surface site. This trapped state is equivalent to a bound OH<sup>0</sup> radical and is strongly favored under 4.9-eV radiation by transitions i and j, which promote electrons from the OH<sup>-</sup> site to a higher lying electron trap, either the Fe<sup>3+</sup> or the S' center. The additional 4.9-eV transition k, promotion of an electron from an intrinsic surface oxygen state to a surface Fe<sup>3+</sup> state, cannot be ruled out for it can produce OH<sup>0</sup> by the energetically favorable secondary reaction on the surface



Equation 9 corresponds to transition n. This transition could contribute to the visible fluorescence following irradiation at 4.9 eV.

Transitions e and m at 4.8–4.9 eV have catalytic possibilities in an indirect manner. Transition e has been identified as that leading to the formation of the

$V_1$  center, which correlates with catalytic activity. Either of these hole traps near the surface may directly or indirectly receive an electron from surface  $\text{OH}^-$  and  $\text{O}^{2-}$  groups, in effect transferring a hole to the surface and creating the active site. These secondary transitions are labeled a and a' on the band diagram.

A large number of possible transitions at 4.9 eV probably accounts for a large intensity of this peak in the reaction rate spectrum. Transitions at the other energies are more limited; thus the lower peak in the catalyst at 4.0 eV probably corresponds to transitions of type h in Figure 5. This is a surface process yielding directly the proposed active surface radical. The 5.7-eV response seems to have only one correlation, designated by transition f, creating another hole trap which may be filled either thermally from the surface state, leading to catalyst activity, or by photoprocess from the valence band, leading to photoconductivity. The broad nature of many of the peaks may be explained by the presence of many impurities or defects with energies close to each other, by local inhomogeneities causing variations of the electron energy near the same impurity or defect, and also by the altering of electron states due to varying distances from the surface. In summary, the most plausible transitions to associate with mechanism II activity in the photocatalytic response curve of Figure 3 are outlined in Table I.

Table I

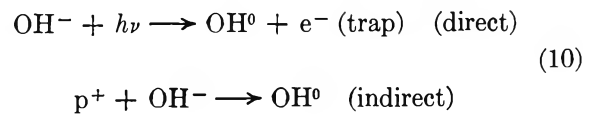
Energy, eV	Transi-tion	Effect
~4.9	k	$\text{O}^-$ produced by excitation of electron from $\text{O}^{2-}$ to a surface impurity which then forms $\text{OH}^0$ by transition n and fluorescence
~4.9	h	$\text{OH}^0$ produced on a surface by excitation to a surface impurity, e.g., $\text{Fe}^{3+}$
~4.9	i, j	$\text{OH}^0$ produced on surface by excitation to an $S'$ center or to an impurity below the surface
~4.9	e	A $V_1$ center formed near the surface which then receives an electron from $\text{OH}^-$ forming $\text{OH}^0$
5.7	f	A $V_1$ center formed near the surface which then receives an electron from $\text{OH}^-$ forming $\text{OH}^0$
4.0	h	$\text{OH}^0$ formed directly by excitation from $\text{OH}^-$ to a surface impurity

2. Mechanism I, the Photoinsensitive Case. Under strong preheating, around 500°, almost all surface water will have been removed, eliminating the  $\text{OH}^-$  sites from the band diagram. Furthermore, some loss of oxygen from the crystal will have occurred and more anion vacancies will exist. The larger increase in positive charge on the surface and a deeper space charge region will skew the surface edge of the band diagram

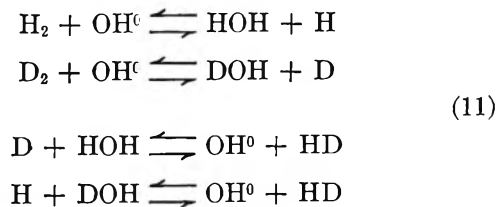
over a longer distance than in the preceding case. With oxygen removal, electrons are available to reduce the original number of  $\text{Fe}^{3+}$  and  $\text{Y}^{3+}$  states in the crystal. As a precursor to oxygen removal, the  $\text{O}^{2-}$  surface state may lose electrons stepwise by transition a to the nearby  $\text{Y}^{3+}$  defect level, leaving an  $\text{O}^-$  site. This site is a hole trapped at a surface  $\text{O}^{2-}$  which becomes the active site upon which hydrogen-deuterium exchange may now occur, since no  $\text{OH}^-$  ions are available. The fact that both the uv-absorption peaks at 5.7 and 4.8 eV and the uv-enhanced catalytic activity both disappear simultaneously and completely upon strong vacuum heating is additional evidence of the  $\text{Fe}^{3+}$  state as a necessary secondary component in the photosensitive catalyst. The stronger vacuum heating and shift to mechanism I catalyst tends to remove the  $\text{Fe}^{3+}$  state and thus prevents transitions e, f, g and k. Transitions h, i, and j are also removed, since  $\text{OH}^-$  disappears by eq 8. Consequently, the uv excitation cannot take place, since both the required electron donors and acceptors no longer exist.

3. Chemical Reaction Mechanism. We have proposed that the catalytic site for the ultraviolet-sensitive mechanism II catalyst is primarily the  $\text{OH}^0$  and the active site for the mechanism I catalyst is the surface  $\text{O}^-$  anion. They are common in the sense that both are equivalent to a trapped hole in the highest level hole traps on the two types of catalyst surface. The actual mechanism I site is chemically different, however, as reflected in the lower activation energy for mechanism I exchange.

The mechanism occurring on the  $\text{OH}^-$  site (mechanism II catalyst) seems to be rather straightforward. Activation of this site is given by direct production of surface holes and by indirect migration of holes to the surface



The exchange reaction occurring on that site is given by the series of equations representing the interaction of holes with  $\text{H}_2$  and  $\text{D}_2$



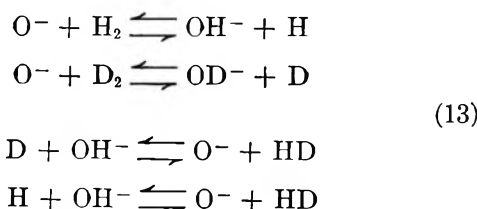
It should be pointed out that the  $\text{OH}^0$  group proposed here as an active site has never been detected in esr studies. This does not preclude its existence at very low concentrations. Lunsford<sup>16</sup> is the only one who has reported looking for it on catalysts activated under moderate conditions where it is most likely to be

found. Nelson, Tench, and Harmsworth<sup>20</sup> also looked for OH<sup>0</sup> but their samples were preheated at 900°, a treatment procedure removing most OH<sup>-</sup> groups from the surface.

A plausible activation of the O<sup>-</sup> active site is given by the following solid-state reaction indicated by transition a in Figure 5 which represents production of surface holes by

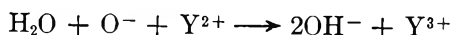


and the chemical reaction occurring on that site for hydrogen-deuterium exchange is given by a series of four equations



Undoubtedly, mechanism I would occur to some extent simultaneously with mechanism II on catalysts receiving the moderate heat treatment.

*4. Catalytic Deactivation by Water Poisoning and Thermal Annealing.* The poisoning of both mechanisms by large amounts of absorbed water would be partly due to surface blockage. The specific poisoning of mechanism I is explained by the removal of the O<sup>-</sup> active site *via* the reaction



The ultraviolet sensitivity of mechanism II is also removed if large concentrations of OH<sup>-</sup> remove surface traps. This would be the case if large OH<sup>-</sup> concentrations cause the filling of the anion vacancies which form S' centers on ultraviolet irradiation or if the excess OH<sup>-</sup> ions involve Fe<sup>3+</sup> acceptors in hydroxide formation at the surface.

Thermal annealing between 100 and 300° apparently removes the uv effects in a completely reversible manner simply by thermal excitation of carriers out of their traps and decay to the original sources. The uv-induced surface sites are destroyed by electron capture to reform the original surface states that existed before uv excitation. Such processes in the bulk, particularly among the iron impurity ions, have been followed by Hansler and Segelken<sup>30</sup> in thermoluminescence studies, and it is logical to suppose that such processes also occur upon the surface. We observed a green luminescence in our photosensitive catalyst samples during irradiation around 4.9 eV. Whether this corresponds to a bulk phenomenon, *i.e.*, the 2.2-eV transition between the Fe<sup>3+</sup>-Fe<sup>2+</sup> state, or to a surface transition such as n, has not been determined.

*5. Two-Frequency Photocatalysis.* An interesting set of auxiliary experiments can be performed by utilizing

irradiation at two frequencies. As an example, photosensitive catalysts were irradiated for a short time with 2537-Å (5-eV) light and then exposed without annealing to 3660-Å (4-eV) light. It was found that the photoenhancement at 3660 Å was about twice what it would have been had there been no preexposure to the higher energy radiation, or had there been sufficient annealing between exposures. Such two-frequency irradiation effects can be explained in terms of Figure 5, wherein transition b following 5-eV irradiation increases the number of Fe<sup>3+</sup> traps near the surface, providing more acceptors for transition h following irradiation at 4 eV and generation of the active OH<sup>0</sup> site.

## V. Conclusions

This work has shown that the location and density of imperfection levels in an insulator may be semiquantitatively determined by surface irradiations at controlled frequencies to obtain in effect a reaction rate spectrometer. It shows also the importance of having detailed knowledge of the band structure at the catalyst surface. We have suggested that the general active site on this insulator catalyst is a surface trapped hole, even though the actual mechanism of the reaction may change, depending upon the chemical nature of the species trapping the hole. The concentration of such active sites is, in turn, the result of an equilibrium with the large number of other secondary levels within the catalyst surface and subsurface phases. It is clear that one should not necessarily think of an active site as a unique chemical species or a particular structural feature. For example, the chemical species introduced by adsorbed water on the surface acts as a poison unless it traps a hole, in which case it becomes an active site for the reaction. An active site in this sense cannot function independently of its surroundings on or near the surface. This work shows for insulator catalysts that the minority energy levels are important and must be taken into consideration in an electronic theory of catalysis very much as Gray<sup>36</sup> has shown this for semiconductor catalysts. This work especially emphasizes the importance of intrinsic surface levels in photocatalytic reactions in much the same manner in with Mark<sup>34</sup> initially emphasized their importance in the photoadsorption step.

These conclusions are not entirely general for all catalytic reactions, for there are cases in which the active site is more distinctly local and depends more specifically upon its chemical nature. However, the relationship between the electronic structure of solids and their catalytic activity is undoubtedly more complicated than previous work has treated. Often it is the total electronic structure and the distribution of carriers in that structure that is important, not the type of carrier alone or any other single solid-state parameter. Expecting that a wide group of semiconductor and in-

(36) T. J. Gray, *Chem. Eng. News*, **46**, 42 (1968).

sulator catalysts will be found to act similarly in principle to the system studied here, one might look to future work in the field detailing the total electronic structure of many solid catalysts.

*Acknowledgments.* We wish to thank the National Aeronautics and Space Administration for partial

support of this research under Grant No. NSG-6-59 for research on physics of solid materials at Rice University; Shell Development Co. for help in spectroscopic analysis of the MgO sample impurities; Dr. J. W. Hightower for his help with the mass spectrometry experiments; and Dr. J. H. Lunsford for several helpful discussions.

## Binary Diffusion Studies with a Wedge Interferometer

by J. L. Duda, W. L. Sigelko, and J. S. Vrentas

*Process Fundamentals Research Laboratory, The Dow Chemical Company, Midland, Michigan 48640  
(Received July 19, 1968)*

By conducting a free-diffusion experiment in a thin wedge formed by two partially reflecting glass plates, binary diffusion coefficients in liquid systems can be determined from an analysis of the interference patterns which are induced when this optical wedge is illuminated by monochromatic light. The accuracy, limitations, and potential problems associated with this technique are investigated, and innovations in experimental techniques, cell design, and data analysis are disclosed. Measurements of the concentration-dependent diffusion coefficient for the binary system of sucrose-water at 25° demonstrate that diffusivity data accurate to 3% or less can be obtained with the wedge interferometer technique. This study shows that it is deceptively easy to produce data with a wedge interferometer but rather difficult to obtain accurate data because there are several points in this type of diffusion experiment where significant errors can be introduced if certain precautions are not taken.

### Introduction

Several types of optical interference methods have been developed for the measurement of refractive index distributions that are associated with free-diffusion experiments. Although the conventional interferometers such as the Rayleigh and Gouy differ from each other in their optical configurations, the actual free diffusion takes place in a cell which to a large degree is not dependent on the particular method used to determine the concentration or concentration-gradient distribution. Therefore, these conventional methods have many common characteristics and limitations.

One of the significant limitations of these techniques is the fact that they are inefficient for the measurement of the small, strongly concentration dependent diffusivities exhibited by concentrated polymer solutions. In recent years, a new type of interferometric technique based on the formation of interference patterns by a thin wedge has appeared in the literature.<sup>1</sup> In this apparatus the diffusion cell is an integral part of the interferometer, for light interference is induced by partially metallized cell walls which are arranged to form a thin wedge in which free diffusion takes place. Since concentration distributions over very small distances can be measured in the wedge apparatus, this technique ap-

pears to be particularly applicable to the study of diffusion in polymer systems because even for these systems the time of the experiment can be kept short. This method possesses other apparent advantages, for it involves relatively simple experimental apparatus and does not require extremely accurate temperature control since the diffusion takes place in a thin channel in which natural convection currents are strongly suppressed.

Although the wedge interferometer appears to have great potential as a method of measuring diffusion coefficients in liquid systems, it apparently has not received wide recognition. This lack of acceptance is no doubt partially due to the fact that even though numerous data have been obtained with this method, the accuracy of the measured diffusivities has never been adequately determined. In this study, the accuracy of the wedge technique is established by measurement of the concentration-dependent diffusion coefficient for the binary system of sucrose-water at 25°. This particular

(1) Typical studies which give references to previous work: D. R. Paul, *Ind. Eng. Chem. Fundam.*, **6**, 217 (1967); R. M. Secor, *J. Polymer Sci., Part A-2*, **5**, 323 (1967); A. Ye. Chalykh and R. M. Vasenin, *Vysokomol. Soedin.*, **8**, 1908 (1966); *Polym. Sci. (USSR)*, **8**, 2107 (1966).

system was chosen because accurate, widely accepted diffusion data over a concentration range are available for comparison. The limitations and potential problems associated with this method are also investigated, and innovations in experimental technique, cell design, and data analysis are disclosed.

### Experimental Technique

In previous studies the wedge interferometer has consisted of two partially metallized glass slides separated by a spacer at one end to form a wedge. This optical wedge is situated on a microscope stage and is illuminated from below by collimated monochromatic light.<sup>2</sup> This configuration produces interference fringes which may be viewed and photographed through the eyepiece of the microscope. When the wedge is filled with a material of constant refractive index, the fringes are evenly spaced straight lines which run parallel to the axis of the wedge. More details of the conventional wedge interferometer are available in several publications<sup>1</sup> and the theory of the optical wedge has been treated by Searle.<sup>3</sup> For the relatively small wedge angles employed in this study, the adjustable aperture technique devised by Ambrose<sup>4</sup> was found to be unnecessary for the formation of sharp fringes.

An investigation of various types of glass slides and coatings has revealed that the accuracy of the wedge interferometer can be significantly improved by changes in these basic components. It was found that glass plates optically flat to a quarter of a wavelength are necessary to produce sharp, unrippled fringes at small wedge angles. Optically flat plates were recommended by Berg<sup>5</sup> in his pioneering study of the wedge interferometer and have been used by O'Brien,<sup>6</sup> however, most recent investigators have not followed this recommendation. A multilayered coating<sup>7</sup> which reflects approximately 85% of sodium D line wavelength light (5893 Å) proved to be an excellent coating for these interferometric studies. This coating will produce sharp fringes with a highly illuminated background, and good quality pictures can be obtained with exposure times as low as  $\frac{1}{8}$  sec using 3000-speed, Type 57 Polaroid film. This particular coating is also highly resistant to wear and corrosion.

The most difficult step in a free-diffusion experiment is the initiation of the diffusion process with a sharp interface between the adjacent phases. Ideally, the two phases would have straight boundaries at right angles to the interference fringes when they contact each other; in addition, the phases should come together in such a manner that their concentration distributions are not distorted by the contacting process. Several types of diffusion cells which suppress the initial boundary disturbances have been developed for use with the more conventional interferometric techniques.<sup>8</sup> However, with the wedge interferometer it has been common practice to initiate diffusion by simply allowing two

drops of different compositions to come together at an interface which is perpendicular to the axis of the wedge. In the first wedge interferometer studies of liquid systems,<sup>9</sup> the two liquid drops were placed near each other on the lower glass plate and were subsequently forced together by lowering the upper plate into place. These first investigators also modified this technique by introducing one of the solutions into the wedge through a small capillary tube. Secor<sup>10</sup> improved these procedures by first forming the wedge around one drop of solution and then using surface tension forces to draw the second drop into contact.

None of these techniques is completely satisfactory, for, especially when dealing with low viscosity solutions such as employed in this study, these procedures must be repeated many times before a straight initial interface which is perpendicular to the interference fringes is obtained. The principal problem with these procedures is the fact that the solutions are unconstrained and can flow freely in any direction within the wedge. Therefore, it is to a large degree just a random chance that the two droplets will flow toward each other to form the desired interfacial shape and orientation. The chances of forming the desired interface are greatly improved if a channel is used to guide the flow of the solutions. In these studies a small amount of powdered graphite was built up on the bottom plate to form a rectangular channel which is open at the edge of the plate and closed on the other three sides.

To start an experiment the first drop of known concentration is placed in the channel near the closed end. The upper slide is then rotated down toward the open end of the channel to contact the solution and form the wedge. Finally, the second drop of the solution can be drawn into contact by capillary action from the open end of the channel. Graphite is an excellent inert material for this purpose since it controls the flow of the solutions but is permeable to the air which is trapped between the two solutions. Also, graphite powder will freely deform to the shape of the wedge and can easily be removed without damaging the coating. Whereas graphite appears to be ideal for use in the wedge for aqueous solutions, the nature of some solvents may be such that the channel must be formed from some other material.

- (2) In this study a Leitz Ortholux microscope with a spectacle lens condenser was used. The light source was a 24-W sodium vapor lamp in a Leitz Universal Lamp Housing No. 250.
- (3) G. F. C. Searle, *Phil. Mag.*, **37**, 361 (1946).
- (4) E. J. Ambrose, *J. Sci. Instrum.*, **25**, 134 (1948).
- (5) W. F. Berg, *Proc. Roy. Soc. (London)*, **A164**, 79 (1938).
- (6) R. N. O'Brien, *Rev. Sci. Instrum.*, **35**, 803 (1964).
- (7) Hi-Efficiency Coating No. 801, supplied by Liberty Mirror Division of Libby-Owens Ford Company, Inc., Brackenridge, Pa.
- (8) Various types of cells are described by A. L. Geddes in "Physical Methods of Organic Chemistry," Vol. I, A. Weissberger, Ed., Interscience Publishers, New York, N. Y., 1960.
- (9) Y. Nishijima and G. Oster, *J. Polym. Sci.*, **19**, 337 (1956).
- (10) R. M. Secor, *A.I.Ch.E. J.*, **11**, 452 (1965).

The graphite-channel technique helps to form the boundary configuration which is desired in a free-diffusion experiment; however, initial mixing of the two solutions due to boundary disturbances upon contacting of the two drops must also be eliminated for the realization of a pure molecular-diffusion type process. If the idealized free-diffusion conditions of a sharp initial boundary and one-dimensional unrestricted diffusion are satisfied, then it has been shown<sup>11</sup> that for all cases the concentration in the diffusion field is a function only of the variable  $\eta = x/2t^{1/2}$ . This variable is defined such that  $x$  is the distance from the initial boundary at which contact occurs and  $t$  is the time which passed since the two solutions made their initial contact. The fact that concentration is a function only of the  $\eta$  variable in a perfect free-diffusion experiment can be used to test for the presence of initial mixing in the wedge apparatus. Results of this investigation show that the previous methods of initiating the free-diffusion process in the wedge produce significant interfacial mixing. Preliminary experiments with the sucrose-water system showed that this initial mixing is substantially reduced by decreasing the wedge angle, and all the data reported in this study were obtained from a wedge with an angle of  $0.10^\circ$ , which is small compared with the angles which have been previously used. For the sucrose-water system it was not possible to form an initial boundary with a tolerable amount of mixing when larger wedge angles were employed; however, it is quite possible that larger wedge angles can be utilized when dealing with high-viscosity solutions such as a typical polymer solution.

In Figure 1, concentration distributions at various times are shown for run 1 whose characteristics are presented in Table I. The changing of the concentration *vs.*  $\eta$  curves with time indicates that the initial boundary for this run was diffuse owing to boundary disturbances when the solutions were contacted. This particular run was the best that could be attained by the conventional contacting technique, and numerous attempts were necessary before a run with this limited amount of mixing was realized. Figure 1 indicates that the data tend to converge to a common curve as time is increased. Although no completely general theoretical proof exists, the calculations of Mijnlieff and Vreedenberg<sup>12</sup> indicate that the concentration *vs.*  $\eta$  curves resulting from a diffuse initial boundary will eventually approach the distribution which would issue from an exact step function initial distribution. Therefore, it appears that accurate diffusion coefficients can be obtained from experiments with a diffuse initial boundary if the final, unchanging concentration-distribution data are used. Calculations based on early concentration-distribution data taken before the distribution has relaxed to its final form will yield highly inaccurate diffusion coefficients which are larger than the actual values. It is discouraging to note that in most pre-

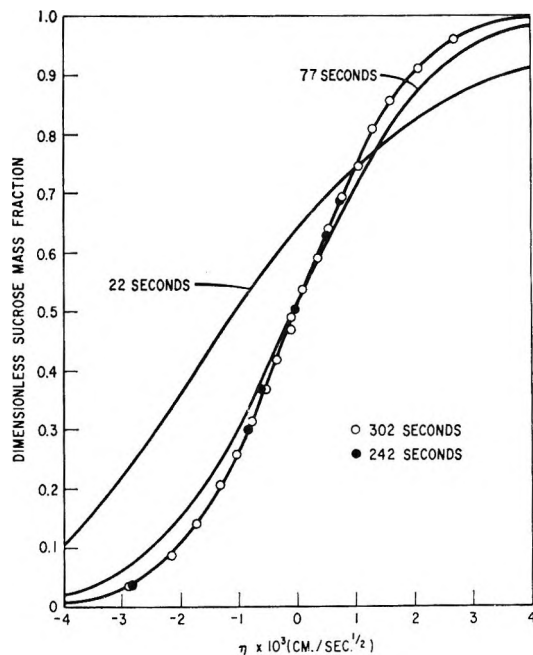


Figure 1. Effect of initial mixing on concentration distribution for run 1.

vious diffusion studies with the wedge interferometer the data were apparently not checked for the effects of initial mixing.

Table I: Summary of Wedge Interferometer Runs

Run no.	Wt fraction	
	At limit where velocity is zero	At other limit
1	0	0.0962
2	0	0.299
3	0	0.297

Although the concentration distribution for any experiment should eventually relax to a form which can be correctly analyzed, the degree of initial mixing which can be tolerated in the wedge experiment is quite limited. In the wedge apparatus, it is conceivable that the free-diffusion field can be disturbed by the finite extent of the liquid drops and by concentration changes due to evaporation before the concentration distribution has had enough time to relax to its final form. The liquid drops within the wedge come together with relatively large velocities when the conventional techniques are used, and it is not surprising that this type of collision often produces large boundary disturbances which

(11) This follows from utilization of a similarity transformation. For example, see J. L. Duda and J. S. Vrentas, *Ind. Eng. Chem. Fundam.*, 4, 301 (1965).

(12) P. F. Mijnlieff and H. A. Vreedenberg, *J. Phys. Chem.*, 70, 2158 (1966).

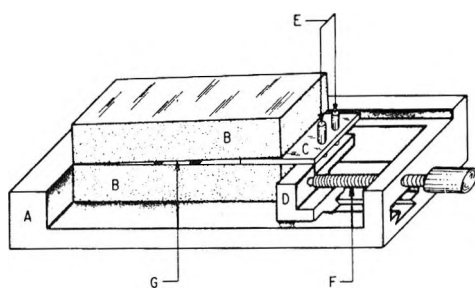


Figure 2. Schematic diagram of adjustable-angle wedge interferometer: A, cell which is positioned on microscope stage; B, optically flat, coated glass plates (approximately  $25 \times 75$  mm); C, wedge spacer which determines the wedge angle; D, positioning block which slides horizontally in a dovetail channel; E, pins connecting wedge spacer to positioning block; F, screw for adjustment of wedge angle; G, open end of graphite channel.

cannot be tolerated. Operation of the wedge apparatus would be greatly facilitated if the experimentalist could exert greater control over the contacting of the drops. To achieve finer control, a new type of wedge cell was devised.

The modified cell used in this study, which is shown in Figure 2, has provisions for manually changing the wedge angle after the wedge has been formed. In using this new cell, the first step is to bring the two solutions into the general vicinity of each other in the graphite channel by conventional means. Next, the actual contacting is achieved by slowly turning the adjustment screw in order to decrease the wedge angle. As the wedge angle is decreased, the solutions are forced to flow toward each other and their velocities upon contacting can be very accurately controlled. With this technique the mixing associated with the formation of the initial boundary can be minimized for a given wedge angle and it is not necessary to perform numerous trial runs. This adjustable angle technique was used to produce runs 2 and 3 of this study.

### Interpretation of Interference Patterns

During the course of a free-diffusion experiment in a wedge interferometer, the interference pattern is photographed at different times. In order to obtain concentration distribution data these interferograms must be analyzed to obtain information concerning the distribution of the refractive index within the diffusion field. This analysis is based on the fact that the fringes are contours of constant optical thickness, and any increase in refractive index along a fringe must be accompanied by a decrease in the thickness of the wedge. The wedge interferograms are analyzed by relating the refractive index at a given point to the known refractive indices which exist at the extremes of the diffusion field.

Two techniques for the interpretation of wedge interference data have been developed, and the accuracy and problems associated with both of these techniques were considered in this study. A technique in which mea-

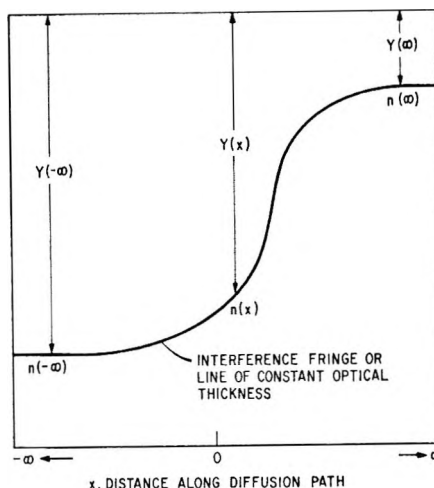


Figure 3. Constant optical thickness technique for interpretation of wedge interferograms.

surements are taken along a path of constant optical thickness was first employed by Hayes and Park<sup>13</sup> and more recently by Paul.<sup>1</sup> In this method, the displacement of one interference fringe from a reference line which is parallel to the wedge axis is measured as a function of distance along the diffusion path. A typical fringe and the basic measurements in this technique are shown in Figure 3. In the regions on the far right and left, the fringes are straight lines, since the diffusion process has not changed the concentrations at these two extremes, and the refractive indices,  $n(-\infty)$  and  $n(\infty)$ , are known, for they correspond to the refractive indices of the original solutions. The refractive index at any position  $x$  in the diffusion field can be related to the refractive indices at the two limits by an equation derived by Paul<sup>1</sup>

$$\frac{n(x) - n(\infty)}{n(-\infty) - n(\infty)} = \frac{1 - \xi}{\left[ \frac{n(-\infty)}{n(\infty)} - 1 \right] \xi + 1} \quad (1)$$

where  $\xi = [Y(x) - Y(-\infty)]/[Y(\infty) - Y(-\infty)]$ .

Instead of measuring along one fringe or a path of constant optical thickness, other investigators<sup>9,10</sup> have interpreted wedge fringe patterns by noting the position and number of fringe intersections along a reference line which is parallel to the axis of the wedge in the direction of diffusion. Since the wedge thickness is constant along this reference line, the refractive index difference between any two adjacent fringe intersections is constant. In the previous studies the refractive index,  $n_I$ , at the position where the  $I$ th fringe crosses through or intersects the line of constant thickness has been calculated from the equation

$$n_I = n(-\infty) + I \frac{n(\infty) - n(-\infty)}{K + 1} \quad (2)$$

(13) M. J. Hayes and G. S. Park, *Trans. Faraday Soc.*, **52**, 949 (1956).

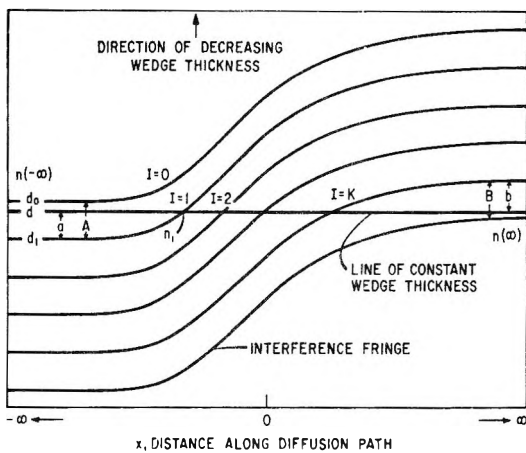


Figure 4. Constant wedge thickness technique for interpretation of wedge interferograms.

where  $K$  is the total number of fringe intersections between the two limits of the diffusion field. However, as will be shown in the following development, eq 2 is exact only when the reference line which follows the path of constant wedge thickness coincides with fringes at both extremes of the diffusion field.

The two ends of a typical interferogram are depicted in Figure 4. The straight line crossing through the fringe pattern represents a line of constant wedge thickness,  $d$ , which is parallel to the axis of the wedge. It can be shown that fringes associated with an optical wedge satisfy the relationship

$$nd = \frac{\nu\lambda}{2} \quad (3)$$

where  $\lambda$  is the wavelength of the monochromatic light,  $\nu$  is an integer, and  $d$  is the thickness of the wedge at the position where interference occurs in a medium in which the refractive index is  $n$ . If we consider the fringe in Figure 4 which is designated as  $I = 1$ , it follows from this equation that the refractive index,  $n_i$ , at the point where this fringe intersects the constant-thickness reference line can be related to the known refractive index at the one limit by the equation

$$n(-\infty)d_1 = n_id_1 \quad (4)$$

From geometrical considerations, the following relationship between the thicknesses at the various positions shown in Figure 4 can be derived

$$d = d_1 - \frac{a}{A}(d_1 - d_0) \quad (5)$$

and eq 4 and 5 can be combined to give

$$n_i = n(-\infty) \left[ 1 + \frac{a}{A} \frac{(d_1 - d_0)}{d} \right] \quad (6)$$

From eq 3 the difference in wedge thickness,  $d_1 - d_0$ , between the adjacent fringes  $I = 0$  and  $I = 1$  can be shown to be

$$d_1 - d_0 = \frac{\lambda}{2n(-\infty)} \quad (7)$$

Substitution of eq 7 into eq 6 gives an expression for the refractive index at the point where this first fringe intersects the reference line in terms of the refractive index at the extreme where  $x \rightarrow -\infty$

$$n_i = n(-\infty) + \frac{a\lambda}{2dA} \quad (8)$$

Following this same procedure, an expression can be derived for the refractive index,  $n_i$ , at the point where the  $I$ th fringe intersects the reference line

$$n_i = n(-\infty) + \left( I - 1 + \frac{a}{A} \right) \left( \frac{\lambda}{2d} \right) \quad (9)$$

By an analogous procedure we can relate the refractive index,  $n_i$ , to the refractive index at the other infinite limit by the equation

$$n_i = n(\infty) - \left( K - I + \frac{b}{B} \right) \left( \frac{\lambda}{2d} \right) \quad (10)$$

where  $K$  again is the total number of fringes which intersect the constant-thickness reference line. Equations 9 and 10 can be combined to yield

$$n_i = n(-\infty) + \frac{\left( I - 1 + \frac{a}{A} \right) [n(\infty) - n(-\infty)]}{K - 1 + \frac{a}{A} + \frac{b}{B}} \quad (11)$$

Equation 11 is an exact equation for determining the refractive index at points of intersection in terms of the known refractive indices and easily measured quantities. This relationship reduces to eq 2 only when the fractions  $a/A$  and  $b/B$  are both equal to 1, which occurs when the reference line coincides with fringes at both limits of the diffusion field. This condition is realized only when

$$\frac{2d[n(\infty) - n(-\infty)]}{\lambda} = N \quad (12)$$

where  $N$  is an integer. The error introduced when the approximate eq 2 is employed instead of eq 11 is most significant when the number of intersecting fringes,  $K$ , is small, such as occurs when thin wedges are employed to suppress initial mixing. In practice, eq 11 is used to calculate the refractive index as a function of the distance,  $x$ , along the diffusion path. By using more than one reference line of constant thickness, an unlimited number of  $n$  vs.  $x$  points can be obtained from one interferogram.

Comparison of the constant optical thickness and constant wedge thickness methods has shown that although a large number of  $n$  vs.  $x$  points can more easily be obtained with the constant optical thickness

technique, this technique has a greater susceptibility to error. For equivalent accuracy, the diffusion must be perfectly one dimensional over a broader front when the constant optical thickness method is used, for the fringe lines which are followed traverse a large segment of the diffusion field. On the other hand, the constant wedge thickness method can be used to analyze a rather narrow diffusion field and is not as sensitive to diffusion perpendicular in direction to the desired free-diffusion path. This undesired diffusion is produced by evaporation from the surfaces of the solution which are parallel to the path of the free diffusion. The constant optical thickness method was also found to be sensitive to errors in the measurement of the distances  $Y(-\infty)$  and  $Y(\infty)$ , which can be troublesome to determine accurately since they are approached asymptotically as the limits of the diffusion field become effectively infinite in extent. Although the fractions  $a/A$  and  $b/B$  in the constant wedge thickness technique are also approached asymptotically, the effect of errors in these fractions on most of the concentration distribution curve is not as great. Finally, it should be noted that with proper care accurate refractive index distribution data by either method can be obtained if the measurements are performed with a traveling microscope which has an accurate traversing mechanism in two directions.

For the above reasons, the data presented in this study were obtained with a traveling microscope using the constant wedge thickness technique, and this technique is recommended in preference to the constant optical thickness method. Although it is possible to obtain accurate data with the constant optical thickness technique, it involves considerably more care during experimentation and measurement.

### Determination of Diffusion Coefficients

The wedge interferograms yield the refractive index distribution as a function of time in the infinite free-diffusion field. From knowledge of the refractive index as a function of concentration, the preliminary interferometer data can easily be converted to give the form of the concentration distribution at each time that an interferogram is obtained. In the wedge diffusion experiment, the position of the initial interface,  $x = 0$ , cannot be accurately determined experimentally. However, a procedure is available<sup>14</sup> for calculating this position from concentration distribution data which have been measured with respect to an arbitrary reference plane in the diffusion field. After the  $x$ -coordinate system has been properly established from interferograms for which initial mixing is no longer a factor, the concentration *vs.*  $x$  data for these times are combined to form a single concentration *vs.*  $\eta$  curve.

The free-diffusion process was first analyzed by Boltzmann,<sup>15</sup> and it is possible from this analysis to determine the diffusivity-concentration functional dependence from the concentration distribution data. This analy-

sis has recently been generalized to include the effect of volume change on mixing, and it has been shown that in some instances this effect can be quite significant.<sup>11</sup> A convenient form of the generalized equation for the analysis of wedge data is

$$D = \frac{1}{\rho} \frac{d\eta}{d\omega_1} \left( - \int_{\rho_{10}}^{\rho_1} 2\eta d\rho_1 + \omega_1 \int_{\rho_0}^{\rho} 2\eta d\rho \right) \quad (13)$$

where  $D$  is the binary diffusion coefficient when the mass density of species 1 is  $\rho_1$ ;  $\rho$  and  $\omega_1$  are the total solution density and the mass fraction of species 1 at this composition, respectively; and  $\rho_0$  and  $\rho_{10}$  are the total density and species density, respectively, at the limit of the diffusion field where the solution velocity is zero. In this study, the closed end of the graphite channel served as a constraining boundary which maintained a zero velocity at this limit of the free-diffusion field. In the determination of diffusion coefficients from eq 13, auxiliary data which describe the functional dependence of the total density of the solution on the concentration must be available in addition to the concentration distribution data.

In the application of eq 13, concentration *vs.*  $\eta$  data which are free of initial mixing effects must be integrated and differentiated. The calculated diffusion coefficients can be quite dependent on the way these operations are performed, especially on the differentiation process when only a limited number of data points which contain random experimental error are treated. Some investigators have performed these operations graphically<sup>13</sup> and others<sup>1,10</sup> have smoothed out the data using various analytical approximations to the curves.

To test various techniques for treating the concentration distribution data without the complications associated with experimental measurements, theoretical  $\omega_1$  *vs.*  $\eta$  points were obtained from a numerical solution of the equations describing the free-diffusion process. These test-data points were obtained for the case of a diffusivity which is a linear function of weight fraction, closely approximating the diffusivity behavior for the water-sucrose system. The numerical technique employed to solve the diffusion equation in an infinite medium has been described elsewhere.<sup>16</sup> Comparison of the diffusivity-concentration relationship calculated from the test data using eq 13 with the original diffusivity function which was used to generate the test distribution data permitted evaluation of various techniques for performing differentiation and integration operations.

The following three methods were evaluated as to their accuracy when used to perform the necessary

(14) J. L. Duda and J. S. Vrentas, *Ind. Eng. Chem. Fundam.*, 5, 434 (1966).

(15) L. Boltzmann, *Ann. Phys. (Leipzig)*, 53, 959 (1894).

(16) J. L. Duda and J. S. Vrentas, *Ind. Eng. Chem. Fundam.*, 5, 69 (1966).

differentiation and integration steps: numerical integration and differentiation; approximation of the concentration distribution function by an S-shaped curve, as proposed by Secor,<sup>10</sup> and modification of the analytical approximation technique suggested by Paul.<sup>1</sup> For the latter two, analytical differentiation and integration of the empirical fitting functions give the desired derivatives and integrals. Among these three, definitely the most accurate technique for analyzing free-diffusion data was found to be the third method which was based on finding analytical approximations for the two ends and for the center of the concentration distribution curve. The basic steps of the method can be described as follows. First, the weight fraction distribution data are transformed using a variable suggested by Hall<sup>17</sup>

$$u(\eta) = \text{inverf} (2W - 1) \quad (14)$$

where  $W = [\omega_1 - \omega_1(-\infty)] / [\omega_1(\infty) - \omega_1(-\infty)]$  is the normalized weight fraction and where  $\text{inverf } \beta$  is defined such that  $\beta = \text{erf} (\text{inverf } \beta)$ . When  $u(\eta)$  is plotted as a function of  $\eta$ , the curve consists of two straight lines at the extremes of the concentration distribution connected by a curved portion in the center. The two linear portions are fit with straight lines, and these linear approximations are used to perform the integration and differentiation steps analytically in these regions. Next, the weight fraction distribution curve is transformed using the variable

$$U(\eta) = \text{invtanh} (2W - 1) \quad (15)$$

where  $\text{invtanh } \beta$  is defined such that  $\beta = \tanh (\text{invtanh } \beta)$ . The function  $U(\eta)$  is then fit with the polynominal approximation

$$U = a_0 + a_1\eta + a_2\eta^2 + a_3\eta^3 + a_4\eta^4 \quad (16)$$

using the data in the center portion and a few points at the ends which are used in the previous fits. Finally, eq 15 and 16 are used to perform integrations and differentiations analytically in the region which is not described by the error function approximations.

The above procedure is similar to the technique suggested by Paul except that it was determined by testing various modifications of this basic approach that, for the greatest accuracy, it is necessary to fit the variable  $U(\eta)$  with a five-coefficient polynomial function of  $\eta$ , using all the data in the center portion and a few points on the ends which are also used to fit the two straight lines in these regions. This was done to ensure smoothness between the center region and the two end regions. Paul fit the center with a straight-line approximation, apparently using only the points in this region. By the above technique, the diffusion coefficients calculated from the test data agreed with the original diffusivity function with an error no greater than 0.4% over more than 95% of the concentration range. Since this technique was the best method found for analyzing the

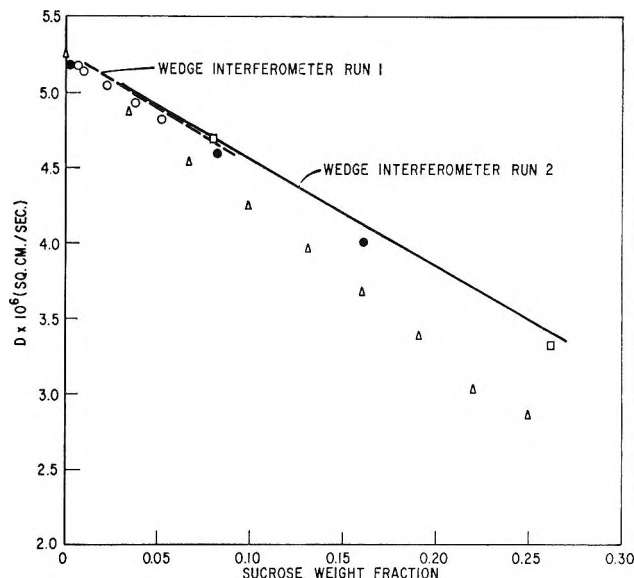


Figure 5. Comparison of wedge interferometer data for sucrose-water system with previous data: O, Gosting and Morris;<sup>19</sup> ●, Ellerton and Dunlop;<sup>20</sup> △, Irani and Adamson;<sup>21</sup> □, Henrion.<sup>22</sup>

test data, all diffusivity calculations reported in this study were obtained in this manner.

Because of the nature of the concentration distribution curve, there is less accuracy in the derivatives and integrals used in eq 13 when they are evaluated at the two extremes of the curve than when calculated for the center portion. Consequently, it seems appropriate to follow the suggestion of Chalykh and Vasenin<sup>13</sup> and not report diffusivity data for the complete concentration range studied. A reasonable and safe practice would be to claim accurate experimental diffusion coefficients over the middle 80% of the concentration range. Attempts to obtain diffusion coefficients at the two concentration limits by extrapolation of empirical fits of the data, as proposed by Paul,<sup>1</sup> led to inaccurate results for the data of this study, and extrapolation procedures of this type should be used with caution.

## Results and Conclusions

Three diffusion runs with the wedge interferometer were performed for the sucrose-water system at  $25 \pm 0.1^\circ$  and the characteristics of these runs are presented in Table I. The diffusivity results from the first two runs are shown in Figure 5 along with some previous data from the literature. The data points of Gosting and Morris<sup>19</sup> as well as those of Ellerton and Dunlop<sup>20</sup> were taken with a Gouy interferometer, and the data of Irani and Adamson<sup>21</sup> and the experimental results of

(17) L. D. Hall, *J. Chem. Phys.*, **21**, 87 (1953).

(18) A. Ye. Chalykh and R. M. Vasenin, *Vysokomol. Soedin.*, **7**, 586 (1965); *Polymer Sci. (USSR)*, **7**, 642 (1966).

(19) L. J. Gosting and M. S. Morris, *J. Amer. Chem. Soc.*, **71**, 1998 (1949).

(20) H. D. Ellerton and P. J. Dunlop, *J. Phys. Chem.*, **71**, 1291 (1967).

(21) R. R. Irani and A. W. Adamson, *ibid.*, **62**, 1517 (1958).

Henion<sup>22</sup> were obtained with the diaphragm cell technique. Gouy interferometer data are generally considered to be very accurate; for example, the data of Gosting and Morris have been carefully checked by several investigators<sup>23-25</sup> and are thought to be accurate to  $\pm 0.1\%$ . Consequently, the Gouy interferometer data can serve as a standard for determining the accuracy of diffusion data for liquid systems.

Table II: Diffusion Coefficients for Sucrose-Water System at 25°<sup>a</sup>

Wt fraction	Gouy interferometer	Wedge interferometer		
		Run 1	Run 2	Run 3
0.010	5.148 <sup>b</sup>	5.20	...	...
0.023	5.049 <sup>b</sup>	5.10	...	...
0.038	4.934 <sup>b</sup>	4.99	5.00	4.89
0.052	4.821 <sup>b</sup>	4.89	4.90	4.83
0.082	4.588 <sup>c</sup>	4.66	4.69	4.65
0.161	4.007 <sup>c</sup>	...	4.14	4.11

<sup>a</sup> Diffusion coefficients are in units of  $\text{cm}^2/\text{sec}$ . <sup>b</sup> Data of Gosting and Morris.<sup>19</sup> <sup>c</sup> Data of Ellerton and Dunlop.<sup>20</sup>

In Table II, a comparison of the Gouy interferometer data with the wedge interferometer data is presented. The important fact that this table shows is that, over the middle 80% of the concentration range where the wedge data are considered accurate, the maximum deviation between the Gouy and wedge interferometer data is approximately 3%. This is perhaps the first attempt to determine the degree of accuracy which can be obtained from the wedge technique. From the above three runs, the precision of the wedge interferometer is seen to be no worse than about  $\pm 2\%$ .

Figure 5 and Table II indicate that the diffusion coefficients obtained from the wedge interferometer have a tendency to be slightly too large. This trend suggests that some small effect of the initial mixing is still present even at the longest experimental times where the concentration distribution appears to have relaxed to its final form. Although the practice of obtaining diffusivities from concentration *vs.*  $\eta$  data which appear to be unchanging with respect to time is quite satisfactory, the possibility exists that the accuracy of the wedge interferometer could be further improved by a method of extrapolating the diffusivity data to essentially infinite time in a manner somewhat similar to the technique employed in the analysis of Guoy interferometer data.<sup>19</sup> This was not done in the present study since it was felt that not enough is yet known about the relaxation of the concentration profile to its final distribution for the case of concentration-dependent diffusion coefficients.

Although experiments on conventional interferometers yield more accurate data since measurements

can be taken over a very small concentration range, one carefully executed wedge interferometer experiment will give diffusivity data over a wide concentration range with an accuracy which is acceptable for most purposes. In addition, the wedge appears to be better suited to the study of polymer solutions than conventional interferometers. On the other hand, for obvious reasons, very volatile solvents cannot be studied with a wedge apparatus. Finally, although accurate data can be obtained with the wedge technique, it should be emphasized that the characteristics of this method are such that it is deceptively easy to obtain data but rather difficult to obtain accurate data.

This study clearly shows that there are several points in a wedge interferometer diffusion experiment where significant errors can be introduced if certain precautions are not followed. It is very critical that all wedge diffusion data be tested for the presence of initial mixing effects. A plot such as Figure 1 seems to be a relatively sensitive method for detecting these effects which lead to high values for the diffusion coefficients. For example, the data for run 1 shown in Figure 5 were obtained from an analysis of the 242 and 302-sec data points shown in Figure 1. If the data taken at 77 sec are analyzed, the resulting diffusivities are in error by a minimum of 20%. Also, significant errors can sometimes be introduced by neglecting the volume change on mixing in the data analysis. In this case, however, neglect of the volume change introduces only about 1% error.

This investigation also shows that the analysis of the concentration distribution data with eq 13 is critical. Although the scheme followed in the analysis of the sucrose-water system is very accurate, there are no guarantees that it will be as successful in the treatment of data from other systems. However, alternative schemes can be proposed and easily evaluated in the manner described above. This critical step can be checked by comparing an  $\omega_1$  *vs.*  $\eta$  curve which has been numerically generated from the calculated diffusivities with the original concentration distribution data. For example, the solid curve through the data in Figure 1 was obtained from a numerical solution based on the diffusivity data for run 1 presented in Figure 5. The good agreement between this curve and the original data indicates that these data have been properly analyzed. Since a relatively simple technique is available for the numerical solution of the free-diffusion problem,<sup>16</sup> it seems reasonable that all such diffusion data should be checked in this manner.

(22) P. N. Henrion, *Trans. Faraday Soc.*, **60**, 72 (1964).

(23) D. F. Akeley and L. J. Gosting, *J. Amer. Chem. Soc.*, **75**, 5685 (1953).

(24) J. M. Creeth, *ibid.*, **77**, 6428 (1955).

(25) E. L. Cussler and P. J. Dunlop, *J. Phys. Chem.*, **70**, 1880 (1966).

In conclusion, this study shows that diffusivity data accurate to 3% or less can be obtained from the wedge interferometer. Further refinements could conceivably decrease the magnitude of the error. However, there are several steps in a wedge diffusion experiment which should be carefully checked, and the results of some previous studies are open to question since some of the

potential sources of error have apparently been overlooked. Finally, the new cell design presented here makes it much simpler to perform accurate diffusion measurements. It is hoped that future work, possibly on methods to extrapolate the data to infinite time, will make the wedge interferometer more accurate than this investigation has shown it to be.

## The Entropies of the Hydrates of Sodium Hydroxide. II.

### Low-Temperature Heat Capacities and Heats of Fusion of $\text{NaOH} \cdot 2\text{H}_2\text{O}$ and $\text{NaOH} \cdot 3.5\text{H}_2\text{O}^1$

by P. R. Siemens and W. F. Giauque

*Low Temperature Laboratory, Departments of Chemistry and Chemical Engineering,  
University of California, Berkeley, California 94720 (Received July 19, 1968)*

The heat capacity of  $\text{NaOH} \cdot 2\text{H}_2\text{O}$  has been measured from 12 to 345°K. It has a peritectic point with  $\text{NaOH} \cdot \text{H}_2\text{O}$  and solution at  $285.73 \pm 0.02^\circ\text{K}$ . Its heat of fusion was found to be  $3859 \pm 12$  cal/mol at its unstable melting point,  $286.5^\circ\text{K}$ . The heat capacity of  $\text{NaOH} \cdot 3.5\text{H}_2\text{O}$  has been measured from 12 to 300°K. Its heat of fusion was found to be  $5380 \pm 7$  cal/mol at its melting point,  $288.53 \pm 0.01^\circ\text{K}$ . Using the third-law entropy value of Murch and Giauque for  $\text{NaOH}$  as a reference and combining it with available free energy and enthalpy data, the entropy of  $\text{NaOH} \cdot 2\text{H}_2\text{O}$  was calculated to be 46.86 gibbs/mol at 298.15°K, in agreement with the value 46.84 gibbs/mol obtained from  $\int C_p d \ln T$ . Similarly the entropy value for  $\text{NaOH} \cdot 3.5\text{H}_2\text{O}$  calculated from data at ordinary temperatures, 68.44 gibbs/mol, agrees with the value 68.35 gibbs/mol from  $\int C_p d \ln T$  at 298.15°K. The entropies of  $\text{NaOH} \cdot 3\text{H}_2\text{O}$ ,  $\text{NaOH} \cdot 4\text{H}_2\text{O}$ ,  $\text{NaOH} \cdot 5\text{H}_2\text{O}$ , and  $\text{NaOH} \cdot 7\text{H}_2\text{O}$  were found to be 60.99, 76.17, 92.27, and 125.80 gibbs/mol, respectively, at 298.15°K. The free energy and enthalpy changes accompanying hydration of sodium hydroxide have been summarized for all of the hydrates. The thermodynamic properties of  $\text{NaOH} \cdot 2\text{H}_2\text{O}$  and  $\text{NaOH} \cdot 3.5\text{H}_2\text{O}$  have been tabulated. The solubility of  $\text{NaOH} \cdot \text{H}_2\text{O}$  has been measured as  $52.208 \pm 0.003$  wt %  $\text{NaOH}$  or  $\text{NaOH} \cdot (2.0324 \pm 0.0004)\text{H}_2\text{O}$  at 298.15°K.

The freezing point-solubility curves of the sodium hydroxide-water system were investigated by Pickering.<sup>2</sup> He made measurements on the hydrates  $\text{NaOH} \cdot \text{H}_2\text{O}$ ,  $\text{NaOH} \cdot 2\text{H}_2\text{O}$ ,  $\text{NaOH} \cdot 3\text{H}_2\text{O}$ ,  $\text{NaOH} \cdot 3.5\text{H}_2\text{O}$ ,  $\alpha\text{-NaOH} \cdot 4\text{H}_2\text{O}$ ,  $\beta\text{-NaOH} \cdot 4\text{H}_2\text{O}$ ,  $\text{NaOH} \cdot 5\text{H}_2\text{O}$ , and  $\text{NaOH} \cdot 7\text{H}_2\text{O}$ . Of these only  $\text{NaOH} \cdot \text{H}_2\text{O}$  and  $\text{NaOH} \cdot 3.5\text{H}_2\text{O}$  have thermodynamically stable melting points. However, aqueous sodium hydroxide solutions supercool rather easily so that the other hydrates may be obtained by suitable control of temperature, concentration, and the patience of the experimenter.

Murch and Giauque<sup>3</sup> measured the low-temperature heat capacities and heats of solution of anhydrous  $\text{NaOH}$  and  $\text{NaOH} \cdot \text{H}_2\text{O}$ . They also investigated the heats of solution of various compositions of the solid mixtures between  $\text{NaOH}$  and  $\text{NaOH} \cdot \text{H}_2\text{O}$ , partly to dispose of various uncertain suggestions that  $\text{NaOH} \cdot 1/2\text{-}$

$\text{H}_2\text{O}$  and  $\text{NaOH} \cdot 2/3\text{H}_2\text{O}$  exist. Such suggestions were based on similar but less accurate data and it was concluded that no evidence for these fractional hydrates exists. This conclusion was reinforced by Brodale and Giauque,<sup>4</sup> who investigated the freezing point-solubility curve for the region  $\text{NaOH}-\text{NaOH} \cdot \text{H}_2\text{O}$ . Murch and Giauque<sup>3</sup> combined their calorimetric data with measurements of Baxter and Starkweather<sup>5</sup> on the dissociation pressure over  $\text{NaOH}-\text{NaOH} \cdot \text{H}_2\text{O}$  and used the

(1) This work was supported in part by National Science Foundation Grant GP-8137.

(2) S. U. Pickering, *J. Chem. Soc.*, 890 (1893).

(3) L. E. Murch and W. F. Giauque, *J. Phys. Chem.*, **66**, 2052 (1962).

(4) G. E. Brodale and W. F. Giauque, *ibid.*, **66**, 2051 (1962).

(5) P. Baxter and H. W. Starkweather, *J. Amer. Chem. Soc.*, **38**, 2038 (1916).

third law of thermodynamics to reach the conclusion that  $\text{NaOH}\cdot\text{H}_2\text{O}$  approached zero entropy at low temperatures (nuclear spin contributions excepted as conventional).

The present work uses the known entropy of  $\text{NaOH}$  as an anchor for use of available free energy and heat of solution data on the aqueous solutions of sodium hydroxide to calculate the entropies of all of the hydrates at 298.15°K. This has been done. With these entropy values for reference, low-temperature heat capacity measurements on any sodium hydroxide hydrate should decide whether or not it approaches a state of perfect order at limiting low temperatures. The present work includes low-temperature heat capacity measurements on  $\text{NaOH}\cdot 2\text{H}_2\text{O}$  and  $\text{NaOH}\cdot 3.5\text{H}_2\text{O}$  and reaches the conclusion that each of these substances approaches zero entropy at limiting low temperatures.

*Low-Temperature Calorimeter.* The calorimeter used has been described by Murch and Giauque.<sup>3</sup> Briefly, it is made of gold 1-mm thick, with a length of 11.5 cm and a 4.2-cm o.d. There are eight radial vanes and an axial well, attached to the bottom, to contain a standard platinum resistance thermometer. The outer wall of the calorimeter is wound with a gold thermometer-heater. The calorimeter has the laboratory designation gold calorimeter VI. The Leeds and Northrup strain-free platinum resistance thermometer, No. 1215-333, had been calibrated at the Bureau of Standards. After the investigation of each hydrate it was checked at the ice point and found to be 0.03° high each time. Appropriate corrections were made; 1 cal (defined) was taken as 4.1840 J (absolute) and 0°C = 273.15°K.

*Preparation and Analysis of the Samples.* The sodium hydroxide was prepared from Baker and Adamson reagent grade metallic sodium which contains less than 0.01 mol % of impurities. The reaction was controlled by passing humidified  $\text{CO}_2$ -free nitrogen through the gas-tight glove box used in connection with the preparation and transfer of the samples. The preparation was essentially the same as that described by Murch and Giauque.<sup>3</sup> Weight buret titration with sulfuric acid, standardized as a constant boiling solution as described by Kunzler,<sup>6</sup> was used for analyses. The carbonate, which was less than 0.01 mol %, was determined by precipitation of  $\text{BaCO}_3$  followed by centrifuging and visual comparison with reference standards as described previously.<sup>3</sup> Difficulty in keeping the  $\text{NaOH}$  solutions relatively free of impurity over long periods made it desirable to repeat the reaction process for each of the three samples used.

The product of the original reaction, which was collected in a platinum dish, had an approximate concentration of  $\text{NaOH}\cdot 1.3\text{H}_2\text{O}$ . It was diluted with  $\text{CO}_2$ -free water to the desired concentrations in Pyrex flasks after an investigation to make certain that the glass would not introduce an amount of impurity that could

not be tolerated. The flasks used for the calorimetric samples were treated with concentrated  $\text{NaOH}$  solutions for about 1 month prior to testing. Periodic cleaning, drying, and weighing over a period of 61 days showed that the loss in weight was about  $5 \times 10^{-3}$  mg/cm<sup>2</sup> day or 1.8 mg/day for a 500-ml flask. The rate was essentially the same over the concentration range of the present work.

In anticipation of later work a test was run on Hastelloy C alloy.<sup>7</sup> A sample, held in  $\text{NaOH}\cdot 2\text{H}_2\text{O}$  for 2 months at 45–47°, lost only 0.4 mg from 18.6-cm<sup>2</sup> surface.

The calorimeter was filled with 192.459 g of "NaOH·2H<sub>2</sub>O" by means of a weight buret in the glove box which was maintained at 30–35° to prevent crystallization. Analysis gave the result  $\text{NaOH}\cdot 1.9997\text{H}_2\text{O}$ , with 0.007 mol % carbonate.

In the later work with  $\text{NaOH}\cdot 3.5\text{H}_2\text{O}$ , which was easily crystallized, it was possible to obtain some purification by recrystallization. A 452-g sample of  $\text{NaOH}\cdot (3.500 \pm 0.005)\text{H}_2\text{O}$  was prepared by dilution. With some 90–95% of the material crystallized in large, well-formed crystals, the liquid portion was removed. All but a few seed crystals were then melted and the process was repeated three times. The amounts removed were 43, 20, 20, and 23 g, respectively, over a period of 33 hr. A 175.600-g portion of the "NaOH·3.5H<sub>2</sub>O" sample, from the melted crystals, was run into the calorimeter from a weight buret. Analysis of the samples gave the result  $\text{NaOH}\cdot (3.4973 \pm 0.0006)\text{H}_2\text{O}$ , which we were not inclined to accept because the samples were taken in the completely dry glove box, which was a mistake, since the nitrogen atmosphere could easily have been brought into approximate equilibrium with the solution, which has a vapor pressure of 5.265 torr at 25°. Other procedures also caused a short delay in capping the samples. In this situation it was decided to use a calorimetric analysis instead of the above result. The analysis for carbonate gave 0.005 mol %, which of course was not affected by a small loss of water.

During later heat capacity measurements on the "NaOH·3.5H<sub>2</sub>O" a premelting of 1.8 cal/mol occurred below 280.5°K. This can be attributed to either the  $\alpha\text{-NaOH}\cdot 4\text{H}_2\text{O}-\text{NaOH}\cdot 3.5\text{H}_2\text{O}$  solution peritectic point (excess water) or to the  $\text{NaOH}\cdot 2\text{H}_2\text{O}-\text{NaOH}\cdot 3.5\text{H}_2\text{O}$  eutectic point (deficient water), each of which has approximately the same temperature. In either case the 1.8 cal/mol indicates that the  $\text{NaOH}\cdot 3.5\text{H}_2\text{O}$  was a very close approximation of the composition, and rough estimates of the heat effects at the above points lead us to estimate the purity of this recrystallized sample of hydrate as  $\text{NaOH}\cdot (3.5000 \pm 0.0003)\text{H}_2\text{O}$ . If both meltings occurred, which of course would be possible if some concentration displacement was present, the

(6) J. E. Kunzler, *Anal. Chem.*, **25**, 93 (1953).

(7) Union Carbide Stellite Co., Kokomo, Ind.

0.0003H<sub>2</sub>O would be further reduced over-all. During the later determination of the melting point the pre-melting data indicated a liquid-soluble-solid-insoluble impurity of 0.018 mol % for the recrystallized sample.

A similar technique was used for determining the composition of the "NaOH·2H<sub>2</sub>O" calorimetrically. After holding the sample near the peritectic temperature for about 2 weeks, with several partial meltings and recrystallizations, an eutectic melting of  $4.7 \pm 1.2$  cal/mol of NaOH·2H<sub>2</sub>O was observed below 278°K, the NaOH·2H<sub>2</sub>O-NaOH·3.5H<sub>2</sub>O eutectic temperature. Taking the eutectic composition as 45.4 wt % from Pickering,<sup>2</sup> our later heats of fusion of NaOH·2H<sub>2</sub>O and NaOH·3.5H<sub>2</sub>O, and heats of solution and heat capacities from Bertetti and McCabe,<sup>8,9</sup> we determined, using a sufficiently accurate estimate of the eutectic heat of fusion, the composition of the sample to be NaOH·2.0007H<sub>2</sub>O. We believe this to be more accurate than the sample analyses which gave NaOH·1.9997H<sub>2</sub>O, since some water was probably also lost in sampling this material in the dry glove box. However, the agreement is such that the composition has been taken as NaOH·2H<sub>2</sub>O exactly, within the limits of error. The estimate of impurity may be made by adding 0.007 mol % carbonate, 0.01 mol % from the sodium metal, and 0.013 "mol %" from the glass, for a total of some 0.03 mol %.

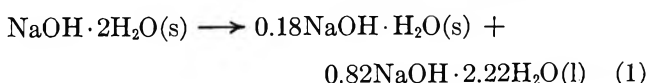
The unoccupied space in the calorimeter was filled with helium at 1 atm in the case of each hydrate.

*Heat Capacity of NaOH·2H<sub>2</sub>O.* Obtaining a crystalline sample of sodium hydroxide dihydrate is complicated by the fact that it forms a peritectic with the monohydrate and the equilibrium solution. On cooling, a liquid with the composition NaOH·2H<sub>2</sub>O should split into solid NaOH·H<sub>2</sub>O and solution, with reconstitution to form pure solid dihydrate when cooled to the peritectic temperature. This is quite impracticable within a calorimeter since the monohydrate sinks to the bottom, leaving the diluted residual solution in the upper portion. This happened during the first crystallization of the dihydrate, and it was necessary to stir the liquid to restore a uniform concentration. This can ordinarily be done by supplying heat to the lower part of a calorimeter to produce convection in the liquefied sample. However, the calorimeter had been built to measure solids and the gold thermometer-heater extended over nearly the entire length without a tap to enable use of a lower section. After 2 months of alternately heating and cooling the calorimeter failed to produce a uniform concentration. The calorimeter was then removed and a heat lamp used to obtain sufficient unsymmetrical heating to provide the necessary convection over 12–15-day periods for the two occasions when this was necessary. The calorimeter could not be stirred by shaking it because the solution would have made contact with the soldered closure at the top.

Fortunately sodium hydroxide solutions, like most substances with OH groups, supercool readily. Thus the calorimeter could be cooled well below the peritectic temperature before any crystallization occurred. In order to cool the well-stirred solution as rapidly as possible, the evacuated apparatus was surrounded by liquid nitrogen while the calorimeter was heated. Radiation cooled the heavy metal block which surrounded the calorimeter. When the block temperature reached about 170°K, the vacuum was broken with hydrogen and the calorimeter heater was turned off. A period of 12 min was required to cool the calorimeter from 300–302 to 255–258°, at which point crystallization began. It was complete in 9–10 min while the temperature remained below 273°K, some 12° below the peritectic temperature. There was some cooling curve evidence that a small amount of monohydrate had been formed and this was supported by some 200 cal/mol of heat evolution when the calorimeter was heated to 279.9°K, and later measurements indicated a 16.5-cal/mol melting at the NaOH·2H<sub>2</sub>O-NaOH·3.5H<sub>2</sub>O eutectic. The heat evolution was evidently due to the reconstitution of NaOH·H<sub>2</sub>O with solution which did not have much chance to separate owing to the rapidity of the crystallization. The sample was then held near the peritectic temperature for 2 weeks with alternate heating and cooling to complete the reconstitution. The eutectic melting was then found to be  $4.7 \pm 1.2$  cal/mol, a value which was repeated for a later recrystallization and which was evidently an equilibrium value. This corresponds to NaOH·(2.0007 ± 0.0002)H<sub>2</sub>O.

The heat capacity measurements on the above preparation are given in Table I. In order to obtain the heat capacity of the liquid before any crystallization occurred, measurements of series I were made over the range 300–328°K. These measurements permitted a reliable extrapolation through the 10° supercooled region to the unstable melting point of NaOH·2H<sub>2</sub>O.

*Heat of Fusion of NaOH·2H<sub>2</sub>O.* The heat of fusion of NaOH·2H<sub>2</sub>O is complicated by the fact that it decomposes as a peritectic to give approximately



Heat input must be continued until the higher melting NaOH·H<sub>2</sub>O is also liquefied. However, during the process at the peritectic temperature the crystals of NaOH·H<sub>2</sub>O sink toward the bottom of the calorimeter. Later melting of the monohydrate near the bottom leads to a situation in which the liquid near the bottom part of the calorimeter is more concentrated than that in the upper portion. Mixing the several concentrations will evolve heat, fortunately, a very small amount,

(8) J. W. Bertetti and W. L. McCabe, *Ind. Eng. Chem.*, **28**, 247 (1936).

(9) J. W. Bertetti and W. L. McCabe, *ibid.*, **28**, 375 (1936).

**Table I:** Heat Capacities of  $\text{NaOH}\cdot 2\text{H}_2\text{O}$  (Experimental)<sup>a</sup>

$T, ^\circ\text{K}$	$C_p$	$T, ^\circ\text{K}$	$C_p$	$T, ^\circ\text{K}$	$C_p$
Series 1		37.737	3.417	171.095	20.626
303.970	57.093 <sup>b</sup>	41.425	4.094	177.675	21.126
310.846	57.025 <sup>b</sup>	45.405	4.842	184.469	21.671
317.726	56.831 <sup>b</sup>	49.891	5.691	191.932	22.201
324.367	56.831 <sup>b</sup>	54.821	6.600	199.231	22.710
		60.620	7.682	206.424	23.236
Series 2		66.916	8.822	213.539	23.742
12.619 <sup>d</sup>	0.182	73.676	9.936	220.439	24.221
11.997	0.156	80.171	10.963	227.611	24.740
13.438	0.224	85.775	11.822	235.108	25.237
14.788	0.305	93.043	12.837	242.452	25.717
16.203	0.416	100.843	13.835	242.411	25.745
17.874	0.543	107.223	14.679	249.635	26.239
19.669	0.710	114.052	15.371	256.831	26.717
22.021	0.960	121.140	16.152	263.900	27.196
24.127	1.209	128.492	16.905	270.109	27.712
25.547	1.445 <sup>c</sup>	135.636	17.604	276.745	29.002
26.623	1.563	142.736	18.260		
28.348	1.824	150.016	18.895	Melted	
31.364	2.316	157.045	19.495	335.806	56.587
34.463	2.849	164.069	20.064	342.351	56.551

<sup>a</sup> Units of  $C_p$  are gibbs per mole (1 gibbs = 1 cal (defined)/deg (defined); the molecular weight of  $\text{NaOH}\cdot 2\text{H}_2\text{O}$  is 76.028.

<sup>b</sup> Measurements were made on the liquid before any crystallization was allowed to occur. <sup>c</sup> Not used in drawing smoothed curve, 2.8% high. <sup>d</sup> Sample recooled and series 2 restarted.

which must be evaluated and subtracted from the heat input before correcting for  $\int C_p dT$  to obtain the heat of fusion of the dihydrate.

One way to do this would be to stop heat input just above the peritectic temperature and wait until the  $\text{NaOH}\cdot \text{H}_2\text{O}$  settled into a rather compact layer at the bottom. Further heat input would then lead to a liquid layer which would contain about 0.18 mol of liquid near the concentration of the monohydrate at the bottom with some 0.82 mol of NaOH in the peritectic liquid at the top. Since the heat would come primarily from above, there should be little mixing. The mixing heat could then be estimated. We decided against the above procedure in this case since it would have involved heating the calorimeter above the melting point of  $\text{NaOH}\cdot \text{H}_2\text{O}$ ,  $338.25^\circ\text{K}$ ,<sup>3</sup> with increased heat leak correction.

It was found that continuous heating from below the peritectic temperature to about  $328^\circ\text{K}$  completed the melting. In order to find the correction for the concentration dislocation which accompanied the process, visual observation of the melting process was carried out in Pyrex glass tubes. A sample of  $\text{NaOH}\cdot 2\text{H}_2\text{O}$  containing less than 0.1%  $\text{Na}_2\text{CO}_3$  was crystallized in a cylinder of height comparable with the liquid in the calorimeter. After the  $\text{NaOH}\cdot \text{H}_2\text{O}(s)$  was formed from the decomposition of the  $\text{NaOH}\cdot 2\text{H}_2\text{O}$ , it stayed in place, with little or no settling until a temperature of  $296^\circ\text{K}$  had been reached. Above  $296^\circ\text{K}$  settling was

rapid, and by  $300^\circ\text{K}$  all of the solid that remained was contained in a bottom section which was 20% of the total sample height. As heating continued above  $300^\circ\text{K}$ , the  $\text{NaOH}\cdot \text{H}_2\text{O}$  continued to settle and melt until the process was complete below  $330^\circ\text{K}$ .

It was then assumed that the composition of the upper 80% by volume was  $\text{NaOH}\cdot 2.066\text{H}_2\text{O}(l)$ , estimated from the solubility curve at  $296^\circ\text{K}$ , and that the average composition of the bottom 20 vol % was  $\text{NaOH}\cdot 1.761\text{H}_2\text{O}$ . In order to calculate the heat of mixing, the composition of the lower layer was assumed to vary linearly from  $\text{NaOH}\cdot 2.066\text{H}_2\text{O}$  to  $\text{NaOH}\cdot 1.455\text{H}_2\text{O}$ , which was consistent with the observed settling and melting above  $300^\circ\text{K}$ . The total mixing correction, based on available density and enthalpy data, was only -7.2 cal/mol, and this was applied to each of the two heats of fusion measured. The small amount of heat at the  $\text{NaOH}\cdot 2\text{H}_2\text{O}-\text{NaOH}\cdot 3.5\text{H}_2\text{O}$  eutectic was added to the total heat input as premelting.

The details of the heat of fusion measurements are summarized in Table II. The accepted value was  $3859 \pm 12$  cal/mol.

**Table II:** Heat of Fusion of  $\text{NaOH}\cdot 2\text{H}_2\text{O}$ <sup>a</sup>

$T_{\text{initial}}, ^\circ\text{K}$	279.548	280.593
$T_{\text{final}}, ^\circ\text{K}$	328.989	332.445
Premelting	6.5	8.6
$\int C_p(s) dT$	198.3	168.8
$\int C_p(l) dT$	2424.0	2620.0
Heat added to substance	6459.9	6653.0
Correction for concentration dislocation	-7.2	-7.2
$\Delta H_F^b$	$3837 \pm 25^c$	$3866 \pm 8$

<sup>a</sup> All heat quantity units are calories per mole. <sup>b</sup> The accepted value is  $\Delta H_F = 3859 \pm 12$  cal/mol (mp  $286.5^\circ\text{K}$ ).

<sup>c</sup> Heat leak correction was three times as large as in the second determination, which was thus given triple weight.

*The Peritectic and Melting Points of  $\text{NaOH}\cdot 2\text{H}_2\text{O}$ .* It is sometimes possible to observe an unstable melting point before peritectic decomposition occurs; however, the melting point was not observed in the present case. By accounting for the amount of heat added, the peritectic temperature was observed as  $285.73 \pm 0.02^\circ\text{K}$ , when about half of the sample was present as peritectic liquid.

From a solubility determination of  $\text{NaOH}\cdot \text{H}_2\text{O}$  at  $25^\circ$ , to be presented below, we have corrected Pickering's<sup>2</sup> peritectic liquid composition to be  $\text{NaOH}\cdot 2.22\text{H}_2\text{O}$ . With this value and the slope of his  $\text{NaOH}\cdot 2\text{H}_2\text{O}$  freezing point-solubility curve, the unstable melting point of  $\text{NaOH}\cdot 2\text{H}_2\text{O}$  has been estimated to be about  $0.8^\circ$  above the peritectic temperature, or  $286.5 \pm 0.2^\circ\text{K}$ .

*Heat Capacity of  $\text{NaOH}\cdot 3.5\text{H}_2\text{O}$ .* Since  $\text{NaOH}\cdot 3.5\text{H}_2\text{O}$  has a stable melting point, it seemed like a straight-

forward matter to crystallize it and measure its heat capacity. However, it did not happen this way. The sample was held some 5–6° below its melting point for 10 days without crystallizing. The temperature was then lowered an additional 10° to 273°K without effect, a somewhat hazardous procedure since either  $\alpha\text{-NaOH}\cdot 4\text{H}_2\text{O}$  or  $\text{NaOH}\cdot 3\text{H}_2\text{O}$  could have appeared under these conditions. The sample was then cooled rapidly in the range below its melting point until crystallization began at 260°K. The temperature rose to 270°K in 5 min and then suddenly to the melting point of  $\text{NaOH}\cdot 3.5\text{H}_2\text{O}$ . It appears certain that at least one other hydrate appeared prior to the crystallization of the  $\text{NaOH}\cdot 3.5\text{H}_2\text{O}$  but that it did not have time to separate sufficiently in the viscous solution to cause more than a very small concentration dislocation. The sample was then melted completely and heated to about 50°. After cooling it was held about 6° below the melting point for 12 hr but again did not crystallize, so that the previous sequence of cooling rapidly to 260°K was repeated with a similar result. Crystallization required about 100 min after the sample heated itself to the melting point. The heat capacities given in Table III were then measured. The premelting ob-

in one location must be balanced by an excess in some other location. As mentioned above, Pickering's phase diagram<sup>2</sup> shows a peritectic between  $\alpha\text{-NaOH}\cdot 4\text{H}_2\text{O}$  and  $\text{NaOH}\cdot 3.5\text{H}_2\text{O}$  and also a eutectic between  $\text{NaOH}\cdot 3.5\text{H}_2\text{O}$  and  $\text{NaOH}\cdot 2\text{H}_2\text{O}$ , each at about 278°K, within his limit of accuracy. An inspection of Pickering's<sup>2</sup> freezing point-solubility diagram, shown as his Figure 1, is almost essential in understanding the possible complications in supercooled  $\text{NaOH}\cdot 3.5\text{H}_2\text{O}$ . There is additional reason to believe that the first stages of crystallization involved the production of one or more crystalline forms which had a greater density than solid  $\text{NaOH}\cdot 3.5\text{H}_2\text{O}$ . This eventually led to the development of strain in the calorimeter at temperatures above 240°K. That the substance was expanding the calorimeter became evident from the behavior of the gold resistance thermometer on its exterior surface during the heat capacity measurements. Its use as a heater was continued, but it was necessary to use the standard platinum resistance thermometer to record the temperature drifts above 240°K. It appears that conversion of the one or more solid hydrates to solid  $\text{NaOH}\cdot 3.5\text{H}_2\text{O}$  involved an increase in volume near 270°K. When the calorimeter was cooled below 240°K the normal shrinkage of the solid with temperature released the strain, which was not observed at lower temperatures. After several repetitions of the crystallization the thermometer-heater eventually broke on the lower part of the calorimeter, but fortunately not until the data essential to the present research had been completed. It seems safe to conclude that both  $\alpha\text{-NaOH}\cdot 4\text{H}_2\text{O}$  and  $\text{NaOH}\cdot 2\text{H}_2\text{O}$  phases were present during the heat capacity measurements on  $\text{NaOH}\cdot 3.5\text{H}_2\text{O}$ . However, the total amounts are estimated to be appreciably less than 0.1%. Since hydrate heat capacities ordinarily average to give nearly the values of intermediates, it would be difficult to conclude that the small concentration dislocation would lead to an error of more than the order of 0.01%.

*Heat of Fusion of  $\text{NaOH}\cdot 3.5\text{H}_2\text{O}$ .* The heat of fusion of  $\text{NaOH}\cdot 3.5\text{H}_2\text{O}$  was much more straightforward than that of  $\text{NaOH}\cdot 2\text{H}_2\text{O}$ . The principal complication was the presence of very small amounts of  $\alpha\text{-NaOH}\cdot 4\text{H}_2\text{O}$  and  $\text{NaOH}\cdot 2\text{H}_2\text{O}$ . All premelting heat due to these substances and any attributable to the small amount of impurity was added to the total heat required for fusion. The details of the two measurements are given in Table IV. The larger amount of premelting during the first run includes not only the heats of peritectic and eutectic melting but also the additional melting of  $\text{NaOH}\cdot 3.5\text{H}_2\text{O}$  along the freezing point curve due to these dislocated regions. Before the second measurement the concentration had become uniform throughout to a high degree, thus the small total premelting heat. The accepted weighted result is taken as  $5380 \pm 7$  cal/mol.

*Melting Point of  $\text{NaOH}\cdot 3.5\text{H}_2\text{O}$ .* Since  $\text{NaOH}\cdot 3.5\text{H}_2\text{O}$  has a stable melting point, it was possible to obtain

Table III: Heat Capacities of  $\text{NaOH}\cdot 3.5\text{H}_2\text{O}$  (Experimental)<sup>a</sup>

T, °K	C <sub>p</sub>	T, °K	C <sub>p</sub>	T, °K	C <sub>p</sub>
Series 1		45.488	6.890	182.452	32.908
285.958	83.982 <sup>b</sup>	49.352	7.965	189.828	33.844
292.097	84.319 <sup>b</sup>	53.713	9.145	197.131	34.756
298.502	84.734 <sup>b</sup>	59.006	10.617	203.840	35.577
		64.912	12.197	210.959	36.451
		70.765	13.651	217.756	37.270
Series 2		76.283	14.983	224.936	38.163
12.810	0.261	82.392	16.441	232.313	39.031
14.371	0.386	89.221	17.932	239.749	39.921
16.030	0.540	96.804	19.482	246.759	40.700
17.697	0.715	104.502	20.979	253.714	41.464 <sup>c</sup>
19.460	0.941	112.757	22.468	258.389	42.027 <sup>c</sup>
21.498	1.236	121.274	23.938	264.214	42.679 <sup>c</sup>
23.710	1.600	129.307	25.269	270.500	43.770 <sup>c</sup>
26.249	2.066	137.028	26.498	277.040	46.329 <sup>c</sup>
29.072	2.698	144.679	27.642	283.460	47.878 <sup>c</sup>
31.837	3.326	152.316	28.746		
34.808	4.063	160.022	29.856		
38.091	4.903	167.791	30.888	Melted	
41.653	5.838	175.287	31.941	296.036	84.709 <sup>c</sup>

<sup>a</sup> Units of C<sub>p</sub> are gibbs per mole. <sup>b</sup> Measurements were made on the liquid before any crystallization occurred. <sup>c</sup> Platinum resistance thermometer used for drifts because of strain in the gold thermometer-heater.

served in the three runs below 280.5°K amounted to 18.6 cal/mol and this was primarily due to some small concentration dislocation. Since the discussion of purity given above gives evidence that the sample was  $\text{NaOH}\cdot(3.5000 \pm 0.003)\text{H}_2\text{O}$ , any deficiency of water

**Table IV:** Heat of Fusion of  $\text{NaOH} \cdot 3.5\text{H}_2\text{O}^a$ 

$T_{\text{initial}}$ , °K	286.535	280.523
$T_{\text{final}}$ , °K	292.893	292.524
Premelting	33.9	1.8
$\int C_p(s) dT$	90.4	360.0
$\int C_p(l) dT$	367.7	336.5
Heat added to substance	5809.6	6065.3
$\Delta H_F^b$	$5385 \pm 6$	$5370 \pm 10^c$

<sup>a</sup> All heat quantity units are calories per mole. <sup>b</sup> The accepted value is  $\Delta H_F = 5380 \pm 7$  cal/mol (mp 288.53 ± 0.01 °K). <sup>c</sup> The increased error is due to uncertain heat leak correction, thus first determination has been given double weight.

an estimate of the impurity, other than an excess of  $\text{H}_2\text{O}$  or  $\text{NaOH}$ , as well as the melting point of the pure substance. As usual this is done by measuring the melting temperature as a function of the fraction melted,  $f$ . A plot of  $T_{\text{obsd}} \text{ vs. } 1/f$  extrapolated to zero gives the melting point for the pure substance. There is one precaution that must be taken in using this procedure, namely, that it should be restricted to less than 50% of the sample melted. The reason for this is that for a high percentage melted the denser solid falls to the bottom of the calorimeter where it melts to give pure liquid. The equilibrium between the pure solid and liquid controls the temperature of the whole calorimeter which rises to the true melting point for a high percentage melted. In effect the operation of gravity leaves the impurity in the upper liquid and purifies the bottom portion. The data are given in Table V. Since the components of  $\text{NaOH} \cdot 3.5\text{H}_2\text{O}$  are in almost exact proportion, the freezing point lowering is due to unrelated impurity and the straight line  $T \text{ vs. } 1/f$  rule is expected to hold. The first three values fall on a straight line within the limit of error and the last two are 0.005 and 0.008°, respectively, above it. They are, however, very close to the straight-line limit, 288.53 ± 0.01 °K, which is taken as the melting point of the pure substance.

*The Thermodynamic Properties of  $\text{NaOH} \cdot 2\text{H}_2\text{O}$  and  $\text{NaOH} \cdot 3.5\text{H}_2\text{O}$ .* The heat capacity data have been used to calculate the thermodynamic properties of  $\text{NaOH} \cdot 2\text{H}_2\text{O}$  and  $\text{NaOH} \cdot 3.5\text{H}_2\text{O}$  on the assumption,

**Table V:** Melting Point of  $\text{NaOH} \cdot 3.5\text{H}_2\text{O}^a$ 

Fraction melted	$T$ , °K
0.106	288.478
0.156	288.493
0.253	288.507
0.491	288.523
0.669	288.529
(∞)	(288.529)

<sup>a</sup> The accepted value is 288.53 ± 0.01 °K.

**Table VI:** Thermodynamic Properties of  $\text{NaOH} \cdot 2\text{H}_2\text{O}^a$ 

$T$ , °K	$C_p$ , °	$S$ , °	$(H^\circ - H_0^\circ)/T$	$-(F^\circ - F_0^\circ)/T$
10	(0.087)	(0.028)	(0.021)	(0.007)
15	0.320	0.101	0.076	0.024
20	0.742	0.247	0.187	0.060
25	1.331	0.472	0.354	0.119
30	2.088	0.780	0.578	0.202
35	2.937	1.165	0.854	0.311
40	3.827	1.615	1.169	0.446
45	4.766	2.119	1.516	0.603
50	5.702	2.670	1.888	0.782
55	6.636	3.257	2.277	0.980
60	7.569	3.875	2.680	1.195
70	9.350	5.178	3.507	1.670
80	10.957	6.533	4.340	2.193
90	12.416	7.909	5.157	2.752
100	13.737	9.287	5.951	3.336
110	14.928	10.653	6.713	3.939
120	16.029	12.000	7.444	4.555
130	17.058	13.324	8.145	5.179
140	18.012	14.623	8.816	5.807
150	18.897	15.896	9.459	6.438
160	19.739	17.143	10.075	7.068
170	20.540	18.364	10.667	7.697
180	21.314	19.560	11.238	8.323
190	22.064	20.733	11.788	8.945
200	22.793	21.883	12.320	9.563
210	23.505	23.012	12.836	10.177
220	24.204	24.122	13.337	10.786
230	24.894	25.213	13.824	11.389
240	25.577	26.287	14.300	11.988
250	26.256	27.345	14.764	12.581
260	26.934	28.388	15.219	13.169
270	27.610	29.417	15.666	13.752
273.15	27.823	29.739	15.805	13.934
280	28.286	30.434	16.104	14.329
285.73	28.673	31.010	16.353	14.658
286.5	28.725	31.088	16.386	14.702
Mp	...	...	...	...
286.5	57.396 <sup>b</sup>	44.557	29.855	14.702
290	57.343 <sup>b</sup>	45.254	30.187	15.067
298.15	57.215 <sup>b</sup>	46.841	30.928	15.914
300	57.186 <sup>b</sup>	47.195	31.090	16.105
310	57.029	49.068	31.929	17.139
320	56.872	50.876	32.711	18.165
330	56.715	52.644	33.461	19.183
340	56.558	54.335	34.143	20.192
350	56.401	55.972	34.781	21.191

<sup>a</sup> Units are gibbs per mole. <sup>b</sup> Supercooled liquid.

later justified, that their entropies approach zero at limiting low temperatures. The data were extrapolated below 12°K by means of plots of  $C_p/T$  vs.  $T^2$ . The smoothed data are given in Tables VI and VII.

*The Entropies of Hydration of the Sodium Hydroxide Hydrates.* The entropies of hydration of all of the sodium hydroxide hydrates can be calculated from free energy and enthalpy data at ordinary temperatures

$$\Delta S = (\Delta H - \Delta F)/T \quad (2)$$

The typical isotherm reaction is



where  $A$  represents the moles of water in the particular hydrate. All of the hydrates are in the form of liquid solutions at 25° except the mono- and dihydrates

$$S(\text{NaOH}\cdot A\text{H}_2\text{O}) = \Delta S(\text{eq 3}) +$$

$$S(\text{NaOH(s)}) + AS(\text{H}_2\text{O(l)}) \quad (4)$$

Before the above equations can be applied the free energies and enthalpies of hydration must be evaluated.

*The Free Energies of Hydration of the Sodium Hydroxide Hydrates.* For the reaction



Table VII: Thermodynamic Properties of  $\text{NaOH}\cdot 3.5\text{H}_2\text{O}^a$

$T, ^\circ\text{K}$	$C_p, ^\circ$	$S, ^\circ$	$(H^\circ - H_0^\circ)/T$	$-(F^\circ - H_0^\circ)/T$
10	(0.132)	(0.044)	(0.033)	(0.011)
15	0.444	0.149	0.111	0.037
20	1.015	0.348	0.260	0.088
25	1.836	0.659	0.490	0.169
30	2.904	1.085	0.800	0.284
35	4.106	1.621	1.185	0.436
40	5.403	2.253	1.631	0.623
45	6.761	2.968	2.125	0.843
50	8.137	3.751	2.657	1.094
55	9.516	4.591	3.218	1.373
60	10.889	5.478	3.800	1.678
70	13.493	7.355	5.002	2.354
80	15.890	9.316	6.215	3.101
90	18.097	11.316	7.414	3.902
100	20.120	13.330	8.585	4.744
110	21.981	15.336	9.719	5.616
120	23.727	17.324	10.815	6.509
130	25.382	19.289	11.872	7.417
140	26.948	21.228	12.894	8.334
150	28.433	23.138	13.881	9.258
160	29.854	25.019	14.835	10.184
170	31.226	26.870	15.759	11.111
180	32.559	28.693	16.655	12.038
190	33.858	30.488	17.527	12.961
200	35.126	32.257	18.375	13.882
210	36.367	34.001	19.202	14.799
220	37.578	35.721	20.010	15.711
230	38.764	37.418	20.300	16.618
240	39.929	39.092	21.573	17.519
250	41.074	40.745	22.330	18.415
260	42.206	42.379	23.073	19.306
270	43.331	43.992	23.802	20.190
273.15	43.686	44.497	24.029	20.468
280	44.457	45.589	24.520	21.069
288.53	45.417	46.937	25.123	21.814
Mp	...	...	...	...
288.53	84.134	65.583	43.770	21.814
290	84.222	66.011	43.974	22.037
298.15	84.708	68.352	45.081	23.271
300	84.819	68.876	45.326	23.550
310	(85.416)	(71.667)	(46.610)	(25.058)
320	(86.013)	(74.389)	(47.832)	(26.557)
330	(86.610)	(77.045)	(48.998)	(28.047)

<sup>a</sup> The units are gibbs per mole.

the data of Murch and Giauque<sup>3</sup> give  $\Delta H_{298.15} = -5519$  cal/mol. Baxter and Starkweather<sup>10</sup> measured the equilibrium pressure of water vapor over the solids NaOH and  $\text{NaOH}\cdot \text{H}_2\text{O}$ . The pressure,  $1.15 \pm 0.01$  torr, at 50°, was large enough to give accuracy. The equation

$$\frac{d(\Delta F/T)}{dT} = - \frac{\Delta H}{T^2} \quad (6)$$

in combination with the free energy change at 323.15°K, the available enthalpy, and heat capacity, gives  $\Delta F_{298.15^\circ\text{K}} = -3036 \pm 5$  cal/mol for eq 5.

The isopiestic data of Stokes<sup>11</sup> on aqueous sodium hydroxide solutions at 25°, from 1.988 to 28.745 M NaOH, against the equilibrium sulfuric acid solutions, which range from 1.673 to 21.650 M  $\text{H}_2\text{SO}_4$ , supply most of the additional information needed. However, the solubility data of Pickering<sup>2</sup> are not accurate enough to give the concentration of the aqueous solution in equilibrium with solid  $\text{NaOH}\cdot \text{H}_2\text{O}$  at 25°. This solubility was measured during the present experiment as follows.

Some of the sodium hydroxide prepared from metallic sodium, as described above, was diluted with  $\text{CO}_2$ -free water until about half the sample was liquid at 25°. About 350 ml of the mixture was placed in a 500-ml round-bottomed Pyrex flask. The flask was attached to a rocker and submerged in a thermostat at 25°. To protect the solution from atmospheric  $\text{CO}_2$  an overpressure of several centimeters of pure nitrogen was maintained over the mixture. Samples were removed by using nitrogen pressure to force the solution to rise into a weight buret. The samples were protected from solid inclusion by means of a sintered-glass filter. Two samples were taken after 9 and 13 days, respectively. The results are summarized in Table VIII.

Sample 2 was analyzed for carbonate, which was found to be present to the extent of 0.014 mol %. Adding this to 0.01 mol % of impurity from the sodium

Table VIII: Solubility of  $\text{NaOH}\cdot \text{H}_2\text{O}$  at  $298.15 \pm 0.01^\circ\text{K}$

Sample	Equilibrium time, days	$A$ (by analysis), <sup>a</sup> mol of $\text{H}_2\text{C}/$ mol of NaOH
1	9	2.0333
1	9	2.0324
1	9	2.0317
2	13	2.0324
2	13	2.0322

<sup>a</sup> The accepted average  $A = 2.0324 \pm 0.0004 \text{H}_2\text{O}$  or  $52.208 \pm 0.003$  wt % NaOH.

(10) P. Baxter and H. W. Starkweather, *J. Amer. Chem. Soc.*, **38**, 2038 (1916).

(11) R. H. Stokes, *ibid.*, **67**, 1689 (1945).

**Table IX:** Corrections to Smoothed Molal Thermodynamic Properties of NaOH and NaOH·H<sub>2</sub>O<sup>a</sup>

Compd	Temp range, °K	<i>C<sub>p</sub></i> <sup>b</sup>	<i>S</i> <sup>b</sup>	( <i>H</i> <sup>°</sup> − <i>H</i> <sub>0</sub> <sup>°</sup> )/ <i>T</i>	−( <i>F</i> <sup>°</sup> − <i>H</i> <sub>0</sub> <sup>°</sup> )/ <i>T</i>	Factor for change in mol wt to <sup>12</sup> C basis
NaOH	15–315	0.002	0.0054(log <i>T</i> ) − 0.0056	(0.0024 − 0.026)/ <i>T</i>	−(0.0054(log <i>T</i> ) − 0.026)/ <i>T</i> + 0.0080	−0.00020 <i>x</i> <sup>c</sup>
NaOH·H <sub>2</sub> O	15–338.25	0.004	0.0093(log <i>T</i> ) − 0.0096	(0.0041 − 0.046)/ <i>T</i>	−(0.0093(log <i>T</i> ) − 0.046)/ <i>T</i> + 0.0137	−0.00016 <i>x</i> <sup>c</sup>

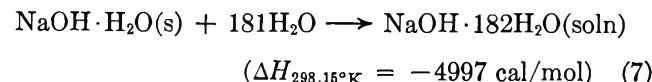
<sup>a</sup> Reference 3. <sup>b</sup> Units are gibbs per mole. <sup>c</sup> *x* represents the values of *C<sub>p</sub>*<sup>°</sup>, *S*<sup>°</sup>, (*H*<sup>°</sup> − *H*<sub>0</sub><sup>°</sup>)/*T*, or (*F*<sup>°</sup> − *H*<sub>0</sub><sup>°</sup>)/*T*.

metal and 0.022 "mol %" estimated as glass dissolved from the flask and the fritted-glass filter, the total impurity was estimated as 0.046%, which should not affect the result beyond the spread of the analyses.

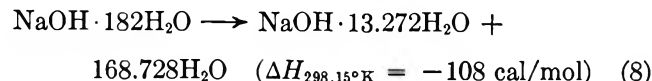
Unstable liquid NaOH·2H<sub>2</sub>O at 25° resulting from the melting of the dihydrate is supersaturated with respect to solid NaOH·H<sub>2</sub>O. However, Stokes<sup>11</sup> isopiestic data require no extrapolation in covering the range between *A* = 2 and the solution *A* = 2.0324, which is in equilibrium with NaOH·H<sub>2</sub>O at 25°, since they extend to *A* = 1.9310 in the supersaturated region.

The tables of Giauque, Hornung, Kunzler, and Rubin,<sup>12</sup> on the thermodynamic properties of aqueous sulfuric acid solutions, include the partial molal free energy of water as a function of acid concentration. These tables were used with the isopiestic data of Stokes<sup>11</sup> on NaOH-H<sub>2</sub>SO<sub>4</sub> solutions to calculate the free energy of hydration for NaOH·2H<sub>2</sub>O, NaOH·3H<sub>2</sub>O, NaOH·3.5H<sub>2</sub>O, NaOH·4H<sub>2</sub>O, NaOH·5H<sub>2</sub>O, and NaOH·7H<sub>2</sub>O at 298.15°K. The resulting values are tabulated later.

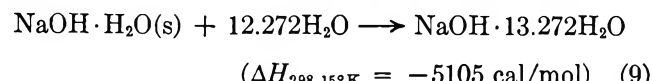
*The Enthalpy of Hydration of NaOH.* The enthalpy of formation of NaOH·H<sub>2</sub>O(s) from NaOH(s) has been quoted as  $\Delta H_{298.15^\circ\text{K}} = -5519 \text{ cal/mol}$ .<sup>3</sup> Murch and Giauque<sup>3</sup> also give a connection with the more dilute solutions by means of the determination



To bring this within connecting range of enthalpy data for the compositions corresponding to several hydrates, the results of Sturtevant<sup>13</sup> were interpolated to give

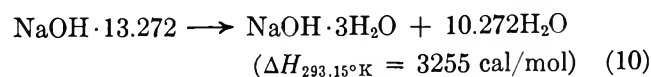


Combining eq 7 and 8 gives



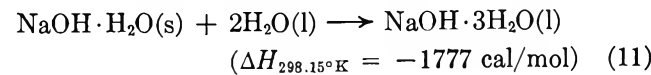
and brings the connection within the range of the

enthalpy and heat capacity data of Bertetti and McCabe.<sup>8,9</sup> The trihydrate may be used as a typical example within the range of Bertetti and McCabe's work.



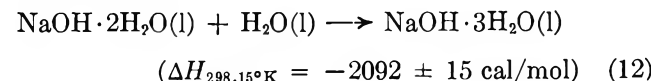
and with the assistance of their heat capacity data  $\Delta H_{298.15^\circ\text{K}} = 3328 \text{ cal/mol}$ .

Adding eq 9 and 10



By means of a similar procedure the data of Bertetti and McCabe<sup>8,9</sup> give the connection between NaOH·H<sub>2</sub>O(s) and all of the other hydrates, except the supersaturated NaOH·2H<sub>2</sub>O, which required more involved considerations.

In order to extrapolate the enthalpy data of Bertetti and McCabe from 48 to 52.609% NaOH·2H<sub>2</sub>O(l) it was desirable to have points, not necessarily highly accurate, in more concentrated solutions to direct the short extrapolation above 48%. Several such guide points were calculated from the data of Wilson and McCabe,<sup>14</sup> with an additional extension to 68.946% NaOH·H<sub>2</sub>O by means of the data of Murch and Giauque.<sup>3</sup> Since the heat of fusion,  $3776 \pm 30 \text{ cal/mol}$ , and the heat capacity of the liquid monohydrate were known,<sup>3</sup> the enthalpy of NaOH·H<sub>2</sub>O as a supercooled liquid at 298.15°K could be calculated as a guide point of the extrapolation of the enthalpy data of Bertetti and McCabe.<sup>8,9</sup> The extrapolation gives



This completes the necessary enthalpy connections between anhydrous NaOH and all of its hydrates.

(12) W. F. Giauque, E. W. Hornung, J. E. Kunzler, and T. R. Rubin, *J. Amer. Chem. Soc.*, **82**, 62 (1960).

(13) J. M. Sturtevant, *ibid.*, **62**, 2276 (1940).

(14) H. R. Wilson and W. L. McCabe, *Ind. Eng. Chem.*, **34**, 555 (1942).

*Comparison of the Entropies of the Sodium Hydroxide Hydrates by Means of the Third Law of Thermodynamics.* Using the third-law value of the entropy of anhydrous NaOH, 15.405 gibbs/mol, obtained by Murch and Giauque,<sup>3</sup> as a reference, the values of the entropies of all of the known hydrates of sodium hydroxide may be calculated from the second law and the enthalpy and free energy data given above. There are two very minor corrections to the results of Murch and Giauque.<sup>3</sup> Their data books indicate that when the heat capacity of the "empty" calorimeter was measured it contained helium which was sealed in to the amount of 1 atm at about 20°. Thus when the heat capacities of NaOH and NaOH·H<sub>2</sub>O were measured, the published results were low by the heat capacity of the helium displaced by the solid. The volume of NaOH was taken as 18.8 ml/mol and that of NaOH·H<sub>2</sub>O as 33.7 ml/mol. The helium corrections for the several properties are given in Table IX. In addition the change in molecular weights in the 1962 table (<sup>12</sup>C scale)<sup>15</sup> reduces the several properties by 0.020% for NaOH and by 0.016% for NaOH·H<sub>2</sub>O. The net result of the two corrections is to increase the entropy of NaOH by 0.005 gibbs/mol and that of NaOH·H<sub>2</sub>O by 0.010 gibbs/mol, each at 298.15°K. These corrections have been applied. The results are collected in Table X, where they are compared with the several values from  $\int C_p d \ln T$  which have been measured. The agreements are all within the limits of accuracy of the data and indicate that there is no disorder in the crystals at limiting low temperatures.

By combining the data in Tables VI and VII for

**Table X:** Hydration of Sodium Hydroxide at 298.15°K<sup>a</sup>  
((NaOH(s) + AH<sub>2</sub>O(l) → NaOH·AH<sub>2</sub>O, S(H<sub>2</sub>O)(l))<sub>298.15°K</sub> = 16.71 gibbs/mol)<sup>b</sup>

A	-ΔH	-ΔF	ΔS	S	
				2nd law	3rd law
O (s)	0	0	0	(15.405)	15.405 <sup>c</sup>
1 (s)	5,519	3036	8.328	23.79	23.78 <sup>c</sup>
2 (l)	5,204	4617	1.969	46.86	46.84 <sup>d</sup>
3 (l)	7,296	5942	4.541	60.99	...
3.5 (l)	8,059	6434	5.450	68.44	68.35
4 (l)	8,651	6839	6.077	76.17	...
5 (l)	9,443	7451	6.681	92.27	...
7 (l)	10,175	8214	6.577	125.80	...

<sup>a</sup> H and F are in calories per mole; S is in gibbs per mole; A is the moles of H<sub>2</sub>O per mole of NaOH. <sup>b</sup> Reference 12. <sup>c</sup> Measurements from Murch and Giauque.<sup>3</sup> <sup>d</sup> Liquid NaOH·2H<sub>2</sub>O is supersaturated with respect to NaOH·H<sub>2</sub>O(s) at 298.15°K. <sup>e</sup> It may be possible to obtain separate third-law values from α-NaOH·4H<sub>2</sub>O and β-NaOH·4H<sub>2</sub>O.

NaOH·2H<sub>2</sub>O and NaOH·3.5H<sub>2</sub>O and the similar table of Murch and Giauque<sup>3</sup> for NaOH·H<sub>2</sub>O with the data in Table X, it may be shown that solid NaOH·2H<sub>2</sub>O is thermodynamically stable with respect to decomposition into the solids NaOH·H<sub>2</sub>O and NaOH·3.5H<sub>2</sub>O at all temperatures.

*Acknowledgment.* We thank J. A. Duisman and R. H. Lamoreaux for assistance with the experimental measurements.

(15) A. E. Cameron and E. Wickers, *J. Amer. Chem. Soc.*, **84**, 4175 (1962).

# Transport Processes in Hydrogen-Bonding Solvents. II. Conductance of Tetraalkylammonium Salts in 1-Butanol and 1-Pentanol at 25°

by D. Fennell Evans<sup>1</sup> and Philip Gardam

*Department of Chemistry, Case Western Reserve University, Cleveland Ohio 44106 (Received July 24, 1968)*

Conductance measurements are reported for  $\text{Me}_4\text{NCl}$ ,  $\text{Bu}_4\text{NCl}$ ,  $\text{Me}_4\text{NBr}$ ,  $\text{Et}_4\text{NBr}$ ,  $\text{Pr}_4\text{NBr}$ ,  $\text{Bu}_4\text{NBr}$ ,  $\text{Et}_4\text{NI}$ ,  $\text{Pr}_4\text{NI}$ ,  $\text{Bu}_4\text{NI}$ ,  $i\text{-Am}_3\text{BuNI}$ ,  $\text{Hept}_4\text{NI}$ , and  $\text{Bu}_4\text{NClO}_4$  in 1-butanol and  $\text{Bu}_4\text{NBr}$ ,  $\text{Bu}_4\text{NI}$ ,  $i\text{-Am}_3\text{BuNI}$ , and  $\text{Hept}_4\text{NI}$  in 1-pentanol at 25°. The data were analyzed by the Fuoss-Onsager equation. The extent of ionic association was found to increase with increasing size of the anion and is discussed in terms of a multiple-step association process. The variation of ionic mobilities in methanol, ethanol, 1-propanol, and 1-butanol is compared to that predicted by the Zwanzig equation and found to agree only in a qualitative manner.

## Introduction

This is the second in a series of papers discussing the transport properties of electrolytes in hydrogen-bonded solvents. In the first paper,<sup>2</sup> the conductances of the tetraalkylammonium salts in ethanol and propanol at 25° were reported. Contrary to the predictions of electrostatic theory, ionic association of these salts was found to increase with increasing anion size. In an effort to obtain further information about this homologous series of solvents, we have extended the measurements to the higher alcohols 1-butanol and 1-pentanol.

## Experimental Section

The tetraalkylammonium salts were purified by recrystallization. The solvents used in the recrystallization and the temperature at which the salts were dried have been given elsewhere.<sup>2-4</sup>

Conductivity grade 1-butanol and 1-pentanol were prepared by drying Fisher reagent grade alcohol over calcium oxide for several days and then distilling from a fresh batch of calcium oxide. The distillations were carried out in a 1.3-m Stedman column under nitrogen, and only the middle fraction was retained. The densities of butanol and pentanol at 25° were found to be 0.80576 and 0.81096, respectively. These values are in agreement with those given in the literature, 0.80572 for butanol<sup>5</sup> and 0.8110 for pentanol.<sup>5</sup> The viscosities of butanol and pentanol, 0.02589 and 0.03476 P, respectively, were determined in two Cannon Ubbelohde viscometers.

The dielectric constants were measured in the all-glass platinum cells described by Kay and Vidulich.<sup>6</sup> The value of  $\epsilon_{25}$  17.45 found for butanol is in agreement with that given by Dannhauser and Bahe,<sup>7</sup>  $\epsilon_{25}$  17.51. The value of  $\epsilon_{25}$  15.04 was determined for pentanol.

The electrical equipment, conductance cells, and techniques were similar to those reported previously.<sup>2-4,8</sup> Briefly, the measurements were carried out

in Kraus-type conductance cells and increments of salt were added to the cell in small Pyrex cups with the aid of the Hawes-Kay cup-dropping device,<sup>9</sup> except for runs II for  $\text{Me}_4\text{NCl}$  and  $\text{Bu}_4\text{NCl}$ . Because of the extreme hygroscopic nature of these salts and the difficulties in weighing (with sufficient accuracy) the small amounts required, the results obtained with the cup-dropping device were checked using a Kimax weight buret with Teflon stopcock. The cell was initially filled with solvent to a level above that of the tubes which connect the electrode compartments to the erlenmeyer flask. A concentrated stock solution was added to the conductance cell from the weight buret in small increments. The manipulations were held to a minimum and were accomplished rapidly to minimize contamination by atmospheric moisture.<sup>10</sup>

## Results

The measured equivalent conductances and the corresponding electrolyte concentrations in moles per liter are shown in Table I for 1-butanol and Table II for 1-pentanol. Also given is  $A$ , the density increment used to calculate the volume concentration. These increments were obtained by density measurements on the most concentrated solutions used in the conductance

- (1) To whom all correspondence should be directed.
- (2) D. F. Evans and P. Gardam, *J. Phys. Chem.*, **72**, 3281 (1968).
- (3) D. F. Evans, C. Zawoyski, and R. L. Kay, *ibid.*, **69**, 3878 (1965).
- (4) R. L. Kay, C. Zawoyski, and D. F. Evans, *ibid.*, **69**, 4208 (1965).
- (5) J. Timmermans, "Physico-chemical Constants of Pure Organic Compounds," Elsevier Publishing Co., New York, N. Y., 1950.
- (6) G. A. Vidulich and R. L. Kay, *Rev. Sci. Instrum.*, **37**, 1662 (1966). We wish to thank Professor Kay for the use of the facilities of his laboratory and for his help in carrying out the measurements.
- (7) W. Dannhauser and L. W. Bahe, *J. Chem. Phys.*, **40**, 3058 (1964).
- (8) C. G. Swain and D. F. Evans, *J. Amer. Chem. Soc.*, **88**, 383 (1966).
- (9) J. L. Hawes and R. L. Kay, *J. Phys. Chem.*, **69**, 2420 (1965).
- (10) T. L. Broadwater, Ph.D. Thesis, Case Western Reserve University, 1968.

**Table I:** Equivalent Conductances in Butanol at 25°

$10^4 C$	$\Lambda$	$10^4 C$	$\Lambda$	$10^4 C$	$\Lambda$	$10^4 C$	$\Lambda$
$\text{Me}_2\text{NCl}$		$\text{Me}_2\text{NBr}$		$\text{Et}_4\text{NI}$		$\text{Hept}_4\text{NI}$	
$A = 0.03$		$A = 0.07$		$A = 0.11$		$A = 0.10$	
Run I							
2.981	11.953	3.231	12.070	3.616	14.132	2.636	11.875
8.062	9.262	5.196	10.793	7.757	11.957	6.244	10.041
15.160	7.071	7.276	9.861	12.232	10.600	9.887	8.959
22.561	6.721	9.657	9.081	17.105	9.660	13.539	8.230
30.347	6.085	12.455	8.412	22.124	8.969	17.276	7.677
38.750	5.597	15.054	7.933	27.843	8.361	20.968	7.249
48.113	5.194	17.843	7.517	33.942	7.868	25.152	6.858
Run II							
2.030	12.873	$\text{Et}_4\text{NBr}$		$\text{Pr}_4\text{NI}$		$\text{Bu}_4\text{NClO}_4$	
5.044	10.535	$A = 0.07$		$A = 0.10$		$A = 0.08$	
8.484	9.140	4.285	13.082	4.756	12.677	3.435	12.623
12.262	8.188	7.894	11.411	9.885	10.736	7.852	10.193
18.841	7.148	12.026	10.245	14.855	9.643	13.369	8.689
24.157	6.586	17.386	9.250	20.229	8.843	18.951	7.766
31.723	6.008	22.006	8.639	26.193	8.197	25.225	7.054
34.988	5.812	27.057	8.124	32.341	7.692	32.493	6.466
		32.571	7.676	38.834	7.265	40.089	6.009
		39.141	7.255	45.989	6.897	48.697	5.607
$\text{Bu}_4\text{NCl}$		$\text{Pr}_4\text{NBr}$		$\text{Bu}_4\text{NI}$			
$A = 0.05$		$A = 0.08$		$A = 0.10$			
Run I		3.724	12.867	3.548	12.620		
2.400	12.870	7.784	11.163	7.286	10.859		
7.136	10.913	12.266	10.037	11.103	9.797		
12.106	9.803	16.958	9.237	15.940	8.878		
17.075	9.061	22.196	8.588	20.684	8.238		
22.530	8.463	27.560	8.081	26.126	7.684		
27.472	8.039	33.276	7.654	31.521	7.256		
33.165	7.650	40.103	7.245	37.135	6.896		
39.864	7.276						
Run II		$\text{Bu}_4\text{NBr}$		$i\text{-Am}_3\text{BuNI}$			
1.215	13.828	$A = 0.07$		$A = 0.12$			
3.408	12.398	2.712	12.814	3.281	12.398		
6.343	11.235	6.375	11.080	7.240	10.455		
11.128	10.055	10.153	10.007	11.496	9.277		
15.614	9.313	14.385	9.190	16.684	8.357		
20.931	8.678	18.741	8.578	21.943	7.705		
26.216	8.194	23.731	8.042	27.475	7.193		
30.077	7.903	29.225	7.582	33.583	6.752		
		35.041	7.195	40.325	6.369		

measurements and were assumed to follow the relationship  $d = d_0 + A\bar{m}$ , where  $\bar{m}$  represents the moles of salt per kilogram of solution.

The data were analyzed with the Fuoss-Onsager equation in the form<sup>9,11</sup>

$$\Lambda = \Lambda_0 - S(c\gamma)^{1/2} - Ec\gamma \ln(c\gamma) + (J - BA\gamma)c\gamma - K_A f^2 c\gamma\Lambda \quad (1)$$

The value of  $B$ , which corrects for the effect of the added electrolyte on the viscosity of the solvent, was set equal to zero. The value of  $B$  does not affect the limiting conductance or the association constant. In all nonaqueous solvents where the  $B$  correction has been determined, the value of  $\bar{d}$  was increased by the con-

stant amount of  $0.2 \text{ \AA}$  for all of the tetraalkylammonium halides.

Shown in Table III are the parameters obtained from the Fuoss-Onsager equation by a least-squares computer program.<sup>12</sup> Included are the standard deviations in each parameter and the standard deviation,  $\sigma\Lambda$ , of the individual points.

Some indication of the precision of the measurement can be obtained from the iodide — bromide difference of  $1.07 \pm 0.04$  for the  $\text{Et}_4\text{N}^+$ ,  $\text{Pr}_4\text{N}^+$ , and  $\text{Bu}_4\text{N}^+$  salts. The corresponding bromide — chloride difference for the

(11) R. M. Fuoss and F. Accascina, "Electrolyte Conductance," Interscience Publishers, New York, N. Y., 1959.

(12) R. L. Kay, *J. Amer. Chem. Soc.*, **82**, 2099 (1960).

**Table II:** Equivalent Conductances in Pentanol at 25°

$10^4 C$	$\Delta$	$10^4 C$	$\Delta$
$Bu_4NBr$			Hept <sub>4</sub> NI
$A = 0.07$			$A = 0.11$
3.350	7.188	2.326	7.077
7.615	5.780	5.748	5.588
12.397	4.998	9.154	4.848
18.228	4.416	12.827	4.354
23.823	4.045	16.574	3.995
29.347	3.774	20.857	3.689
35.108	3.556	25.186	3.455
41.224	3.375	30.032	3.249
$Bu_4NI$			$i\text{-Am}_3BuNI$
$A = 0.09$			$A = 0.10$
3.266	7.329	2.426	7.556
6.698	6.008	5.141	6.231
10.934	5.173	8.943	5.268
15.220	4.643	13.514	4.615
20.647	4.188	18.118	4.181
26.042	3.870	22.746	3.865
31.838	3.613	27.683	3.611
39.861	3.345	34.707	3.339

**Table III:** Conductance Parameters in Butanol and Pentanol at 25°, Calculated from Eq 1

Salt	$\Lambda_0$	$\delta$	$K_A$	$\sigma\Delta$
Butanol				
$Me_4NCl$	$17.61 \pm 0.07$	$6.9 \pm 0.2$	$2270 \pm 30$	0.02
	$17.49 \pm 0.01$	$7.09 \pm 0.07$	$2200 \pm 10$	0.005
$Bu_4NCl$	$15.41 \pm 0.03$	$5.2 \pm 0.1$	$620 \pm 10$	0.02
	$15.55 \pm 0.01$	$5.5 \pm 0.08$	$640 \pm 5$	0.007
$Me_4NBr$	$17.88 \pm 0.04$	$6.3 \pm 0.5$	$2110 \pm 30$	0.02
$Et_4NBr$	$18.70 \pm 0.04$	$6.3 \pm 0.1$	$1330 \pm 10$	0.01
$Pr_4NBr$	$17.01 \pm 0.02$	$5.4 \pm 0.1$	$920 \pm 10$	0.007
$Bu_4NBr$	$16.07 \pm 0.01$	$5.4 \pm 0.1$	$860 \pm 5$	0.005
$Et_4NI$	$19.72 \pm 0.08$	$6.4 \pm 0.3$	$1410 \pm 30$	0.02
$Pr_4NI$	$18.12 \pm 0.05$	$5.5 \pm 0.1$	$1160 \pm 15$	0.01
$Bu_4NI$	$17.16 \pm 0.03$	$5.5 \pm 0.1$	$1180 \pm 10$	0.01
$i\text{-Am}_3BuNI$	$16.99 \pm 0.03$	$5.9 \pm 0.1$	$1360 \pm 15$	0.01
$Hept_4NI$	$15.57 \pm 0.02$	$5.5 \pm 0.1$	$1260 \pm 10$	0.007
$Bu_4NClO_4$	$19.06 \pm 0.05$	$5.7 \pm 0.1$	$2200 \pm 20$	0.01
Pentanol				
$Bu_4NBr$	$11.31 \pm 0.03$	$6.82 \pm 0.09$	$2520 \pm 30$	0.008
$Bu_4NI$	$12.00 \pm 0.05$	$6.5 \pm 0.1$	$3220 \pm 40$	0.01
$i\text{-Am}BuNI$	$11.62 \pm 0.03$	$6.8 \pm 0.1$	$3290 \pm 30$	0.01
$Hept_4NI$	$10.76 \pm 0.03$	$6.6 \pm 0.2$	$3220 \pm 40$	0.09

$Me_4N^+$  and  $Bu_4N^+$  salts is  $0.51 \pm 0.06$ . The conductance of  $Bu_4NI$  in butanol at 0, 25, and 50° has been determined by Venkatasetty and Brown.<sup>13</sup> The agreement of their result at 25° with that given here is within the precision of their measurements.

The lack of transference numbers prevents the data given in Table III from being unambiguously split into limiting ionic conductances. In a previous paper,<sup>2</sup> it was shown that the limiting ionic conductances for the large tetraalkylammonium ions in ethanol could be

calculated from the corresponding values in methanol using the Walden product. When the calculated values were compared with those obtained from transference numbers, they agreed to within 1%. The limiting ionic conductances for ions in butanol given in Table IV were estimated by a similar procedure using the limiting ionic conductance for  $i\text{-Am}_3BuN^+$  and  $He_4N^+$  ions in ethanol and the ethanol-butanol viscosity ratio. An iodide value of  $9.32 \pm 0.01$  was obtained from  $\Lambda_0(i\text{-Am}_3BuNI) - \lambda_0(i\text{-Am}_3BuN^+)$  and  $\Lambda_0(Hept_4NI) - \lambda_0(Hept_4N^+)$ .

**Table IV:** Estimated Limiting Ionic Conductances in Butanol

$Me_4N^+$	9.67	$Hept_4N^+$	6.25
$Et_4N^+$	10.40	$Cl^-$	7.76
$Pr_4N^+$	8.80	$Br^-$	8.23
$Bu_4N^+$	7.84	$I^-$	9.32
$i\text{-Am}_3BuN^+$	7.67	$ClO_4^-$	11.22

## Discussion

**Limiting Ionic Conductances.** Shown in Figure 1 is a plot of  $\lambda_0\eta$  vs.  $1/r_z$ , the reciprocal of the estimated crystallographic radius of an ion, for ions in the four alcohols, methanol,<sup>4</sup> ethanol,<sup>2</sup> propanol,<sup>2</sup> and butanol. The  $\lambda_0\eta$  product in the alcohols shows considerable variation for the smaller ions. This is the type of behavior to be expected from solvation, since the mobility of the ions should decrease as the size of the solvent molecules increases. However, a decrease in mobility with decreasing dielectric constant,  $\epsilon_0$ , and increasing relaxation time,  $\tau$ , is also in accord with the predictions of the Boyd-Zwanzig equation<sup>14</sup>

$$\lambda_0\eta = F^2/N(6\pi r + B/r^3) \quad (2)$$

where  $B$  is a function of solvent properties only and is given by  $B = (2e^2/3)(\tau/\eta)[(\epsilon_0 - \epsilon)/\epsilon_0^2]$ . This theory takes into account the retardation due to the relaxation of solvent dipoles around a moving ion and is in essence a correction to Stokes law. Equation 2 is based on continuum theory and is at present the most complete solution to the problem of ionic mobilities based on this model. In a recent discussion of this theory,<sup>15</sup> it was demonstrated that it will not account for (1) the temperature dependence of ionic mobilities in aqueous solution, where structural effects are present, (2) the variation in mobilities in nonaqueous solvents such as methanol, ethanol, and acetonitrile, which appear to be determined by specific ion-solvent interactions, and (3) the change in ion mobility in  $H_2O-EtOH$  or  $H_2O$ -dioxane mixtures, where solvent struc-

(13) H. V. Venkatasetty and G. H. Brown, *J. Phys. Chem.*, **67**, 954 (1963).

(14) R. Zwanzig, *J. Chem. Phys.*, **38**, 1603 (1963).

(15) R. L. Kay, G. P. Cunningham, and D. F. Evans in "Hydrogen Bonded Solvent Systems," A. Covington and P. Jones, Ed., Taylor and Francis, Ltd., London, 1968, in press.

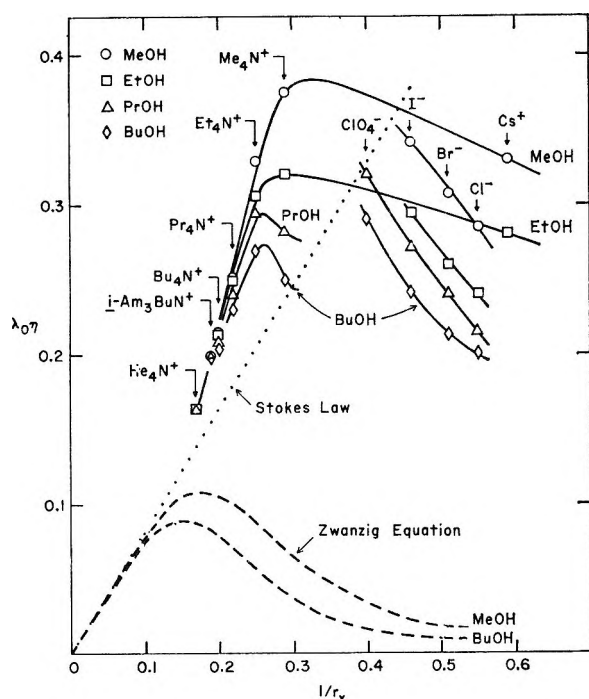


Figure 1. The limiting Walden product for the tetraalkylammonium halide and perchlorate ions as a function of crystallographic size in MeOH, EtOH, PrOH, and BuOH. Theoretical predictions are shown by the dotted curves.

ture and preferential solvation are important. A more favorable examination, in terms of the predictions of this continuum theory, would be the variation of ionic mobilities in the homologous alcohols. Since the functional group of the solvent is common to all, the system would be expected to provide optimum conditions to test the theory.

The variation of  $\lambda_0\eta$  with ionic size for methanol and butanol, as calculated from eq 2, is shown in Figure 1. The values of  $\tau$ , the relaxation time of the solvent, and the dielectric constant at infinite frequency were taken from the compilation of Buckley and Maryott.<sup>16</sup> The static dielectric constant,  $\epsilon_0$ , and viscosity,  $\eta$ , are the values given in this paper and the preceding ones.<sup>2,4</sup> The predicted value of  $\lambda_0\eta$  is too small by almost a factor of 3. Frank has shown that there is no value of  $\dot{r}$  which, when substituted into eq 2, will reproduce the magnitude of the measured  $\lambda_0\eta$  in aqueous solution,<sup>17</sup> and the same argument applies here. The equation predicts a maximum at  $\dot{r}_{\max} = (B/2\pi)^{1/4}$ , which corresponds to a value of  $\dot{r} = 5.7 \text{ \AA}$  in methanol and  $\dot{r} = 6.85 \text{ \AA}$  in butanol. The experimental curves do exhibit a maximum which moves to larger values of  $\dot{r}$  as the series MeOH, EtOH, PrOH, and BuOH is ascended. However, the experimentally determined maxima are at approximately 2.9 Å for MeOH and 4.2 Å for BuOH.

An alternate form in which eq 2 can be used when comparing results in a number of solvents is in the linear form

$$15.5/\lambda_0\eta = 18.8\dot{r} + (15.3 \times 10^{12}/\dot{r}^3)[(\tau/\eta)(\epsilon_0 - \epsilon_\infty)/\epsilon_0^2]$$

suggested by Atkinson and Mori.<sup>18</sup> This can be expressed more succinctly as  $L^* = 18.8\dot{r} + (15.3 \times 10^{12}/\dot{r}^3)R^*$  and a plot of  $L^*$  vs.  $R^*$  should be linear. A value of  $\dot{r}$  can be obtained from both the intercept and slope. Shown in Figure 2 is a plot of  $L^*$  vs.  $R^*$  for cations and anions in the four alcohols, and the points for a given ion are scattered about a straight line. The extent to which this scatter reflects the failure of eq 2, or to what extent it reflects the uncertainty in  $\tau$  and consequently in  $R^*$ , cannot be determined at this time. This scatter indicates an uncertainty of about 20% in  $\tau$ . However, any line drawn within the scatter of the points will still give values of  $\dot{r}$  from the slope which differ from those determined from the intercept by a factor of 3 to 10. For example, two lines drawn through the points for the bromides, with the maximum and minimum slope possible, gave  $\dot{r}(\text{slope}) = 6.55$  and  $\dot{r}(\text{intercept}) = 2.01$ , and  $\dot{r}(\text{slope}) = 8.15$  and  $\dot{r}(\text{intercept}) = 2.34$ , respectively. Therefore even in this

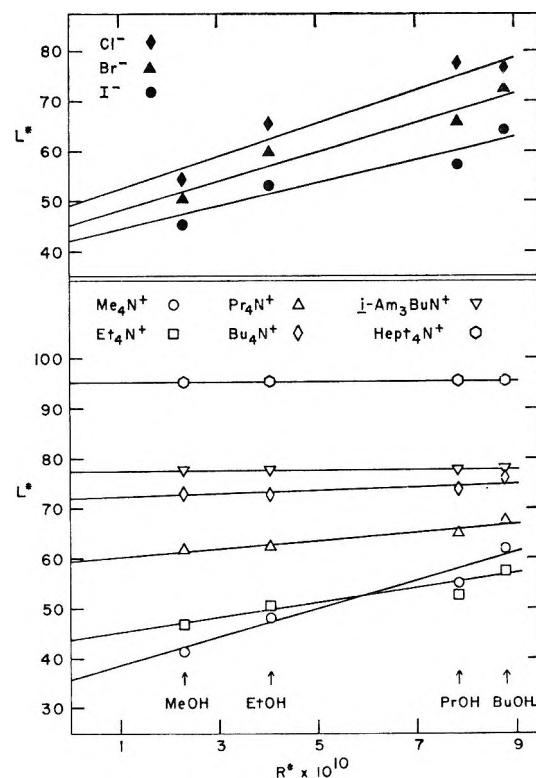


Figure 2. A plot of  $L^*$  vs.  $R^*$  for ions in the alcohols MeOH, EtOH, PrOH, and BuOH.

(16) F. Buckley and A. A. Maryott, National Bureau of Standards Circular No. 589, U. S. Government Printing Office, Washington, D. C., 1958.

(17) H. S. Frank, "Chemical Physics of Ionic Solutions," B. E. Conway and R. G. Barradas, Ed., John Wiley and Sons, Inc., New York, N. Y., 1966, p 61.

(18) G. Atkinson and Y. Mori, *J. Phys. Chem.*, **71**, 3525 (1967).

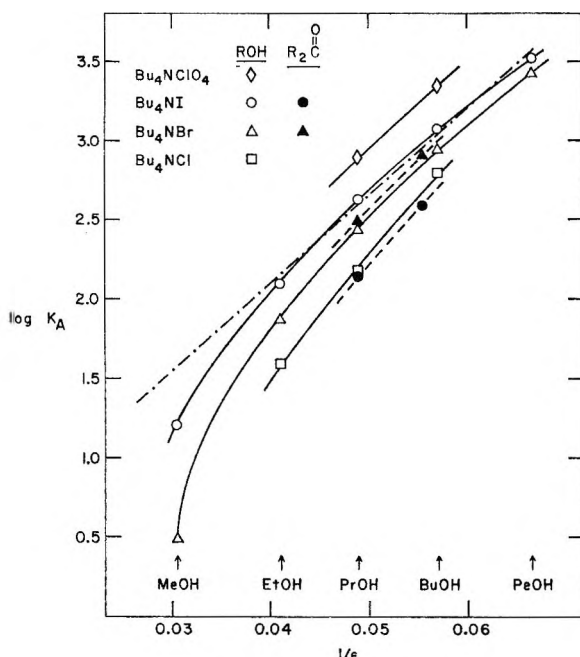


Figure 3. The variation of  $\log K_A$  as a function of  $1/\epsilon$  for tetrabutylammonium salts in the alcohols and ketones.

most advantageous case, the Zwanzig equation does not account quantitatively for the change in mobility in the alcohols. Although there is no doubt that this relaxation effect occurs in the alcohols, these results indicate that specific factors such as solvation, which are ignored in the continuum model, play an important role in determining ionic mobilities.

*Ionic Association.* Previously it was shown that the pattern of ionic association of the tetraalkylammonium salts in methanol<sup>4</sup> and in ethanol and propanol<sup>2</sup> does not exhibit the simple dependence upon ionic size predicted by electrostatic theory. The unusual feature was that, for a given cation, the association constant increased with increasing anion size. Inspection of Table III shows that this same pattern is manifested in the higher alcohols, butanol and pentanol. Before attributing this behavior to solvent effects, the extent to which the results are compatible with continuum theory will be discussed.

#### Coulombic theory<sup>19,20</sup>

$$K_A = K_A^0 e^{(\epsilon^2 / \delta_K \epsilon RT)} \quad (3)$$

predicts that a plot of  $\log K_A$  vs.  $1/\epsilon$  for any given salt should be a straight line whose slope is proportional to  $1/\delta_K$ . Such a plot is shown in Figure 3 for the tetrabutylammonium halides and the perchlorate in the alcohols. Within a good approximation, a straight line is obtained for all of the salts in EtOH, PrOH, BuOH, and PeOH. The values of  $\delta_K$  calculated from the slope (see Table V) are somewhat small but, except for  $Bu_4NCIO_4$ , reasonably constant,  $\delta_K = 3.2 \pm 0.4$ . The same quantitative results are obtained for  $Bu_4NI$ ,  $Pr_4NI$ , and  $Bu_4NBr$  in acetone<sup>21</sup> and methyl ethyl ke-

tone (MEK),<sup>22</sup> except for the fact that the bromides are more associated than the iodides in these solvents. Thus it would appear that salts in the alcohols follow the simple exponential law predicted by electrostatics, as is the case with the ketones, and that only the magnitude of  $K_A$  needs to be explained.

Table V

	ROH		$R_2C=O$	
	$\delta_K$ (slope)	(intercept)	$\delta_K$ (slope)	(intercept)
$Me_4NCl$	3.2	3.3		
$Bu_4NCl$	3.3	2.4		
$Me_4NBr$	3.3	4.2		
$Et_4NBr$	3.6	4.1		
$Pr_4NBr$	3.6	3.6		
$Bu_4NBr$	3.6	3.6	2.7	3.8
$Et_4NI$	2.8	5.1		
$Pr_4NI$	2.8	5.1		
$Bu_4NI$	2.8	5.1	2.8	3.5
$i\text{-Am}_3BuNI$	2.8	5.1		
$Hept_4NI$	2.8	5.1		
$Bu_4NCIO_4$	4.2	7.2		

The preexponential factor of eq 3,  $K_A^0$ , contains the contribution to association for all factors, except the long-range Coulombic interactions. The excluded volume theory<sup>20</sup> predicts that

$$K_A^0 = 4\pi N \delta_K^3 / 3000 \quad (4)$$

From the intercepts of the lines in Figure 3, values of  $K_A^0$  are obtained and using eq 4, the values of  $\delta_K$  (Table V) are calculated. They are small and vary in a manner which only reflects the peculiar association pattern in the alcohols, and it appears that some factor other than size affects the magnitude of  $K_A^0$ .

For the alcohols alone, this type of behavior could possibly be explained within the framework of simple continuum theory, but with the assumption that anion solvation was the predominant factor controlling the extent of ion pairing. However, the extremely high association of tetrabutylammonium perchlorate in propanol compared to its association in the isodielectric solvent, acetone, makes this explanation unlikely.<sup>2</sup>

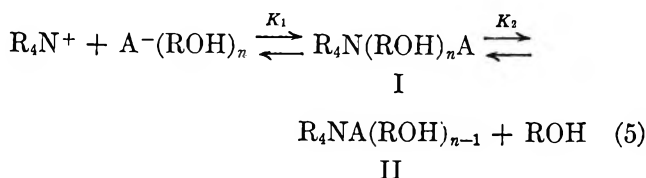
We feel that the best alternative is an explanation based on a multiple-step association process, i.e., solvent-separated and contact ion pairs. A simple mechanism which takes into account the sensitivity of  $K_A$  to anions in the case of the tetraalkylammonium salts is

(19) W. R. Gilkerson, *J. Chem. Phys.*, **25**, 1199 (1956).

(20) R. Fuoss, *J. Amer. Chem. Soc.*, **80**, 5059 (1958).

(21) M. B. Reynolds and C. A. Kraus, *ibid.*, **70**, 1709 (1948); M. J. McDowell and C. A. Kraus, *ibid.*, **73**, 3293 (1951).

(22) S. R. C. Hughes and D. H. Price, *J. Chem. Soc.*, 1093 (1967).



the association constant being given by

$$K_\Sigma = \frac{\sum C_{(\text{ion pairs})}}{(C_{\text{R}_4\text{N}^+})(C_{\text{A}^-(\text{ROH})_n})} = K_1(1 + K_2) \quad (6)$$

The value of  $K_\Sigma$  can be determined from conductance measurements while  $K_1$  and  $K_2$  are in principle accessible from relaxation measurements. This latter information is not available for this solvent system; however,  $K_1$  and  $K_2$  can be estimated in the following way. The magnitude of  $K_1$  is generally estimated from

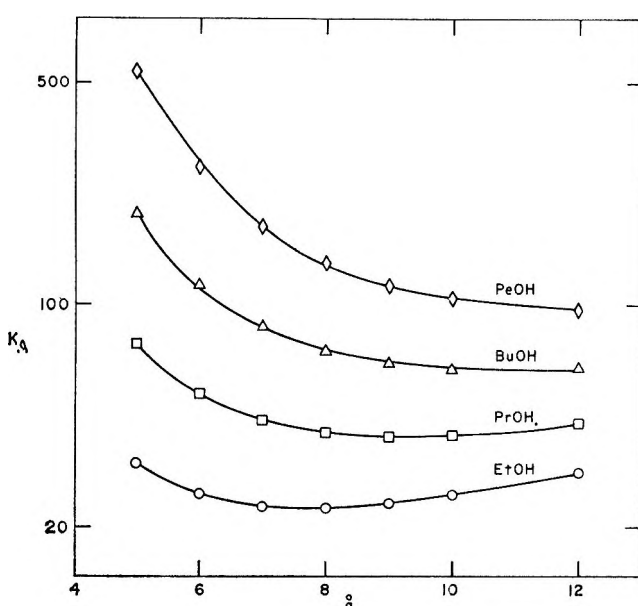


Figure 4. The change of  $K_1$  with  $\bar{a}$  as predicted by eq 3 and 4.

eq 3 and 4 and is thought to be reliable within a factor of 2 or 3.<sup>23</sup> The exponential dependence on  $1/\delta_K$  combined with the preexponential cubic dependence of eq 4 results in a value of  $K_1$  which is nearly independent of  $\delta_K$  over some finite region of ion sizes. This is shown in Figure 4, and the region over which  $K_1$  shows little variation corresponds to that for the cation-anion separation of  $\text{R}_4\text{N}$  salts of species I in eq 5. Using the average values of 25, 40, and 65 for  $K_1$  in EtOH, PrOH, and BuOH, respectively, and the values given in Table III for  $K_\Sigma$ ,  $K_2$  can be estimated from eq 6. The values for the tetrabutylammonium salts alone are shown in Table VI since they serve to illustrate the

Table VI: Estimated Values of  $K_2$  for Tetrabutylammonium Salts from Eq 6

	EtOH	PrOH	BuOH
$\text{Bu}_4\text{NCl}$	0.6	3	9
$\text{Bu}_4\text{NBr}$	2	6	12
$\text{Bu}_4\text{NI}$	4	9	17
$\text{Bu}_4\text{NClO}_4$		18	33

following general features. First, the change of  $K_2$  with size is consistent with the expected relative ease of desolvation of the anion which occurs in the transformation from species I to species II of eq 6. Secondly, this type of multiple-step mechanism accounts for the large values of the  $K_A$  and the distinctive association pattern observed in the alcohols. More concrete evidence for this multiple-step process is being obtained by relaxation measurements on this solvent system.

*Acknowledgment.* This work was supported by Contract No. 14-01-0001-1281 with the Office of Saline Water, U. S. Department of the Interior.

(23) G. G. Hammes and J. I. Steinfeld, *J. Amer. Chem. Soc.*, **84**, 4639 (1962).

# Partial Molal Volume of $[Bu_3N-(CH_2)_8-NBu_3]Br_2$ , a Large Bolaform

Electrolyte, in Water at 10 and 25°

by T. L. Broadwater and D. Fennell Evans<sup>1</sup>

*Department of Chemistry, Case Western Reserve University, Cleveland, Ohio 44106 (Received August 19, 1968)*

The apparent,  $\phi_2$ , and partial,  $\bar{V}_2$ , molal volumes were determined for octane-1,8-bis(*tri-n*-butylammonium) dibromide ( $DiBuBr_2$ ) in water at 10 and 25°. Over the concentration range studied (0.3–1.2 M), the volume behavior was similar to that observed for  $Bu_4NBr$ , with  $\phi_2$  and  $\bar{V}_2$  decreasing to a minimum,  $\phi_2(\min) = DiBuBr_2 \cdot 100H_2O$ , and then increasing as the concentration increased. The partial molal expansibilities,  $\phi_E$ , of  $(\phi_E - \phi_E^0)$  were positive, went through a maximum at the concentration where  $\phi_2$  is at a minimum, and then decreased. The observed effects, including clathrate formation, all indicate that this large divalent salt affects water structure in the same manner as  $Bu_4NBr$ .

## Introduction

The partial molal volume behavior of symmetrical tetraalkylammonium halides has been investigated in aqueous<sup>2–8</sup> as well as nonaqueous solvents.<sup>9,10</sup> It is firmly established from these studies as well as numerous others<sup>11,12</sup> that the unusual concentration dependence of salts having ions with large hydrophobic surfaces arises from water structural effects. However, there is no general agreement on the exact nature of the ion–solvent interactions. Ion pairing,<sup>3,4,6</sup> micelle formation,<sup>13</sup> hydrophobic bonding,<sup>14</sup> salting-in,<sup>5,15</sup> and cation–cation pairing<sup>2,7</sup> have been suggested to explain the anomalous concentration behavior. It has been pointed out that the first three alternatives listed above do not explain the observed volume behavior.<sup>7</sup> The compound studied here allows the implications of the last suggestion to be explored more thoroughly since  $DiBuBr_2$  should serve as a good model for the  $Bu_4N^+$  cation–cation pair.

A second paper in this series will report the conductance behavior of cations with the general formula  $[(C_nH_{2n+1})_3N^+-(CH_2)_{2n}-N^+(C_nH_{2n+1})_3]$ , where  $n = 2, 3$ , or  $4$ .<sup>16</sup>

## Experimental Section

Density measurements were carried out below 0.5 M with two 25-ml Weld and three 30-ml capillary pycnometers. Above this concentration, three 5-ml Weld pycnometers were used. All calibrations were carried out using conductivity grade water, and the procedure of Weissberger<sup>17</sup> was used for measurements with the Weld pycnometers. Capillary pycnometers were filled with syringes equipped with long needles, and the unfilled portions of the capillaries were wiped clean with lens paper. The constant temperature baths were maintained at  $25.000 \pm 0.005$  and  $10.00 \pm 0.01^\circ$ .

The salt was made by refluxing an excess of tributylamine with 1,8-dibromo-octane in ethanol. The excess amine was removed by extraction with ether and re-

crystallizations were carried out in methanol–ether mixtures (mp 123–125°). *Anal.* Calcd for  $C_{32}H_{70}Br_2N_2$ : C, 59.80; H, 10.98; Br, 24.87. Found: C, 59.57; H, 10.68; Br, 24.63.

## Results

The densities and molal concentrations at 25 and 10° are given in Table I, along with the corresponding values of  $\phi_2$ . The latter were calculated from the density data using the equation

$$\phi_2 = \frac{1}{m_2} \left( \frac{1000 + m_2 M}{d} - \frac{1000}{d_0} \right)$$

where  $m_2$  is the molal concentration of the solute,  $M$  is its molecular weight,  $d$  is the density of the solution, and  $d_0$  is the density of the solvent.

- (1) To whom all correspondence should be directed.
- (2) W. Y. Wen and S. Saito, *J. Phys. Chem.*, **68**, 2639 (1964).
- (3) L. G. Hepler, J. M. Stokes, and R. H. Stokes, *Trans. Faraday Soc.*, **61**, 20 (1965).
- (4) B. J. Levien, *Aust. J. Chem.*, **18**, 1161 (1965).
- (5) (a) B. E. Conway, R. E. Verrall, and J. E. Desnoyers, *Trans. Faraday Soc.*, **62**, 2738 (1966); (b) R. E. Verrall, unpublished Ph.D. dissertation, University of Ottawa, 1966.
- (6) H. E. Wirth, *J. Phys. Chem.*, **71**, 2922 (1967).
- (7) F. Franks and H. T. Smith, *Trans. Faraday Soc.*, **63**, 2586 (1967).
- (8) R. Gopal and M. A. Siddiqi, *J. Phys. Chem.*, **72**, 1814 (1968).
- (9) J. Padova and I. Abrahamer, *ibid.*, **71**, 2112 (1967).
- (10) W. Y. Wen, "Saline Water Conversion Report," Office of Saline Water, U. S. Department of the Interior, 1966, p 13.
- (11) T. L. Broadwater, Ph.D. Dissertation, Case Western Reserve University, 1968.
- (12) All of the pertinent references are too numerous to be conveniently listed here, but are given in ref 11.
- (13) S. Lindenbaum and G. E. Boyd, *J. Phys. Chem.*, **68**, 911 (1964).
- (14) F. Franks and H. T. Smith, *ibid.*, **68**, 3581 (1964).
- (15) J. E. Desnoyers and M. Arel, *Can. J. Chem.*, **45**, 359 (1967).
- (16) D. F. Evans and T. L. Broadwater, to be published.
- (17) A. Weissberger, "Physical Methods of Organic Chemistry," 2nd ed., Vol. I, Part 1, Interscience Publishers, New York, N. Y., 1949.

**Table I:** Densities, Molalities, and Apparent Molal Volumes for DiBuBr<sub>2</sub>

m	25°		10°	
	Density	$\phi_2$	Density	$\phi_2$
7.232	1.08592	580.6	1.09620	574.2
5.037	1.08061	579.4	1.09119	572.4
3.755	1.07589	577.9	1.08680	570.1
2.615	1.06911	575.2	1.07993	566.8
2.342	1.06695	574.4	1.07807	565.2
1.740	1.05911	573.1	1.06967	563.3
1.543	1.05622	572.2	1.06700	561.6
1.512	1.05543	572.3	1.06602	561.8
1.303	1.05132	571.7	1.06156	560.8
1.174	1.04862	571.0	1.05860	559.8
0.9842	1.04356	570.5	1.05265	559.5
0.7289	1.03488	570.8	1.04299	559.3
0.6499	1.03181	571.0	...	...
0.6471	1.03184	570.7	1.03925	559.7
0.5420	1.02728	571.3	1.03391	560.7
0.4887	1.02485	571.6	...	...
0.4241	1.02167	572.2	1.02744	562.0
0.3989	1.02047	572.2	1.02606	562.1
0.3494	1.01793	572.6	1.02314	562.7
0.3096	1.01568	573.4	1.02076	563.1
0.2932	1.01484	573.5	1.01960	563.9
0.2476	1.01216	574.6	1.01676	564.5
0.2400	1.01185	574.2	1.01622	564.9
0.2212	1.01076	574.5	1.01497	565.4
0.2092	1.01011	574.4	1.01425	565.3
0.2026	1.00976	574.4	1.01382	565.4
0.1900	1.00895	574.9	1.01289	566.2
0.1115	1.00423	575.9	1.00762	567.4
0.0932	1.00310	576.1	1.00636	568.0
0.0883	1.00278	576.5	1.00599	568.5
0.0799	1.00224	576.6	...	...
0.0756	1.00195	576.9	...	...
0.0631	1.00115	577.3	...	...
0.0427	0.99985	577.6	...	...
0.0317	0.99914	577.8	...	...

Partial molal volumes were calculated from the  $\phi_2$  data using the relationship

$$\bar{V}_2 = \phi_2 + \left( \frac{1000 - C\phi_2}{2000 + C\sqrt{C} \frac{\partial \phi_2}{\partial \sqrt{C}}} \right) \sqrt{C} \frac{\partial \phi_2}{\partial \sqrt{C}}$$

Values of  $\partial \phi / \partial \sqrt{C}$  were determined graphically from curves drawn through the  $\phi_2$  data. Plotted in Figure 1 is the concentration dependence of  $\phi_2$  and  $\bar{V}_2$  at 25 and 10°.

Partial molal expansibilities,  $\phi_E$ , were calculated at different concentrations from the  $\phi_2$  data at 25 and 10°. The resulting curve is plotted in Figure 2, along with data for Bu<sub>4</sub>NBr, Na<sub>2</sub>SO<sub>4</sub>, and KCl.

## Discussion

The partial molal volume of tetraalkylammonium compounds has been studied over a large concentration range and as a function of temperature.<sup>2-8</sup> Above a concentration of  $\sim 0.01 M$ ,  $\phi_2$  and  $\bar{V}_2$  for the larger of

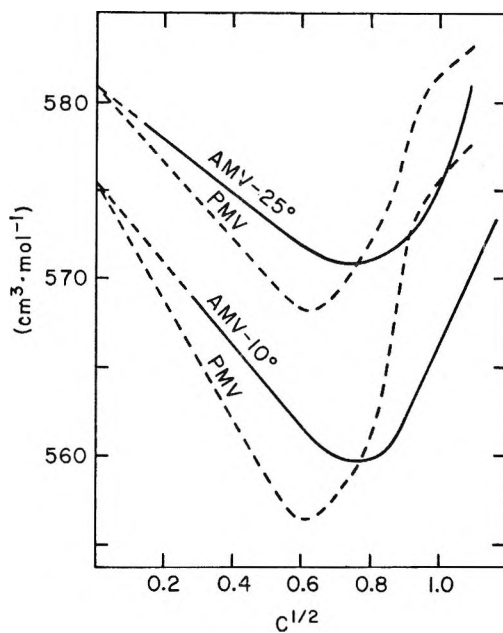


Figure 1. Apparent molal volume (AMV) and partial molal volume (PMV) for DiBuBr<sub>2</sub> at 10 and 25°.

these salts decrease, go through a minimum, and then begin to increase. The value of  $\bar{V}_2^0$  becomes smaller and the minima become more pronounced as the temperature decreases.<sup>2</sup> In contrast, for salts which are small and electrostrictively hydrated, the increase of  $\bar{V}_2$  with concentration is reasonably linear.<sup>7</sup> Shown in Figure 1 are the apparent and partial molal volumes of DiBuBr<sub>2</sub> at 10 and 25°. The curves display a dependence upon concentration similar to that observed for the large univalent tetraalkylammonium salts.

The aqueous solution behavior has been explained for R<sub>4</sub>N<sup>+</sup> halides in terms of cation-cation pairing.<sup>2,7</sup> It was proposed that the increasing concentration of these large ions eventually led to cooperative networks in which the cations were forced to share sheaths of water. Time-averaged solution structures similar to the crystalline clathrates studied by Jeffrey and his associates<sup>18</sup> were assumed to make a contribution. The sharing of water layers would place the cations in close proximity and presumably the anions would participate in the structure to reduce the coulombic repulsion. The decrease in  $\phi_2$  was attributed to the association of more and more ions until the minimum, corresponding to a maximum solution structure, was reached. A further increase in concentration would break down the open hydrogen-bonded structure.

Further evidence for cation-cation pairing has recently been offered by Wen and Nara<sup>19</sup> from data on the

(18) D. Feil and G. A. Jeffrey, *J. Chem. Phys.*, **35**, 1863 (1961); M. Bonamico, R. K. McMullan, and G. A. Jeffrey, *ibid.*, **37**, 2219 (1962); **39**, 3295 (1963).

(19) W. Y. Wen and K. Nara, *J. Phys. Chem.*, **71**, 3907 (1967); **72**, 1137 (1968); W. Y. Wen, K. Nara, and R. H. Wood, *ibid.*, **72**, 3048 (1968).

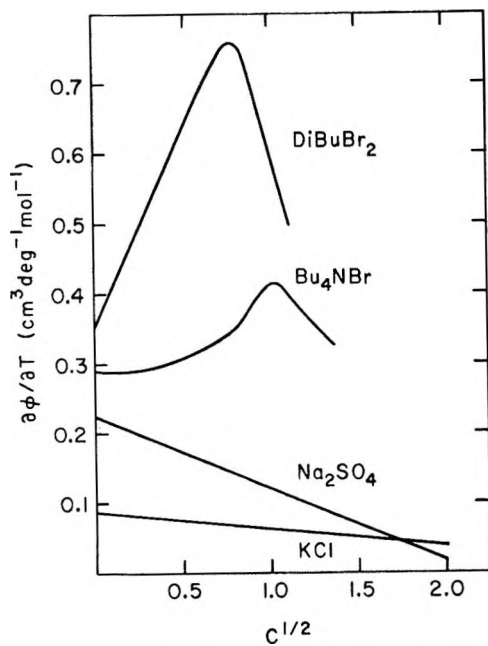


Figure 2. Apparent molal expansibilities of  $\text{DiBuBr}_2$ ,  $\text{Bu}_4\text{NBr}$ ,  $\text{Na}_2\text{SO}_4$ , and  $\text{KCl}$ .

volume increases observed when  $\text{R}_4\text{N}$  halides are mixed with alkali metal halides. The data were analyzed in terms of Friedman's ionic solution theory,<sup>20</sup> which, when applied to the mixing of salts AX and BX, describes the volume change in terms of structural parameters due to an ion i in the vicinity of an ion j. The term involving  $i = j = \text{R}_4\text{N}^+$  was found to be predominant where  $\text{Pr}_4\text{N}^+$  and  $\text{Bu}_4\text{N}^+$  were studied.

In Figure 3, the concentration dependences of  $\text{Bu}_4\text{NBr}$  and  $\text{DiBuBr}_2$  are compared and the similarities in behavior are evident. The curve for the larger salt has the more negative slope and undergoes a larger decrease in  $\phi_2$ . This is probably a reflection of the fact that more water per ion is being affected. The minima in the  $\phi_2$  curves correspond to  $\text{Bu}_4\text{NBr} \cdot 55\text{H}_2\text{O}$  and  $\text{DiBuBr}_2 \cdot 100\text{H}_2\text{O}$ .

The partial molal volumes at infinite dilution, obtained by extrapolating the negative portion of the  $\phi_2$  curve to  $C = 0$ , were  $(\bar{V}_2^0)_{25} = 580.9 \pm 0.5$  and  $(\bar{V}_2^0)_{10} = 575.4 \pm 0.5$ . The large uncertainties are due to scatter in the density data at low concentrations. In addition, the values obtained are too large because the extrapolation to zero concentration ignores the contribution from the limiting Debye-Hückel term which produces a positive slope for the region below 0.01 M. The magnitude of this error can be estimated by constructing the limiting slope of 9.66<sup>21</sup> so that it intersects the  $\phi_2$  curve at  $C^{1/2} = 0.16$ , this being the approximate concentration where the theoretical and the extrapolated experimental curves intersect for  $\text{Pr}_4\text{NBr}$  and  $\text{Bu}_4\text{NBr}$ .<sup>7</sup> At 25°, this procedure gives  $\bar{V}_2^0 = 577.9$ , a value which is 3.0 cm<sup>3</sup>/mol lower than the linear extrapolation. The value of  $\bar{V}_2^0$  for

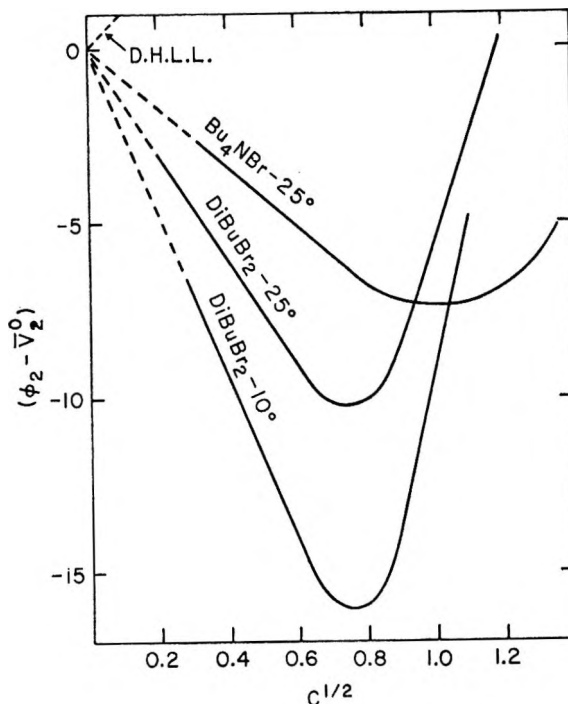


Figure 3. Concentration dependence of the partial molal volume for  $\text{Bu}_4\text{NBr}$  and  $\text{DiBuBr}_2$ .

$\text{Pr}_4\text{NBr}$  and  $\text{Bu}_4\text{NBr}$ , obtained by Wen and Saito<sup>2</sup> by linear extrapolation, is too large by a value of 2.6 cm<sup>3</sup>/mol, as can be determined from the data of Franks and Smith.<sup>7</sup> Subtracting the value of  $\bar{V}_2^0(\text{Br}^-) = 30.2$  gives a ratio  $\bar{V}_2^0(\text{DiBu}^{2+})/\bar{V}_2^0(\text{Bu}_4\text{N}^+) = 517.5/270.2 = 1.91$ . The volume decrease on the formation of a cation-cation pair for  $\text{Bu}_4\text{N}^+$  ions has been evaluated by Wen, Nara, and Wood<sup>19</sup> to be 3.7–7.3, 5.4–9.2, and 7.2–11.5 cm<sup>3</sup>/mol at ionic strengths of 1, 0.5, and 0.2, respectively. A value at infinite dilution of  $11 \pm 2$  cm<sup>3</sup>/mol can be estimated by extrapolating to zero concentration the values at 0.5 and 0.2  $\mu$ . An independent estimate of this volume decrease can be gained from the following simple calculation:  $[(2)(270.2) - 517.5] = 22.9$  cm<sup>3</sup>/mol. The magnitude of the value obtained for  $\text{DiBu}^{2+}$  gives credence to our contention that this ion is a good model for a  $\text{Bu}_4\text{N}^+$  cation-cation pair.

The similarities in behavior of the two cations are further emphasized by the fact that a crystalline clathrate was found for  $\text{DiBuF}_2$  which melts at 5° and has approximately 40 waters as determined by the Karl Fischer titration method. The exact number of waters is uncertain because of the difficulties of obtaining a sample for titration free of adsorbed water. The exact composition can probably be resolved by X-ray analysis.

The apparent molal expansibilities for  $\text{DiBuBr}_2$  are

(20) H. L. Friedman, *J. Chem. Phys.*, **32**, 1134 (1960); H. L. Friedman, "Ionic Solution Theory," Interscience Publishers, New York, N. Y., 1962.

(21) O. Redlich and D. M. Meyer, *Chem. Rev.*, **64**, 221 (1964).

plotted in Figure 2 along with data for  $\text{Bu}_4\text{NBr}$ ,  $\text{Na}_2\text{SO}_4$ , and  $\text{KCl}$ .<sup>2,22</sup> The curves for both  $\text{Bu}_4\text{NBr}$  and  $\text{DiBuBr}_2$  differ from the others in that they are positive, go through a maximum, and then decrease. The maximum for both curves occurs at the concentration where the  $\phi_2$  data pass through a minimum. The behavior shown for  $\text{KCl}$  and  $\text{Na}_2\text{SO}_4$  is typical of small electrolytes.<sup>22</sup> The curve for  $\text{KCl}$  does become positive at low concentrations ( $<0.04\text{ M}$ ).<sup>7</sup>

The apparent molal expansibility at infinite dilution,

$\phi_E^0$ , for the alkali halides decreases with increasing radius, while the opposite trend occurs for  $\text{R}_4\text{N}^+$  salts. There does not appear to be a direct correlation, however, between  $\phi_E^0$  and the number of carbon atoms in the ammonium compounds since  $\phi_E^0(\text{Bu}_4\text{NBr}) = 0.29^2$  (or 0.24),<sup>7</sup> while  $\phi_E^0(\text{DiBuBr}_2) = 0.37$ .

(22) H. S. Harned and B. B. Owen, "The Physical Chemistry of Electrolyte Solutions," 3rd ed., Reinhold Publishing Corp., New York, N. Y., 1958, p 373.

## A Dimensionless Constant Characteristic of Gases, Equations of State, and Intermolecular Potentials

by Eugene M. Holleran

Chemistry Department, St. John's University, Jamaica, New York 11432 (Received July 24, 1968)

The ratio of the Boyle volume and the unit compressibility law volume is introduced as a characteristic dimensionless constant. Tables of values are presented for various gases and mixtures, simple equations of state, and intermolecular potentials. The constant can be used as: (a) an indication of the suitability of any two-constant equation of state or intermolecular potential to a given gas, (b) an adjustable explicit parameter in equations of state with more than two constants, (c) a simple means of determining, for a given gas, the necessary value of the third parameter of an intermolecular potential, and (d) the third constant in a three-constant system of corresponding states. In a useful version of the latter, the ratio of the constants of two gases determines the relative deviation from ideality of their reduced properties at equal reduced temperatures and densities.

### Introduction

The two-parameter version of the principle of corresponding states assumes that any two substances at the same reduced temperature and volume are in corresponding states and have the same values of other reduced properties. Various constant-temperature-volume pairs have been used as reducing factors, including the critical constants  $T_c$  and  $V_c$ , the molecular parameters  $\epsilon/k$  and  $b_0$  of various intermolecular potentials, and others to be discussed below. In this two-parameter form the corresponding-states principle is not generally valid, as illustrated for example by the fact that the compressibility factor at the critical point ( $Z_c = P_c V_c / RT_c$ ) has different values for different substances. However, groups of substances having similar values of this dimensionless constant are assumed to correspond in other properties also, and this assumption is an example of the three-parameter version of corresponding states. Several third parameters besides  $Z_c$ , notably the acentricity factor,<sup>1</sup> have been used.<sup>2</sup>

In addition to characterizing substances for corresponding-states groupings, the constant  $Z_c$  also serves to characterize simple equations of state. Two-parameter equations such as van der Waals' require a single constant value of  $Z_c$ , and equations with more than two constants have adjustable  $Z_c$ . It would be useful if  $Z_c$  could also be evaluated for intermolecular potentials. Although approximations are available,<sup>3-5</sup> the exact relation between this constant and the various potentials is unknown.

The purpose of this paper is to introduce and discuss the potential uses of a new dimensionless constant which is characteristic of real gases and mixtures, simple equations of state, and intermolecular potentials.

- (1) K. S. Pitzer, *J. Amer. Chem. Soc.*, **77**, 3427 (1955).
- (2) R. C. Reid and T. K. Sherwood, "The Properties of Gases and Liquids," McGraw-Hill Book Co., New York, N. Y., 1966, p 54 ff.
- (3) J. A. Barker and D. Henderson, *Can. J. Phys.*, **45**, 3959 (1967).
- (4) L. I. Stiel and G. Thodos, *J. Chem. Eng. Data*, **7**, 234 (1962).
- (5) J. S. Rowlinson, *J. Chem. Phys.*, **19**, 831 (1951).

### The Boyle and Unit Compressibility Law Constants

Two related sets of reducing constants for corresponding states have come into use relatively recently. They are the Boyle constants,  $T_B$  and  $V_B$ , and the unit compressibility law (UCL) constants,  $T_B$  and  $V_0$ . The Boyle temperature,  $T_B$ , shared by both systems, is the temperature at which the second virial coefficient  $B(T)$  is zero. The Boyle volume,  $V_B$ , introduced by Kihara,<sup>6</sup> is defined as

$$V_B = (TdB/dT)_{T_B} \quad (1)$$

The UCL volume  $V_0$  is defined by the unit compressibility law<sup>7</sup> as

$$V_0 = V_1[1 - (T_1/T_B)] \quad (2)$$

where  $T_1$  and  $V_1$  are the temperature and molar volume, respectively, of any state for which the compressibility factor  $Z$  equals unity.

The Boyle constants have been used by a number of authors<sup>8–11</sup> in corresponding-states treatments and in comparing theory with experiment. In particular, an accurate correspondence of experimental second virial coefficients has been shown by graphs of  $B/V_B$  vs.  $T/T_B$  by Munn<sup>12</sup> for Ne, Ar, Kr, and Xe and by Douslin, Harrison, and Moore<sup>13</sup> for Ar, Kr, CH<sub>4</sub>, CF<sub>4</sub>, and the cross-term coefficient  $B_{12}$  for mixtures of the last two. Also, Hamann and Lambert<sup>14</sup> and Munn<sup>12</sup> have shown that plots of  $B/V_B$  vs.  $T/T_B$  for various common intermolecular potentials are nearly indistinguishable except at temperatures far above and below  $T_B$ . As a result, second virial coefficient data in the usual experimental temperature range have proved insufficient for the unambiguous selection of a potential function for a given gas. Also, it can be expected that the Boyle constants  $V_B$  and  $T_B$  will continue to prove useful as reducing constants for correlating this property and possibly others such as viscosity.<sup>15</sup>

The UCL constants have been used as reducing factors in comparing the compressibility and residual thermodynamic properties of argon with those of xenon<sup>16</sup> and methane.<sup>17</sup> By introducing as a third constant the ratio of the deviations from ideality of the two gases, it was found that the compressibility factor of methane could be calculated from argon data over a wide range of temperature and density with an average deviation of only 4 parts/10,000. The UCL constants are therefore proving very useful in the correlation of compressibility and related properties.

### Definition of the Constant $k_B$

The Boyle constants and the UCL constants both enjoy the great advantage over earlier sets of reducing factors in that they can be found both experimentally and in terms of an assumed intermolecular potential. Which of these two closely related systems will prove to be more fundamental for corresponding-states correlations remains to be seen. However, it is evident that

the ratio of the two characteristic volumes represents a distinctive dimensionless constant.

Accordingly, we defined a constant  $k_B$  as

$$k_B = V_B/V_0 \quad (3)$$

which may be viewed as the Boyle volume reduced by the UCL volume or the UCL density reduced by the Boyle density.

Additional expressions for  $k_B$  can be found as follows. The unit compressibility law implies an interrelation of the virial coefficients,<sup>18</sup> one consequence of which is a simple relation among  $V_B$ ,  $V_0$ , and  $C_B$ , the third virial coefficient at the Boyle temperature. Briefly, this is found from eq 2 and the virial equation of state

$$Z = 1 + Bd + Cd^2 + \dots \quad (4)$$

from which we see that  $B + C[1 - (T/T_B)]/V_0 + \dots = 0$ . Differentiation and introduction of eq 1 then gives

$$V_0 = C_B/V_B \quad (5)$$

This equation permits the evaluation of  $V_0$  for equations of state which disobey the unit compressibility law and for intermolecular potentials; in both cases  $C_B$  rather than  $V_0$  is directly determinable. Equation 5 thus gives rise to two alternative definitions for the constant  $k_B$

$$k_B = C_B/V_0^2 = V_B^2/C_B \quad (6)$$

Any two of the three quantities,  $V_B$ ,  $V_0$ , and  $C_B$ , therefore suffice to determine  $k_B$ . According to the last expression in eq 6,  $k_B$  is a property of the Boyle point, hence the subscript.

### The Constant for Gases and Mixtures

The accurate experimental determination of  $k_B$  for any substance or mixture requires high-quality *PVT* data, from which are derived the virial coefficients on the one hand and the unit compressibility law constants on the other. For the latter, the temperatures and volumes,  $T_1$  and  $V_1$ , at which the compressibility factor  $Z$  is unity are found by interpolation in the data and

- (6) T. Kihara, *Rev. Mod. Phys.*, **25**, 831 (1953).
- (7) E. M. Holleran, *J. Chem. Phys.*, **47**, 5318 (1967).
- (8) S. F. Boys and I. Shavitt, *Proc. Roy. Soc.*, **A254**, 499 (1960).
- (9) F. J. Smith, E. A. Mason, and R. J. Munn, *J. Chem. Phys.*, **42**, 1334 (1965).
- (10) A. E. Sherwood, A. G. DeRocco, and E. A. Mason, *ibid.*, **44**, 2984 (1966).
- (11) J. P. O'Connell and J. M. Prausnitz, *J. Phys. Chem.*, **72**, 632 (1968).
- (12) R. J. Munn, *J. Chem. Phys.*, **40**, 1439 (1964).
- (13) D. R. Douslin, R. H. Harrison, and R. T. Moore, *J. Phys. Chem.*, **71**, 3477 (1967).
- (14) S. D. Hamann and J. A. Lambert, *Aust. J. Chem.*, **7**, 1 (1954).
- (15) R. J. Munn, *Discussions Faraday Soc.*, **40**, 130 (1965).
- (16) E. M. Holleran, *J. Phys. Chem.*, **72**, 1230 (1968).
- (17) E. M. Holleran and G. J. Gerardi, *ibid.*, **72**, 3559 (1968).
- (18) E. M. Holleran, *J. Chem. Phys.*, **49**, 39 (1968).

**Table I:** The Constant for Some Gases and Mixtures

Gas	$T_B$ , °K	$V_B$ , cm³/m	$V_0$ , cm³/m	$10^{-2}C_B$ , cm⁶/m²	$k_B$	$Z_c^a$	Ref for $B$ or $V_B$
Argon	408.2	39.9	21.4	8.53	1.86	0.290	b
Krypton	580	46.9	26.4	12.4	1.78	0.291	b
Xenon	793	68.7	33.7	23.2	2.04	0.290	c
Nitrogen	326	52.3	24.6	12.9	2.13	0.291	c
Carbon dioxide	722	63.2	24.4	15.4	2.59	0.274	c
Methane	509.2	54.3	28.0	15.2	1.94	0.290	b
0.75 CH <sub>4</sub> -0.25 CF <sub>4</sub>	490.5	67.5	30.4	20.5	2.22		b
0.50 CH <sub>4</sub> -0.50 CF <sub>4</sub>	493.1	78.9	32.5	25.6	2.43		b
0.25 CH <sub>4</sub> -0.75 CF <sub>4</sub>	505.0	90.5	34.6	31.3	2.62		b
Tetrafluoromethane	521	104.1	36.1	37.6	2.88	0.272	b

<sup>a</sup> Reference 2. <sup>b</sup> Reference 13. <sup>c</sup> Reference 6.

then fit by least squares to eq 2, thereby obtaining  $T_B$  and  $V_0$ .

For the former,  $B(T)$  can be found as the zero density limit of  $(Z - 1)V$  at various temperatures.  $T_B$  then follows as the temperature at which  $B$  is zero, and its value should agree with that found from eq 2.  $V_B$  may be found either by differentiation of an empirical equation for  $B(T)$ ,<sup>12</sup> or from a fit of the data to an intermolecular potential,<sup>10,13</sup> or by interpolation at  $T_B$  of smoothed values of  $B/(T - T_B)$  or  $TB/(T - T_B)$ .<sup>18</sup> The third virial coefficient  $C(T)$  may be found as the zero density limit of  $[Z - 1 - (B/V)]V^2$  for each experimental isotherm. Its value interpolated at  $T_B$  is  $C_B$ , and this should agree with  $C_B$  found as  $V_0 V_B$ .

The further these procedures lead from the original *PVT* data the less reliable are the results, and it is probable that at present most published experimental values of  $C_B$  will not yield accurate values of  $k_B$ . For this reason it is preferable to use  $V_0$  and  $V_B$ , although these also are highly sensitive to errors in the data.

Table I lists  $T_B$ ,  $V_B$ ,  $V_0$ ,  $C_B$ , and  $k_B$  for several gases and mixtures. The values of  $T_B$  and  $V_0$  were obtained from the unit compressibility law, which holds for all these systems.<sup>7,19</sup> Values of  $V_B$  were calculated from an empirical equation for  $B(T)$ . The  $C_B$  values listed represent the product  $V_0 V_B$  and are probably more reliable than  $C_B$  found from experimental  $C(T)$ , where they differ. In the case of CH<sub>4</sub>, CF<sub>4</sub>, and their mixtures, the data were adjusted within experimental error to provide a consistent set of constants, with the UCL values of  $T_B$  and  $V_0$  agreeing with the values of  $T_B$  and  $C_B/V_B$  derived from the virial coefficients.<sup>20</sup> For these gases, and for Ar, the listed values of  $k_B$  calculated as  $V_B/V_0$  are probably accurate to within  $\pm 0.01$ . In other cases, such as Kr, the error could be several per cent. It seems unlikely, however, that uncertainties are sufficient to account for the apparent inversion in the Ar, Kr, and Xe series. The list of  $k_B$  values and their accuracy can of course be extended in the future, particularly if compressibility

measurements are made with the specific objective of determining  $V_B$  and  $V_0$ .

Table I also includes values of  $Z_c$  for comparison. Several advantages of  $k_B$  are apparent. In the first place, a "pseudocritical"  $Z_c$  is required for mixtures,<sup>2</sup> whereas  $k_B$  can be found by the same procedure used for pure gases. (Also,  $k_B$  for CH<sub>4</sub>-CF<sub>4</sub> mixtures can be estimated from the pure-gas values to within about 1% as linear in mole fraction.) Second, it is evident that  $k_B$  exhibits a greater range and is more distinctive than  $Z_c$ . For CH<sub>4</sub> and CF<sub>4</sub>,  $Z_c$  differs by only 7%, while  $k_B$  differs by 50%. Also, such gases as N<sub>2</sub>, CH<sub>4</sub>, and Ar, which have nearly the same  $Z_c$  (and small acentricity factors also<sup>2</sup>), are definitely distinguished by their  $k_B$  values. One consequence of this is that, although these gases would be grouped together in the  $T_c$ ,  $V_c$ , and  $Z_c$  system of corresponding states, their *PVT* properties, e.g.,  $k_B$ , cannot correspond accurately in this system. A three-parameter system of corresponding states based on  $T_B$ ,  $V_0$ , and  $k_B$  therefore appears promising and is discussed in a later section.

### The Constant for Equations of State

For an equation of state  $k_B$  is found as  $V_B^2/C_B$ . The equation is expanded in powers of the density to identify  $B$  and  $C$  as functions of  $T$ , from which  $T_B$ ,  $V_B$ , and  $C_B$  follow without difficulty.  $V_0$  is given as  $C_B/V_B$ , but since most analytic equations of state (van der Waals is an exception) do not obey the unit compressibility law,<sup>7</sup> this  $V_0$  does not have the physical significance implied by eq 2.

For two-parameter equations of state the constant  $k_B$  is characteristic; that is, it is independent of the two parameters. Table II lists the values of  $T_B$ ,  $V_B$ ,  $C_B$ ,  $V_0$ ,  $Z_c$ , and  $k_B$  for the equations of van der Waals,  $[P + (a/V^2)](V - b) = RT$ ; Berthelot,  $[P + (a/TV^2)](V - b) = RT$ ; Dieterici,  $(Pe^{a/VRT})(V - b) =$

(19) E. M. Holleran and G. J. Gerardi, *J. Phys. Chem.*, in press.

(20) E. M. Holleran, unpublished data.

**Table II:** The Constant for Simple Equations of State

Eq	$T_B$	$V_B$	$C_B$	$V_0$	$k_B$
van der Waals	$a/bR$	$b$	$b^2$	$b$	1
Berthelot	$(a/bR)^{1/2}$	$2b$	$b^2$	$b/2$	4
Dieterici	$a/bR$	$b$	$b^2/2$	$b/2$	2
Redlich-Kwong	$(a/bR)^{2/3}$	$3b/2$	$2b^2$	$4b/3$	9/8

$RT$ ; and Redlich-Kwong,  $[P + a/T^{1/2}V(V + b)] \cdot (V - b) = RT$ . Here again the wider range of  $k_B$  compared with  $Z_c$  is evident. Comparison of these values of  $k_B$  with those for the various gases in Table I shows that Dieterici's equation gives the best value for  $k_B$ , as it does also for  $Z_c$ . However, this does not imply that it is necessarily best in other ways; for example, van der Waals' equation is better by the criterion of obeying the unit compressibility law. Of course two-constant equations, like two-parameter systems of corresponding states, are not generally valid.

Equations of state with three or more parameters have  $k_B$  values which depend on the values of the parameters. One example is the Wohl equation<sup>2</sup>

$$\{P + [a_1/V(V - b)] - (a_2/V^3)\}(V - b) = RT$$

for which we find that  $(1 - k_B)/k_B = a_2/a_1b$ . The equation can therefore be written in terms of two of the original constants and an independent  $k_B$ , and this  $k_B$  can be made to agree with the experimental value for any substance. The equation may also be written in terms of the three parameters  $T_B$ ,  $V_B$ , and  $k_B$  by using the additional relations  $b = V_0$  and  $a_1 = V_B RT_B$ . Although the Wohl equation is not much better than van der Waals', we may anticipate that an accurate three-constant equation of state, explicit in  $T_B$ ,  $k_B$ , and  $V_B$  ( $= V_0 k_B$ ), can be devised if the corresponding-states system based on these three parameters should prove fruitful.

In a similar way, these three parameters can also be made explicit in more complex equations. For example the Beattie-Bridgman equation<sup>21</sup> contains five parameters

$$Z = [1 + (B_0/V) - (bB_0/V^2)] \times [1 - (c/VT^3)] - A_0[1 - (a/V)]/RTV \quad (7)$$

Three of these parameters can be eliminated in favor of  $T_B$ ,  $V_B$ , and  $k_B$  by using the equations

$$(A_0/RT_B) + (c/T_B^3) = B_0$$

$$(A_0/RT_B) + (3c/T_B^3) = V_B \quad (8)$$

$$a(V_B - 3B_0) = V_B^2/k_B + B_0(V_B - 4B_0 - b)$$

An incidental result from these equations is the observation that the Beattie-Bridgman constants found for methane<sup>22</sup> in the usual way<sup>21</sup> are not consistent with the Boyle constants.

In a recent discussion by Martin,<sup>23</sup>  $T_B$  and  $C_B$  are included among the experimental quantities used to help evaluate the constants in multiconstant equations of state. It is suggested that  $k_B$  and  $V_B$  or  $V_0$  should also prove useful for this purpose, and in many cases it may be preferable to have them appear explicitly.

### The Constant for Intermolecular Potentials

All realistic intermolecular potentials possess two basic parameters:  $\epsilon/k$ , a temperature which determines the depth of the potential well, and  $b_0$ , a molecular volume. Most potentials in common use possess a third parameter also, such as the repulsive index,  $n$ , for the Lennard-Jones  $n$ -6 potential. For specified values of the third parameter, the virial coefficients for such potentials are calculated by statistical-mechanical methods and tabulated as  $B^*$ ,  $C^*$ , ..., functions of  $T^*$ , where  $B^* = B/b_0$ ,  $C^* = C/b_0^2$ , ..., and  $T^* = kT/\epsilon$ . From these tables  $T_B^*$  can be found as the  $T^*$  for which  $B^* = 0$ ;  $V_B^*$  can be found as  $T^*B^*/(T^* - T_B^*)$  interpolated as  $T_B^*$  or from  $T^*(dB^*/dT^*)$  if this quantity is also tabulated; and  $C_B^*$  can be found by interpolation of  $C^*$  at  $T_B^*$ . From these we calculate  $k_B$  as  $V_B^{*2}/C_B^*$  and  $V_0^*$  as  $C_B^*/V_B^*$ .

For two-parameter potentials,  $k_B$  is a constant characteristic of the potential, independent of the parameters. The agreement of this  $k_B$  with an experimental value may be taken as a necessary condition for the suitability of a potential for a given substance. For three-parameter potentials,  $k_B$  depends on the third parameter, as illustrated for several potentials in Tables III-VI. The value of  $k_B$  for such potentials can therefore be made to fit an experimental value by adjusting the third parameter, and this is the simplest and perhaps the best way to fix the value of this parameter.

Table III gives  $k_B$  for the exp 6 potential for which the potential  $\phi$  is represented by

$$\phi = \{\epsilon/[1 - (6/\gamma)]\}\{(6/\gamma) \times \exp\{\gamma[(1 - (r/r_m)]\} - (r/r_m)^6\} \quad (9)$$

for intermolecular separations,  $r$ , greater than the value for which the above function reaches a maximum; at smaller  $r$ ,  $\phi$  is taken as infinite. The parameter  $r_m$  is the value of  $r$  at which  $\phi = -\epsilon$ . The intermolecular volume  $b_0$  is the volume of the positive potential; that is,  $b_0 = 2\pi N r_0^3/3$ , where  $r_0$  is the separation at which  $\phi = 0$ . The relation between  $r_m$  and  $r_0$  is given in a table by Sherwood and Prausnitz,<sup>24</sup> who have also calculated  $C^*$  for this potential. Additional values of

(21) J. A. Beattie and O. C. Bridgman, *Proc. Amer. Acad. Arts Sci.*, **63**, 229 (1928).

(22) D. R. Douslin, R. H. Harrison, R. T. Moore, and J. P. McCullough, *J. Chem. Eng. Data*, **9**, 358 (1964).

(23) J. J. Martin, *Ind. Eng. Chem.*, **59**, 34 (1967).

(24) A. E. Sherwood and J. M. Prausnitz, *J. Chem. Phys.*, **41**, 413 (1964).

**Table III:** The Constant for the Exp 6 Potential

$\gamma$	$T_B^*$	$V_B^*$	$C_B^*$	$V_0^*$	$k_B$
12	3.921	0.727	0.316	0.435	1.67
13.5	3.424	0.783	0.329	0.420	1.86
15	3.098	0.825	0.334	0.405	2.04
16	2.935	0.848	0.337	0.398	2.13
18	2.687	0.883	0.340	0.385	2.29
20	2.368	0.913	0.341	0.374	2.44
24	2.258	0.955	0.342	0.359	2.66
30	2.031	0.997	0.341	0.342	2.91
60	1.618	1.083	0.331	0.306	3.54
$\infty$	1.171	1.174	0.350	0.411	3.94

**Table IV:** The Constant for the Kihara Potential

$a^*$	$T_B^*$	$V_B^*$	$C_B^*$	$V_0^*$	$k_B$
0.00	3.418	0.8112	0.3385	0.4173	1.944
0.05	3.126	0.839	0.341	0.407	2.06
0.10	2.880	0.865	0.343	0.396	2.18
0.15	2.671	0.889	0.343	0.386	2.31
0.20	2.491	0.911	0.342	0.375	2.43
0.25	2.335	0.932	0.340	0.365	2.55
0.30	2.198	0.952	0.339	0.355	2.68
0.35	2.077	0.971	0.336	0.346	2.81
0.40	1.970	0.989	0.333	0.337	2.94
0.45	1.874	1.007	0.331	0.328	3.07
0.50	1.788	1.023	0.328	0.320	3.20
0.55	1.711	1.039	0.324	0.312	3.33
0.60	1.641	1.055	0.321	0.304	3.47
0.65	1.577	1.070	0.318	0.297	3.60
0.70	1.518	1.084	0.315	0.290	3.74
0.75	1.464	1.098	0.312	0.284	3.87
0.80	1.415	1.112	0.308	0.277	4.01
0.85	1.369	1.126	0.305	0.271	4.16

**Table V:** The Constant for the Stockmayer Potential

$t^*$	$T_B^*$	$V_B^*$	$C_B^*$	$V_0^*$	$k_B$
0.0	3.418	0.8112	0.3384	0.4172	1.944
0.2	3.471	0.820	0.349	0.425	1.93
0.4	3.622	0.845	0.380	0.450	1.88
0.6	3.855	0.879	0.426	0.485	1.81
0.8	4.151	0.914	0.482	0.527	1.73
1.0	4.495	0.948	0.538	0.567	1.67
1.2	4.876	0.979	0.580	0.592	1.65

$C^*$  are given by Bergeon.<sup>25</sup> The second coefficient  $B^*$  has been given by Rice and Hirschfelder<sup>26</sup> and by Sherwood and Prausnitz.<sup>27</sup> Table III shows the dependence of  $k_B$  on the third parameter  $\gamma$ , which determines the steepness of the repulsive core. The constant increases with  $\gamma$ , reaching 3.94 for  $\gamma = \infty$ , which is the Sutherland potential.

The Kihara potential<sup>6</sup> with a spherical hard core of radius  $a$  surrounded by a Lennard-Jones 12-6 potential is  $\infty$  for  $r \leq 2a$ , and for larger  $r$  is given by

$$\phi = 4\epsilon(X^{12} - X^6) \quad (10)$$

**Table VI:** The Constant for the Square-Well Potential

$\sigma$	$T_B^*$	$V_B^*$	$C_B^*$	$V_0^*$	$k_B$
1.4	2.206	1.244	0.3617	0.2908	4.276
1.5	2.846	1.186	0.4151	0.3500	3.388
1.6	3.573	1.146	0.4657	0.4062	2.822
1.7	4.394	1.118	0.5119	0.4578	2.442
1.8	5.316	1.097	0.5522	0.5033	2.179
1.9	6.346	1.081	0.5851	0.5413	1.997
2.0	7.489	1.068	0.6093	0.5704	1.873
2.1	8.751	1.058	0.6245	0.5902	1.793
2.2	10.140	1.050	0.6336	0.6034	1.740
2.3	11.660	1.044	0.6390	0.6124	1.704
2.4	13.318	1.038	0.6421	0.6186	1.678
2.6	17.071	1.030	0.6445	0.6260	1.645
3.0	26.497	1.019	0.6431	0.6311	1.615
$\infty$	$\infty$	1.000	0.6250	0.6250	1.600

where  $X = (r_0 - 2a)/(r - 2a)$ . For various values of the reduced core parameter defined as  $a^* = 2a/(r_0 - 2a)$ , Sherwood, DeRocco, and Mason<sup>10</sup> gave  $T_B^*$  and  $V_B^*$ , and Sherwood and Prausnitz<sup>24</sup> tabulated  $C^*$ . Table IV lists  $k_B$  as a function of  $a^*$ , and it is seen that  $k_B$  increases with increasing core size. For zero core radius, this model reduces to the Lennard-Jones 12-6 potential whose  $k_B = 1.944$ . It is therefore clear that such gases as argon and krypton, whose  $k_B$ 's are less than 1.944, cannot be adequately represented by this potential, although several attempts have been made (see ref 11, for example). One way of correcting for this inadequacy is to modify the results for the potential by including an estimate of the nonadditive three-body effects, as was done by Sherwood and Prausnitz.<sup>24,27</sup> Another way, which may be preferable since the nonadditive effects are not known accurately, is to modify the additive potential to give the experimentally correct  $C_B$  and  $k_B$ . A hard core with a softer surrounding potential could provide lower values of  $k_B$ , as seen from the fact that the Lennard-Jones 9-6 potential<sup>28,29</sup> has  $k_B = 1.611$ .

This latter result also shows what may be expected from the Lennard-Jones  $n$ -6 potential, whose virial coefficients have not been tabulated in general. In agreement with the results of the exp 6 potential,  $k_B$  appears to increase with increasing steepness of the repulsive potential, represented by  $n$ .

The Stockmayer potential was designed<sup>30</sup> to represent polar molecules and consists of a Lennard-Jones 12-6 potential with an added attractive term depending on

(25) R. Bergeon, *J. Rech. Centre Natl. Rech. Sci. Lab. Bellevue*, **9**, 171 (1958).

(26) W. E. Rice and J. O. Hirschfelder, *J. Chem. Phys.*, **22**, 187 (1954).

(27) A. E. Sherwood and J. M. Prausnitz, *ibid.*, **41**, 429 (1964).

(28) L. F. Epstein and C. J. Hibbert, *ibid.*, **20**, 752 (1952).

(29) L. F. Epstein, C. J. Hibbert, M. D. Powers, and G. M. Roe, *ibid.*, **22**, 464 (1954).

(30) W. H. Stockmayer, *ibid.*, **9**, 398 (1941).

the dipole moment through a third parameter  $t^*$ .  $C^*$  for this potential was given by Rowlinson<sup>31</sup> and was tabulated along with  $B^*$  by Curtiss, Hirschfelder, and Bird.<sup>32</sup> Table V gives  $k_B$  as a function of  $t^*$  and shows that  $k_B$  decreases from the nonpolar Lennard-Jones 12-6 value of 1.944 as the polarity increases. This polar model is therefore inadequate for gases having  $k_B$  above 1.944. Modifications that would permit larger  $k_B$  would be an added Kihara core or the substitution of a Lennard-Jones potential with a stronger repulsive index,  $n$ .

The square-well potential is infinite for  $r \gtrsim r_0, -\infty$  for  $r$  between  $r_0$  and  $gr_0$ , and zero for larger separations. The third parameter,  $g$ , is the ratio of the outer diameter to the inner diameter of the potential well. This model is less realistic than the foregoing, but it is rather versatile, and the dependence of  $k_B$  on  $g$  is known analytically. Kihara<sup>6</sup> has given expressions for  $B^*$ ,  $T_B^*$ ,  $V_B^*$ , and  $C^*$ , from which we find that

$$k_B = [2g(g^3 - 1)]^3 \{ \ln [g^3/(g^3 - 1)] \}^{2/3} / D \quad (11)$$

where  $D = 1 - 18g^2 - 5g^3 + 5g^6$  for  $g \gtrsim 2$  and  $D = 1 - 18g^2 + 27g^3 - 27g^6 - 18g^8 - g^9$  for  $g \leq 2$ . These expressions are evaluated in Table VI for  $g$  from 1.4 to  $\infty$ , in which limit  $C_B$  assumes the hard-sphere value of  $5/8$ . This model can provide any value of  $k_B$  above 1.6, and it is interesting to note that, as far as  $k_B$  is concerned, the broad potential wells represented by large  $g$  can simulate the extended attractive fields of polar molecules with their low  $k_B$ 's, while the relatively narrow wells and wide cores represented by small  $g$  can provide the same large  $k_B$ 's given by the Kihara model with large cores.

From this survey of the  $k_B$  values provided by some common intermolecular potentials, the usefulness of  $k_B$  in selecting an appropriate potential model is apparent. The correct  $k_B$  is, however, a necessary but probably not a sufficient condition for the suitability of a potential to a gas. For example,  $\text{CF}_4$ , with its  $k_B$  of about 2.9, cannot be represented by the Lennard-Jones 12-6 or 9-6 potentials or by the Stockmayer potential but could be represented by the square-well potential with  $g$  a little less than 1.6, by the Kihara potential with  $a^* \approx 0.38$ , and by the exp 6 potential with  $\gamma \approx 30$ . Presumably, all potentials that provide the correct  $k_B$  will differ somewhat in their predictions of at least some other properties, and these differences will ultimately determine the best potential.

It is interesting to observe that, with this use of  $k_B$ , there exists a 1:1 correspondence between the three experimental  $PVT$  constants,  $T_B$ ,  $V_B$ , or  $V_0$ , and  $k_B$  on the one hand and the parameters of any three-parameter potential on the other. Thus the Boyle temperature determines  $\epsilon/k$  as  $T_B/T_B^*$ ; the UCL volume or the Boyle volume determines  $b_0$  as  $V_0/V_0^*$  or  $V_B/V_B^*$ ; and  $k_B$  fixes the third parameter at the only value for which that potential form gives the same  $b_0$

from both  $V_0$  and  $V_B$ . Thus we see that, assuming additivity, all three parameters of a given potential form can be evaluated unambiguously from sufficiently accurate compressibility data alone, measured over a relatively small temperature range in the vicinity of  $T_B$ .

### The Three-Constant System of Corresponding States

As noted earlier, an important potential use of  $k_B$  is as the third constant, along with  $T_B$  and  $V_0$ , in a three-constant system of corresponding states. In its general form, this system would assume that two gases having the same  $k_B$  should correspond in all their properly reduced properties at equal reduced temperatures and reduced volumes. Gases with different  $k_B$ 's would not so correspond, but the reduced properties as functions of  $T/T_B$  and  $V/V_0$  could be tabulated for a series of different  $k_B$  values. However, a particular form of this three-constant system is available, in which the effect of the third constant is shown in an explicit, analytic manner, thereby eliminating the need for multiple tabulations.

This highly useful version was introduced in ref 17, where the very accurate correlation of the compressibility factors of argon and methane mentioned earlier was obtained with the two UCL constants and a third constant defined as the ratio of the deviations from ideality for the two gases at equal reduced temperatures and densities. Considering this third constant as the ratio of two constants,  $k$ , characteristic of the two gases, it was assumed that  $(Z - 1)/k$  is a corresponding property for different gases at equal reduced  $T$  and  $V$ .

We can easily relate this constant  $k$  to our constant  $k_B$ . The virial equation of state, eq 4, can be written as

$$(Z - 1)/k = (B/kV_0)\delta + (C/kV_0^2)\delta^2 + \dots \quad (12)$$

where  $\delta$  is the reduced density,  $d/d_0 = dV_0$ , and the virial coefficients,  $B, C, \dots$ , are functions of temperature but not density. From the assumption that  $(Z - 1)/k$  is a universal function of  $\theta = T/T_B$  and  $\delta$ , it therefore follows that  $B/kV_0$  and  $C/kV_0^2$  are universal functions of  $\theta$  only. From the definition of  $V_B$ , eq 1, we see that  $V_B$  is  $dB/d\theta$  evaluated at  $\theta = 1$ , so that  $V_B/V_0k$  should be a universal constant. Because we are dealing usually with ratios of  $k$ , we can set the constant  $V_B/V_0k$  equal to unity for convenience, allowing us to identify  $k_B$  with  $k$ , according to eq 3. Thus the ratio of  $k_B$  for two gases determines the relative deviation of their compressibilities from ideality at equal  $\theta$ 's and  $\delta$ 's. The constant ratio of  $(Z - 1)$ 's producing the best correspondence of the compressibilities of  $\text{CH}_4$  and Ar

(31) J. S. Rowlinson, *J. Chem. Phys.*, **19**, 827 (1951).

(32) J. O. Hirschfelder, C. F. Curtiss, and R. B. Bird, "Molecular Theory of Gases and Liquids," John Wiley & Sons, Inc., New York, N. Y., 1954.

over the fairly extended range of  $\theta$  between 0.54 and 1.22 and  $\delta$  up to 0.36 was found in ref 17 to be 1.044, and the agreement of this with the ratio of  $k_B$ 's from Table I ( $1.94/1.86 = 1.04$ ) is quite satisfactory. Comparison of the deviations from ideality of a given gas and a standard such as Ar or CH<sub>4</sub> can therefore provide reliable experimental values of  $k_B$ .

It will be of interest in the future to find the extent of the validity of this interpretation of  $k_B$ . It predicts, for example, that the more polar of two Stockmayer gases (cf. Table V) will show the smaller deviation from ideality at equal  $\theta$  and  $\delta$ . Further implications can be seen from the following. With the help of eq 3, we can write eq 12 as

$$Z = 1 + (B/V_B)\delta + (C/C_B)\delta^2 + \dots \quad (13)$$

This equation shows that the assumption that  $(Z - 1)/k_B$  is a universal function of  $\theta$  and  $\delta$  implies the previously mentioned correspondence of  $B/V_B$  at equal  $\theta$  which has been observed both for experimental values and for those calculated from various intermolecular potential models. The deviations of the calculated values for different potentials at very high and low temperatures indicate that our assumption would be in error at extreme temperatures.

Taking the consequences of our assumption one step further, we note that eq 13 implies that  $C/C_B$  should also be a universal function of  $\theta$ . A good test of this is provided by the experimental data of Douslin, Harrison, and Moore for CH<sub>4</sub>, CF<sub>4</sub>, and their mixtures,<sup>13</sup> for which  $C_B$  and  $k_B$  cover a wide range of values, as seen in Table I. A single empirical equation

$$C/C_B = 1 - 0.6y + 0.4y^2 - 0.15y^3 \quad (14)$$

in which  $y = 1 - (1/\theta)$ , fits the 80  $C$  values of the 5 gases (2 pure gases and 3 mixtures) given in ref 13 with a maximum deviation of 5%, which is probably within experimental error.

As far as theoretical calculations are concerned, an inspection of the figures in ref 6, 10, 24, and 27 shows that  $C^*(T^*)$  for the various intermolecular potentials all have similar shapes, so that  $C^*/C_B^*$  vs.  $T^*/T_B^*$  will correspond well at temperatures not too far removed

from  $T_B^*$ . However, at very low temperatures the correspondence is poor, since  $C^*$  drops sharply and becomes negative at different  $\theta$  for different potentials. At a  $\theta$  for which one potential gives a large positive  $C^*$  and another a large negative  $C^*$ , the  $Z$  or  $(Z - 1)/k_B$  vs.  $\delta$  isotherms cannot be superimposable because they will have opposite curvatures at low  $\delta$ . However, it appears that the calculated  $C^*(\theta)$  will agree much better for potentials having the same  $k_B$  values. For example, the Kihara potential with  $a^* = 0.15$  and the exp 6 potential with  $\gamma = 18$  have nearly the same  $k_B$  of 2.3 and from the tables in ref 24 can be seen to correspond in  $C/C_B$  within 2 or 3% over the entire range of  $T^*$  from 0.5 to 10 and in particular to become negative at about the same  $\theta$ . This suggests that at the extremes of temperature the general three-constant system of corresponding states may be much more accurate than the particular version in which the effect of  $k_B$  is given analytically as in eq 12. This is not a practical concern, however, since few if any experimental measurements of  $C$  have been made at temperatures low enough to observe the theoretically predicted drop below zero, except for highly associated fluids.

It therefore appears that the  $T_B$ ,  $V_0$ , and  $k_B$  system of corresponding states with explicit  $k_B$  dependence may prove very useful in the usual experimental range of *PVT* measurements. If successful, this system will permit the accurate calculation of equilibrium and possibly nonequilibrium properties of any gas from tabular or empirical analytic representations of these properties as universal function of  $\theta$  and  $\delta$ , simply from a knowledge of the three characteristic constants,  $T_B$ ,  $V_0$ , and  $k_B$ , for that gas.

In ref 17 it was shown that the correspondence of  $(Z - 1)/k_B$  at equal  $\theta$  and  $\delta$  produces an analogous correspondence in the residual thermodynamic properties, provided they are divided by  $k_B$  and also reduced by the dimensionally proper combination of  $R$ ,  $T_B$ , and  $V_0$ . It is interesting to note that  $V_0$  rather than  $V_B$  is the required reducing volume. In the case of the second virial coefficient, reduction of  $B/k_B$  by  $V_0$  is equivalent to the reduction of  $B$  by  $V_B$ , but for other properties such as  $C/k_B$  the equivalency disappears, and  $V_0$  is the more fundamental reference volume.

## Thermodynamic Properties of Nonaqueous Solutions. VI.

### Enthalpies of Solution of Some Tetraalkylammonium

### Iodides in Water and N,N-Dimethylformamide at 25°

by Om N. Bhatnagar and Cecil M. Criss<sup>1</sup>

*Department of Chemistry, University of Miami, Coral Gables, Florida 33124 (Received July 29, 1968)*

Heats of solution of  $(\text{CH}_3)_4\text{NI}$ ,  $(\text{C}_2\text{H}_5)_4\text{NI}$ , and  $(\text{C}_3\text{H}_7)_4\text{NI}$  have been measured in N,N-dimethylformamide (DMF) and in water in the concentration range  $3.5 \times 10^{-4}$  to  $5 \times 10^{-3} \text{ m}$  and have been extrapolated to infinite dilution by the simple Debye-Hückel equation in order to obtain standard heats of solution in the two solvents. Enthalpies of transfer,  $\Delta H_{tr}^{\circ}$ , of the salts from water to DMF have been calculated and compared with other  $\Delta H_{tr}^{\circ}$  data taken from the literature. Although in every case examined there is an unexpectedly large change in  $\Delta H_{tr}^{\circ}$  between  $\text{CsI}$  and  $(\text{CH}_3)_4\text{NI}$ , it is shown that this change cannot be fully explained in terms of the ice-like structure of water molecules around the tetraalkylammonium ions. The modified Born equation is shown to be inadequate to explain, even qualitatively, the behavior of the enthalpies of transfer for these salts and the alkali metal iodides from water to DMF and other solvents, or between two nonaqueous solvents.

#### Introduction

Tetraalkylammonium halides have attracted much attention in the past few years because of their abnormal behavior in aqueous solutions.<sup>2,3</sup> Most generally the abnormal properties have been attributed to the structural changes in water which occur in the vicinity of the  $\text{R}_4\text{N}^+$  species. While these salts have been of considerable interest generally, only a few enthalpy-of-solution data exist for these compounds in either aqueous or nonaqueous systems at 25°. Latimer, Pitzer, and Coulter<sup>4</sup> reported heats of solution of  $(\text{CH}_3)_4\text{NI}$  in water and Samoilov<sup>5</sup> reported a heat of solution in water at one concentration for  $(\text{CH}_3)_4\text{NBr}$ . More recently Arnett and McKelvey<sup>6</sup> have measured heats of solution of the tetraethylammonium halides in water and in dimethyl sulfoxide (DMSO); Wu and Friedman<sup>7</sup> reported heat data for tetramethyl- and tetraethylammonium halides in water and propylene carbonate (PC); and Boyd and Wang<sup>8</sup> have made similar measurements in water, methanol, and acetonitrile. In all these latter investigations, heats of transfer from water to the nonaqueous solvent were evaluated. No heat-of-solution data have been reported for  $(\text{C}_3\text{H}_7)_4\text{NI}$  in water or for any tetraalkylammonium salts in dimethylformamide (DMF). In continuation of our enthalpy measurements in nonaqueous solutions,<sup>9,10</sup> it appeared worthwhile to measure heats of solution of the tetraalkylammonium iodides in water and DMF, to evaluate the enthalpies of transfer, and to compare them with enthalpies of transfer for other solvent pairs.

#### Experimental Section

**Salts.** Eastman Kodak's  $(\text{CH}_3)_4\text{NI}$  and  $(\text{C}_3\text{H}_7)_4\text{NI}$  and Baker's  $(\text{C}_2\text{H}_5)_4\text{NI}$  were used in the experiments.

$(\text{C}_2\text{H}_5)_4\text{NI}$  and  $(\text{C}_3\text{H}_7)_4\text{NI}$  were recrystallized twice from a chloroform-ether mixture and  $(\text{CH}_3)_4\text{NI}$  was recrystallized twice from a methanol-ether mixture. The salts were dried at 70° in a vacuum oven for 3–4 days, then in a vacuum desiccator for 3 days. Because of the hygroscopic nature of the salts, they were immediately transferred to a vacuum drybox under a dry nitrogen atmosphere. The iodide content for all three salts, determined gravimetrically by  $\text{AgI}$ , was 99.6% of the theoretical value.

**Solvents.** Singly distilled water, which was passed through a deionizing column, was used for all the aqueous studies. Eastman's DMF was distilled at 65° and 15 mm of pressure through a distillation column filled with glass helices. The distillate was dried over freshly heated  $\text{BaO}$  for 8–10 hr, the contents being shaken intermittently. The liquid phase was removed and distilled again from  $\text{BaO}$ . This process was repeated until the conductance was  $2 \times 10^{-7} \text{ ohm}^{-1} \text{ cm}^{-1}$  or below. The amount of water in the DMF, as deter-

- (1) To whom correspondence should be directed.
- (2) W. Y. Wen and S. Saito, *J. Phys. Chem.*, **68**, 2639 (1964).
- (3) R. H. Wood, H. L. Anderson, J. D. Beck, J. R. France, W. E. de Vry, and L. J. Soltzberg, *ibid.*, **71**, 2149 (1967).
- (4) W. M. Latimer, K. S. Pitzer, and L. V. Coulter, *J. Amer. Chem. Soc.*, **62**, 2845 (1940).
- (5) O. Y. Samoilov, *Dokl. Akad. Nauk SSSR*, **81**, 641 (1951).
- (6) E. M. Arnett and D. R. McKelvey, *J. Amer. Chem. Soc.*, **88**, 2598 (1966).
- (7) Y. C. Wu and H. L. Friedman, *J. Phys. Chem.*, **70**, 2020 (1966).
- (8) R. H. Boyd and P. S. Wang, Abstracts of Papers, 155th National Meeting of the American Chemical Society, San Francisco, Calif., April 1968. See also P. S. Wang, M.S. Thesis, Utah State University, Logan, Utah, 1967.
- (9) R. P. Held and C. M. Criss, *J. Phys. Chem.*, **69**, 2611 (1965).
- (10) R. P. Held and C. M. Criss, *ibid.*, **71**, 2487 (1967).

mined by a Luft Karl Fischer titrator, never exceeded 0.01%.

*Apparatus and Procedure.* The calorimeter, associated instrumentation, and procedure have been described in detail.<sup>9</sup> The same precautions were taken to avoid contact of DMF with atmospheric moisture. Because of the low decomposition temperature of the tetraalkylammonium salts, the thin-walled sample bulbs were immersed in ice water to the base of the neck while being sealed by a torch under vacuum.

Originally it was planned to measure heats of solution of  $(C_4H_9)_4NI$ , but this salt was observed to float on the surface of the solvent causing an extremely uncertain dissolution time.

### Results and Discussion

The results are given in Tables I and II. The data were extrapolated to infinite dilution in accordance with the simple Debye-Hückel theory, although in some cases it did not represent the best straight line through the data. The resultant standard heats of solution are listed in Table III, along with the standard deviation of the data from the curve. A Debye-Hückel limiting slope of  $1740 \text{ cal kg}^{1/2} \text{ mol}^{-1/2}$ <sup>10</sup> was used in extrapolating the DMF solutions. Within the limits of experimental error, the observed slopes in both solvents were not significantly different from theory. The tetraalkylammonium salts, like other electrolytes,<sup>10</sup> exhibit much smaller heats of solution in DMF than in water.

From the standard heats of solution, standard enthalpies of transfer of the electrolytes from water to DMF have been calculated and are listed in Table IV.

**Table I:** Integral Heats of Solution of Tetraalkylammonium Iodides in DMF at 25°

$10^4m$ , mol/kg of DMF	$10^2m^{1/2}$	$\Delta H_s$ , kcal/mol
$(CH_3)_4NI$		
2.77	1.66	4.04
3.01	1.74	4.02
4.20	2.05	4.06
8.78	2.96	4.05
23.3	4.83	4.06
$(C_2H_5)_4NI$		
7.58	2.75	3.46
9.42	3.07	3.44
21.9	4.68	3.49
30.7	5.54	3.49
42.5	6.52	3.49
52.0	7.21	3.50
$(C_3H_7)_4NI$		
2.51	1.58	2.01
4.21	2.05	2.06
13.8	3.72	2.02
19.6	4.43	2.07
38.1	6.17	2.08
44.8	6.69	2.07

**Table II:** Integral Heats of Solution of Tetraalkylammonium Iodides in Water at 25°

$10^4m$ , mol/kg of $H_2O$	$10^2m^{1/2}$	$\Delta H_s$ , kcal/mol
$(CH_3)_4NI$		
8.19	2.86	9.92
8.33	2.87	9.92
15.1	3.89	10.00
21.7	4.66	9.98
24.1	4.91	9.99
38.9	6.24	10.05
54.8	7.40	10.03
$(C_2H_5)_4NI$		
3.50	1.87	6.70
4.49	2.12	6.62
5.71	2.39	6.71
11.3	3.36	6.81
16.2	4.02	6.75
20.0	4.47	6.78
29.5	5.43	6.73
$(C_3H_7)_4NI$		
3.72	1.93	2.79
9.20	3.03	2.74
17.6	4.20	2.75
19.2	4.38	2.76
33.3	5.77	2.78
49.8	7.06	2.80

**Table III:** Standard Heats of Solution of Tetraalkylammonium Iodides in DMF and Water at 25°

	$\Delta H_s^\circ$ , kcal/mol	DMF	$H_2O^a$	$H_2O^b$
$(CH_3)_4NI$	$4.010 \pm 0.014$	9.99	$\pm 0.05$	10.13 (10.050)
$(C_2H_5)_4NI$	$3.420 \pm 0.025$	6.74	$\pm 0.06$	6.86
$(C_3H_7)_4NI$	$1.996 \pm 0.021$	2.765	$\pm 0.025$	

<sup>a</sup> This work. <sup>b</sup> Reference 8 except value in parentheses, which is from ref 4.

Table IV also lists standard enthalpies of transfer of alkali metal iodides from water to DMF, calculated from data in the literature,<sup>10-12</sup> as well as heats of transfer from water to other solvents, also reported in the literature.<sup>6-8</sup>

The derivative of the Bcrn equation, as modified by Latimer, Pitzer, and Slansky,<sup>13</sup> gives for the enthalpy of solvation the expression<sup>10</sup>

$$\Delta H_i^\circ = -\frac{e_i^2[1 - (1/\epsilon)]}{2(r_i + \delta)} \times \left[ 1 - \frac{T(\partial\epsilon/\partial T)}{\epsilon(\epsilon - 1)} + \frac{T}{(r_i + \delta)} \left( \frac{\partial\delta}{\partial T} \right) \right] \quad (1)$$

(11) L. Weeda and G. Somsen, *Rec. Trav. Chim.*, **86**, 893 (1967).

(12) V. B. Parker, "Thermal Properties of Aqueous Uni-univalent Electrolytes," National Bureau of Standards Report NSRDS-NBS 2, U. S. Government Printing Office, Washington, D. C., April 1965.

(13) W. M. Latimer, K. S. Pitzer, and C. M. Slansky, *J. Chem. Phys.*, **7**, 108 (1939).

**Table IV:** Standard Enthalpies of Transfer from Water to Various Nonaqueous Solvents at 25°<sup>a</sup>

Salt	$\Delta H_{tr}^{\circ}$ (solvent $\leftarrow$ H <sub>2</sub> O), kcal/mol			
	DMF <sup>a</sup>	PC <sup>a</sup>	DMSO <sup>f</sup>	CH <sub>3</sub> OH
LiI	-3.97 <sup>b</sup> (-11.8) <sup>c</sup>	-0.10		
NaI	-11.35 <sup>b</sup> (-12.15) <sup>d</sup>	-3.22	-9.67	-6.21 <sup>e</sup>
KI	-12.90 <sup>b</sup>	-6.02	-11.36	
CsI	-12.22 <sup>b</sup> (-12.22) <sup>d</sup>	-7.18	-10.30	-3.82 <sup>a</sup>
(CH <sub>3</sub> ) <sub>4</sub> NI	-5.98	-4.74		-0.39 <sup>h</sup>
(C <sub>2</sub> H <sub>5</sub> ) <sub>4</sub> NI	-3.32	-0.59	-1.97	1.25 <sup>h</sup>
(C <sub>3</sub> H <sub>7</sub> ) <sub>4</sub> NI	-0.769			

<sup>a</sup> Where only heats of solution in the nonaqueous solvent have been reported, the heats of solution in water, used in calculating the heats of transfer, have been taken from ref 12. <sup>b</sup> Heat-of-solution data taken from ref 11. <sup>c</sup> Calculated from heat-of-solution data of NaI, NaBr, and LiBr taken from ref 10. The standard heat of solution of LiBr was obtained from an extrapolation of the data from concentrations  $> 3 \times 10^{-4}$  m. The standard heats of formation of the crystalline salts used in the calculation are from W. M. Latimer, "The Oxidation States of the Elements and Their Potentials in Aqueous Solutions," 2nd ed, Prentice-Hall, Inc., Englewood Cliffs, N. J., 1952. <sup>d</sup> Heat-of-solution data taken from ref 10. <sup>e</sup> Reference 7. <sup>f</sup> Reference 6. <sup>g</sup> S. I. Drakin and C. Yu-min, *Russ. J. Phys. Chem.*, **38**, 1526 (1964). <sup>h</sup> Reference 8.

where  $e_i$  and  $r_i$  are the charge and crystal radius of the ion, respectively;  $\epsilon$  is the dielectric constant of the solvent; and  $\delta$  is a parameter which depends upon the sign of the charge on the ion and the solvent. The difference in the enthalpy of solvation for a given ionic species in two solvents, X and Y, gives the enthalpy of transfer of the corresponding ion between the two solvents. Consequently, if one assumes that  $\partial\delta/\partial T$  is negligibly small, one can obtain for the enthalpy of transfer of ions from solvent X to solvent Y the expression

$$\Delta H_{tr}^{\circ} = -\frac{e_i^2}{2} \left( \frac{K_Y}{r_i + \delta_Y} - \frac{K_X}{r_i + \delta_X} \right) \quad (2)$$

where  $K_X$  and  $K_Y$  are constants characteristic of the solvent and equal  $[1 - (1/\epsilon)] \{ 1 - [T(\partial\epsilon/\partial T)/\epsilon(\epsilon - 1)] \}$  where  $\epsilon$  is the dielectric constant of the respective solvent.

For cations,  $\delta$  is approximately constant for the solvents H<sub>2</sub>O, DMF, and PC.<sup>10,14</sup> If this generally true, eq 2 can be written as

$$\Delta H_{tr}^{\circ} = -\frac{e_i^2(K_Y - K_X)}{2(r_i + \delta)} \quad (3)$$

where  $\delta \approx \delta_X \approx \delta_Y$ . Consequently, the enthalpies of transfer should be a linear function of  $1/(r_i + \delta)$  for cations.

Wu and Friedman<sup>7</sup> and Friedman<sup>15</sup> have shown that the enthalpies of transfer of ions between water and propylene carbonate decrease with increasing radius for the alkali metal ions but there is an interruption of this trend between Cs<sup>+</sup> and the tetraalkylammonium ions.

They explain this phenomenon in terms of the iceberg effect proposed by Frank and Evans,<sup>16</sup> in which water molecules are more highly ordered in the vicinity of hydrocarbons. Presumably, the hydrocarbon qualities of the tetraalkylammonium ions give the extra stabilization for iceberg formation in aqueous solutions.

An examination of enthalpies of transfer of salts from water to DMF and DMSO, listed in Table IV, shows that there is neither a continuous increase nor a decrease of  $\Delta H_{tr}$  with increasing radius as predicted by eq 3, even for the alkali metal ions. The lack of a trend consistent with eq 3 is also observed for enthalpies of transfer of the alkali metal ions from water to formamide and N-methylformamide.<sup>17</sup>

Even though, in general, the alkali metal ions do not follow the trend predicted by eq 3, there is, nevertheless, surprisingly large changes in the enthalpies of transfer between CsI and (CH<sub>3</sub>)<sub>4</sub>NI for each of the solvents listed in Table IV. On first consideration one might conclude that these large changes are caused by the unique structure of water around the tetraalkylammonium ions as suggested by Wu and Friedman<sup>7</sup> for the H<sub>2</sub>O-PC solvent pair. While this argument is appealing, it probably is not the complete explanation, since interruptions can also be observed between CsI and (CH<sub>3</sub>)<sub>4</sub>NI for solvent pairs not involving water. Table V lists enthalpies of transfer of electrolytes between nonaqueous solvents. Although the sparsity of data makes trends more difficult to discern, there nevertheless

**Table V:** Standard Enthalpies of Transfer between Various Nonaqueous Solvents at 25°<sup>a</sup>

	PC	DMSO	CH <sub>3</sub> OH
Solvent $\leftarrow$ DMF			
LiI	3.87 (11.7)		
NaI	8.13 (8.93)	1.68 (2.48)	5.14 (5.94)
KI	6.88	1.54	
CsI	5.04 (5.04)	1.92	8.40 (8.40)
(CH <sub>3</sub> ) <sub>4</sub> NI	1.24		5.59
(C <sub>2</sub> H <sub>5</sub> ) <sub>4</sub> NI	2.73	1.35	4.57
Solvent $\leftarrow$ PC			
NaI		-6.45	-2.99
KI		-5.34	
CsI		-3.12	3.36
(CH <sub>3</sub> ) <sub>4</sub> NI			4.35
(C <sub>2</sub> H <sub>5</sub> ) <sub>4</sub> NI		-1.38	1.84
Solvent $\leftarrow$ DMSO			
NaI			3.46
CsI			6.48
(C <sub>2</sub> H <sub>5</sub> ) <sub>4</sub> NI			3.22

<sup>a</sup> See Table IV for sources of data.

(14) Y. C. Wu and H. L. Friedman, *J. Phys. Chem.*, **70**, 501 (1966).

(15) H. L. Friedman, *ibid.*, **71**, 1723 (1967).

(16) H. S. Frank and M. W. Evans, *J. Chem. Phys.*, **13**, 507 (1945).

(17) L. Weeda and G. Somsen, *Rec. Trav. Chim.*, **85**, 159 (1966).

less appear to be interruptions between  $\text{CsI}$  and  $(\text{CH}_3)_4\text{NI}$  for the DMF-PC,  $\text{CH}_3\text{OH}-\text{DMF}$ , and  $\text{CH}_3\text{OH}-\text{DMSO}$  solvent pairs. The interruption for the  $\text{CH}_3\text{OH}-\text{PC}$  solvent pair occurs between  $(\text{CH}_3)_4\text{NI}$  and  $(\text{C}_2\text{H}_5)_4\text{NI}$ . At the present time it appears that no general statement can be made in terms of solvent structure to explain the  $\Delta H_{tr}^\circ$  data for the various solvent pairs.

We conclude that (1) the modified Born equation, satisfactory as it may be in describing free energies of solvation,<sup>13,18</sup> as it is now expressed is not suitable for predicting heats of transfer of cations even qualitatively, and (2) the large change observed in  $\Delta H_{tr}^\circ$  as one proceeds from  $\text{Cs}^+$  to  $(\text{CH}_3)_4\text{N}^+$  is not explained by the water structure alone but is the result of special interactions of the tetraalkylammonium ions with solvents in general.

Weeda and Somsen<sup>17</sup> have applied the van Eck theory<sup>19</sup> to enthalpies of transfer of alkali metal iodides and have found  $\Delta H_{tr}^\circ$  to be relatively constant, as predicted by the theory, for sodium, potassium, rubidium, and cesium iodides between water and formamide but not constant for the same salts upon transfer from water to N-methylformamide. Table IV shows that, in general, the van Eck theory is not consistent with  $\Delta H_{tr}^\circ$  data.

*Acknowledgment.* The authors are grateful to the National Science Foundation for their financial support through Grant GP-7870.

(18) C. M. Criss and E. Lukška, *J. Phys. Chem.*, **72**, 2966 (1968).

(19) C. L. van P. van Eck, Thesis, University of Leiden, Leiden, The Netherlands, 1958.

## The Pyrolysis of Biacetyl and the Third-Body Effect on the Combination of Methyl Radicals

by K. J. Hole and M. F. R. Mulcahy

CSIRO Division of Mineral Chemistry, Coal Research Laboratory, Chatswood, NSW, Australia (Received July 29, 1968)

The kinetics of pyrolysis of biacetyl at 677–776°K and 0.6–45 torr have been investigated by the stirred-flow method. The decomposition (to carbon monoxide, methane, ketene, acetone, ethane, and 2,3-pentanedione) is shown to be a chain reaction initiated by reaction 1, propagated by reactions 3 and 8, and terminated mainly by reaction 6, which is strongly pressure dependent. The following kinetics data were obtained ( $k$  and  $A$  being in  $\text{cm}^3 \text{mol}^{-1} \text{sec}^{-1}$ )

	Order	$k$ (at 730°K)	$\log A$	$E, \text{kcal mol}^{-1}$
(1) $(\text{CH}_3\text{CO})_2 \rightarrow 2\text{CH}_3\text{CO}$	1	$7.6 \times 10^{-5}$	16.0	$67.2 \pm 3.3$
(3) $\text{CH}_3 + (\text{CH}_3\text{CO})_2 \rightarrow \text{CH}_4 + \text{CH}_2\text{COCOCH}_3$	2	$1.2 \times 10^9$	11.8	9.1
(6) $\text{CH}_3 + \text{CH}_3 (+\text{M}) \rightarrow \text{C}_2\text{H}_6 (+\text{M})$	3	$1.6 \times 10^{20}$	16.3	$\sim -13$
(8) $\text{CH}_3 + (\text{CH}_3\text{CO})_2 \rightarrow (\text{CH}_3)_2\text{CO} + \text{CH}_3\text{CO}$	2	$2.6 \times 10^8$	10.3	6.3

Pressures of biacetyl, at which the second-order rate constant for reaction 6 is half its limiting high-pressure value, increase from 14 torr at 677°K to 30 torr at 776°K and are in satisfactory agreement with values calculated by previous authors on the basis of the RRKM theory assuming a "loose" activated complex and strong deactivating collisions. The presence of a trace of 2-hydroxy-2-methylbutan-3-one in the products is regarded as evidence that reaction 8 proceeds through formation of the radical  $(\text{CH}_3)_2\text{C}(\text{O}\cdot)\text{COCH}_3$ . The heat of formation of the gaseous acetyl radical is estimated to be  $-5.1 \pm 2.0 \text{ kcal mol}^{-1}$  at 298°K.

### Introduction

Much of the recent progress in understanding the kinetics of pyrolytic and free-radical reactions has been achieved from studies of the same elementary reactions in different reaction systems. Translation of an elementary reaction from one environment to another may bring into prominence in the second system kinetic features which are vestigial or absent in the first;

important examples of this are the occurrence of pressure dependence in recombinations<sup>1–3</sup> and the unimolecular decompositions<sup>4–6</sup> of radicals. The study of biacetyl reported here was carried out with a twofold pur-

- (1) R. E. Dodd and E. W. R. Steacie, *Proc. Roy. Soc., A223*, 283 (1954).
- (2) N. L. Arthur and T. N. Bell, *Chem. Commun.*, **9**, 166 (1965).
- (3) L. F. Loucks, *Can. J. Chem.*, **45**, 2775 (1967).

pose: first, to examine the behavior of methyl and acetyl radicals in a somewhat different system from those hitherto investigated, and, second, to test the suitability of biacetyl as a pyrolytic source of methyl radicals for studies at higher temperatures than are available to less stable sources such as di-*t*-butyl peroxide and azomethane.

Rice and Walters<sup>7,8</sup> have established that the pyrolysis of biacetyl is a homogeneous first-order chain reaction at 650–740°K and about 200 torr, and Taylor<sup>9</sup> has applied the toluene-carrier technique to obtain Arrhenius parameters for the initial unimolecular fission of the molecule. A detailed kinetic analysis of the over-all reaction does not seem to have been carried out previously.

### Experimental Section

The pyrolysis was carried out at 404–503° and 0.6–45 torr in a stirred-flow apparatus of the type described previously.<sup>10–13</sup> The pressure in the reactor was measured by a dibutyl phthalate manometer,<sup>14</sup> via a N<sub>2</sub> buffer. There was no carrier gas. Products and excess biacetyl passed successively through a trap at –78° and a Ward-LeRoy still at –175°. Products volatile at –175° passed to a calibrated volume and were analyzed by gas chromatography ( $\pm 2\%$  for each gas). A fraction, consisting solely of ketene (as determined by ir spectroscopy and gas chromatography), was distilled from the Ward still at –125° and was determined volumetrically ( $\pm 2\%$ ). The liquid collected at –78° contained acetone and 2,3-pentanedione (pd) together with traces of 2-hydroxy-2-methylbutan-3-one (HMB) and an unidentified substance in a large excess of biacetyl. The liquid was weighed and analyzed by gas chromatography on a 3 ft  $\times$   $1/8$  in. Poropak Q column with a flame ionization detector (acetone to  $\pm 5\%$ ). This column, chosen after trying a number of others, gave fair resolution of 0.01–0.1% pd from the bulk of biacetyl, but the accuracy of determination was not better than  $\pm 10\%$ . The presence of HMB was established by identical retention times with those of an authentic sample on Poropak Q and on Ucon 5% on Chromosorb G (80–100 M), respectively. The unknown trace product had a retention time on Poropak Q double that of 2-hydroxy-2-methylbutan-3-one; its mass spectrum (AEI, MS9) suggested 2-hydroxy-3-methoxy-2,3-dimethylbutane, but the small amount of product available prevented conclusive identification.

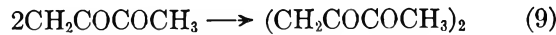
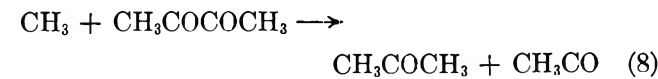
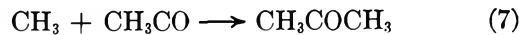
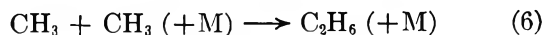
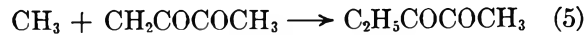
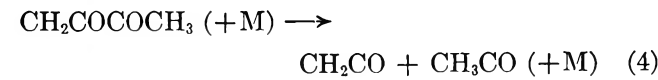
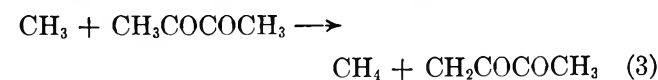
Biacetyl (BDH) was purified by preparative gas chromatography on Ucon (20%)-Chromosorb W (36–44 M) (24 ft  $\times$  0.5 in.). No impurity ( $\geq 0.01\%$ ) could be detected in the purified product on an analytical column.

### Results and Discussion

*Products and Stoichiometry.* The main products of pyrolysis (each greater than 5 mol % of the total) were found to be carbon monoxide, methane, ketene, and

acetone; minor products (<5, >0.3%) were ethane and 2,3-pentanedione. Traces (<0.3%) of ethylene, carbon dioxide, propane, 2-hydroxy-2-methylbutan-3-one, and possibly 2-hydroxy-3-methoxy-2,3-dimethylbutane were also found.

Primary kinetic data are given in Table I. The experiments identified by P in column 1 were carried out with a reactor containing 14 g of quartz wool; this increased the surface:volume ratio tenfold. Unless otherwise indicated, the following discussion refers to the unpacked reactor. Since the decomposition was not carried beyond 5% and frequently was <2%, the rates of disappearance of biacetyl and the formation of products could not be compared accurately. However, element balances H:C:O taken over the total products were always close to 3:2:1 (see Table II); it is therefore improbable that a major product was missed in the analysis. Stoichiometrically the products are accounted for by reactions 1–8 of the mechanism



which is essentially that proposed by Blacet and Bell<sup>15,16</sup>

- (4) E. O'Neal and S. W. Benson, *J. Chem. Phys.*, **36**, 2196 (1962).
- (5) M. Flowers, L. Batt, and S. W. Benson, *ibid.*, **37**, 2662 (1962).
- (6) M. F. R. Mulcahy and D. J. Williams, *Aust. J. Chem.*, **17**, 1291 (1964).
- (7) F. O. Rice and W. D. Walters, *J. Chem. Phys.*, **7**, 1015 (1939).
- (8) W. D. Walters, *J. Amer. Chem. Soc.*, **62**, 880 (1940).
- (9) J. W. Taylor, Ph.D. Thesis, Manchester, 1953, quoted by A. F. Trotman-Dickenson, "Gas Kinetics," Butterworth and Co. Ltd., London, 1955, p 111.
- (10) M. F. R. Mulcahy and D. J. Williams, *Aust. J. Chem.*, **14**, 534 (1961).
- (11) J. de Graaf and H. Kwart, *J. Phys. Chem.*, **67**, 1458 (1963).
- (12) M. F. R. Mulcahy, D. J. Williams, and J. R. Wilmshurst, *Aust. J. Chem.*, **17**, 1329 (1964).
- (13) M. F. R. Mulcahy, B. G. Tucker, D. J. Williams, and J. R. Wilmshurst, *ibid.*, **20**, 1155 (1967).
- (14) A. T. J. Hayward, *J. Sci. Instrum.*, **40**, 173 (1963).
- (15) F. E. Blacet and W. E. Bell, *Discussions Faraday Soc.*, **14**, 70 (1953).
- (16) W. E. Bell and F. E. Blacet, *J. Amer. Chem. Soc.*, **76**, 5332 (1954).

Table I: Kinetic Data for Pyrolysis of Biacetyl<sup>a</sup>

Experiment no.	Temp, °C	P, torr	10 <sup>9</sup> × efflux of products ( $n_i$ ), mol sec <sup>-1</sup>					
			$n_{CO}$	$n_m$	$n_e$	$n_k$	$n_{at}$	$n_{pd}$
81	403.0	6.30	4.62	4.29	0.08	4.20	1.05	
82	403.2	32.0	37.6	29.9	0.18	28.0	7.79	
83	404.1	58.4	63.6	51.0	0.18	45.5	14.0	1.1
84	404.9	21.4	27.0	20.7	0.17	20.3	7.86	
85	404.0	4.65	4.29	3.62	0.08	4.04	0.95	
86	404.5	31.7	28.7	22.3	0.12	20.2	5.53	
87	404.0	41.8	28.7	22.6	0.08	22.3	5.48	
88	404.1	13.3	13.9	11.3	0.11	10.7	2.49	0.2
89	404.1	3.52	2.96	2.46	0.05	2.06	0.69	
90	443.0	3.30	18.8	14.6	0.66	12.5	3.81	0.2
91	442.6	5.75	30.1	23.2	0.86	21.0	5.55	0.5
92	443.0	13.8	93.1	72.0	1.85	63.0	16.5	1.0
93	443.0	22.1	159	127	2.34	116	27.5	1.5
95	440.0	44.0	209	165	1.72	149	38.0	5.3
123	442.3	41.3	244	180	1.85	170	44.0	3.4
124	442.4	22.7	162	122	2.27	112	32.8	1.6
125	442.5	13.2	85.8	65.6	1.44	57.6	16.0	0.9
142P	443.0	13.8	48.6	30.1	0.35	25.5	11.5	5.45
143P	443.0	5.21	16.8	8.45	0.19	11.2	4.9	2.34
97	464.8	3.44	49.3	37.2	2.80	34.2	8.72	0.3
98	464.1	3.18	36.9	26.9	2.15	24.2	5.50	1.1
99	463.5	12.8	246	181	8.20	159	39.8	3.2
100	463.5	24.5	465	343	11.9	329	75.4	4.0
101	464.0	3.60	49.5	37.2	2.61	34.4	8.29	0.4
126	463.2	13.4	271	201	9.65	186	42.2	1.3
127	463.7	16.4	332	249	9.93	229	52.4	1.8
112	478.0	5.45	162	119	9.70	110	24.5	
113	478.8	2.84	78.0	55.6	5.69	50.3	11.5	0.3
114	478.7	13.1	485	345	22.5	333	72.1	1.9
115	478.0	22.2	809	591	30.7	565	120	5.8
139P	478.3	23.9	512	332	8.82	284	67.7	67.2
140P	477.0	5.62	97.2	61.5	2.24	52.9	17.7	10.6
141P	478.4	13.8	306	182	5.71	159	49.8	40.5
116	488.3	0.64	24.0	17.9	1.59	13.7	4.10	0.19
117	489.1	2.83	108	72.5	7.18	65.7	14.7	0.8
118	489.2	5.34	243	162	15.2	154	32.5	1.7
128	989.6	32.2	2006	1481	91.7	1381	295	14
129	488.6	5.16	237	169	16.5	152	33.2	0.28
130	489.6	11.9	635	452	37.0	423	88.2	1.9
119	503.4	5.50	421	279	34.2	261	52.3	2.8
120	502.3	2.80	194	122	16.9	115	23.4	0.6
121	502.0	13.7	1186	788	77.0	743	150	8.7
122	503.5	0.60	48.4	32.6	5.78	25.8	7.51	0.5
131	501.6	24.4	1851	1275	105	1175	240	11
132	503.4	27.0	2400	1623	135	1453	305	16
133	503.5	14.2	1370	889	96.8	839	170	5.6
134P	502.0	25.9	1591	983	47.0	769	...	108
135P	506.0	3.93	260	152	14.0	158	37.1	22.3
136P	501.0	14.8	970	566	36.2	485	127	108
137P	505.2	2.95	195	116	10.9	120	32.0	14.7
138P	501.5	22.8	1433	832	42.3	688	192	131
								7.23

<sup>a</sup> m, methane; e, ethane; k, ketene; at, acetone; pd, 2,3-pentanedione; en, ethylene; P, packed reactor. The volume of the reactor (packed and unpacked) is 283 cm<sup>3</sup>.

for the photolysis at 300–470°K. These reactions require the stoichiometric relations

$$n_{CO}/\Sigma_1 = 1$$

(I)

and

$$n_m/\Sigma_2 = 1 \quad (\text{II})$$

where  $\Sigma_1 = n_m + n_{at} + 2n_e + n_{pd}$ ,  $\Sigma_2 = n_k + n_{pd}$ ,

**Table II:** Stoichiometric Relations and Kinetic Parameters

Temp. °K	Pressure range, torr	Element balance		$n_{CO}/\Sigma_1$	$n_m/\Sigma_2$	$n_e/n_{pd}$ range	Order	$p_{1/2},$ torr	$10^{-20}k_0,$ $\text{cm}^6$ $\text{mol}^{-2}$ $\text{sec}^{-1}$
		C:O	H:O						
677	3.5-58.0	2.00 ± 0.03	3.05 ± 0.07	0.96 ± 0.08	1.05 ± 0.08	0.2-0.6	1.08 ± 0.02	13.5	3
716	3.3-44.0	2.00 ± 0.01	3.02 ± 0.09	1.00 ± 0.03	1.09 ± 0.03	0.4-3	1.09 ± 0.02	21	2
737	3.1-24.5	2.01 ± 0.07	3.03 ± 0.17	1.01 ± 0.04	1.08 ± 0.10	2-8	1.24 ± 0.02	24	1.7
751	2.8-22.2	1.99 ± 0.02	2.99 ± 0.09	1.00 ± 0.09	1.05 ± 0.03	5-20	1.15 ± 0.01	26.5	1.2
762	0.6-32.2	1.99 ± 0.03	2.96 ± 0.13	1.02 ± 0.05	1.11 ± 0.09	7-20	1.15 ± 0.02	29.5	1.0
776	0.6-24.4	1.97 ± 0.02	2.92 ± 0.08	1.04 ± 0.06	1.09 ± 0.12	9-25	1.04 ± 0.02	30	0.9

and  $n_i$  (in moles per second) is the rate of formation of product i (the meanings of the subscripts m, at, etc., are given in Table I). Evidence that reaction 9 can generally be neglected will be discussed later. The values given in Table II show that eq I is vindicated very well by the data. The experimental values of  $n_m/\Sigma_2$  are 5-10% higher than required by eq II, probably because of a small degree of polymerization of the ketene.<sup>17</sup> (The small amounts of CO<sub>2</sub> and C<sub>2</sub>H<sub>4</sub> found in the products probably arise from the pyrolysis of ketene,<sup>18</sup> but they are insufficient to account for the discrepancy.)

**Kinetic Analysis. Reaction Order.** The over-all rate of decomposition  $-n_B$  was taken as half the total rate of appearance of O in the products. Plots of  $\log -n_B$  against  $\log [B]$  gave straight lines, yielding the reaction orders given in Table II. The order is thus a little greater than 1 over the whole range of conditions. Neglecting the discrepancy from unity, the over-all first-order rate constant can be expressed approximately by

$$-n_B/(V[B]) = k_{ov} = 10^{11.4} \exp(-47,140/RT) \text{ sec}^{-1} \quad (III)$$

The Arrhenius plot is shown in Figure 1 (curve 1). In the "packed" reactor the order remained close to 1; the values of  $(k_{ov})_P$  at 443, 478, and 503°, respectively, were 35, 27, and 18% less than the corresponding values of  $k_{ov}$ , showing that the surface exerts little effect on the over-all kinetics in the unpacked reactor.

Assuming that the above chain reaction scheme is basically correct, the reaction order considered in light of the principles of rate theory gives a preliminary guide to possible main terminating reactions. According to RRK theory, the pressure at which a unimolecular reaction such as reaction 1 begins to become second order decreases as  $(E_1/SRT)^{S-1}$  increases,<sup>19</sup> where S is the number of active Kassel oscillators. The known behavior<sup>6</sup> of other molecules with about 12 atoms and similar values of  $E/SRT$  indicates that reaction 1 is probably substantially first order under the present experimental conditions. In this case first-order kinetics for the over-all decomposition require  $\beta\mu$ - or  $\beta\beta M$ -type termination reactions.<sup>20</sup> All  $\beta\beta M$ -

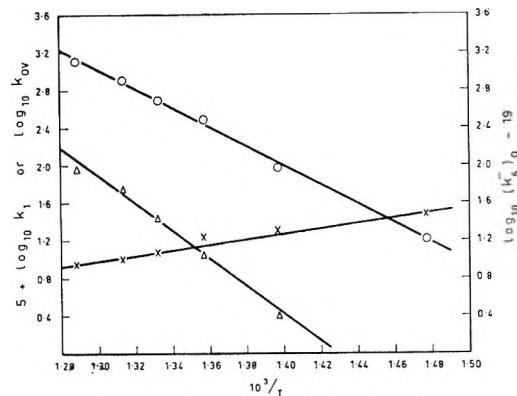
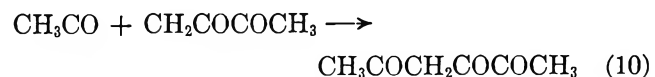


Figure 1. Arrhenius plots of  $k_1$ ,  $k_{ov}$ , and  $(k_6''')_0$ :  $\Delta$ ,  $\log k_1$ ;  $\circ$ ,  $\log k_{ov}$ ;  $\times$ ,  $\log (k_6''')_0$ .

type reactions can be eliminated on the grounds that  $S$  and  $-\Delta H$  are too high, except reaction 6 and, possibly, the third-order version of reaction 7. Hence possible main terminating reactions at this stage are reactions 5, 6, 10, and perhaps 7.



**Origin of Acetone and the Role of the Acetyl Radical.** The maximum rate of production of acetone by reaction 7 is given by

$$(n_{at})_7 = V k_7 [\text{CH}_3][\text{CH}_3\text{CO}] \quad (IV)$$

where  $V$  is the volume of the reactor and  $k_7$  can be taken as approximately equal to the high-pressure limiting value of  $k_6$ . Assuming that ethane is formed exclusively by reaction 6,  $[\text{CH}_3]$  for any experiment can be calculated from  $n_e$  and  $k_6$  (the latter from ref 21 and data to be presented later);  $[\text{CH}_3\text{CO}]$  can be derived from  $n_{CO}$  and the data relating to reaction 2 obtained by O'Neal and Benson.<sup>4</sup>

(17) R. K. Brinton, *J. Amer. Chem. Soc.*, **83**, 1541 (1961).

(18) W. B. Guenther and W. D. Walters, *ibid.*, **81**, 1310 (1959).

(19) S. W. Benson, "The Foundations of Chemical Kinetics," McGraw-Hill Book Co., Inc., New York, N. Y., 1960, Chapter XI.

(20) K. J. Laidler and D. J. McKenney in "The Chemistry of the Ether Linkage," S. Patai, Ed., Interscience Publishers Ltd., London, 1967, p 169.

(21) A. Shepp, *J. Chem. Phys.*, **24**, 939 (1956).

Table III: Calculated Rates of Formation of  $(CH_3)_2CO$  by Reaction 7 Compared with Experimental Rates

Experiment no.	$(n_{at})_7, \text{ mol sec}^{-1}$	
	Calcd	Exptl
87	$2 \times 10^{-12}$	$5.5 \times 10^{-9}$
123	$6 \times 10^{-11}$	$4.4 \times 10^{-8}$
125	$7 \times 10^{-11}$	$1.6 \times 10^{-8}$
120	$2.5 \times 10^{-9}$	$2.3 \times 10^{-8}$
131	$3 \times 10^{-9}$	$2.4 \times 10^{-7}$

By extrapolating their results we estimate that the pressure at which the first-order constant ( $k_2$ )<sub>0</sub> falls to half its limiting high-pressure value is about 270 torr at 673°K and 430 torr at 773°K. Hence reaction 2 is effectively second order under the present conditions. Therefore

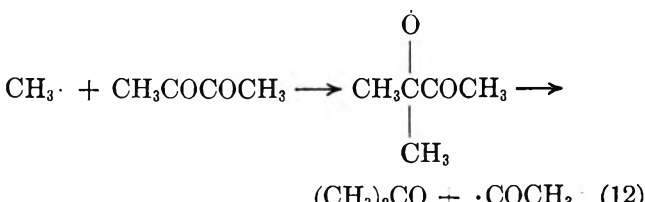
$$[CH_3CO] = n_{CO}/V(k_2)_0[M] \quad (V)$$

where [M] is the total molecular concentration. The representative values of ( $n_{at}$ )<sub>7</sub> given in Table III were calculated from the present data via eq IV and V using values of ( $k_2$ )<sub>0</sub> calculated from the Arrhenius parameters given by O'Neal and Benson.<sup>4</sup> First, they are notably less than the experimental values and another source of acetone must therefore be found. Second, they are much smaller than the experimental rates of formation of ethane (Table I); hence reaction 7 cannot be the main terminating reaction. Third, in general they are also smaller than  $n_{pd}$  (Table I); this means that, except for reaction 2, the acetyl radical plays an insignificant role in determining the kinetics, thereby eliminating reaction 10 as a possible terminating reaction.

Reaction 8, which occurs in the photolysis of biacetyl,<sup>15,16</sup> is the most likely source of acetone. If so, assuming the methane is produced by reaction 3, we should find  $n_{at} \propto n_m$ . Figure 2 shows that this is the case. An analogous reaction



has been proposed to account for the formation of acetone in the pyrolysis of acetaldehyde.<sup>22,23</sup> The production of a trace of  $(CH_3)_2C(OH)COCH_3$  by biacetyl suggests that reaction 8 occurs in two steps, as proposed earlier by Darwent<sup>24</sup>



the intermediate radicals being sufficiently long lived for a few of them to abstract a hydrogen from biacetyl.

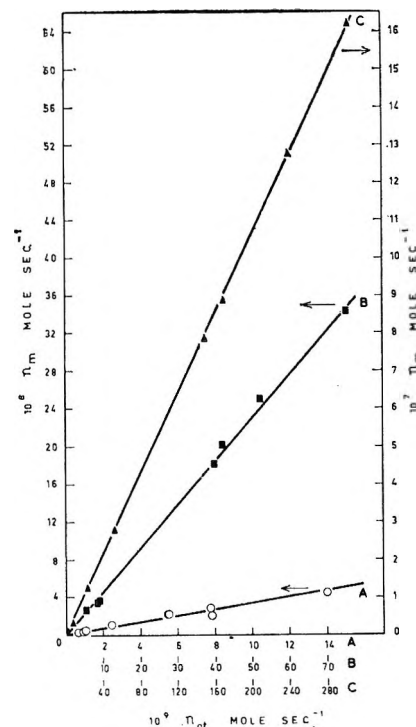
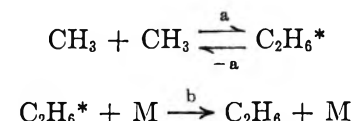


Figure 2. Typical plots of  $n_m$  against  $n_{at}$ :  
▲, 776°K; ■, 737°K; ○, 677°K.

Batt<sup>25</sup> has discussed evidence that reaction 11 also occurs by this mechanism.

*Reactions 3, 4, 6, and 8.* The  $\beta$ -propagating reactions 3 and 8 are related kinetically by their common participant  $CH_3$  to reaction 6, which, from its behavior at lower temperatures, is expected to be pressure dependent. Assuming a Lindemann-Hinshelwood mechanism



the following relation applies

$$\frac{n_\beta^2}{n_e[B]^2} = \frac{V k_\beta^2}{k_a} \left\{ 1 + \frac{k_{-a}}{k_b} \frac{1}{[B]} \right\} = \frac{V k_\beta^2}{k_b''} \quad (VI)$$

where  $\beta$  refers either to reaction 3 or reaction 8, [B], the biacetyl concentration, is equated to [M], and  $k_b''$  is the pressure-dependent bimolecular constant. That curves rather than straight lines are obtained by plotting  $n_\beta^2/(n_e[B]^2)$  against  $1/[B]$  (Figures 3 and 4) shows that the Lindemann-Hinshelwood mechanism should be replaced by one which takes account of the variation of the lifetime of  $C_2H_6^*$  with its energy content, as found previously by Shaw, Menczel, and Toby<sup>26</sup> (see

(22) M. Eusuf and K. J. Laidler, *Can. J. Chem.*, **42**, 1851 (1964).  
(23) K. J. Laidler and M. T. H. Lin, *Proc. Roy. Soc., A* **297**, 365 (1967).

(24) B. deB Darwent, *Discussions Faraday Soc.*, **14**, 129 (1953).

(25) L. Batt, *J. Chem. Phys.*, **47**, 3674 (1967).

(26) H. Shaw, J. H. Menczel, and S. Toby, *J. Phys. Chem.*, **71**, 4180 (1967).

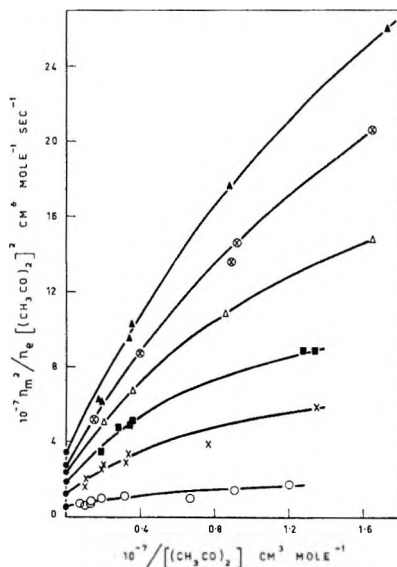


Figure 3. Plots of  $n_m^2/n_e[(\text{CH}_3\text{CO})_2]^2$  against  $1/[(\text{CH}_3\text{CO})_2]$ :  $\blacktriangle$ , 776°K;  $\odot$ , 762°K;  $\Delta$ , 751°K;  $\blacksquare$ , 737°K;  $\times$ , 716°K;  $\circ$ , 677°K;  $\bullet$ , extrapolated from photolysis, R. Ausloos and E. W. R. Steacie, *Can. J. Chem.*, **33**, 39 (1955).

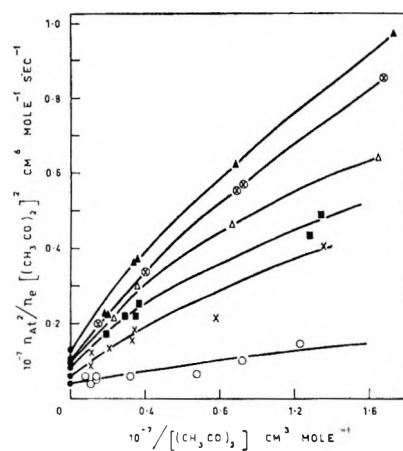


Figure 4. Plots of  $n_\alpha^2/n_e[(\text{CH}_3\text{CO})_2]^2$  against  $1/[(\text{CH}_3\text{CO})_2]$ :  $\blacktriangle$ , 776°K;  $\odot$ , 762°K;  $\Delta$ , 751°K;  $\blacksquare$ , 737°K;  $\times$ , 716°K;  $\circ$ , 677°K;  $\bullet$ , extrapolated from photolysis (Blacet and Bell<sup>16</sup>).

also ref 27 and 28). The points on the ordinates were obtained by extrapolating, by means of Arrhenius plots, values of  $Vk_\beta^2/(k_6'')_\infty$  derived from photolytic data<sup>16,29</sup> at 300–470°K and 20–50 torr, reaction 6 being assumed to be at its high-pressure limit under these conditions. The points are seen to be consistent with the present data, as was verified by extrapolating the latter to the ordinates without prior knowledge of the photolysis data. These extrapolated values, when combined with those derived from the photolysis, gave 9.1 and 6.3 kcal mol<sup>-1</sup> for  $E_3$  and  $E_8$ , respectively, which may be compared with 8.5<sup>29</sup> and 6.6<sup>16</sup> kcal mol<sup>-1</sup> based on the photolytic data alone.

Values of  $p_{1/2}$ , the pressure at which  $k_6''$  has the value  $0.5(k_6'')_\infty$ , interpolated from Figure 3 are given in Table II. Values derived from the acetone–ethane

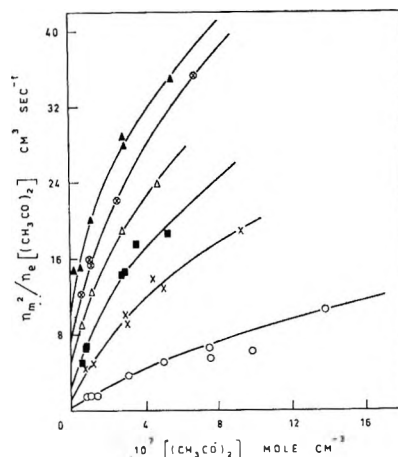


Figure 5. Plots of  $n_m^2/n_e[(\text{CH}_3\text{CO})_2]$  against  $[(\text{CH}_3\text{CO})_2]$ :  $\odot$ , 677°K;  $\times$ , 716°K;  $\blacksquare$ , 737°K;  $\Delta$ , 751°K;  $\odot$ , 762°K;  $\blacktriangle$ , 776°K.

data (Figure 4), though expected to be of lower accuracy, were in fact all within  $\pm 10\%$  of these. Further reference to  $p_{1/2}$  will be made later.

Plots according to eq VI emphasize the results obtained at the high end of the pressure range. Rearrangement of eq VI to give

$$\frac{n_\beta^2}{n_e[B]} = \frac{V k_\beta^2}{k_a k_b} \{k_{-a} + k_b[B]\} = \frac{V k_\beta^2}{k_6''' \quad (\text{VII})}$$

produces the contrary effect (where  $k_6'''$  is the termolecular constant).

Figure 5 shows  $n_m^2/(n_e[B])$  as a function of [B]. Extrapolation to the ordinate yields  $V k_3^2/(k_6''')_0$ , from which, with the values of  $V k_3^3/(k_6'')_\infty$  determined above and Shepp's value<sup>30</sup> of  $(k_6'')_\infty$ , the approximate values of  $(k_6''')_0$  given in Table II were derived. Similar treatment of the acetone–ethane data gave values of  $(k_6''')_0$  within 15% of these. Although the absolute values are subject to the uncertainties of the extrapolations, there is little doubt that the inverse effect of temperature on  $(k_6''')_0$  is genuine. The best Arrhenius line gives  $E_6''' = -13$  kcal mol<sup>-1</sup> and  $\log A_6 = 16.3$  cm<sup>6</sup> mol<sup>-2</sup> sec<sup>-1</sup> (see Figure 1). The results may also be expressed by the relation  $(k_6''')_0 = 10^{46.6} T^{-9.2} \text{ cm}^6 \text{ mol}^{-2} \text{ sec}^{-1}$ . The absolute values of  $(k_6''')_0$  agree well with the value  $\gtrsim 3 \times 10^{20} \text{ cm}^6 \text{ mol}^{-2} \text{ sec}^{-1}$  derived<sup>31,32</sup> from the photolysis of acetone at 473°K.<sup>1</sup> Estimates of -11.7 and -9.8 kcal mol<sup>-1</sup> made by Laidler, et al.,<sup>33</sup> from photolytic data<sup>1,17</sup> are also compatible with the

- (27) A. B. Trenwith, *Trans. Faraday Soc.*, **62**, 1538 (1966).
- (28) M. C. Lin and M. H. Back, *Can. J. Chem.*, **44**, 2357 (1966).
- (29) P. Ausloos and E. W. R. Steacie, *ibid.*, **33**, 39 (1955).
- (30) A. Shepp, *J. Chem. Phys.*, **24**, 939 (1956).
- (31) D. E. Hoare and A. D. Walsh, *Trans. Faraday Soc.*, **53**, 1102 (1957).
- (32) E. K. Gill and K. J. Laidler, *Proc. Roy. Soc.*, **A250**, 121 (1959).
- (33) See ref 20, p 195.

present figure for  $E_6'''$ . Further reference will be made to reaction 6 later.

An investigation of reaction 4 was attempted by means of the relation  $n_k[\text{CH}_3]/n_{pd} = k_4'f([M])/k_5$  (where  $f([M])$  is a function of  $[M]$ ) but the results were inconclusive, probably because of insufficient precision in the determination of  $n_{pd}$  and the intervention of a surface effect in reaction 5 (as described later).

*Initiation and Termination.* Elimination of the acetyl radical from consideration leaves reactions 5 and 6 (the latter third order) as the only plausible termination reactions compatible with over-all first-order kinetics. From the values of  $n_e/n_{pd}$  listed in Table II it appears that reaction 5 is the main terminating reaction at 677°K but gives way to reaction 6 at higher temperature. Since the pressure in the great majority of the experiments above 677°K was less than  $p_{1/2}$ , it is legitimate to regard reaction 6 as substantially third order at these temperatures. The positive deviations from unity observed in the over-all order doubtless reflect the fact that the reaction is not actually at its third-order limit. Since the rates of termination and initiation must be equal (irrespective of order) the following relation should apply

$$V k_1[B] = n_e + n_{pd} + n_x \quad (\text{VIII})$$

where  $x$  is the product of reaction 9.

The term  $n_x$  is added because  $[\text{CH}_3]$  and  $[\text{CH}_2\text{COCOCH}_3]$  were of comparable magnitudes in experiments at 677 and 716°K. Its magnitude, calculated from  $n_e$  and  $n_{pd}$  on the assumption that  $(k_6''')_0/(k_5 k_9)^{1/2} = 2$ , was found to be negligible in all but a few experiments. Figure 6 shows that  $n_e + n_{pd} + n_x$  is in fact linearly related to  $[B]$ . This vindicates the previous conclusion that reaction 1 is first order; furthermore, the fact that the lines pass through the origin shows that there is no appreciable contribution to the over-all reaction from an intramolecular decomposition. The Arrhenius plot of the slopes of the lines in Figure 6 shown in Figure 1 yields

$$k_1 = 10^{16.0} \exp[-(67200 \pm 3300)/RT] \text{ sec}^{-1} \quad (\text{IX})$$

in good agreement with the values  $A = 5 \times 10^{15} \text{ sec}^{-1}$  and  $E = 66.0 \text{ kcal mol}^{-1}$  obtained by Taylor<sup>9</sup> by the toluene-carrier method. Absolute values of  $k_1$  calculated from Taylor's parameters are within 20% of the present figures. The value of  $E_1$  in eq IX may be used to obtain a second value for  $E_6'''$ . Since the chain length is of the order of 15–35 and reaction 6 is the dominant terminating reaction above 677°K, it follows that  $E_{ov} \approx 1/2(E_1 - E_6''') + E_\beta$ . An empirical value was found for  $E_\beta$  (namely, 7.5 kcal mol<sup>-1</sup>) from a plot of  $\log(k_3 + k_8)$  against  $1/T$ . Hence with  $E_{ov} = 47.1 \text{ kcal mol}^{-1}$  and  $E_7 = 67.2 \text{ kcal mol}^{-1}$ , we find  $E_6''' = -12 \text{ kcal mol}^{-1}$ , comparing well with the value of  $-13 \text{ kcal mol}^{-1}$  found from  $(k_6''')_0$  directly.

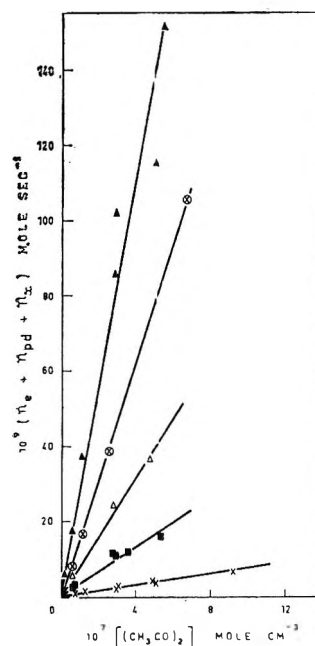


Figure 6. The total rate of formation of termination products as a function of  $[(\text{CH}_3\text{CO})_2]$ : ▲, 776°K; ⊖, 762°K; △, 751°K; ■, 737°K; ×, 716°K.

*Effect of Surface.* Increasing the surface:volume ratio tenfold reduced the rates of formation of CO,  $\text{CH}_4$ , and  $\text{CH}_2\text{CO}$  by up to 50%,  $(\text{CH}_3)_2\text{CO}$  by 25%, and  $\text{C}_2\text{H}_6$  by up to 75% (see Table I). The rate of production of  $\text{CH}_3\text{CH}_2\text{COCOCH}_3$ , however, increased 10–15-fold. Formation of  $\text{CO}_2$  and  $\text{C}_2\text{H}_4$ , which are probably decomposition products of  $\text{CH}_2\text{CO}$ , also increased notably. Table IV shows that  $n_m^2/n_e$  was unaffected apart from a small increase at low pressures, but  $n_{at}^2/n_e$  showed a distinct increase. The increase in  $n_{pd}$  is interesting because it suggests that reaction 5 occurs mainly at the surface. This would cause the stationary concentration of  $\text{CH}_3\cdot$  to decrease in the packed vessel and thus lower the values of  $n_m$ ,  $n_e$ , and  $n_{at}$ , as observed. The increase in  $n_{at}^2/n_e$  may also be indicative of surface catalysis of reaction 7. However, the constancy of  $n_m^2/n_e$  shows that reaction 6 is not appreciably catalyzed by the surface. Since surface catalysis of a radical combination presumably requires absorption of one or both radicals, it may be expected to increase with increasing molecular weight and polar character of the radicals.

*Heat of Formation of the Acetyl Radical,  $\Delta H_f^\circ(\text{CH}_3\text{CO})$ .* Recent determinations of  $\Delta H_f^\circ(\text{CH}_3\text{CO})$  by several more-or-less indirect methods have given values ranging from  $-6.5^{34}$  to  $-3 \text{ kcal mol}^{-1}$ <sup>35</sup> and three "best values" have been derived from various com-

(34) E. Murad and M. G. Inghram, *J. Chem. Phys.*, **41**, 404 (1964).

(35) J. G. Calvert and J. T. Gruver, *J. Amer. Chem. Soc.*, **80**, 1313 (1958).

**Table IV:** Effect on Product Ratios of Increasing Surface:Volume by a Factor of 10 (the Volume of Packed and Unpacked Vessels Is 283 cm<sup>3</sup>)

Temp; °K	Pressure; torr	$10^8 n_m^2/n_e$ , mol sec <sup>-1</sup>		$10^7 n_{pd}^2/n_e$ , mol sec <sup>-1</sup>		$n_e/n_{pd}$	
		Unpacked <sup>a</sup>	Packed	Unpacked <sup>a</sup>	Packed	Unpacked <sup>a</sup>	Packed
776	25.9	2.03	2.17	...	...	8.7	0.43
	22.8	1.68	1.68	5.88	8.74	9.9	0.32
	14.8	0.89	0.89	3.10	4.38	17.2	0.33
	3.9	0.14	0.16	0.51	0.99	12.2	0.63
	2.95	0.09	0.12	0.35	0.94	26.4	0.75
751	23.9	1.25	1.25	4.88	5.19	5.3	0.13
	13.8	0.57	0.62	2.16	4.34	11.9	0.14
	5.6	0.15	0.17	0.67	1.40	...	...
716	13.8	0.29	0.26	1.51	3.83	1.6	0.06
	5.2	0.07	0.06	0.43	1.29	1.6	0.08

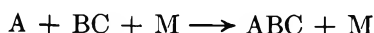
<sup>a</sup> Interpolated.

binations of these, namely,  $-5.4 \pm 0.8$ ,<sup>36</sup>  $-4 \pm 2$ ,<sup>37,38</sup> and  $-4.3$  kcal mol<sup>-1</sup>.<sup>39</sup> Intrinsically the most reliable of the individual values seems to be that of  $-4.7 \pm 0.7$  kcal mol<sup>-1</sup> found by Walsh and Benson,<sup>36</sup> though it rests on the assumption that  $E = 0$  for the reaction  $\text{CH}_3\text{CO} + \text{I}_2 \rightarrow \text{CH}_3\text{COI} + \text{I}$ . The present work yields a value directly, if it is assumed only that fission of the biacetyl molecule occurs at the central C-C bond and that  $E_{-1} = 0$ . Thus

$$\Delta H_f^\circ(\text{CH}_3\text{CO}) = \frac{1}{2} \{ E_1 + \Delta H_f^\circ[(\text{CH}_3\text{CO})_2(\text{g})] + \Delta(H^\circ_{730} - H^\circ_{298}) \}$$

The value of  $H^\circ_{730} - H^\circ_{298}$  for biacetyl was taken as equal to the value for *n*-butane<sup>40</sup> and that for the acetyl radical was calculated using a mean specific heat of 17 cal deg<sup>-1</sup> mol<sup>-1</sup> (after Walsh and Benson<sup>36</sup>). Hence with  $\Delta H_f^\circ[(\text{CH}_3\text{CO})_2(\text{g})] = -78.10$ <sup>37</sup> and  $E_1 = 67.2 \pm 3.3$  kcal mol<sup>-1</sup> we find  $\Delta H_f^\circ(\text{CH}_3\text{CO}) = -5.1 \pm 2.0$  kcal mol<sup>-1</sup>.

*Combination of Methyl Radicals.* The fact that both  $(k_6''')_0$  and its negative temperature coefficient are notably larger than the corresponding values for combinations between simpler species is in accord with the RRK theory,<sup>41</sup> which predicts an increase in both quantities with increasing complexity of the combining species (as well as with increasing exothermicity of the combination). A semiquantitative correlation has been found<sup>41,42</sup> between the rates and  $-\Delta H$  of reactions of the type



On this basis,  $(k_6''')_0$  for such a reaction with  $-\Delta H = -\Delta H_6 = 84$  kcal mol<sup>-1</sup> and M a simple molecule would be  $10^{16}$  to  $10^{17}$  at 298°K. The major part of the difference between this value and  $(k_6''')_0 \rightarrow 10^{22}$  at 298°K may be attributed to the greater complexity of the methyl radicals. (The greater efficiency of biacetyl

as third body is unlikely to involve more than a factor of  $10^2$ ; cf. ref 1.) Temperature coefficients for the triatomic combinations, as expressed by  $E$ , fall between  $-0.5$  and  $-2$  kcal mol<sup>-1</sup>.<sup>43</sup> Although the considerably greater value of  $E_6$  ( $-13$  kcal mol<sup>-1</sup>) may owe a little to the nature of the third body,<sup>44</sup> it seems likely that here again the complexity of the combined species is mainly responsible.<sup>45-47</sup> RRK theory leads to the relation

$$\log p_{1/2} = a + (S - 1/2) \log T \quad (\text{X})$$

where  $a$  is almost independent of  $T$ . Figure 7 shows values of  $\log p_{1/2}$  derived from several sources. Those at the five highest temperatures relate to the reverse of reaction 6, namely, the pyrolysis of ethane<sup>27,28</sup>; apart from the present results, and that of ref 48, the remainder were obtained from photolytic work. The present results are compatible with eq X and when extrapolated to lower temperatures agree well with the values obtained by Dodd and Steacie,<sup>1,26</sup> though the

- (36) R. Walsh and S. W. Benson, *J. Phys. Chem.*, **70**, 3651 (1966).
- (37) J. A. Kerr, *Chem. Rev.*, **66**, 465 (1966).
- (38) D. M. Golden, R. Walsh, and S. W. Benson, *J. Amer. Chem. Soc.*, **87**, 4053 (1965).
- (39) J. G. Calvert and J. N. Pitts, "Photochemistry," John Wiley & Sons, New York, N. Y., 1966, p 820.
- (40) National Bureau of Standards Circular C461, U. S. Government Printing Office, Washington, D. C., 1947.
- (41) S. W. Benson, "The Foundations of Chemical Kinetics," McGraw-Hill Book Co., Inc., New York, N. Y., 1960, p 312.
- (42) M. A. A. Clyne, D. J. McKenney, and B. A. Thrush, *Trans. Faraday Soc.*, **61**, 2701 (1965).
- (43) T. C. Clark, M. A. A. Clyne, and D. H. Stedman, *ibid.*, **62**, 3354 (1966).
- (44) G. Porter and J. A. Smith, *Proc. Roy. Soc.*, **A261**, 28 (1961).
- (45) On the other hand, two independent sets of data yield<sup>48</sup>  $E \approx 1$  kcal mol<sup>-1</sup> for the reaction  $\text{CH}_3 + \text{O}_2 + \text{M} \rightarrow \text{CH}_3\text{O}_2 + \text{M}$  (where M is  $(\text{CH}_3)_2\text{CO}$  or  $(\text{CH}_3)_2\text{N}_2$ ), whereas the value<sup>49</sup> for the about equally exothermic reaction  $\text{O} + \text{O}_2 + \text{CO}_2 \rightarrow \text{O}_3 + \text{CO}_2$  is  $-1.5$  kcal mol<sup>-1</sup>.
- (46) W. C. Sleppy and S. G. Calvert, *J. Amer. Chem. Soc.*, **81**, 769 (1959).
- (47) M. F. R. Mulcahy and D. J. Williams, *Trans. Faraday Soc.*, **64**, 59 (1968).
- (48) M. Krech and S. J. W. Price, *Can. J. Chem.*, **45**, 157 (1967).

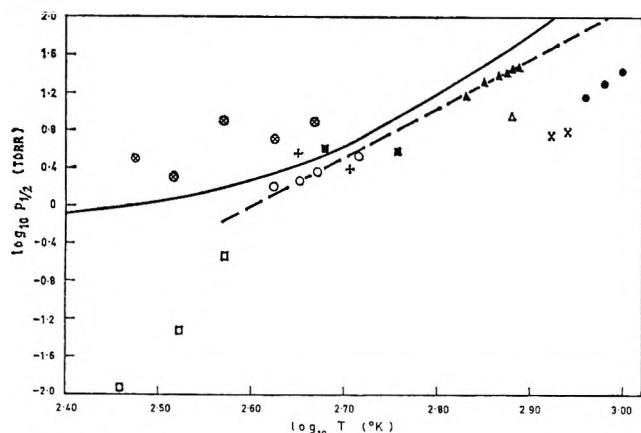


Figure 7. The dependence of  $\log p_{1/2}$  on  $\log T$ :  
 ---,  $\log p_{1/2} = (\text{constant}) + 5.2 \log T$ ; —,  $\log p_{1/2}$ ,  
 RRKM absolute calculation (B. S. Rabinovitch and D. W.  
 Setser, *Advan. Photochem.*, **3**, 1 (1964); J. Grotewald, E. A.  
 Lissi, and M. G. Neumann, *J. Chem. Soc., A*, **2**, 375  
 (1968)). Third body: biacetyl, ▲; acetone: +, G. B.  
 Kistiakowsky and E. K. Roberts, *J. Chem. Phys.*, **21**, 1637  
 (1953); O, Dodd and Steacie;<sup>1</sup> azomethane-azoethane: □,  
 J. Grotewald, E. A. Lissi, and M. G. Neumann, *J. Chem.  
 Soc., A*, **2**, 375 (1968); ⊗, S. Toby and B. H. Weiss,  
*J. Phys. Chem.*, **68**, 2492 (1964); dimethyl ether: ■,  
 Loucks<sup>3</sup>; benzene: Δ, M. Krech and S. J. W. Price,  
*Can. J. Chem.*, **45**, 157 (1967); ethane: X, Lin and Back,<sup>28</sup>  
 ●, Trenwith.<sup>27</sup>

agreement may be to some degree fortuitous. The broken line has the slope corresponding to  $S = 6$ . This is lower than, but according to RRK theory should be equal to, the value derived from the temperature coefficient of  $(k_6''')_0$ , namely,  $S = 10$ . Extrapolation of the present values of  $p_{1/2}$  to higher temperatures leads to values 4–10 times greater than those derived from ethane pyrolysis. Errors in the present determinations of  $p_{1/2}$  are more likely to cause the values to

be too low rather than too high. The results could be reconciled by postulating a specifically high third-body efficiency for ethane (due to a resonance effect). However, experience with the recombination of I atoms<sup>49</sup> and with the reaction



where M is  $\text{O}_3$ ,  $\text{CO}_2$ , etc.,<sup>50,51</sup> suggests that such an effect, if it exists,<sup>52</sup> may well be outweighed by that of the weaker van der Waals' field of ethane compared with biacetyl. Further evidence of a genuine discrepancy between the present and the pyrolytic results comes from calculations of the absolute values of  $p_{1/2}$  on the basis of the RRKM theory.<sup>53</sup> These are shown as the unbroken line in Figure 7 and were made<sup>53,54</sup> assuming a "loose" activated complex (*i.e.*, tumbling methyls) and strong deactivating collisions. The agreement with the present values (and those of Dodd and Steacie<sup>1</sup>) is remarkably good, the maximum difference between theory and experiment being a factor of 1.6. This seems to dispose of misgivings<sup>54</sup> concerning the validity of the loose activated complex model for the recombination, at least in the range 430–800°K.

*Acknowledgment.* The authors are grateful to Dr. J. R. Wilmshurst for advice on gas chromatographic methods.

- (49) M. I. Christie, *J. Amer. Chem. Soc.*, **84**, 4066 (1962).
- (50) S. W. Benson and A. E. Axworthy, *J. Chem. Phys.*, **42**, 2614 (1965).
- (51) F. Kaufman and J. R. Kelso, *ibid.*, **46**, 4541 (1967).
- (52) J. W. Linnett and N. J. Selley, *Z. Phys. Chem. (Frankfurt)*, **37**, 402 (1963).
- (53) B. S. Rabinovich and D. W. Setser, *Advan. Photochem.*, **3**, 1 (1964).
- (54) J. Grotewald, E. A. Lissi, and M. G. Neumann, *J. Chem. Soc., A*, **2**, 375 (1968).

## Diffusion in Binary Liquid Mixtures

by T. Loflin and E. McLaughlin<sup>1,2</sup>

*Department of Chemical Engineering, Louisiana State University, Baton Rouge, Louisiana* (Received July 31, 1968)

Several expressions previously proposed for the mutual diffusion coefficient of a binary liquid system are shown to follow from the Bearman theory when a geometric-mean relationship between certain friction coefficients is assumed. The Rice–Allnatt extension of the Rice–Kirkwood theory, which can be tested without the introduction of this assumption, is shown to give virtually quantitative agreement with experiment for both viscosity and diffusion when the binary system is close to ideality. Under these conditions, however, their equations likewise approximate closely to the assumption of a geometric-mean relationship between the friction constants.

### I. Introduction

In the study of the transport properties of mixtures of dense fluids, considerable effort has been devoted to the coefficient of mutual diffusion,  $D$ , from both the experimental<sup>3</sup> and the theoretical points of view. On the theoretical side a number of equations have been proposed relating the mutual diffusion coefficient to other properties of the mixture. It is the purpose of the present article to show a common route to the derivation of these equations which have, as a necessary condition for validity, a geometric-mean relationship between certain friction coefficients. In addition a check is made on the recent theory of Rice and Allnatt<sup>4</sup> which can be evaluated without the introduction of this assumption.

### II. Theories of Diffusion

In the development of the theory of transport properties of mixtures, a significant step was taken by Bearman and Kirkwood,<sup>5</sup> who on the basis of the statistical-mechanical analogs of the conservation equations of fluid mechanics showed that introduction of perturbations to the singlet and pair space distribution functions linearized in the temperature gradient, diffusion velocities and the local rate of shear lead, in the stationary state, to the linear relationships of irreversible thermodynamics between the gradients of temperature and chemical potential and the fluxes of heat and mass.

This theory was subsequently developed by Bearman,<sup>6</sup> who for the case of diffusion derived the following equations for the mutual ( $D$ ) and self-diffusion ( $D_i$ ) coefficients in a two-component fluid

$$D = (\bar{v}_1 k T / \xi_{12}) [1 + (\partial \ln f_2 / \partial \ln c_2)_{T,p}] \quad (1a)$$

$$= (\bar{v}_2 k T / \xi_{12}) [1 + (\partial \ln f_1 / \partial \ln c_1)_{T,p}] \quad (1b)$$

$$D_i = k T / \xi_i \quad (2)$$

$$\xi_i = \sum_{j=1}^2 c_j \xi_{ij} \quad (3)$$

where  $f_1$  and  $f_2$  are the activity coefficients;  $c_1$  and  $c_2$  are the concentrations (number of molecules per unit volume) of species 1 and 2, respectively;  $\bar{v}_1$  and  $\bar{v}_2$  are the

partial molecular volumes;  $k$  is the Boltzmann constant; and the various  $\xi$  are the friction constants. These equations are based only on the combination of statistical mechanics with the phenomenological theory of irreversible processes and do not contain empirical combining laws for either thermodynamic or transport properties of mixtures. The equivalence of eq 1a and 1b follows from the thermodynamic identity

$$\left( \frac{\partial \ln a_1}{\partial \ln c_1} \right)_{T,p} \bar{v}_2 = \left( \frac{\partial \ln a_2}{\partial \ln c_2} \right)_{T,p} \bar{v}_1 \quad (4)$$

where  $a_i$  is the activity of species  $i$ .

In general in the study of diffusion in binary systems a substantial effort has been devoted to relating the mutual diffusion coefficient  $D$  to  $D_1$  and  $D_2$ , which from eq 2 and 3 are given by

$$D_1 = v k T / (x_1 \xi_{11} + x_2 \xi_{12}) \quad (5)$$

$$D_2 = v k T / (x_2 \xi_{22} + x_1 \xi_{12}) \quad (6)$$

where  $x_1$  and  $x_2$  are the mole fractions related to the concentrations by  $c_1 = x_1/v$  and  $c_2 = x_2/v$ , where  $v = x_1 \bar{v}_1 + x_2 \bar{v}_2$ .

Combination of eq 1, 5, and 6 gives

$$D = \left( \frac{\partial \ln a_1}{\partial \ln x_1} \right)_{T,p} (x_1 D_2 + x_2 D_1) \times \left\{ \frac{x_1 \xi_{12}}{x_1 \xi_{12} + x_2 \xi_{22}} + \frac{x_2 \xi_{12}}{x_2 \xi_{12} + x_1 \xi_{11}} \right\}^{-1} \quad (7)$$

which reduces to the form

$$D = \left( \frac{\partial \ln a_1}{\partial \ln x_1} \right)_{T,p} (x_1 D_2 + x_2 D_1) \quad (8)$$

(1) Department of Chemical Engineering and Chemical Technology, Imperial College, S. Kensington, London.

(2) National Science Foundation Senior Foreign Scientist Fellow.

(3) P. A. Johnson and A. L. Babb, *Chem. Rev.*, **56**, 387 (1956).

(4) S. A. Rice and A. R. Allnatt, *J. Chem. Phys.*, **34**, 409 (1961).

(5) R. J. Bearman and J. G. Kirkwood, *ibid.*, **28**, 136 (1958).

(6) R. J. Bearman, *ibid.*, **32**, 1308 (1960).

when

$$\xi_{12} = (\xi_{11}\xi_{22})^{1/2} \quad (9)$$

Equation 8 resembles the equation proposed by Hartley and Crank,<sup>7</sup> and the form of this equation in comparison with similar equations has been discussed extensively by Bearman.<sup>8</sup> Condition 9 has also been given by Tyrrell.<sup>9</sup>

In addition to equations which have the form of eq 8, other equations have been suggested, and hence it is of interest to see under what conditions they are derivable from the Bearman-Kirkwood theory.

Equation 2 can be rearranged to the form

$$\frac{1}{D_1} = \frac{1}{v} \left[ \frac{x_1 \xi_{11}}{kT} + \frac{x_2 v_2}{D} \left( \frac{\partial \ln a_1}{\partial \ln c_1} \right)_{T,p} \right] \quad (10)$$

on using eq 1b, and to

$$\frac{1}{D_1} = \frac{1}{v} \left[ \frac{x_1 v_1}{D_1^0} + \frac{x_2 v}{D} \left( \frac{\partial \ln a_1}{\partial \ln x_1} \right)_{T,p} \right] \quad (11)$$

by virtue of the thermodynamic relation

$$\left( \frac{\partial \ln a_1}{\partial \ln c_1} \right)_{T,p} = \left( \frac{\partial \ln a_1}{\partial \ln x_1} \right)_{T,p} \frac{x_1}{v_2 c_1} \quad (12)$$

and the assumption  $D_1^0 = v_1 kT / \xi_{11}$ , where  $D_1^0$  is the self-diffusion coefficient of pure species 1. Equation 11 has been proposed by Lamm<sup>10</sup> and its validity rests on the assumption that  $D_1^0 = v_1 kT / \xi_{11}$ , which implies that the friction constant  $\xi_{11}$  is independent of composition.

Equation 11 is also of interest for the case of a dilute gas, for which it reduces to

$$\frac{1}{D_1} = \frac{x_1}{D_1^0} + \frac{x_2}{D} \quad (13)$$

which was previously suggested by Meyer<sup>11</sup> on the basis of gas kinetic theory and was confirmed experimentally by Miller and Carman,<sup>12</sup> who showed that for a number of gas mixtures  $1/D_1$  was linear in  $x_1$ ; as in the gas phase,  $D$  is substantially composition independent.

Returning to the liquid state, Bearman<sup>8</sup> has shown that for the case of regular solutions, where there is no volume change on mixing ( $v = x_1 v_1 + x_2 v_2$ ) and where the radial distribution function is independent of composition, then

$$\xi_{11}/\xi_{12} = v_1/v_2; \quad \xi_{22}/\xi_{12} = v_2/v_1 \quad (14)$$

and hence from eq 5 and 6

$$(D_1/D_2) = v_2/v_1; \quad \xi_{22}/\xi_{11} = (D_1/D_2)^2 \quad (15)$$

Equation 14 satisfies condition 9, and hence  $D$  under these conditions reduces from eq 7 to eq 8. In addition Bearman and Jones have shown that  $\eta D_1$  is a constant<sup>13</sup> which under these conditions is given by<sup>14</sup>

$$\eta D_1 = \eta_1 D_1^0 = \eta_2 D_2^{\infty 1} \quad (16)$$

and likewise

$$\eta D_2 = \eta_2 D_2^0 = \eta_1 D_2^{\infty 2} \quad (17)$$

hence eq 8 may be rewritten

$$D = \left( \frac{\partial \ln a_1}{\partial \ln x_1} \right)_{T,p} \frac{1}{\eta} [x_1 \eta_1 D_2^{\infty 1} + x_2 \eta_2 D_1^{\infty 2}] \quad (18)$$

which has been proposed previously by Carman and Stein.<sup>15</sup>  $\eta$  is the shear viscosity of the mixture and  $\eta_1$  and  $\eta_2$  are the viscosities of the pure components.  $D_1^{\infty 2}$  and  $D_2^{\infty 1}$  are the values of the mutual diffusion coefficient at infinite dilution by species 2 and 1, respectively, at which points they correspond with the self-diffusion coefficients<sup>16</sup> at infinite dilution.

In general it is well known that for the liquid state none of the above approximate equations is completely satisfactory for the representation of experimental data and attempts at improvement rest on modification of eq 9. This can be approached either on the basis of empirical correlations or by using theoretical relationships between the friction constants.

To date the only theory which can be readily evaluated is the Rice and Allnatt<sup>17</sup> extension of the approximate Rice-Kirkwood theory<sup>18</sup> to binary mixtures. In this theory

$$\xi_{12} = \Lambda_{12} m_{12} [(1/\xi_1) + (1/\xi_2)] \quad (19)$$

where

$$\Lambda_{12} = \frac{1}{3} \int \nabla_{R_{12}}^2 \phi_{12}(R_{12}) g_{12}^{(2,0)}(R_{12}) d^3 R_{12} \quad (20)$$

and  $\phi_{12}(R_{12})$  and  $g_{12}^{(2,0)}(R_{12})$  are the intermolecular potential and pair correlation function, respectively, with  $m_{12}$  as the reduced mass. Equations 1-3 are also applicable. From eq 19 and its analog for the pure fluid

$$\begin{aligned} \frac{\xi_{11}}{\xi_{12}} &= \frac{\Lambda_{11}}{\Lambda_{12}} \frac{m_1}{m_{12}} \left( \frac{D_1}{D_1 + D_2} \right); \\ \frac{\xi_{22}}{\xi_{12}} &= \frac{\Lambda_{22}}{\Lambda_{12}} \frac{m_2}{m_{12}} \left( \frac{D_2}{D_1 + D_2} \right) \end{aligned} \quad (21)$$

so that, provided  $\Lambda_{11}/\Lambda_{12}$  and  $\Lambda_{22}/\Lambda_{12}$  can be obtained and  $D_1$  and  $D_2$  are known,  $D$  can be calculated from eq 7.

- (7) G. S. Hartley and J. Crank, *Trans. Faraday Soc.*, **45**, 801 (1949).
- (8) R. J. Bearman, *J. Phys. Chem.*, **65**, 1961 (1961).
- (9) H. J. V. Tyrrell, *J. Chem. Soc.*, 1599 (1963).
- (10) O. Lamm, *Acta Chem. Scand.*, **3**, 1120 (1954).
- (11) D. E. Meyer, "Kinetic Theory of Gases," Longmans, Green and Co., London, 1899.
- (12) L. Miller and P. C. Carman, *Trans. Faraday Soc.*, **57**, 2143 (1961).
- (13) R. J. Bearman and P. F. Jones, *J. Chem. Phys.*, **33**, 1432 (1960).
- (14) J. K. Horrocks and E. McLaughlin, *Trans. Faraday Soc.*, **88**, 1357 (1962).
- (15) P. C. Carman and L. H. Stein, *ibid.*, **52**, 619 (1956).
- (16) R. J. Bearman, *J. Chem. Phys.*, **29**, 1278 (1958).
- (17) S. A. Rice and A. R. Allnatt, *ibid.*, **34**, 409 (1961).
- (18) S. A. Rice and J. G. Kirkwood, *ibid.*, **31**, 901 (1958).

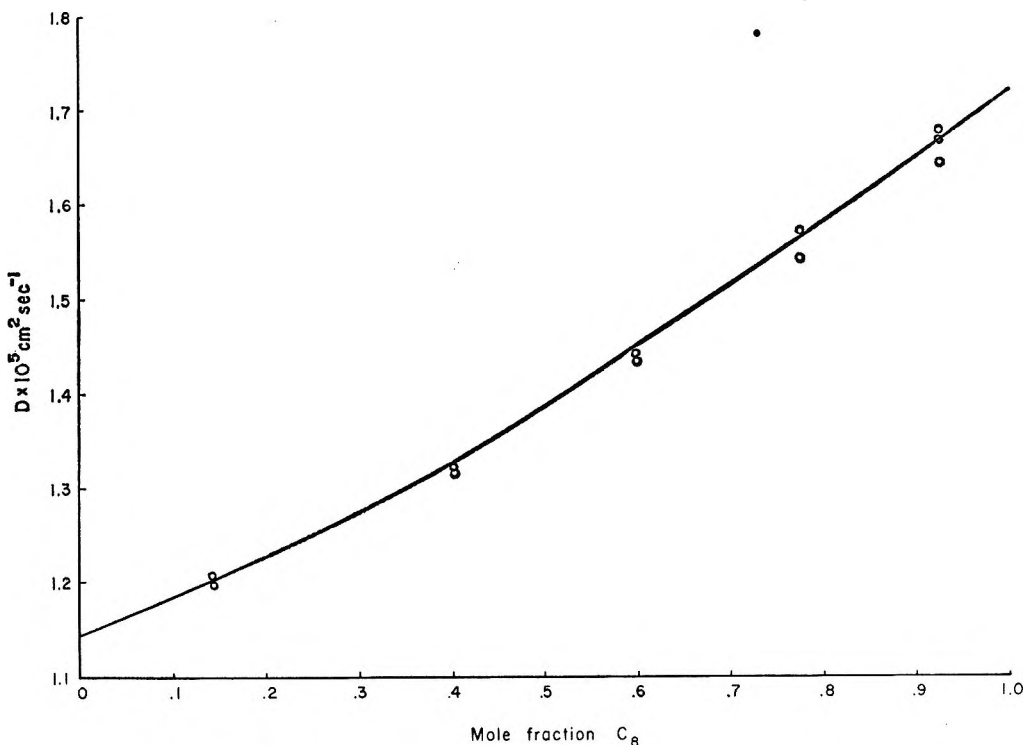


Figure 1. Comparison of calculated (Rice-Allnatt theory) and experimental mutual diffusion coefficients of the system *n*-octane-*n*-dodecane at 25°.

By rewriting<sup>19</sup> the integral in eq 20 as

$$\Lambda_{12} \simeq \frac{1}{3\sigma_{12}^2} \int R_{12}^{-2} \nabla_{R_{12}}^2 \phi_{12}(R_{12}) g_{12}^{(2,0)}(R_{12}) d^3 R_{12} \quad (22)$$

and using the corresponding-states argument of Rice and Allnatt

$$\frac{B_m^{(1,2)}}{B_m^{(1,1)}} = \left( \frac{\epsilon_{12}}{\epsilon_{11}} \right) \left( \frac{x_2}{x_1} \right) \left( \frac{v_1^*}{v_2^*} \right)^{1/2} \left( \frac{\sigma_{12}}{\sigma_{11}} \right)^3 \quad (23)$$

where

$$B_m^{(1,2)} = 4\epsilon_{12} \frac{N_1 N_2}{(v_1^* v_2^*)^{1/2}} \int \left( \frac{\sigma_{12}}{R_{12}} \right)^m g_{12}^{(2,0)} d^3 R_{12} \quad (24)$$

and  $v_1^*$  and  $v_2^*$  are the volumes containing  $N_1$  molecules of species 1 and  $N_2$  molecules of species 2, respectively, and the intermolecular potential is of the Lennard-Jones 12:6 form

$$\phi_{12}(R_{12}) = 4\epsilon_{12} [(\sigma_{12}/R_{12})^{12} - (\sigma_{12}/R_{12})^6] \quad (25)$$

then

$$\frac{\Lambda_{11}}{\Lambda_{12}} = \left( \frac{\epsilon_{11}}{\epsilon_{12}} \right) \left( \frac{\sigma_{11}}{\sigma_{12}} \right); \quad \frac{\Lambda_{22}}{\Lambda_{12}} = \left( \frac{\epsilon_{22}}{\epsilon_{12}} \right) \left( \frac{\sigma_{22}}{\sigma_{12}} \right) \quad (26)$$

so that

$$\frac{\xi_{11}}{\xi_{12}} = \left( \frac{\epsilon_{11}}{\epsilon_{12}} \right) \left( \frac{\sigma_{11}}{\sigma_{12}} \right) \left( \frac{m_1 + m_2}{m_2} \right) \left( \frac{D_1}{D_1 + D_2} \right) \quad (27)$$

$$\frac{\xi_{22}}{\xi_{12}} = \left( \frac{\epsilon_{22}}{\epsilon_{12}} \right) \left( \frac{\sigma_{22}}{\sigma_{12}} \right) \left( \frac{m_1 + m_2}{m_1} \right) \left( \frac{D_2}{D_1 + D_2} \right) \quad (28)$$

and hence

$$\xi_{11}\xi_{22} = \xi_{12}^2 \left( \frac{\epsilon_{11}\epsilon_{22}}{\epsilon_{12}^2} \right) \left( \frac{\sigma_{11}\sigma_{22}}{\sigma_{12}^2} \right) \frac{(m_1 + m_2)^2}{m_1 m_2} \frac{D_1 D_2}{(D_1 + D_2)^2} \quad (29)$$

Equations 27 and 28 therefore provide an alternative prescription for the evaluation of eq 7 from thermodynamic and self-diffusion data, and eq 29 indicates the conditions that must be fulfilled before eq 9 holds. If the usual geometric-combining rule for the  $\epsilon$ 's and the arithmetic-mean rule for the molecular diameters is assumed, then

$$\xi_{11}\xi_{22} = 4\xi_{12}^2 \frac{\sigma_{11}\sigma_{22}}{(\sigma_{11} + \sigma_{22})^2} \frac{(m_1 + m_2)^2}{m_1 m_2} \frac{D_1 D_2}{(D_1 + D_2)^2} \quad (30)$$

so that for systems composed of molecules of comparable molecular weight and size we know  $D_1$  and  $D_2$  are then comparable in magnitude; hence, eq 30 will approximate to eq 9.

In order to show this, calculated and experimental results for  $D$  for the system *n*-octane + *n*-dodecane are given in Figure 1. The diffusion data were obtained by Van Geet and Adamson<sup>20</sup> and the thermodynamic data by Brønsted and Koefoed.<sup>21</sup> Force constants were

(19) J. S. Rowlinson, *Mol. Phys.*, **7**, 477 (1964).

(20) A. L. Van Geet and A. W. Adamson, *J. Phys. Chem.*, **68**, 238 (1964).

(21) J. N. Brønsted and J. Koefoed, *Kgl. Danske Videnskab. Selskab. Mat. Fys. Medd.*, **22**, 1 (1946).

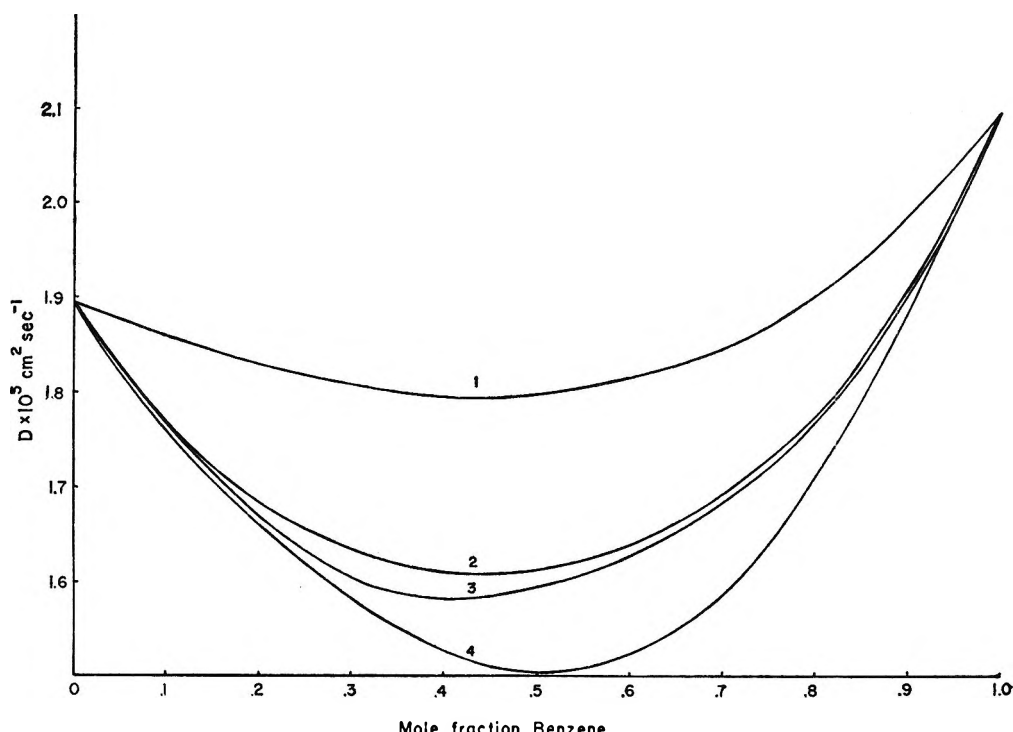


Figure 2. Comparison of calculated and experimental values of the mutual diffusion coefficient of the benzene-cyclohexane system at 25°: 1, experimental; 2, Rice-Allnatt theory; 3, eq 8; 4, Vignes correlation.

estimated by the correlation of Stiel and Thodos.<sup>22</sup> Agreement is seen to be quantitative, but Van Geet and Adamson<sup>20</sup> have already pointed out that eq 8 is also satisfactory.

For the system benzene and cyclohexane,  $D$  has been measured by Lyons and Rodwin<sup>23</sup> and the self-diffusion data by Mills<sup>24</sup> and by Kamal and McLaughlin.<sup>25</sup> (Dr. Mills has kindly pointed out that his reported coefficients<sup>24</sup> at infinite dilution are measured values and not extrapolated as assumed in ref 25. Values in Table 3 of ref 25 should therefore be replaced by his values  $10^5 D_1 \approx 2 = 1.895 \text{ cm}^2 \text{ sec}^{-1}$  and  $10^5 D_2 \approx 1 = 2.104 \text{ cm}^2 \text{ sec}^{-1}$  and the text adjusted accordingly.) Using the latter results together with the values of  $(\partial \ln a_1 / \partial \ln x_1)_{T,p}$  calculated by Douglass and McCall<sup>26</sup> from the experimental work of Scatchard, Wood, and Mochel,<sup>27</sup> the mutual diffusion coefficient  $D$  has been calculated from eq 8 and 7 together with eq 27 and 28. The improve-

ment on the Rice-Allnatt theory is only marginal, as would be expected in view of the comments already made about eq 30. Included also in Figure 2 is the calculated value of  $D$  according to the recent empirical equation of Vignes<sup>28</sup> which shows no improvement

$$D = \left( \frac{\partial \ln a_1}{\partial \ln x_1} \right)_{T,p} (D_1 \approx 2)^{x_2} (D_2 \approx 1)^{x_1} \quad (31)$$

The same situation holds for the Rice-Allnatt equation

$$\eta = \left( \frac{v_1^*}{v} \right)^2 \eta_1 \frac{D_1}{D_1^0} \left[ 1 + 2 \frac{m_2}{m_1 + m_2} \left( \frac{\epsilon_{22}}{\epsilon_{11}} \right)^{1/2} \left( \frac{x_2}{x_1} \right) \left( \frac{\sigma_{12}}{\sigma_{11}} \right)^3 \right] + \left( \frac{v_2^*}{v} \right)^2 \eta_2 \frac{D_2}{D_2^0} \left[ 1 + \frac{2m_1}{m_1 + m_2} \left( \frac{\epsilon_{11}}{\epsilon_{22}} \right)^{1/2} \left( \frac{x_1}{x_2} \right) \left( \frac{\sigma_{12}}{\sigma_{22}} \right)^3 \right] \quad (32)$$

which is used to calculate the viscosity of binary mixtures.  $\eta$  is the viscosity of the mixture and  $\eta_1$  and  $\eta_2$  are the viscosities of pure 1 and 2, respectively. When applied to benzene and toluene mixtures, the results obtained using the self-diffusion data of Kamal and McLaughlin show almost quantitative agreement with experiment (Table I). For benzene and cyclohexane the results are poor.

(22) L. Stiel and G. Thodos, *J. Chem. Eng. Data*, **7**, 234 (1962).

(23) Quoted by H. S. Harned, *Discussions Faraday Soc.*, **24**, 7 (1947).

(24) R. Mills, *J. Phys. Chem.*, **69**, 3116 (1965).

(25) I. Kamal and E. McLaughlin, *Trans. Faraday Soc.*, **62**, 1762 (1966).

(26) D. C. Douglass and D. McCall, *J. Phys. Chem.*, **71**, 987 (1967).

(27) G. Scatchard, S. E. Wood, and J. M. Mochel, *ibid.*, **43**, 119 (1939).

(28) A. Vignes, *Ind. Eng. Chem., Fundam.*, **5**, 189 (1966).

Table I: Calculated and Experimental Viscosities of the System Benzene and Toluene at 25°

	Mole fraction of benzene					
	0	0.1	0.2	0.3	0.4	0.5
$10^3 \eta, \text{P}$						
Calcd	5.82	5.90	5.96	6.03	6.10	6.15
Exptl	5.82	5.88	5.92	5.97	6.02	6.08
	Mole fraction of benzene					
	0.6	0.7	0.8	0.9	1.0	
Calcd	6.21	6.24	6.26	6.29	6.27	
Exptl	6.10	6.16	6.20	6.24	6.27	

**Table II:** Force Constants and Self-Diffusion Coefficients of Simple Organic Molecules at 25°

	$\epsilon/k$ , °K	$\sigma$ , Å	$10^6 D_i^0$ , cm <sup>2</sup> sec <sup>-1</sup>	Ref
(1) Benzene	367	5.492	2.12	a
(2) Cyclohexane	324	6.093	1.41	a
(3) Toluene	395	5.727	2.23	b
(4) Carbon tetrachloride	327	5.881	1.41	c

<sup>a</sup> Reference 25. <sup>b</sup> I. Kamal and E. McLaughlin, Proceedings of the Fourth Symposium on Thermophysical Properties, J. R. Moszynski, Ed., American Society of Mechanical Engineers, New York, N. Y., 1968, p 278. <sup>c</sup> H. Watts, B. J. Alder, and J. H. Hildebrand, *J. Chem. Phys.*, **21**, 1601 (1953).

As well as looking at the variation with composition of the calculated mutual diffusion coefficient, it is also useful to look at the values at extreme dilution, particularly when only self-diffusion measurements have been made. According to eq 27 we may write

$$\frac{2a^2}{1+a} = \left( \frac{\epsilon_{ff}}{\epsilon_{ii}} \right)^{1/2} \left( 1 + \frac{\sigma_{ff}}{\sigma_{ii}} \right) \left( \frac{m_f}{m_i + m_f} \right) \quad (33)$$

where  $a = D_i^0/D_f^{\infty i}$ , so that if  $D_i^0$  is known  $D_f^{\infty i}$  can be calculated. Table II lists the self-diffusion coefficient and intermolecular force constants used to calculate the mutual diffusion coefficients at extreme dilution for a series of pairs of simple binary organic mixtures. The results are compared in Table III with experimental values. Agreement in most cases is only moderate.

### Conclusions

In summary it can be seen that for mixtures which approximate closely to regular-solution theory, the geometric-mean relationship between the friction coefficients is approximately true and eq 8 can be used with confidence. For still less ideal solutions, the  $(\partial \ln$

**Table III:** Calculated and Experimental Mutual Diffusion Coefficients in Infinite Dilution at 25°

—Benzene (1) and cyclohexane (2) <sup>a</sup> —		
	$D_1^{\infty 1}$	$D_2^{\infty 1}$
Calcd	1.44	2.08
Exptl	1.88	2.07
—Benzene (1) and toluene (3) <sup>b</sup> —		
	$D_1^{\infty 1}$	$D_3^{\infty 1}$
Calcd	2.45	1.93
Exptl	2.33	2.03
—Benzene (1) and $\text{CCl}_4$ (4) <sup>c</sup> —		
	$D_1^{\infty 1}$	$D_4^{\infty 1}$
Calcd	1.80	1.78
Exptl	1.41	1.92
—Cyclohexane (2) and toluene (3) <sup>b</sup> —		
	$D_2^{\infty 2}$	$D_3^{\infty 2}$
Calcd	2.41	1.31
Exptl	2.07	1.69
—Cyclohexane (2) and $\text{CCl}_4$ (4) <sup>d</sup> —		
	$D_2^{\infty 2}$	$D_4^{\infty 2}$
Calcd	1.75	1.20
Exptl	1.27	1.49

<sup>a</sup> Reference 25. <sup>b</sup> I. Kamal and E. McLaughlin, Proceedings of the Fourth Symposium on Thermophysical Properties, J. R. Moszynski, Ed., American Society of Mechanical Engineers, New York, N. Y., 1968, p 278. <sup>c</sup> C. S. Caldwell and A. L. Babb, *J. Phys. Chem.*, **60**, 51 (1956). <sup>d</sup> B. R. Hammond and R. H. Stokes, *Trans. Faraday Soc.*, **52**, 781 (1956).

$a_1/\partial \ln x_1)_{T,p}$  term in eq 8 overcorrects the effect of the  $x_1 D_2 + x_2 D_1$  term and at present there is no satisfactory method of evaluating the final term in eq 7 which reduces this correction.

*Acknowledgments.* E. McL. wishes to thank the National Science Foundation for the award of a Senior Foreign Scientist Fellowship and the faculty, particularly Professors J. Coates and P. Murrill, of the Louisiana State University Chemical Engineering Department at Baton Rouge for their hospitality.

## Mass Spectrometric Study of the Reactions of Atomic Oxygen with Ethylene and Formaldehyde<sup>1</sup>

### Oxygen with Ethylene and Formaldehyde<sup>1</sup>

by John T. Herron and Ralph D. Penzhorn

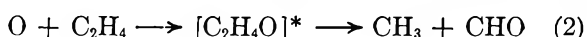
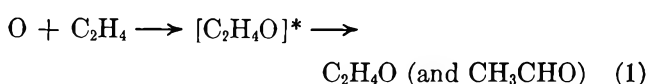
National Bureau of Standards, Washington, D. C. 20234 (Received August 1, 1968)

A mass spectrometric study has been made of the reactions of atomic oxygen with ethylene and formaldehyde. The formation of formaldehyde in the ethylene reaction is shown to be independent of the presence of molecular oxygen and is attributed to a reaction between atomic oxygen and methyl radicals. The rate constant for the reaction of atomic oxygen with formaldehyde is  $9.0 \times 10^{10} \text{ cm}^3 \text{ mol}^{-1} \text{ sec}^{-1}$  at 300°K.

### Introduction

The reaction of atomic oxygen with ethylene has been studied over a wide range of temperature and total pressure. Aside from some interpretative difficulties in the case of the low-pressure flow experiments, a consistent reaction mechanism seems to be applicable.

This mechanism, due primarily to Cvetanovic,<sup>2,3</sup> may be presented in a simplified form as



Thus when oxygen atoms react with solid ethylene films at 65–69°K, ethylene oxide and acetaldehyde are the only products found.<sup>4</sup> At higher temperatures where the reaction has been studied in the gas phase over a wide range of total pressure, using a photolytic source of atomic oxygen, it was found that although some ethylene oxide and acetaldehyde were formed, many other products were formed which could be interpreted as arising from reaction 2 followed by reactions of the primary products. Secondary atomic oxygen reactions could be discounted. Formaldehyde was not found as a product.

Finally, experiments in electrical discharge-flow systems at total pressures of several torr showed that under these conditions, the final products were formaldehyde and carbon monoxide<sup>5</sup> with a very small amount of acetaldehyde. Either formaldehyde could be a primary product of the reaction, thus disproving the Cvetanovic mechanism, or it could arise from a secondary reaction of the methyl radicals produced in reaction 2.

The present study was undertaken in an attempt to clarify the mechanism of the low-pressure flow experiments and to see if they could be interpreted in terms of the general mechanism represented by reactions 1 and 2.

The formaldehyde reaction was included in view of its importance as a final product in the ethylene reaction and its importance in combustion chemistry in general.

### Experimental Section

The reaction was studied using a flow system attached to a mass spectrometer as described elsewhere.<sup>6</sup> Oxygen atoms were generated by either of two methods. In the first, argon gas at about 2 torr of total pressure, containing about 3% O<sub>2</sub>, was passed through a 2450-MHz electrodeless discharge to yield directly oxygen atoms. In the second, pure nitrogen gas at about 2 torr of total pressure was passed through the discharge, resulting in the production of nitrogen atoms which then reacted with nitric oxide to yield oxygen atoms via the very fast reaction



In some experiments <sup>15</sup>NO was used to avoid interference at mass 30 in the mass spectrum.

The partial pressures of reactants and products were continuously monitored with the mass spectrometer. The oxygen measurements, and in some few cases hydrogen atom measurements, were put on an absolute basis by using the NO<sub>2</sub>-titration technique.<sup>7</sup> The reaction time could be varied by adjusting the distance between the reactant inlet and the sampling orifice of the mass spectrometer. All experiments were carried out at room temperature (300°K).

Formaldehyde, prepared after the method of Spence and Wilde<sup>8</sup> by the thermal decomposition of  $\alpha$ -poly(oxymethylene), was generated continuously as required.

### Results and Discussion

#### 1. Mechanism of the Ethylene Reaction. Figure 1

- (1) Contribution of the National Bureau of Standards, not subject to copyright.
- (2) R. J. Cvetanovic, *J. Chem. Phys.*, **23**, 1375 (1955).
- (3) R. J. Cvetanovic, *Advan. Photochem.*, **1**, 115 (1963).
- (4) A. N. Ponomarev, *Kinet. Katal.*, **7**, 237 (1966).
- (5) L. I. Avramenko, R. V. Kolesnikova, and G. I. Savinova, *Izv. Akad. Nauk SSSR, Otd. Khim. Nauk*, **36** (1963).
- (6) F. S. Klein and J. T. Herron, *J. Chem. Phys.*, **41**, 1285 (1964).
- (7) F. Kaufman, *Progr. Reaction Kinetics*, **1**, 1 (1961).
- (8) R. Spence and W. Wilde, *J. Chem. Soc.*, 338 (1935).

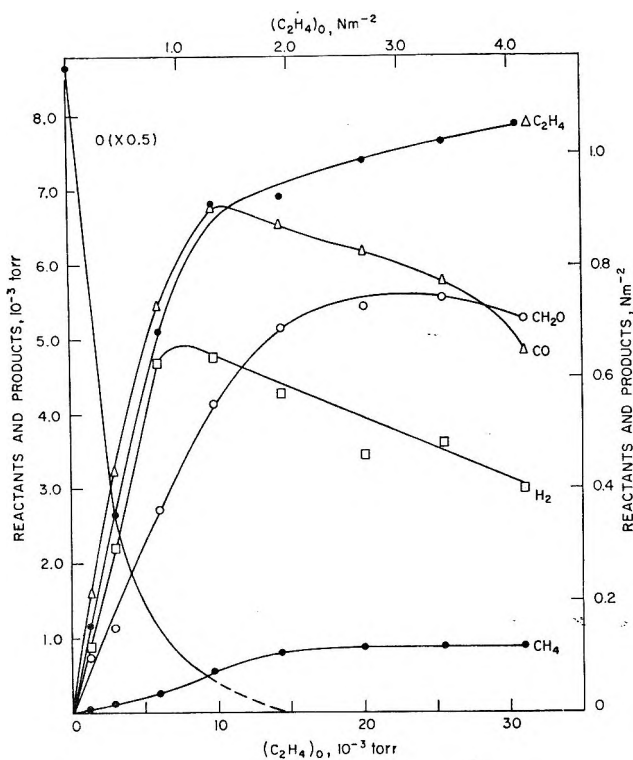


Figure 1. Ethylene reaction. Partial pressure of reactants and products as a function of the initial ethylene partial pressure. The reaction time is 0.02 sec.

gives the partial pressures<sup>9</sup> of reactants and products as a function of the initial ethylene partial pressure with a fixed reaction time and initial atomic oxygen partial pressure. The atomic oxygen in this case was prepared from the oxygen in the argon mixture. The carbon balance for these data is about 85%. Additional minor products were identified in the mass range 40–44 but were not quantitatively evaluated. Using deuterioethylene, we observed a shift in the mass range of up to 48, which suggests the presence of acetaldehyde (or ethylene oxide).

The methane measurements are based on the mass-15 peak in the spectrum. This was checked by using deuterioethylene and noting the formation of deuteriomethane at mass 20. Water was not detected as a product.

These experiments were repeated using atomic oxygen generated from the  $N-^{16}NO$  reaction. The results were essentially the same, except that carbon monoxide was not determinable because its nominal mass coincides with that of molecular nitrogen.

The accuracy of the formaldehyde measurements is severely limited owing to the unusual behavior of the mass spectral peak corresponding to mass 30. When the discharge was turned on, with no reactant present, this peak showed a considerable increase. Upon addition of a reactant removing oxygen atoms, the 30 peak dropped off again. Obviously if we attempt to analyze for formaldehyde using the mass-30 peak, the

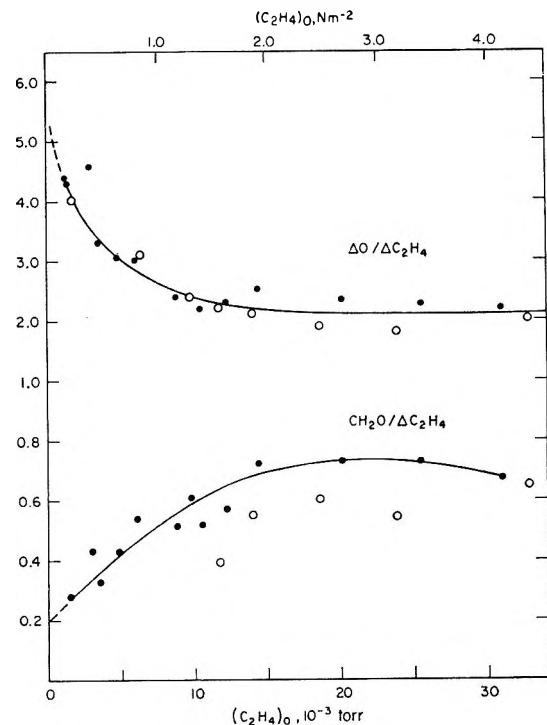
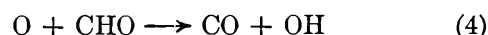
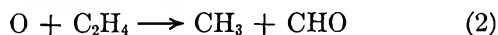


Figure 2. Ethylene reaction. Ratios of atomic oxygen to ethylene consumed and formaldehyde formed to ethylene consumed. Open circles represent systems free of molecular oxygen.

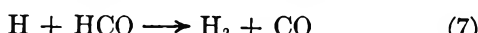
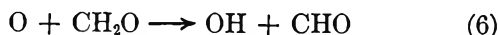
result will be in error. Our data are based on both 29 and 30 mass spectral peaks, with the former being relied on completely at low flows. At higher flows we have relied more on the 30 peak, since mass 29, unlike 30, corresponds to a major peak in the mass spectrum of many compounds. At high reactant flows there was an excess at mass 29 over that due to formaldehyde, and when deuterioethylene was used as a reactant, a shift to mass 34 (*i.e.*,  $\text{C}_2\text{D}_5^+$ ) resulted. Both observations are compatible with the formation of acetaldehyde or ethylene oxide.

In the case of the  $N-^{16}NO$  experiments no quantitative analysis for  $\text{CH}_2\text{O}$  was possible at the lowest flow rates because of the large background peak at mass 29. The results we give, based on the mass-30 peak, may be expected to be low by about 25%.

The stoichiometry with respect to atomic oxygen, ethylene, and formaldehyde is shown in Figure 2. Although the reaction is complex, the observations are in accord with the simplified mechanism



(9) Partial pressures are given in torr and newtons per square meter (1 torr = 133.32 N m<sup>-2</sup>).



In addition there will be reactions of atomic hydrogen with ethylene<sup>10</sup> and formaldehyde and possibly additional reactions involving hydroxyl radicals.

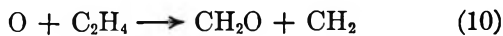
At initial ethylene partial pressures approaching zero, this mechanism predicts a ratio of  $\Delta[\text{O}]/\Delta[\text{C}_2\text{H}_4]$ , the ratio of atomic oxygen consumed to ethylene consumed, of between 4 and 7, depending on the extent of reaction of formaldehyde, in reasonable agreement with the observed ratio of about 5. (The observed yield at high ethylene partial pressures cannot be related to the mechanism until the atomic hydrogen reactions are better understood.)

Reactions 7–9 were originally proposed by Cvetanovic.<sup>11</sup> Further evidence for reactions 8 and 9 comes from a study of the photolysis of methyl formate, from which rate constants  $k_8 = 3.8 \times 10^{12} \text{ cm}^3 \text{ mol}^{-1} \text{ sec}^{-1}$  and  $k_9 = 2.2 \times 10^{13} \text{ cm}^3 \text{ mol}^{-1} \text{ sec}^{-1}$  (independent of temperature from 304 to 377°K) were derived.<sup>12</sup> If this mechanism is correct, then the formation of methane would be expected to show a dependence on the square of the ethylene consumed. As shown in Figure 3 this is the case within the limits of experimental error.

The main point is that formaldehyde is formed in the absence of molecular oxygen, and if we accept reaction 2, it follows that formaldehyde is produced directly from a reaction of atomic oxygen with methyl radicals. Fenimore and Jones<sup>13</sup> have also concluded that the reaction of atomic oxygen with methyl radicals is important and have proposed that  $k_3 = (1.9 \pm 0.3) \times 10^{13} \text{ cm}^3 \text{ mol}^{-1} \text{ sec}^{-1}$  from about 1500 to 2000°K.

The main argument against the occurrence of reaction 3 is that formaldehyde has not been found as a product of the atomic oxygen–methane reaction in the absence of molecular oxygen.<sup>14,15</sup> Westenberg and de Haas<sup>15</sup> argued that inasmuch as the initial step in the methane reaction almost certainly is  $\text{O} + \text{CH}_4 \rightarrow \text{CH}_3 + \text{OH}$ , failure to detect formaldehyde indicates that reaction 3 is unimportant.

This in turn strongly implies that in the case of the ethylene reaction, formaldehyde is a primary reaction product, *i.e.*



However, these experiments were carried out under flow conditions, using a mass spectrometer to analyze the products. Our own experience indicates that this is an extremely insensitive method of looking for formaldehyde, particularly as it is the product of a very slow reaction and reacts much more rapidly with atomic oxygen than does methane. Furthermore, it requires

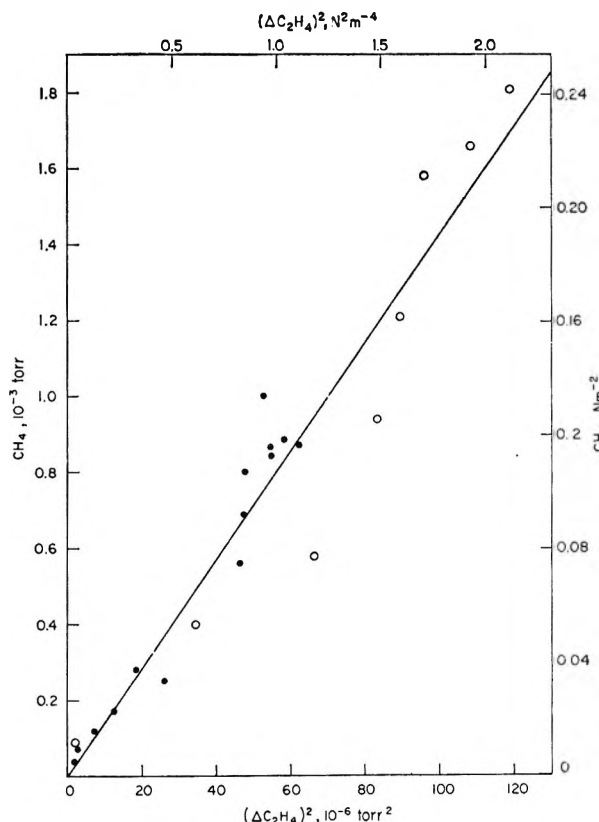


Figure 3. Ethylene reaction. Methane production as a function of the square of the ethylene consumed. Open circles represent systems free of molecular oxygen.

that the photolytic work on the atomic oxygen–ethylene reaction<sup>2</sup> be in considerable error. Thus the principal product of the reaction, formaldehyde, would have had to be almost completely missed, as well as the secondary products such as cyclopropane and ethane that would arise from secondary reactions of  $\text{CH}_2$  radicals produced in reaction 10.

The question would be resolved if a simple chemical source of methyl radicals were available. We have looked for such a source in reactions of atomic oxygen with the methyl halides and have found a possible source in methyl iodide, which, unlike the other methyl halides, reacts extremely rapidly with atomic oxygen at room temperature.

The only products of the reaction that we have detected are formaldehyde and an oxide, or mixture of

(10) By analogy with reaction 3, the formation of acetaldehyde could be explained by the sequence  $\text{H} + \text{C}_2\text{H}_4 \rightarrow \text{C}_2\text{H}_5$  and  $\text{O} + \text{C}_2\text{H}_5 \rightarrow \text{CH}_3\text{CHO} + \text{H}$ .

(11) R. J. Cvetanovic, *Can. J. Chem.*, **33**, 1684 (1955).

(12) M. J. Yee Quee and J. C. J. Thynne, *Ber. Bunsenges. Phys. Chem.*, **72**, 211 (1968); see also F. P. Lossing, *Can. J. Chem.*, **35**, 305 (1957).

(13) C. P. Fenimore and G. W. Jones, *J. Phys. Chem.*, **65**, 1532 (1961).

(14) E. L. Wong and A. E. Potter, Jr., *Can. J. Chem.*, **45**, 367 (1967).

(15) A. A. Westenberg and N. de Haas, *J. Chem. Phys.*, **46**, 490 (1967).

**Table I:** Isotopic Distribution of Formaldehydes Formed in the Reactions of Atomic Oxygen with Deuterated Ethylenes<sup>a</sup>

Reactant	CH <sub>2</sub> O	CHDO	CD <sub>2</sub> O
C <sub>2</sub> H <sub>3</sub> D	1.21	1.00	0.22
CHDCHD	~0.5	1.00	0.49
CH <sub>2</sub> CD <sub>2</sub>	0.56	1.00	0.78
C <sub>2</sub> HD <sub>3</sub>	0.25	1.00	1.92
C <sub>2</sub> H <sub>4</sub> -C <sub>2</sub> D <sub>4</sub> (equimolar mixture)	1.00	1.00	2.00

<sup>a</sup> These data are based on experiments in which ethylene was in excess and atomic oxygen was completely consumed. Typical reactant partial pressures were  $(O)_0 \approx 15 \times 10^{-3}$  torr,  $(\text{ethylene})_0 \approx 30 \times 10^{-3}$  torr, and  $\Delta(\text{ethylene}) \approx 7.5 \times 10^{-3}$  torr. The same results were obtained in the case of the C<sub>2</sub>H<sub>4</sub>-C<sub>2</sub>D<sub>4</sub> mixture when  $(O)_0 \approx 15 \times 10^{-3}$  torr,  $(\text{ethylene})_0 \approx 10 \times 10^{-3}$  torr, and  $\Delta(\text{ethylene}) \approx 5 \times 10^{-3}$  torr.

oxides, of iodine which deposited on the walls of the reactor (but which is readily washed off with water). The rapidity of the reaction is suggestive of a chain mechanism, and although the nature of the initiating step is not apparent,<sup>16</sup> reaction 3 is certainly the most likely source of the formaldehyde.

In principle it would seem that some of these mechanistic problems could be resolved by the use of labeled ethylenes. We have attempted to do this by collecting the reaction products for various deuterium-labeled ethylenes and by determining the isotopic distribution of the formaldehydes. The results, shown in Table I, are not compatible with any single mechanism. However, it is clear that these data do not support a predominantly molecular origin for formaldehyde (reaction 10). Qualitatively at least, the data can be explained on the basis of established exchange reactions of atomic hydrogen with methyl radicals<sup>17</sup> and ethylene,<sup>18</sup> of the type D + CH<sub>3</sub> → H + CH<sub>2</sub>D and D + C<sub>2</sub>H<sub>4</sub> → H + C<sub>2</sub>H<sub>3</sub>D, which could lead to the observed isotopic mixing of the product formaldehydes.

*2. Mechanism of the Formaldehyde Reaction.* Experiments were made in which the partial pressures of reactants and products were followed as functions either of initial reactant partial pressure or of reaction time. Only in the case of the latter experiments was an attempt made to measure the atomic hydrogen partial pressure.

Figure 4 gives the partial pressures of reactants consumed and products formed as a function of the initial formaldehyde partial pressure at a fixed reaction time and initial atomic oxygen partial pressure. Only the formaldehyde, carbon monoxide, atomic oxygen, and molecular hydrogen partial pressures were measured directly. Water was readily detected, but it was not possible to calibrate the mass spectrometer for water vapor to make a quantitative measurement. However, it is possible to calculate an upper limit to the

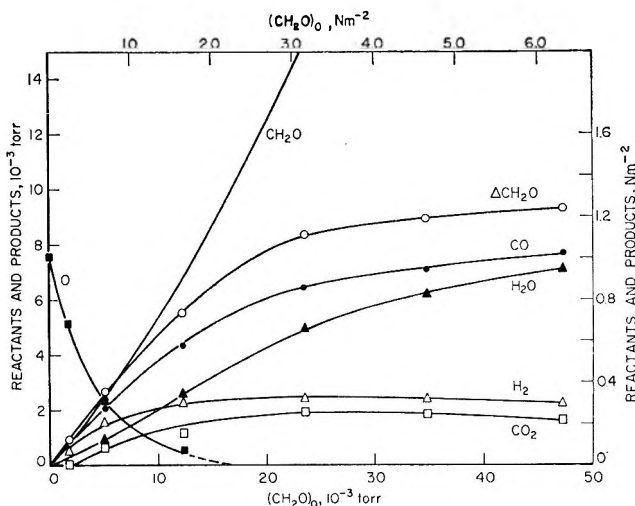


Figure 4. Formaldehyde reaction. Partial pressure of reactants and products as a function of the initial formaldehyde partial pressure. The reaction time is 0.02 sec.

amount of water produced from the stoichiometry of the reaction. At the highest initial formaldehyde partial pressure, hydrogen atoms produced in the reaction will react at least partially to yield molecular hydrogen (see below), and in the absence of any other hydrogen-containing products,  $(H_2O) \leq \Delta(CH_2O) - (H_2)$ . This calculated water partial pressure in conjunction with the measured intensity of the water peak in the mass spectrum permits us to calculate the sensitivity of water and hence to calculate the water partial pressure at any point. Allowing for the presence of some atomic hydrogen, the true water yield will be lower by a constant factor.

In the case of carbon dioxide, some carbon dioxide is formed in the absence of added formaldehyde, indicating that oxygen atoms are probably reacting on the surfaces of the reactor or the ion source. At higher formaldehyde flows where all the atoms are consumed, this problem is minimized and a reasonably accurate value for carbon dioxide can be found. At high initial formaldehyde partial pressure, the carbon dioxide produced is equal, within the experimental uncertainty, to  $\Delta[CH_2O] - [CO]$ . The latter quantity is used throughout as the carbon dioxide yield. No other carbon-containing products were found.

Figure 5 gives the partial pressures of reactants and products as functions of reaction time. The data for water were too uncertain here to be of value and are omitted. As in the case of ethylene, the reaction is complex. This may be seen from Figure 6, where the ratio  $\Delta[O]/\Delta[CH_2O]$ , the ratio of atomic oxygen consumed to formaldehyde consumed, from the data of

(16) The reaction of atomic oxygen with CF<sub>3</sub>I is also extremely fast and, as in the case of CH<sub>3</sub>I, is apparently endothermic in terms of the abstraction of an iodine atom.

(17) R. Berisford and D. J. LeRoy, *Can. J. Chem.*, 36, 983 (1958).

(18) A. H. Turner and R. J. Cvetanovic, *ibid.*, 37, 1075 (1959).

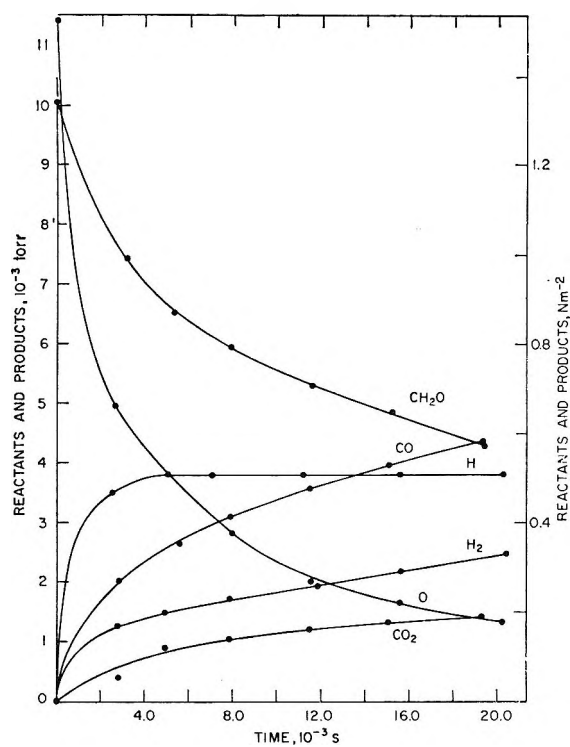
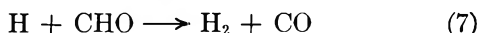
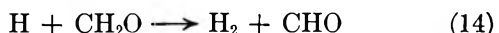
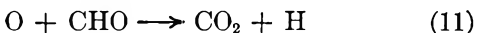
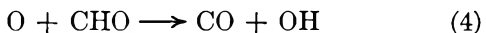
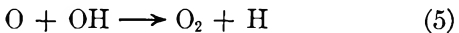
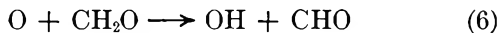


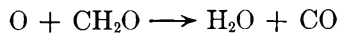
Figure 5. Formaldehyde reaction. Partial pressure of reactants and products as a function of reaction time.

Figure 4 is shown as a function of  $(\text{CH}_2\text{O})_0$ . The fact that this ratio approaches a value between 3 and 4 as  $(\text{CH}_2\text{O})_0 \rightarrow 0$  is indicative of reactions of oxygen atoms with the reaction products. At higher formaldehyde flows, this ratio drops to less than unity, which suggests that reaction products may also be reacting with formaldehyde. This conclusion is supported by the rate measurements discussed in the next section.

We suggest the following mechanism to account for the observed products



Reaction 6 was originally postulated by Geib<sup>19</sup> and has been confirmed by Niki<sup>20</sup> in a study similar to ours. The mechanism suggested by Avramenko and Lorentzo<sup>21</sup>



is clearly inadequate to explain the observations.

Reaction 11 has been tentatively adopted from

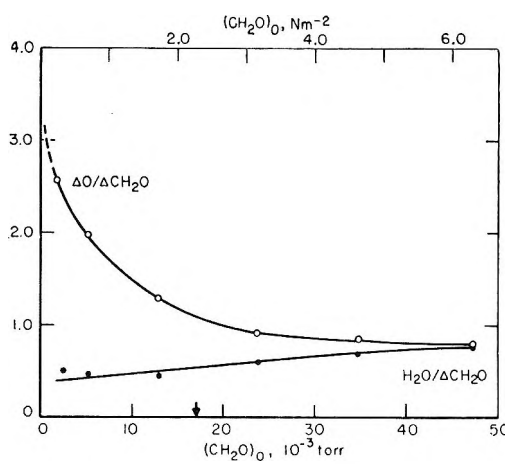


Figure 6. Formaldehyde reaction. Ratio of atomic oxygen to formaldehyde consumed and of water produced to formaldehyde consumed as a function of the initial formaldehyde partial pressure. Data from Figure 4. The arrow indicates the formaldehyde partial pressure at which all atomic oxygen is consumed.

Brennen, *et al.*,<sup>22</sup> and Niki<sup>20</sup> to explain the formation of carbon dioxide. The reaction between carbon monoxide and hydroxyl radicals is much too slow to account for the amount of carbon dioxide formed.

Although water may be formed in reaction 12 or 13, we believe that reaction 12 is the major source of water. In Figure 6 the ratio  $[\text{H}_2\text{O}] / \Delta[\text{CH}_2\text{O}]$ , the ratio of water produced to formaldehyde consumed, is shown as a function of  $(\text{CH}_2\text{O})_0$ . This quantity approaches unity at high formaldehyde flow rates, which is not unexpected on the basis of the above mechanism. However, it is surprisingly large at low formaldehyde flow rates. Under the latter conditions, where oxygen atoms are not completely consumed,  $[\text{OH}] \ll [\text{O}]$ , and since  $k_{13} \approx 0.09k_5$ , the rate of loss of OH in reaction 13 would be negligible in comparison with its rate of loss in reaction 5. However, as can be seen from Figure 6, a significant amount of water is produced under these conditions.

According to Avramenko and Lorentzo,<sup>23</sup> reaction 12 has a rate constant at room temperature of about  $6 \times 10^{10} \text{ cm}^3 \text{ mol}^{-1} \text{ sec}^{-1}$ , and under conditions such that  $(\text{O}) \approx (\text{CH}_2\text{O})$ , the loss of OH in reaction 12 would be slight compared with its loss in reaction 5, so that again the formation of significant amounts of water would not be expected. However, there is reason to doubt that the experimental technique of Avramenko and Lorentzo

(19) K. H. Geib, *Ergeb. Exakt. Naturw.*, **15**, 15, 44 (1936).

(20) H. Niki, *J. Chem. Phys.*, **45**, 2330 (1966).

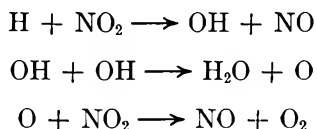
(21) L. I. Avramenko and R. V. Lorentzo, *Zh. Fiz. Khim.*, **26**, 1084 (1952).

(22) W. R. Brennen, I. D. Gay, G. P. Glass, and H. Niki, *ibid.*, **43**, 2569 (1965).

(23) L. I. Avramenko and R. V. Lorentzo, *Dokl. Akad. Nauk SSSR*, **69**, 205 (1949).

is valid,<sup>24,25</sup> and we have therefore attempted to make a direct check of the rate of reaction 12.

By treating hydrogen atoms with nitrogen dioxide, it is possible to generate hydroxyl radicals.<sup>25</sup> With an excess of nitrogen dioxide the reaction sequence is



the over-all stoichiometry being  $\text{H} + 1.5\text{NO}_2 \rightarrow 1.5\text{NO} + 0.5\text{H}_2\text{O} + 0.5\text{O}_2$ .<sup>26</sup> From the stoichiometry,  $[\text{OH}]_0$ , the initial hydroxyl radical concentration, can be determined.

Addition of formaldehyde causes a sharp increase in the water yield and leads to the consumption of most of the formaldehyde; *e.g.*, with  $[\text{OH}]_0 = 1.8 \times 10^{-10} \text{ mol cm}^{-3}$  and  $[\text{CH}_2\text{O}]_0 = 3.8 \times 10^{-11} \text{ mol cm}^{-3}$ , 90% of the formaldehyde is consumed in 0.02 sec.

If we assume that formaldehyde is consumed only through reaction with hydroxyl radicals, then the rate constant for reaction 12 may be written as  $k_{12} = \ln \{ [\text{CH}_2\text{O}]_0 / [\text{CH}_2\text{O}]_t \} / \int_0^t [\text{OH}] dt$ . With no reactant present, hydroxyl radicals are lost primarily through reaction 13. Under these conditions, we can compute  $\left\{ \int_0^t [\text{OH}] dt \right\}_{[\text{CH}_2\text{O}] = 0}$ , knowing  $k_{13}$ ,  $[\text{OH}]_0$ , and the reaction time,  $t$ . With added formaldehyde  $\int_0^t [\text{OH}] dt$  can only be smaller; hence  $k_{12} \geq \ln \{ [\text{CH}_2\text{O}]_0 / [\text{CH}_2\text{O}]_t \} / \left\{ \int_0^t [\text{OH}] dt \right\}_{[\text{CH}_2\text{O}] = 0}$ . Using the above data and  $k_{13} = 1.55 \times 10^{12} \text{ cm}^3 \text{ mol}^{-1} \text{ sec}^{-1}$ ,<sup>27</sup>  $\left\{ \int_0^t [\text{OH}] dt \right\}_{[\text{CH}_2\text{O}] = 0} \approx 8.9 \times 10^{-13} \text{ mol sec cm}^{-3}$ , and hence  $k_{12} \geq 4 \times 10^{12} \text{ cm}^3 \text{ mol}^{-1} \text{ sec}^{-1}$ .

If  $k_{12}$  is this large, then reaction 12 is competitive with reaction 5 and the formation of water is explicable. It follows that the rate constant  $k_{12}$  reported in ref 23 is in error by a factor of about 100.

*3. Rate of the Formaldehyde Reaction.* If formaldehyde is consumed only through reaction with oxygen

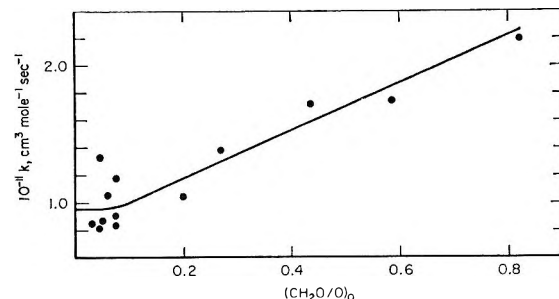


Figure 7. Formaldehyde reaction. Apparent rate constant as a function of the ratio of the initial partial pressure of formaldehyde to the initial partial pressure of atomic oxygen.

atoms, then  $-d[\text{CH}_2\text{O}]/dt = k_6[\text{O}][\text{CH}_2\text{O}]$ , which on integrating yields the expression

$$k_6 = \ln \{ [\text{CH}_2\text{O}]_0 / [\text{CH}_2\text{O}]_t \} / \int_0^t [\text{O}] dt$$

where the subscripts refer to time zero and time  $t$ . The integral is graphically evaluated by measuring the atomic oxygen concentration as a function of time.

In Figure 7 rate constants calculated from this equation are shown as a function of  $[\text{CH}_2\text{O}]_0 / [\text{O}]_0$ . As would be expected for a reaction in which the products in turn can react with formaldehyde, the calculated rate constant increases with increasing  $[\text{CH}_2\text{O}]_0 / [\text{O}]_0$ .<sup>28</sup> In the limit  $[\text{CH}_2\text{O}]_0 / [\text{O}]_0 = 0$ , such secondary reactions are of negligible importance and the true rate is the value obtained at  $[\text{CH}_2\text{O}]_0 / [\text{O}]_0 = 0$ . The value so obtained is  $9.0 \times 10^{10} \text{ cm}^3 \text{ mol}^{-1} \text{ sec}^{-1}$ , with an estimated uncertainty of  $\pm 30\%$ .<sup>29</sup>

(24) F. P. Del Greco and F. Kaufman, *J. Chem. Phys.*, **35**, 1895 (1961).

(25) F. P. Del Greco and F. Kaufman, *Discussions Faraday Soc.*, **33**, 128 (1962).

(26) L. F. Phillips and H. I. Schiff, *J. Chem. Phys.*, **37**, 1233 (1962).

(27) G. Dixon-Lewis, W. E. Wilson, and A. A. Westenberg, *ibid.*, **44**, 2877 (1966).

(28) However, the reaction is exothermic, so that some increase in rate might be brought about by an increase in temperature at the point of mixing.

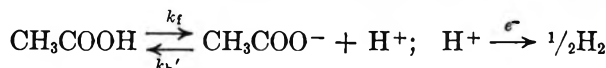
(29) Some of the observations reported here have been independently arrived at by H. Niki, private communication, 1968, and H. Niki, E. E. Daby, and B. Weinstock, *J. Chem. Phys.*, **48**, 5729 (1968).

## Application of the Potentiostatic Method. Determination of the Rate Constant for the Dissociation of Acetic Acid<sup>1</sup>

by Ronald R. Schroeder<sup>2</sup> and Irving Shain

*Department of Chemistry, University of Wisconsin, Madison, Wisconsin 53706 (Received August 1, 1968)*

The rate constant for the dissociation of acetic acid in aqueous solutions was determined by conducting potentiostatic investigations on several acetate-acetic acid solutions of low buffering capacity. The current which was measured resulted from the discharge of the hydrogen ions which were produced by the acid dissociation.



Using existing theories for preceding reaction mechanisms, an apparent rate constant was determined for each of five acetic acid-acetate anion concentrations. The values of the apparent rate constant were found to depend on the thickness of the reaction layer in which the net chemical reaction occurs, relative to the thickness of the electrical double layer in which the reaction is influenced by the potentials and the electric field. A graphical correction procedure was developed which involved plotting the product of the apparent rate constant times the reaction layer thickness against the reaction layer thickness. From the slope of this plot, it was possible to evaluate the characteristics of that portion of the reaction occurring outside of the double layer. Using this correction procedure, a value of the rate constant of  $k_d = 1.58 \times 10^5 \text{ sec}^{-1}$  was obtained.

When the reactant at an electrode is obtained from a chemical reaction in the bulk of the solution, the current is a function of the rate of the chemical reaction. Early work on kinetic systems of this type involved polarographic studies.<sup>3-5</sup> Subsequently, the other electrochemical methods were also applied in the investigation of such reactions. These included the galvanostatic method,<sup>6,7</sup> the potentiostatic method,<sup>8</sup> and many others.<sup>9,10</sup>

Among the early studies were investigations of weak acid systems where an easily reduced acid molecule is produced in the solution by the recombination of the less easily reducible acid anion with hydrogen ions. Several acids were studied and their dissociation and recombination rate constants were reported.<sup>11,12</sup> However, rates obtained electrochemically were often in conflict with the earlier theories of Debye<sup>13</sup> and Onsager<sup>14</sup> which had established upper limits on attainable recombination rates. These limiting theories were confirmed when nonelectrochemical methods were applied to fast reaction studies and the general validity of electrochemically measured rates was questioned.

Possible sources of error in electrochemical measurements were discussed by Delahay and Vielstich<sup>8</sup> and by Strehlow.<sup>15</sup> They were thought to arise from the inadequacies of the diffusion equations for describing the mass transfer in fast kinetic systems and from the effect of the electric field of the double layer on the reaction rates (second Wein effect).

The first of these problems was resolved, in part, by considering the effect of the electrical double layer on mass transfer.<sup>16</sup> The second problem, the effect of the

electric field on rate constants, was considered by Nürnberg,<sup>17</sup> who reported a study of fast reactions in which the second Wein effect was taken into account. In other work,<sup>18</sup> he also corrected his measured values for mass transfer effects in the double layer and thus

- (1) From the Ph.D. thesis of R. R. Schroeder, University of Wisconsin, 1967; presented in part at the 155th National Meeting of the American Chemical Society, San Francisco, Calif., April 1968.
- (2) National Institutes of Health Predoctoral Fellow, 1966.
- (3) R. Brdicka and K. Wiesner, *Collect. Czech. Chem. Commun.*, **12**, 138 (1947).
- (4) J. Koutecky and R. Brdicka, *ibid.*, **12**, 337 (1947).
- (5) J. Koutecky, *ibid.*, **18**, 597 (1953); **19**, 857 (1954).
- (6) P. Delahay and W. Vielstich, *J. Amer. Chem. Soc.*, **77**, 4955 (1955).
- (7) H. Gerischer and M. Krause, *Z. Phys. Chem. (Frankfurt am Main)*, **10**, 264 (1967).
- (8) P. Delahay and S. Oka, *J. Amer. Chem. Soc.*, **82**, 329 (1960).
- (9) P. Delahay, "New Instrumental Methods in Electrochemistry," Interscience Publishers, New York, N. Y., 1954.
- (10) P. Delahay, "Advances in Electrochemistry and Electrochemical Engineering," Vol. I, P. Delahay, Ed., Interscience Publishers, New York, N. Y., 1961, p 233.
- (11) R. Brdicka, "Advances in Polarography," Vol. II, I. S. Longmuir, Ed., Pergamon Press, New York, N. Y., 1960, p 655.
- (12) H. Strehlow in "Technique of Organic Chemistry," Vol. VIII, A. Weissberger, Ed., Interscience Publishers, New York, N. Y., 1963, p 799.
- (13) P. Debye, *Trans. Electrochem. Soc.*, **82**, 262 (1942).
- (14) L. Onsager, *J. Chem. Phys.*, **2**, 599 (1934).
- (15) H. Strehlow, *Z. Elektrochem.*, **64**, 45 (1960).
- (16) L. Gierst in "Transactions of the Symposium on Electrode Processes, Philadelphia, 1959," E. Yeager, Ed., John Wiley & Sons, Inc., New York, N. Y., 1961.
- (17) H. W. Nürnberg, *Discussions Faraday Soc.*, **136** (1965).
- (18) H. W. Nürnberg in "Polarography 1964," G. J. Hills, Ed., Macmillan and Co., Ltd., London, 1966, p 149.

obtained rate constant values which were independent of electrode effects.

The study of weak acid systems has been one of the principal applications of electrochemical methods in the area of fast reactions. However, the methods used in early studies required that the product of the chemical reaction be electroactive, and thus the recombination rates of common nonreducible acids, such as acetic acid, could not be determined. The dissociation of these acids produces hydrogen ion which does react at the electrode, but its polarographic wave is very drawn out and appears at potentials where most supporting electrolytes are also reduced. Ruetschi<sup>19</sup> used an indirect method which involved a material (azobenzene) whose reduction requires hydrogen ion. Solution conditions were adjusted such that the rate of the dissociation of the acid limited the current. The value obtained for the rate constant for the dissociation of acetic acid in ethanol-water was  $k_d = 2.1 \times 10^5 \text{ sec}^{-1}$ , uncorrected for specific electrode effects. Using the same chemical system in chronopotentiometry, Delahay and Vielstich<sup>6</sup> obtained  $k_d = 2.9 \times 10^5 \text{ sec}^{-1}$ , also uncorrected for electrode effects.

In the first studies carried out directly on the dissociation of nonreducible organic acids, Nürnberg<sup>17, 18, 20</sup> used lithium salts as the indifferent electrolyte, thereby decreasing the interference between the reduction current for hydrogen ion and the residual current. Although significant blank corrections were still necessary, it was possible to make measurements using high-level faradaic rectification, apply additional corrections for electrode effects, and obtain a value of  $k_d = 1.39 \times 10^6 \text{ sec}^{-1}$  for acetic acid. Other values of  $k_d$  for acetic acid ranging from  $5 \times 10^5$  to  $3 \times 10^6 \text{ sec}^{-1}$  have been obtained<sup>21</sup> using various relaxation methods.

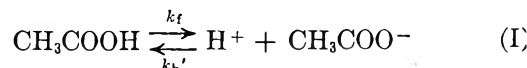
Only one application of the potentiostatic technique to the kinetic study of acids has been reported. Delahay and Oka<sup>8</sup> used the azobenzene system to measure the dissociation rate of monochloroacetic acid in an ethanol-water mixture. A fast-rise potentiostat was used, and data were obtained a few milliseconds after application of the potential. The theories of Koutecky and Brdicka,<sup>4</sup> Koutecky,<sup>5</sup> and Matsuda<sup>22</sup> were applied, and a value of  $k_d = 1.77 \times 10^6 \text{ sec}^{-1}$  (without double-layer corrections) was reported.

In this work, the potentiostatic method was used to study the dissociation rate of acetic acid in aqueous solution by determining the current-time characteristics of hydrogen ion discharge from a series of acetate buffer solutions. Interference from the residual current was essentially eliminated by using tetramethylammonium chloride as the indifferent electrolyte. This work was done to evaluate the capabilities of a specially constructed potentiostat-cell apparatus<sup>23</sup> and to demonstrate the applicability of the potentiostatic method to the study of an important kinetic system involving fast reactions. Although the acetic acid system does not

involve rate constants quite fast enough to test the full capabilities of the instrumentation, the measurements reported here are one or more orders of magnitude faster than previous measurements of reasonable reliability using the potentiostatic method. Correction for double-layer effects on the rate constants was made, and the results are in reasonable agreement with data obtained by other methods.

### Theory

*Boundary Value Problem.* The general boundary value problem for a system in which a chemical reaction precedes a charge transfer has been considered several times.<sup>9</sup> For the acetic acid system, the reactions are



For the general case, the rate constant,  $k_b'$ , for the recombination reaction would be second order, and this would make it impossible to obtain an analytical solution to the boundary value problem. However, in potentiostatic experiments it is feasible to maintain the concentration of the acetate ions constant and large compared with the concentrations of the other species. Under these circumstances a pseudo-first-order rate constant can be defined and used in the derivation

$$k_b = k_b' C^{*A^-} \quad (1)$$

where  $C^{*A^-}$  is the concentration of acetate ions in the bulk of the solution.

Even with this assumption, however, a completely rigorous solution to the boundary value problem can be obtained only if it is assumed that all diffusion coefficients are equal. The result is<sup>5, 8, 9</sup>

$$i_k = (nFAC^{*A^-} \sqrt{D_{HA}/t}) \lambda \exp(\lambda^2) \operatorname{erfc}(\lambda) \quad (2)$$

where

$$\lambda = \sqrt{k_t K t} \quad (3)$$

and

$$K = \frac{k_t}{k_b} = \frac{C_{H^+}}{C_{HA}} \quad (4)$$

Here,  $i_k$  is the kinetic current,  $A$  is the electrode area,  $t$  is the time,  $C_{H^+}$  and  $C_{HA}$  are the concentrations of hydrogen ions and acetic acid, respectively,  $C^{*A^-}$  is the bulk concentration of acetic acid,  $D_{HA}$  is the dif-

(19) P. Ruetschi, *Z. Phys. Chem.* (Frankfurt am Main), **5**, 323 (1955).

(20) H. W. Nürnberg and G. C. Barker, *Naturwissenschaften*, **15**, 191 (1964).

(21) E. F. Caldin, "Fast Reactions in Solution," John Wiley & Sons, Inc., New York, N. Y., 1964.

(22) H. Matsuda, *J. Amer. Chem. Soc.*, **82**, 331 (1960).

(23) R. R. Schroeder, Ph.D. Thesis, University of Wisconsin, 1967.

fusion coefficient of the acetic acid, and the other terms have their usual significance. The equilibrium constant,  $K$ , which is dependent on the concentration of acetate ion, is related to the acid dissociation constant for acetic acid by  $K_d = KC^{*_{\text{A}^-}}$ .

For a system such as acetic acid, eq 2 cannot be applied directly, since the diffusion coefficient of hydrogen ion differs greatly from that of the other materials involved in the reaction. If the differences in the diffusion coefficients are taken into account, an approximate solution can be obtained<sup>5,22</sup> which is of exactly the same form as eq 2, except that in this case

$$\lambda = (D/D_{\text{HA}}) \sqrt{D_{\text{H}^+}/D_{\text{HA}}} K \sqrt{(k_f + k_b)t} \quad (5)$$

and

$$D = \frac{KD_{\text{H}^+} + D_{\text{HA}}}{K + 1} \quad (6)$$

This can be simplified further, since for most experimental situations where the potentiostatic method would be applied (including the acetic acid system studied here),  $C^{*_{\text{H}^+}} \ll C^{*_{\text{HA}}}$ ,  $k_f \ll k_b$ , and  $K \ll 1$ , and therefore  $D \approx D_{\text{HA}}$ . Under these conditions,  $\lambda$  can be simplified to

$$\lambda = \sqrt{k_f K t D_{\text{H}^+}/D_{\text{HA}}} \quad (7)$$

The normal way of evaluating potentiostatic data from these systems involves comparing the kinetic current,  $i_k$ , as given by eq 2, with the diffusion current,  $i_d$ , which would be observed if the rate constants were very large

$$i_d = nFAC^{*_{\text{HA}}} \sqrt{D_{\text{HA}}/\pi t} \quad (8)$$

$$\frac{i_k}{i_d} = \sqrt{\pi} \lambda \exp(-\lambda^2) \operatorname{erfc}(\lambda) \quad (9)$$

$$= f(\lambda) \quad (10)$$

Values of the function  $f(\lambda)$  can be obtained from tables and approximation methods.<sup>24</sup> For values of  $\lambda$  less than 0.01,  $f(\lambda)$  reduces to  $\sqrt{\pi} \lambda$ , and from eq 2, for small values of  $\lambda$  (short times), the current is constant and its value is dependent primarily on the kinetic parameters,  $k_f$  and  $K$ .

For large values of  $\lambda$  (greater than 7),  $f(\lambda)$  becomes unity and the kinetic and diffusion currents are identical (eq 10). Between the limits  $0.01 < \lambda < 7$  the current is controlled by both diffusion and the kinetic parameters.

*Range of Applicability.* The range of magnitudes of the kinetic parameters which can be determined by the potentiostatic method depends on the time scale over which the faradaic current can be measured. For very fast reactions, the current must be measured at very short times before it becomes diffusion controlled. Thus, the electrical double layer must be charged very rapidly so that the charging current will be negligibly small at the short times when the faradaic current must

be measured. Furthermore, it must be possible to make current measurements of kinetic significance over a time interval of at least one order of magnitude. Thus, for an initial current measurement at  $10 \mu\text{sec}$ , partial kinetic control must be observed up to at least  $100 \mu\text{sec}$ . Then, if  $i_k/i_d = 0.9$  is set as an upper limit at which the kinetic current can be distinguished from the diffusion current (corresponding to a value of  $\lambda$  of about 2), for an initial measurement at  $10 \mu\text{sec}$  a kinetic parameter  $k_f K$  (eq 3) of  $4 \times 10^4 \text{ sec}^{-1}$  can be measured. For a typical value of  $K$  equal to  $10^{-4}$ , this parameter corresponds to a rate constant of  $4 \times 10^8 \text{ sec}^{-1}$ . For faster charging rates or smaller equilibrium constants correspondingly faster rate constants can be determined.

At the other extreme, for the determination of small rate constants, the limits of the potentiostatic method arise from a different source. It is generally desirable to evaluate the kinetic parameters by comparing the kinetic current to the diffusion current obtained at longer times. That is, if the ratio  $i_k/i_d$  (eq 9) can be obtained, it is not necessary to know several other parameters (particularly  $D_{\text{HA}}$ ) in order to obtain the kinetic terms from the current-time data. When small rate constants are to be measured, the eventual appearance of a diffusion-controlled current at long times is precluded by the onset of convection, generally at about 10–20 sec from the start of the experiment. If this occurs, it becomes impossible to measure  $i_d$ , and to evaluate kinetic data, eq 2 must be used, which requires that the value of the diffusion coefficient,  $D_{\text{HA}}$ , be known. This information is generally not available and the use of eq 2 is thereby limited. When employing eq 9, a lower limit on measurable rate constants can be estimated by considering the need for diffusion control (*i.e.*,  $\lambda = 7$ ) at times between 1 and 10 sec. This value of  $\lambda$  corresponds to a kinetic parameter  $k_f K$  of about 50, and, since  $K$  must be much smaller than unity, values of  $k_f$  smaller than  $5 \times 10^3 \text{ sec}^{-1}$  are difficult to measure.

In potentiostatic investigations employing mercury drop electrodes (such as the study reported here), convection may occur at considerably shorter times since stirring is caused by the movement of the electrode. This movement can be attributed to the change in surface tension upon application of the potential jump. Further stirring may occur when hydrogen gas is evolved at the electrode. In this work these two effects caused convection at times as short as 20 msec in some cases.

*Double-Layer Effects.* Chemical rate constants which are measured by electrochemical methods may be subject to errors introduced by the presence of the electrode and the electrical double layer in the region of the

(24) "National Bureau of Standards Handbook of Mathematical Functions," U. S. Department of Commerce, Washington, D. C., 1965.

solution where the chemical reaction occurs. To obtain true rate constants which correspond to those which would be measured in a homogeneous solution, these errors must be eliminated. Experimentally, the specific effects which cause these errors cannot be eliminated, so it is necessary to employ some theoretical means to account for them in the calculations of the rate constants. Nürnberg<sup>18</sup> proposed a method for obtaining true solution rate constants from electrochemical data, and a similar method was developed independently in this laboratory. Both methods rely on the consideration that the double-layer effects occur in a region of the solution very close to the electrode surface (diffuse double layer), while some of the chemical reaction occurs outside this region.

*Nature of the Diffuse Double Layer.* The properties of the double layer can, in this case, be described by the applied potential,  $E_a$ , the potential at the outer Helmholtz plane,  $\psi_H$  (as calculated from known values of the double-layer capacitance using Gouy-Chapman theory), and the half-thickness of the diffuse layer,  $1/\kappa$  (*i.e.*, the distance,  $x$ , at which the potential is  $\psi_H/2$ , equivalent to the Debye-Hückel radius of the charge atmosphere). Of principal interest here is the distance  $1/\kappa$  from which the size of the diffuse layer can be inferred<sup>25</sup>

$$\frac{1}{\kappa} = \left( \frac{8\pi z^2 F^2 C_s}{RTd} \right)^{-1/2} \quad (11)$$

Here,  $z$  is the charge of the ions of a symmetrical electrolyte of concentration  $C_s$ ,  $d$  is the dielectric constant, and  $R$ ,  $T$ , and  $F$  have their usual significance. For an aqueous solution at 25° this becomes<sup>16</sup>

$$\frac{1}{\kappa} = \frac{3.04 \times 10^{-8}}{z\sqrt{C_s}} \quad (12)$$

or, for a 1.5 M solution containing a 1-1 electrolyte,  $1/\kappa \approx 2.5 \text{ \AA}$ . The potential at any point in the diffuse double layer can be given when  $\psi_H$  is small and when  $x > 1/\kappa$  by

$$\psi = \psi_H \exp(-\kappa x) \quad (13)$$

and for  $x > 4/\kappa$  the potential is negligibly small ( $\psi < 0.02\psi_H$ ). For the same conditions, the electric field is obtained by differentiating eq 13 to give

$$\frac{d\psi}{dx} = -\psi_H \kappa \exp(-\kappa x) \quad (14)$$

and for typical values of  $\psi_H = 0.033 \text{ V}$  and  $\kappa = 3 \times 10^7 \text{ cm}^{-1}$ , fields greater than  $10^5 \text{ V/cm}$  are possible. However, the field decays rapidly and at  $x = 4/\kappa$  the field magnitude is too small to affect homogeneous reactions. The concentrations,  $C$ , of ions of charge  $z$  at any point in the double layer are given by<sup>10</sup>

$$C = C^* \exp(-zF\psi/RT) \quad (15)$$

and for  $x > 4/\kappa$  the concentrations approach their bulk values  $C^*$ . This, in effect, defines the thickness of the diffuse part of the double layer.

When specific ion adsorption is present, the compact layer will contain ionic charges in accordance with the adsorption isotherm for the species involved. In general, the potentials and charge population in the diffuse layer will be lowered. The values for the parameter describing the diffuse layer can still be determined from the Gouy-Chapman theory but a new capacitance must be considered when calculating  $\psi_H$ . Nevertheless, eq 11 remains valid for calculating  $1/\kappa$ , and although  $\psi_H$  is changed, the forms of eq 14 and 15 remain the same. For most cases the distance limit for the influence of the potentials remains  $x \approx 4/\kappa$ .

*Reaction Layer.* The reaction layer is the small region around the electrode where net chemical reaction is assumed to occur and where the chemical system is not at equilibrium. The thickness  $\mu$  of the reaction layer can be estimated for the acetic acid system as

$$\mu = \sqrt{D_{H^+}/k_b} \quad (16)$$

$$= \sqrt{D_{H^+}/k_b' C_A^-} \quad (17)$$

and it is considered that all hydrogen ions produced between the plane defined by  $\mu$  and the electrode surface will react at the electrode surface and produce faradaic current. The size of the reaction layer cannot be calculated without prior knowledge of  $k_b'$ , the rate constant for recombination. However, for many acids, this recombination rate is nearly diffusion controlled and a value of  $5 \times 10^{10} (\text{mol/l.})^{-1} \text{ sec}^{-1}$  can be assumed for the acetic acid case.

Under these circumstances, for  $D_{H^+} \approx 10^{-4} \text{ cm}^2/\text{sec}$  and  $C_A^- \approx 1 \text{ M}$ ,  $\mu$  will be approximately  $4.5 \text{ \AA}$ . Thus, for large anion concentrations  $\mu$  can be of the same magnitude as  $4/\kappa$ , the effective double-layer thickness, in which case all the chemical reaction will occur in a region influenced by the double-layer potentials and the electric field. On the other hand, at a lower anion concentration but the same ionic strength,  $\mu$  becomes much larger than  $4/\kappa$ . For example, for  $C_A^- \approx 0.01 \text{ M}$ ,  $\mu$  will be about  $45 \text{ \AA}$ , and much of the chemical reaction will occur in a field-free region of the solution.

*Correction for Double-Layer Effects.* When a chemical rate constant is calculated from electrochemical data neglecting double-layer effects, the result will be an apparent rate constant,  $k_a$ , which will differ from the true chemical rate constant,  $k_t$ , since the region in which the chemical reaction occurs is not homogeneous. The inhomogeneity introduced by the double layer will be reflected by one or more specific effects which may include alteration of the ionic concentrations in

(25) P. Delahay, "Double Layer and Electrode Kinetics," Interscience Publishers, New York, N. Y., 1965.

the double layer from their bulk values (eq 15), enhancement of the dissociation rate by the electric field<sup>14</sup> (eq 14), alteration of the rate and equilibrium expressions by dielectric saturation,<sup>25</sup> and acceleration or inhibition of mass transfer of ionic material by the potential and the electric field.<sup>16</sup> None of these effects has been considered in the derivation of the boundary value problem in which it was assumed that  $k_t$ ,  $K$ , and  $C_{A^-}$  were all constant, independent of distance and time. A rigorous derivation in which these parameters are considered as functions of distance would be difficult. An alternate approach is to estimate the magnitude of these effects on the apparent kinetic parameter,  $(k_t K)_a$ .

The apparent kinetic parameter as determined from the experimental data represents a mean value of the actual parameter within the reaction layer. Since within this layer the individual parameters,  $k_t$  and  $K (=K_d/C_{A^-})$ , are functions of distance, this mean value is given by

$$(k_t K)_a = \left( \frac{1}{\mu} \right) \int_0^\mu \left[ \frac{k_t(x) K_d(x)}{C_{A^-}(x)} \right] dx \quad (18)$$

or considering the kinetic parameter as a single function

$$(k_t K)_a = \left( \frac{1}{\mu} \right) \int_0^\mu \left( \frac{k_t K_d}{C_{A^-}} \right)_x dx \quad (19)$$

At distances greater than  $4/\kappa$  (the effective double-layer thickness), the kinetic parameter assumes its bulk value which is independent of distance and, if the experiment is carried out in a system where  $\mu$  is large compared to the dimensions of the double layer—i.e.,  $\mu > 4/\kappa$ —the integral can be separated

$$\mu(k_t K)_a = \int_0^{4/\kappa} \left( \frac{k_t K_d}{C_{A^-}} \right)_x dx + \left( \frac{k_t K_d}{C_{A^-}^*} \right) \int_{4/\kappa}^\mu dx \quad (20)$$

Rearranging the limits of integration

$$\begin{aligned} \mu(k_t K)_a = & \int_0^{4/\kappa} \left( \frac{k_t K_d}{C_{A^-}} \right)_x dx + \\ & \left( \frac{k_t K_d}{C_{A^-}^*} \right) \left( \int_0^\mu dx - \int_0^{4/\kappa} dx \right) \end{aligned} \quad (21)$$

and collecting terms and simplifying, one obtains

$$\begin{aligned} \mu(k_t K)_a = & \mu \left( \frac{k_t K_d}{C_{A^-}^*} \right) + \int_0^{4/\kappa} \left[ \left( \frac{k_t K_d}{C_{A^-}} \right)_x - \frac{k_t K_d}{C_{A^-}^*} \right] dx \\ & \quad (22) \end{aligned}$$

The remaining integral could be evaluated if  $k_t(x)$ ,  $K_d(x)$ , and  $C_{A^-}(x)$  were known; if  $\mu$  were not greater than  $4/\kappa$ , this integral would have to be evaluated to obtain the bulk parameters. However, it suffices here to note that this term represents the difference between the average kinetic parameter within the double layer and the kinetic parameter in the bulk of the solu-

tion and contains all the specific effects introduced in the experiment. Thus, representing this integral term as  $(k_t K_d/C_{A^-})_{dl}$ , eq 22 becomes

$$\mu(k_t K)_a = \mu \left( \frac{k_t K_d}{C_{A^-}^*} \right) + \left( \frac{k_t K_d}{C_{A^-}} \right)_{dl} \quad (23)$$

Dividing each term by  $K_d/C_{A^-}^*$  gives

$$\mu k_a = \mu k_t + (k_t)_{dl} \quad (24)$$

For a series of experiments performed at constant ionic strength,  $(k_t)_{dl}$  will be constant, and if  $\mu$  is varied by employing several different anion concentrations, several different values of  $k_a$  will be obtained. Provided that  $\mu > 4/\kappa$ , a plot of the values of  $\mu k_a$  vs.  $\mu$  will provide a value of  $k_t$  from the slope. Since  $\mu$  cannot be calculated before  $k_t$  is known, it suffices to assume that  $k_b$  and  $D_{H^+}$  are constant and, in accord with eq 17, to plot  $k_a/\sqrt{C_{A^-}}$  vs.  $1/\sqrt{C_{A^-}}$ , again obtaining  $k_t$  from the slope.

## Experimental Section

One of the major aspects of this work was the development of instrumentation capable of charging the double layer very rapidly, so that reliable measurements of the faradaic current could be made at times as short as 10  $\mu$ sec. A detailed discussion of this portion of the work will be presented elsewhere.<sup>26</sup>

*Instrumentation. Cell.* The cell used for potentiostatic experiments was designed to eliminate undesired impedances (lead inductance, contact resistance, etc.) and was arranged so that electrode placement was reproducible. The working electrode was a stationary mercury drop supported on a J-shaped electrode, the counter electrode was a platinum wire immersed in the test solution, and the reference electrode was a saturated calomel electrode which contacted the test solution through a salt bridge and a Luggin capillary. For potentiostatic and stationary electrode polarography experiments, a microburet-type electrode (Brinkmann Instruments) was used to supply mercury drops. For all experiments the solution temperature was determined using a thermometer mounted in the cell lid and immersed in the solution. Room temperature was changed as a means of controlling the cell temperature, and all experiments were carried out at solution temperatures of  $25 \pm 0.5^\circ$ .

*Potentiostat and Signal Sources.* For potentiostatic experiments a circuit similar to that shown in Figure 15a of ref 27 was used. Positive feedback was used to correct for the uncompensated cell resistance and was obtained by overcompensating the  $iR$  drop in a small resistor placed in series with the working electrode.

(26) In preparation; see also ref 23. The principles involved have been discussed by G. L. Boaman and W. B. Holbrook, *Anal. Chem.*, **35**, 1793 (1963); **37**, 795 (1965); the subject has been reviewed by R. R. Schroeder and I. Shain, *Chem. Instrum.*, in press.

(27) W. M. Schwarz and I. Shain, *Anal. Chem.*, **35**, 1770 (1963).

The adder-controller amplifier was a Burr-Brown 1607B operational amplifier driving a Burr-Brown 1634A booster amplifier. The voltage follower was an Analog Devices 102C operational amplifier and was mounted as close to the reference electrode as possible. The inverter-compensator used to provide the positive feedback was a Philbrick P45A operational amplifier. Circuit details and operating characteristics will be presented elsewhere.<sup>26</sup> The signal used to supply the cell potential was derived from a Hewlett-Packard 214A pulse generator. A Tektronix 545A oscilloscope equipped with a Type W differential comparator plug-in was used for signal monitoring and recording of the current-time curves. The pulse generator used to apply the cell potential signal also functioned as the main timing device for the experimental system. Oscilloscope base line drift problems were overcome by providing a second triggering sequence which initiated the oscilloscope sweep and delayed the main pulse by a time equivalent to one graticule division on the oscilloscope face. Thus, the first time division on the resulting photograph presented a zero current base line for reference.

Polarographic experiments were performed employing conventional three-electrode methods. For stationary electrode polarography a circuit similar to Figure 4 of ref 28 was employed. The input signals required to impose linear and triangular potential functions on the cell were obtained from a circuit which converted the time base sweep signal from the oscilloscope into triangular signals of the proper magnitude and slope.<sup>23</sup>

**Reagents. Chemicals.** The chemicals used were of the best available quality (reagent grade when possible) and, except for the supporting electrolyte material, were used without further purification. Tetramethylammonium chloride, TMACl (Eastman Organic Chemicals), was purified by recrystallization from 95% ethanol. Tetramethylammonium hydroxide, TMAOH (Eastman Organic Chemicals), was titrated with standard hydrochloric acid and an exact weight:equivalent ratio was determined. Two solutions of acetic acid (0.173 and 3.46 F) were prepared and standardized against a sodium hydroxide solution which was, in turn, standardized using potassium acid phthalate. Triply distilled water was used for the preparation of solutions and the rinsing of all glassware.

The nitrogen, which was bubbled through the solution in the cell to remove oxygen, was of high purity and was further purified by passing it through solutions of vanadous sulfate and sodium hydroxide and finally through a solution of the supporting electrolyte. The mercury used for both stationary and dropping mercury electrodes was purified by rinsing several times alternately with 1 M nitric acid, 1 M sodium hydroxide with potassium cyanide added, and tripoly distilled water. This chemically purified mercury was then

**Table I:** Concentrations of Acetic Acid, Tetramethylammonium Acetate, Tetramethylammonium Chloride, and Hydrogen Ion for the Test Solutions

Solution	$C_{\text{HA}}$ , mM	$C_{\text{A}}$ , M	$C_{\text{TMACl}}$ , M	pH
I	2.17	0.025	1.475	5.80
II	4.32	0.049	1.450	5.81
III	8.65	0.100	1.40	5.78
IV	17.3	0.200	1.30	5.83
V	34.6	0.400	1.10	5.78

distilled at reduced pressure to remove inert, refractory materials.

**Solution Preparation.** Solutions for the electrochemical investigations were prepared by weighing out an appropriate amount of 10% aqueous TMAOH, titrating this to equivalence with 3.46 and 0.173 F acetic acid, adding a predetermined excess of 0.173 F acetic acid and sufficient solid TMACl for a final ionic strength of 1.5, and finally diluting to the appropriate volume. In all, five different solutions (Table I) were prepared in this manner.

**Procedure for Electrochemical Experiments. Preparation.** The cell was filled and nitrogen was bubbled through the solution for at least 10 min. Then the capillary leading to the reference electrode was filled by drawing solution from the cell into the capillary. A center compartment of the reference electrode salt bridge was filled with concentrated TMACl solution.

**Determining Electrode Positions and Recording Conditions.** The cell and the potentiostat were matched as closely as possible by analyzing the transfer functions of the components and adjusting the interelectrode spacings to obtain the best possible frequency response without instability.<sup>26</sup> Final positioning of the electrodes was done using either blank or test solutions. The pulse generator was triggered and the current-time function was observed on the oscilloscope screen. Then the reference electrode capillary position was adjusted until the most rapid current decay was observed.

When optimum conditions had been established on blank solutions, an estimate was made of the shortest time at which accurate faradaic current measurements could be made. The value of the charging current which could be considered negligible was different for the various solutions employed, but, in general, a current of less than 100  $\mu\text{A}$  introduced negligible error and was usually attained at times between 20 and 40  $\mu\text{sec}$ .

**Recording Current-Time Curves.** Several curves were included on the same photograph by vertically spacing the base lines and curves. Generally, three or four curves were obtained on the same electrode with 2-min delays between them. A new mercury

(28) W. L. Underkofler and I. Shain, *Anal. Chem.*, **35**, 1778 (1963).

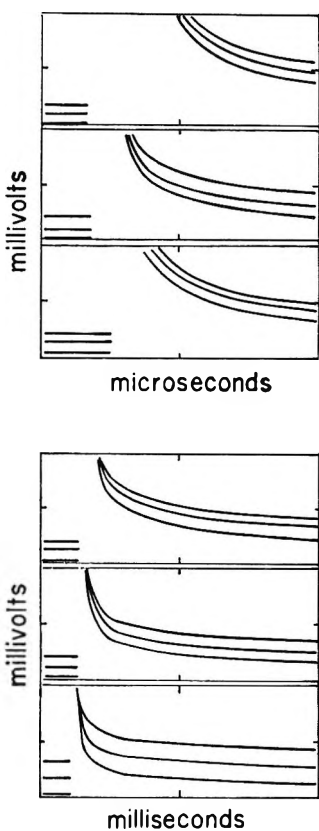


Figure 1. Typical current-time curves obtained on test solution I. Solution composition: 0.025 M TMAOAc, 2.17 mM HOAc, 1.475 M TMACl; load resistor, 300 ohms; oscilloscope settings: upper photograph, top: 20  $\mu$ sec/div, 200 mV/div; middle: 50  $\mu$ sec/div, 200 mV/div; bottom: 100  $\mu$ sec/div, 100 mV/div; lower photograph, top: 200  $\mu$ sec/div, 100 mV/div; middle: 500  $\mu$ sec/div, 100 mV/div; bottom: 1 msec/div, 100 mV/div.

drop electrode was collected after the third or fourth run. Since three separate photographs could be taken on each film, 9–12 separate current-time curves were recorded on each picture. Typical curves are shown in Figure 1.

**Time Range.** Experiments on each solution were conducted over several time ranges corresponding to oscilloscope time base settings of from 100  $\mu$ sec to 20 msec full scale. The time scales used in the experiments were limited by the onset of convective mass transfer at about 40–50 msec after the application of the potential step. Observation of the electrode, using a microscope, showed that this stirring was caused by two effects. Upon application of the pulse the mercury drop moved because of surface tension changes, and also because large volumes of hydrogen were liberated. The form of the current-time curves indicates, however, that these processes were rather slow compared to the time scales employed and that the stirring did not affect the currents during the first few milliseconds after the potential change. At times longer than 100 msec, the stirring caused the current to increase slightly and eventually to become constant. The 20-msec time

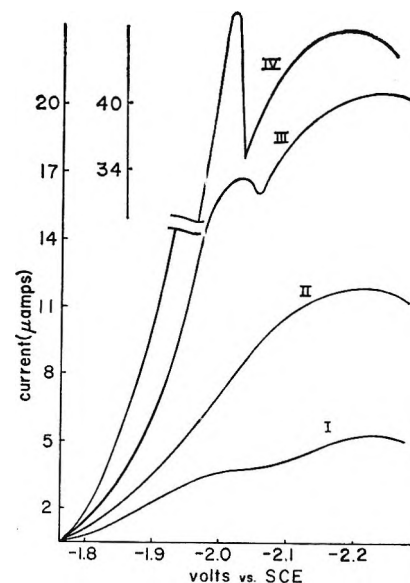


Figure 2. Polarograms of test solutions; composition as in Table I.

limit on accurate current measurement made it nearly impossible to observe a diffusion-controlled current which would have made it possible to use eq 10. For each current-time curve, 7–10 points equally spaced on the time axis were selected and their horizontal and vertical coordinates were measured.

**Initial and Final Potentials.** The potentials employed in the potentiostatic experiment were selected from the current-potential data obtained by polarography. In polarographic experiments with the dme, the waves obtained were, in general, poorly shaped and exhibited maxima and adsorption phenomena for most of the solution concentrations employed (Figure 2). In order to determine a suitable final potential for the potentiostatic experiments, stationary electrode polarography had to be used. The stationary electrode polarograms (Figure 3) did not exhibit maxima or other anomalies. The processes which cause the poorly shaped dme polarograms were probably related to the motion of the drop at these very negative potentials.

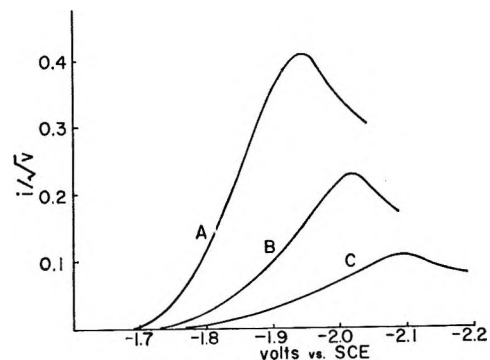


Figure 3. Stationary electrode polarograms on solution I. Scan rates: curve A, 0.41 V/sec; curve B, 4.10 V/sec; curve C, 41.0 V/sec.

The potential values employed for the potentiostatic work were an initial potential of  $-1.5$  V and a final potential of  $-2.1$  V (vs. sce).

## Results and Discussion

*Computation Procedures. Graphical Determination of the Rate Constant.* The simplest manner in which the current-time data can be used to obtain the parameter  $\lambda$  and the kinetic term  $k_t K$  involves a graphical procedure based on rearranging eq 10, in which  $i_k \sqrt{t}$  is graphed vs.  $\sqrt{t}$ .

In actually applying this method, however, there are several serious limitations. Values of  $f(\lambda)$  are obtained point by point, and any scatter in the data results in a substantial uncertainty in the calculated values of the kinetic parameters. A second factor is that experimental data must be available for times at which the current is diffusion controlled. When the limiting values of  $i_k \sqrt{t}$  are not experimentally obtainable, the problem of determining  $k_t K$  becomes complex. Theoretical diffusion currents can be calculated (eq 8) but this requires that the diffusion coefficient  $D_{HA}$  be known accurately. In some cases, values of the diffusion coefficient can be obtained from polarographic data, but this approach could not be used in this work, since the polarographic waves were poorly shaped. Thus, an alternate procedure was sought which would not be so sensitive to the scattered data and which would not depend so directly on the value of  $i_d$  or  $D_{HA}$ .

*Curve-Fitting Method for Determining the Rate Constant.* When current-time data are available over a reasonably wide range of experimental times, a graphical method can be used which relies on the magnitude and time dependence of the kinetic current. For this method, eq 9 can be used to calculate theoretical kinetic current-time curves assuming convenient values of  $k_t K$  and  $i_d$ . Three principal regions in the resulting curves are obtained corresponding to the short-time, the midrange, and the long-time limits of  $f(\lambda)$ . At very short times (small  $\lambda$ ) the current is constant, while at long times (large  $\lambda$ ),  $i_k \rightarrow i_d$ . On log-log plots, such as Figure 4, these curves appear as a constant current at short times, then a transition region where the currents gradually decrease, and finally a straight-line region corresponding to a limiting slope of  $-1/2$ . However, all three regions can be seen for a single curve only if a very wide range of times is included.

Then experimental current-time data are plotted in a similar fashion, and the experimental curves are matched with one of the theoretical current-time curves. The matching can be done by superimposing one graph over the other and moving one in a vertical or horizontal direction until the experimental and calculated curves show the best fit. The matched curves imply that the values of  $\lambda$  for the two current-time curves are the same, *i.e.*,  $\lambda_{\text{calcd}} = \lambda_{\text{exptl}}$ . In the matching process, the graphs become shifted relative to each

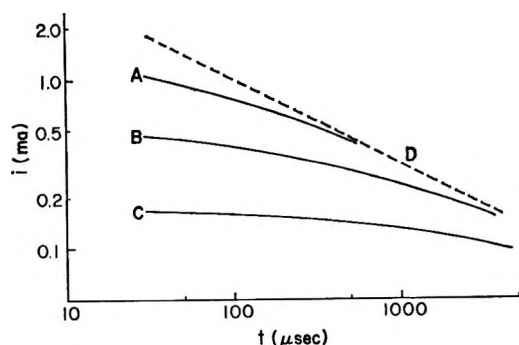


Figure 4. Theoretical kinetic current-time curves. The kinetic parameters are: A,  $k_t K = 10^4 \text{ sec}^{-1}$ ; B,  $k_t K = 10^3 \text{ sec}^{-1}$ ; C,  $k_t K = 10^2 \text{ sec}^{-1}$ ; D,  $i_d \sqrt{t} = 10^{-5} \text{ A sec}^{1/2}$  ( $k_t K \rightarrow \infty$ ).

other on the time scale. The ratio  $t_{\text{calcd}}/t_{\text{exptl}}$  is easily determined by comparing the time scales. Since  $\lambda_{\text{calcd}}/\lambda_{\text{exptl}} = 1$ , it follows from the definition of  $\lambda$  (eq 7) that

$$\frac{(\gamma k_t K)_{\text{exptl}}}{(k_t K)_{\text{calcd}}} = \frac{t_{\text{calcd}}}{t_{\text{exptl}}} \quad (25)$$

where  $\gamma = D_{H^+}/D_{HA}$ . Then the experimental kinetic parameter can be calculated from the value of  $k_t K$  which was used to generate the theoretical curve.

When this method is used, the current-time data along the entire curve are used simultaneously, and scatter in the data introduces much less error in the calculation of the kinetic parameters. In addition, it is much easier to estimate the limiting value of the current-time data at long times, and only the ratio  $D_{H^+}/D_{HA}$  need to be known explicitly. This ratio was taken as equal to the ratio of the limiting equivalent conductances of  $H^+$  and  $CH_3COO^-$ , 8.55.<sup>29</sup>

*Determination of Equilibrium Constant.* The equilibrium constant for the dissociation of acetic acid in concentrated solutions of tetramethylammonium chloride has not been reported previously and had to be determined for this work. Acetic acid-tetramethylammonium acetate buffers of several concentration ratios were prepared and their pH was measured. Also, dilute solutions of hydrochloric acid were made up and tetramethylammonium chloride was added to make the ionic strength 1.5. The pH of these solutions was also measured. The chemical equilibrium constant was then determined from the relation

$$K_d = C_A(C_H/C_{HA}) \quad (26)$$

or

$$K_d = (C_A/C_{HA})(a_H/f_H) \quad (27)$$

where  $a_H$  and  $f_H$  are the activity and activity coefficient for hydrogen ion. A value of  $K_d = 2.28 \times 10^{-5} \text{ mol/l}$ . was found.

(29) L. Meites, Ed., "Handbook of Analytical Chemistry," McGraw-Hill Book Co., Inc., New York, N. Y., 1963.

**Table II:** Typical Potentiostatic Current-Time Data Obtained from Solution IV

100 $\mu\text{sec}^a$		200 $\mu\text{sec}^a$		500 $\mu\text{sec}^a$	
$t_i$ $\mu\text{sec}$	$i_i$ mA	$t_i$ $\mu\text{sec}$	$i_i$ mA	$t_i$ $\mu\text{sec}$	$i_i$ mA
23	8.40	40	1.97	50	2.26
33	2.11	60	1.83	100	1.54
43	2.00	80	1.63	150	1.37
53	1.92	100	1.54	200	1.21
63	1.73	120	1.47	250	1.09
73	1.57	140	1.40	300	1.01
83	1.46	160	1.33	350	0.941
93	1.34	180	1.24	400	0.876
1 msec <sup>a</sup>		5 msec <sup>a</sup>		10 msec <sup>a</sup>	
$t_i$ $\mu\text{sec}$	$i_i$ mA	$t_i$ $\mu\text{sec}$	$i_i$ mA	$t_i$ $\mu\text{sec}$	$i_i$ mA
86	1.58	0.50	0.822	1.00	0.621
186	1.25	1.00	0.637	2.00	0.476
286	1.03	1.50	0.548	3.00	0.404
386	0.899	2.00	0.490	4.00	0.357
486	0.801	2.50	0.452	5.00	0.328
586	0.745	3.00	0.418	6.00	0.306
686	0.697	3.50	0.389	7.00	0.288
786	0.660	4.00	0.368	8.00	0.272
886	0.622	4.50	0.350	9.00	0.257

<sup>a</sup> Full-scale.

## Experimental Results

In all, 31 sets of current-time data were obtained on the five solutions listed in Table I. Each set consisted of a series of replicate current-time curves obtained over the time range from 10  $\mu\text{sec}$  to 10 msec. Usually, this time range was covered in six groups of current-time curves: 0–100  $\mu\text{sec}$ ; 0–200  $\mu\text{sec}$ ; 0–500  $\mu\text{sec}$ , 0–1 msec; 0–5 msec; and 0–10 msec; three or four curves were obtained within each group. Thus, each set of data for a particular solution required the analysis of from 18 to 24 individual current-time curves.

In the normal procedure, the three or four replicate current-time curves for a particular time range were averaged, and data were tabulated for seven to ten different values of the time. A typical set of such tabulated current-time data is shown in Table II. Then each set provided a single composite log-log plot of the current as a function of time. Typical plots (one for each solution) are shown in Figure 5. The plots of the experimental currents correspond closely to the theoretical curves of Figure 4 except at very short times, where the currents are higher than predicted. A major portion of the current at these short times is due to the charging of the electrical double layer. Simultaneous adsorption of tetramethylammonium ions appears to extend the charging current to longer times than encountered for solutions of perchloric acid or lithium salts. An additional contribution to this initial current is caused by the reduction of the free hydrogen ions present at the start of the experiment. Although these processes were not considered in the boundary value

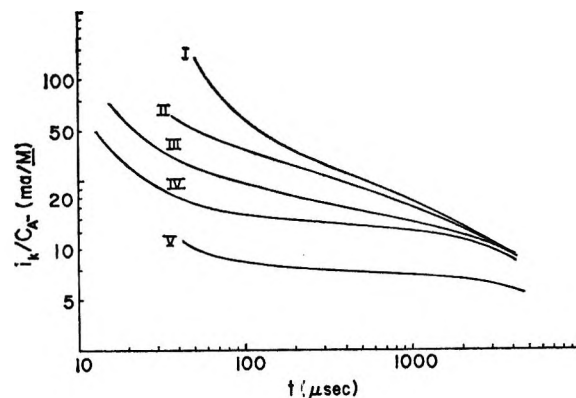


Figure 5. Experimental current-time data on log-log plots; solution composition as in Table I.

**Table III:** The Apparent Rate Constants and Equilibrium Constants for the Five Solutions

Solu-	$C_A$ , $M$	$K \times 10^4$	$k_a \times 10^{-6}$ , $\text{sec}^{-1}$	Std dev $\times 10^{-6}$	No. of deter-
I	0.025	9.12	11.0	2.0	6
II	0.049	4.56	10.0	0.3	7
III	0.100	2.28	4.8	0.4	10
IV	0.200	1.14	3.2	0.1	5
V	0.400	0.57	1.5	0.1	3

problem, they did not extend to times long enough to interfere with the analysis of the kinetic data, *i.e.*, times longer than about 10–20  $\mu\text{sec}$ .

Each of these log-log current-time plots was treated as discussed above, and an experimental value of the apparent rate constant  $k_a$  was calculated. The values obtained on each solution were averaged, and these results are summarized in Table III.

*Correction for Double-Layer Effects.* With these values of  $k_a$  and the appropriate acetate concentrations, eq 24 was employed to obtain the true rate constant by plotting  $k_a/\sqrt{C_{A^-}}$  vs.  $1/\sqrt{C_{A^-}}$  (Figure 6). The slope, calculated by the method of least squares, gave a value for  $k_f$  of  $1.58 \times 10^6 \text{ sec}^{-1}$ .

To test the validity of this approach to the determination of the true value of the rate constant  $k_f$ , it was

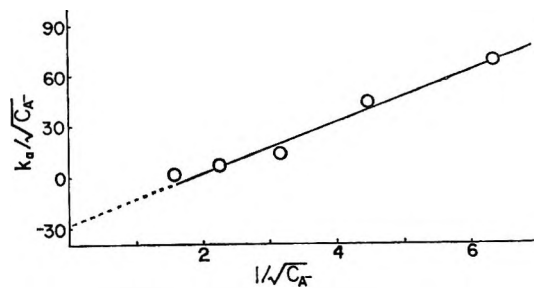


Figure 6. Graphical correction for double-layer effects. Units are  $k_a/\sqrt{C_{A^-}}$  ( $\times 10^{-6}$ ),  $\text{sec}^{-1}$ , vs.  $1/\sqrt{C_{A^-}}$ ,  $\text{M}^{-1/2}$ .

necessary to determine the value of the reaction layer thickness for each of the five solutions to confirm that the variation of  $k_a$  with acetate concentration could in fact be accounted for by field effects. This was done by calculating  $k_b$  from eq 4, assuming  $D_{H^+} = 10^{-4}$  cm<sup>2</sup>/sec and substituting these values in eq 16. The calculated values of  $\mu$  were 24, 17, 12, 8.5, and 6.0 Å for solutions I-V, respectively. Since the effective thickness of the diffuse part of the double layer was estimated at  $4/\kappa \approx 10$  Å, it is apparent that a substantial portion of the chemical reaction must take place in a region of strong potential fields. Thus, the extrapolation technique is valid and the  $k_f$  determined in this experiment represents a true chemical rate constant.

*Discussion of Error.* The uncertainty in the value of the rate constant can be assessed qualitatively in terms of the experimental errors. The principal sources of error in the experiment are the oscilloscope, uncertainty in the value of the equilibrium constant and the diffusion coefficients, and the method of calculation. The measurement error ( $\pm 3\%$  on each axis of the oscilloscope) was reduced by data averaging, although some scatter in the current-time data remained. In general, the error introduced by the curve-fitting method is determined by the time range over which experimental data are available. In this case, sufficient data were available so that the curve-fitting procedure itself introduced only minor error; the major error was the uncertainty introduced by the lack of exact values for  $D_{HA}$  (or  $i_d$ ).

Thus, the uncertainty in the quantities  $K_d$  and  $D_{HA}$  are the largest sources of error. The error in these terms is not readily calculable, but for the determination of  $K_d$ , a  $\pm 12\%$  error could be introduced by read-

ing errors of 0.05 pH unit. The error in the value of  $D_{H^+}/D_{HA}$  cannot be assessed, but assuming 20% possible error, an estimated error in  $k_f$  would be  $\pm 30\%$ . The final result would then be a value of  $k_f$  equal to  $1.6 (\pm 0.5) \times 10^6$  sec<sup>-1</sup>.

*Significance of the Double-Layer Correction.* Although the magnitude of the estimated error precludes any quantitative interpretation of the double-layer effects, the form of the plot in Figure 6 merits comment. For the effects of accelerated dissociation and/or deviation from pseudo-first-order nature for the recombination, an increase in the rate constant with small  $\mu$  would be expected. That is, the last term in eq 24 would be positive, but actually the opposite effect, a decreased value of  $k_f$  is observed, indicating that the double layer inhibits the net reaction.

One possible explanation for this would be the specific adsorption of the tetramethylammonium ion which could cause a decrease in the dielectric constant near the electrode surface and also a significant change in the potentials within the double layer. That is, because of the specific adsorption of cations, the potential in the electrical double layer would be less negative than anticipated from merely considering the cell potential. The last term in eq 24 would be negative, indicating that the kinetic parameter within the double-layer region is smaller than its bulk value. Thus, from the form of the correction term in eq 24, a negative intercept in the plot of  $k_f\mu$  vs.  $\mu$  is reasonable in the system studied.

*Acknowledgments.* The authors are grateful to the National Science Foundation, which supported this work in part through Grant No. GP-3907, and the U. S. Atomic Energy Commission, which supported this work in part through Contract No. AT(11-1)-1083.

# A Correlation of Molecular Flexibility with Volume and Heat of Mixing of Organic Solutes with Water and Glycol-Water Mixture

by K. R. Brower, John Peslak, Jr., and James Elrod

*Department of Chemistry, New Mexico Institute of Mining and Technology, Socorro, New Mexico 87801  
(Received August 5, 1968)*

The presence of unsaturation, small rings, and especially aromatic rings causes the volume of mixing of organic compounds to tend toward zero. Evidence is presented to show that the space requirement of methylene groups is approximately 2 ml/mol greater when they are conformationally free than when they are restricted, and it is hypothesized that the net mixing volume for open-chain compounds results from an interference with their rotational freedom by the cohesive forces of water. The volume of mixing appears to be unrelated to icelike structure formation because it is independent of temperature over a range of 80° and is nearly the same for the glycol-water mixture in which the solutes have normal heat capacities. Mixing is more exothermic for flexible molecules, and the magnitude of the variation is comparable with the  $P\Delta V$  work done by the internal pressure.

## General Discussion

In connection with a long-term study of the effect of pressure on reaction rates, we have needed to take account of the change of volume which accompanies the mixing of a variety of organic compounds with water. For the sake of brevity this quantity will hereafter be called the mixing volume. Most liquids mix with a change of volume of the order of 1 ml/mol or less, but it is characteristic of water that dissolution of polar organic liquids causes a contraction which may be as large as 2 ml/carbon atom. For hydrocarbons the contraction is even larger. This phenomenon has stimulated a large number of measurements and interpretations.<sup>1-10</sup>

According to the "flickering-cluster" model for the structure of liquid water,<sup>8</sup> there are large empty spaces within the hydrogen-bonded framework, and the contraction on mixing is due to the occupation of these spaces by solute molecules. A quantitative estimate of the volume change is made by multiplying three terms: (1) the number of water molecules surrounding the solute molecule (estimated from molecular models), (2) the fraction of tetrahydrogen-bonded molecules, these being the only ones supposed to undergo an increase of coordination number, and (3) an empirical value of -43 ml/24 water molecules in ethane hydrate. The measured mixing volumes are about twice as great as the calculated values. The predicted temperature dependence is for the mixing volume to decrease to about half for a 65° rise, and this is in disagreement with observation as shown by the data of Table I.

It has been suggested by Masterton<sup>7</sup> that the contraction results from compression of the solute molecule by the powerful cohesive forces of water. He shows that the partial molal volumes of methane and ethane in water at 25° (internal pressure, 12,000 atm) are, respec-

Table I: Effect of Temperature on Volume of Mixing with Water

Compd	Temp. °C	$-\Delta V$ ml/mol
<i>t</i> -Butyl alcohol	80	10.9 ± 0.5
	25	9.0 ± 0.5
	5	9.8 ± 0.5
Cyclohexanol	80	3.0 ± 1.0
	25	2.0 ± 1.0
Benzyl alcohol	80	0.0 ± 1.0
	25	0.0 ± 1.0
Pyridine	80	1.9 ± 0.5
	25	2.3 ± 0.5
Dioxane	80	5.6 ± 0.5
	25	5.1 ± 0.5
	0	6.0 ± 0.5

tively, 54 and 62% of their values in perfluoro-*n*-heptane (internal pressure, 1430 atm). It should be noted that ordinary liquids are only compressed to about 85% of their original volume by a corresponding change of external pressure, and the high apparent partial molal compressibility of methane and ethane may result from

- (1) F. Franks and D. J. G. Ives, *Quart. Rev. (London)*, **20**, 1 (1966).
- (2) M. E. Friedman and H. A. Scheraga, *J. Phys. Chem.*, **69**, 3795 (1965).
- (3) J. E. Desnoyers and M. Arel, *Can. J. Chem.*, **45**, 35€ (1967).
- (4) F. Franks, *Ann. N. Y. Acad. Sci.*, **125**, 277 (1965).
- (5) K. Nakanishi, *Bull. Chem. Soc. Jap.*, **33**, 793 (1960).
- (6) W. Wen and S. Saito, *J. Phys. Chem.*, **68**, 2639 (1964).
- (7) W. L. Masterton, *J. Chem. Phys.*, **22**, 1830 (1954).
- (8) G. Nemethy and H. A. Scheraga, *ibid.*, **36**, 3401 (1962).
- (9) J. L. Kavanau, "Water and Solute-Water Interactions," Holden-Day Inc., San Francisco, Calif., 1964, p 26.
- (10) F. Franks, "Physico-Chemical Processes in Mixed Aqueous Solvents," Elsevier Publishing Co., Inc., New York, N. Y., 1967, p 60.

the temperature being far above their normal boiling point.

A third factor which might contribute to the total volume change is the formation of an icelike structure in the water immediately surrounding the solute molecules. The concept of "iceberg formation" was introduced by Frank and Evans<sup>11</sup> to account for the generally exothermic mixing of organic compounds with water and the large excess heat capacities of the solutions. The hypothesis has had wide acceptance and is mentioned in all but one of ref 1-10. Because there is no basis for choice among a number of different ice structures, it is not possible to predict the effect on volume. To the extent that the "icebergs" resemble ordinary ice, there would be an expansion.

In view of the independence of the three effects mentioned above, it might appear hopeless to attempt a prediction of the sign, let alone the magnitude, of the mixing volume. Nevertheless, some regularities have been noted. In a homologous series the decrement of mixing volume per methylene group is 1-2 ml.<sup>2,3,6</sup> Indeed it can be seen from the data of Table II that even when aliphatic compounds with different oxygen-containing functions are compared, the decrement of mixing volume per carbon atom is nearly constant.

The compounds of Table II can conveniently be divided into three groups for the purpose of comparison by structural type as open chain, saturated ring, or aromatic compounds. The mixing volumes for the first group can be estimated by multiplying the number of carbon atoms by -2 ml. The aromatic compounds have mixing volumes close to zero, and the compounds with saturated rings have intermediate values. This result suggested to us that the relevant property is freedom of internal rotation, and three further comparisons were then undertaken. First, allyl alcohol and propargyl alcohol were found to have mixing volumes of -5.6 and -2.6 ml compared with -6.6 ml for *n*-propyl alcohol; second, glycidol (2,3-epoxy-1-propanol) with a mixing volume of -1.5 ml was compared with *n*-propyl alcohol; and third, cyclopropanecarboxylic acid with a value of -5.0 ml was compared with butyric acid with -7.9 ml. The restriction of internal rotation whether by introduction of unsaturation or three-membered rings is associated with a mixing volume nearer to zero.

In a further effort to isolate the cause of the variation of mixing volume with structure, we explored the possibility that the differences arise in the icelike region of the solvent. One approach was to determine the temperature dependence of the mixing volume, since according to the Frank-Evans hypothesis, the large excess heat capacity of the solutions is due to melting of the icebergs with rising temperature. Representatives of all three groups of solutes were tested, and the results are shown in Table III. No correlation is evident. It is difficult to estimate the fraction of the icelike

Table II: Heats and Volumes of Mixing with Water at 26.5°

Compd	$-\Delta H$ , cal/mol	$-\Delta V$ , ml/mol
Methanol	1850	2.8
Ethanol	2270	5.0
1-Propanol	2416	6.6
2-Propanol	3166	7.1
1-Butanol	2408	6.4
2-Butanol	2864	6.8
Isobutyl alcohol	2313	8.1
<i>t</i> -Butyl alcohol	4172	8.5
1,2-Propanediol	2437	3.2
2-Chloroethanol	954	2.8
Propanone	2407	6.5
Butanone	2518	7.4
2-Pentanone	...	9.3
2,4-Pentanedione	...	9.2
Ethyl acetate	2192	8.8
1,2-Dimethoxyethane	...	9.4
Allyl alcohol	1625	5.6
Propargyl alcohol	222	2.6
Butyric acid	...	7.9
<i>sec</i> -Butylamine	6847	12.0
<i>t</i> -Butylamine	9428	15.8
Diethylamine	8354	15.3
Triethylamine	8460	21.8
Glycidol	...	1.5
Cyclopropane carboxylic acid	...	5.0
Cyclopentanol	2533	2.9
Cyclopentanone	5365	4.5
Tetrahydrofuran	3533	2.9
Pyrrolidine	...	7.0
Cyclohexanol	2082	2.0
Cyclohexanone	5365	4.5
Dioxane	2381	5.0
Paraldehyde	...	10.5
Furfuryl alcohol	325	0.7
Pyrrole	...	2.8
Phenol	-380	1.8
Benzyl alcohol	0	0.0
Aniline	-376	2.0
Pyridine	2245	2.3
Benzylamine	2901	3.2

structure which would be destroyed by a temperature rise of 80°, but it can be said that the change in enthalpy of mixing calculated from the excess heat capacity of *t*-butyl alcohol, for example, would suffice to melt more than 3 mol of ordinary ice. This must surely be a substantial fraction of the total icelikeness. As mentioned earlier, the flickering-cluster model calls for the mole fraction of tetrahydrogen-bonded water in the first layer to decrease by about half over a 65° interval. We conclude from the insensitivity of mixing volume to temperature that the origin of the variation with structural type is not in the surrounding solvent region and furthermore that the density of the Frank-Evans icebergs is about the same as that of bulk water.

(11) H. S. Frank and M. W. Evans, *J. Chem. Phys.*, **13**, 507 (1945).

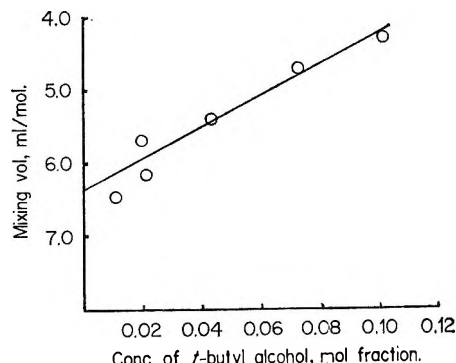
**Table III:** Temperature Dependence of the Heat of Mixing with Water

Compd	$\Delta H$ , cal/mol		
	At 26°	At 62°	$\Delta\Delta H/\Delta T$
Ethanol	2270	1250	28.4 <sup>a</sup>
<i>t</i> -Butyl alcohol	4172	2200	54.8 <sup>a</sup>
Propargyl alcohol	222	-368	16.4
Diethylamine	8354	5625	75.7
Tetrahydrofuran	3533	1720	50.4
Dioxane	2381	1535	23.5
Cyclohexanol	2082	-260	65.2
Furfuryl alcohol	325	-808	31.5
Benzyl alcohol	0	-1600	44.5
Pyridine	2245	960	35.5

<sup>a</sup> In a narrow range near 26° the excess heat capacities for ethanol and *t*-butyl alcohol are 32 and 61 cal/mol deg, respectively.

Assuming the correctness of Masterton's suggestions that the contraction on mixing is due to the exceptionally strong cohesive force of water, we investigated other solvents having high cohesive energy density (heat of vaporization per milliliter). Dimethyl sulfoxide, triethanolamine, and ethylene glycol were tested, and the largest contraction was 3.1 ml/mol for *t*-butyl alcohol in glycol. Since there is still a large difference in cohesive energy density between water (22,000 atm) and glycol (7050 atm), we also tried a solution of 33 mol % glycol in water (14,100 atm). In this medium the mixing volume of *t*-butyl alcohol was -6.4 ml, and in pure water it is -8.9 ml. Figure 1 gives the variation of mixing volume with composition and there is no sign of a shallow minimum as is sometimes noted for organic solutes in water. This result suggests that the minima are linked to changes in water structure.

Although we were disappointed by the necessity of including a substantial amount of water in order to preserve the large mixing volumes, it seemed likely that there would be no promotion of structure such as that caused by organic solutes in pure water. Measurement of the heats of mixing for representative compounds in

Figure 1. Volume of mixing of *t*-butyl alcohol with glycol-water.**Table IV:** Heats and Volumes of Mixing with Glycol-Water<sup>a</sup> at 26.5°

Compd	$\Delta H$ , cal/mol	$-\Delta V$ , ml/mol
Methanol	-300	2.3
Ethanol	0	3.7
1-Propanol	481	...
2-Propanol	132	...
1-Butanol	948	...
2-Butanol	550	...
<i>t</i> -Butyl alcohol	61	6.4
2-Pentanol	1047	4.4
<i>t</i> -Amyl alcohol	168	5.5
Propanone	135	...
Butanone	500	6.9
2-Ethoxyethanol	-56	...
1,2-Dimethoxyethane	-1290	7.7
Allyl alcohol	517	...
Propargyl alcohol	642	...
Propionic acid	1068	...
Butyric acid	1450	4.0
Triethylamine	-3204	...
Cyclopropanecarboxylic acid	1296	...
Cyclopentanol	862	0.4
Cyclopentanone	625	1.9
Tetrahydrofuran	-333	3.9
Cyclohexanol	817	...
Cyclohexanone	784	2.5
Dioxane	259	...
Paraldehyde	298	...
Piperidine	-3325	...
Furfuryl alcohol	875	...
Phenol	925	...
p-Cresol	1032	0
Benzyl alcohol	1785	0.1
Pyridine	-959	2.2
Aniline	765	...

<sup>a</sup> The ratio is 1 mol of glycol:2 mol of water.

the water-glycol solvent showed that mixing is usually endothermic, as would be expected on general theoretical principles.<sup>12</sup> Furthermore, the heats of mixing for *t*-butyl alcohol, benzyl alcohol, and dioxane remained the same within experimental error on changing the temperature from 26 to 63°. Thus we note the absence of the two conspicuous phenomena, exothermicity and a large excess heat capacity of mixing, which the Frank-Evans iceberg hypothesis was designed to explain.

Table IV gives the mixing volumes for the glycol-water solvent (33 mol % glycol). The values are slightly smaller but more or less parallel to those for pure water in Table II. For substances of comparable molar volume and carbon number, it is seen that the mixing volume becomes larger in the sequence aromatic < saturated ring < aliphatic.

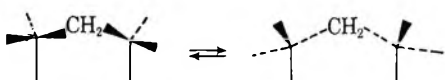
(12) J. H. Hildebrand and R. L. Scott, "The Solubility of Non-electrolytes," 3rd ed, Dover Publications, Inc., New York, N. Y., 1964, p 162.

### Interpretation of the Mixing Volumes

We propose that organic molecules in any intensely cohesive solvent will experience a greatly increased barrier to internal rotation and that the mixing volume arises from the different space requirements of rotatable and "frozen" methylene groups. The hypothesis of environmental interference with rotation has been advanced by Aranow and Witten<sup>13</sup> to account for the effect of chain length of solubility ratios, Traube's rule of surface tension, and critical micelle formation.

In order to test the notion that freedom of rotation is correlated with the molar volume, we have searched for processes other than mixing which would cause a significant change in rotational freedom. For example, let us define the volume of hydrogenation,  $V_H$ , as the difference in molar volume between an olefin and the parent hydrocarbon. There is, of course, no rotation about the double bond of the olefin, but the two new methylene groups created by hydrogenation might be conformationally free in some cases and not in others. The restriction might arise, for example, from inclusion in a small ring. For eight randomly chosen alkenes we found  $V_H = 7.9$  ml with a mean deviation of 1.0 ml; whereas for cyclobutene, cyclopentene, and cyclohexene,  $V_H = 5.9$ , 5.2, and 6.6 ml, respectively. The difference in the two averages is 2.0 or 1.0 ml/methylene group.

A second process which can effect a significant change of rotational freedom is structural isomerization. Because branching always leads to an increased volume and because this might have little or nothing to do with internal rotation, we have confined our attention to cases in which the degree of branching does not change. The following diagram may assist the visualization of the writhing motion of a three-atom chain segment



In a condensed medium the interconversion of rotamers probably occurs with minimum translational displacement of the atoms belonging to the segment as the drawing is intended to suggest. Motion of this type is not possible in 2-butene or 2-butyne because there are no three-carbon segments with a methylene group in the middle, but 1-butene and 1-butyne do contain such segments. The increase of volume on isomerizing the unsaturated group from the central to the terminal position is 3.9 ml for butyne and 1.6 and 4.1 ml for the *trans*- and *cis*-butenes, respectively. The pentadienes also exhibit the effect. The two allenic isomers, 1,2 and 2,3, show a volume increase of 2.1 ml on moving the allenic group from the central to the terminal position, and there is an increase of 3.5 ml on changing 1,3 to 1,4, of which only the latter contains a methylene group flanked by other carbons. We think it justifiable to neglect the effect of rotation about the 2,3 bond of the

former because resonance would heighten the barrier by several kilocalories.

A third process which converts rotatable methylene groups into ones of fixed conformation is the freezing of polyethylene. The entropy of fusion arises largely from the onset of rotational isomerism,<sup>14</sup> and one may infer that changes in other properties are likewise associated with rotation. The change of volume is 3.1 ml/CH<sub>2</sub> at ordinary pressure and 137°.

### Interpretation of the Heats of Mixing

The heat of mixing, like the volume of mixing, is a composite of quantities which we are unable to measure individually. The interaction energy of water and the hydrocarbon portion of the solute, the hydrogen-bonding energy, and the energy of iceberg formation are expected to amount to several kilocalories each. It is interesting that in spite of the complexities the heats of mixing with water show a degree of predictability. The dissolution of aliphatic compounds is strongly exothermic, and the magnitude shows a general increase with carbon number. For the aromatic compounds phenol, aniline, benzyl alcohol, and furfuryl alcohol, the heats of mixing are close to zero. The same is true of propargyl alcohol. The anomalous values for piperidine, pyridine, and triethylamine we attribute to the strong hydrogen bonding from oxygen to nitrogen. One would expect the anomaly to increase with basicity (*cf.* aniline and benzylamine) and to be especially large for tertiary amines, since hydrogen bonding would be absent in the organic liquid (*cf.* pyridine and aniline).

When the solvent is changed to a water-glycol mixture, the mixing is usually endothermic, which is to be expected of liquids which do not react chemically. In the absence of iceberg formation, the differences in hydrogen-bonding capacity for the various oxygen-containing functional groups are more distinct. The ketones and especially the ethers are exothermic relative to the alcohols of similar molecular weight, probably because they engage in one-way hydrogen bonding after mixing. A familiar textbook example of nonideality arising from this cause is the mixture of acetone and chloroform which shows negative deviation from Raoult's law. In a homologous series the increment of enthalpy per methylene group is more constant than for water solutions. The heats of mixing for the 1-alkanols, ketones, and carboxylic acids provide seven values of the increment for which the mean is 416 cal and the mean deviation is 56 cal. Owing to the variation with functional type, it is harder to isolate the factor of conformational freedom, but there are signs that rigid molecules are exothermic relative to flexible ones. The series 1-propanol, allyl alcohol, and propargyl alcohol gives values of 481, 517, and 642 cal, respectively. One is tempted to point to tetrahydrofuran and furfuryl

(13) R. H. Aranow and L. Witten, *J. Phys. Chem.*, **64**, 1643 (1960)

(14) H. W. Starkweather, Jr., and R. H. Boyd, *ibid.*, **64**, 410 (1960).

alcohol, but the spectacular difference is probably due largely to the low basicity of the ring oxygen in the latter. The aromatic compounds are generally highly endothermic, and benzyl alcohol is the most endothermic of all compounds tested. The case of the cycloalkanols and cycloalkanones is curious. The increment of heat of mixing per methylene group is -33 cal for the former and 159 cal for the latter. It is possible that the great deviation from the value of 416 cal for aliphatic compounds is due to the considerable increase in flexibility on passing from a five-membered to a six-membered ring.

It is possible that the greater heat liberated by flexible solute molecules is directly related to the fact that their mixing volumes are greater. In order to make this clear, let us consider a rigid molecule and a flexible molecule of equal molar volume, but let the mixing volume of the rigid molecule be nearly zero as we have often observed and let the flexible molecule dissolve with a contraction of 4 ml. In the aqueous medium let us then create two equal void spaces into which we insert the solute molecules. In the case of the rigid molecule there is no contraction and no  $PV$  work, but the flexible molecule undergoes a compression of 4 ml. This would cause a temperature rise which we might hope to estimate roughly. We have elected to determine empirically the temperature rise which results from an irreversible surge of pressure by suddenly opening a valve between a large reservoir at high pressure and a smaller vessel containing a thermocouple. For motor oil the increase of heat in the small vessel amounted to 0.69.  $P\Delta V$ , where  $P$  is the upper pressure. If we now assume a value of 4 ml for  $\Delta V$  and let  $P$  be the difference in cohesive energy density between water and the organic liquid ( $\sim 8000$  atm), then the extra heat of solution for the flexible molecule would be 540 cal.

## Experimental Section

*Heats of Mixing.* Our calorimeter and experimental procedure is modeled after that of O'Hara, Wu, and Hepler,<sup>15</sup> but the water bath has been replaced by an ingot of aluminum ( $8 \times 8 \times 12$  in.). A 3.5-in. hole bored through the long dimension contains the dewar flask, and the ends of the hole are closed by removable 2 in. thick aluminum plugs. The upper plug has holes for the stirrer and electrical leads to the thermistor bridge and heater. The temperature was controlled by pumping water through loops of copper tubing attached to each of the four large faces.

The uncertainty in the temperature drift corresponds to an error of 0.5 cal in 4 min, which is the duration of a typical measurement. The sample size was commonly near 0.02 mol, and the mean deviation from the mean for all samples was 23 cal/mol. Comparison of several of our data with recorded values might help to assess the

reliability. For the specific heat of ethanol at 25° a value of 0.581 is recorded and we found 0.588. A recent report of the excess heat capacity of ethanol in water<sup>16</sup> gives 28.5 cal/mol deg, and we found 28.4 cal/mol. For the heat of mixing of ethanol with water we found -2311 cal/mol at 25°, and a modern literature value<sup>17</sup> is -2390 cal/mol. Other recorded values have a spread of 190 cal.

In view of the high dilution (final concentration,  $\sim 0.06 M$ ) we believe the heat of infinite dilution may be safely neglected. Published data for the propyl alcohols<sup>18</sup> indicate that the heat of dilution from 0.06  $M$  is approximately 5 cal/mol.

*Volumes of Mixing.* Volume changes were calculated from the following equation, in which  $m$  represents mass,  $M$  is the molecular weight,  $d$  is the density at 25°, and subscripts 1, 2, and 3 denote the organic liquid, solvent, and solution, respectively

$$-\Delta V = [(m_1/d_1) + (m_2/d_2) - (m_1 + m_2)/d_3]M_1/m_1$$

The mole fraction of solute was usually 0.01–0.02. Some solutes, notably the alcohols, have a shallow minimum in partial molal volume in the region of 0.02–0.10 mol fraction,<sup>5</sup> and our neglect of this phenomenon could lead to a discrepancy possibly as large as 1.0 ml/mol between our results and the true partial molal volume at infinite dilution. In view of the fact that the precision of our pycnometer (1 part/10,000) limits the reproducibility of the mixing volume to about 0.5 ml, we did not think it profitable to attempt extrapolations to infinite dilution in most cases. For the aliphatic alcohols Friedman and Scheraga<sup>2</sup> have reported densities of aqueous solutions below a mole fraction of 0.01. We have calculated apparent molal volumes for the highest concentrations, usually about 2 wt %, and found that they differ from the partial molal volume at infinite dilution by less than 0.5 ml for ethanol, propanol, and butanol. For *t*-butyl alcohol in glycol–water we did explore a considerable range of concentration as shown in Figure 1. Assuming a linear relation between mixing volume and mole fraction, one would predict a difference of 0.3 ml for the values at infinite dilution and a mole fraction of 0.02.

*Materials.* The ethylene glycol and various solutes used in this study were Eastman White Label grade and were used without further purification.

*Acknowledgment.* The authors are indebted to the National Science Foundation which supported this work through Grant GP-7020.

(15) W. F. O'Hara, C. Wu, and L. G. Hepler, *J. Chem. Ed.*, **38**, 512 (1961).

(16) S. L. Rivkin and A. N. Vinnikova, *Teploenergetika*, **11**, 59 (1964).

(17) R. Aveyard and A. S. C. Lawrence, *Trans. Faraday Soc.*, **60**, 2265 (1964).

(18) W. Dimmling and E. Lange, *Elektrochem.*, **55**, 322 (1951).

# Silver and Sodium Ion Transport Numbers into Pyrex from Binary Nitrate Melts<sup>1</sup>

by A. G. Keenan and W. H. Duewer

*Department of Chemistry, University of Miami, Coral Gables, Florida 33124 (Received August 5, 1968)*

The cation transport numbers of sodium and silver ion from mixed melts of the nitrates into a Pyrex membrane at 318° are found to be accurately equal to the corresponding cation mole fractions in the melt over the whole range of compositions. This result is explainable on the basis of a simple liquid-junction model without surface exchange for the membrane. This is in contrast with the previous equilibrium membrane potential studies which required an ion-exchange model. The reasons for this are discussed.

Ionic mobilities in glass are of interest from many points of view. In two recent publications<sup>2,3</sup> it has been demonstrated that the ion-exchange equation<sup>4</sup> satisfactorily fits Pyrex membrane potential data in fused salts. The selectivity constants so determined involve mobility ratios. Mobilities in glasses and fused salts may be measured in a variety of known ways, such as conductance, diffusion, tracer diffusion, and transport experiments.<sup>5</sup> The coefficients so determined are not necessarily equivalent.

No systematic study seems to have been made of macroscopic electric transport of cations into glass from fused salts since the very early work of Schultze<sup>6</sup> and Kraus and Darby.<sup>7</sup> Their results were largely qualitative, although they are still much quoted. We have now found that over the whole range of composition from pure silver nitrate to sodium nitrate, the cation transport fractions into a Pyrex glass membrane are equal to their mole fractions in the melt. This somewhat startling result can be explained on the basis of a liquid-junction model for the membrane in contradiction to the equilibrium emf data.

## Experimental Section

The transport experiments were carried out in a direct manner by measuring the weight change of a Pyrex bulb containing, and immersed in, silver nitrate-sodium nitrate melts through which a measured current was passed for a measured time. The Pyrex bulbs were about 20 mm in diameter and 0.2 mm thick, blown on the end of 10-mm tubing. Their dc resistances varied from 2 to 15 kohms. A cathode of pure silver wire was immersed in the internal solution, which was an equimolar mixture of analytical reagent grade silver and sodium nitrates. The external solution was a similar melt of variable composition. It contained a massive pure silver anode of several square centimeters in surface area. The external melt was held in a 30-mm Pyrex test tube, which in turn was immersed in a constant-temperature bath. Temperature control and measurement have been previously described.<sup>2,3</sup>

The dc voltage was obtained from a 110-V ac supply through a constant-voltage transformer followed by a Variac and was rectified with a 1.8-A full-wave silicon bridge rectifier. A 10.5-H choke and a 30 μF dual-section capacitor were used as a π filter, followed by a 100-ohm power resistor. Up to 74 V (dc) were available with an ac ripple of less than 0.1% as measured on an oscilloscope. The charge passed through the transport cell was obtained by integrating the potential across a 1-ohm standard series resistor as a function of time. This was done by means of an electronic potentiometric recorder of 5-mV full-scale sensitivity provided with a ball-and-disk integrator. Runs ranged from 2 to 24 hr. The current was usually about 10 mA and remained constant within a few per cent after the first 5 min.

The salt mixtures were melted before a run and were sparged with pure nitrogen for 2 hr to remove water. The inner bulb containing the salt and electrode was carefully weighed with all the usual precautions before and after the electrolysis. Blank runs indicated that weighing errors were no more than 2%. The weight changes were taken to result solely from passage of sodium and silver ions into the glass, since it is well established<sup>8,9</sup> that current in the glass phase is carried only by cations. From the data, the silver:sodium ratio and hence the transference numbers could be calculated. The experimental method obviously gives the electrical transport fractions passing from the melt

- (1) This work was supported by the Office of Naval Research, Power Program, under Contract Nonr-4008(07).
- (2) K. Notz and A. G. Keenan, *J. Phys. Chem.*, **70**, 662 (1966).
- (3) A. G. Keenan, K. Notz, and F. L. Wilcox, *ibid.*, **72**, 1085 (1968).
- (4) F. Conti and G. Eisenman, *Biophys. J.*, **5**, 247, 511 (1965).
- (5) R. W. Laity and M. P. Miller, *J. Phys. Chem.*, **68**, 2145 (1964).
- (6) G. Schultze, *Ann. Physik*, **40**, 335 (1913).
- (7) C. A. Kraus and E. H. Darby, *J. Amer. Chem. Soc.*, **44**, 2783 (1922).
- (8) G. Eisenman, *Advan. Anal. Chem. Instr.*, **4**, 213 (1965).
- (9) J. O. Isard in "Glass Electrodes for Hydrogen and Other Cations," G. Eisenman, Ed., Marcel Dekker, Inc., New York, N. Y., 1967, p 51.

**Table I:** Transport Data into Pyrex Glass for a Silver Nitrate-Sodium Nitrate Melt at 318°

Mole fraction of AgNO <sub>3</sub> in melt	Q, C	ΔW, mg	t <sub>Ag</sub>
0.000	100.0	23.9	0.002
0.100	79.1	29.8	0.157
0.100	75.2	24.3	0.097
0.222	124.2	59.0	0.269
0.222	89.5	37.9	0.211
0.350	128.9	68.5	0.333
0.350	58.9	33.3	0.372
0.358	71.6	42.0	0.396
0.500	106.0	71.0	0.491
0.506	128.0	89.9	0.528
0.700	96.8	83.2	0.706
0.700	143.5	118.7	0.669
0.900	113.9	123.5	0.962
0.900	51.8	51.5	0.859
0.900	51.9	51.4	0.855
1.000	96.5	108.0	1.001
1.000	162.5	184.6	1.020

into the glass. Blank experiments with zero current showed that ion exchange and thermal diffusion contributed negligible weight changes. In some cases the glass of the bulbs after electrolysis was ground in a stainless steel mill, was dissolved in hydrofluoric and nitric acids, and was analyzed for sodium, potassium, and silver with an atomic absorption spectrometer.<sup>10</sup>

## Results

The transport data for the silver-sodium system are given in Table I. A graph of average values of  $t_{Ag}$  against rounded concentrations is shown in Figure 1. The standard deviation from the line  $t_{Ag} = X_{Ag}$  is 0.034 and the average deviation from the line is +0.007. The optimum fit of third order or less as determined by a least-squares computer program is  $t_{Ag} = 0.956X_{Ag} + 0.027$  and has a standard deviation of 0.031, so that no statistical justification exists for an attempt to fit the data with any other type of curve. No significant correlation between the amount of charge transported or the duration of a run and the magnitude or sign of the deviations from  $t_{Ag} = X_{Ag}$  exists. Transport numbers of sodium and silver ion into Pyrex are thus equal to their respective mole fractions in the binary-nitrate melt.

No attempt was made to carry out systematic analyses of glass composition changes for all runs, but the data obtained showed that, as expected,<sup>7</sup> replacement of sodium by silver was on an equivalent basis. Up to 50% replacement occurred in the longer runs. The glass changed color but did not appear to lose appreciable mechanical strength.

## Discussion

The general flux equation for ion transport is<sup>4,11-13</sup>

$$J_i = -C_i u_i (dV_i/dx) \quad (1)$$

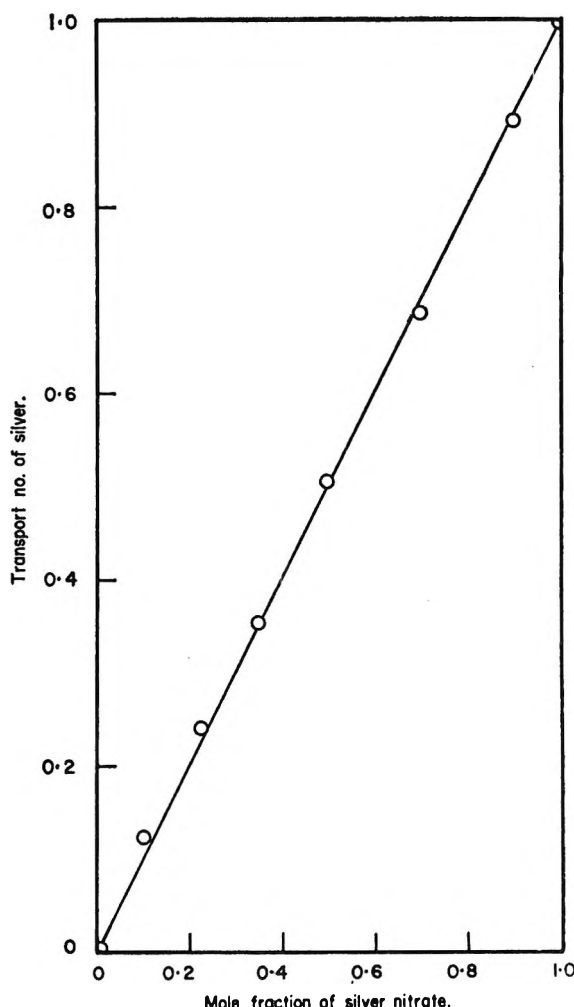


Figure 1. Transport number of silver ion into Pyrex membrane vs. mole fraction of silver nitrate in a NaNO<sub>3</sub>-AgNO<sub>3</sub> melt at 318°.

where  $J_i$  is the flux, in  $\text{mcl cm}^{-2} \text{ sec}^{-1}$ , of component  $i$  in the  $x$  direction;  $C_i$  is the concentration, in  $\text{mol cm}^{-3}$ ;  $V_i$  is the electrochemical potential, in volts; and  $u_i$  is the mobility in the glass. The electrochemical potential is given by

$$V_i = \mu_i^0 + RT \ln a_i + z_i F \psi \quad (2)$$

where the first two terms are the chemical potential,  $z_i$  is the charge,  $F$  is the faraday, and  $\psi$  is the electrical potential. In the present system the electrical potential was of the order of 70 V. The chemical potential is equal to the equilibrium membrane potential in emf measurements and is therefore of the order of millivolts<sup>3</sup> and is negligible. Thus the gradient of the electrochemical potential in the flux equation is the same for both univalent cations and cancels out below.

(10) We are indebted to Mr. O. Joensuu of the Institute of Marine Science for these analyses.

(11) R. W. Laity, *J. Phys. Chem.*, **67**, 671 (1963).

(12) R. W. Laity, *J. Chem. Phys.*, **30**, 682 (1959).

(13) L. Onsager, *Trans. N. Y. Acad. Sci.*, **46**, 241 (1945).

From its definition,<sup>14</sup> the transport number  $t_i$  may then be written

$$t_i = \frac{z_i J_i}{\sum_k z_k J_k} = \frac{C_i u_i}{\sum_k C_k u_k} \quad (3)$$

If  $t_i$  is taken as the transport number into the Pyrex membrane, then  $C_i$  is the concentration in the membrane surface. Experimentally it has just been shown for the  $\text{NaNO}_3\text{-AgNO}_3$  system that  $t_i = X_i$ , where  $X_i$  is the mole fraction in the melt.

The above relations are general. It remains to investigate the applicability of various physical models of the membrane to the observed results. In prior publications<sup>2,3</sup> it has been shown that membrane potential data for Pyrex in fused nitrates fit the ion-exchange model<sup>4</sup> and not the classical liquid-junction model.<sup>15</sup> According to the ion-exchange model, the concentrations  $C_i$  in eq 3 are established by ion exchange with the melt. Assuming that the exchange processes are much faster than transport through the glass,<sup>4</sup> the former may be considered to be in equilibrium and governed by a constant of the form<sup>4</sup>

$$K_{1,i} = \frac{C_i a_i}{C_1 a_1} \quad (4)$$

where  $a_i$  is the activity in the melt. A ratio of fluxes may now be written as

$$\frac{J_i}{J_1} = \frac{C_i u_i}{C_1 u_1} = \frac{a_i u_i K_{1,i}}{a_1 u_1} = \frac{a_i k_i}{a_1} \quad (5)$$

where  $k_i$  is the "selectivity constant" of the ion-exchange theory.<sup>2-4</sup> Using eq 3, the transport number in the two-cation system is

$$t_{\text{Ag}} = \frac{a_{\text{Ag}} k_{\text{Ag}}}{a_{\text{Ag}} k_{\text{Ag}} + a_{\text{Na}}} = \frac{\gamma_{\text{Ag}} X_{\text{Ag}} k_{\text{Ag}}}{\gamma_{\text{Ag}} X_{\text{Ag}} k_{\text{Ag}} + \gamma_{\text{Na}} X_{\text{Na}}} \quad (6)$$

where  $\gamma$  is the activity coefficient. Introducing the experimental fact that  $t_{\text{Ag}} = X_{\text{Ag}}$  leads to the condition  $k_{\text{Ag}} = \gamma_{\text{Na}}/\gamma_{\text{Ag}}$ .

This activity ratio for cation pairs in the melt may be taken<sup>16</sup> equal to the ratio of molar activity coefficients. This varies over a threefold range (from 0.6 to 1.8 at 350°) for this system.<sup>3</sup> On the other hand, the ion-exchange model accounts for the emf data with a constant value of  $k_{\text{Ag}}$  (0.78 at 350°). Thus the present transport data are not consistent with an ion-exchange model.

The liquid-junction model does not recognize the existence of surface phenomena. Thus it implies that the  $C_i$  of eq 3 is the concentration in the melt at the membrane surface. The ratios may therefore be replaced by mole fractions ( $X_i$ ) in the melt, leading to the equation

$$t_{\text{Ag}} = X_{\text{Ag}} = \frac{u_{\text{Ag}} X_{\text{Ag}}}{u_{\text{Ag}} X_{\text{Ag}} + u_{\text{Na}} X_{\text{Na}}} \quad (7)$$

This equation has the unique solution  $u_{\text{Ag}} = u_{\text{Na}}$ , these mobilities applying to the membrane. It is, of course, known that for a homogeneous, mixed fused salt, equal mobilities require transport numbers to be equal to mole fractions.<sup>14</sup>

It has already been shown by others<sup>17-19</sup> that the mobilities of silver and sodium ions are equal in the mixed nitrate melt. The present transport data thus indicate on this basis that the equality of cation mobilities persists into the membrane, which simply acts as a barrier to prevent anion migration. That surface-exchange phenomena may be negligible in the present transport experiments, in contrast to the equilibrium emf type of measurement, is understandable in view of the high electric field present and the gross transport of material through the surface.

Although the crystal radii of sodium and silver ions are rather different ( $r_{\text{Na}} = 0.95 \text{ \AA}$  and  $r_{\text{Ag}} = 1.26 \text{ \AA}$ ), these cations show interesting similarities in transport and other properties. Thus while cation mobilities are in general not equal in mixed fused salts,<sup>19-21</sup> they are so for the pairs  $\text{NaNO}_3\text{-AgNO}_3$  and  $\text{NaCl}\text{-AgCl}$ .<sup>19</sup> This has been stated in other terms by showing that the friction coefficients of sodium and silver relative to nitrate are equal.<sup>22</sup> This independence of mobility ratio on the anion environment appears to carry over into the borosilicate lattice. There is also precedent for cation mobility ratios in glass being in general independent of the concentration ratios in the glass.<sup>8</sup> Fused sodium and silver nitrates are also similar in that the conductivities and molar volumes are equal and the latter are equal to the partial molar volumes in all intermediate mixtures.<sup>22</sup> Finally, the tracer diffusion coefficients of sodium and silver relative to nitrate are equal in fused salts.<sup>23</sup>

(14) R. W. Laity in "Encyclopedia of Electrochemistry," C. A. Hampel, Ed., Reinhold Publishing Corp., New York, N. Y., 1964, p 653.

(15) D. A. McInnes, "The Principles of Electrochemistry," Reinhold Publishing Corp., New York, N. Y., 1939, p 220.

(16) R. W. Laity in "Reference Electrodes," D. J. G. Ives and G. J. Janz, Ed., Academic Press, New York, N. Y., 1961, p 543.

(17) F. R. Duke, R. W. Laity, and B. Owens, *J. Electrochem. Soc.*, **104**, 299 (1957).

(18) R. W. Laity, *J. Amer. Chem. Soc.*, **79**, 1849 (1957).

(19) R. W. Laity and C. T. Moynihan, *J. Phys. Chem.*, **67**, 723 (1963).

(20) C. R. Moynihan and R. W. Laity, *ibid.*, **68**, 3312 (1964).

(21) A. Berlin, F. Menes, S. Forcheri, and C. Monfrini, *ibid.*, **67**, 2505 (1963).

(22) R. W. Laity, *Ann N. Y. Acad. Sci.*, **79**, 997 (1960).

(23) B. R. Sundheim in "Fused Salts," B. R. Sundheim, Ed., McGraw-Hill Book Co., New York, N. Y., 1964, p 165.

# Electron Spin Resonance Spectroscopy of the 1-Methylphenalenyl and the 1-Phenylphenalenyl Radicals

by I. C. Lewis and L. S. Singer

Union Carbide Corporation, Carbon Products Division, Parma Technical Center, Parma, Ohio 44180  
(Received August 6, 1968)

Electron spin resonance measurements have been made of the stable free radicals 1-methylphenalenyl and 1-phenylphenalenyl in solution. Analyses of the proton hyperfine structure indicate that the unpaired spin densities at the unsubstituted positions are only slightly affected by the presence of a methyl or phenyl group. The observed large methyl proton splittings prove the existence of a significant hyperconjugation effect. The small phenyl-ring splittings in 1-phenylphenalenyl are consistent with a nonplanar conformation of the radical.

## Introduction

The phenalenyl (perinaphthyl) radical (I) which was first observed in 1957 by Sogo, Nakazaki, and Calvin<sup>1</sup> is one of the best known examples of a stable neutral hydrocarbon radical. Phenalenyl can be formed at room temperature by the dissociation of hydrogen from the hydrocarbon perinaphthene and has been ob-



I

served in petroleum distillates<sup>2,3</sup> and in the pyrolysates of aromatic hydrocarbons.<sup>4</sup> There have been a number of recent esr studies of phenalenyl in both ordinary<sup>5,6</sup> and liquid crystal solvents.<sup>7,8</sup> The magnitudes and signs of the spin densities for I have been of general theoretical interest.<sup>9,10</sup>

No substituted phenalenyl radicals have been prepared by dissociation reactions. Weiss, *et al.*,<sup>11</sup> have identified a hydroxylphenalenyl radical formed during the photolysis of perinaphthenones. We have now prepared the 1-methyl and 1-phenyl derivatives of I by simple dissociation reactions and have measured their esr spectra in solution.

The methyl and phenyl groups are of particular interest as substituents in phenalenyl. The magnitude of the hyperfine interaction for the protons of methyl groups in aromatic ions has been taken as direct evidence for hyperconjugation.<sup>12,13</sup> Large hyperfine splittings have also been observed for the methyl protons in substituted neutral triphenylmethyl radicals.<sup>14</sup> The magnitude of the hyperfine interaction of the methyl protons in the methylphenalenyl radical would provide a significant test of this hyperconjugation effect. In the case of 1-phenylphenalenyl, molecular models show that the phenyl group cannot be coplanar with the phenalenyl ring system. It should be possible to con-

firm this conformational effect by determining the unpaired spin distribution in the radical.

In this paper, the isotropic esr hyperfine spectra for the 1-methylphenalenyl and 1-phenylphenalenyl radicals are presented. The proton hyperfine coupling constants for these radicals have been determined and compared with those for phenalenyl. The chemical implications of the coupling constants are discussed.

## Experimental Section

*Preparation of Radicals.* (1) *Phenalenyl.* The phenalenyl radical was obtained directly from perinaphthene in solution at room temperature.<sup>1</sup> The perinaphthene was prepared by the reduction of perinaphthenone tosylhydrazone with NaBH<sub>4</sub>.<sup>15</sup> This method proved to be more effective than the direct reduction of perinaphthenone with LiAlH<sub>4</sub>.<sup>16</sup>

(2) *1-Methylphenalenyl.* The 1-methylphenalenyl radical was obtained from 1-methylperinaphthene in solution at room temperature. The 1-methylperi-

- (1) P. B. Sogo, M. Nakazaki, and M. Calvin, *J. Chem. Phys.*, **26**, 1343 (1957).
- (2) J. E. Bennett, *Proc. Chem. Soc.*, 144 (1961).
- (3) F. C. Stehling and K. W. Bartz, *J. Chem. Phys.*, **34**, 1076 (1961).
- (4) L. S. Singer and I. C. Lewis, *Carbon*, **2**, 115 (1964).
- (5) F. Gerson, *Helv. Chim. Acta*, **49**, 1463 (1966).
- (6) B. G. Segal, M. Kaplan, and G. K. Fraenkel, *J. Chem. Phys.*, **43**, 4191 (1965).
- (7) S. H. Glarum and J. H. Marshall, *ibid.*, **44**, 2884 (1966).
- (8) H. R. Falle and G. R. Luckhurst, *Mol. Phys.*, **11**, 299 (1966).
- (9) R. Lefebvre, H. H. Dearman, and H. M. McConnell, *J. Chem. Phys.*, **32**, 176 (1960).
- (10) L. C. Snyder and T. Amos, *J. Chem. Phys.*, **42**, 3670 (1965).
- (11) G. P. Rabold, K. H. Bar-Eli, E. Reid, and K. Weiss, *ibid.*, **42**, 2438 (1965).
- (12) J. R. Bolton, A. Carrington, and A. D. McLachlan, *Mol. Phys.*, **5**, 31 (1962).
- (13) E. deBoer and J. P. Colpa, *J. Phys. Chem.*, **71**, 21 (1967).
- (14) H. Judeikis and D. Kivelson, *J. Amer. Chem. Soc.*, **84**, 1132 (1962).
- (15) L. Caglioti and P. Grasselli, *Chem. Ind. (London)*, 153 (1964).
- (16) V. Boekelheide and C. E. Larrabee, *J. Amer. Chem. Soc.*, **72**, 1245 (1950).

**Table I:** Experimental Proton Coupling Constants for Phenalenyl Radical (I)

Solvent	Measuring temp., °C	$a_1$ , G	$a_2$ , G	Ref
CCl <sub>4</sub>	25	6.32 ± 0.01	1.81 ± 0.01	This work
CCl <sub>4</sub>	25	6.306 ± 0.002	1.821 ± 0.003	6
DME <sup>a</sup>	25	6.333 ± 0.002	1.823 ± 0.002	6
DME <sup>a</sup>	20	6.336	1.826	7
CCl <sub>4</sub>	25	6.29 ± 0.04	1.805 ± 0.015	5
Petroleum distillate	25	6.3 ± 0.1	1.82 ± 0.05	2
p-Azoxyanisole	102	6.280	1.822	8
p-Azoxyanisole	145	6.270	1.833	7
m-Quinquephenyl	150	6.27	1.81	4

<sup>a</sup> DME, dimethoxyethane.

naphthalene was produced from the Grignard reaction of perinaphthenone with CH<sub>3</sub>MgBr.<sup>17,18</sup>

(3) *1-Phenylphenalenyl and 1-Phenyl-d<sub>5</sub>-phenalenyl.* The 1-phenylphenalenyl radical was formed from 1-phenylperinaphthene in solution at room temperature. The 1-phenylperinaphthene was prepared from the Grignard reaction of perinaphthenone with C<sub>6</sub>H<sub>5</sub>MgBr. The deuterated radical, 1-phenyl-d<sub>5</sub>-phenalenyl, was prepared from perinaphthenone with C<sub>6</sub>D<sub>5</sub>MgBr (Merck Sharp and Dohme).

*Esr Measurements.* The esr spectrum for phenalenyl was obtained for a degassed solution of radical in CCl<sub>4</sub> at room temperature. The spectrum for 1-methylphenalenyl was measured for a degassed, 10<sup>-3</sup> M solution of the radical in dimethoxyethane at -50°. These conditions have been used by Segal, Kaplan, and Fraenkel in obtaining excellent resolution of the phenalenyl radical spectrum.<sup>6</sup> The esr spectra for 1-phenylphenalenyl and 1-phenyl-d<sub>5</sub>-phenalenyl were measured on degassed 10<sup>-4</sup> M solutions of the radical in C<sub>6</sub>H<sub>6</sub> at 25°.

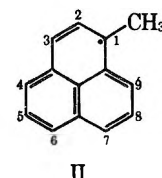
The spectra were measured with an X-band esr spectrometer employing superheterodyne detection at a microwave power of 0.1 mW. Low-temperature measurements were performed with the Varian variable-temperature cavity.

## Results

*Phenalenyl Radical (I).* The esr spectrum of phenalenyl shows a large hyperfine interaction from the six

equivalent protons at the active positions and a small splitting by the three equivalent protons at the inactive positions.<sup>19</sup> The coupling constants which we have determined for phenalenyl (I) in CCl<sub>4</sub> at 25° are: 6 H, 6.32 ± 0.01 G; and 3 H, 1.81 ± 0.01 G. These values are in good agreement with those obtained in other recent investigations. Table I lists the recent proton coupling constant data that have been reported for I. The magnitudes of the hyperfine splittings show a slight dependence on solvent and temperature.

### 1-Methylphenalenyl Radical (II).



II

The 1-methylphenalenyl radical (II) is observed immediately after the dissolution of the parent hydrocarbon 1-methylperinaphthene at room temperature. The extreme ease with which the hydrogen dissociation from methylperinaphthene to form the radical II takes place is indicative of the high stability of radicals incorporating the phenalenyl ring system. Since the methyl group in II is substituted at one of the active starred positions, one would expect an appreciable hyperfine interaction by the three methyl protons. In addition, large hyperfine splittings are expected for the five protons at the remaining active ring sites.

Figure 1a shows the esr spectrum obtained for the 1-methylphenalenyl radical formed in a dimethoxyethane solution approximately 10<sup>-3</sup> M in methylperinaphthene. The spectrum contains 116 resolvable lines with an individual line width of 0.1 G. This spectrum has been reduced to the following coupling constants: 1 H, 6.48 ± 0.02 G; 3 H, 6.27 ± 0.01 G;

(17) L. F. Fieser and L. W. Newton, *J. Amer. Chem. Soc.*, **64**, 917 (1942).

(18) L. C. Craig, W. A. Jacobs, and G. I. Lavin, *J. Biol. Chem.*, **139**, 277 (1941).

(19) A. Streitwieser, "Molecular Orbital Theory for Organic Chemists," John Wiley & Sons, Inc., New York, N. Y., 1961, p 46.

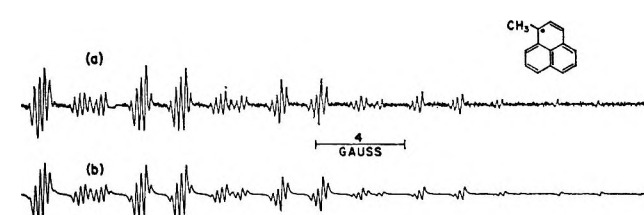


Figure 1. Comparison of the experimental curve (a) and the computed curve (b) for the 1-methylphenalenyl free radical. Computed values: 1 H, 6.48 G; 3 H, 6.27 G; 4 H, 6.05 G; 3 H, 1.77 G.

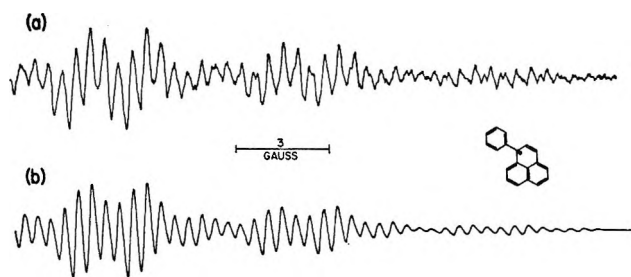
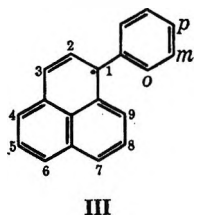


Figure 2. Comparison of the experimental curve (a) and the computed curve (b) for the 1-phenylphenalenyl free radical. Computed values: 5 H, 6.12 G; 3 H, 1.78 G; 3 H, 0.48 G; 2 H, 0.39 G.

4 H,  $6.05 \pm 0.01$  G; and 3 H,  $1.77 \pm 0.01$  G. A spectrum simulated from this assignment is shown in Figure 1b.

The assignment of these coupling constants to the specific ring positions of II can be made from a comparison with the coupling constants for the unsubstituted phenalenyl radical. The splitting of 6.27 G must be assigned to the three equivalent protons of the methyl group. The small splitting of 1.77 G is attributed to the three protons at the inactive 2, 5, and 8 positions. Of the five remaining protons in the molecule, the 4, 6, 7, and 9 protons are the most similar chemically. The coupling constant of 6.05 G can, therefore, be assigned to these protons, leaving the single splitting of 6.48 G for the proton at the 3 position.

**1-Phenylphenalenyl (III).** An intense esr spectrum for the phenylphenalenyl radical



was observed for solutions of phenylperinaphthene at room temperature. Figure 2a shows the esr spectrum observed for a  $10^{-4} M$  solution of III in benzene at  $25^\circ$ . Since this spectrum is incompletely resolved and since there is considerable ambiguity in its analysis, we have also obtained an esr spectrum for the 1-phenyl- $d_5$ -phenalenyl radical prepared from 1-phenyl- $d_5$ -perinaphthene. The splittings by the protons in the phenyl ring are expected to be small in comparison with those for the protons of the phenalenyl ring. Deuteration of the phenyl ring should, therefore, result in a simplified spectrum.

Figure 3a shows the esr spectrum obtained for a solution of 1-phenyl- $d_5$ -phenalenyl radical in benzene at  $25^\circ$ . A simple pattern of 24 hyperfine lines 0.36 G wide is observed. This spectrum can readily be reduced to the following coupling constant assignment: 5 H,  $6.12 \pm 0.01$  G and 3 H,  $1.781 \pm 0.003$  G. A stick plot from these values is shown in Figure 3b.

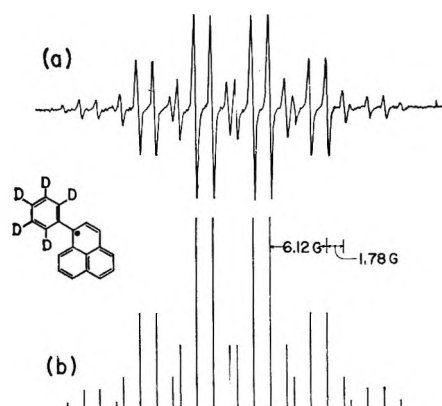


Figure 3. Comparison of the experimental curve (a) and the computed stick plot (b) for the 1-phenyl- $d_5$ -phenalenyl free radical. Computed values: 5 H, 6.12 G; 3 H, 1.781 G.

The hyperfine splittings by the deuteriums of the phenyl group are considerably less than 0.36 G and are not resolved. With the aid of the results for the deuterated radical, we have been able to analyze the spectrum for III in terms of the following coupling constants: 5 H, 6.12 G; 3 H, 1.78 G; 3 H, 0.48 G; and 2 H, 0.39 G. An esr curve computed from these values is shown in Figure 2b. The slight additional resolution apparent in the experimental curve indicates that the assumed proton equivalences are not exact.

### Discussion

The ease of formation of the substituted phenalenyl radicals from both 1-methylperinaphthene and 1-phenylperinaphthene is further confirmation of the extreme stability of radicals incorporating the phenalenyl ring system. The coupling constants obtained for the phenalenyl, methylphenalenyl, and phenylphenalenyl radicals are summarized in Table II. The close similarity in the values for the different radicals makes the assignment to ring positions relatively unambiguous.

The most interesting aspects of the coupling constant

Table II: Comparison of Coupling Constants in Gauss for Phenalenyl, 1-Methylphenalenyl, and 1-Phenylphenalenyl Radicals

Position	Phenalenyl (I)	1-Methylphenalenyl (II)	1-Phenylphenalenyl (III)
1	6.32	6.27 ( $\text{CH}_3$ )	0.48 ( <i>p</i> ) 0.48 ( <i>o</i> ) 0.39 ( <i>m</i> )
2	1.81	1.77	1.78
3	6.32	6.48	6.12
4	6.32	6.05	6.12
5	1.81	1.77	1.78
6	6.32	6.05	6.12
7	6.32	6.05	6.12
8	1.81	1.77	1.78
9	6.32	6.05	6.12

data for the methylphenalenyl radical are the large hyperfine splittings for the methyl protons. The magnitude of the methyl splitting is approximately the same as that for the ring protons in unsubstituted phenalenyl. Large methyl proton splittings have been observed in methyl-substituted aromatic ions.<sup>12,13</sup> This effect has been described in terms of a combined inductive and hyperconjugation mechanism. The large methyl splitting in II demonstrates the importance of these mechanisms in aromatic neutral radicals.

An examination of the coupling constant data for II shows only a small perturbation by the methyl group on the unpaired electron distribution in the remainder of the molecule. The splittings at the inactive posi-

tions, which are positions of negative spin density,<sup>7,8</sup> are virtually unchanged by the methyl substituent. The hyperfine interactions at the remaining active positions are altered only slightly by the 1-methyl substituent.

The phenyl substituent in III effects a slight reduction in the magnitude of the hyperfine interaction at all the phenalenyl ring positions. The splittings by the phenyl protons are in turn quite small, a result which is consistent with the sterically enforced nonplanar conformation of the phenyl group.

*Acknowledgments.* We wish to thank Mrs. S. B. Wallon for synthesizing the compounds.

## Estimation of the Bisulfate Ion Dissociation in Solutions of Sulfuric Acid and Sodium Bisulfate

by Richard E. Lindstrom and Henry E. Wirth

Department of Chemistry, Syracuse University, Syracuse, New York 13210 (Received August 7, 1968)

Young's rule was applied to the observed mean apparent molal volumes of sulfuric acid and sodium bisulfate to obtain estimates of the dissociation quotient ( $Q_v$ ) in the volume ionic strength ( $\mu_v$ ) range 0–4. The results in sulfuric acid solution are given by the equation  $\log Q_v = \log 0.0102 + 2.036\mu_v^{1/2} - 1.376\mu_v + 0.8862\mu_v^{3/2} - 0.2171\mu_v^2$  and in sodium bisulfate solution by the equation  $\log Q_v = \log 0.0102 + 2.036\mu_v^{1/2} - 1.543\mu_v + 0.8297\mu_v^{1/2} - 0.1703\mu_v^2$ . The volume change at infinite dilution ( $\Delta v^\theta$ ) for the process  $H^+ + SO_4^{2-} \rightarrow HSO_4^-$  was found to be 21.6 ml.

Some years ago Klotz and Eckert<sup>1</sup> investigated the dissociation of the bisulfate ion in sulfuric acid solutions utilizing apparent molar volumes. Their approach was to assume that a bisulfate solution is a mixture of two electrolytes: the completely dissociated species,  $H^+$ ,  $H^+, SO_4^{2-}$ , and the undissociated species,  $H^+, HSO_4^-$ . The observed or mean apparent molar volume,  $\Phi$ , could then be expressed as a function of the mole fraction and apparent molar volumes of the two solute species.

This relationship is essentially that defined more explicitly by Young and Smith<sup>2</sup> and tested by Wirth and coworkers.<sup>3</sup> It is

$$\Phi = \frac{C_2\phi_2 + C_3\phi_3}{C_2 + C_3} \quad (1)$$

where  $\Phi$  is the mean or observed apparent molar volume of the solute at ionic strength  $\mu_v$ ,  $\phi_2$  is the apparent molar volume of  $H^+, H^+, SO_4^{2-}$  in a pure solution of the same ionic strength  $\mu_v$ , and  $\phi_3$  is the apparent molar volume of  $H^+, HSO_4^-$  also in a pure solution at ionic strength  $\mu_v$ .

$C_2$  and  $C_3$  are the molar concentrations of the dissociated and undissociated species, respectively.

In terms of the degree of dissociation ( $\alpha$ ), eq 1 becomes

$$\Phi = \alpha\phi_2 + (1 - \alpha)\phi_3 \quad (2)$$

The ionic strength at a total solute molarity ( $C$ ) is

$$\mu_v = (1 + 2\alpha)C \quad (3)$$

Simultaneous solution of eq 2 and 3 yields an  $\alpha$  which may be used to calculate the dissociation quotient,  $Q_v$ , at the given ionic strength where

$$Q_v = \frac{[H^+][SO_4^{2-}]}{[HSO_4^-]} = \frac{\alpha(1 + \alpha)C}{1 - \alpha} \quad (4)$$

(1) I. M. Klotz and C. F. Eckert, *J. Amer. Chem. Soc.*, **64**, 1878 (1942).

(2) T. F. Young and M. B. Smith, *J. Phys. Chem.*, **58**, 716 (1954).

(3) H. E. Wirth, R. E. Lindstrom, and J. N. Johnson, *ibid.*, **67**, 2339 (1963).

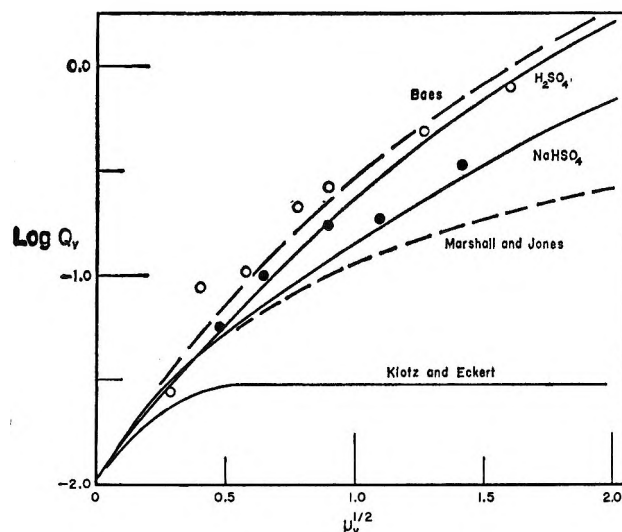


Figure 1. The bisulfate ion dissociation quotient ( $Q_v$ ) as a function of ionic strength in solutions of sulfuric acid and of sodium bisulfate (solid curves), compared with the results of C. F. Baes, Jr., *J. Amer. Chem. Soc.*, **79**, 5611 (1957), of W. L. Marshall and E. V. Jones, *J. Phys. Chem.*, **70**, 4028 (1966), and of Klotz and Eckert<sup>1</sup> for sulfuric acid. The experimental points are the Raman results of Young in sulfuric acid (○) and in sodium bisulfate (●) quoted by Baes.

Klotz and Eckert<sup>1</sup> used known values of  $Q_v$  to establish  $\phi_3$  in the concentration range 0–0.14 $\mu_v$ . From 0.4 to 3.2 $\mu_v$  they found that values of  $Q_v$  between 0.01 and 0.09 gave reasonable values for the apparent molar volume of  $H^+,HSO_4^-$ . They chose  $Q_v = 0.03$  as the best value. However, the Raman data of Young<sup>4</sup> give much higher values of  $Q_v$  in this concentration range (*cf.* Figure 1) and larger values of  $\phi_3$  are therefore required. Thus either the slope of  $\phi_3$  vs.  $\mu_v^{1/2}$  is greater than that of a normal 1:1 electrolyte, or the value of  $\phi_3^0$  estimated by Klotz and Eckert is too small. In the present work we have found that both a larger slope and a larger value of  $\phi_3^0$  is required to give reasonable values of  $Q_v$ .

In this investigation the apparent molar volumes of both sulfuric acid and sodium bisulfate were obtained by density and dilatometric methods, with emphasis on the dilute concentration range (0.001–0.01C).

### Experimental Section

Stock solutions of sulfuric acid and sodium bisulfate were prepared from CP chemicals. The stock sulfuric acid solution was analyzed by weight titration using a National Bureau of Standards standardized sulfuric acid solution as the reference standard. The stock sodium bisulfate solution was prepared by solution of sodium sulfate, previously dried at 110°, on a mole for mole basis in the stock sulfuric acid. Dilute solutions of both salts were prepared as required by weight dilution of the initial stock solutions. The density of each solution thus prepared was determined by the sinker method.<sup>5</sup>

Apparent molar volumes for solutions of varying bisulfate concentration were obtained using a dilatometric technique.<sup>3</sup> In the present investigation, a calibrated capillary was added to the dilatometer system to provide additional precision in measuring volume changes at low concentration. By careful control of the pressure ( $\pm 0.1$  mm) on the system and of the temperature of the thermostated bath ( $\pm 0.0005^\circ$ ), the experimental uncertainty in the observed volume changes was estimated to be reduced to  $\pm 6 \times 10^{-5}$  ml. This corresponds to an uncertainty of  $\pm 0.06$  ml in the molar volumes in the most dilute solution.

The apparent molar volume,  $\Phi$ , of a given solution within the mixing chamber of the dilatometer is given by

$$\Phi = \Phi_2 + \frac{\Delta_{\text{vol}}}{n_2} \quad (5)$$

where  $\Phi_2$  is the apparent molar volume of the stock solution,  $n_2$  is the number of moles of solute in the chamber, and  $\Delta_{\text{vol}}$  is the volume change noted on mixing the volume of stock solution containing  $n_2$  mol of salt with a known amount of water.

The data obtained are given in Tables I and II. Figure 2 illustrates the agreement of the experimental results of this investigation with the values obtained by Klotz and Eckert.<sup>2</sup>

### Results and Discussion

Interpretation of the mean apparent molar volume of an electrolyte solution by the mixture rule of Young requires knowledge of this property for the contributing salts. Thus it was necessary to evaluate the apparent molar volumes of the dissociated salt,  $X^+,H^+,SO_4^{2-}$ , and undissociated salt,  $X^+,HSO_4^-$ , as a function of ionic strength. Since direct experimental determination is not possible, the required information was obtained on the assumption that apparent molar volumes of electrolytes are additive, even to relatively high concentration.

*Evaluation of  $\phi_2$  for  $X^+,H^+,SO_4^{2-}$ .* The apparent molar volumes of the theoretical, completely dissociated bisulfates may be represented by

$$\begin{aligned} \phi_2(Na^+,H^+,SO_4^{2-}) &= \\ \phi(Na_2SO_4) + \phi(HCl) - \phi(NaCl) &= \end{aligned} \quad (6)$$

$$\begin{aligned} \phi_2(H^+,H^+,SO_4^{2-}) &= \\ \phi(Na_2SO_4) + 2\phi(HCl) - 2\phi(NaCl) &= \end{aligned} \quad (7)$$

where each  $\phi$  is the apparent molar volume of the respective salt at a given ionic strength. Utilizing these equations, the hydrochloric acid and sodium chloride data of Wirth<sup>5</sup> and the sodium sulfate data of Gibson<sup>6</sup>

(4) T. F. Young, *Rec. Chem. Prog.*, **12**, 81 (1951).

(5) H. E. Wirth and F. N. Collier, Jr., *J. Amer. Chem. Soc.*, **72**, 5292 (1950).

(6) R. E. Gibson, *J. Phys. Chem.*, **31**, 496 (1927).

**Table I:** Apparent Molal Volumes of Sodium Bisulfate in Water

<i>m</i>	<i>C</i>	$\Phi$
0	0	(12.86)
0.001019	0.001016	14.12
0.002010	0.002004	15.23
0.004848	0.004833	16.79
0.011611	0.011574	19.322
0.017461	0.017404	20.769
0.028894	0.028792	22.254
0.057435	0.057186	24.554
0.085643	0.085203	25.909
0.10000	0.099446	26.320
0.11340	0.11273	26.806
0.14073	0.13978	27.486
0.22006	0.21803	28.905
0.41510	0.40867	30.845
0.59109	0.57846	31.955
0.75073	0.73062	32.746
0.89607	0.86759	33.359
1.0291	0.99163	33.860
1.1511	1.1043	34.280
1.2636	1.2072	34.641
1.3674	1.3014	34.956
1.4523	1.3778	35.210
1.4637	1.3882	35.233
1.5512	1.4663	35.483
1.5531	1.4679	35.478
1.6365	1.5419	35.702
1.6644	1.5666	35.783
1.7143	1.6104	35.903
1.7956	1.6816	36.113
1.9492	1.8149	36.486
2.1315	1.9707	36.898
2.3514	2.1556	37.369
2.6220	2.3786	37.911
2.9627	2.6521	38.539
3.4058	2.9961	39.293
4.0040	3.4402	40.206

**Table II:** Apparent Molal Volumes of Sulfuric Acid in Water

<i>m</i>	<i>C</i>	$\Phi$
0.0	0	(14.08)
0.001257	0.001254	17.58
0.002485	0.002478	19.07
0.005998	0.005979	22.44
0.009299	0.009270	24.247
0.017159	0.017101	26.726
0.023933	0.023847	27.964
0.029823	0.029710	28.775
0.034997	0.034859	29.327
0.11470	0.11394	32.757
0.01347	0.01343	25.50 <sup>a</sup>
0.05283	0.05259	30.66 <sup>a</sup>
0.1147	0.1139	32.78 <sup>a</sup>
0.3442	0.3591	35.02 <sup>a</sup>
0.7917	0.7674	36.36 <sup>a</sup>
1.4561	1.3774	37.21 <sup>a</sup>
2.3359	2.1393	38.08 <sup>a</sup>

<sup>a</sup> Determined by the sinker method.<sup>5</sup>

limited ionic strength range, it is then possible to determine  $\phi_3^0$  for  $\text{Na}^+, \text{HSO}_4^-$  and  $\text{H}^+, \text{HSO}_4^-$ .

Working first with sodium bisulfate, the approach was to pick both a  $\phi_2$  at some ionic strength below 0.04 and an observed apparent molar volume,  $\Phi$ , at a concentration, *C*, thought to approximate the same ionic strength. Equation 3 then gave an  $\alpha$ , which on substitution into eq 2 gave the corresponding  $\phi_3$ . The same steps were followed for sulfuric acid, using the identical ionic strength. The entire procedure was repeated as necessary to find  $\phi_3$  values of both solutes giving the best agreement in  $\Delta v$  at that ionic strength.

The  $\Delta v$  values obtained above were plotted against  $\mu_v^{1/2}$  (Figure 4). A line of slope 1.86, that of a 1:1

were combined to obtain  $\phi_2$  for both theoretical salts. The results are given in Tables III and IV and in Figures 2 and 3.

Because similar data for the  $\text{HSO}_4^-$  ion are not experimentally available, the direct approach could not be used for the undissociated species,  $\text{Na}^+, \text{HSO}_4^-$  and  $\text{H}^+, \text{HSO}_4^-$ . Instead, the  $\phi_3$  vs.  $\mu_v^{1/2}$  curves were obtained by first determining the probable intercept of such a curve for each salt, then completing the evaluation using data for salts with analogous apparent molar volume properties.

*Determination of  $\Delta v^0$ .* The apparent molar volume of  $\text{X}^+, \text{HSO}_4^-$ , at infinite dilution  $\phi_3^0$ , is given by

$$\phi_3^0 = \phi_2^0 + \Delta v^0 \quad (8)$$

where  $\phi_2^0$  is the apparent molar volume of  $\text{X}^+, \text{H}^+, \text{SO}_4^{2-}$  at infinite dilution and  $\Delta v^0$  is the change in apparent molar volume accompanying the process  $\text{H}^+ + \text{SO}_4^{2-} \rightarrow \text{HSO}_4^-$ . Assuming  $\Delta v^0$  is independent of the second cation and that eq 8 holds over a

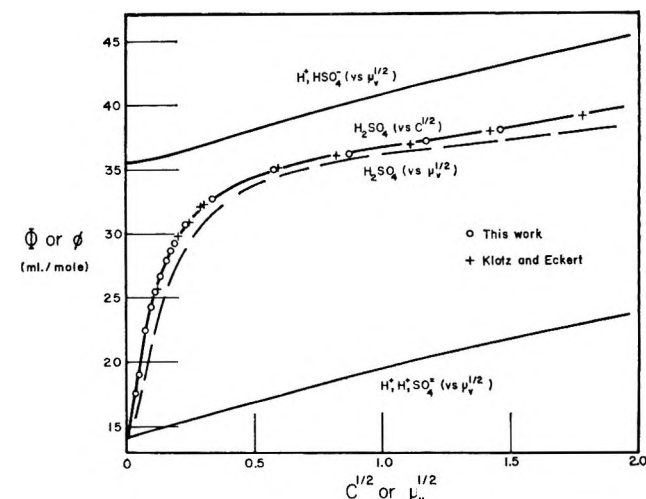


Figure 2. Experimental values for the mean apparent molal volume of sulfuric acid ( $\Phi$ ) vs. the square root of the molarity and vs. the square root of the calculated volume ionic strength (dashed curve). These ionic strengths ( $\mu_v = (1 + 2\alpha)C$ ) are consistent with the values of  $\alpha$  obtained from eq 11.

Table III: Ionization of  $\text{HSO}_4^-$  in Sodium Bisulfate

$\mu_v^{1/2}$	<i>C</i>	$C^{1/2}$	$\phi(\text{Na}^+, \text{HSO}_4^-)$	$\phi(\text{Na}^+, \text{H}^+, \text{SO}_4^-)$	$\Phi(\text{NaHSO}_4)$	<i>a</i>	<i>Q<sup>a</sup></i>	<i>Q<sup>b</sup></i>
0	0	0	(34.46)	(12.86)				
0.05	0.0008681	0.02946	34.56	13.16	14.54	0.940	0.0128	0.0128
0.1	0.003737	0.06113	34.58	13.49	16.48	0.838	0.0162	0.0158
0.2	0.01695	0.1302	35.26	14.10	20.90	0.679	0.0243	0.0229
0.3	0.04163	0.2040	35.88	14.73	23.60	0.581	0.0335	0.0319
0.4	0.07890	0.2809	36.52	15.34	25.64	0.514	0.0430	0.0422
0.6	0.1921	0.4383	37.76	16.59	28.50	0.437	0.0652	0.0679
0.8	0.3532	0.5943	39.02	17.79	30.40	0.406	0.0980	0.1010
1.0	0.5580	0.7470	40.28	18.99	31.84	0.396	0.145	0.145
1.2	0.8045	0.8970	41.54	20.19	33.10	0.395	0.207	0.204
1.4	1.086	1.042	42.80	21.39	34.20	0.402	0.293	0.287
1.6	1.411	1.195	44.06	22.57	35.32	0.407	0.394	0.396
1.8	1.772	1.331	45.32	23.73	36.38	0.414	0.518	0.530
2.0	2.169	1.473	46.58	24.89	37.42	0.422	0.668	0.661

<sup>a</sup> Observed dissociation quotient. <sup>b</sup> Calculated using eq 15.Table IV: Ionization of  $\text{HSO}_4^-$  in Sulfuric Acid

$\mu_v^{1/2}$	<i>C</i>	$C^{1/2}$	$\phi(\text{H}^+, \text{HSO}_4^-)$	$\phi(\text{H}^+, \text{H}^+, \text{SO}_4^-)$	$\Phi(\text{H}_2\text{SO}_4)$	<i>a</i>	<i>Q<sup>a</sup></i>	<i>Q<sup>b</sup></i>
0	0	0	(35.68)	(14.08)				
0.05	0.0009038	0.03006	35.78	14.40	16.90	0.883	0.0128	0.0128
0.1	0.004184	0.06468	35.88	14.72	21.16	0.695	0.0162	0.0159
0.2	0.02186	0.1479	36.48	15.32	27.70	0.415	0.0219	0.0233
0.3	0.05703	0.2388	37.00	15.91	30.90	0.289	0.0299	0.0329
0.4	0.1093	0.3307	37.56	16.48	32.66	0.232	0.0407	0.0451
0.6	0.2586	0.5085	38.62	17.56	34.50	0.196	0.0754	0.0791
0.8	0.4591	0.6776	39.99	18.57	35.50	0.197	0.135	0.132
1.0	0.7022	0.8380	40.68	19.54	36.20	0.212	0.229	0.240
1.2	0.9756	0.9877	41.72	20.47	36.66	0.238	0.377	0.356
1.4	1.279	1.131	42.70	21.38	37.02	0.266	0.587	0.576
1.6	1.618	1.272	43.70	22.27	37.46	0.291	0.857	0.894
1.8	1.990	1.411	44.68	23.17	37.92	0.314	1.20	1.27
2.0	2.387	1.545	45.66	24.09	38.36	0.338	1.63	1.56

<sup>a</sup> Observed dissociation quotient. <sup>b</sup> Calculated using eq 14.

electrolyte, extrapolated through these points gave  $\Delta v^0 = 21.6 \text{ ml}$ , a value 1.4 ml greater than that reported by Klotz and Eckert.<sup>1</sup> Equation 8 gave  $\phi_3^0$  for  $\text{Na}^+$ ,  $\text{HSO}_4^-$  and  $\text{H}^+$ ,  $\text{HSO}_4^-$  as 34.46 and 35.68 ml, respectively.

*Evaluation of  $\phi_3$  for  $X^+$ ,  $\text{HSO}_4^-$ .* Having established  $\phi_3^0$  for  $\text{H}^+$ ,  $\text{HSO}_4^-$  and  $\text{Na}^+$ ,  $\text{HSO}_4^-$ , it was expected that  $\phi_3$  at higher concentrations could be obtained by using  $\text{HClO}_4$  or  $\text{HCl}$  and  $\text{NaClO}_4$  as model electrolytes (*i.e.*, at a given ionic strength,  $\phi(\text{H}^+, \text{HSO}_4^-) = \phi^0(\text{H}^+, \text{HSO}_4^-) + [\phi(\text{HClO}_4) - \phi^0(\text{HClO}_4)]$ ). Values of  $\phi_3$  thus obtained were found to approach the experimental values for sulfuric acid and sodium bisulfate at the highest concentrations studied, indicating very little dissociation. To be in agreement with the work of Young,<sup>4</sup> the slope of the  $\phi_3$  vs.  $\mu_v^{1/2}$  curve must be three to four times that usual for a 1:1 electrolyte.

A similar phenomenon was observed by Wirth and Shapiro<sup>7</sup> in their work with potassium dihydrogen

phosphate,  $\text{KH}_2\text{PO}_4$ . After correcting for possible hydrolysis and dissociation, they found that the apparent molar volumes of this salt, in the 0.25–1.6 ionic strength range, varied nearly linearly with  $\mu_v^{1/2}$ , with a slope of 5.88.

No explanation is apparent for this observation, but it does parallel the relationship indicated for the undissociated bisulfate salts. This prompted the choice of  $\text{H}_2\text{PO}_4^-$  as the model for the bisulfate ion. A qualitative appraisal of the over-all  $\phi_3$  vs.  $\mu_v^{1/2}$  relationship would then show a transition from the limiting slope of 1.86 in dilute solution to the larger slope predicted by the  $\text{H}_2\text{PO}_4^-$  model.

Curves for both solutes at ionic strengths above 0.02 were constructed, using the relations

$$\begin{aligned} \phi(\text{Na}^+, \text{H}_2\text{PO}_4^-) &= \phi(\text{K}^+, \text{H}_2\text{PO}_4^-) + \\ &\quad \phi(\text{Na}^+, \text{Cl}^-) - \phi(\text{K}^+, \text{Cl}^-) \quad (9) \end{aligned}$$

(7) H. E. Wirth and S. Shapiro, unpublished work, 1964.

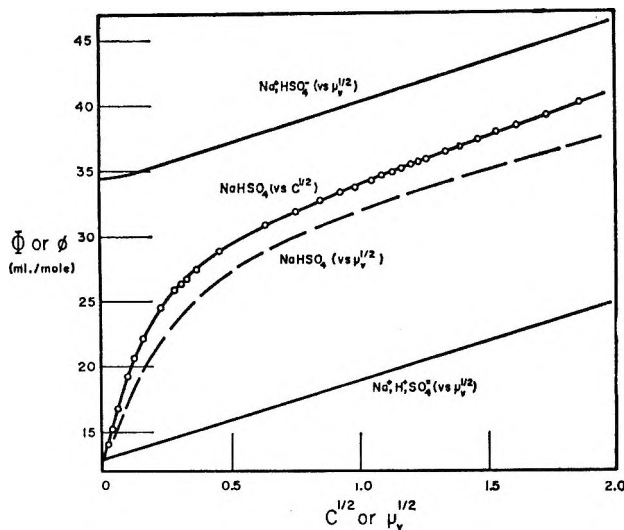
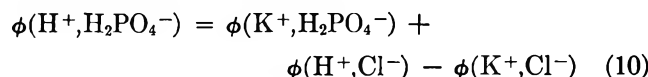


Figure 3. Experimental values for the mean apparent molar volume of sodium bisulfate ( $\Phi$ ) vs. the square root of the molarity and vs. the square root of the calculated volume ionic strength (dashed curve). These ionic strengths ( $\mu_v = (1 + 2\alpha)C$ ) are consistent with the values of  $\alpha$  obtained from eq 11.



The sodium chloride, hydrochloric acid, and potassium chloride data of Wirth<sup>5,8</sup> and the potassium dihydrogen phosphate data of Wirth and Shapiro were used for the calculations. These curves were then adjusted to fit the  $\phi_3^0$  values determined earlier for  $Na^+, HSO_4^-$  and  $H^+, HSO_4^-$ . This fitting established the final  $\phi_3$  vs.  $\mu_v^{1/2}$  relationships used in the remainder of this investigation. The results are given in Figures 2 and 3 and in Tables III and IV.

*Estimation of Dissociation Quotients, Q<sub>v</sub>.* It was now possible to proceed with a determination of  $\alpha$  as a function of ionic strength.  $\phi_2$  and  $\phi_3$  values for the salts at a given ionic strength were read from  $\phi$  vs.  $\mu_v^{1/2}$  plots to  $\pm 0.02$  ml and introduced into the equation

$$\alpha = \frac{\phi_3 - \Phi}{\phi_3 - \phi_2} \quad (11)$$

where  $\Phi$  was an observed apparent molar volume estimated to be near the correct value.

Substituting this  $\alpha$  into eq 3 gave  $C$  which was used to obtain a second  $\Phi$ . This process was repeated until the  $C$  obtained in eq 3 corresponded to the  $\Phi$  used in calculating  $\alpha$ . At this point,  $Q_v$ , the dissociation quotient at ionic strength  $\mu_v$  was calculated using the equations

$$Q_v(NaHSO_4) = \frac{\alpha^2 C}{1 - \alpha} \quad (12)$$

$$Q_v(H_2SO_4) = \frac{(1 + \alpha)\alpha C}{1 - \alpha} \quad (13)$$

The results are summarized in Tables III and IV.

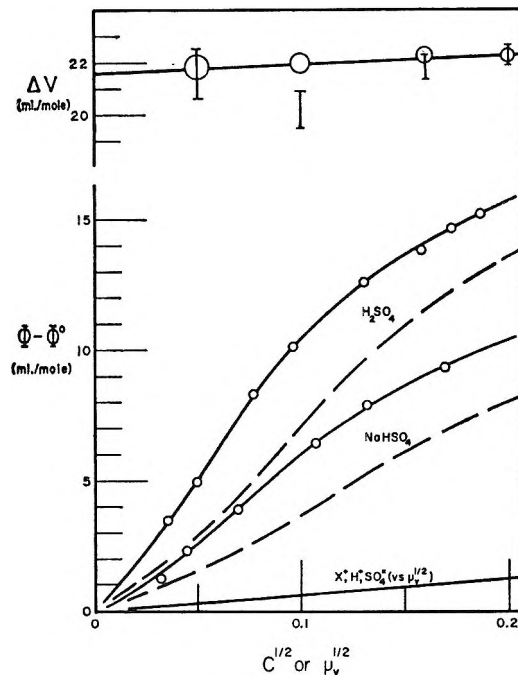


Figure 4. Upper curve: volume change ( $\Delta v$ ) for the process  $H^+ + SO_4^{2-} \rightarrow HSO_4^-$  at low ionic strengths, calculated for sulfuric acid (O) and for sodium bisulfate (I) (the size of the symbols represents the error in the estimated value of  $\Delta v$ ); lower curve: experimental values of  $\Phi - \Phi^0$  for sulfuric acid and for sodium bisulfate vs. the square root of the molarity and vs. the square root of the calculated ionic strength (dashed curves). The values of  $\alpha$  used in calculating  $\mu_v$  are consistent with the modified form of eq 11 ( $\alpha = [(\phi_3 - \phi_3^0) - (\Phi - \Phi^0)]/\Delta v$ ).

The results of this investigation are compared in Figure 1 with those of Baes<sup>9</sup> and those of Marshall and Jones,<sup>10</sup> as well as the original estimates of Klotz and Eckert.<sup>1</sup> The agreement with the recent results is considered to be satisfactory in view of the number of assumptions necessarily made in this work. The experimental results can be represented by the equations

$$\log Q_v = \log 0.0102 + 2.036\mu_v^{1/2} - 1.376\mu_v + 0.8862\mu_v^{3/2} - 0.217\mu_v^2 \quad (\text{in } H_2SO_4) \quad (14)$$

$$\log Q_v = \log 0.0102 + 2.036\mu_v^{1/2} - 1.543\mu_v + 0.8297\mu_v^{3/2} - 0.1703\mu_v^2 \quad (\text{in } NaHSO_4) \quad (15)$$

The quantity 0.0102 is the thermodynamic dissociation constant ( $K$ ) at 25°, which we have taken from Baes.<sup>9</sup> This value is in good agreement with the results of Dunsmore and Nancollas<sup>11</sup> ( $K = 0.0103 \pm 0.0001$ ), Covington, Dobson, and Wynn-Jones<sup>12</sup> ( $K = 0.0106 \pm$

(8) H. E. Wirth, *J. Amer. Chem. Soc.*, **59**, 2549 (1937).

(9) C. F. Baes, Jr., *ibid.*, **79**, 5611 (1957).

(10) W. L. Marshall and E. V. Jones, *J. Phys. Chem.*, **70**, 4028 (1966).

(11) H. S. Dunsmore and G. N. Nancollas, *ibid.*, **68**, 1579 (1964).

(12) A. K. Covington, J. V. Dobson, and W. F. K. Wynn-Jones, *Trans. Faraday Soc.*, **61**, 2057 (1965).

0.0009), Marshall and Jones<sup>10</sup> ( $K = 0.01028 \pm 0.0002$ ), and Klotz<sup>13</sup> ( $K = 0.01015$ ). However, Wallace<sup>14</sup> found  $K = 0.0131 \pm 0.0002$  in his Donnan membrane equilibrium studies. The coefficient of  $\mu_v^{1/2}$  is the Debye-Hückel limiting slope.

Other authors<sup>9-12</sup> have used the equation<sup>15</sup>

$$\log Q = \log K + \frac{2.036\mu^{1/2}}{1 + A\mu^{1/2}} + B\mu \quad (16)$$

with  $A$  values ranging from 0.4 (Baes) to 0.94 (Marshall and Jones) with  $B = 0$ , while Covington, Dobson, and Wynn-Jones use  $A = 1.0$  and 1.7 with a finite value of

*B.* In dilute solutions, our equations correspond to an  $A$  value of *ca.* 0.7.

*Acknowledgment.* The authors gratefully acknowledge the facilities, time, and funds provided by the Frank J. Seiler Research Laboratory, Office of Aerospace Research, United States Air Force Academy, Colorado, where the greater portion of the research for this investigation was accomplished.

(13) I. M. Klotz, *Chem. Rev.*, **41**, 373 (1947).

(14) R. M. Wallace, *J. Phys. Chem.*, **70**, 3922 (1966).

(15) It should be noted that a plot of  $\log Q$  vs.  $\mu^{1/2}$  (on a molal basis) coincides within experimental error with a plot of  $\log Q_v$  vs.  $\mu_v^{1/2}$  (molar basis) even in concentrated solutions.

## Electrolyte-Solvent Interaction. XIX. Solvation by Molecular Picric Acid

by Alessandro D'Aprano<sup>1</sup> and Raymond M. Fuoss

Sterling Chemistry Laboratory, Yale University, New Haven, Connecticut 06520 (Received August 12, 1968)

The conductances in acetonitrile at 25° of solutions of tetrabutylammonium picrate and tetramethylammonium picrate and tetramethylammonium bromide to which picric acid was added have been measured. The conductance of the salts is decreased by the picric acid. If a specific preferential solvation of the anions by picric acid molecules, to give a complex with lower mobility, is assumed, the data can be quantitatively described in terms of an equilibrium between ions solvated by picric acid and ions surrounded only by acetonitrile. In purifying the acetonitrile, it was found that traces of ammonia can give spurious conductances for picric acid solutions, due to formation of ammonium picrate. For ammonium picrate in acetonitrile, the limiting conductance is 174.4 and the association constant is 185. A 1-ppm concentration of ammonia in acetonitrile of conductance of the order of  $10^{-8}$  gives a specific conductance of  $1.5 \times 10^{-5}$  upon addition of picric acid.

In order to account for the decrease in conductance produced by the addition of *p*-nitroaniline (PNA) to solutions of various electrolytes in acetonitrile,<sup>2</sup> we proposed that PNA, with its larger dipole moment, displaced acetonitrile solvate, thereby forming a bulkier and slower ionic species. Other cases of specific ion-solvent interaction have since been reported.<sup>3</sup> With the nitrophenols,<sup>4</sup> much larger effects than for PNA were observed for the *meta* and *para* isomers, while *o*-nitrophenol caused only a very slight decrease. Picric acid (trinitrophenol) decreased the conductance of tetrabutylammonium bromide even more than *p*-nitrophenol did. Since PNA and *p*-nitrophenol have about the same dipole moment, the greater effect of the latter must be due to a difference between the hydroxyl and the amino group. These results suggested that hydrogen bonding, rather than ion-dipole attraction, was the mechanism of solvation in the case of the nitrophenols; we therefore investigated the effect of adding picric acid to several other electrolytes

and again found markedly decreased conductances. In the course of the work, it became clear that the conductance of picric acid in pure acetonitrile is extremely low and that what we (and others) have used as the specific conductance of picric acid in acetonitrile is actually the conductance of dilute solutions of picrates of basic impurities in the acetonitrile, ammonia and water being the most probable. We present here a summary of a study of the conductance of picric acid in "dry" acetonitrile, in "pure" acetonitrile, and in acetonitrile containing controlled amounts of water or ammonia. A 1-ppm concentration of ammonia will

(1) NATO Postdoctoral Research Fellow, 1966-1967. On leave of absence from the University of Palermo, Palermo, Italy.

(2) A. D'Aprano and R. M. Fuoss, *J. Phys. Chem.*, **67**, 1722, 1871 (1963).

(3) W. R. Gilkerson and J. B. Ezell, *J. Amer. Chem. Soc.*, **87**, 3812 (1965); W. R. Gilkerson and E. K. Ralph, *ibid.*, **87**, 175 (1965); J. B. Ezell and W. R. Gilkerson, *ibid.*, **88**, 3486 (1966).

(4) C. Treiner, M. Quintin, and R. M. Fuoss, *J. Chim. Phys.*, **63**, 320 (1966).

give a specific conductance of about  $1.5 \times 10^{-5}$  to acetonitrile containing picric acid. Then it will be shown that picric acid decreases the conductance of solutions of tetrabutylammonium picrate ( $\text{Bu}_4\text{NPI}$ ), tetramethylammonium picrate ( $\text{Me}_4\text{NPI}$ ), and tetramethylammonium bromide by amounts which correspond to a 1:1 addition of picric acid to the anions of these salts. The equilibrium constant for solvation by picric acid is of the order of 3000–4000.

### Experimental Section

Picric acid was recrystallized twice from ethanol, was dried 2 days under vacuum at  $40^\circ$ , and was kept in a desiccator with phosphorus pentoxide. Conductance measurements were made in a cell with constant  $0.15033 \text{ cm}^{-1}$ . Electrical apparatus and measuring techniques were as described before.<sup>2</sup> The precision in the specific conductances is 0.01%. All data refer to  $25 \pm 0.002^\circ$ .

Salt solutions were made up by weight; after determining the conductance of the salt solution, successive portions of dry picric acid (PA) were added, and the conductance remeasured, after rocking the cell (which was kept under the thermostat oil so that the temperature did not change) to dissolve the acid. The conductances became steady as soon as the acid was all in solution; no drift in resistance was observed. In order to calculate the change in conductance due to the picric acid, the resistances of a series of solutions of picric acid in acetonitrile were also determined. The results are summarized in Table I, where  $c$  is the concentration

**Table I:** Conductances of Salts Plus Picric Acid in Acetonitrile at  $25^\circ$

$10^4 c$	$10^4 C$	$10^6 \sigma(c, C)$	$10^6 \sigma(C)$	$-10^6 \Delta \sigma$
Picric Acid				
0.0	24.8	...	9.51	...
0.0	51.9	...	12.74	...
0.0	73.1	...	14.46	...
0.0	103.3	...	16.47	...
$\text{Bu}_4\text{NPI} + \text{PA}$				
8.479	0.00	110.78	0.00	...
8.471	33.33	112.64	10.65	8.83
8.465	57.58	112.96	13.25	11.11
8.457	87.37	113.37	15.75	12.91
8.451	110.18	113.62	16.95	14.05
$\text{Me}_4\text{NPI} + \text{PA}$				
4.221	0.00	66.85	0.00	...
4.216	38.87	69.45	11.30	8.75
4.212	77.05	70.35	14.80	11.30
4.208	107.92	70.86	16.80	12.79
4.202	152.84	71.52	19.05	14.43
$\text{Me}_4\text{NBr} + \text{PA}$				
7.600	0.00	130.95	0.00	...
7.589	50.52	133.15	13.00	10.40
7.583	73.84	133.09	14.60	12.46
7.578	100.05	132.98	16.30	14.27

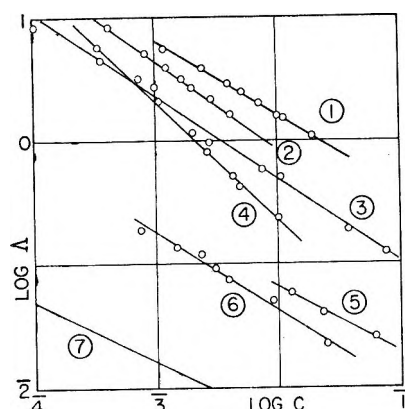


Figure 1. Conductances of picric acid in acetonitrile.

of the salt (equiv/l.) and  $C$  is the concentration of picric acid. The symbol  $\sigma(c, C)$  designates the specific conductance of a solution containing salt and acid at concentrations  $c$  and  $C$ , respectively, while  $\Delta\sigma$  represents the difference between  $\sigma(c, C)$  and the sum of the conductances of the components taken separately

$$\Delta\sigma = \sigma(c, C) - [\sigma(c) + \sigma(C)] \quad (1)$$

Obviously  $\Delta\sigma$  would be zero if the conductances were additive; as seen in the table, net conductance decreases on adding picric acid to the salt solutions. In Table I,  $\sigma(C)$  is the conductance of picric acid alone at concentration  $C$ , interpolated from the data on picric acid. These values agree very closely with those of Treiner.<sup>4</sup>

After the above measurements on salts plus picric acid had been made, an analysis of the data was started. We expected, of course, to make a correction for the common-ion effect in the case of the two picrates, for which the dissociation constant of picric acid is needed. The values in the literature for the  $pK$  of picric acid range from French and Roe's value<sup>5</sup> of 5.6 to Kolthoff and Chantooni's value<sup>6</sup> of 11.0! The latter (potentiometric) is the correct one. Conductance data for picric acid in acetonitrile are summarized in Figure 1, where  $\log \Delta\sigma$  is plotted against  $\log C$ . The top line represents the data for picric acid from Table I, combined with those of Treiner.<sup>4</sup> Lines 2 and 6 are further data obtained in this laboratory and will be discussed later. Line 3 is based on the data of Römberg and Cruse;<sup>7</sup> line 4, French and Roe;<sup>5</sup> line 5, the earlier work of Kolthoff.<sup>8</sup> Line 7 is calculated, using Kolthoff's value  $pK = 11.0$  and his estimate<sup>8</sup>  $\Lambda_0 = 160$  for the limiting conductance of picric acid in acetonitrile and the ap-

(5) C. M. French and I. G. Roe, *Trans. Faraday Soc.*, **49**, 314 (1953).

(6) See Table XII, I. M. Kolthoff and M. K. Chantooni, *J. Amer. Chem. Soc.*, **87**, 4428 (1965).

(7) E. Römberg and K. Cruse, *Z. Elektrochem.*, **63**, 404 (1959).

(8) I. M. Kolthoff, S. Bruckenstein, and M. K. Chantooni, *J. Amer. Chem. Soc.*, **83**, 3927 (1961).

proximate Arrhenius equation  $c\Lambda^2 = K\Lambda_0^2$ . We note that all the other lines on Figure 1 are steeper than line 7, which has the theoretical slope of  $-0.5$ . Line 4 has a slope of  $-1$ ; this implies that the product  $c\Lambda$  is constant and gives the clue to the puzzle. Constant  $c\Lambda$  means constant specific conductance. French and Roe used the dilution method; that is, successive portions of acetonitrile were added to the initial solution of picric acid. Suppose the solvent contained a trace of strong base X; it would be a latent electrolyte and would produce its picrate on contact with picric acid. By hypothesis, the picric acid is far in excess over the trace impurity; therefore, the concentration of X-picrate would be constant in a dilution run and the  $c\Lambda$  product would not change. For systems which give slopes between  $-0.5$  and  $-1.0$ , we must postulate at least two impurities, one a strong base and one a weak base. Ammonia (from hydrolysis of acetonitrile) and water are prime suspects; the experiments described below were made to test their effects on the conductance of picric acid in acetonitrile.

The acetonitrile used for the data of Table I had been dried by refluxing for 12 hr over Drierite, after standing over potassium carbonate to remove acetic acid. Treiner's<sup>4</sup> solvent had also been dried in the same way. Analysis by vapor-phase chromatography, using a hot-wire detector, showed the presence of 0.10% water; this is 0.043 equiv/l. of water and is very much higher than the concentrations of picric acid used in our work. In order to obtain a lower water content, 500 ml of acetonitrile (Matheson Coleman and Bell) was stirred over calcium hydride for 2 days and then distilled from phosphorus pentoxide.<sup>9</sup> Vpc showed the presence of 0.035% water. The conductance was  $3.7 \times 10^{-8}$ ; on standing in a closed conductance cell for 96 hr, the conductance gradually increased to  $4.1 \times 10^{-8}$ . Upon addition of picric acid, solutions whose conductance increased with time were obtained. Other workers have also reported that the conductance of picric acid in acetonitrile changes on standing.<sup>5-8</sup> Several examples are shown in Figure 2, where curve 1 gives the resistance in a cell of constant  $k = 0.03876 \text{ cm}^{-1}$  of a solution with  $C = 8.42 \times 10^{-4}$  in acetonitrile with a water content of 0.035%. In 2.5 hr, the resistance dropped by about 6%, and in a most peculiar pattern: at about 1 hr, the resistance seemed to be approaching constancy, and then a second slower process appeared. Curve 2 is for  $C = 2.02 \times 10^{-3}$  in a cell with  $k = 0.11772 \text{ cm}^{-1}$ , in acetonitrile to which water had been added to give 0.135% water. Curve 3 is for  $C = 1.167 \times 10^{-3}$  in a cell with  $k = 0.15033 \text{ cm}^{-1}$  in acetonitrile with 0.535% water. Cusps appeared in all our PA-MeCN-H<sub>2</sub>O systems. Clearly, two processes are occurring, and the second can only begin after the first has reduced the concentration of some inhibitor below a critical level. We were unable to find any correlation between the rates of either process or the time of ap-

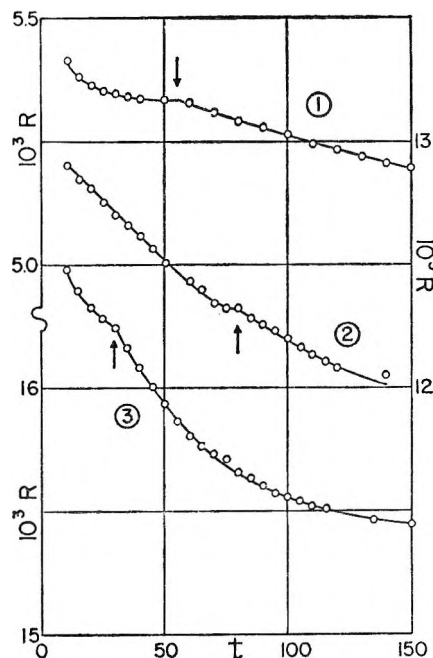


Figure 2. Change of resistance with time (minutes) for picric acid in acetonitrile containing water.

pearance of the cusp and the concentration of either water or picric acid.

If the variable resistances are extrapolated back to zero time, for picric acid in acetonitrile containing controlled amounts of water, conductance curves are obtained which lie between lines 1 and 6 of Figure 1. Line 1 of Figure 1 is for 0.10% water in acetonitrile that had been treated with Drierite. Line 2 is for acetonitrile that had been distilled from calcium hydride; this solvent also containing 0.10% water. Line 6 averages a set of points for picric acid in acetonitrile that had been dried with special care (3 days over calcium hydride, 12 hr over phosphorus pentoxide, fractionally distilled, middle cut used, and dry nitrogen in still, receiver, and cell). The water content of this solvent was 0.018%. Picric acid solutions in this solvent were a faint greenish yellow. Each point represents a separate determination: picric acid was weighed into solvent in the cell, and resistance was measured every 5 min for 3 hr. The points represent the extrapolated zero-time conductances. This conductance curve comes nearest to line 7, which represents picric acid in an ideal acetonitrile which contains no trace whatsoever of basic impurity. We obtained a number of other conductance curves, which lie between line 1 and 6; in general the higher the water content, the higher the line in the figure, but frequently a high curve would be found for a solvent with low water content. At this stage, we may draw conclusions: (1) dissociation constants of weak acids cannot be determined in aprotic solvents conductimetrically, and (2) the erratic be-

(9) J. F. Coetzee, G. P. Cunningham, D. K. McGuire, and G. R. Padmanabhan, *Anal. Chem.*, **34**, 1139 (1962).

havior of picric acid in acetonitrile with a controlled water content suggests the presence of a base which is stronger than water with respect to picric acid in acetonitrile.

In some of the methods of "purifying" acetonitrile, potassium carbonate or hydroxide was used to remove acetic acid. However, if even a trace of the acetonitrile had previously hydrolyzed to acetamide and then to ammonium acetate, treatment with alkali will give ammonia. We found ammonia by a positive Nessler test in acetonitrile distilled from potassium hydroxide. Upon addition of picric acid, a yellow solution was obtained, which showed strong absorption at  $420 \text{ m}\mu$ , where the picrate ion absorbs, and which had a high conductance. When nitrogen was bubbled through the solution overnight, both color and conductance decreased appreciably. If the ammonia is not removed, it will, of course, form ammonium picrate upon addition of picric acid. The conductance of ammonium picrate in acetonitrile was therefore determined, with the expectation that it would be orders of magnitude higher than that of picric acid (line 7, Figure 1). A solution of ammonia in acetonitrile was made by passing dry gas into the solvent; the solution was standardized by titration against aqueous 0.1 *N* hydrochloric acid. To this 0.0465 *N* solution of ammonia was added an exact equivalent of dry picric acid. This solution was then diluted to give the starting solution for a conductance run. The results are given in Table II. The salt is

Table II: Conductance of Ammonium Picrate in Acetonitrile at 25°

$10^4 c$	$\Lambda$
7.89	147.96
15.15	135.56
25.78	123.28
37.45	113.69
53.75	104.96

moderately associated, because the phoreogram (Figure 3) lies well below the limiting tangent. From the data, we find by using the 1965 conductance equation<sup>10</sup> that  $\Lambda_0 = 174.4$  and  $K_A = 185$  for ammonium picrate in acetonitrile. To show that ammonia or picric acid is conductimetrically almost invisible in the presence of ammonium picrate, two more conductance runs were made. In the first, the solvent was a 0.0465 *N* solution of ammonia in acetonitrile; for the initial solution for a dilution run, about 0.1 equiv of picric acid was added to a portion of the solvent to give a solution 0.005846 *N* in ammonium picrate. In the second, to a 0.003093 *N* solution of ammonium picrate in acetonitrile was added picric acid to make the solution 0.01362 *N* in acid. A dilution run with acetonitrile was then made with the mixed solution. In Figure 3, the open circles

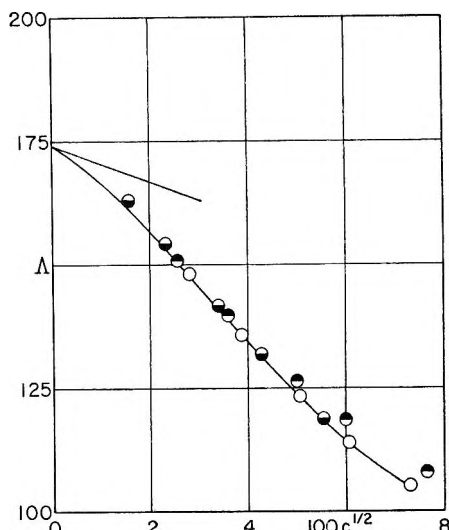


Figure 3. Conductance of ammonium picrate in acetonitrile ( $\circ$ ), in the presence of excess ammonia ( $\bullet$ ), and in the presence of excess picric acid ( $\ominus$ ).

represent the conductance of ammonium picrate in acetonitrile, and the half-shaded circles ammonium picrate in the presence of excess ammonia or picric acid; up to about 0.002 *N*, the three curves coincide. From these experiments, we conclude that traces of ammonia, which of course would be undetectable in the solvent conductance, are converted to a highly conducting salt upon addition of acid, and here we have the explanation of the erratic results summarized in Figure 1.

## Discussion

The results of Table I, as well as earlier work,<sup>2,4</sup> show that conductance is in general decreased<sup>11</sup> when a substance more polar than the solvent is added to an electrolytic solution. In the case of *p*-nitroaniline, the proposed mechanism was solvation of the anions by ion-dipole attraction to give a bulky ion-dipole aggregate which naturally has a lower mobility than the anion solvated by acetonitrile. In the case of the nitrophenols (including picric acid, of course), hydrogen bonding then stabilizes the complex after electrostatic forces have brought ion and dipole together, because the decrease in conductance for a given molar ratio of added dipole:ion is much greater for the phenols than for the aniline. Since the molar volumes of aniline and phenol are not greatly different, the difference in effect must be due to a higher stability of the ion-dipole complex for the phenols.

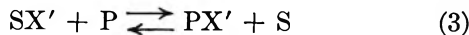
(10) See eq 2.4, R. M. Fuoss, L. Onsager, and J. F. Skinner, *J. Phys. Chem.*, **69**, 2581 (1965).

(11) Given the large increases in conductance produced by traces of ammonia, we now ascribe the increases in conductance reported<sup>4</sup> for *p*-nitrophenol and tetrabutylammonium tetraphenylboride or picrate to the formation of the ammonium salt of the phenol, in amounts sufficient to mask the decrease produced by the normal ion-dipole effect.

A simple mass-action treatment can be applied. Consider the equilibrium



where  $S_nX'$  represents an anion  $X'$  solvated by  $n$  molecules of solvent  $S$  and  $P$  represents an added dipolar molecule such as picric acid. (Of course  $n$  may be zero; there is no way of determining  $n$  from our measurements, and in any case, its value is irrelevant.) To simplify the algebra, we shall set  $n$  equal to 1, giving



which is described by the mass-action equation

$$[PX'][S]/[SX'][P] = K \quad (4)$$

If the stoichiometric concentration of the salt (and cation) is denoted by  $c$  and the concentration of  $PX'$  by  $x$ , the equation is easily solved for  $x$ , giving

$$x = KcC/(S + KC) \quad (5)$$

where  $C$  and  $S$  denote concentrations of added dipolar material (e.g., picric acid) and of solvent. The specific conductance  $\sigma$  is given by

$$10^3\sigma = c\lambda_1 + (c - x)\lambda_2 + x\lambda_3 \quad (6)$$

where  $\lambda_1$ ,  $\lambda_2$ , and  $\lambda_3$  are, respectively, the equivalent conductances at concentration  $c$  of the cation, the ordinary anion, and the solvated anion  $PX'$ . Using eq 5, this becomes

$$10^3\sigma = c[\lambda_1 + \lambda_2 - (\lambda_2 - \lambda_3)KC/(S + KC)] \quad (7)$$

The observed specific conductance  $\sigma(c, C)$  is the sum of the conductance (eq 7) due to the salt and picric acid plus the conductance  $\sigma_0$  due to the ammonium picrate produced from the impurities in the solvent (neglecting interaction between ammonium picrate and picric acid, as is justified by the results shown in Figure 3). The "solvent conductance"  $\sigma_0$  also includes the conductance due to  $H_3O^+$ -picrate and that due to any other extraneous electrolytes in the solvent. Since all of the data of Table I were obtained using the same batch of aceto-

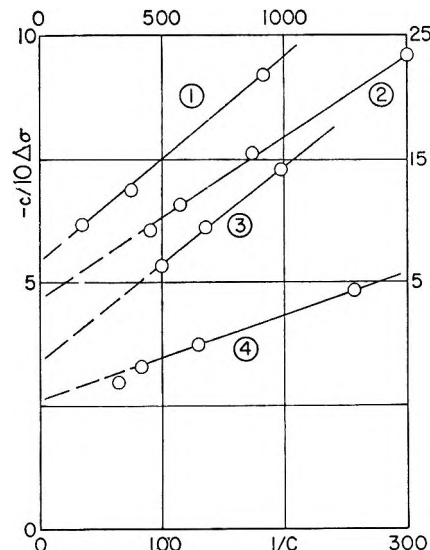


Figure 4. Test of eq 9: 1, tetrabutylammonium bromide (coordinates top and right); 2, tetrabutylammonium picrate; 3, tetramethylammonium bromide; 4, tetramethylammonium picrate.

nitrile, we assume that  $\sigma(C) = \sigma_0$ . Then the observed  $\Delta\sigma$  is given by

$$10^3\Delta\sigma = -(\lambda_2 - \lambda_3)KcC/(S + KC) \quad (8)$$

which rearranges to a form convenient for plotting

$$-c/10^3\Delta\sigma = (1/\Delta\lambda) + (S/K\Delta\lambda)C^{-1} \quad (9)$$

where  $\Delta\lambda$  is  $\lambda_2 - \lambda_3$ , the difference at concentration  $c$  between the conductances of anions surrounded by acetonitrile and anions solvated by picric acid. Figure 4 shows a plot of  $c/10\Delta\lambda$  against the reciprocal of picric acid concentration for the three salts of Table I; Treiner's data<sup>4</sup> for tetrabutylammonium bromide plus picric acid are also included. The plots are linear, in conformity with eq 9, which is based on the hypothesis of specific solvation by picric acid. The intercepts give values of 15–38 for the difference  $\lambda_2 - \lambda_3$ , which seems to be a reasonable value for the decrease in ionic conductance due to solvation by a molecule of picric acid. From the slopes, the solvation constant  $K$  calculates to 3000–4000.

# The Rotatory Properties of Molecules Containing Two Peptide Groups: Theory<sup>1</sup>

by Peter M. Bayley, Eigil B. Nielsen, and John A. Schellman

*Department of Chemistry, University of Oregon, Eugene, Oregon 97403 (Received July 1, 1968)*

A general matrix formulation for the rotatory strength is given which incorporates all previously considered mechanisms in a systematic way. The general equations are reduced to a very simple form for the treatment of molecules containing two peptide units, each assumed to possess only the two lowest excited states (the  $n,\pi^*$  and  $\pi,\pi^*$  transitions of the peptide group). The four rotatory strengths of the resulting dimer are calculated as a function of the conformational angles  $\varphi$  and  $\psi$  for a number of structural situations which arise in polypeptide problems. It is shown that the optical rotation is derived simultaneously from three interaction mechanisms and that the relative roles of these mechanisms are very sensitive to conformation. The procedures have been developed for specific application to a number of experimental investigations of diamide models which will appear in a later work. The present paper concentrates on general results and on a qualitative application of the rotatory strength maps to the  $n,\pi^*$  transition of helical polymers.

A study of the rotatory properties of molecules containing two peptide groups possesses many features of interest. Experimentally, the results have a bearing on the important problem of protein and polypeptide conformations. Theoretically, the close proximity of  $n,\pi^*$  and  $\pi,\pi^*$  transitions in two similar chromophores presents the possibility for an elaborate interplay of mechanisms of interaction. Indeed, there is no aspect of the mechanistic possibilities associated with the names of Kuhn,<sup>2</sup> Kirkwood,<sup>3</sup> Condon, Altar, and Eyring,<sup>4</sup> Moffitt,<sup>5</sup> and Tinoco<sup>6</sup> that does not arise in the seemingly simple problem of two peptide units, even when the number of excited states is drastically limited in the calculations.

In order to be prepared for the variety of contingencies which arise in the practical calculation of rotatory strengths in these molecules, we have found it advisable to go back to the fundamental equations for rotatory strength, which incorporate all mechanisms, and derive from general considerations the relations necessary for the interpretation. In so doing, we are essentially covering the ground of the very thorough paper of Tinoco,<sup>6</sup> though the treatment differs in that matrix methods rather than perturbation methods are used. In this way, first-order perturbation methods are avoided, which could be seriously in error with the almost degenerate bands of dipeptides, and a very compact notation is achieved.

The plan of the work is as follows. In section I a general matrix formulation of optical rotation is developed. In section II the formula is made tractable by limiting the electronic configurations which enter the theory to those which are accessible to ground-state spectroscopy. In section III the details of wave functions, parameters, and computational methods are given, and in section IV the results are applied to the

two-peptide case as a function of conformational angles.

## I. General Theory

The basic problem is to express the rotatory strengths of the electronic transitions of a molecule in terms of all the electronic transitions of its  $N$  constituent groups. These groups are assumed to possess independently defined electronic eigenstates which are perturbed in the assembled molecule by group-group interactions. These interactions can lead to mixing of states within a given group as well as to coupling of states in different groups. The groups themselves are supposed to have planes or centers of symmetry so that they are not intrinsically optically active. Electron exchange among the groups is ignored. Consequently, the model is inappropriate for molecules containing inherently dissymmetric chromophores or exhibiting intergroup charge-transfer spectra.

To minimize complex notation, we use a matrix formulation. The electronic states of each group, specified by  $\lambda$ ,  $\mu$ , etc., provide a local set of energy eigenfunctions. Initial basis functions for the whole molecule are formed as products of these local functions, the product being designated by bracket notation; *i.e.*,  $|0\rangle$  refers to all groups in their ground state and other basis functions are designated solely in terms of their excitations, *e.g.*,  $|\lambda_i\rangle$  and  $|\lambda_i\mu_j\rangle$ . Sub-

(1) This work was supported by grants from the National Science Foundation and the National Cancer Institute, CA04216.

(2) W. Kuhn in "Stereochemie," K. Freudenberg, Ed., Deuticke, Leipzig, 1933, p 317.

(3) J. G. Kirkwood, *J. Chem. Phys.*, **5**, 479 (1937).

(4) E. U. Condon, W. Altar, and H. Eyring, *ibid.*, **5**, 753 (1937).

(5) W. Moffitt, *ibid.*, **25**, 467 (1956).

(6) I. Tinoco, *Advan. Chem. Phys.*, **4**, 113 (1962).

scripts designate the group which is excited. Though this notation is most useful in specifying the physical significance of the states, it produces cumbersome expressions in the matrix equations which follow. To avoid this, we assume that an ordering convention has been established, so that each may be symbolized by a single integer,  $I^0, J^0$ , regardless of the complexity of the excitation. A convenient ordering is: ground state, all excited states of group 1, all excited states of group 2, etc., on through double and triple and higher excited states. The Hamiltonian for the molecule is given by

$$H + H^0 + V = \sum_i H_i^0 + V \quad (1)$$

where  $H_i^0$  is the local Hamiltonian for the  $i$ th group and  $V$  is the intergroup potential for the entire molecule. The diagonal elements of the Hamiltonian matrix are of the form  $H_{I^0, I^0} + V_{I^0, I^0} = E_{I^0} + V_{I^0, I^0}$ , where  $E_{I^0}$  is the energy of the state  $I^0$  when the groups are isolated from one another and  $V_{I^0, I^0}$  is the alteration in this energy produced by the interactions of the groups (the crystal shift of the exciton theory). It is usually possible to estimate the diagonal elements directly from the spectroscopy of the groups in appropriate solvents. Because of the selection of basis functions, all off-diagonal elements are of the form  $V_{I^0, J^0}$ .

The Hamiltonian matrix is diagonalizable by a unitary matrix  $C$

$$C^{-1}HC = H_{\text{diag}} \quad (2)$$

The electric and magnetic dipole matrices in the new representation are given by

$$\vec{\mu} = C^{-1}\vec{\mu}^0C; \quad \vec{M} = C^{-1}\vec{M}^0C \quad (3)$$

where  $\vec{\mu}^0$  and  $\vec{M}^0$  are the electric and magnetic transition moment matrices in the original representation.  $\vec{\mu}^0$  and  $\vec{M}^0$  contain all the electric and magnetic transition moments of the individual groups. These conform to the selection rules determined by the local symmetry. The elements of these matrices are vector quantities which are, in principle, obtainable from experiment or theory. In practice, only a few elements of these matrices are accessible for most chemical groups, usually those connecting the ground state to the first few excited states. The elements of  $\vec{M}^0$  have an origin dependence which will be discussed later.

The rotatory strength matrix for the molecule is given by

$$R = \text{Im}\{\vec{\mu} : \vec{M}'\} \quad (4)$$

$$R_{I,J} = \text{Im}\{\vec{\mu}_{I,J} \cdot \vec{M}'_{J,I}\}$$

where the symbol  $:$  means that scalar products are formed element by element and the prime indicates transposition. We use capital letters without super-

scripts to designate states in the final (diagonal) energy representation.

This is the most general expression for the rotatory strength which can be obtained from the model. Combining eq 3 and 4, a typical rotatory strength is given by

$$R_{0K} = \text{Im} \left( \sum_{I^0, J^0} C_{0I^0}^{-1} \vec{\mu}^0_{I^0, J^0} C_{J^0 K} \right) - \left( \sum_{L^0, M^0} C_{K L^0}^{-1} \vec{M}^0_{L^0, M^0} C_{M^0 0} \right) \quad (5)$$

$$= \text{Im} \sum_{I^0, J^0} C_{I^0 0}^* C_{M^0 0} C_{L^0 K}^* C_{J^0 K} \vec{\mu}^0_{I^0, J^0} \cdot \vec{M}^0_{L^0, M^0}$$

Thus, in principle, each rotatory strength  $R_{0K}$  involves *all* of the electric and magnetic transition moments connecting all possible excited states of the groups.

Equivalently, the dipole strength matrix for the molecule is given by

$$D = \vec{\mu} : \vec{\mu}' \quad (6)$$

$$D_{I,J} = \vec{\mu}_{I,J} \cdot \vec{\mu}_{J,I}$$

These equations account for intensity transfer among the absorption bands (hyper- and hypochromicity) and for exciton selection rules.

Equation 4 contains implicitly the specialized mechanisms proposed by Kirkwood, Kuhn, Moffitt, and Condon, Altar, and Eyring. We will now outline the formal procedure for the simplification to produce the special models of optical activity. (1) Retain only those parts of the Hamiltonian which couple nondegenerate, electrically allowed excitation of different groups. Expand to first-order perturbation theory. (Provided that all elements  $V_{I,J}$  of the original Hamiltonian are small,  $C$  can be regarded as an infinitesimal unitary transformation with  $C_{II} \cong 1$  and  $C_{I^0, J^0} = -V_{I^0, J^0}/(E_{I^0} - E_{J^0})$ . This is equivalent to first-order perturbation theory.) This is the Kirkwood theory.<sup>3</sup> (2) The same as in step 1, but the states which are coupled are degenerate. Retain the secular equation as in the degenerate perturbation theory. This is the exciton theory of Moffitt,<sup>5</sup> as extended by Tinoco and coworkers.<sup>6</sup> (3) Retain only those parts of the Hamiltonian which are associated with the mixing of different states of excitation of the same group. Expand to first-order perturbation theory. Electrically and magnetically allowed states thus combined to give rotatory strength via the Condon, Altar, and Eyring theory.<sup>4</sup>

## II. A RESTRICTED THEORY OF OPTICAL ROTATION BASED ON SPECTROSCOPICALLY OBSERVABLE STATES

With molecules containing two or more peptide linkages, the absorption bands which are susceptible of measurement are either degenerate or very close to it and are of both the electric and magnetic type ( $\pi, \pi^*$  and  $n, \pi^*$  transitions). As will be shown, in this case

we are simultaneously confronted with substantial contributions from all of the mechanisms cited above. It is not satisfactory to try to estimate the contributions of the various terms one at a time because it can be shown that they are not additive. The approach adopted for this work is one which incorporates all mechanistic possibilities but which remains simple and tractable by virtue of two simplifying assumptions. The first is that the electronic states of individual groups are limited to a finite set, usually those which are well established by ground-state spectroscopy. This procedure is not recommended for molecules with isolated or very widely spread energy levels but appears to be a good approximation for the almost degenerate transitions of polypeptides.

The second approximation is that all parts of the secular equation are ignored except for those which pertain to singly excited states of the entire molecule. In particular, the ground configuration is excluded from the scheme of interaction as well as configurations involving the simultaneous excitation of two separate groups. This approximation is standard in many fields of spectroscopy but leads to a minor difficulty in the theory of optical rotation. It can be shown that the omission of simultaneously excited states in the coupling of nondegenerate electric transition moments leads either to an origin dependence of rotatory strength or to rotatory strengths which do not sum to zero, depending on the manner in which the approximation is introduced. The problem does not arise for degenerate levels and causes only small discrepancies for a limited energy span. This point will be discussed further in the section dealing with magnetic transition moments. In this fashion, the Hamiltonian matrix is reduced to the form

$$H = \begin{pmatrix} E_0 & \dots & \dots & \dots \\ \vdots & (1-1)(1-2) & \dots & (1-N) \\ \vdots & (2-1)(2-2) & \dots & (2-N) \\ \vdots & \dots & \dots & \dots \\ \vdots & (N-1)(N-2) & \dots & (N-N) \end{pmatrix} \quad (7)$$

in which  $E_0$ , the ground-state energy, is conventionally taken as zero. The reason that the ground state is retained even though it plays no part in the diagonalization process is that the ground state plays a fundamental role in the companion matrices  $\vec{\mu}$  and  $\vec{M}$  which are required for optical rotation calculations.  $H$  has been partitioned into submatrices representing specific group-group interactions. For example, (1-1) has the typical off-diagonal element  $(\lambda_1|V|\mu_1)$ , where  $\lambda$  and  $\mu$  represent different excited states of group 1. This element leads to the *mixing* of the states  $\lambda$  and  $\mu$  by virtue of the static, ground-state field of the rest of the groups. A typical element of (1-2) is  $(\lambda_1|V|\mu_2)$ , which leads to a *coupling* of the transition  $0 \rightarrow \lambda$  of group 1 with the transition  $0 \rightarrow \mu$  of group 2. This partitioning

and the physical interpretation of the matrix elements is illustrated in a simple example in the next section.

These assumptions lead to a considerable simplification of the problem. The transformation matrix  $C$  will now have all elements of the first row and column equal to zero ( $C_{0r} = C_{r0} = 0$ ), except  $C_{00} = 1$ . Hence, electric and magnetic transition moments from the ground state are given by

$$\begin{aligned} \vec{\mu}_{0K} &= \sum_{I^0, J^0} C_{0I^0}^{-1} \vec{\mu}^0_{I^0 J^0} C_{J^0 K} \\ &= \sum_{J^0} \vec{\mu}^0_{0 J^0} C_{J^0 K} \\ \vec{M}_{K0} &= \sum_{I^0, J^0} C_{KI^0}^{-1} \vec{M}^0_{I^0 J^0} C_{J^0 0} \\ &= \sum_{I^0} \vec{M}^0_{I^0 0} C^*_{I^0 K} \end{aligned} \quad (8)$$

It is now to be observed that only transition moments from the ground state appear in these expressions. This permits us to limit consideration to the first row of  $\vec{\mu}$  and  $\vec{M}$  and treat them as row vectors. We define

$$\vec{M}^0_{I^0} = \vec{M}^0_{I^0 0}; \quad \vec{\mu}^0_{I^0} = \vec{\mu}^0_{0 I^0}$$

It should be remembered that the ordering of subscripts is important for  $M$ , since  $\vec{M}^0_{I^0 0} = -\vec{M}^0_{0 I^0}$  for real wave functions. We then have

$$\vec{u} = \vec{\mu}^0 C; \quad \vec{M} = \vec{M}^0 C^* \quad (9)$$

These equations have a simple physical interpretation.  $\vec{\mu}^0$  and  $\vec{M}^0$  contain all the transition moments of the individual groups from the ground state. In principle, these moments are obtainable from ground-state spectroscopy. The transition moments of the assembled molecule are linear combinations of the original set with coefficients obtainable from the columns of  $C$ . In practice,  $C$  is usually a real matrix so that the electric and magnetic transition moments transform with the same coefficients. Thus the approximation embodied in eq 7 reduces the evaluation of the molecular electric and magnetic transition moments to an intuitively simple, linear vector transformation of those group moments which are obtainable from experiment or for which the most accurate theoretical work is available.

The rotatory and dipole strengths are given by

$$\begin{aligned} R &= \vec{u} : \vec{M}' = (\vec{\mu}^0 C) : (\vec{M}^0 C^*)' \\ R_K &= (\sum C_{I^0 K} \vec{\mu}^0_I) \cdot (\sum C_{I^0 K} \vec{M}^0_I) \end{aligned} \quad (10)$$

$$= \sum_{I^0, J^0} C_{I^0 K} C^*_{J^0 K} (\mu_{I^0} \cdot \vec{M}_{J^0})$$

$$D = \vec{u} \cdot \vec{u}' = (\vec{\mu}^0 C) : (\vec{\mu}^0 C)' \quad (11)$$

$$D_K = \sum_{I^0, J^0} C_{I^0 K} C^*_{J^0 K} (\mu_{I^0} \cdot \mu^*_{J^0})$$

The symbol : has the same significance as previously, so that  $R$  and  $D$  are row vectors with components equal to the rotatory and dipole strengths of the individual transitions of the entire molecule.

The magnetic transition moment requires further comment since it possesses an origin dependence of considerable importance. Neglecting spin magnetic moments, the magnetic moment operator is

$$\vec{M} = \frac{e}{2mc} \sum_a \vec{r}_a \times \vec{p}_a$$

where  $\vec{r}$  is the distance from an arbitrarily selected origin and  $\vec{p}$  is the operator for linear momentum. The summation is over electrons. In order to separate intrinsically magnetic transitions from those which acquire magnetic moment only by virtue of the separation of linear displacements,  $r_a$  is expressed as

$$r_a = \vec{R}_i + \vec{p}_{ia}$$

where  $\vec{R}_i$  is the position vector of a selected local origin in the  $i$ th group and  $\vec{p}_{ia}$  is the position vector of the electron relative to this new origin. The magnetic moment operator is then given by

$$\begin{aligned} \vec{M} &= \frac{e}{2mc} \sum_a \vec{p}_{ia} \times \vec{p}_a + \frac{e}{2mc} \vec{R}_i \times \sum_a \vec{p}_a \\ &= \vec{m}_i + \frac{e}{2mc} \vec{R}_i \times \vec{P} \end{aligned} \quad (12)$$

The first term is the intrinsic magnetic moment referred to group  $i$ . The appropriate group  $i$  is automatically selected in the process of forming matrix elements. Because  $\vec{M}$  is a one-electron operator and by assumption there is no electron exchange between groups, each matrix element in the original set specifies a localized excitation. The position of the local origin  $\vec{R}_i$  is chosen so as to minimize the value of the matrix element of  $\vec{m}_i$  for the given transition. Transitions for which this quantity cannot be made to vanish are called intrinsically magnetic transitions. Any arbitrariness which remains after the minimization of the matrix element of  $\vec{m}$  can be removed by minimizing the magnitudes of the quadrupole or higher multipole components. The selection of local origin can often be made on the basis of group symmetry. With groups of very low symmetry,  $\vec{R}_i$  will vary depending on the transition under consideration. The subscript  $i$  will hereafter be dropped in expressions for the matrix elements.

The formalism will now be rewritten to take into account the two sources of magnetic moment. The magnetic moment associated with transition  $K$  of the molecule is given by

$$\vec{M}_{K0} \equiv \vec{M}_K = (\vec{m})_K + \left( \frac{e}{2mc} R \times P \right)_K$$

since

$$\vec{P}_K = \vec{P}_{K0} = \frac{im\omega_{K0}}{e} \vec{\mu}_{K0} \quad (13)$$

we have

$$\vec{M}_K = \vec{m}_K + \frac{i\omega_{K0}}{2c} (R \times \mu)_K \quad (14)$$

where  $\omega_{K0}$  is the circular frequency associated with the transition  $K$ . The components of  $\vec{m}$  and  $\vec{R} \times \vec{\mu}$  required in eq 13 are found from the transformation equations (eq 8), as

$$\vec{m} = \vec{m}^0 C^*; \quad (\vec{R} \times \vec{\mu}) = (\vec{R} \times \vec{\mu})^0 C^* \quad (15)$$

It would appear more direct to write

$$\vec{M} = \left( \vec{m} + \frac{e}{2mc} \vec{R} \times \vec{p} \right)^0 C^* \quad (16)$$

rather than eq 13 and 14. The two formalisms differ only in that in the text the Heisenberg transformation (eq 13) is applied to the final eigenstates, whereas in eq 16 it is applied in the original basis set. If the problem were being solved rigorously, it would not make any difference at which level the transformation is made. However, because of the use of a limited basis set, the following difficulties arise when the electrically allowed transitions of the zeroth-order system are not degenerate. If the transformation  $\vec{p} \rightarrow \vec{\mu}$  is made in the original set, rotatory strength is conserved (*i.e.*, sums to zero<sup>7</sup>), but the optical rotation is origin dependent. If it is made in the final set, there is no origin dependence, but the rotatory strength does not sum to zero for all the transitions. The problem does not arise with degenerate electrically allowed transitions, nor does it arise in other similar optical problems such as the borrowing of intensity, energy transfer, etc. The inclusion of double excited states which mix with the ground state eliminates these difficulties but increases enormously the computational problem involved, while making only small changes in the results. The procedure of the text which gives no origin dependence and slightly nonconservative rotatory strengths is adopted in this work.

This completes the formal development of the theory. The basic approximation of this section has been to reduce the set of interacting states to a finite set of singly excited states of the entire molecule. The major consequence of this approximation is that all components of the  $\vec{\mu}$  and  $\vec{M}$  matrices other than those in the first row drop out of the problem. As a result,  $\vec{\mu}$  and  $\vec{M}$  transform like vectors in the passage from the basis functions describing transitions isolated in individual groups to the final functions describing excitations extending over the molecule. (The transformation is linear in the elements of the transformation matrix  $C$  in eq 9, rather than bilinear as in eq 3.) There is thus a strong formal resemblance between this treatment and the classical mechanical treatment of an assembly of coupled oscillators. The elimination of matrix elements of  $\vec{\mu}$  and  $\vec{M}$  other than the first row and column

(7) C. A. Bush and J. Brahms, *J. Chem. Phys.*, **46**, 79 (1967).

appears to be necessary at this stage of development of the subject, since practically all information available at present is restricted to transitions from the ground state.

The set of excited states to be used for a given group must include as a minimum all the states which can be observed polarimetrically. Often there are fairly well characterized states in the Schumann region of the ultraviolet which can be added to this minimal set. There remains then the question of all the remaining transitions to states of very high energy. These may be introduced into the formalism as effective transitions deep in the ultraviolet with transition moments and energies selected to reproduce (together with the known transitions) the polarizability and anisotropy of polarizability of the group under consideration. This method of inclusion was introduced by Fitts and Kirkwood<sup>8</sup> and has been consistently utilized by Tinoco and his collaborators for a number of years. Another procedure (which is used in this work) is to ignore all lower bands and see how far one can go in interpreting the optical rotation of molecules in terms of known spectral transitions. A necessary condition for the use of this approach is that the rotatory strengths of the observed transitions should sum approximately to zero. A practical criterion is to evaluate  $\sum R_i / \sum |R_i|$  experimentally. If the observed Cotton effects are all of one sign, or predominantly of one sign, this will be nonzero, and lower bands must be included in the theory; if this parameter is much smaller than 1, say of the order of 0.1, then the lower bands may be ignored as a first approximation. The condition is not sufficient, since it is possible that an interchange of rotatory strength takes place between the observed and unobserved bands which is significant but sums to zero.

In either case, the method is open to cumulative improvement. Each newly characterized absorption of the molecule may be accommodated by adding elements to  $\vec{u}^0, \vec{M}^0$ , and  $H$ , leading to revised values for the elements of  $\vec{u}, \vec{M}, R, D$ , and  $H_{\text{diag}}$ .

### III. Theory for Two Peptide Groups

We now apply the theory outlined above to the problem of two peptide groups. The absorption bands whose rotatory properties can be observed experimentally are the  $\pi, \pi^*$  and  $n, \pi^*$  transitions. The position of these bands depends on solvent and substitution. Wave functions, transition moments, etc., appropriate for these transitions have been discussed in a separate work<sup>9</sup> and are briefly summarized in Table I. Other peptide absorption bands have been assigned at lower wavelengths,<sup>10</sup> and there have been recent suggestions of another band at long wavelengths.<sup>11,12</sup> Because of the lack of quantitative information concerning these bands, they cannot be included in the calculations without an unpleasant depreciation in the level of accuracy of the work. To the extent that the optical

**Table I:** Amide Parameters for a Typical Calculation  
 $(E_{n,\pi^*} = 47,170 \text{ cm}^{-1} (212 \text{ m}\mu)^a$  and  
 $E_{\pi,\pi^*} = 52,630 \text{ cm}^{-1} (190 \text{ m}\mu)^b)^c$

Description	Position and moment vectors			Charge <sup>d</sup>	
	x	y	z		
1	$\vec{R}_{C'}$	1.53	0	0	2.04
2	$\vec{R}_H$	1.58	2.02	0	1.25
3	$\vec{R}_N$	2.13	1.18	0	-1.44
4	$\vec{R}_O$	2.16	-1.05	0	-1.87
5	$\vec{\mu}_{\pi,\pi^*}$	-0.435	-3.019	0	...
6	$\vec{R}_\mu$	2.15	0.02	0	...
7	$\vec{m}_{n,\pi^*}$	0.68	1.12	0	...
8	$\vec{R}_1$	2.540	-0.847	0.440	-0.40
9	$\vec{R}_2$	2.540	-0.847	-0.440	0.40
10	$Q_O \begin{cases} \vec{R}_3 \\ \vec{R}_4 \end{cases}$	1.786	-1.281	-0.440	-0.40
11	$\vec{R}_4$	1.768	-1.281	0.440	0.40
12	$\vec{R}_1$	1.907	0.227	0.440	-0.60
13	$Q_C \begin{cases} \vec{R}_2 \\ \vec{R}_3 \end{cases}$	1.907	0.227	-0.440	0.60
14	$\vec{R}_3$	1.153	-0.227	-0.440	-0.60
15	$\vec{R}_4$	1.135	-0.227	0.440	0.60
16	$C_\alpha'$	1.53	0	0.707	0.41
17	$C'_b$	1.53	0	-0.707	0.41
18	$N_a$	2.13	1.18	0.589	-0.86
19	$N_b$	2.13	1.18	-0.589	-0.86
20	$O_a$	2.16	-1.05	0.505	0.45
21	$O_b$	2.16	-1.05	-0.505	0.45

<sup>a</sup> This wavelength is appropriate for a simple secondary amide unit in aqueous solution, as judged from curve fitting a number of Cotton effects in model systems. The  $n, \pi^*$  transition seems to be 3–5 m $\mu$  higher in structureless polypeptides. <sup>b</sup> This wavelength is appropriate for a secondary amide in aqueous solution (E. B. Nielsen and J. A. Schellman, *J. Phys. Chem.*, **71**, 2297 (1967)). <sup>c</sup> Rows 1–4 are the position vectors of the atoms with their assumed static charges. Rows 5 and 6 give the components of the  $\pi, \pi^*$  electric transition moment (in Debye units) and the assumed position of this moment. Row 7 gives the  $n, \pi^*$  magnetic transition moment vector in Bohr magnetons. Rows 8–15 give the positions and charges of the distributed monopoles comprising the transition quadrupoles of the O and C atoms. These are the atomic  $P_y \rightarrow P_z$  quadrupole charges and are multiplied by the appropriate coefficients during calculation.<sup>8</sup> It should be noted that  $(\pi, \pi^* | Q | n, \pi^*)$  is used in the Condon mechanism and  $(0 | Q | n, \pi^*)$  is used in the  $\mu-m$  mechanism. See ref 9. <sup>d</sup> These coordinates refer to a convention in which the origin is at the  $\alpha$  carbon, the positive  $x$  axis goes from  $C_\alpha$  to  $C'$ , and the amide group lies in the  $xy$  plane with N in the first quadrant. The units are Ångströms. <sup>e</sup> The units of charge are  $10^{-10}$  esu; i.e., the charge of the electron in these units is -4.8.

rotatory properties are dominated by the interaction of the two chosen bands, the theory outlined here will be a faithful representation of the problem. In many

- (8) D. D. Fitts and J. G. Kirkwood, *Proc. Nat. Acad. Sci. U. S.*, **43**, 1046 (1957).
- (9) J. A. Schellman and E. B. Nielsen, *J. Phys. Chem.*, **71**, 3914 (1967).
- (10) E. E. Barnes and W. T. Simpson, *J. Chem. Phys.*, **39**, 670 (1963).
- (11) H. Basch, M. B. Robin, and N. A. Kuebler, *ibid.*, **47**, 1201 (1967).
- (12) D. G. Barnes and W. Rhodes, *ibid.*, **48**, 817 (1968).

$$H = \begin{pmatrix} \begin{pmatrix} E_{\alpha_1} & \langle \alpha_1 | V | \beta_1 \rangle \\ \langle \beta_1 | V | \alpha_1 \rangle & E_{\beta_1} \end{pmatrix} & \begin{pmatrix} \langle \alpha_1 | V | \alpha_2 \rangle & \langle \alpha_1 | V | \beta_2 \rangle \\ \langle \beta_1 | V | \alpha_2 \rangle & \langle \beta_1 | V | \beta_2 \rangle \end{pmatrix} \\ \begin{pmatrix} \langle \alpha_2 | V | \alpha_1 \rangle & \langle \alpha_2 | V | \beta_1 \rangle \\ \langle \beta_2 | V | \alpha_1 \rangle & \langle \beta_2 | V | \beta_1 \rangle \end{pmatrix} & \begin{pmatrix} E_{\alpha_2} & \langle \alpha_2 | V | \beta_2 \rangle \\ \langle \beta_2 | V | \alpha_2 \rangle & E_{\beta_2} \end{pmatrix} \end{pmatrix} \quad (17)$$

instances, the experimentally determined rotatory strengths satisfy the criteria discussed in the preceding paragraph, presumably because of the near degeneracy of the  $n, \pi^*$  and  $\pi, \pi^*$  bands. The ultimate test of the approximations is in the comparison of predictions with experimental results, and here the situation looks promising.

*The Secular Determinant.* With two states for each peptide, the Hamiltonian (eq 7) reduces to the form

$$\begin{pmatrix} (1-1) & (1-2) \\ (2-1) & (2-2) \end{pmatrix}$$

where each of the submatrices is  $2 \times 2$ . The ground state has been deleted, since it remains invariant by assumption. There are four singly excited states of the dimer:  $|\alpha_1\rangle$ ,  $|\beta_1\rangle$ ,  $|\alpha_2\rangle$ ,  $|\beta_2\rangle$ . The symbols 0,  $\alpha$ , and  $\beta$ , designate, respectively, the ground,  $n, \pi^*$  and  $\pi, \pi^*$  states. Written out in full, the Hamiltonian matrix is as shown in eq 17. We shall now examine in detail the relationship of the elements of this matrix with the various theories of optical rotation which were outlined in general in the first section. The only off-diagonal element in (1-1) is

$$\int \varphi_1^\alpha \varphi_1^\beta V(\varphi_2^0)^2 d\tau_1 d\tau_2$$

This is seen to involve the mixing of the  $n, \pi^*$  and  $\pi, \pi^*$  states of group 1 by the perturbing field of group 2 in its ground state. The mixed state accordingly has the magnetic transition moment of the  $\alpha_1$  and the electric moment of the  $\beta_1$  leading to optical rotation. This is the static or one-electron mechanism of Condon, Altar, and Eyring (CAE). The off-diagonal element of (2-2) has a similar interpretation with the roles of the groups reversed.

The elements of (1-2) and (2-1) are of three types:  $\int \varphi_1^0 \varphi_1^\beta V \varphi_2^0 \varphi_2^\beta d\tau_1 d\tau_2$ ,  $\int \varphi_1^0 \varphi_1^\beta V \varphi_2^0 \varphi_2^\alpha d\tau_1 d\tau_2$ , and  $\int \varphi_1^0 \varphi_1^\alpha V \varphi_2^0 \varphi_2^\alpha d\tau_1 d\tau_2$ . The first involves the coupling of the electric transition moments of the two  $\pi, \pi^*$  transitions. This interaction (K) plays the fundamental role in the theories of Kirkwood, Kuhn, and Moffitt. The second type involves the coupling of the  $n, \pi^*$  transition of one group with the  $\pi, \pi^*$  transition of the other. This possibility, though long realized,<sup>13</sup> has only been incorporated in more recent calculations of optical rotation.<sup>14-17</sup> The energy of interaction arises between the quadrupolar charge distribution of the  $n, \pi^*$  transition of one group and the dipolar charge distribution of the  $\pi, \pi^*$  transition of the other. This mech-

anism, here designated as  $\mu-m$ , is of fundamental importance in the interpretation of the optical rotation of two peptide groups, since it is seen by calculation that it adds to, deletes from, or completely overshadows the CAE mechanism, depending on conformation. The energy arising from the third type of matrix element involve the direct coupling of the  $n, \pi^*$  transition of the two groups and is so small that it is neglected in our calculations. With these mechanistic definitions we may paraphrase the Hamiltonian matrix as

$$\begin{pmatrix} \begin{pmatrix} E_{\alpha_1} & \text{CAE} \\ \text{CAE} & E_{\beta_1} \end{pmatrix} & \begin{pmatrix} 0 & \mu_1 m_1 \\ \mu_1 m_2 & K \end{pmatrix} \\ \begin{pmatrix} 0 & \mu_1 m_2 \\ \mu_2 m_1 & K \end{pmatrix} & \begin{pmatrix} E_{\alpha_2} & \text{CAE} \\ \text{CAE} & E_{\beta_2} \end{pmatrix} \end{pmatrix}$$

where the symbols now refer to the optical rotation mechanism to which the elements contribute. By appropriate deletions it is possible to establish approximately the relative contributions of the various mechanisms, though they are not additive.

*Evaluation of the Matrix Elements.* The off-diagonal matrix elements of  $H$  were evaluated by the London method of monopoles. Since a complete description of the application of this method to the peptide group has recently been given by Woody and Tinoco,<sup>14</sup> we will list only the instances where our approximations differ from theirs. (1) We have used the wave functions derived in eq 9 rather than the LCAO orbitals of Nagakura. A major difference arises from the delocalization of the  $n$  orbital (Table I). This leads to a small change in the value for the magnetic moment of the  $n, \pi^*$  transition and to a pair of quadrupolar charge distributions centered about the C and O atoms rather than the single distribution about O which was used by Woody and Tinoco. (2) The positions of the monopoles of the  $n, \pi^*$  transition were located using the numerical integration of Hartree-Fock functions rather than Slater orbitals. Regions close to the nucleus make a major contribution to these integrals, and it is in this

(13) W. J. Kauzmann, J. E. Walter, and H. Eyring, *Chem. Rev.*, **26**, 339 (1940).

(14) R. W. Woody and I. Tinoco, *J. Chem. Phys.*, **46**, 4927 (1967); R. W. Woody, Ph.D. Thesis, University of California, Berkeley, Calif., 1962.

(15) D. J. Caldwell and H. Eyring, *Rev. Mod. Phys.*, **35**, 577 (1963).

(16) J. Schellman and E. B. Nielsen in "The Conformation of Biopolymers," G. N. Ramachandran, Ed., Academic Press, New York, N. Y., 1967.

(17) E. G. Höhn and O. E. Weigang, *J. Chem. Phys.*, **48**, 1127 (1968).

region that Slater orbitals tend to be least accurate. The charges and their positions are given in Table I. (3) The same method was used to establish the distribution over atoms of the  $\pi, \pi^*$  transition moment. However, these were not localized on the nuclei but were divided between the centers of the contacting spheres of the Parr approximation.<sup>18</sup> This leads to differences in results only when there is virtual contact of the  $\pi$  electron clouds of the two groups.

*Computational Methods.* All the off-diagonal elements of  $H$  depend on the relative positions and orientations of the two peptide groups. In our calculations, the conformation is not fixed but is allowed to vary throughout the range of structural possibilities of the compound. The positions of the atoms within the peptide groups are taken from X-ray investigations of appropriate compounds or from the assignments of Pauling and Corey. The bond angle at the  $\alpha$ -carbon atom is set at  $110^\circ$  unless the molecule under consideration has a specialized structure (*e.g.*, diketopiperazines). *cis*-Peptide and *trans*-peptide are considered as separate problems, so that the conformation of the dimer is determined by the values of the conformational angles  $\varphi$  and  $\psi$ .<sup>19</sup>

The emphasis of the present studies, both experiment and theory, is the exploration of the functional dependence of the rotatory strength on the values of  $\varphi$  and  $\psi$ . Experimentally, this is done by the study of model compounds which are limited to different regions of the  $\varphi, \psi$  plane. Theoretically, these angles are variable parameters in the calculation.

The numerical calculations are performed with a digital computer using a program which combines the conformational and optical aspects of the problem. The input consists of experimentally determined<sup>20</sup> energies for the various transitions, the components of the electric and magnetic transition moments, position vectors for all charge monopoles required in the calculation, position vectors for the electric transition moments, and values, or ranges of values, for the angles  $\varphi$  and  $\psi$ .

The calculations are performed in the following steps. (1) All position and moment vectors are transformed into a common coordinate system. The transformation matrix depends on the chosen value of the bond angle connecting the peptide groups and the current value of  $\varphi$  and  $\psi$ . These angles are arranged to vary by selected intervals to explore any region of the conformational map. (2) For energy calculations, all off-diagonal elements of the Hamiltonian are calculated as well as the electrostatic conformational energy. The latter is not a part of the optical calculations but helps to find regions of electrostatic stability. This is often of importance when  $\varphi$  or  $\psi$  can vary in a molecule. This calculation, plus a standard exclusion calculation, is of great help in deciding the most probable conformation of a molecule with one degree of freedom. (3) The Hamiltonian is diagonalized by a standard method for

symmetric matrices which simultaneously computes the elements of the  $C$  matrix. The column vectors of this matrix are the eigenvectors of the interaction problem. (4) The optical properties are calculated as described in the first section

$$\vec{m} = \vec{m}^0 C; \quad \vec{u} = \vec{u}^0 C; \quad (\vec{R} \times \vec{u}) = (\vec{R} \times \vec{u})^0 C; \quad D = \vec{u} : \vec{u}' ; \quad R = \text{Im} (\vec{u} : \vec{M}')$$

Here  $\vec{m}$ ,  $\vec{u}$ ,  $R$ , and  $D$  are row vectors with elements for each of the four transitions, and the complex-conjugate sign on  $C$  has been dropped since it is a real matrix in the calculation.

The full output for a given calculation consists of the current value of  $\varphi$  and  $\psi$ , the electrostatic energy, and the energies, wavelengths, eigenvectors, dipole strengths, and rotatory strengths of each of the four transitions. In the reporting of results the  $n, \pi^*$  transitions are combined since they remain essentially degenerate. Alternatively, the optical properties may be mapped as a function of  $\varphi$  and  $\psi$  in tabular form. The maps shown in Figure 2 *et seq.* were obtained in this way.

The program is extendable with minor variations to cover any number of chromophores in any number of groups. There is an obvious practical limitation of the number of degrees of freedom which can be tolerated.

#### IV. Results

A brief calculation shows that even so simple a system as a pair of peptide units connected by an  $\alpha$ -carbon atom presents 20 separate problems. These arise because of the possibilities that either of the peptide units can be *cis* or *trans* and that they can be primary, secondary, or tertiary amide groups. The distinction between *cis* and *trans* produces considerable changes in transition moment geometry and in the allowed regions of conformational space (as may be seen from the standard exclusion diagrams (Figure 1)) but little change in energy levels. On the other hand, the principal effect of substitution on the amide group is in the change in energy levels of the  $\pi, \pi^*$  state.<sup>20</sup> In addition to these variations, we have those which are caused by solvent. We are not speaking here of the effect of solvent on conformation but of its effect on the energy levels. For example, a solvent shift which brings the  $n, \pi^*$  and  $\pi, \pi^*$  bands closer together will increase the effect of a given perturbation at constant conformation, producing substantial changes in optical rotatory properties. Of all possible systems, four have been

(18) R. G. Parr, *J. Chem. Phys.*, **20**, 1499 (1952).

(19) J. T. Edsall, P. J. Flory, J. C. Kendrew, A. M. Liquori, G. Nementy, G. N. Ramachandran, and H. A. Scheraga, *Biopolymers*, **4**, 121 (1966).

(20) E. B. Nielsen and J. A. Schellman, *J. Phys. Chem.*, **71**, 2297 (1967).

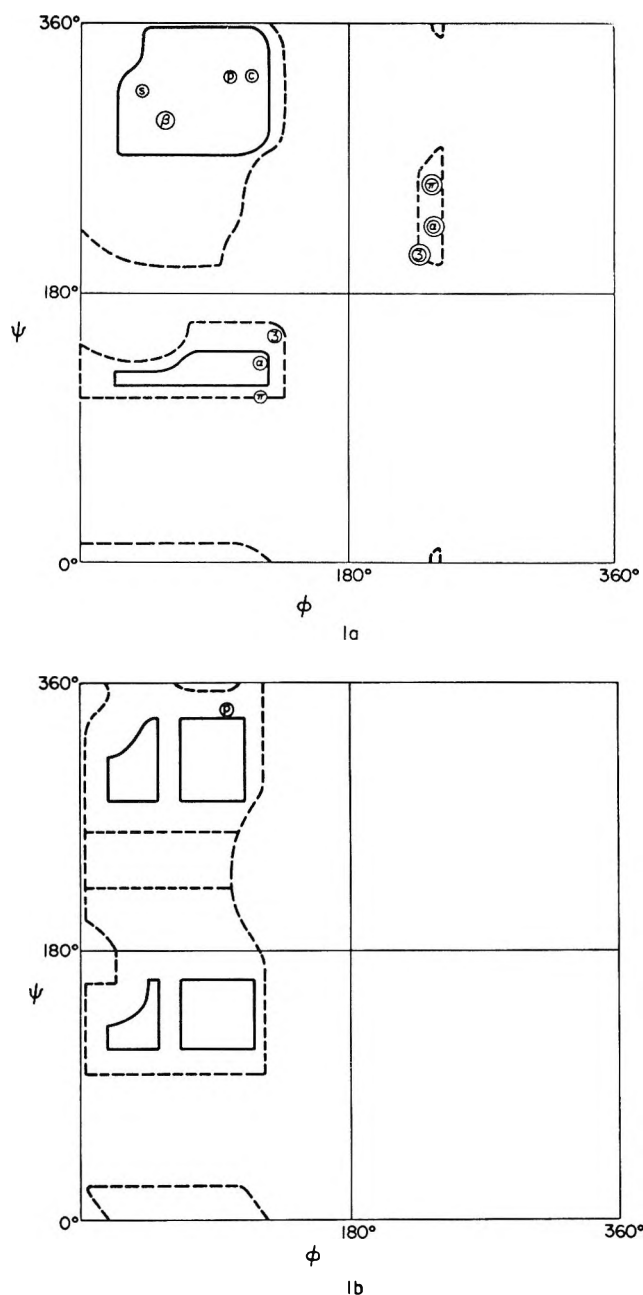


Figure 1. Standard exclusion diagrams (Ramachandran) for two peptide units in (a) *trans-trans* and (b) *cis-cis* conformation (G. N. Ramachandran, *Advan. Protein Chem.*, in press): ( $\alpha$ ),  $\alpha$  helix; ( $\pi$ ),  $\pi$  helix; ( $3_{10}$ ),  $3_{10}$  helix; ( $\beta$ ),  $\beta$  structure; ( $s$ ), silk fibroin structure; ( $p$ ), polyproline; ( $c$ ), collagen.

selected for general discussion: (1) the *trans-trans* case, with two secondary amide groups (this corresponds to a dimer segment of an ordinary polypeptide chain); (2) the *trans-trans* case, with a tertiary amide followed by a secondary amide (this corresponds to the appearance of a proline residue in a polypeptide chain and is used as a model for the nondegenerate case); (3) two tertiary residues, both of which are *trans* (representing a segment of polyproline II and poly(N-methyl-L-alanine)); and (4) two tertiary residues, both of which are *cis* (representing a segment of polyproline I). Though

these four cases correspond to important sequential situations of biopolymers, it must be emphasized that the calculations to be presented are for the dimer case only. Only those optical properties which depend predominantly on the interactions of sequential neighbors can be extrapolated from the dimer to the polymer. For example, all exciton effects in ordered polymers will be misrepresented by the dimer calculations. In this sharply limited context, a few qualitative conclusions concerning biopolymers will be drawn in the last section of this discussion.

As outlined in the previous section, the method is to solve the secular equation and calculate the optical properties of all four transitions of the dipeptide as a function of the conformational angles  $\varphi$  and  $\psi$ . In practice, the two  $n, \pi^*$  transitions are not split by the weak interactions which produce their optical rotation, and the total  $n, \pi^*$  rotatory strength is recorded as the sum of the two overlapping transitions. The results are then the rotatory strengths of three transitions as a function of  $\varphi$  and  $\psi$ . Because  $R$  is essentially conservative in the calculations (exactly conservative for the degenerate cases), it is only necessary to report the rotatory strength of two of the transitions, usually the  $n, \pi^*$  combination and the longest wavelength  $\pi, \pi^*$ . Since all four transitions are combined in the diamide molecule, the designations  $\pi, \pi^*$  and  $n, \pi^*$  are not exact. The mixing of these two types of transitions is in general rather small, so that they retain their identity to a considerable extent, as may be seen by looking at the computed coefficients of the matrix  $C$ . The effect is in fact rarely measurable experimentally with other optical properties which do not depend explicitly on the mixing of predominantly magnetically allowed transitions with electrically allowed transitions. Even with these reductions, the results are generally too voluminous to report in quantitative form. Instead, they will be presented as qualitative diagrams over the angular phase space (Figure 2). The + and - signs designate the sign of the rotatory strength in the regions specified and the curved lines are nodal lines, where the rotatory strength is predicted to vanish. When the conformational variation is reduced to one angle, it becomes easy to present the data in a quantitative fashion and this will be done in a few cases.

With regard to comparison with experiment, the only meaningful result is that which is obtained by solving the full secular equation which combines all three of the mechanisms. However, for heuristic purposes, we shall present results of calculations in which certain off-diagonal elements of the secular equation are set equal to zero so that it is possible to explore the general pattern of behavior produced by the separate mechanisms. In these simplified calculations one is dealing with only two molecular transitions and a single interaction. The rotatory strength then turns out to be a product of two factors: one which describes the geometry of the electric and

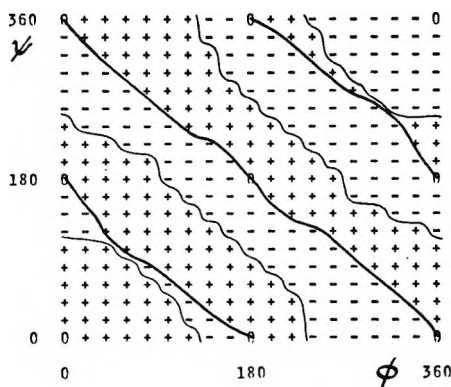


Figure 2. Map of  $\pi, \pi^*$  rotational strength (*trans, trans*-peptides, secondary-secondary combination, i.e., degenerate case, Kirkwood terms only). The sign refers to the nearest (low-energy)  $\pi, \pi^*$  transition. Heavy and light lines refer to optical and interaction nodes, respectively.

magnetic transition dipole moments (this will be called the optical factor) and the other (the interaction factor) which represents the perturbation energy which couples or mixes the electric and magnetic dipoles and is the origin of exciton splits and spectral shifts. The optical factors for the three mechanisms are

$$\vec{R}_{ij} \cdot \vec{\mu}_i \times \vec{\mu}_j \quad (\text{Kirkwood-Moffitt})$$

$$\vec{\mu}_i \cdot \vec{m}_j \quad (\mu-m \text{ mechanism})$$

$$\vec{\mu}_i \cdot \vec{m}_i \quad (\text{CAE mechanism})$$

where  $i$  and  $j$  represent the groups in which the transition dipoles  $\mu$  and  $m$  arise and  $\vec{R}_{ij} = \vec{R}_i - \vec{R}_j$ . In the first expression, certain constants independent of geometry have been suppressed.

The interaction factors are the off-diagonal elements of the original Hamiltonian and their form depends on the degree of sophistication of the calculations. The multipole approximation is given (for example) in ref 21. The monopole method described in section III is more accurate and is used in this work. It is easy to see how the three types of optical factor arise in the present formalism by constructing the various types of products contained in the rotatory strength *via* eq 9 and 14.

In some of the figures, nodal lines for the rotatory strength will be separately designated as "optical nodes" when the optical factor vanishes and as "interaction nodes" when the coupling or mixing energy vanishes. (Note that in the present treatment the optical factor for the CAE mechanism is invariant to changes in conformation so that there are only interaction nodes.) When contributions to a rotatory strength arise from a number of interactions or mechanisms, the rotatory strength is a sum of products of optical and interaction factors, and the interpretation of nodal lines loses its simplicity. It should be emphasized that, although the contributions of these mechanisms are additive in the approximation of the

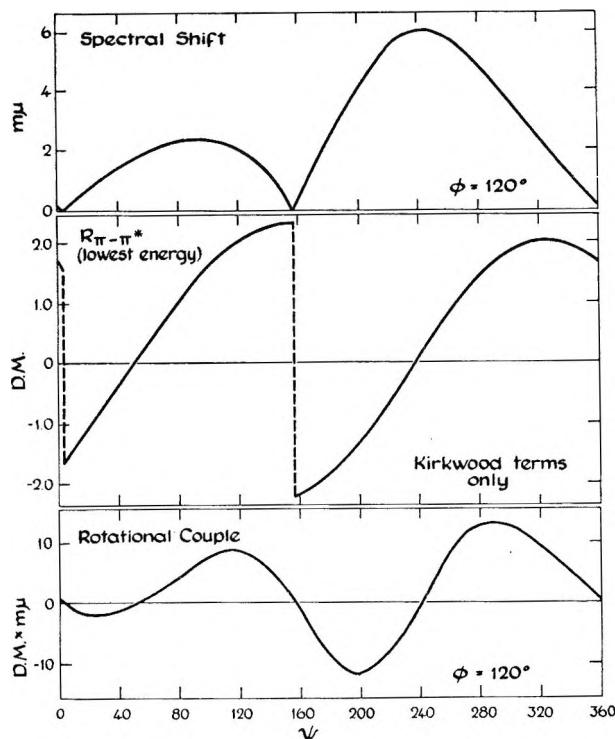


Figure 3. Details of Figure 2, for  $\varphi = 120^\circ$ ,  $\psi$  varied (Kirkwood terms only): (a) Spectral shift, interaction energy, (total  $\pi, \pi^*$  separation is twice the shift); (b) rotational strength of nearest  $\pi, \pi^*$  transition; (c) rotational couple (units,  $DM \text{ m}\mu$ ).

first-order perturbation theory, this is not true with a complete-diagonalization procedure. For example, the two  $n, \pi^*$  transitions are very inefficiently coupled to one another directly because of the smallness of quadrupole-quadrupole interactions. On the other hand, each  $n, \pi^*$  transition is mixed with the  $\pi, \pi^*$  transition of the same group, which is strongly coupled to the other chromophore, leading to an effective coupling of the  $n, \pi^*$  transitions.

*trans, trans-Peptides.* 1. *Secondary-Secondary Combination.* Calculations were performed for a secondary-secondary amide combination with  $E_{\alpha_1} = E_{\alpha_2} = 47,600 \text{ cm}^{-1}$  (210 m $\mu$ ) and  $E_{\beta_1} = E_{\beta_2} = 52,600 \text{ cm}^{-1}$  (190 m $\mu$ ). Figure 2 shows the qualitative behavior of the  $\pi, \pi^*$  transition when the calculation is restricted to the dipole-dipole coupling mechanism. Since the rotatory strengths of the two transitions are equal and opposite in sign, only the rotatory strength of the longest wavelength band of the exciton split is shown. Because of the identity of the assumed initial  $\pi, \pi^*$  energies, this is a case of degenerate interaction. The "optical" and "interaction" nodes are designated by heavy and light lines, respectively. A clear representation of the meaning of optical and interaction nodes in the degenerate case may be obtained by viewing the quantitative results for a line segment of the two-dimensional diagram. Figure 3 shows the behavior as

(21) J. A. Schellman, *Accounts Chem. Res.*, 1, 144 (1968).

one proceeds up the  $\varphi$ - $\psi$  diagram along the line  $\varphi = 120^\circ$ . The upper part of the graph shows the energy of the exciton splitting, in millimicrons, as predicted by the calculations. The splitting energy is twice the interaction energy. The second part of the figure shows the rotational strength of the lowest energy transition as a function of  $\psi$ . There are two genuine nodes in this function, at about 50 and  $240^\circ$ , which are the optical nodes discussed above. The discontinuities at 2 and  $160^\circ$  correspond to the interaction nodes and result from the following. There are two fully coupled dimer transitions in the exciton case, differing by a phase factor. Both have large rotatory strengths in the region of  $\psi = 2$  and  $160^\circ$  but are opposite in sign. At these points, they occur at the same wavelength because the perturbation energy is zero. The net rotatory strength at the common wavelength vanishes. When one proceeds to the other side, the two transitions have exchanged roles, leading to a change in sign of the nearest wavelength Cotton effect.

It can be shown that, when two absorption bands of opposite and equal rotatory strength are closer to one another than a half-band-width, the experimentally observable quantity is the rotatory couple, that is, the magnitude of the rotatory strength multiplied by the difference in wavelength of the two bands. The third part of the figure shows a plot of the rotatory couple as a function of  $\psi$ . It is seen to vanish at both the optical and energetic nodes.

Figure 4 shows the qualitative behavior of the  $n, \pi^*$  rotational strength as a function of the different mechanisms. Only the left half is shown; the right half may be obtained by symmetry by rotation about ( $\varphi = 180^\circ, \psi = 180^\circ$ ) and reversing the plus and minus signs. Figure 4a shows the rotational strength deriving from a pure CAE mechanism. In this calculation the rotatory strength arises as separate contributions from the two groups. Only mixing between the transitions of the group is produced, the perturbation being the asymmetric electrostatic field of the other group. Certain correlations may be seen with the map of Figure 2. When both  $\varphi$  and  $\psi$  are any multiple of  $180^\circ$ , the  $n, \pi^*$  rotatory strength, like the  $\pi, \pi^*$  rotatory strength, is zero because of symmetry. Apart from this, the  $n, \pi^*$  rotatory strength in Figure 4a only roughly parallels the nodes of Figure 2. This is because (1) the rotatory strength plotted in Figure 4a is the sum of the rotatory strength developed in the two groups (the symmetry relations at the two groups are nonequivalent because of the directional property of the polypeptide chain); (2) the absence of optical nodes in the CAE case; and (3) the different forms for the perturbation energy function. In Figure 4b the effect of including both the CAE and Kirkwood mechanisms is shown. With few exceptions, the map is qualitatively identical with Figure 4a, and the magnitude of the predicted rotatory strength is affected in only a minor way. This

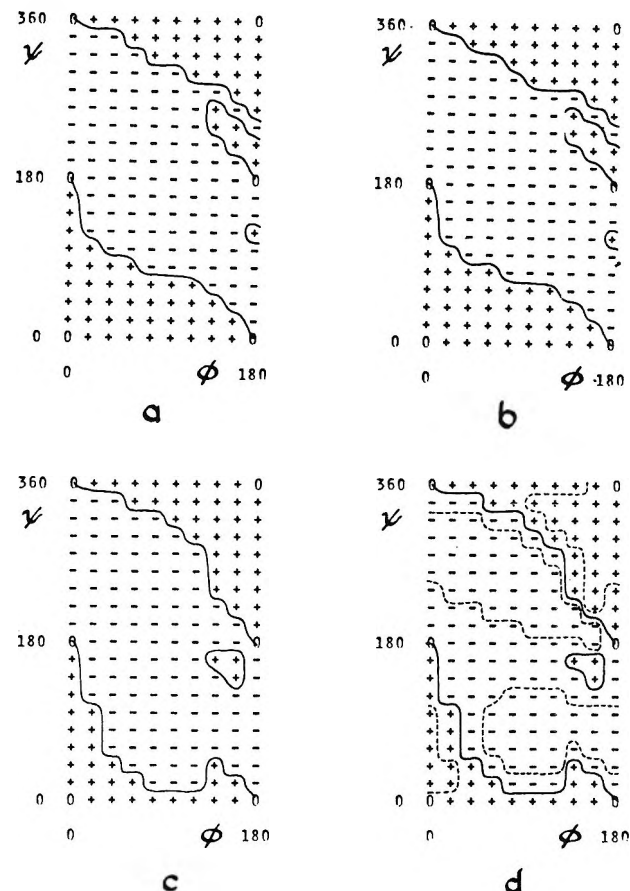


Figure 4. Maps of total  $n, \pi^*$  rotational strength (*trans, trans-peptides, secondary-secondary combination*). Development of  $n, \pi^*$  rotational strength by: (a) CAE mechanism, (b) CAE + K mechanism, (c) CAE + K -  $\mu$ - $m$  mechanism (full theory), (d) nodes as in c (dotted lines are contours for  $R = \pm 0.1$  DM).

shows that the CAE and Kirkwood-Moffitt calculations are essentially superimposable, at this level. This fact provided the rationale for the grafting of the  $n, \pi^*$  transition onto the exciton theory of the optical rotation of the  $\alpha$  helix in an earlier work.<sup>22</sup> By contrast, Figure 4c shows clearly that the direct coupling of  $\alpha_1$ - $\beta_2$  and  $\alpha_2$ - $\beta_1$  which is provided by the  $\mu$ - $m$  mechanism leads to substantial changes in the pattern. The two positive regions in the upper half of the map now coincide, and a new region appears around  $(150^\circ, 150^\circ)$ . Inspection of the exclusion map (Figure 1) or the calculated electrostatic energy shows this region to be strictly forbidden, owing to unfavorable proximity of the carbonyl groups. In Figure 4c the general course of the nodes is not regular, since it is determined by the sum of all the interactions in both groups, as represented by the full secular matrix of eq 17. Also, the magnitude of the predicted rotatory strength is considerably different in many cases, as may be seen from the course of the contours in Figure 4d and as will be seen later in consideration of specific conformations.

(22) J. A. Schellman and P. J. Oriel, *J. Chem. Phys.*, **37**, 2114 (1962).

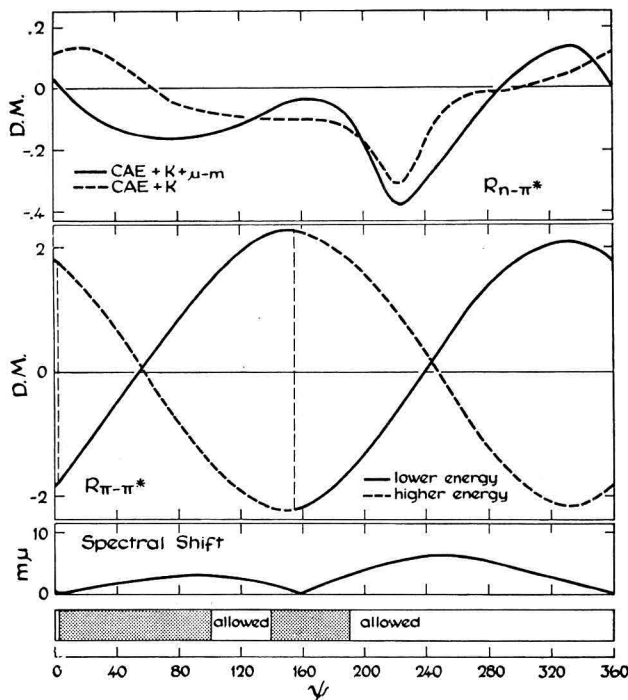


Figure 5. Details of full theory for  $\varphi = 120^\circ$ ,  $\psi$  varied (*trans, trans*-peptides, secondary-secondary combination):  
(a) contributions of different mechanisms to the total  $n, n^*$  rotational strength; (b) rotational strength of the  $\pi, \pi^*$  system;  
(c) spectral shift of each  $\pi, \pi^*$  transition; (d) the allowed regions of conformational space for this combination.

The quantitative results of the solution of the full secular equation are illustrated in Figure 5 with the section taken at  $\varphi = 120^\circ$ . The upper figure represents the rotatory strength in Debye magnetons of the  $n, n^*$  transition as a function of  $\psi$ . The contributions of the different mechanistic approximations to the full theory can readily be seen. We wish to call attention to the fact that the magnitude of the  $n, n^*$  Cotton effect is predicted to exceed 0.1 DM over a good portion of the allowed region on the line segment (illustrated in Figure 5). These values are in accord with experimental determinations of the rotatory strengths of this transition, both in simple model compounds and in helices. In previous calculations<sup>14, 22, 23</sup>  $n, n^*$  Cotton effects were always predicted to be about one order of magnitude too low. We attribute this improvement to the use of improved wave functions. It appears especially that the delocalization of the  $n, n^*$  transition improves agreement with experiment. It is emphasized, however, that all wave functions and parameters were selected in advance of calculation to give the best representation of the electronic structure of the peptide group according to criteria set up in other fields, and no parameters were varied with the intention of improving optical rotation calculations.

The middle section of the figure shows the behavior of the two  $\pi, \pi^*$  transitions. The heavy line indicates the rotatory strength of the long-wavelength transition,

and the dashed line represents that of the lower wavelength transition. The appearance is superficially that of a two-component exciton, but, in fact, the curves are not reflections of one another. In the four-transition calculation, the  $\pi, \pi^*$  transitions exchange rotatory strength with the  $n, n^*$  transitions and only the total of all four vanishes. It is worth pointing out that, although the rotatory strengths of the  $\pi, \pi^*$  transitions appear to be very much larger than those of the  $n, n^*$  transitions, they largely cancel one another, so that the order of magnitude of rotation produced by the two transitions is frequently the same. The splitting is essentially the same as that shown in Figure 4, since this derives almost entirely from the coupling of the two  $\pi, \pi^*$  transitions.

**2. Tertiary-Secondary Combination.** Repeating these calculations for a tertiary-secondary combination with  $E_{\beta_1} = 50,300 \text{ cm}^{-1}$  (199 m $\mu$ ),  $E_{\beta_2} = 52,600 \text{ cm}^{-1}$  (190 m $\mu$ ), and  $E_{\alpha_1} = E_{\alpha_2} = 47,600 \text{ cm}^{-1}$  (210 m $\mu$ ), the effect of having nondegenerate  $\pi, \pi^*$  transitions may be examined. All other parameters but the diagonal energies remain the same. Figure 6 shows the results for the pure Kirkwood mechanism (compare with Figure 3 for the degenerate case). In the upper part of the figure is shown the spectral shift  $\Delta\lambda$ . In accordance with the results of the perturbation theory, the shifts of the energy levels are smaller than in the degenerate case and are always in the direction to produce a greater separation. The nodes of the shift depend on the nondiagonal elements of the Hamiltonian and are in the same position as for the degenerate case. This is also true for the optical nodes of the rotatory strength of the nearest  $\pi, \pi^*$  transition, as may be seen in the central portion of Figure 6. One important difference may be noted: at the energetic nodes  $R$  tends to zero and is not discontinuous as in the degenerate case. As emphasized before, for cases where the total spectral separation is less than the half-band-width the observable quantity is not the individual rotational strength, but the rotational couple. This condition is met for most values of  $\psi$ , even given the initial separation of 9 m $\mu$  between  $\beta_1$  and  $\beta_2$ . The calculated couple is shown in the lowest figure. This is seen to be identical with the couple in the degenerate case, although the centering will be different. This result is in agreement with theoretical predictions which will be discussed in a subsequent work. The meaning of this result is that, provided two coupled transitions are close enough so that they cannot be resolved (*i.e.*, the separation of peaks and troughs depends on band-width and not separation), it does not matter whether the levels are initially truly degenerate or not. The experimental results for true and near degeneracy are the same. Extending the calculations for the tertiary-secondary combination to the treatment by the full theory, the

(23) E. S. Pysh, *Proc. Nat. Acad. Sci. U. S.*, **56**, 825 (1966).

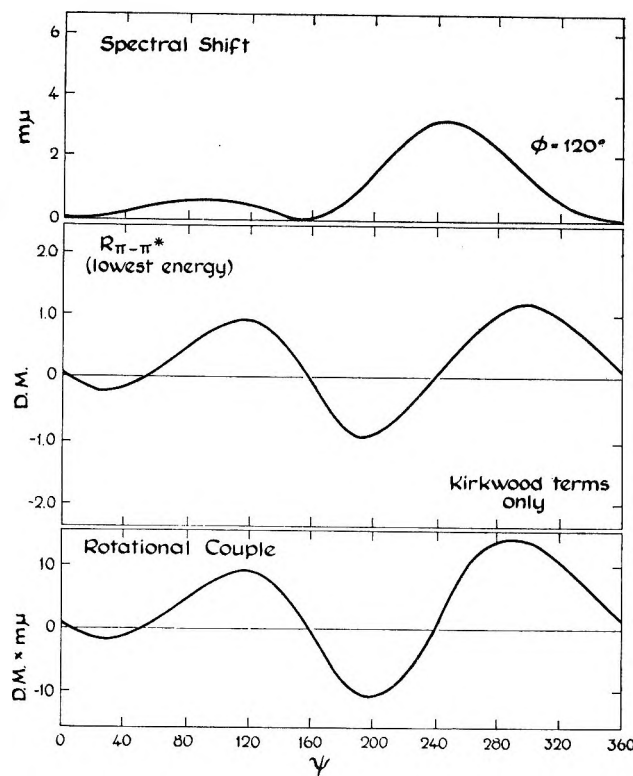


Figure 6. Rotational strength for  $\varphi = 120^\circ$ ,  $\psi$  varied (*trans,trans*-peptides, tertiary-secondary combination, i.e., nondegenerate case, Kirkwood terms only): (a) spectral shift (total  $\pi,\pi^*$  separation twice the shift plus the initial nondegeneracy); (b) rotational strength of the nearest  $\pi,\pi^*$  transition; (c) rotational couple.

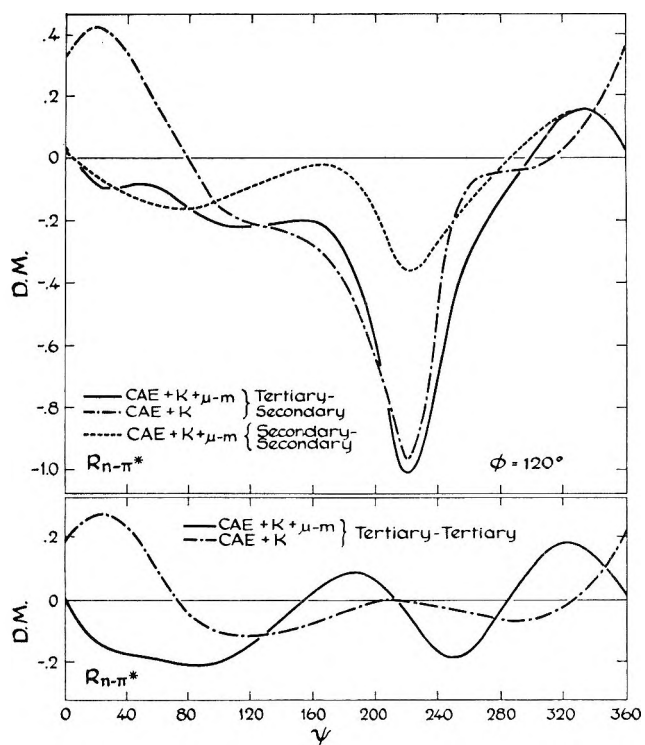


Figure 8. Contributions of different mechanisms to the total  $n,\pi^*$  rotational strength for  $\varphi = 120^\circ$ ,  $\psi$  varied (*trans,trans*-peptides in various combinations).

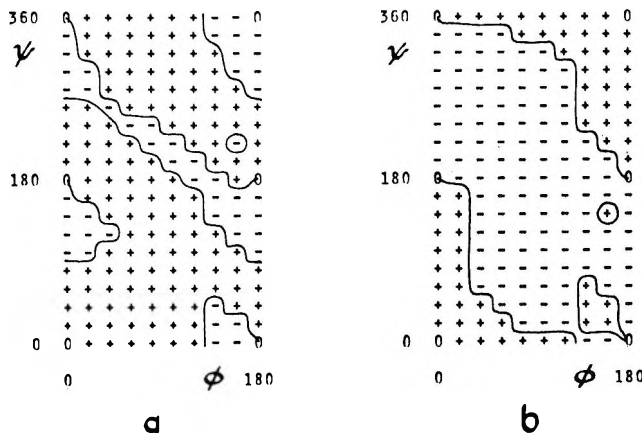


Figure 7. Maps of rotational strength (*trans,trans*-peptides, tertiary-secondary combination, i.e., nondegenerate case, full theory): (a) nearest  $\pi,\pi^*$  transition, (b) total  $n,\pi^*$  rotational strength.

$\pi,\pi^*$  system shows some changes in the nodal patterns as depicted in Figure 7a (*cf.* the degenerate case where the nodes for  $\pi,\pi^*$  in K, CAE + K, and CAE + K +  $\mu-m$  were roughly the same). This is brought about by the appearance in this combination of regions which give rise to very high rotational strengths in the  $n,\pi^*$  transitions. The map of the  $n,\pi^*$  transitions is given

in Figure 7b. This shows substantially the same pattern as the  $n,\pi^*$  (full theory) for the degenerate transitions, Figure 4c, but the magnitudes of the rotational strength are in this case greatly enhanced. This is shown most clearly for  $\varphi = 120^\circ$  in Figure 8a. The curve shows a minimum at  $\psi = 220^\circ$  with a magnitude three times greater than in the case of the secondary-secondary combination. Also, it may be seen that this minimum derives mainly from the CAE mechanism. Since the perturbation (by group 2) is in both cases due to the secondary amide, the effect arises entirely from the energy separation of  $\alpha_1$  and  $\beta_1$ . In the secondary-secondary case these were 210 and 190 m $\mu$ ; in the tertiary-secondary case, 210 and 199 m $\mu$ . The smaller separation brought about by the increased substitution on the nitrogen atom predicts a striking change in the  $n,\pi^*$  Cotton effect. Because of the nonequivalence of group 1 and 2 relative to the direction of the peptide links, the combination secondary-tertiary will not be the same as tertiary-secondary.

3. *Tertiary-Tertiary Combination.* For these calculations the  $n,\pi^*$  wavelengths are both at 210 m $\mu$ ; the  $\pi,\pi^*$  are both at 199 m $\mu$ . Since this represents another degenerate case, the previous discussion is directly applicable for the pure Kirkwood mechanism. In CAE + K and CAE + K +  $\mu-m$ , the interaction between  $n,\pi^*$  and  $\pi,\pi^*$  is somewhat enhanced because of the relative proximity of their energies. However, the most interesting feature is the  $n,\pi^*$  predicted by the

full theory. This is shown in Figure 8b. The predicted rotational strengths are of lesser magnitude than either secondary-secondary or tertiary-secondary (Figure 8a), in spite of the proximity of  $\alpha$  and  $\beta$ . This is due to the much reduced contribution from the CAE mechanism which depends upon the electrostatic charges present. Tertiary amides are less polar (Table II or III), and hence the final pattern is set mainly by the  $\mu-m$  mechanism whose off-diagonal terms are effectively independent of the degree of substitution. This change in behavior is of only academic interest, since the substituent groups of tertiary-tertiary amides make this conformational region inaccessible.

**Table II:** Rotatory Contributions of the Dipeptide for ( $\varphi = 120^\circ$ ,  $\psi = 120^\circ$ ) (the  $\alpha$ -helical conformation is (122, 132)<sup>a</sup>

Transition	Terms used in calcn			
	CAE	K	CAE + K	CAE + K + $\mu-m$
1				
$\lambda_1$	210	...	210	210
$R_1$	-0.038	...	-0.044	-0.022
2				
$\lambda_2$	190	187.9	187.9	187.9
$R_2$	0.038	-2.06	-1.97	-1.96
$D_2$	9.30	13.6	13.6	13.6
3				
$\lambda_3$	210	...	210	210
$R_3$	-0.061	...	-0.046	-0.083
4				
$\lambda_4$	190	192.1	192.1	192.1
$R_4$	0.061	2.06	2.06	2.06
$D_4$	9.30	5.0	5.0	5.0
$R_{n,\pi^*}$	-0.099 (= $R_1 + R_3$ )	...	-0.090	-0.104

<sup>a</sup> Units are as follows:  $\lambda$  in  $m\mu$ ; R in Debye magnetons; D in Debye units squared.

**Table III:** Predicted  $n,\pi^*$  Rotatory Strengths for Dimers in the Four Conformations which Have Been Proposed for Poly(N-methylalanine) (parameters for *trans-trans*, tertiary-tertiary case (units as in Table II)

$(\varphi, \psi)$	Conformation			
	I	II	III	IV
$\lambda_1, \lambda_3$	(30, 250)	(210, 250)	(80, 345)	(240, 345)
$R_1 + R_3$	210	210	210	210
$R_1 + R_3$	-0.220	+0.110	+0.066	+0.14
$\lambda_2$	198	197.4	195.3	198.1
$R_2$	1.45	0.88	-1.74	-1.43
$\lambda_4$	200	200.5	202.2	199.5
$R_4$	-1.23	-0.99	1.68	1.29
Helix sense				
Residues/turn	R 2.9	L -3.59	L -2.82	R 4.88
Ångströms/residue <sup>a</sup>	2.86	1.67	3.34	2.40

<sup>a</sup> G. N. Ramachandran, *Advan. Protein Chem.*, in press.

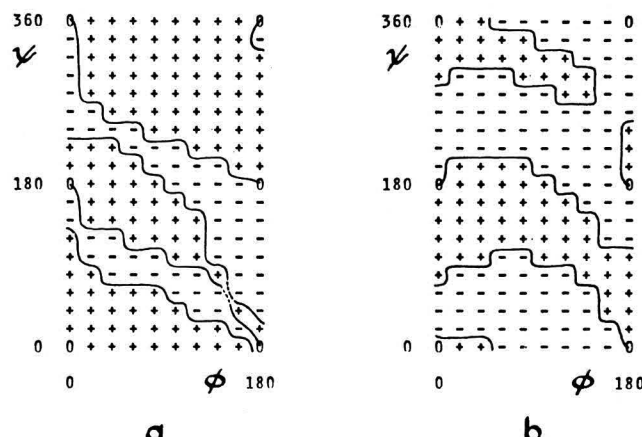


Figure 9. Maps of rotational strength (*cis,cis*-peptides, tertiary-tertiary combination, full theory): (a) nearest  $\pi,\pi^*$  transition, (b) total  $n,\pi^*$  rotational strength.

**4. *cis,cis*-Peptides.** The calculations were repeated for a dipeptide with the *cis* orientation of the peptide groups. This change has a considerable effect upon the excluded volume (see Figure 1b). For the case under consideration, the tertiary-tertiary combination, the C=O in group 1, and all the dependent moments and monopoles required are rotated 180° about the C-N bond. (In group 2, changes are minimal; for secondary amides a carbon and hydrogen atom are rotated, which involves only static electric charges.) The results for the full theory are shown in Figure 9. The repositioning of charges and moments in group 1 leads to a new conformational dependence of the rotatory strength, as shown by the extensive changes in the nodal curves. The sign of the  $n,\pi^*$  rotatory strength shows more variability in this case; a line segment of the results is shown for  $\varphi = 120^\circ$  in Figure 10. The angular dependence of  $n,\pi^*$  and  $\pi,\pi^*$  rotational strength and exciton split have changed considerably upon introduction of the *cis* conformation. The phenomena exhibited here parallel those shown for the degenerate *trans-trans* case (secondary-secondary) in Figure 5, but the positions of the optical nodes and energetic nodes are different in conformity with the new conditions of symmetry and intergroup geometry obtaining in the *cis* conformation.

**Applications.** The calculations which have been presented have their purpose in the interpretation of the optical rotation of specific compounds containing two peptide units. These applications will be discussed in detail in subsequent publications. One would expect, as well, that the results would be valuable for any polypeptide situation in which the optical rotation could be regarded as being developed from pairwise interactions of peptide units. It may be demonstrated that, for a weak transition like the  $n,\pi^*$  transition, the interactions producing rotatory strength are local and essentially unaffected by long-range order in the polypeptide system. This comes from a theorem which

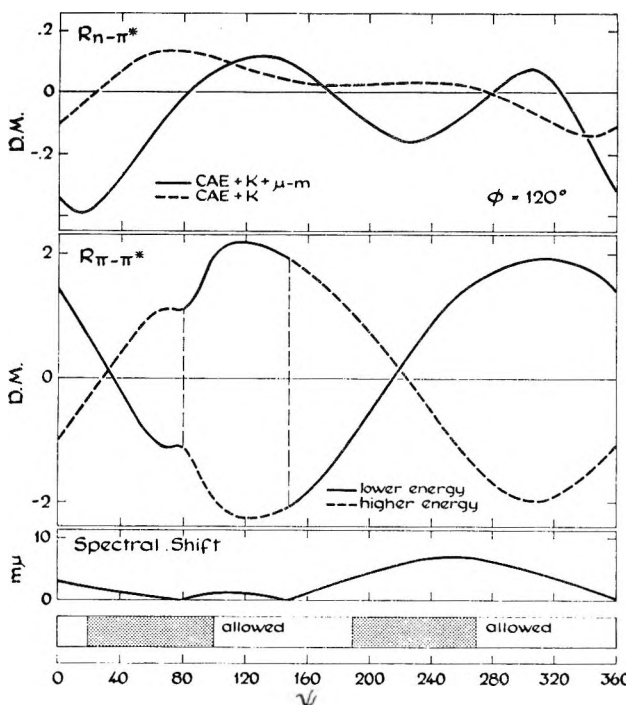


Figure 10. Details of full theory for  $\varphi = 120^\circ$ ,  $\psi$  varied (*cis,cis*-peptides, tertiary-tertiary combination):  
(a) contributions of different mechanisms to the total  $n, \pi^*$  rotational strength; (b) rotational strength of the  $\pi, \pi^*$  system;  
(c) spectral shift of each  $\pi, \pi^*$  transition; (d) allowed regions of conformational space for this combination.

states that, in the absence of effective splitting, the spectral behavior of an exciton system is the same as that of the uncoupled monomers. To the extent that the rotatory strength of the  $n, \pi^*$  transition is dominated by nearest neighbor interactions in polypeptides, the maps which have been shown are helpful in determining the behavior of this transition. A detailed look into the interactions which are effective in perturbing the  $n, \pi^*$  transition of peptides shows that very often the principal interactions do come from nearest neighbors. A comparison of the rotatory strengths which have been observed by experiment with those predicted by the maps given above shows that the correct sign is predicted for the  $\alpha$  helix, polyproline I, polyproline II, and the collagen fold.

**$\alpha$ -Helical Conformation.** Details of the results for the dimer near the  $\alpha$ -helical conformation are given in Table II. The four transitions represent the final (combined) states of excitation derived from the initial set  $\alpha_1, \beta_1, \alpha_2, \beta_2$ . Inspection of column 4 shows that the full theory predicts an  $n, \pi^*$  Cotton effect of the sign and order of magnitude of that observed in the  $\alpha$  helix ( $R_1 + R_3$  (dimer, theoretical) = -0.1 DM and  $R$  ( $n, \pi^*$ ,  $\alpha$  helix, experimental)<sup>24</sup> = -0.2 DM). It should be noted, however, that the dimer calculations are appropriate for an aqueous environment,  $\lambda_{n, \pi^*}$  210 m $\mu$ , whereas in the helix  $\lambda_{n, \pi^*}$  equals 222 m $\mu$ . This difference does not interfere with qualitative comparisons.

The  $\pi, \pi^*$  Cotton effects, on the other hand, bear no resemblance to those observed in an  $\alpha$  helix. Woody and Tinoco<sup>14</sup> have studied the development of the  $\pi, \pi^*$  rotatory strength of helices as a function of helical length showing that somewhere between 5 and 10 units are required before the appearance of a typical  $\alpha$ -helical pattern of rotatory strengths.

Table II also gives a breakdown of the origins of the rotatory strengths. For the  $\alpha$ -helical conformation,  $R_1$  and  $R_3$  are of the same sign but differ in magnitude because of the nonequivalence of groups 1 and 2 in the dimer structure. Other features to be observed are (1) the split in the original  $\pi, \pi^*$  transitions, (2) the inequality of the dipole strength in the two bands, and (3) the dominance of the CAE mechanism over the  $\mu-m$  mechanism for this conformation.

**The Disordered Polypeptide Chain.** The experimental results<sup>25,26</sup> for the disordered polypeptide chain suggest a very weak contribution to the circular dichroism at about 235 m $\mu$  ( $R = -0.01$  DM) and a weak positive contribution at 217 m $\mu$  ( $R = 0.1$  DM). The upper band may represent a very weak transition other than  $n, \pi^*$  and  $\pi, \pi^*$ ,<sup>11,12</sup> the presence of a small population of peptide residues with chromophores totally sequestered from the polar solvent,<sup>20</sup> or a computational artifact resulting from very broad negative bands at lower wavelengths which still persist at long wavelengths and do not follow the Gaussian shape assigned to them in the analysis. In any event, the effect is small and beyond the scope of our calculations. The 217-m $\mu$  band may be assigned to the  $n, \pi^*$  transition. In small molecules this band appears at  $212 \pm 2$  m $\mu$  in aqueous solution but appears to be shifted up about 5 m $\mu$  in the disordered polypeptide chain.

Comparing the map Figure 4c with the Ramachandran diagram of Figure 1a, it is seen that diarnides distributed randomly over the available angular space would acquire negative rotatory strength of the  $n, \pi^*$  transition in the  $\alpha$ -helical region and both positive and negative rotatory strength from the upper allowed region. The potential energy calculations of Brant, Miller, and Flory<sup>27</sup> show that randomly coiled polyalanine is distributed in three principal regions of angular space. Region I (near  $\psi = 120^\circ$ ) is electrostatically undesirable and contributes negative rotatory strength at a potential energy minimum near  $\varphi = 120^\circ$  (the  $\alpha$  helix) and positive rotatory strength at a minimum near  $\varphi = 20^\circ$ . Region II (near  $(240^\circ, 240^\circ)$ , the left-hand  $\alpha$  helix) gives rotatory strength of positive sign and, to the extent it is present, cancels out the

(24) G. Holzwarth and P. Doty, *J. Amer. Chem. Soc.*, **87**, 218 (1965).

(25) J. Carver, E. Shechter, and E. Blout, *ibid.*, **88**, 2550 (1966).

(26) S. Timasheff, H. Susi, R. Townend, L. Stevens, M. Gorbunoff, and T. Kumosinski in "The Conformation of Biopolymers," G. N. Ramachandran, Ed., Academic Press, New York, N. Y., 1967, p 173.

(27) D. A. Brant, W. G. Miller, and P. Flory, *J. Mol. Biol.*, **23**, 47 (1967).

contribution of an equivalent amount of the right-handed helix. Region III contains a broad minimum, ( $90\text{--}110^\circ$ ,  $290\text{--}330^\circ$ ), which contributes both positively and negatively. The appearance of a positive  $n,\pi^*$  Cotton effect indicates the dominance of conformations in the positive regions of Figure 4c, presumably in the neighborhood of the collagen conformations, ( $110^\circ$ ,  $340^\circ$ ). The rotatory strength pattern of the random polypeptide chain and collagen are strikingly similar.<sup>26</sup>

*Poly(N-methyl-L-analine).* The optical properties of this polymer were recently reported by Goodman and Fried.<sup>28</sup> Nmr evidence was presented to show the presence of *trans*- rather than *cis*-peptides. We therefore utilize calculations for the *trans-trans* tertiary-tertiary combination. A full map has not been presented for this case, but required values are given in Table III. In an initial attempt at conformational analysis of this polymer by the theoretical stereochemical approach, four conformations were isolated as representing energy minima of helical conformations: I, ( $30^\circ$ ,  $250^\circ$ ); II, ( $210^\circ$ ,  $250^\circ$ ); III, ( $80^\circ$ ,  $345^\circ$ ); and IV, ( $240^\circ$ ,  $345^\circ$ ).<sup>29</sup>

Inspection of the circular dichroism curve indicates a strong negative band at  $222\text{ m}\mu$ . Transitions at this wavelength are unlikely to derive from the  $\pi,\pi^*$  system, and we assign this region as representing a strong negative  $n,\pi^*$  Cotton effect. Comparing the four conformations above with our calculations for dipeptides, we find (Table III) that only conformation I has the predicted sign for the  $n,\pi^*$  Cotton effect. In addition, the theory predicts that the rotational strength will be strong. In all other conformations, the theory predicts a positive rotational strength. This conclusion is in agreement with recent publications of Goodman, *et al.*,<sup>30</sup> and Liquori,<sup>31</sup> who have computed the energetically preferred conformation and on purely stereochemical grounds have concluded that conformation I is preferred.

*Polyproline I.* The experimental circular dichroism for poly(L-proline) in *n*-propyl alcohol shows a very weak, poorly defined negative band at  $236\text{ m}\mu$ , a strong positive band at  $214\text{ m}\mu$ , and a strong negative band at  $200\text{ m}\mu$ .<sup>26</sup> The weak negative band is presumably assignable to the  $n,\pi^*$  transition which is shifted to the red in a nonaqueous environment. The  $214\text{-m}\mu$  band has been assigned by Pysh to the  $\pi,\pi^*$  exciton system.<sup>32</sup> This form of polyproline contains *cis* residues and the conformational angles are ( $100^\circ$ ,  $340^\circ$ ).<sup>33</sup> The  $n,\pi^*$  rotatory strength calculated successively with the CAE, CAE + K, and CAE + K +  $\mu-m$  terms of the theory is  $-0.11$ ,  $-0.14$ , and  $-0.01$ . The CAE and  $\mu-m$  contributions are in opposition and the resultant is effectively zero. Although the agreement with experiment (a very weak negative band) is good, the result is very sensitive to small changes in conformation. This is illustrated in Table IV, where the breakdown shows that both groups are affected differently and by

both mechanisms. Consequently, the agreement could be improved or destroyed with relatively small changes in the assignment of conformation or small inaccuracies in the calculations. The aspect of interest is the suggestion that polyproline I has a small  $n,\pi^*$  rotatory strength because of the cancellation of the two mechanisms.

**Table IV:** Predicted  $n,\pi^*$  Rotatory Strengths for the Dimer Near the Polyproline I Conformation (units as in Table II)

$\psi$	100		120	
	CAE + K	CAE + K + $\mu-m$	CAE	CAE + K + $\mu-m$
340				
$R_1$	-0.024	0.017	-0.002	-0.004
$R_3$	-0.113	-0.023	-0.140	-0.150
$R_1 + R_3$	-0.137	-0.006	-0.142	-0.153
320				
$R_1$	-0.020	0.086	-0.013	0.043
$R_3$	-0.066	0.035	-0.098	-0.015
$R_1 + R_3$	-0.086	0.121	-0.111	0.028

*Polyproline II.* The experimental circular dichroism for polyproline II (the *trans* form) in aqueous solution shows a positive band at  $221\text{ m}\mu$  and a stronger negative band at  $207\text{ m}\mu$ .<sup>26</sup> In this form of the polymer the peptide units are *trans* and the conformational angles are ( $112^\circ$ ,  $330^\circ$ ).<sup>34</sup> Calculations were performed over the region ( $100\text{--}120^\circ$ ,  $320\text{--}340^\circ$ ). The prediction of the full theory for ( $110^\circ$ ,  $330^\circ$ ) is a positive  $n,\pi^*$  (+0.13 DM), in fair agreement in sign and magnitude with the experimental value of 0.065. It is rare that theory exceeds experiment for an  $n,\pi^*$  transition. In this case, the explanation probably lies in the imperfect rigidity of this polymer.

Investigations of the different contributions for the  $n,\pi^*$  rotatory strength indicates that the CAE mechanism is weak in this region, while the  $\mu-m$  mechanism is the determining influence, providing a strong positive contribution which is relatively insensitive to changes of  $\pm 10^\circ$  in  $\varphi$  or  $\psi$ .

## V. Conclusion

The purpose of this paper has been to present a formalism for calculating optical rotation which is applicable to a wide variety of problems. Although the procedures were developed for application to a number

(28) M. Goodman and M. Fried, *J. Amer. Chem. Soc.*, **89**, 1264 (1967).

(29) J. E. Mark and M. Goodman, *ibid.*, **89**, 1267 (1967).

(30) J. E. Mark and M. Goodman, *Biopolymers*, **5**, 809 (1967).

(31) A. M. Liquori and P. DeSantis, *ibid.*, **5**, 815 (1967).

(32) E. S. Pysh, *J. Mol. Biol.*, **23**, 857 (1967).

(33) W. Traub and U. Shmueli in "Aspects of Protein Structure," G. N. Ramachandran, Ed., Academic Press, New York, N. Y., 1963, p 81.

(34) G. N. Ramachandran, *Advan. Protein Chem.*, in press.

of experimental investigations of specific substances containing two peptide groups in a variety of conformations, the accent in this paper has been placed on treating rotatory strengths as functions of two variables, in this case the angles  $\varphi$  and  $\psi$ . The applications given in the last section have taken advantage of the fact that the Cotton effects of the  $n,\pi^*$  transition in polypeptides, as well as in dimers, are largely vicinal in character and depend principally on nearest neighbors. The general semiquantitative agreement which is obtained between experiment and calculation for these polymers as well as for specific model diamides indicates that the maps obtained give at least a coarse-grained description of the rotatory strength over the  $\varphi-\psi$  plane. These maps are presumably most accurate where strong rotatory strengths are predicted and least accurate near nodal lines which are produced by the cancellation of large contributions from several mechanisms. Continuation of this work with the rotatory strengths of polypeptides as functions of chain length and conformation is now well under way.

It should be emphasized that the methods of sections III and IV are strictly applicable only to two peptide units and that the ultimate purpose of their presentation here is to provide an interpretation to a number of experimental studies on diamide models which have been performed in our laboratory. Experimental and theoretical results on these compounds will be presented later.

Polymeric systems (helical or disordered) may be treated with no difficulty by the methods of section II and a number of such calculations have already been performed.<sup>35</sup> The discussion of polymers given in section IV serves only to illustrate that a useful qualitative picture of the dependence on  $\varphi$  and  $\psi$  of the  $n,\pi^*$  rotatory strength may be obtained from the dimer maps. No such correlations are possible with the  $\pi,\tau^*$  transition because it is extensively delocalized and therefore sensitive to total polymer geometry.

(35) V. Madison, unpublished work.

## The Relation between the Amounts of Chemisorbed and Physisorbed Water on Metal Oxides

by Tetsuo Morimoto, Mahiko Nagao, and Fujiko Tokuda

*Department of Chemistry, Faculty of Science, Okayama University, Tsushima, Okayama, Japan* (Received August 23, 1968)

The first and second water adsorption isotherms and the water content on the metal oxide surfaces have been measured for samples of  $TiO_2$  (rutile) and  $\alpha-Fe_2O_3$  (hematite). After the first adsorption isotherm had been obtained, the sample was degassed under a reduced pressure of  $10^{-5}$  torr at room temperature for 4 hr, and then the second adsorption isotherm was measured at the same temperature as before. The determination of water content was carried out by the successive ignition-loss method. The amounts of physisorbed water ( $V_p$ ) and chemisorbed water ( $V_c$ ) were estimated from the two isotherms. The total amount of chemisorbed water was obtained by adding the water content ( $V_h$ ) to the value of  $V_c$ . The sum of  $V_c$  and  $V_h$  decreases slightly with an increase in the temperature of pretreatment of the sample, which indicates that the extent of reversible rehydroxylation of the sites dehydrated at higher temperatures is somewhat diminished. The ratio of  $V_p$ , expressed in the number of water molecules per unit area, to the sum of  $V_c$  and  $V_h$ , both of which are expressed in the number of hydroxyl groups per unit area, was found to be about 1:2 for all samples used, which indicates that a water molecule is adsorbed on two hydroxyl groups through hydrogen bonding.

### Introduction

It has been made clear that the surfaces of most metal oxides have hydroxyl groups in the atmosphere which play important roles in such surface phenomena as catalytic action, selective adsorbability, hydrophilicity, surface electrification, etc.

Recently, the properties of the surface hydroxyl

groups have been investigated from the following standpoints. Surface hydroxyl groups can generally be removed by condensation dehydration at higher temperature *in vacuo*, but the removal temperature considerably differs depending on the nature of the solid substrate.<sup>1</sup> On the other hand, the rehydroxylation of the dehydrated surface can proceed in the

saturated water vapor at a rate possible to follow experimentally, which may also be different with a variety of solid substrates.<sup>2,3</sup> The energy of surface rehydroxylation has been determined by heat-of-immersion calorimetry for several oxides and has been found to be different for each substance.<sup>4-6</sup>

Infrared spectroscopic studies have shown that water molecules are adsorbed on the surface of oxides through hydrogen bonding with surface hydroxyl groups.<sup>7-13</sup>

The purposes of the present paper are to investigate quantitatively the relation between the amount of water chemisorbed as surface hydroxyl groups and the amount of water physisorbed on these groups and to discern the structure of the adsorbed layer of water on metal oxides. Hollabaugh and Chessick<sup>14</sup> have discussed the ratio of the number of physisorbed water molecules to the number of surface hydroxyl groups on metal oxides. However, a measurement of hydroxyl groups remaining on the oxide surfaces was not made in their study, so that the discussion seems insufficient. In the present paper, the true relation between the amounts of physisorbed and chemisorbed water has been dealt with, the latter including the number of hydroxyl groups remaining on the surface in addition to the amount of chemisorbed water determined from the adsorption isotherm of water. Using these data, we can consider the detailed structure of the adsorbed layer of water on metal oxide surfaces, as will be described later.

## Experimental Section

**Materials.** The samples used in this study were  $\text{TiO}_2$  (rutile) and two kinds of  $\alpha\text{-Fe}_2\text{O}_3$  (hematite). The original sample of rutile, obtained from Teikoku Kako Co., was a commercial one prepared from titanium sulfate solution. One of the hematite samples, which was obtained from Nippon Bengara Co., was made by the calcination of  $\text{FeSO}_4 \cdot 7\text{H}_2\text{O}$  at 800° for 7 hr ( $\text{Fe}_2\text{O}_3(\text{I})$ ). These two samples were treated with 0.1 N nitric acid several times to remove basic impurities, were washed repeatedly with 0.1 N ammonia to remove acidic impurities, then were thoroughly washed with distilled water, and finally were dried at 110° for 8 hr. Another sample of hematite was prepared by calcination of  $\alpha\text{-FeOOH}$  (goethite) at 800° in air for 5 hr, the latter having been precipitated by the oxidation of an aqueous solution of ferrous sulfate by hydrogen peroxide and washed with distilled water. The second sample of hematite was immersed in hot water at 80° for 3 days and then was dried at 110° for 8 hr ( $\text{Fe}_2\text{O}_3(\text{II})$ ).

**Surface Area Measurement.** The surface areas of samples were determined by applying the BET theory to the nitrogen adsorption data obtained at liquid nitrogen temperature, assuming the molecular area of nitrogen to be 16.2 Å<sup>2</sup>.

**Water Vapor Adsorption Isotherm.** The adsorption isotherm of water on metal oxides was determined

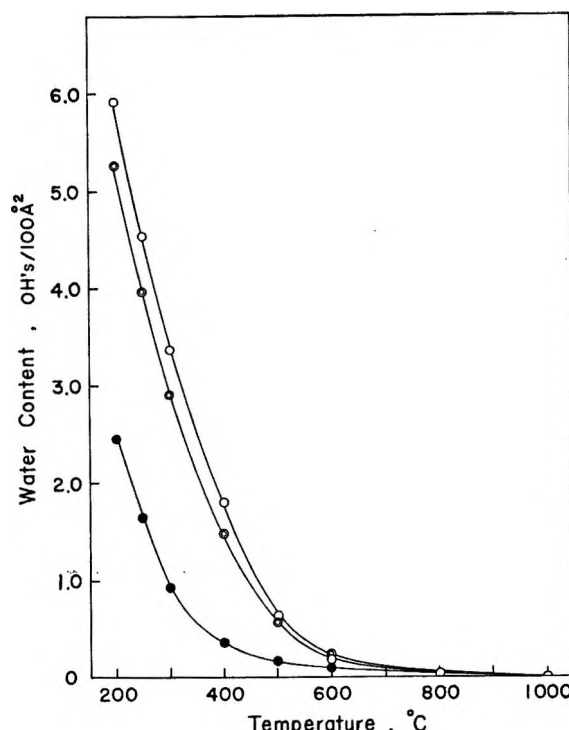


Figure 1. Water content of oxide surfaces at various temperatures: ●,  $\text{TiO}_2$  (rutile); ○,  $\alpha\text{-Fe}_2\text{O}_3(\text{I})$ ; ◎,  $\alpha\text{-Fe}_2\text{O}_3(\text{II})$ .

volumetrically by using an adsorption apparatus which was equipped with an oil manometer to measure sensitively the equilibrium pressure. The sample taken for every run was about 10 m<sup>2</sup>. Prior to the adsorption measurement, the sample was treated at a given temperature (250, 600, and 900° for  $\text{TiO}_2$  and 250, 600, and 800° for  $\alpha\text{-Fe}_2\text{O}_3$ ) under a reduced pressure of  $10^{-5}$  torr for 4 hr. The adsorption measurement was made at 18° for  $\text{TiO}_2$  and at 25° for  $\alpha\text{-Fe}_2\text{O}_3$ , and the adsorption equilibrium was usually established within 30 min for every addition of water vapor to the adsorption system. The desorption measurement carried out as a

- (1) T. Morimoto, M. Nagao, and F. Tokuda, *Bull. Chem. Soc. Jap.*, **40**, 2723 (1967).
- (2) T. Morimoto and M. Nagao, *Kolloid-Z. Z. Polym.*, **224**, 62 (1968).
- (3) Unpublished data.
- (4) G. J. Young and T. P. Bursh, *J. Colloid Sci.*, **15**, 361 (1960).
- (5) T. Morimoto, K. Shiomi, and H. Tanaka, *Bull. Chem. Soc. Jap.*, **37**, 392 (1964).
- (6) T. Morimoto, M. Nagao, and M. Hirata, *Kolloid-Z. Z. Polym.*, **225**, 29 (1968).
- (7) A. V. Kiselev and V. I. Lygin, *Kolloid. Zhur.*, **21**, 561 (1959).
- (8) J. H. Anderson, Jr., and K. A. Wickersheim, *Proc. Int. Congr. Phys. Chem. Solid Surfaces*, North Holland, Amsterdam, 252 (1964).
- (9) G. J. Young, *J. Colloid Sci.*, **13**, 67 (1958).
- (10) D. J. C. Yates, *J. Phys. Chem.*, **65**, 746 (1961).
- (11) K. E. Lewis and G. D. Parfitt, *Trans. Faraday Soc.*, **62**, 204 (1966).
- (12) G. Blyholder and E. A. Richardson, *J. Phys. Chem.*, **66**, 2597 (1962).
- (13) G. Blyholder and E. A. Richardson, *ibid.*, **68**, 3882 (1964).
- (14) C. M. Hollabaugh and J. J. Chessick, *ibid.*, **65**, 109 (1961).

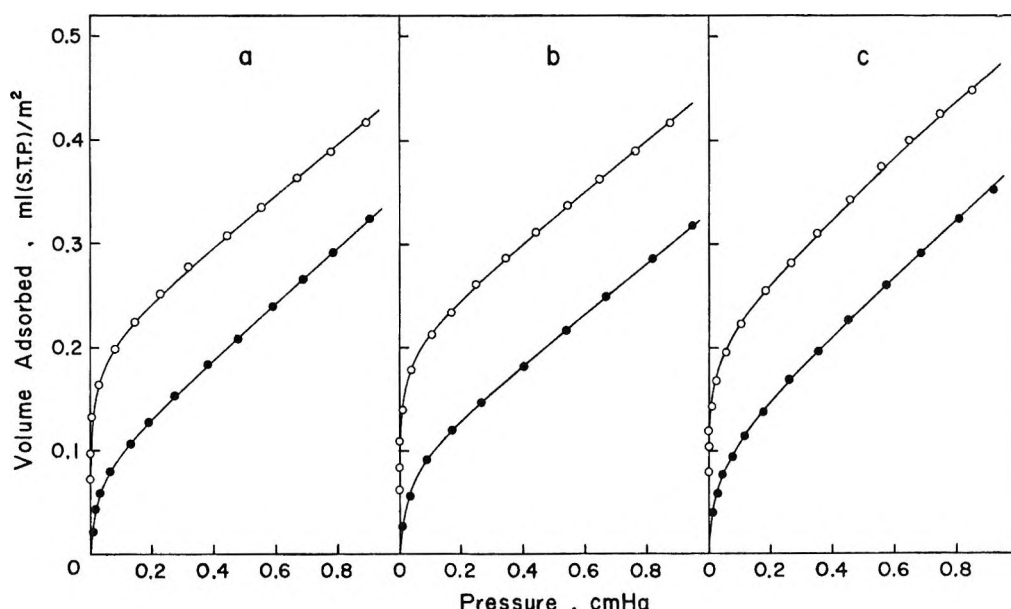


Figure 2. Adsorption isotherms of water on  $\text{TiO}_2$  (rutile) at  $18^\circ$ , pretreated at  $250^\circ$ , a;  $600^\circ$ , b; and  $900^\circ$ , ○, first adsorption; ●, second adsorption.

preliminary test for each adsorbent showed no hysteresis, indicating that the samples examined were nonporous.

After the first adsorption isotherm of water had been obtained, the sample was placed under a reduced pressure of  $10^{-5}$  torr at room temperature for 4 hr, and then the second adsorption was carried out at the same temperature as before. In the case of rutile it has been reported that partial reduction of the sample occurs when it is treated *in vacuo* at an elevated temperature.<sup>14,15</sup> In the present case, the color of the sample changed slightly to light gray after treatment *in vacuo* at temperatures higher than  $600^\circ$ , but we utilized the sample in this state for the adsorption measurement. The BET plots<sup>16</sup> of the water adsorption data on every sample showed a linear relation in the range of relative pressure from 0.05 to 0.35, and the monolayer capacity of water was calculated from the linear part of the plot.

**Water Content Measurement.** The surface hydroxyl groups can be removed by condensation dehydration upon heat treatment of the sample *in vacuo*, but the removal temperature differs depending on the nature of the metal oxides.<sup>1</sup> By employing the apparatus for the measurement of water adsorption isotherms, the remaining water content of the samples treated at a given temperature was measured by the successive ignition-loss method as described previously.<sup>5</sup>

When the powdered samples were treated at higher temperature *in vacuo*, not only water vapor but also other volatile gases were found to be expelled. Accordingly, during the measurement of water content, all the gases evolved at a given temperature were trapped as a first step in a bulb kept at liquid nitrogen tem-

perature and were determined volumetrically after reevaporation at room temperature. Then most of the reevaporated gases could be trapped again in the bulb at  $-72^\circ$ , where the remaining gases were determined in the same way as described above. When only water vapor was present in the measuring system, the vapor was completely retrapped by this procedure, the pressure of the remaining gas being zero. When the sample was treated at  $300^\circ$ , the amount of these remaining gases was negligibly small and increased with an increase in the temperature of treatment of the samples. If the detected values are expressed in molecules per  $100 \text{ \AA}^2$ , they are, for example, 0.54 at  $900^\circ$  for  $\text{TiO}_2$ , and 0.76 and 0.29 at  $800^\circ$  for  $\text{Fe}_2\text{O}_3(\text{I})$  and  $\text{Fe}_2\text{O}_3(\text{II})$ , respectively. The water content values illustrated in Figure 1 of this paper are those free from these contaminations.

### Results and Discussion

The water content obtained at various temperatures is given in Figure 1; the value is expressed in OH groups/ $100 \text{ \AA}^2$ . This value means the number of hydroxyl groups remaining on the surface at the temperature indicated. The data show that, with rising temperature of treatment, the water content decreases linearly up to about  $400^\circ$  and decreases exponentially at higher temperature. At  $800^\circ$  the remaining number of hydroxyl groups is negligibly small in every sample. The water content of the two kinds of  $\alpha\text{-Fe}_2\text{O}_3$  is similar over the whole range of treatment temperature, in spite of their differences in origin and history. The

(15) J. Gebhardt and K. Herrington, *J. Phys. Chem.*, 62, 120 (1958).

(16) S. Brunauer, D. H. Emmett, and E. Teller, *J. Amer. Chem. Soc.*, 60, 309 (1938).

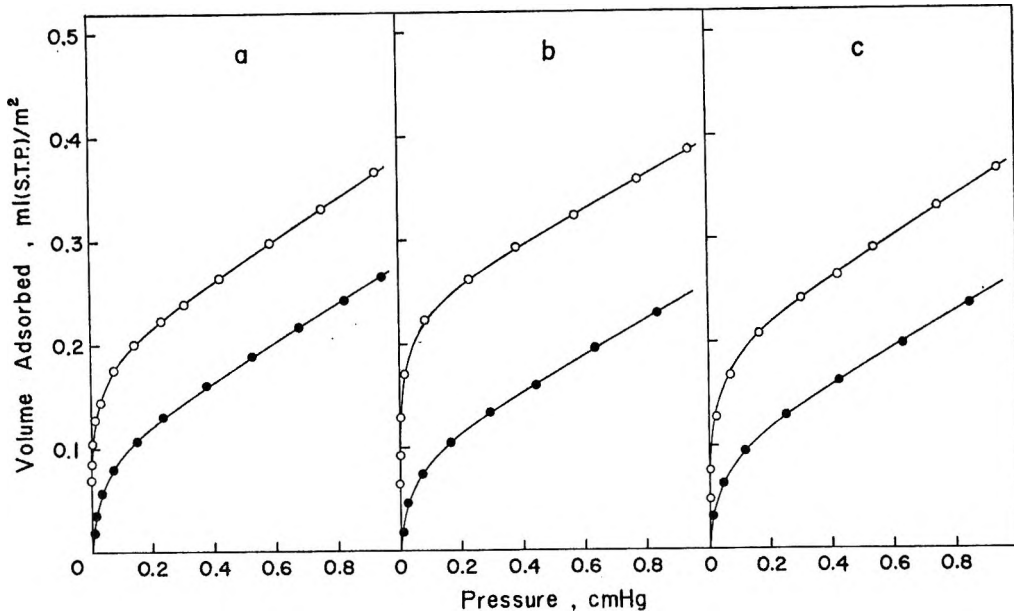


Figure 3. Adsorption isotherms of water on  $\alpha\text{-Fe}_2\text{O}_3$ (I) at 25°, pretreated at 250°, a; 600°, b; and 800°, c: ○, first adsorption; ●, second adsorption.

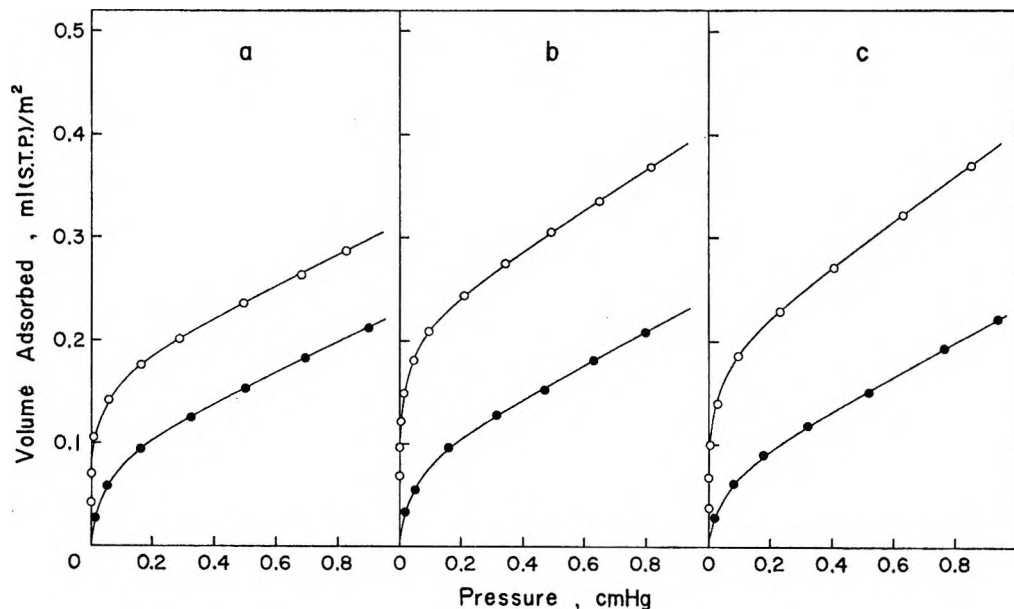


Figure 4. Adsorption isotherms of water on  $\alpha\text{-Fe}_2\text{O}_3$ (II) at 25°, pretreated at 250°, a: 600°, b; and 800°, c: ○, first adsorption; ●, second adsorption.

water content of  $\text{TiO}_2$  is considerably smaller than that of  $\alpha\text{-Fe}_2\text{O}_3$  over the whole range of temperature, which may reasonably result from the fact that the removal of surface hydroxyl groups starts at different temperatures depending on the nature of the substrate; they can be removed from  $\text{TiO}_2$  at a lower temperature than from  $\alpha\text{-Fe}_2\text{O}_3$ .<sup>17</sup>

In Figure 2, the water adsorption isotherms obtained at 18° on  $\text{TiO}_2$  are shown, the pretreatment temperatures of which were 250, 600, and 900°. The adsorption isotherms of  $\alpha\text{-Fe}_2\text{O}_3$  pretreated at 250, 600, and 800° are given in Figures 3 and 4. The adsorption

curves of both substances show a similar tendency that represents multimolecular adsorption. In all cases the second adsorption isotherm is lower than the first one by a definite amount specified by the condition of treatment, the difference being due to the irreversible adsorption of water.

Calculated data are summarized in Table I.  $S_{N_2}$  is the specific surface area of the sample obtained by nitrogen adsorption. The data of  $S_{N_2}$  show that the heat treat-

(17) T. Morimoto, M. Nagao, and F. Tokuda, *Bull. Chem. Soc. Jap.*, **41**, 1533 (1968).

Table I: The Relation between the Amounts of Water Chemisorbed and Physisorbed on  $\text{TiO}_2$  (Rutile) and  $\alpha\text{-Fe}_2\text{O}_3$  (Hematite)

Sample	Treat- ment temp., $^{\circ}\text{C}$	Adsorp- tion temp., $^{\circ}\text{C}$	$S_{\text{N}_2}$ , $\text{m}^2/\text{g}$	$V_m$ , ml (STP)/ $\text{m}^2$	$V_p$ , $\text{H}_2\text{O}$ molecules/ $100 \text{ \AA}^2$	$V_c$ , OH groups/ $100 \text{ \AA}^2$	$V_h$ , OH groups/ $100 \text{ \AA}^2$	$V_c + V_h$ , OH groups/ $100 \text{ \AA}^2$	$\frac{V_p}{(V_c + V_h)}$ , $\text{H}_2\text{O}$ molecules/ OH groups
$\text{TiO}_2$	250	18	9.94	0.213	4.30	5.91	1.65	7.56	0.57
	600	18	9.38	0.233	4.14	6.35	0.10	6.45	0.64
	900	18	4.60	0.231	4.51	6.76	0.01	6.77	0.67
$\alpha\text{-Fe}_2\text{O}_3(\text{I})$	250	25	14.5	0.242	4.71	5.70	4.53	10.23	0.46
	600	25	14.0	0.253	4.25	7.59	0.17	7.76	0.55
	800	25	6.41	0.237	4.45	6.73	0.06	6.79	0.66
$\alpha\text{-Fe}_2\text{O}_3(\text{II})$	250	25	21.2	0.194	3.81	4.57	3.95	8.52	0.45
	600	25	20.0	0.254	4.04	7.91	0.22	8.13	0.50
	800	25	14.9	0.247	3.75	7.91	0.03	7.94	0.47

ment of samples at higher temperatures leads to the large depression of specific surface areas, which indicates the occurrence of appreciable sintering.

$V_m$  is the monolayer capacity of water obtained by applying the BET theory to the first adsorption isotherms. This value is found to vary slightly with the treatment temperature of the samples, and the value of the 600° treated sample is the largest of the three in every sample. The  $V_m$  value calculated from the application of the BET theory should contain the amount of chemisorbed water in addition to that of the first layer of physisorbed water. In order to estimate the amounts of the two kinds of adsorbed water separately, Jurinak<sup>18</sup> determined the first and second adsorption isotherms of water on  $\alpha\text{-Fe}_2\text{O}_3$ ,  $\alpha\text{-FeOOH}$ , and  $\text{TiO}_2$  (anatase), taking the difference of the two resulting  $V_m$  values to be the chemisorbed amount of water. Hollabaugh and Chessick,<sup>14</sup> on the other hand, obtained the irreversibly adsorbed amount of water on  $\text{TiO}_2$  (rutile) by subtracting the value of the second adsorption isotherm from that of the first adsorption isotherm at the relative pressure of 0.2. These authors assumed that the second adsorption isotherm, when measured after degassing the sample at room temperature, contains only physical adsorption of water. Indeed, this is true of  $\alpha\text{-Fe}_2\text{O}_3$  and  $\text{TiO}_2$  (rutile).<sup>17</sup>

Also in the present investigation the monolayer capacity of physically adsorbed water,  $V_p$ , was calculated by applying the BET theory to the second adsorption isotherm, and is expressed in  $\text{H}_2\text{O}$  molecules/ $100 \text{ \AA}^2$ , as shown in Table I. The value of  $V_p$  is almost the same on each sample, independent of the temperature of pretreatment. This suggests that the number of sites for physical adsorption of water does not depend on the temperature of pretreatment.

If it is assumed that the area of a water molecule physisorbed on the oxide surfaces is  $10.8 \text{ \AA}^2$ , the number of water molecules which can possibly exist geometrically on the surface can be estimated as 9.2  $\text{H}_2\text{O}$  molecules/ $100 \text{ \AA}^2$ . The values obtained experimentally for  $\alpha\text{-Fe}_2\text{O}_3$  and  $\text{TiO}_2$  are 41–48% of this number, which shows the water molecules in the first physically adsorbed layer to be in a loosely packed state. Jurinak<sup>18</sup> and Healey, *et al.*,<sup>19</sup> reported that only two-thirds of the hematite surfaces were effective for the physical adsorption of water, a figure larger than the present results.

As described above, it seems that there is a definite interval between the first and second adsorption isotherms on each sample, which can be considered the amount of irreversibly adsorbed water, *i.e.*, the chemisorbed water. We have regarded the difference of each pair of isotherms at the relative pressure of 0.2 as the amount of newly chemisorbed water ( $V_c$ ) during the adsorption process, as Hollabaugh and Chessick<sup>14</sup> did in their work. Since a water molecule is considered to be chemisorbed on the oxide surfaces to form two hydroxyl groups, the value of  $V_c$  is expressed in OH groups/ $100 \text{ \AA}^2$ . The  $V_c$  values for the 250° treated samples are smaller than those of the samples treated at higher temperatures.

The amount of the remaining surface hydroxyl groups can be read from Figure 1, and the results are listed in column 8 of Table I. The sum of  $V_c$  and  $V_h$  should be the total number of surface hydroxyl groups at the end of the adsorption process. The total amount of chemisorbed water on  $\text{TiO}_2$ , generally, seems to be different from that on  $\alpha\text{-Fe}_2\text{O}_3$ : the latter is slightly larger than the former. Taking into account the lattice constants, we can estimate the number of hydroxyl groups which are able to exist crystallographically on the oxide surfaces. In this estimation, we assume that only one hydroxyl group is formed on each surface metal atom. The calculated value amounts to about 8 OH groups/ $100 \text{ \AA}^2$  for the average of the (100) and (110) planes of  $\text{TiO}_2$  (rutile), whose cleavage is

(18) J. J. Jurinak, *J. Colloid Sci.*, **19**, 477 (1964).  
 (19) F. H. Healey, J. J. Chessick, and A. V. Fraioli, *J. Phys. Chem.*, **60**, 1001 (1956).

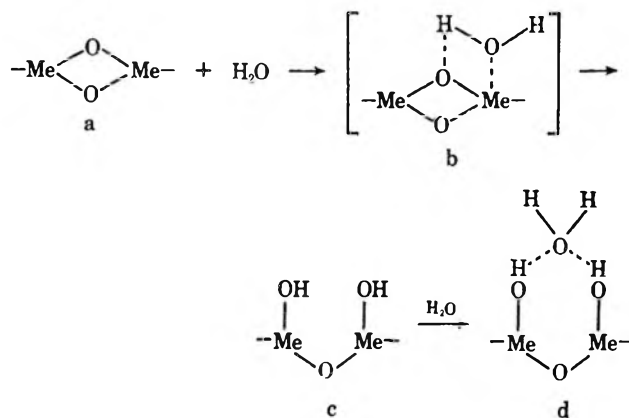
known to be perfect, and to about 9 OH groups/100 Å<sup>2</sup> for the (001) plane of α-Fe<sub>2</sub>O<sub>3</sub>.<sup>20</sup> As a whole, these values are nearly equal to the maximum value of the total chemisorbed water in Table I, which means that the surfaces are completely hydroxylated after the adsorption process.

If we examine the data in Table I in detail, it is found that the sum of  $V_c$  and  $V_h$ , or the total amount of chemisorbed water, decreases slightly with the rising temperature of pretreatment of the sample. In the previous paper,<sup>17</sup> alternate repetition of the adsorption measurement and degassing treatment showed that the reversible chemisorption occurs on dehydrated sites of the oxide surfaces, when the degassing treatment of oxide samples is carried out at temperatures lower than 500°. The present result implies that the rehydroxylation of the oxide surfaces dehydrated at higher temperatures than 600° *in vacuo* is not perfect. It is known that most metal oxides reveal the maximum in the plot of heat of immersion in water against pretreatment temperature at a temperature of 400–600°.<sup>4–6</sup> This fact has been explained in terms of the stabilization of oxide structure, which would occur at higher temperature of treatment; the stabilization results in the retardation of rehydroxylation upon immersion of the oxide surfaces in water. The present results seem to support the above explanation for the phenomenon-of-immersion anomaly. The change in the total amount of chemisorbed water by the pretreatment temperature is larger with α-Fe<sub>2</sub>O<sub>3</sub>(I) than with α-Fe<sub>2</sub>O<sub>3</sub>(II), as seen in Table I, which indicates that the extent of rehydroxylation may depend upon the origin and/or the history of the sample.

The ratio of the first-layer capacity of physical adsorption ( $V_p$ ) to the total number of underlying hydroxyl groups ( $V_c + V_h$ ) is nearly equal to 1:2, as shown in Table I, except in the case of TiO<sub>2</sub> pretreated at extremely high temperature. This suggests that a water molecule is adsorbed on two surface hydroxyl groups in most cases. Kiselev and Lygin,<sup>7</sup> who studied the adsorbed state of water molecules on silica by means of infrared spectroscopy, concluded that a water molecule is adsorbed on two surface hydroxyl groups through the formation of a hydrogen bond between the oxygen atom of the water molecule and two hydrogen atoms of

the neighboring hydroxyl groups. The quantitative demonstration for their conclusion has not been given. Also, on the surfaces of TiO<sub>2</sub> and Fe<sub>2</sub>O<sub>3</sub> it has been found by infrared spectroscopic investigation<sup>10–13</sup> that the physical adsorption of water occurs through hydrogen bonding to the surface hydroxyl groups, while the quantitative relation between the two kinds of surface species has not become clear. The fact that the cross-sectional area of the water molecule in the monolayer on TiO<sub>2</sub> (rutile) was extremely large, 23.5 Å<sup>2</sup>/H<sub>2</sub>O molecule, made Hoilabaugh and Chessick<sup>14</sup> infer that the physical adsorption of water would occur through the localization of a molecule on two surface hydroxyl groups. In the case of TiO<sub>2</sub> pretreated at an extremely high temperature, the ratio  $V_p : V_c + V_h$  was found to be nearly 1:2 as in other cases, despite the possibility of partial reduction and the resultant nonstoichiometric structure of the surface.

Thus we can, generally, conclude that the adsorption mechanism of water on the surfaces of TiO<sub>2</sub> and α-Fe<sub>2</sub>O<sub>3</sub> is



At the first stage of adsorption, a water molecule will be physically adsorbed on an activated site (a) to form an adsorption complex (b), which will subsequently transfer to surface hydroxyl groups (c). Next, another water molecule will come to be adsorbed through hydrogen bonding on the two neighboring hydroxyl groups as shown in d.

(20) E. S. Dana and W. E. Ford, "A Textbook of Mineralogy," John Wiley & Sons, Inc., New York, N. Y., 1960, pp 483, 498.

# Liquid Ion-Exchange Membranes with Weakly Ionized Groups. I.

## A Theoretical Study of Their Steady-State Properties<sup>1</sup>

by John Sandblom<sup>2</sup>

*Department of Physiology and Committee on Mathematical Biology, University of Chicago,  
Chicago, Illinois 60637 (Received September 1, 1967)*

The behavior of liquid ion-exchange membranes with weakly ionized groups is examined by applying previous theories of mobile-site membranes to the case of strong association, *i.e.*, when the number of ions is small compared with the number of ion pairs. By introducing a number of idealizing assumptions, the flux equations are integrated for a multicomponent system of univalent electrolytes, and the profiles, fluxes, and membrane resistance are expressed in terms of the electric current. It is shown that the current-voltage relationship is practically linear for intermediate fields, whereas higher fields give rise to a nonlinearity which depends not only on the mobilities of the counterions but also on their dissociation constants. Comparisons are also made between membranes with weakly and strongly ionized groups, between liquid and solid ion-exchange membranes, and between heterogeneous and homogeneous membranes. Finally a special case is considered, namely, the simultaneous presence of completely dissociated and strongly associated ions, which is shown to possess "apparent" limiting conductances for intermediate fields.

### Introduction

A liquid ion-exchange membrane consists of a water-immiscible solvent in which is dissolved an ionic component with a high affinity for the membrane phase.<sup>3</sup> The properties of such a membrane are similar in many ways to those of a solid ion-exchange membrane, *e.g.*, with respect to the restriction of ionic movement,<sup>4</sup> the large degree of selectivity,<sup>3,5</sup> and the ability to function as an ion-specific electrode.<sup>6</sup> On the other hand, a liquid exchange membrane is also distinguished from its solid counterpart by its partial solubility in the aqueous phases<sup>4</sup> and by the movement of dissociated ion pairs in the membrane interior.<sup>5,7</sup>

Although they have attracted considerable interest, liquid ion-exchange membranes have mostly been studied under such experimental conditions that a steady state has not been attained,<sup>4,5,7-10</sup> which is the reason why a complete description of the steady-state properties analogous to that which has been developed for fixed-site membranes<sup>11-16</sup> is presently lacking. The first attempt, however, at describing the steady-state behavior of liquid membranes was made by Conti and Eisenman,<sup>16</sup> who studied a membrane containing mobile sites with complete dissociation between sites and counterions. Their theory was later extended by Sandblom, Eisenman, and Walker,<sup>17</sup> who included the effects of association by assuming that sites and counterions combined to form electroneutral ion pairs within the membrane. This added considerable complexity to the mathematical treatment, although explicit solutions were obtained for the current-voltage relationship in the case of a single counterion<sup>17b</sup> and for the membrane potential at zero current in the case of two strongly associated counterions.<sup>17a</sup> The

theory for the single-counterion case was also verified experimentally.<sup>18</sup>

The present paper continues the treatment by Sandblom, *et al.*,<sup>17</sup> and considers a multicomponent system with the purpose of presenting a complete steady-state description of the membrane properties including fluxes, profiles, and current-voltage relationships for the limiting case of strong association between sites and counterions. This is a case of practical importance, since most

(1) This work was supported by research grant GB-4039 from the National Science Foundation and was aided by U. S. Public Health Service General Research Support Grant FR-5367 and Training Grant 5-T1-GM-833.

(2) Department of Physiology and Medical Biophysics, University of Uppsala, Uppsala, Sweden.

(3) K. Sollner and G. M. Shean, *J. Amer. Chem. Soc.*, **86**, 1901 (1964); G. M. Shean and K. Sollner, *Ann. N. Y. Acad. Sci.*, **137**, 759 (1966).

(4) K. F. Bonhoeffer, M. Kahlweit, and H. Strehlow, *Z. Phys. Chem. (Frankfurt am Main)*, **1**, 21 (1954).

(5) O. D. Bonner and J. Lunney, *J. Phys. Chem.*, **70**, 1140 (1966).

(6) J. W. Ross, Bulletin 92-81, Orion Research Inc., 1967.

(7) M. Kahlweit, *Arch. Ges. Physiol.*, **271**, 139 (1960).

(8) G. Eisenman, *Anal. Chem.*, **40**, 310 (1968).

(9) M. Dupeyrat, *J. Chim. Phys.*, **61**, 306, 323 (1964).

(10) H. L. Rosano, P. Duby, and J. H. Schulman, *J. Phys. Chem.*, **65**, 1704 (1961).

(11) T. Teorell, *Progr. Biophys. Biophys. Chem.*, **3**, 305 (1953).

(12) R. Schlogl, *Z. Phys. Chem. (Frankfurt am Main)*, **1**, 305 (1954).

(13) F. Helfferich, "Ion Exchange," McGraw-Hill Book Co., Inc., New York, N. Y., 1962.

(14) Y. Kobatake, *J. Chem. Phys.*, **28**, 146 (1958).

(15) F. Conti and G. Eisenman, *Biophys. J.*, **5**, 247 (1965).

(16) F. Conti and G. Eisenman, *ibid.*, **6**, 227 (1966).

(17) (a) J. Sandblom, G. Eisenman, and J. L. Walker, Jr., *J. Phys. Chem.*, **71**, 3862 (1967); (b) J. Sandblom, G. Eisenman, and J. L. Walker, Jr., *ibid.*, **71**, 3871 (1967).

(18) J. L. Walker, G. Eisenman, and J. Sandblom, *ibid.*, **72**, 978 (1968).

of the conventional liquid ion-exchange membranes have functional groups which are weakly ionized, owing partly to the relatively low dielectric constants of the organic diluents.<sup>3</sup> A strong association between sites and counterions is therefore expected to be a characteristic property of the unifunctional weakly acidic and basic liquid ion exchangers (*e.g.*, alkylphosphoric acids or alkylamines)<sup>19</sup> in solvents of low dielectric constants (<20). On the other hand, it is doubtful whether this is true for the strongly acidic or basic exchangers such as dinitronaphthalenesulfonic acid<sup>20</sup> and quaternary ammonium salts which may not be sufficiently associated except in solvents of very low dielectric constants (<3). In addition the considerable water solubility of the strongly acidic and basic exchangers will prevent them from being completely trapped within the membrane phase which is one of the basic assumptions of the theory.

Since the main object of the present treatment is to demonstrate the characteristic features which reflect the presence of trapped sites with a high degree of ion pair formation, it is reasonable to make a number of idealizing assumptions in order to simplify the mathematical solutions. The assumptions made here are also justified by the fact that the principle features predicted by the theory have been demonstrated experimentally on a thin membrane formed by dissolving bis(2-ethylhexyl)-phosphoric acid in amyl alcohol. The experimental results are described in part II.

### Theoretical Description

The differential equations describing an idealized liquid ion-exchange membrane with various degrees of association between sites and counterions have been developed by Sandblom, *et al.*,<sup>17a</sup> and the underlying assumptions have been discussed at length elsewhere.<sup>17b</sup>

Briefly, the membrane consists of a homogeneous ideal phase (see Figure 1) in which is dissolved an ionic, univalent component S, which constitutes the sites for exchange and which is assumed to be completely trapped within the membrane boundaries. The concentration of the ionic form of this component,  $c_s$ , is large enough to exclude co-ions; *i.e.*, the membrane is ideally permselective. The system also contains  $n$  number of univalent counterions and any number of impermeable co-ions.

Each component is present partly in its associated form and partly in its dissociated form. Therefore, the total concentration  $c_i^*$  of a component is equal to the sum of all the forms over which this component is distributed, or

$$c_i^* = c_i + c_{is} \quad (1a)$$

$$c_s^* = c_s + \sum_i c_{is} \quad (1b)$$

where  $c_s$  and  $c_i$  represent the dissociated forms of sites and counterions and  $c_{is}$  the corresponding associated

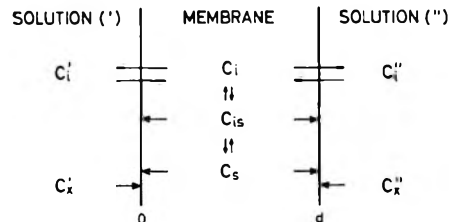


Figure 1. Schematic diagram of the system. The arrows indicate the equilibrium conditions prevailing in the membrane and across the membrane-solution interfaces.

forms. These concentrations are also assumed to be related at every point in the membrane through a set of mass-law equations

$$\frac{c_i c_s}{c_{is}} = K_i \quad (i = 1, \dots, n) \quad (2)$$

where  $K_i$  is the dissociation constant of the  $i$ th reaction (ion pair formation).

*Fluxes.* The fluxes of the various components follow the same additive rule as the concentrations (eq 1), and using the same subscripts this gives

$$J_i^* = J_i + J_{is} \quad (3a)$$

$$J_s^* = J_s + \sum_i J_{is} \quad (3b)$$

The partial fluxes  $J_i$ ,  $J_s$ , and  $J_{is}$  are also related to their electrochemical gradients by

$$J_i = -u_i c_i \frac{d}{dx} (RT \ln c_i + zF\psi) \quad (4a)$$

$$J_s = -u_s c_s \frac{d}{dx} (RT \ln c_s - zF\psi) \quad (4b)$$

$$J_{is} = -u_{is} c_{is} \frac{d}{dx} (RT \ln c_{is}) \quad (4c)$$

where  $u_i$ ,  $u_s$ , and  $u_{is}$  are the mobilities of the dissociated counterions, the dissociated sites, and the undissociated ion pairs, respectively (they are assumed to be constant);  $z$  is the valence of the counterions; and  $\psi$  is the electric potential.

To integrate the flux equations by taking into account the nonlinear mass-law equations (eq 2) is a complicated problem which has only been solved in a number of limiting cases. In this case the limiting case to be considered is that of strong association, by which is implied that the number of dissociated species is negligible compared with the corresponding number of ion pairs. This can be expressed by the inequalities

$$c_i \ll c_{is} \quad (i = 1, \dots, n) \quad (5)$$

(19) R. Kunin and A. G. Winger, *Angew. Chem. Int. Ed.*, **Engl.**, **1**, 149 (1962).

(20) E. Hogfeldt in "Ion Exchange," Vol. I, Marinsky, Ed., Marcel Dekker, Inc., New York, N. Y., 1967.

If eq 2 is applied to these inequalities, they can also be stated in a different way, namely

$$c_s \gg K_i \quad (i = 1, \dots, n) \quad (6)$$

From the last equation it is seen that in order to conform with the assumption of strong association,  $c_s$  must be large compared with  $K_i$ .

For a single salt eq 6 implies that  $\sqrt{\bar{c}_s^*} \gg \sqrt{K}$ , and an approximate criterion for the applicability of the theory is therefore obtained by applying this inequality to the largest of the  $K_i$ . Thus if the largest  $K_i$  is of the order  $10^{-4} M$ , then  $\bar{c}_s^*$  must be about  $1 M$  or larger in order for the theory to apply.

Equation 5 may be used to simplify the problem of integrating the flux equations, which, however, requires a rearrangement of eq 4a-4c. Thus by combining eq 4a-4c and inserting the mass-law equation (eq 2), we get

$$\frac{J_{is}}{u_{is}c_{is}} = \frac{J_i}{u_i c_i} + \frac{J_s}{u_s c_s} \quad (7)$$

Also, by introducing the electric current  $I$  expressed in terms of the ionic fluxes

$$\frac{I}{zF} = \sum_i J_i - J_s = \sum_i J_i^* - J_s^* \quad (8)$$

it becomes possible to express the total flux  $J_i^*$  in terms of  $J_{is}$  and  $I$ . Substituting  $J_i$  and  $J_s$  from eq 7 and 8 into eq 3a gives

$$J_i^* = \frac{It_i}{zF} + \left(1 + \frac{u_i c_i}{u_{is} c_{is}}\right) J_{is} - t_i \sum_i J_{is} \frac{u_i c_i}{u_{is} c_{is}} \quad (9)$$

where the transference number  $t_i$  is defined as

$$t_i = \frac{u_i c_i}{\sum_i u_i c_i + u_s c_s} \quad (10)$$

Finally, when eq 5 is applied to eq 9, we get a simplified expression for the total flux of a counterion

$$J_i^* = \frac{It_i}{zF} + J_{is} \quad (11)$$

This expression is seen to contain two contributions to the total flux, namely, an electrical contribution from the dissociated form and a diffusional contribution from the associated electroneutral form.

*Boundary Conditions.* In deriving the boundary conditions for the counterions, we shall assume that migration in the membrane phase is the rate-limiting step of the transport processes. The continuity of electrochemical potentials may then be applied to the membrane-solution interfaces, and this leads to the following equations relating internal and external quantities<sup>17</sup>

$$c_i(0) = c_s(0) \frac{a_i' k_t}{\sum_i a_i' k_t} \quad (12a)$$

$$c_i(d) = c_s(d) \frac{a_i'' k_t}{\sum_i a_i'' k_t} \quad (12b)$$

and

$$V = \Delta\psi + \frac{RT}{zF} \ln \frac{c_s(d)}{c_s(0)} + \frac{RT}{zF} \ln \frac{\sum_i a_i' k_t}{\sum_i a_i'' k_t} \quad (13)$$

where 0 and  $d$  refer to the two membrane boundaries and the superscripts refer to the two solution phases.  $a_i$  is the activity in the external solutions,  $\Delta\psi$  is the internal potential, and  $V$  is the total membrane potential.  $k_t/k_t$  is the ratio between partition coefficients of the counterions at infinite dilution of sites and counterions in the membrane. This parameter depends therefore exclusively on the properties of the solvent.

The two boundary conditions for the sites are based on the assumption that they are completely trapped within the membrane, which is expressed by the equations

$$J_s^* = 0 \quad (14)$$

$$\frac{1}{d} \int_0^d c_s^* dx = \bar{c}_s^* \quad (15)$$

where  $\bar{c}_s^*$  is the total average concentration of exchanger in the membrane and is a constant, and  $d$  is the thickness of the membrane.

## Results

*Concentration Profiles.* When the electric current is zero, the partial fluxes  $J_{is}$  are seen from eq 11 to be constants, and consequently the profiles of  $c_{is}$  will become linear (see eq 4c). (Although the partial flux  $J_{is}$  may be considered as constant, this is not necessarily true for the partial flux  $J_i$ , which at zero current is negligibly small compared with  $J_i^*$  and  $J_{is}$ .)  $c_s$  is then obtained from  $c_{is}$  by combining eq 2, the mass-law equation, with the condition of electroneutrality

$$\sum_i c_i = c_s \quad (16)$$

which gives

$$c_s^2 = \sum_i K_i c_{is} \quad (17)$$

It is apparent from this equation that when  $c_{is}$  is linear, the quantity  $c_s^2$  will also be a linear function of  $x$ . In other words, the profile of  $c_s$  has a parabolic shape in the case of strong association, in contrast to the linear shape of  $c_s$  in the case of complete dissociation.<sup>16</sup>

With a knowledge of the profiles, eq 11 and 15 may be integrated directly. Inserting the linear profiles of  $c_{is}$  into eq 15 and integrating yields

$$\sum_i c_{is}(d) + \sum_i c_{is}(0) = 2\bar{c}_s^* \quad (18)$$

where  $c_s$  has been neglected in comparison with  $c_{is}$  (cf. eq 5 together with eq 16). A relationship among

$c_s(0)$ ,  $c_s(d)$ , and external-solution conditions is then obtained by substituting eq 2 and 12 into eq 18

$$c_s^2(d) \frac{\sum_i \frac{k_i a_i''}{K_i}}{\sum_i k_i a_i''} + c_s^2(0) \frac{\sum_i \frac{k_i a_i'}{K_i}}{\sum_i k_i a_i'} = 2\bar{c}_s^* \quad (19)$$

A second expression is needed in order to solve explicitly for  $c_s(0)$  and  $c_s(d)$  in terms of the external boundary conditions, and this may be obtained from eq 11. When eq 11 is added, combined with eq 8 and 14, and integrated, we get

$$c_s^2(d) \frac{\sum_i \frac{u_{is} k_i}{K_i} a_i''}{\sum_i k_i a_i''} - c_s^2(0) \frac{\sum_i \frac{u_{is} k_i}{K_i} a_i'}{\sum_i k_i a_i'} = \frac{Id}{zRTF} \int_0^1 t_s d\left(\frac{x}{d}\right) \quad (20)$$

and at zero current the right-hand side of the equation is zero.

Equations 19 and 20 determine  $c_s(0)$  and  $c_s(d)$ .

*Fluxes.* Integrating eq 11 for the total flux of a counterion under zero current conditions gives

$$J_i^* = -\frac{RT u_{is}}{d} [c_{is}(d) - c_{is}(0)] = -\frac{RT u_{is}}{K_i d} [c_i(d)c_s(d) - c_i(0)c_s(0)] \quad (21)$$

where eq 2, the mass law equation, has been used. When the boundary conditions (12), (19), and (20) are inserted, we get, after rearrangement, the total flux expressed in terms of external boundary conditions

$$J_i^* = -\frac{RT u_{is} k_i}{d K_i} \left[ a_i'' \frac{\sum_i \frac{u_{is} k_i}{K_i} a_i'}{\sum_i k_i a_i''} - a_i' \right] \quad (22)$$

where

$$k = \frac{2\bar{c}_s^* \sum_i \frac{u_{is} k_i}{K_i} a_i''}{\sum_i \frac{u_{is} k_i}{K_i} a_i' \sum_i \frac{k_i}{K_i} a_i'' + \frac{u_{is} k_i}{\sum_i K_i} a_i' \sum_i \frac{k_i}{K_i} a_i'}$$

The flux ratio between two counterions, obtained by taking the ratio of eq 22, may be compared with the corresponding flux ratio derived for fixed-site membranes<sup>11,15</sup> or mobile-site membranes with complete dissociation between sites and counterions<sup>16</sup>

$$\frac{J_i^*}{J_j^*} = \frac{u_i K_i a_i'' e^{zFV/RT}}{u_j K_j a_j'' e^{zFV/RT}} \frac{a_i'}{a_j'} \quad (23)$$

where  $V$  is the total membrane potential and  $K$  is the ion-exchange equilibrium constant.

A comparison between eq 22 and 23 shows that it is possible to define an emf from eq 22 corresponding to the total membrane potential,  $V$ , appearing in eq 23. This emf is evidently given by

$$E = \frac{RT}{zF} \ln \frac{\sum_i \frac{u_{is} k_i}{K_i} a_i'}{\sum_i \frac{u_{is} k_i}{K_i} a_i''} \quad (24)$$

Equation 24 has been deduced from more general considerations<sup>21</sup> and has been shown to be the total emf of the diffusion pathway for the ion pairs. (The concept of two diffusion pathways is purely formal and should not be visualized as a geometrical heterogeneity.) The reason for this is that in a membrane with strong association between sites and counterions the larger part of the ionic transport occurs by way of ion pairs. The equilibrium distribution of an ion between the two solution phases will therefore depend on the emf of the ion pair pathway (eq 24) when the ion is strongly associated and on the total membrane potential  $V$  when it is completely dissociated. If these two potentials are of opposite signs, the possibility exists to separate ions which are primarily associated and ions which are primarily dissociated.

*Membrane Resistance.* The total membrane resistance at steady state for strong association has been derived from the general theory and is given by<sup>21</sup>

$$R_0 = \frac{1}{z^2 F^2} \int_0^d \frac{dx}{\sum_i u_i c_i + u_s c_s} \quad (25)$$

The subscript 0 has been added to indicate that the resistance is measured at steady state (although the instantaneous and steady-state resistance have been shown to coincide for strong association).<sup>21</sup> If the numerator and denominator are multiplied by  $c_s$  and the mass-law equation (eq 2) taken into account, we get

$$R_0 = \frac{1}{z^2 F^2} \int_0^d \frac{c_s dx}{\sum_i u_i K_i c_{is} + u_s c_s} \quad (26)$$

With the abbreviations

$$A = \sum_i (u_i + u_s) K_i (c_{is}(d) - c_{is}(0))$$

$$B = \frac{c_s^2(0) \sum_i (u_i + u_s) K_i c_{is}(d) - c_s^2(d) \sum_i (u_i + u_s) K_i c_{is}(0)}{\sum_i (u_i + u_s) K_i (c_{is}(d) - c_{is}(0))}$$

the solution to eq 26 is given by

(21) J. Sandblom, *Ark. Fys.*, **35**, 329 (1967).

$$R_0 = \frac{d}{z^2 F^2} \frac{2}{A} \left[ c_s(d) - c_s(0) - \sqrt{-B} \operatorname{arctg} \frac{c_s(d)}{\sqrt{-B}} + \sqrt{-B} \operatorname{arctg} \frac{c_s(0)}{\sqrt{-B}} \right] \quad (B < 0) \quad (27a)$$

$$R_0 = \frac{d}{z^2 F^2} \frac{2}{A} \left[ c_s(d) - c_s(0) + \frac{\sqrt{B}}{2} \ln \frac{c_s(d) - \sqrt{B}}{c_s(d) + \sqrt{B}} - \frac{\sqrt{B}}{2} \ln \frac{c_s(0) - \sqrt{B}}{c_s(0) + \sqrt{B}} \right] \quad (B > 0) \quad (27b)$$

where the linearities of  $c_s^2$  and  $c_{is}$  have been used in the integration. When all the mobilities  $u_i$  are equal eq 27a and 27b reduce to

$$R_0 = \frac{d}{z^2 F^2 (u_i + u_s)} \frac{2}{c_s(d) + c_s(0)} \quad (28)$$

The values of  $c_s(0)$  and  $c_s(d)$  are again obtained from eq 19 and 20.

It is seen from eq 27 that the membrane resistance does not explicitly depend on the electric field, except through the boundary concentrations of  $c_s$ . This has the important consequence that the resistance is ohmic whenever the site distribution is kept constant. In general, however, the sites will redistribute under the influence of an applied electric field and give rise to a nonlinearity in the resistance.

So far we have only considered the membrane properties at zero current. However, owing to the very high resistance of liquid ion-exchange membranes with strong association, even small currents will give rise to high electric fields. The equations derived for zero current will therefore describe the behavior of the membrane over a broad range of applied potentials, depending of course on the degree of association (see Figure 2). In particular, it follows that the membrane resistance will be ohmic in this range of potentials in spite of the fact that the mobilities may be quite different and the resistance may vary extensively with the external-solution conditions. This phenomenon is due to the large number of ion pairs which are not acted on by an applied electric field but nevertheless affect the resistance through a chemical coupling with the ions expressed by the mass law (eq 2).

When the membrane resistance is ohmic in a fixed-site membrane, the potential at zero current,  $V_0$ , is due entirely to boundary potentials (*cf.* Teorell's<sup>11</sup> eq 38), in contrast to the situation in liquid ion-exchange membranes where the internal potential may be different from zero even when the resistance is ohmic.

The chemical coupling between ions and ion pairs at *every point in the membrane* also brings out the distinction between the geometrical heterogeneity of mosaic membranes and the purely electrical heterogeneity of liquid ion-exchange membranes. The transport of counterions in two different forms, a dissociated and an associated, will impart certain properties of hetero-

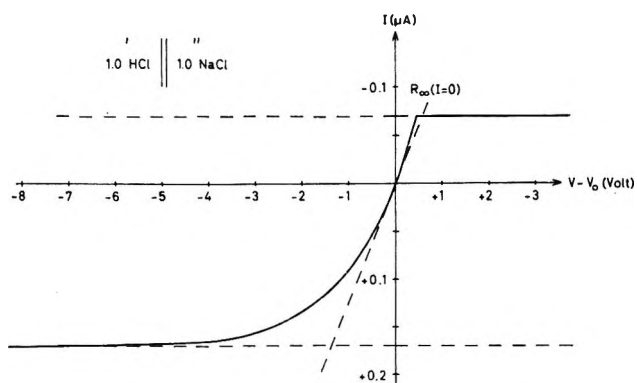


Figure 2. The theoretical current-voltage relationship for a system containing two strongly associated counterions  $H^+$  and  $Na^+$ . The solution on the left-hand side of the membrane contains pure HCl and the solution on the right-hand side contains pure NaCl, as indicated in the figure.  $Cl^-$  is assumed to be impermeable. The following parameters corresponding to the experimental system of part II have been used in the calculations:  $\lambda^0_H = 18.56$ ,  $\lambda^0_{Na} = 1.47$ ,  $\lambda^0_S = 9.99$ ,  $\lambda^0_{NaS} = \lambda^0_H = 2.7$ ,  $K_H = 2.26 \times 10^{-9} \text{ mol/cm}^3$ ,  $K_{Na} = 5.6 \times 10^{-7} \text{ mol/cm}^3$ ,  $c_s^* = 0.3 \times 10^{-3} \text{ mol/cm}^3$ ,  $A(\text{membrane area}) = 0.95 \times 10^{-4} \text{ cm}^2$ ,  $d = 0.065 \text{ cm}$ . The limiting currents and the instantaneous resistance at zero current are indicated by dotted lines. Positive current flows from left to right in the figure and the solution on the left side is considered to have ground potential.

geneity to a geometrically homogeneous membrane, *e.g.*, with respect to the emf,<sup>21</sup> although the chemical coupling between ions and ion pairs is active throughout the membrane. If, on the other hand, dissociated and associated forms move in geometrically separated channels in accordance with a model studied by Finkelstein,<sup>22</sup> their mutual coupling will *only be present at the membrane boundaries*. The ion pairs will then only exert their "buffering" action at the membrane boundaries, maintaining fixed boundary conditions over a large range of applied potentials. This system would therefore retain the rectification properties of the ionic channels in spite of the fact that the inequality (5) is satisfied.

Since the inequality (5) is satisfied whether the system is geometrically homogeneous or whether it is heterogeneous, eq 25 applies to either case, whereas eq 26, which rests on the validity of chemical equilibrium at *all* points in the membrane, only applies to the homogeneous system. *It is this fact which is responsible for the ohmic resistance of a liquid ion-exchange membrane in which all counterions are strongly associated.* At sufficiently high fields, however, the first term in eq 11 can no longer be neglected and the membrane resistance will depart from linearity (see Figure 2).

*Limiting Currents.* A general property of mobile-site membranes with complete co-ion exclusion is the existence of limiting currents.<sup>16,17,23</sup> As the applied current

(22) A. Finkelstein, *Biophys. J.*, **4**, 421 (1964).

(23) G. Eisenman, J. Sandblom, and J. L. Walker, Jr., *Science*, **155**, 965 (1967).

is increased, the sites are depleted and the concentrations are eventually reduced to zero at one end of the membrane. The applied current has then reached a limiting value.

It may be shown that the profiles of  $c_{is}$  which are linear at zero current will also be linear when the limiting current is reached. Multiplying the numerator and the denominator of eq 10 by  $c_s$ , we obtain, using eq 2, the mass-law equation

$$t_i = \frac{\sum_i u_i K_i c_{is}}{\sum_i (u_i + u_s) K_i c_{is}} \quad (29a)$$

$$t_s = \frac{\sum_i u_s K_i c_{is}}{\sum_i (u_i + u_s) K_i c_{is}} \quad (29b)$$

If the profiles of  $c_{is}$  are linear and if moreover they are zero at one end of the membrane, the quantity  $t_i$  will be constant. This is also consistent with eq 11, according to which  $t_i$  must be constant when  $c_{is}$  is linear, except at  $I = 0$ . Equation 11 is therefore satisfied by linear profiles at zero current and at the limiting currents.

Setting, respectively,  $c_s(0)$  and  $c_s(d)$  equal to zero in eq 19 and 20, we obtain for the limiting currents

$$I_l = -\frac{2zRTF\bar{c}_s}{u_sd} * \frac{\sum_i \frac{k_i}{K_i} a_i''}{\sum_i \frac{k_i}{K_i} a_i''} \times \frac{\sum_i (u_i + u_s) k_i a_i''}{\sum_i k_i a_i''} \quad (zV \rightarrow +\infty) \quad (30a)$$

$$I_l = \frac{2zRTF\bar{c}_s}{u_sd} * \frac{\sum_i \frac{u_{is}}{K_i} a_i'}{\sum_i \frac{k_i}{K_i} a_i'} \times \frac{\sum_i (u_i + u_s) k_i a_i'}{\sum_i k_i a_i'} \quad (zV \rightarrow -\infty) \quad (30b)$$

The magnitudes of these are seen to be unaffected by the degree of association and only depend on the ratios of the  $K_i$  values. This dependence will disappear if the mobilities of the different ion pairs are equal (see eq 33), which is likely to be the case in view of their lack of charge and their equal size. Under such circumstances eq 30a and 30b reduce to

$$I_l = -\frac{4zRTF\bar{c}_s}{d} * \frac{\sum_i \frac{u_{is}}{\bar{u}_{is}} k_i a_i''}{\sum_i k_i a_i''} \quad (zV \rightarrow +\infty) \quad (31a)$$

$$I_l = \frac{4zRTF\bar{c}_s}{d} * \frac{\sum_i \frac{u_{is}}{\bar{u}_{is}} k_i a_i'}{\sum_i k_i a_i'} \quad (zV \rightarrow -\infty) \quad (31b)$$

where  $\bar{u}_{is}$  is the mean mobility of the ions defined as

$$\bar{u}_{is} = \frac{2u_i u_s}{u_i + u_s}$$

Thus apart from the ratio  $u_{is}/\bar{u}_{is}$  these expressions are identical with those which apply to a membrane with complete dissociation between sites and counterions (cf. Conti and Eisenman's<sup>16</sup> eq 49 and 50).

*Current-Voltage Relationship.* The complete current-voltage relationship is determined by the steady-state membrane resistance (eq 27), the boundary conditions for the sites (eq 19 and 20), and the membrane potential at zero current. The latter quantity may be derived by combining eq 8 and the inequality (5). Since in the case of two counterions this leads to an expression derived by Sandblom, *et al.*,<sup>17</sup> we shall here only quote their result

$$V_0 = \frac{RT}{zF} (1 - \tau) \ln \frac{\sum_i (u_i + u_s) k_i a_i'}{\sum_i (u_i + u_s) k_i a_i''} + \frac{RT}{zF} \tau \ln \frac{\sum_i \frac{k_i}{K_i} a_i'}{\sum_i \frac{k_i}{K_i} a_i''} \quad (32)$$

where

$$\tau = \frac{u_s(u_{1s}K_2 - u_{2s}K_1)}{(u_2 + u_s)u_{1s}K_2 - (u_1 + u_s)u_{2s}K_1}$$

Figure 2 shows the current-voltage relationship for a cation-selective membrane with a set of parameters that correspond to the experimental system described in part II of this series. The curve has been constructed by inserting these parameters into eq 19, 20, and 27. Each limb of the current-voltage relationship has been calculated with a constant value of  $t_s$ , namely, the value it assumes at the corresponding limiting current. This gives correct values for the  $I$ - $V$  curve close to the limiting currents but also around zero current where the right side of eq 20 is very small.

In the region around zero current a better value for the integral of  $t_s$  is obtained by using the linearity of  $c_{is}$ . The integration of eq 29b then gives

$$\int_0^1 t_s d\left(\frac{x}{d}\right) = \frac{u_s}{A} \times \left[ c_s^2(d) - c_s^2(0) + B \ln \frac{\sum_i (u_i + u_s) K_i c_{is}(d)}{\sum_i (u_i + u_s) K_i c_{is}(0)} \right] \quad (33)$$

where  $A$  and  $B$  have previously been defined.

To calculate the integral of  $t_s$  from eq 33 for each value of the current, an arbitrary value for the right-hand side of eq 20 is chosen from which  $c_s(0)$  and  $c_s(d)$  can be calculated. If these are inserted into eq 33, a

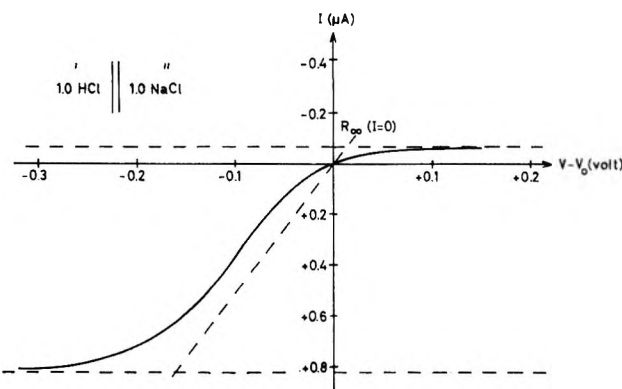


Figure 3. The theoretical current-voltage relationship for the same system as shown in Figure 2, with the exception that  $K_H = K_{Na} = \infty$ . The curve has been calculated from eq 45 of Conti and Eisenman.<sup>16</sup> The instantaneous resistance at zero current was obtained by calculating the instantaneous flux  $J_s$  for potentials corresponding to the linear portion of the steady-state curve. These values of  $J_s$  were then added to the corresponding steady-state currents.

value for the integral is obtained. This is the procedure used in calculating the theoretical curves in the experimental part. (It should be noted, however, that the slope of the  $I$ - $V$  curve at  $I = 0$  is independent of what value for  $t_s$  is used.)

The intermediate sections of the  $I$ - $V$  curve shown in Figure 2 are only approximate, in that  $c_{is}$  is not constant, and eq 19 and 27 therefore are strictly not applicable. Nevertheless, the important features are clearly demonstrated by this figure and it is interesting to compare it with the corresponding figure for a system with complete dissociation between sites and counterions. Figure 3 shows the current-voltage relationship for such a system calculated from the equations of Conti and Eisenman.<sup>16</sup> The same parameters as in Figure 2 are used with the exception of  $K_i$  which is infinite for complete dissociation.

A comparison between Figures 2 and 3 shows that the two systems have approximately the same limiting currents and the same quantitative nonlinearity. On the other hand, some important differences are clearly evident. The scaling factor for the abscissa is quite different in the two cases, and over the same range of applied potentials the system with strong association has a much greater linearity. Moreover, the instantaneous resistance is equal to the steady-state resistance for strong association but quite different from the latter for complete dissociation. This is seen in Figures 2 and 3 where the instantaneous resistances at zero current are indicated by dotted lines. These effects on the steady state and instantaneous resistances introduced by the presence of ion pairs have also been deduced and discussed for the single-counterion case.<sup>17</sup>

Another interesting difference between the two systems is the sharp transition which the resistance undergoes at the limiting currents in the case of strong association. This phenomenon may be explained as follows.

Equation 27 for the membrane resistance is a function which does not tend to infinity as  $c_s(0)$  or  $c_s(d)$  approaches zero, and, therefore, it intercepts the limiting currents. Because, however, the sites must be depleted practically to zero before the dissociated species will predominate over the ion pairs, causing the profiles to shift from a linearity in  $c_s^2$  to a linearity in  $c_s$ , eq 27 is valid except for values which are extremely close to the limiting currents. This becomes more evident by considering the case of a single counterion with  $\bar{u}_{is} = u_{is}$ . The expression for the concentration profile in the case of strong association is then given by (cf. Sandblom, et al.,<sup>17b</sup> eq 17)

$$c_s^2(x) + K c_s(x) = K \bar{c}_s^* \left[ 1 - \frac{I}{I_l} \left( 1 - \frac{2x}{d} \right) \right] \quad (34)$$

where  $I_l$  is the limiting current and  $K$  is the dissociation constant. The transition between a linear  $c_s^2$  and a linear  $c_s$  at one end of the membrane occurs when

$$1 - \frac{I}{I_l} = \frac{2K}{\bar{c}_s^*}$$

which is an exceedingly small quantity, considering that  $\sqrt{\bar{c}_s^*} \gg \sqrt{K}$ .

### The Simultaneous Presence of Completely Dissociated and Strongly Associated Ions

For membrane potentials in the physiological range ( $< 0.5$  V), a strong association between sites and counterions was shown to produce a nearly linear  $I$ - $V$  characteristic (Figure 2), in sharp contrast to the situation in a dissociated system which exhibits a pronounced nonlinear  $I$ - $V$  curve (Figure 3). It is therefore of interest to examine the properties of a system in which both types of ions are present simultaneously. This may also be of some relevance for biological membranes in which ionic carriers have been postulated to exist but where the highly nonlinear current-voltage characteristic makes a strong association between all counterions improbable in view of the results presented in this paper.

An experimental situation with both types of ions present is described in part II of this series. It contains a single electrolyte of sufficient concentration to permit co-ions to pass the membrane. The site and counterion are strongly associated but the co-ion is essentially dissociated. With unequal concentrations of the electrolyte on the two sides of the membrane, this system shows a distinct rectification over a potential range within which a strongly associated system is expected to be practically ohmic.

This can be deduced theoretically from the present treatment and an expression can be obtained for the rectification ratio. If it is assumed that sites and counterions are present in approximately equal amounts, the presence of dissociated co-ions will suppress the ionic forms of the sites by virtue of the mass-law relationship. It therefore follows from eq 3b and 14 that

$$J_{1s} = 0 \quad (35a)$$

for electric potentials satisfying

$$\frac{F\Delta\psi}{RT} \ll \frac{u_{1s}c_{1s}}{u_s c_s} \quad (35b)$$

Equation 35 implies that  $c_{1s}$  is constant throughout the membrane or

$$\frac{c_1 c_s}{K} = c_{1s} = \bar{c}_s^* \quad (36)$$

Consider next the flux of co-ions, labeled  $J_2$ , which is a constant at steady state since the co-ions are completely dissociated. It is also related to the electrochemical gradient by the Nernst–Planck equation

$$J_2 = -u_2 c_2 \frac{d}{dx} (RT \ln c_2 - Fz\psi) \quad (37)$$

Since they are able to pass the membrane in this case, the co-ions contribute to the electric current which is now given by

$$\frac{I}{zF} = J_1 - J_s - J_2 \quad (38)$$

Eliminating  $J_1$  from eq 38 with the aid of eq 7 and 35, we get after rearrangement

$$J_s = -\left(\frac{I}{zF} + J_2\right) \frac{u_s c_s}{u_s c_s + u_1 c_1} = -u_s c_s \frac{d}{dx} (RT \ln c_s - zF\psi) \quad (39)$$

and the flux ratio  $J_s/J_2$  becomes

$$\frac{\frac{I}{zF} + J_2}{J_2} \frac{u_s c_s}{u_s c_s + u_1 c_1} = -\frac{u_s c_s d (RT \ln c_s - zF\psi)}{u_2 c_2 d (RT \ln c_2 - zF\psi)} = -\frac{u_s}{u_2} \frac{dc_s e^{-zF\psi/RT}}{dc_2 e^{-zF\psi/RT}} \quad (40)$$

For large positive or large negative potentials satisfying the inequality (35b), the profiles will be approximately uniform throughout the membrane due to the presence of a dissociated ion with  $J_2$  approaching  $-It_2/zF$ . Applying this to eq 37 and 40, respectively, and integrating yields

$$-\frac{It_2 d}{zF^2 u_2 c_2} = V \quad (41)$$

$$\frac{1 - t_2}{-t_2} \frac{t_s}{1 - t_2} = -\frac{u_s c_s'' e^{-zF\Delta\psi/RT} - c_s'}{u_2 c_2'' e^{-zF\Delta\psi/RT} - c_2'} \quad (42)$$

To insert the proper boundary conditions into eq 42,  $c_s$  is substituted for  $c_1$  recalling that the product  $c_1 c_s$  is constant. Using the continuity of electrochemical potentials of ions 1 and 2 at the boundaries, we then have

$$\frac{S^2}{c_1 c_2} = \frac{\frac{1}{a''} e^{-zFV/RT} - \frac{1}{a'}}{\frac{a''}e^{-zFV/RT} - a'} \quad (43)$$

where  $S$  is the distribution coefficient of the electrolyte between the aqueous solution and the membrane phase

$$c_1 c_2 = S^2 a_{aq}^2$$

Finally  $c_1$  and  $c_2$  are eliminated from eq 41 and 43 by taking into account eq 36 and the electroneutrality condition

$$I = -\frac{zF^2}{d} V \times \frac{(u_1 + u_s) K \bar{c}_s^* + (u_1 + u_2) S^2 \frac{a'' e^{-zFV/RT} - a'}{\frac{1}{a''} e^{-zFV/RT} - \frac{1}{a'}}}{\sqrt{K \bar{c}_s^* + S^2 \frac{a'' e^{-zFV/RT} - a'}{\frac{1}{a''} e^{-zFV/RT} - \frac{1}{a'}}}} \quad (44)$$

The rectification ratio is then obtained directly from eq 44

$$\frac{R(zV \gg -1)}{R(zV \ll +1)} = \frac{\sqrt{K \bar{c}_s^* + S^2 a'^2}}{\sqrt{K c_s^* + S^2 a''^2}} \times \frac{(u_1 + u_s) K \bar{c}_s^* + (u_1 + u_2) S^2 a''^2}{(u_1 + u_s) K \bar{c}_s^* + (u_1 + u_2) S^2 a'^2} \quad (45)$$

and is seen to depend on the ratio between external-solution activities and the concentration  $\bar{c}_s^*$  of exchanger in the membrane. With sufficiently high concentration of the exchanger, the membrane will obviously not exhibit any rectification, whereas in the other limit the rectification will be completely determined by the external solution activities with a direction governed by the movement of co-ions. In this respect the membrane behaves like a negative-fixed-charge membrane described for example by Teorell<sup>11</sup> and Schlogl,<sup>12</sup> where the rectification depends on the fixed-charge density with a direction governed by the co-ions due to a washing-out effect.<sup>12</sup>

It can therefore be concluded from the present treatment that for intermediate applied potentials the membrane will behave as a fixed-charge membrane but for potentials large enough to change the boundary concentrations the behavior will be quite different. If the dissociated ions are counterions, the current will approach limiting values for large applied potentials, but in the presence of dissociated co-ions the membrane resistance will decrease with increasing applied potentials (*cf.* a treatment by Conti and Ciani of a membrane with completely dissociated sites and counterions).<sup>24</sup>

(24) F. Conti and S. Ciani, *Biophysica*, in press.

# Liquid Ion-Exchange Membranes with Weakly Ionized Groups. II.

## The Resistance and Electromotive Force of a Thin Membrane<sup>1</sup>

by John Sandblom<sup>2</sup>

*Department of Physiology and Committee on Mathematical Biology, University of Chicago,  
Chicago, Illinois 60637 (Received September 1, 1967)*

Previously developed theories for liquid ion-exchange membranes, in particular the conclusions of part I, are tested on a thin (0.65-mm) membrane formed by dissolving the acid cation exchanger bis(2-ethylhexyl)-phosphoric acid in amyl alcohol. This system is shown to conform reasonably well with the assumptions on which the theories are based, notably completely trapped sites with weakly ionized groups and a convection-free membrane. The transients of the emf and the membrane resistance are measured simultaneously following step changes in external-solution conditions containing mixtures of HCl and NaCl, from which it is concluded that the emf is established instantaneously long before the profiles have reached their steady states. Measurements are also made of the steady-state resistance for various external solutions and applied electric fields which confirm the theoretical predictions that the resistance is practically independent of the electric field but strongly dependent on the external-solution compositions. The ranges of concentrations in these experiments are chosen such that the co-ions are excluded from the membrane. However, experiments are also performed with HCl in different concentrations on the two sides of the membrane, and a strong rectification tendency is observed when the co-ions are not excluded which is also predicted by the theory.

### Introduction

Liquid ion-exchange membranes have primarily been studied because of their resemblance to cell membranes<sup>3-5</sup> and recently also because of their electrode-specific properties.<sup>6,7</sup> A liquid ion exchanger consists of a water-immiscible organic solvent, usually of low dielectric constant, in which is dissolved an ionic component of proper size and configuration to make it insoluble in water.<sup>8,9</sup> Several types of such systems have been characterized with respect to their physicochemical properties,<sup>10,11</sup> of which the partition coefficients and the complex formation by the ionic constituents are the most important parameters in determining their behavior as membranes.<sup>12,13</sup>

By introducing a number of simplifying assumptions the transport properties of liquid-ion-exchange membranes have also been subject to theoretical analysis, where the membranes have been regarded as mobile-site membranes<sup>14,15</sup> containing varying degrees of ion pair formation.<sup>15,16</sup> In part I of this series a theory for the case of strong association was developed and is expected to describe the behavior of most types of weakly ionized liquid ion-exchange membranes. This as well as earlier treatments, however, have been confined to the steady state which assumes the interior of the membrane to be convection free, and consequently these treatments do not apply to such experimental situations in which the membrane has been deliberately stirred<sup>17,18</sup> or where it has been thick enough to permit convection in the interior.<sup>4,8,19,20</sup> Special experimental arrangements are therefore required to test the steady-state theories, and in the case of a single counterion this has been accomplished in a "model" system designed to

satisfy the idealizing assumptions.<sup>21</sup> By enclosing a solution of HCl-2-propanol in a polyvinyl tubing sealed at both ends with Ag-AgCl electrodes, a model system

- (1) This work was supported by research grant GB-4039 from the National Science Foundation and was aided by U. S. Public Health Service General Research Support Grant FR-5367 and Training Grant 5-T1-GM-833.
- (2) Department of Physiology and Medical Biophysics, University of Uppsala, Uppsala, Sweden.
- (3) R. Beutner, "Physical Chemistry of Living Tissues and Life Processes," Williams and Wilkins, Baltimore, 1933.
- (4) W. J. V. Osterhout, *Cold Spring Harbor Symp. Quant. Biol.*, **8**, 51 (1940).
- (5) K. F. Bonhoeffer, M. Kahlweit, and H. Strehlow, *Z. Phys. Chem.* (Frankfurt am Main), **1**, 21 (1954).
- (6) Data Sheet on Ca<sup>2+</sup> Electrode No. 92-20B, Orion Research Inc., 1966.
- (7) G. Eisenman, *Anal. Chem.*, **40**, 310 (1968).
- (8) G. M. Shean and K. Sollner, *Ann. N. Y. Acad. Sci.*, **137**, 759 (1966).
- (9) R. Kunin and A. G. Winger, *Angew. Chem. Int. Ed., Engl.*, **1**, 149 (1962).
- (10) A. L. Myers, W. J. McDowell, and C. F. Coleman, *J. Inorg. Nucl. Chem.*, **26**, 2005 (1964).
- (11) T. Shedlovsky and H. H. Uhlig, *J. Gen. Physiol.*, **17**, 563 (1933).
- (12) M. Dupeyrat, *J. Chim. Phys.*, **61**, 306, 323 (1964).
- (13) M. Kahlweit, H. Strehlow, and C. S. Hocking, *Z. Phys. Chem.* (Frankfurt am Main), **4**, 212 (1955).
- (14) F. Conti and G. Eisenman, *Biophys. J.*, **6**, 227 (1966).
- (15) J. Sandblom, G. Eisenman, and J. Walker, Jr., *J. Phys. Chem.*, **71**, 3862, 3971 (1967).
- (16) J. Sandblom, *Ark. Fys.*, **35**, 329 (1967).
- (17) O. D. Bonner and J. Lunney, *J. Phys. Chem.*, **70**, 1140 (1966).
- (18) H. L. Rosano, P. Duby, and J. H. Schulman, *ibid.*, **65**, 1704 (1961); H. L. Rosano, K. Breindel, J. Schulman, and A. Eydt, *J. Colloid Sci.*, **22**, 58 (1966).
- (19) M. Kahlweit, *Arch. Ges. Physiol.*, **271**, 139 (1960).
- (20) K. Sollner and G. M. Shean, *J. Amer. Chem. Soc.*, **86**, 1901 (1964).

was obtained which functioned as a mobile-site membrane, the  $H^+$  ions behaving as trapped sites and the  $Cl^-$  ions behaving as permeable counterions.<sup>21</sup> With suitable precautions the interior of this membrane could be kept convection free. The advantage of having well-defined boundary conditions made this system a particularly useful one for testing the basic elements of the theoretical treatments.<sup>21</sup>

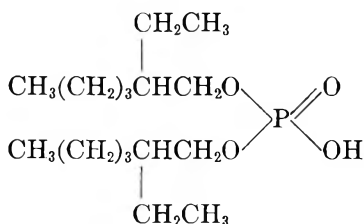
It is also of interest, however, to examine the extent to which the theory can predict the behavior of a liquid ion-exchange membrane in contact with aqueous solutions. For this purpose a membrane has been made from a commercially available liquid ion exchanger and has been studied under such experimental conditions that the requirements of the theory are met. The experiments have been carried out under steady-state conditions with a convection-free membrane, and the results have shown reasonable agreement with the theory.

Studies on this system may therefore be of some relevance to biological membranes in which lipid-soluble carriers have been postulated to exist and where the interior hydrocarbon region is likely to be convection free in view of the bimolecular arrangement. The system should also be useful for comparing liquid and solid ion-exchange membranes with respect to their rectification and other steady-state properties, a comparison which the usual nonconvection-free liquid membranes have not permitted.

*The System Studied.* In preparing a membrane in which the effects of association (ion pair formation) can be conveniently studied, it is desirable to select a system whose chemical properties are simple and well defined. Furthermore, in order to conform with the assumptions of the theories, the experimental system should come as close as possible to meeting the following requirements: (a) the counterions and sites are univalent and behave ideally except insofar as they can associate through a simple law of mass action to form neutral ion pairs; (b) the sites are unable to cross the membrane-solution interfaces; (c) the membrane interior is convection free; and (d) in addition the diffusion of counterions should be membrane controlled.

The property (a) can be obtained by a proper choice of liquid ion exchanger, whereas the properties b-d also depend on the experimental situation.<sup>7,15</sup>

The liquid ion exchanger used was the acid cation exchanger B2EHPA (bis-(2-ethylhexyl)phosphoric acid) having the steric formula<sup>9</sup>



B2EHPA generally forms monomers (ion pairs) or

dimers in organic solvents,<sup>10</sup> and the branching of its hydrocarbon chain makes it sparingly soluble in water. However, it is only in the acid form in which B2EHPA behaves ideally, since ion-exchange studies indicate that the  $Na^+$  salt of B2EHPA forms higher order aggregates of the form  $NAS-3HS$ , where S is the anion of B2EHPA.<sup>10</sup> Furthermore, the  $Na^+$  salt is highly soluble in water, although its affinity for organic solvents is greater than for water.

The properties of a liquid ion exchanger depend to a greater extent on the nature of the solvent, particularly with respect to the dielectric constant and the water content. N-Amyl alcohol was chosen because it combines a relatively low water solubility (2.7 g/100 ml of  $H_2O$ ) with a favorable dielectric constant, which does not cause the ionization of B2EHPA to be unduly suppressed. The conductivity is therefore sufficiently high to permit an evaluation of the limiting conductances and dissociation constants by conductometric methods according to Fuoss and Kraus.<sup>22</sup>

The water content of the membrane will depend on the concentration of B2EHPA and other ions when the membrane is in contact with aqueous solutions. Consequently, the degree of hydration of charged species in the membrane is expected to vary with concentrations. In strong support of this is the observed concentration dependence of the ionic selectivities in a chinolin membrane, which was shown to be a result of variations in the mobilities due to changes in the degree of hydration.<sup>5</sup> Therefore, one might expect deviations from ideal behavior with respect to the mobilities and standard chemical potentials of the ions. On the other hand, it is reasonable to assume that the uncharged species have constant mobilities, since these depend only on the molecular size of the molecules and the viscosity of the membrane which is not expected to vary with small changes in the water content.

*Measurements of Basic Parameters.* The basic parameters in terms of which the membrane properties may be characterized appear in the theoretical treatment of part I, namely, the limiting equivalent conductances ( $\lambda^0_{HS}$  and  $\lambda^0_{Nas}$ ), the dissociation constants ( $K_H$  and  $K_{Na}$ ), the transference numbers ( $t_H$  and  $t_{Na}$ ), the limiting partition coefficients ( $k_H/k_{Na}$ ), and the mobilities of the ion pairs ( $u_{HS}$  and  $u_{Nas}$ ). Except for the mobilities of the ion pairs all these parameters have been determined by classical electrochemical methods (see Table I).

The limiting conductances and dissociation constants for the acid and its sodium salt have been calculated from conductance data by Eisenman.<sup>7</sup> Since these calculations must rely on conductance values which are close to the conductivity of pure amyl alcohol, the

(21) J. L. Walker, Jr., G. Eisenman, and J. Sandblom, *J. Phys. Chem.*, **72**, 978 (1968).

(22) R. A. Fuoss and C. A. Kraus, *J. Amer. Chem. Soc.*, **55**, 476 (1933); **57**, 488 (1935); *Trans. Faraday Soc.*, **32**, 594 (1936).

Table I

	HB2EHPA	NaB2EHPA	HCl	NaCl
$\lambda_0$ , ohm $^{-1}$ cm $^2$ mol $^{-1}$	28.6	11.4	20.83	3.68
$K$ , mol cm $^{-3}$	$2.26 \times 10^{-9}$	$5.6 \times 10^{-7}$	$5.07 \times 10^{-6}$	$3.08 \times 10^{-6}$
$S$	...	...	0.037	0.0031
$t$	0.6	0.8	...	...
$\lambda_0$ (ion pair), ohm $^{-1}$ cm $^2$ mol $^{-1}$	2.7	2.7	...	...

results may not be quite accurate, but the values are consistent with those obtained from conductance measurements of NaCl and HCl in amyl alcohol.<sup>7</sup>

The transference number of hydrogen was measured with glass electrodes according to a method described by Gemant.<sup>23</sup> A liquid junction was formed by bringing two different solutions of B2EHPA in amyl alcohol in contact with each other and measuring the potential difference across the junction with the glass electrodes. The transference number for hydrogen determined by this method was found to be 0.6 from which also  $t_{\text{Na}}$  and  $t_s$  can be calculated, using the values for  $\lambda^0_{\text{HS}}$  and  $\lambda^0_{\text{Nas}}$ .

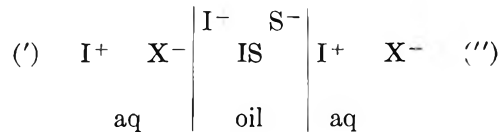
The value for  $k_{\text{H}}/k_{\text{Na}}$  was calculated from the distribution coefficients of HCl and NaCl between water and amyl alcohol. These were measured by equilibrating aqueous solutions of HCl and NaCl with amyl alcohol. Samples of the amyl alcohol were then redissolved in water and analyzed for chloride by electrometric titration. The distribution coefficients  $S$  between alcohol and water obtained this way were 0.037 and 0.0031, respectively, for HCl and NaCl. From conductance measurements Eisenman<sup>7</sup> found these values to be 0.025 and 0.0025, which are in good agreement with the more direct measurements described here. Squaring the ratio of the distribution coefficients gives the value of  $k_{\text{H}}/k_{\text{Na}}$  used in the calculations.

The remaining parameters, namely, the mobilities of the ion pairs ( $u_{\text{HS}}$  and  $u_{\text{Nas}}$ ), may be determined from the limiting currents when all other parameters are known.<sup>21</sup> In view of their size and lack of charge, it seems likely that the ion pairs, whether they contain hydrogen or sodium, have equal mobilities. Being the predominant species in the membrane they will also determine the kinetic behavior; *e.g.*, the time course of relaxation from one steady state to another following a step change in external-solution conditions. These facts provide an easy method to calculate the mobilities of the ion pairs from kinetic measurements as will be described in the section on Results. Table I summarizes the results of all these measurements of the basic parameters.

In order to study the steady-state properties of the B2EHPA-*n*-amyl alcohol system in the form of a thin convection-free membrane, a suitable matrix for the

liquid ion exchanger is required to maintain a stable membrane in contact with aqueous solutions. It was found that Millipore filters did not have the appropriate wetting properties for the system to form such a stable membrane. Instead a method was developed, in collaboration with Eisenman, by which the liquid ion exchanger was placed in a small hole drilled in a Lucite disk where it formed a stable, well-defined membrane in contact with the aqueous solutions. The dimensions of the hole (0.65-mm length and 0.1-mm width) ensured a convection-free interior for which there was also experimental evidence, *e.g.*, the ability of the membrane to rectify the electric current by skewing the profiles. Experiments described in the Methods section were also performed to test requirements b and d.

The following schematic representation illustrates the various components and phase boundaries of the system



where  $\text{X}^-$  is the anion (co-ion),  $\text{I}^+$  is the counterion, and  $\text{S}^-$  is the dissociated bis(2-ethylhexyl)phosphate ion.

Cells of this type were first studied by Beutner and have subsequently been termed Beutner cells with oleophilic salts.<sup>5</sup> It has also been demonstrated that the behavior of these cells depends on the manner in which they are formed, *i.e.*, where the junctions are located and how the various phases are preequilibrated with each other before the junctions are formed.<sup>13</sup> This is not important in our system, however, since the measurements were carried out in the steady state and the external solutions had been preequilibrated with the membrane material.

### Method

The liquid ion exchanger was prepared by dissolving B2EHPA (Union Carbide, 2.99 M) in *n*-amyl alcohol (Baker and Co.) to obtain solutions of 10 and 1 vol % which were subsequently used in the experiments. In all cases these solutions were preequilibrated with  $10^{-2}$  N HCl, but since the membrane, being only 0.65

(23) A. Gemant, *J. Chem. Phys.*, 12, 79 (1944).

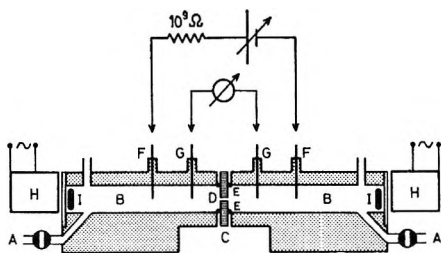


Figure 1. A schematic picture of the chamber and the membrane showing the inlet holes for the solutions (A), the solution compartments (B), the Lucite disk (C) with the hole containing the membrane (D), a set of O rings to clamp the disk (E), current-delivering Ag-AgCl electrodes (F), recording electrodes (G), and magnetic stirrers (H) with magnets (I).

mm thick, equilibrated quickly with the external solutions, the experiments that were carried out at steady state did not require this preequilibration, except that it seemed to increase the stability of the membrane.

The membrane solutions were then placed in a transparent Lucite disk with a thickness of 0.65 mm. A hole had been drilled in the disk (diameter of drill, 0.1 mm) and when a drop of membrane material was placed over the hole it was immediately sucked in. Since the Lucite material was wetted by the amyl alcohol but not by water, the membrane remained stable when the disk was dipped in aqueous solutions which had been preequilibrated with the membrane material. The area of the hole was calibrated by measuring its resistance in  $10^{-2} N$  HCl and the value of  $0.95 \times 10^{-4}$   $\text{cm}^2$  was thus obtained for the area of the hole.

The disk containing the membrane material was mounted in a chamber shown in Figure 1 after which the external compartments of the chamber were filled with the aqueous solutions through the openings (A). The potential was measured between one pair of Ag-AgCl electrodes, the other pair being used for delivering current. At the end of each compartment a magnetic stirrer could be attached as shown in Figure 2, but the stirring appeared to have little effect on the measurements and was not used in most experiments.

The electric potential between the recording electrodes was measured with a Corning pH meter (No. 12) with an input resistance of  $10^{13}$  ohm. Since a continuous recording of the potential was desired, a Rusttrak strip-chart recorder with a chart speed of 1 in./hr was connected to the pH meter.

The current delivered through the membrane was obtained from ordinary dry cells (45 V), and when smaller steps of current were desired a series of nickel cadmium cells were used, each with a stable potential of 1.25 V. The resistance of the membrane varied between  $10^6$  and  $10^8$  ohms, and the batteries were therefore connected via a  $10^9$ -ohm resistor in series with the membrane.

In all cases the aqueous solutions had been pre-

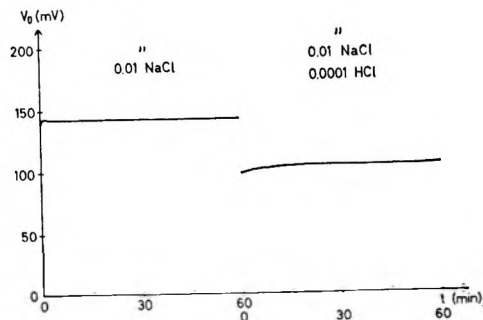


Figure 2a. The time course of the membrane potential at zero current following step changes in the external-solution conditions. The left compartment contained a solution of  $0.01 N$  NaCl, and the membrane, containing a 10% B2EHPA-amyl alcohol solution, was initially preequilibrated with  $10^{-2} N$  HCl. The right compartment was filled with solutions of compositions indicated in the figure.

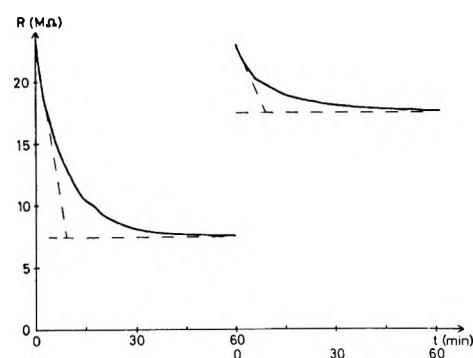


Figure 2b. The time course of the membrane resistance for the corresponding solution compositions of Figure 2a. The resistance changes were measured by applying a constant current of  $5 \times 10^{-8}$  A and recording the electric potential.

equilibrated by vigorous shaking with excess membrane material after which the solutions were allowed to sediment for at least 10 min. The experiments were performed at room temperature.

That the experimental system behaved like a mobile-site membrane fulfilling the requirements a-d was tested by several different methods.

The resistance of the membrane as calculated from the geometry of the system and data obtained by conductance measurements was found to agree with the directly measured values (see Figure 3c), indicating that the resistance of the membrane was determined by its bulk properties.

Next the time constant for establishing the steady-state profiles was measured under identical conditions for two membranes of different thickness (0.5 and 2.5 mm). Decyl alcohol was used instead of amyl alcohol in this experiment, since it had a larger viscosity and therefore a somewhat better stability in the bigger hole. The change in resistance during the exchange of hydrogen for sodium was followed, and the time constant for this process turned out to be approximately propor-

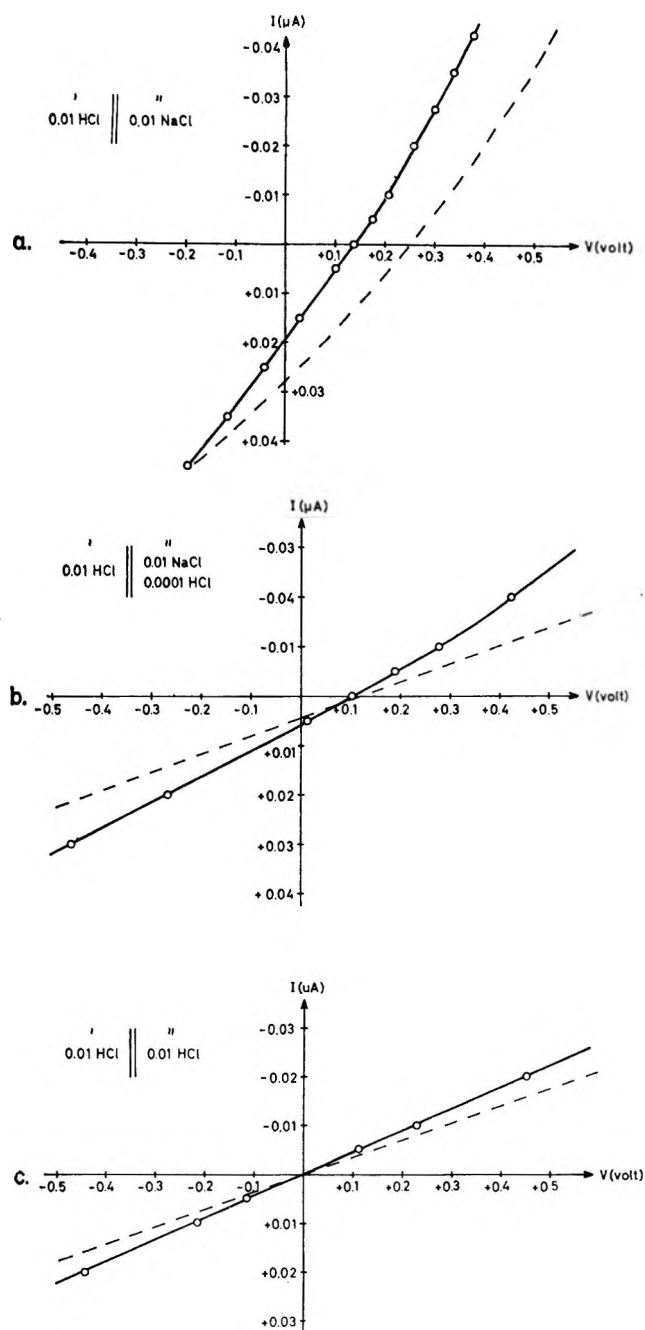


Figure 3. The current-voltage characteristics for various external-solution conditions. The left side of the membrane was exposed to 0.01 *N* HCl and the right side was exposed to the solutions indicated in the figures. Positive current flows from left to right and the left compartment is considered to have ground potential. The circles represent the experimentally measured values and the dotted lines are calculated from the values given in Table I using the equations of part I.

tional to the square of the membrane thickness, further substantiating the fact that the rate-limiting step was determined by diffusion in the membrane phase and not by the exchange across the membrane-solution interfaces. The latter process will, however, be rate limiting for thinner systems, since the activation ener-

gies are much larger for diffusion across the boundaries than for diffusion in the bulk phase of the membrane.<sup>18,24</sup>

The occurrence of concentration-polarization phenomena may be used as experimental evidence for the existence of trapped sites. If the sites have had time to become polarized under the influence of the applied field, a diffusion potential will be produced which gradually decays when the current is turned off. In a dissociated system this polarization potential can reach values of the same order of magnitude as the applied potential,<sup>21</sup> whereas stronger association requires higher applied potentials in order to give the same concentration polarization.<sup>15</sup> In the experiments reported here the polarization potentials varied between 0 and 15 mV, depending on the magnitude of the applied potentials which ranged from 0 to 0.5 V.

An important factor which needs to be controlled is the extent of co-ion exclusion. The external solutions contained HCl and NaCl in different concentrations, and by keeping these sufficiently dilute with respect to the concentration of B2EHPA in the membrane, the Cl<sup>-</sup> ions could be effectively excluded from the membrane phase.

The range of concentrations suitable for the experiments can be determined from a series of potential measurements that were carried out on a thick system at different dilutions of the external solutions (see ref 7, Figure 2). With a 0.3 *M* (10 vol %) concentration of the exchanger in amyl alcohol the potential had a practically ideal Nernst slope (58 mV/tenfold change in concentration) in the concentration range 10–100 mM for both HCl and NaCl. Below 10 mM the effect of the solubility of NaB2EHPA becomes an important factor and above 100 mM the co-ions are no longer effectively excluded.

In some of the experiments the effects of incomplete co-ion exclusion have been studied by diluting the B2EHPA in the membrane and increasing the concentrations of the external solutions.

## Results

**Membrane Potential at Zero Current (*Emf*).** The solutions used in this series of experiments were HCl and NaCl in such amounts that the total concentration on each side of the membrane was kept constant and equal to 0.01 *N*. The membrane phase consisted of a 10% solution of HB2EHPA in amyl alcohol pre-equilibrated with 10<sup>-2</sup> *N* HCl. In each experiment the left compartment was filled with 10<sup>-2</sup> *N* HCl pre-equilibrated with 10% HB2EHPA-amyl alcohol, whereas the right side of the membrane was exposed to solutions containing mixtures of HCl and NaCl. Of these mixtures the pure NaCl solution was preequilibrated with 10% NaB2EHPA-amyl alcohol and the other solution with 10% HB2EHPA-amyl alcohol.

(24) J. T. Davies, *J. Phys. Chem.*, **54**, 185 (1950).

The potential at zero current was measured across the membrane, and the time course of the potential change was recorded beginning immediately after the compartments were filled. Figure 2a shows the typical time course of such a potential change, and the emf is seen to be established essentially instantaneously. In most experiments, however, an initial rapid phase lasting from 0 to 1 min was observed during which the potential rose about 5–15 mV to its final value. This initial phase was always accompanied by an increased membrane resistance, higher than that which would be predicted from the dimensions of the hole. It was therefore attributed to a certain amount of excess membrane material extending beyond the hole which was gradually washed away during the early phase. Further evidence that the emf is established instantaneously in liquid ion-exchange membranes was obtained from measurements on a thick membrane (*ca.* 1 cm). In this system, designed as an electrode, the emf was established within a few minutes, whereas it would take several days to achieve a true steady state in a membrane of this thickness.

To show that the emf had established its final value before the profiles had achieved a steady state, the time course for the corresponding resistance change was recorded simultaneously and is shown in Figure 2b. The resistance was measured by applying a constant current of  $5 \times 10^{-3} \mu\text{A}$  and recording the potential change.

The time constant  $\tau_D$  for the relaxation of the resistance is seen to be *ca.* 10 min and may be used to calculate the mobilities of the ion pairs. It was pointed out that the process which determines the kinetic behavior of the membrane is a simple diffusion of the ion pairs, and, since the mobilities of these are presumably equal, they are related to the time constant  $\tau_D$  by the relationship

$$\tau_D = \frac{d^2}{\pi^2 D} = \frac{(dF)^2}{RT\pi^2\lambda_0}$$

where  $d$  is the membrane thickness,  $D$  is the diffusion coefficient, and  $R$ ,  $T$ , and  $F$  have their usual meaning. Expressed in units of equivalent conductance a value of 2.7 was thus obtained for the mobilities of the ion pairs.

These experiments demonstrate an important phenomenon which was theoretically predicted for liquid ion-exchange membranes with weakly ionized groups,<sup>15</sup> namely, that the instantaneous value for the emf of the membrane following a step change in external-solution conditions is equal to the value which it attains in the steady state. Therefore, *a stationary or quasi-stationary state of the emf is reached immediately following a step change in external-solution conditions, whereas the resistance approaches a steady-state value over a certain period of time which depends on the time constant for establishing the steady-state profiles.* The same phenomenon has also been predicted<sup>25</sup> and observed in dense fixed-site membranes (*e.g.*, glass)<sup>26</sup> and forms the

basis for analyzing their electrode-specific properties.<sup>26</sup> It has therefore been important to test experimentally the predicted agreement between steady-state and instantaneous emf's in liquid ion-exchange membranes since these have also been made into electrodes with ion-selective properties.<sup>6,17</sup> It should be emphasized, however, that this test requires a thin, convection-free membrane in order to achieve a true steady state.

*Current-Voltage Characteristics. HCl-NaCl.* The same experimental arrangement that was used in measuring the emf was also used in measuring the membrane resistance at steady state for various applied potentials. The concentrations of the solutions and of the exchanger were also the same as those used in the previous experiments.

In Figure 3 is shown the current-voltage characteristics for various external-solution conditions. The circles represent the measured values, whereas the dotted lines are calculated from the equations of part I using the values for the parameters given in Table I. The curves in all three figures are seen to have a practically linear shape, exhibiting only a slight nonlinearity which is predicted by the theory. However, a certain deviation from the theory is seen to occur particularly for the case shown in Figure 3a with  $10^{-2} N$  NaCl in the right compartment. This deviation may be explained by possible errors in the parameters of NaB2EHPA, since the measured conductivity of 10% NaB2EHPA–amyl alcohol was found to be 30% higher than that calculated from the values given in Table I. This in turn may be due to the formation of triple ions or other higher order aggregates,<sup>23</sup> but it may also be due to a concentration dependence of  $K$  resulting from changes in the water content of the membrane. In spite of the deviations, however, the theoretically predicted and experimentally measured  $I$ - $V$  curves shown in Figure 3 are quite similar with respect to their general shape. For a fixed-site membrane or a mobile-site membrane with completely ionized sites and counterions, one would expect that the resistance changes observed following changes in external-solution conditions (Figure 2b) would also give rise to a distinct rectification in an interval of about  $\pm 125$  mV around the  $V_0$  potential.<sup>14,25</sup> *The absence of rectification in the actual case is therefore a distinguishing feature of liquid ion-exchange membranes with weakly ionized groups.*

The slight nonlinearity of the  $I$ - $V$  curves in Figures 3a and b is seen to deviate toward higher resistances when the potential is negative and toward lower resistances when the potential is positive. For negative potentials the sodium ions are being carried into the membrane, and in part I it was shown that their higher degree of ionization would give rise to a greater non-

(25) F. Conti and G. Eisenman, *Biophys. J.*, 5, 247 (1965).

(26) G. Eisenman in "The Glass Electrode," Interscience Publishers, New York, N. Y., 1966.

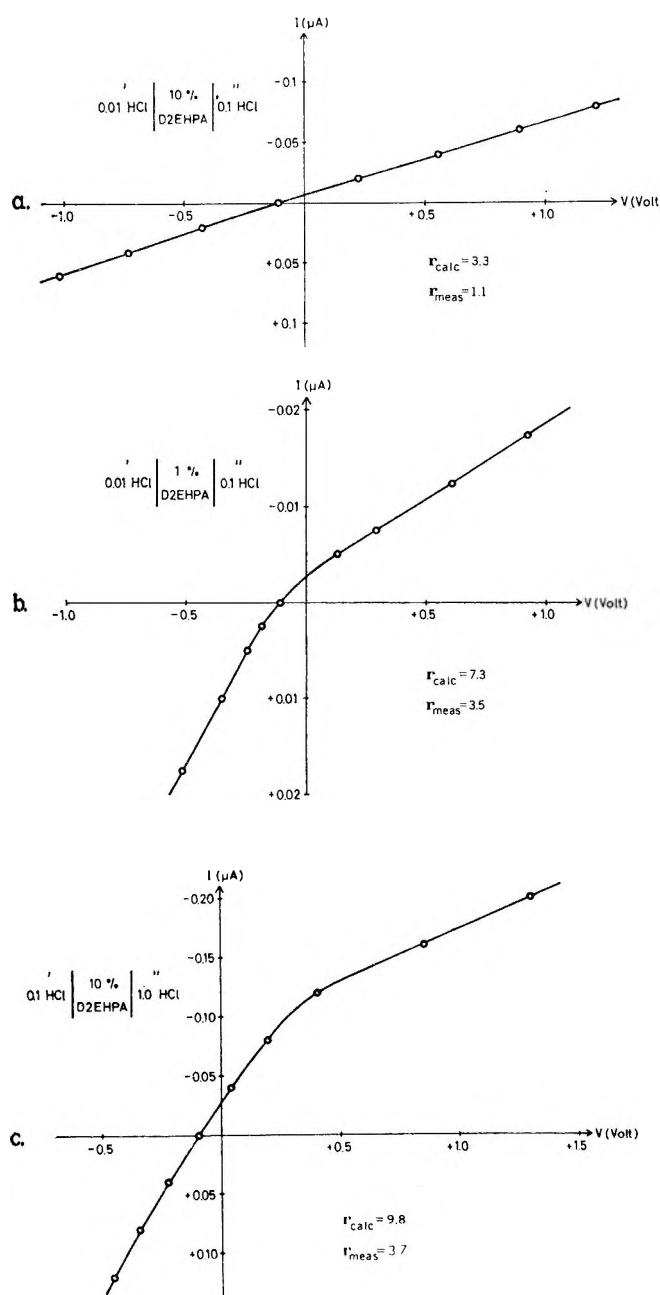


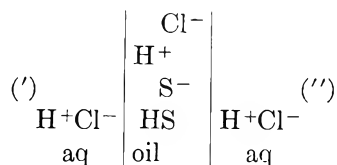
Figure 4. The current-voltage characteristics for external solutions containing various concentrations of HCl. The solution conditions and the concentrations of the exchanger are indicated in the figures. A comparison between the rectification ratio measured directly from the curves and calculated from eq 45 of part I is also shown in the figure. Positive current flows from left to right and the left compartment is considered to have ground potential.

linearity on the negative side which is therefore confirmed experimentally.

The nonlinearity for positive potentials in the direction of decreasing resistance is thought to be an effect of co-ions. These will have a larger tendency to enter the membrane on the left side, where the exchanger is more weakly ionized and the Donnan exclusion is not as effective. An inflow of co-ions will tend to decrease

the membrane resistance, which will therefore continue to decrease as higher fields are applied.

*HCl.* The object with this set of experiments was to examine the effects of co-ions on the electrical properties of the membrane. The conditions were therefore chosen so as not to exclude the co-ions from the membrane phase which is illustrated by the following representation of the cell



The external solutions were maintained at different concentrations levels ( $c''/c' = 10/1$ ).

Figures 4a and b show the current-voltage characteristics at two different concentrations of B2EHPA, 10 and 1%, with the same external-solution conditions. With a membrane concentration of 10% B2EHPA the co-ions are excluded and the current-voltage characteristic shows a distinct rectification (Figure 4a). In the more dilute membrane, however, the co-ions are not completely excluded and the current-voltage characteristic shows a distinct rectification (Figure 4b). In Figure 4c the same phenomenon is demonstrated with 10% B2EHPA and with 10 times higher external-solution concentrations. The resistance of the membrane is seen to be about 10 times lower in Figure 4c than in Figure 4a, whereas the rectification is the same in both cases. This indicates that the factor which determines the rectification tendency of the membrane is the ratio between external-solution concentrations and the concentration of the exchanger.

Moreover, the rectification is in such a direction that the membrane behaves like a fixed-site membrane with negatively charged sites,<sup>27</sup> where the rectification is due to a "washing-out" effect of co-ions.<sup>28</sup> This is understandable from the theoretical conclusions of part I, according to which the strongly associated sites will maintain a fixed distribution owing to the presence of ion pairs.

In Figure 4 are also inserted two values for the rectification ratio, namely,  $r_{\text{meas}}$  which is obtained directly from the curves and  $r_{\text{calcd}}$  which is calculated from eq 45 of part I with the values given in Table I. The calculated values are seen to be considerably higher than the measured ones, which may partly be due to incomplete dissociation of HCl. This is not taken into account in the theoretical derivation which assumes complete dissociation of the  $\text{Cl}^-$  ions. Nevertheless, the relative magnitudes as well as the direction of the rectification agree with the theoretical predictions.

(27) T. Teorell, *Progr. Biophys.*, 3, 305 (1953).

(28) R. Schlogl, *Z. Phys. Chem. (Frankfurt am Main)*, 1, 305 (1954).

## Discussion

The theoretical treatment of part I assumes the exchanger to be weakly ionized and a criterion for this is given by

$$\sqrt{\frac{\bar{c}_s^*}{K_{\max}}} \gg 1$$

where  $\bar{c}_s^*$  is the concentration of the exchanger and  $K_{\max}$  is the largest of the dissociation constants, in this case  $K_{\text{Na}}$ . With 10% B2EHPA ( $\bar{c}_s^* = 0.3 M$ ) the left side of the inequality is equal to 23.5 and a 4% error is therefore made by neglecting the diffusion of dissociated forms (cf. part I).

The errors in the individual determinations of the parameters given in Table I will also influence the quantitative agreement between theory and experiment. The largest error probably lies in the separate determinations of  $\lambda_0$  and  $K$ , whereas the agreement with theory seen in Figure 3c shows that the product  $\lambda_0 \sqrt{K}$  for HB2EHPA is correct.

The largest discrepancy between theory and experiment is seen from Figure 3a to be connected with  $V_0$ , the potential at zero current which is more sensitive than the resistance to errors in the values of  $\lambda_0$  and  $K$ . Although the dissociation constants were calculated from conductance data, an independent check can be obtained by measuring the ion-exchange equilibrium constant  $K_{\text{HN}_a}$  related to the dissociation constants by

$$K_{\text{HN}_a} = \frac{k_{\text{H}}}{k_{\text{Na}}} \frac{K_{\text{Na}}}{K_{\text{H}}}$$

Orme and Sandblom<sup>29</sup> measured this parameter by an extraction procedure and obtained a value ten times lower than that given by Eisenman, which brings the calculated  $V_0$  50 mV closer to the measured value.

It is therefore obvious that the parameters given in Table I contain many errors, and since the theory is also based on a number of idealizing assumptions, an exact agreement between theory and experiment is not to be expected.

Nevertheless, the experiments have shown that the system can adequately serve the purpose for which it was designed, namely, to demonstrate the behavior of a liquid membrane with trapped sites and a convection-free interior. The theory has also proved to be successful in predicting the most important phenomena observed in this system and should therefore be useful as a basic model for liquid ion-exchange membranes.

*Acknowledgment.* I wish to thank professor George Eisenman, with whom this investigation was started, for his many valuable suggestions and for his helpful criticism of the manuscript.

(29) F. Orme and J. Sandblom, unpublished results.

## NOTES

### Onsager's Reciprocal Relation. An Examination of Its Application to a Simple Membrane Transport Process

by E. H. Bresler

Research Division, Veterans Administration Hospital and Department of Medicine, Tulane University School of Medicine, New Orleans, Louisiana 70112

and R. P. Wendt

Department of Chemistry, Loyola University, New Orleans, Louisiana 70118 (Received May 2, 1968)

these theoreticians were met with enthusiasm. However, we feel that there are some fundamental difficulties with the theories which limit their usefulness if they are applied *prima facie*. In particular, we will show that the Onsager reciprocal relation—the most fruitful theorem of nonequilibrium thermodynamics—is not valid as applied by one of the theories to a simple membrane transport process.

Although our criticism may apply with some modification to all of the theories cited above, we will restrict our discussion to the theory developed in 1958

- (1) J. G. Kirkwood in "Ion Transport across Membranes," H. T. Clark, Ed., Academic Press, New York, N. Y., 1954, pp 119-127.
- (2) O. Kedem and A. Katchalsky, *Biochem. Biophys. Acta*, **27**, 229 (1958).
- (3) S. R. de Groot and P. Mazur, "Non-Equilibrium Thermodynamics," North-Holland Publishing Co., Amsterdam, 1962, Chapter XV.
- (4) R. Schlögl, "Stofftransport durch Membranen," Steinkopff Verlag, Darmstadt, 1964.

by Kedem and Katchalsky<sup>2</sup> and described again in detail in a recent textbook.<sup>5</sup> The particular process we consider is that involving bulk flow across an open membrane, *i.e.*, a membrane which is completely nonselective to both the solute and the solvent. The bulk flow is caused by an external pressure difference across the membrane; the two-component solutions in compartments A and B on either side of the membrane are isothermal, dilute in the solute but at different concentrations and are well-stirred. For this process the dissipation function,  $\Phi$ , according to the membrane transport theory under discussion here, is given by

$$\Phi = J_V \Delta P + J_D \Delta \Pi \quad (1)$$

Here  $J_V$  is the time rate of change of volume in compartment B. It is related to the solute and solvent flows  $J_s$  and  $J_w$  (the time rates of change of solute and solvent, respectively, in compartment B) by

$$J_V = \bar{V}_s J_s + \bar{V}_w J_w \quad (2)$$

where  $\bar{V}_s$  and  $\bar{V}_w$  are the partial molal volumes of solute and solvent. The flow  $J_D$  is defined by

$$J_D = (J_s / \bar{c}_s) - J_w \bar{V}_w \quad (3)$$

where

$$\bar{c}_s = (c_s^A - c_s^B) / \ln (c_s^A / c_s^B) \quad (4)$$

The term  $\Delta \Pi$  equals the concentration difference across the membrane multiplied by the gas constant,  $R$ , and the absolute temperature  $T$ .

$$\Delta \Pi = RT(c_s^A - c_s^B) \quad (5)$$

According to a postulate of nonequilibrium thermodynamics, the flows in the entropy dissipation function should be linearly related to the forces for systems sufficiently close to equilibrium; eq 1 therefore implies the form for the linear phenomenological flow equations

$$J_V = L_P \Delta P + L_{PD} \Delta \Pi \quad (6)$$

$$J_D = L_{DP} \Delta P + L_D \Delta \Pi \quad (7)$$

The coefficient  $L_P$  is the mechanical filtration capacity of the membrane,  $L_D$  is related to the permeability of the membrane to the solute when there is no volume flow, and  $L_{PD}$  and  $L_{DP}$  are the cross coefficients. According to the Onsager reciprocity theorem<sup>6</sup>

$$L_{PD} = L_{DP} \quad (8)$$

We offer no criticism of eq 1–6. As derived by Kedem and Katchalsky the dissipation function,  $\Phi$ , when divided by the absolute temperature, is equal to the entropy production in the region between the solutions in compartments A and B. For bulk flow processes this region will in general consist of a boundary layer at face A of the membrane, the membrane itself, and a boundary layer at face B of the membrane. This point is perhaps emphasized more strongly in the approach of de Groot and Mazur.<sup>3</sup> Their derivation

clearly does not depend on the nature of the boundary region between the two solutions A and B: in their eq 57, p 415, they state that the total entropy production of the entire system (solution A, boundary region between the solutions, and solution B) is given by terms which can be reduced to those on the right-hand side of eq 1 in this note.

The latter term on the right-hand side of eq 1, when divided by  $T$ , represents the production of mixing entropy for the system; that is, if  $J_D \Delta \Pi$  were integrated over the entire time of the process, then an expression for the total entropy change due to mixing solution A with solution B would be obtained. Thus if solution A is of different concentration than solution B, so that  $\Delta \Pi$  is nonzero, then the product  $J_D \Delta \Pi$  must not vanish no matter what the nature of the membrane nor how the mixing is produced, because otherwise the entropy of mixing would not be accounted for by eq 1. If  $J_D \Delta \Pi$  does not vanish for any flow process for which  $\Delta \Pi$  is nonzero, then  $J_D$  will not vanish for bulk flow across an open membrane. Thus  $J_D$  cannot be identified in general as a diffusive flow, because a true diffusive flow will vanish for sufficiently rapid bulk flow across an open membrane.<sup>7</sup>

In this interpretation of  $J_D$  we disagree with the generally accepted view<sup>8</sup> and our new interpretation has an important consequence which becomes evident when eq 6 and 7 are examined. Consider again the bulk flow process from one well-stirred compartment to another across the open membrane. For this process the concentration difference will obviously have no effect on the bulk flow rate,  $J_V$ ; hence  $L_{PD}$ , which measures the effect of  $\Delta \Pi$  on  $J_V$ , must be zero for the open membrane:  $L_{PD} = 0$ .  $J_V$  is therefore simply proportional to  $\Delta P$ . However,  $J_D$  must increase as  $J_V$  increases, because the production of entropy due to mixing must increase the faster the solutions are mixed; therefore  $J_D$  depends on  $\Delta P$ , through  $J_V$ . The cross coefficient  $L_{PD}$ , which measures the effect of  $\Delta P$  on  $J_D$ , thus will not vanish even for the open membrane:  $L_{DP} \neq 0$ . Since  $L_{DP} \neq L_{PD} = 0$ , the Onsager reciprocal relation, eq 8, is not satisfied.

The qualitative argument above can be quantitatively expressed as follows. For rapid bulk flow across an open membrane from side A to B the solute flow can be expressed by

$$J_s = c_s^A J_V \quad (9)$$

where the diffusive contribution does not appear because it becomes vanishingly small for sufficiently large

(5) A. Katchalsky and P. F. Curran, "Nonequilibrium Thermodynamics in Biophysics," Harvard University Press, Cambridge, Mass., 1965, Chapter 12.

(6) L. Onsager, *Phys. Rev.*, **37**, 405 (1931); **38**, 2265 (1931).

(7) L. Garby, *Acta Physiol. Scand.*, **40**, Supplement 137 (1957).

(8) Reference 5, p 119.

values for  $J_V$ .<sup>7</sup> We use eq 9 and 2 to find an expression for  $J_D$  in terms of  $J_V$ .

$$J_D = [(c_s^A/\bar{\epsilon}_s - 1) + c_s^A \bar{V}_s] J_V \quad (10)$$

For dilute solutions,  $c_s^A \bar{V}_s \ll 1$  ( $c_s$  has units of moles/cc); by using this approximation, introducing eq 6 for  $J_V$ , and grouping terms in  $\Delta P$  and  $\Delta \Pi$  we obtain

$$J_D = (c_s^A/\bar{\epsilon}_s - 1)L_P \Delta P + (c_s^A/\bar{\epsilon}_s - 1)L_{PD} \Delta \Pi \quad (11)$$

Equating the coefficients of  $\Delta P$  in eq 7 and 11 leads to an expression for  $L_{DP}$ .

$$L_{DP} = (c_s^A/\bar{\epsilon}_s - 1)L_P \quad (12)$$

An expression for  $L_{PD}$  can be inferred from the definition of an open membrane; *i.e.*,  $J_V$  does not depend on  $\Delta \Pi$  but is directly proportional to  $\Delta P$ .

$$J_V = L_P \Delta P \quad (13)$$

From eq 6 and 13 it follows that

$$L_{PD} = 0 \quad (14)$$

From eq 12 and 14 we see that the Onsager relation will be satisfied only if  $c_s^A = \bar{\epsilon}_s$ . This condition is satisfied for the special case of bulk flow across an open membrane on either side of which  $c_s^A = c_s^B = \bar{\epsilon}_s$ , but in general  $c_s^A \neq \bar{\epsilon}_s$  regardless of the fact that the solutions A and B may both be dilute. If  $c_s^A = 0.1 M$  and  $c_s^B = 0.01 M$ , for example, then  $\bar{\epsilon}_s = 0.039$  and  $c_s^A/\bar{\epsilon}_s = 2.56$ . Therefore, except for the special case of bulk flow across an open membrane on either side of which the concentrations are kept at  $c_s^A = c_s^B$ , the Onsager relation cannot be applied here for open membranes.

If we assume the general validity of the Onsager reciprocity theorem when it is properly applied, we must look for assumptions in the membrane transport theory which lead to the apparent invalidity of Onsager's theorem. We find that for bulk flow processes the specified boundary condition of uniform solutions on either side of the membrane, which implies rapid stirring in each compartment, is a characteristic of membrane transport theory which does not appear in the nonequilibrium thermodynamic theory of nonuniform but homogeneous solutions. Now the requirement of stirring is not by itself the source of difficulty, because that condition is specified for diaphragm-cell diffusion experiments in which no bulk flow occurs and where nonequilibrium thermodynamics seems to work quite well.<sup>9</sup> The existence of bulk flow is also not by itself a reason for the invalidity of the Onsager relation, because we have shown that for the process of bulk flow across an open membrane interposed between two identical solutions the Onsager relation is valid, although in a strict sense only a single flux and force exist so that the result is trivial. It is the combination of bulk flow through an open membrane interposed between solutions of different composition, with stirring of the solutions on either side of the membrane, that

causes trouble. For this process the concentration gradient *within the membrane* becomes vanishingly small as bulk flow increases. Thus, although eq 1 accurately describes the total entropy production, the source for the mixing dissipation (the product  $J_D \Delta \Pi$ ) is not located primarily within the structural membrane, where the linear laws and the Onsager relation are expected to be valid;<sup>10</sup> instead it is located in poorly defined layers at each face of the membrane which in principle could be described by the combined application of hydrodynamics and nonequilibrium thermodynamics, although from a practical standpoint this hardly seems possible. In these regions the simple linear laws (eq 6 and 7), and hence the Onsager relation, cannot be expected to hold.

For more important cases of bulk flow across partially selective membranes, *i.e.*, membranes which are neither completely unselective to the solute nor perfectly impermeable to it, we have also derived expressions for  $L_{DP}$  and  $L_{PD}$  which imply that for such processes the Onsager relation is inapplicable. Because of the paucity of good data for such membranes we cannot test rigorously our conclusions. Nevertheless, the failure of the membrane theory we discussed here to describe bulk flow across an open membrane in such a way as to render the Onsager relation valid casts a suspicion on the general validity of this membrane theory. Further theoretical and experimental investigation is needed to establish whether any formulation using the approach of overall entropy production, rather than local entropy production within the membrane, can define transport coefficients which satisfy Onsager's reciprocity principle.

(9) P. J. Dunlop, *J. Phys. Chem.*, **69**, 4276 (1965).

(10) The application of nonequilibrium thermodynamics to processes occurring within the membrane has been discussed by: K. S. Spiegler and O. Kedem, *Desalination*, **1**, 311 (1966); D. C. Mikulicky and S. R. Caplan, *J. Phys. Chem.*, **70**, 3049 (1966); H. J. M. Hanley, *J. Chem. Educ.*, **44**, 717 (1967).

## Nuclear Magnetic Resonance and Thermochemical Studies on the Influence of Urea on Water Structure

by S. Subramanian, D. Balasubramanian,  
and J. C. Ahluwalia

*Department of Chemistry, Indian Institute of Technology,  
Kanpur, India* (Received June 10, 1968)

The effect of urea on the structure of water, on hydrophobic interactions, and hence on protein denaturation has been widely studied but still remains to be explained conclusively. There have been several re-

ports<sup>1-6</sup> on the effect of urea on water structure as to whether it disrupts or enforces water structure. However, it is agreed upon unanimously<sup>7-9</sup> that urea weakens hydrophobic bonds, thereby aiding denaturation of proteins. The mechanism of the action of urea has not yet been interpreted quantitatively with regard to the thermodynamics of urea-water interactions or urea-water-hydrocarbon interactions. Certain important physical properties of aqueous urea solutions indicate that *urea behaves neither as a structure breaker nor as a structure maker but participates with great facility in the mobile hydrogen bonding amidst the "flickering clusters" of water.* The partial molal heat capacity of urea in water ( $\bar{C}_{p_2}^{\circ} \approx C_{p_2}$ ),<sup>1</sup> the slightly positive viscosity  $B$  coefficient,<sup>2</sup> and the enhancement of the dielectric constant of water upon the addition of urea<sup>1</sup> are evidence for the behavior of urea in water as an active participant in the total hydrogen bonding. Disconcertingly enough, the negative heat capacities of transfer of certain amino acids<sup>3</sup> from water to aqueous urea solution and the increments in the critical micelle concentration (cmc)<sup>10</sup> of certain micelles in aqueous urea solutions over the values in aqueous solutions of these surfactants suggest that urea may reduce the cooperative structure of water.

The effect of urea on water structure as inferred from the studies on ternary systems<sup>3,10</sup> may not represent the exact situation, since it is possible that new effects may arise on account of the presence of the third component. So it is more appropriate to study the binary system of urea-water in greater detail to understand the structure of aqueous urea solution. In order to supplement the studies on aqueous urea solutions, we measured the heats of solution of urea at infinite dilution at 25 and 35° and thereby obtained the partial molal heat capacity of urea,  $\bar{C}_{p_2}^{\circ}$ , at 30°. We also measured the chemical shifts of the water proton signal in pure water as well as aqueous urea solutions of several concentrations up to saturation.

## Experimental Section

The calorimeter used to measure the heat of solution of urea in water, the operating procedure, the accessories, and the method of evaluating the integral heats of solution from the measured heats of solution at different molalities have been described elsewhere.<sup>11</sup> The nmr chemical shifts were measured in a Varian HR-100 nmr spectrometer. Acetone was used as an internal standard. The concentration of acetone in water was less than 1 M, which did not alter the chemical shift of water significantly.<sup>12</sup> The chemical shifts were measured at  $32 \pm 1^\circ$ . The internal consistency of the chemical shift values was checked by measuring the chemical shifts of pure water and 4 m aqueous NaBr. The change in the chemical shift of water ( $\Delta\delta$ ) for a solution of 4 m NaBr was  $28 \pm 2$  cps, which agreed perfectly with the values reported (18 cps in a 60-Mcps

instrument) by Hartman.<sup>13</sup> Urea was purchased from May and Baker (assay >99.5%) and was recrystallized twice from water and was dried at 60° for 2 hr. Water used in calorimetric and nmr measurements was doubly distilled conductivity water.

## Results and Discussion

The integral heats of solution of urea at 25 and 35° along with  $\Delta H_s$  values at different molalities are reported in Table I.  $\Delta H_s^{\circ}$  at 25° is  $3734 \pm 15$  cal mol<sup>-1</sup>

**Table I:** Heats of Solution of Urea in Water at 25 and 35°

25.0°		35.0°	
Molality ( $\times 10^3$ )	$\Delta H_s$ , cal mol <sup>-1</sup>	Molality ( $\times 10^3$ )	$\Delta H_s$ , cal mol <sup>-1</sup>
2.197	3730	3.341	3773
4.287	3688	4.305	3721
6.445	3690	5.388	3761
7.437	3725	6.645	3740
8.614	3669	8.132	3753
10.420	3697	9.942	3670
14.710	3642	10.790	3679
16.400	3645	11.600	3707
$\Delta H_s^{\circ a} = 3734 \pm 15$		$\Delta H_s^{\circ a} = 3795 \pm 20$	

<sup>a</sup> Extrapolation to infinite dilution from  $\Delta H_s$  values at the cited molalities was done by a least-squares program in an IBM 7044 computer.

and at 35° is  $3795 \pm 20$  cal mol<sup>-1</sup>. The value at 25° is close to that reported<sup>14</sup> by Egan and Luff. Their value is 3656 at 25°, but we feel that our value is more reliable since we have measured the heat of solution at millimolar concentration range whereas Egan and Luff have extrapolated from 1 m to infinite dilution. Within experimental error the temperature dependence of the enthalpy of dissolution is almost negligible. The  $\Delta C_p^{\circ}$  for urea in water at 30° is  $6.0 \pm 3.0$  cal deg<sup>-1</sup> mol<sup>-1</sup> and  $\bar{C}_{p_2}^{\circ}$ <sup>15</sup> is  $28 \pm 3.0$  cal deg<sup>-1</sup> mol<sup>-1</sup>. This

- (1) M. Abu-Hamidayyah, *J. Phys. Chem.*, **69**, 2720 (1965).
- (2) J. A. Rupley, *ibid.*, **68**, 2002 (1964).
- (3) G. C. Krescheck and L. Benjamin, *ibid.*, **68**, 2476 (1964).
- (4) H. S. Frank, *Federation Proc. Suppl.*, **S-1**, 15 (1965).
- (5) F. Franks and D. L. Clarke, *J. Phys. Chem.*, **71**, 1155 (1967).
- (6) G. E. Walrafen, *J. Chem. Phys.*, **44**, 3726 (1966).
- (7) D. B. Wetlaufer, S. K. Malik, L. Stoller, and R. L. Coffin, *J. Amer. Chem. Soc.*, **86**, 508 (1964).
- (8) P. I. Whitney and C. Tanford, *J. Biol. Chem.*, **237**, 1735 (1962).
- (9) W. Kauzman, *Advan. Protein Chem.*, **14**, 1 (1959).
- (10) M. J. Schick, *J. Phys. Chem.*, **68**, 3585 (1964).
- (11) S. Subramanian and J. C. Ahluwalia, *ibid.*, **72**, 2525 (1968).
- (12) See also von H. G. Hertz and W. Spalthoff, *Z. Elektrochem.*, **63**, 1096 (1959).
- (13) K. A. Hartman, Jr., *J. Phys. Chem.*, **70**, 270 (1966).
- (14) E. P. Egan, Jr., and B. B. Luff, *J. Chem. Eng. Data*, **11**, 192 (1966).
- (15)  $C_p$  of urea at 30° is estimated as  $22.58$  cal deg<sup>-1</sup> mol<sup>-1</sup> from the value reported at different temperatures (R. A. Ruehrwein and H. M. Huffman, *J. Amer. Chem. Soc.*, **68**, 1759 (1946)).

indicates that urea has a tendency to slightly increase water structure in accordance with the concept<sup>16</sup> that structure-making solutes have large positive values for  $\bar{C}_{p_2}^{\circ}$  and structure-breaking ones have negative values. The result is also in accord with the finding<sup>1</sup> that  $C_{p_2} \approx \bar{C}_{p_2}^{\circ}$  for urea in aqueous solution, which means that urea neither decreases nor increases the structure of water.

In aqueous urea solutions, just like any other water molecule urea also forms H bonds to adjacent water molecules. Considering the "flickering-cluster" model<sup>16</sup> for water wherein each water molecule is considered to be an integral part of flickering clusters instead of belonging to monomeric or cluster species solely, the introduction of urea molecules into the heart of the flickering clusters can be achieved without prejudice to the geometry of urea. It is possible that the lifetime of the clusters may be extended and also that the dimensions of the void spaces may be changed on account of interposition of urea in the clusters. Incidentally, this would account for the increased solubility of hydrocarbons<sup>7</sup> in aqueous urea over that in water. It is known<sup>17</sup> that solid urea is extensively H bonded. When it is introduced into water urea-urea H bonds may be broken down; some water-water H bonds may also be destroyed in favor of formation of certain urea-water H bonds. The resultant of all these may leave the total strength of H bonding unaltered, but the energetic balance leads to endothermic dissolution of urea in water. Further studies on the temperature dependence of  $\Delta H_s^{\circ}$  from 0 to 100° would augment the explanation of the action of urea on water structure.

The observation<sup>2</sup> that aqueous urea solutions have anomalously low viscosities is misleading. It is true that the viscosity  $B$  coefficient has only a small positive value, but the viscosity of aqueous urea solutions at all concentrations is greater than that of water.<sup>18</sup> The positive entropy of dilution of aqueous urea solutions ( $\sim 0.034$  eu for 4 M urea) being quoted<sup>2</sup> as evidence of structure-breaking action is not satisfying because firstly the magnitude of the entropy of dilution for urea is very small and secondly it is likely that urea may dimerize or polymerize in concentrated aqueous solutions as revealed<sup>19</sup> by the nonideality of concentrated aqueous urea solutions. The depolymerization would easily account for the small positive entropy of dilution. Studies<sup>20</sup> on autodiffusion of aqueous urea solutions also support the contention that urea in aqueous solutions participates in the formation of H-bonded groups of urea and water molecules.

*Nmr Studies.* It is known<sup>12,13,21</sup> that structure-breaking solutes shift the water pmr signal upfield and structure-making solutes shift it downfield. The chemical shifts of water protons as a function of urea concentration are reported in Table II. It is very interesting to observe that the addition of urea does not alter the chemical shift of water protons until the solute

**Table II:** Proton Chemical Shifts of Water in Aqueous Urea Solutions<sup>a</sup>

Concn of urea, <i>M</i>	$\delta$ , <sup>b</sup> ppm	$\delta(\text{pure water}) -$ $\delta(\text{water in}$ $\text{aqueous urea}),$ ppm
0	$2.42 \pm 0.02$	0
2	$2.42 \pm 0.02$	0
4	$2.41 \pm 0.02$	0.01
6	$2.41 \pm 0.02$	0.01
7	$2.40 \pm 0.02$	0.02
8	$2.38 \pm 0.02$	0.04
10	$2.34 \pm 0.02$	0.08
~12 (satd soln)	$2.33 \pm 0.02$	0.09

<sup>a</sup>  $32 \pm 1.0^{\circ}$ . <sup>b</sup> Chemical shifts from acetone.

concentration is 7 M. Even beyond this concentration the change in the chemical shift is very meager, the magnitude of shift ( $\Delta\delta$ ) being 9 cps for ~12 M urea (in a 100-Mcps instrument). While the change in the chemical shift for water in most other electrolyte solutions is considerable<sup>13</sup> even for moderate concentrations, it is significant that urea does not alter the chemical shift of water much even at the highest concentrations. This further supports the view that urea mixes freely with water molecules and participates in the H bonding with water so as to leave the solution as much structured as water. Only at the highest concentrations does it produce a small upfield shift. This is probably due to the fact that at higher concentrations aggregation of urea molecules might occur which would be responsible for a small upfield shift of water signal.

The temperature dependence of certain physical properties of aqueous urea solutions should be revealing. We are currently studying the thermodynamic properties of certain amphiphilic solutes in water and aqueous urea which we hope would throw more light on the weakening of hydrophobic bonds by urea. The findings should be highly relevant to protein thermodynamics and protein denaturation.

Preliminary measurements on a A60D nmr spectrometer confirmed the observations made in the HR-100 spectrometer with regard to the chemical shift changes of water in urea solutions. We also measured the change of chemical shift of water in NaBPh<sub>4</sub>-water and in NaBPh<sub>4</sub>-water-urea for different concentrations of urea. NaBPh<sub>4</sub> shifts the water signal a little

(16) H. S. Frank and W. Y. Wen, *Discussions Faraday Soc.*, **24**, 133 (1957).

(17) G. C. Pimentel and A. L. McClellan, "The Hydrogen Bond," Freeman, San Francisco, Calif., 1960, Chapter 9.

(18) G. Domes and S. K. Talley, *J. Amer. Chem. Soc.*, **55**, 624 (1933).

(19) R. H. Stokes, *J. Phys. Chem.*, **70**, 1199 (1966).

(20) I. V. Matyash, A. I. Toryanik, and V. V. Kiselnik, *Zh. Strukt. Khim.*, **8**, 418 (1967); *J. Struct. Chem.*, **8**, 371 (1967).

(21) J. C. Hindman, *J. Chem. Phys.*, **36**, 1000 (1962).

downfield, while in the system NaBPh<sub>4</sub>-water-urea the water signal is shifted further downfield than is the case with NaBPh<sub>4</sub>-water. We feel that the downfield shift in the three-component system is due to the disruption of hydrophobic bonds in the aqueous solution of NaBPh<sub>4</sub> by urea. However, further investigation is necessary before anything can be said conclusively. We are pursuing this study in greater detail.

### Isotope Effects in the Diffusion of <sup>12</sup>C- and <sup>14</sup>C-Substituted Molecules in the Liquid Phase

by L. B. Eppstein

*Department of Chemistry, Texas Christian University, Fort Worth, Texas 76129 (Received June 7, 1968)*

Mills and coworkers<sup>1-5</sup> have reported intradiffusion<sup>2</sup> coefficients for several binary systems in which the observed intradiffusion coefficient of the solute at infinite dilution is greater than the limiting mutual-diffusion coefficient of the system. Bearman has shown that for many simple systems at infinite dilution the mutual diffusion and intradiffusion processes are physically identical.<sup>6</sup> From Eyring's treatment of diffusion in liquids, an expression for the self-diffusion coefficient can be written as<sup>7</sup>

$$D^* = \frac{\lambda^2}{V_f^{1/3}} \left( \frac{RT}{2\pi M} \right)^{1/2} \exp(-\Delta E_0/RT) \quad (1)$$

where  $D^*$  is the self-diffusion coefficient,  $V_f$  is the free volume,  $\lambda$  is the jump distance,  $\Delta E_0$  is the energy of activation for the process,  $R$  is the gas constant,  $T$  is the absolute temperature, and  $M$  is the molecular weight of the solute. It seems reasonable to apply eq 1 to the process of intradiffusion at infinite dilution. For an isotopic species where it is assumed that isotope substitution has an extremely small effect upon the intermolecular potential,  $V_f$ ,  $\lambda$ , and  $\Delta E_0$  will be essentially invariant upon isotopic substitution. Then, the ratio of the mutual-diffusion and intradiffusion coefficients at infinite dilution may be written as

$$\frac{D^0}{D^+} = \left( \frac{M^+}{M^0} \right)^{1/2} \quad (2)$$

where  $D^0$  is the limiting mutual-diffusion coefficient,  $D^+$  is the intradiffusion coefficient at infinite dilution,  $M^+$  is the molecular weight of the isotopically substituted species, and  $M^0$  is the molecular weight of the unsubstituted species.

If the assumptions made in obtaining eq 2 are valid, it would be expected that the intradiffusion coefficient at infinite dilution of a compound labeled with <sup>14</sup>C should be smaller than the limiting mutual-diffusion

coefficient of the unlabeled compound. An evaluation of the data obtained by Mills and coworkers indicates that either the assumptions mentioned above are not valid or there is a systematic error in the measurements. Mills and coworkers have consistently calibrated their diaphragm cells with 0.5 M KCl. In this note the deviations of the observed limiting intradiffusion coefficients from the values predicted by eq 2 have been rationalized with the inclusion of a correction for a systematic error arising from "surface effects"<sup>8,9</sup> in the calibration of the diaphragm cell.

A systematic error in the calibration of the diaphragm cell will cause the measured diffusion coefficients to be in error by a factor  $C$ . A correction factor,  $C$ , may be evaluated from

$$C = \frac{D^+_{\text{obsd}}}{D^0} \left( \frac{M^+}{M^0} \right)^{1/2} \quad (3)$$

where  $D^+_{\text{obsd}}$  is the limiting intradiffusion coefficient which has been measured by the diaphragm-cell method,  $D^0$  is the limiting mutual-diffusion coefficient which has been measured by an absolute method such as the Gouy interferometric method,  $M^0$  is the molecular weight of the unlabeled solute species in the mutual-diffusion experiment, and  $M^+$  is the molecular weight of the <sup>14</sup>C-labeled solute species in the intradiffusion experiment. By using the data for the urea-water system<sup>2,10</sup> the correction factor,  $C$ , for Mills's data is found to have a value of 1.020.

An independent evaluation of the factor  $C$  is obtained by the comparison of the mutual-diffusion data for the sucrose-water system obtained by Henrion,<sup>11</sup> who used a diaphragm cell calibrated with 0.5 M KCl, with the mutual-diffusion data obtained by Gosting and Morris,<sup>12</sup> who used the Gouy interferometric method. If a systematic error due to surface effects is present in Mills's data, then a similar error should be found when Henrion's data is compared with the data obtained by Gosting and Morris. The mutual-diffusion data measured by Gosting and Morris have been extrapolated to the lowest concentration at which Henrion measured the diffusion coefficient of the sucrose-water system. At this concentration, 0.2405 M, Henrion obtained  $D = 4.69 \times$

- (1) R. Mills and H. D. Ellerton, *J. Phys. Chem.*, **70**, 4089 (1966).
- (2) J. G. Albright and R. Mills, *ibid.*, **69**, 3120 (1965).
- (3) J. G. Albright, *ibid.*, **70**, 2299 (1966).
- (4) R. Mills, *ibid.*, **69**, 3116 (1965).
- (5) J. F. Tilley and R. Mills, *Trans. Faraday Soc.*, **63**, 2931 (1967).
- (6) R. J. Bearman, *J. Phys. Chem.*, **65**, 1961 (1961).
- (7) A. E. Stern, E. M. Irish, and H. Eyring, *ibid.*, **44**, 981 (1940).
- (8) R. H. Stokes, *J. Amer. Chem. Soc.*, **72**, 2243 (1950).
- (9) I. Altug and M. L. Hair, *J. Phys. Chem.*, **71**, 4260 (1967).
- (10) L. J. Gosting and D. F. Akeley, *J. Amer. Chem. Soc.*, **74**, 2058 (1952).
- (11) P. N. Henrion, *Trans. Faraday Soc.*, **60**, 72 (1964).
- (12) L. J. Gosting and M. S. Morris, *J. Amer. Chem. Soc.*, **71**, 1998 (1949).

$10^{-6}$  cm<sup>2</sup>/sec, while the data of Gosting and Morris extrapolate to  $D = 4.60 \times 10^{-6}$  cm<sup>2</sup>/sec. Since the sucrose used by Henrion was isotopically equivalent to that used by Gosting and Morris, the factor  $C$  becomes the ratio of the diffusion coefficients measured by the respective methods. This gives the same value of 1.020 for the correction factor  $C$ . This agreement provides additional support for the assumption that a systematic error exists when the diffusion of 0.5 M KCl is used to calibrate the diaphragm cell.

Equation 2 will be used to calculate limiting intradiffusion coefficients from available mutual-diffusion coefficients for the systems studied by Mills, *et al.* In order to obtain a valid comparison, the masses of the labeled molecules used by Mills must be applied in eq 2. Specific activity data<sup>13,14</sup> for the various tracer species used in these experiments indicate that the tracer species contained one <sup>14</sup>C atom per molecule. This assumption provides a coherent correlation for the data from the urea, thiourea, mannitol,  $\alpha$ -alanine,  $\beta$ -alanine, benzene, and cyclohexane experiments. The deviation of the corrected limiting intradiffusion coefficient ( $D^+ = 0.515 \times 10^{-5}$  cm<sup>2</sup>/sec) of sucrose<sup>1</sup> from the value calculated from eq 2 ( $D^+_{\text{calcd}} = 0.521 \times 10^{-5}$  cm<sup>2</sup>/sec) with the assumption above and the limiting mutual-diffusion data of Gosting and Morris suggests that the sucrose <sup>14</sup>C used in the experiments contained several <sup>14</sup>C atoms per tracer molecule. Data obtained from the Radiochemical Centre<sup>15</sup> for the sucrose-<sup>14</sup>C used by Mills and Ellerton indicate that this material contained not less than three <sup>14</sup>C atoms per molecule. In Table I, the corrected limiting intradiffusion coefficients are compared with the values calculated from eq 2.

**Table I:** Calculated and Corrected Limiting Intradiffusion Coefficients

	$10^6 D^+_{\text{obsd}}$ , cm <sup>2</sup> /sec	$10^6 D^+$ , cm <sup>2</sup> /sec	$10^6 D^+_{\text{calcd}}$ $(D^0/D^+ = [M^+/M^0]^{1/2})$ , cm <sup>2</sup> /sec	$D^+_{\text{cor}}$ $(= 10^6 D^+_{\text{obsd}}/1.020)$ , cm <sup>2</sup> /sec
Thiourea	1.340 <sup>a</sup>	1.3310 <sup>e</sup>	1.314	1.314
Mannitol	0.670 <sup>a,b</sup>	0.662 <sup>f</sup>	0.658	0.657
Sucrose	0.525 <sup>a</sup>	0.5226 <sup>g</sup>	0.518 <sup>m</sup>	0.515
Benzene	1.890 <sup>c</sup>	1.876 <sup>h</sup>	1.852	1.853
<i>c</i> -C <sub>6</sub> H <sub>12</sub>	2.104 <sup>c</sup>	2.101 <sup>h</sup>	2.076	2.062
$\alpha$ -Alanine	0.928 <sup>d</sup>	0.915 <sup>i</sup>	0.905	0.910
$\beta$ -Alanine	0.944 <sup>d</sup>	0.939 <sup>j</sup>	0.929	0.926
Urea	1.386 <sup>k</sup>	1.382 <sup>l</sup>	1.359	1.359

<sup>a</sup> See ref 5. <sup>b</sup> See ref 1. <sup>c</sup> See ref 4. <sup>d</sup> See ref 3. <sup>e</sup> D. B. Ludlum, R. C. Warner, and H. W. Smith, *J. Phys. Chem.*, **66**, 1540 (1962). <sup>f</sup> P. J. Dunlop, *ibid.*, **69**, 4276 (1965). <sup>g</sup> See ref 12. <sup>h</sup> H. S. Harned, *Discussions Faraday Soc.*, **24**, 7 (1947). <sup>i</sup> F. J. Gutter and G. Kegeles, *J. Amer. Chem. Soc.*, **75**, 3893 (1953). <sup>j</sup> H. C. Donoian and G. Kegeles, *ibid.*, **83**, 255 (1961). <sup>k</sup> See ref 10. <sup>l</sup> See ref 2. <sup>m</sup> Calculated for three <sup>14</sup>C atoms per sucrose-<sup>14</sup>C molecule.

It is striking that agreement between the calculated and corrected  $D^+$  is in all cases within the estimated experimental error of the measurements. Contrary to the suggestion of Mills and Ellerton,<sup>1</sup> this treatment suggests that "surface effects" probably do not increase the rate of diffusion of polar nonelectrolytes through the glass frit in the diaphragm cell. These results indicate the need for applying mass corrections as in eq 2 to the measured limiting intradiffusion coefficients in order to compare these coefficients with the limiting mutual-diffusion coefficients. It should be noted that radiochemical suppliers do not routinely supply any information concerning the molecular distribution of the <sup>14</sup>C in their uniformly labeled compounds. Clearly future investigators in the tracer diffusion field should concisely describe the molecular distribution of <sup>14</sup>C in their tracer species.

*Acknowledgment.* The author wishes to thank Dr. J. G. Albright, Department of Chemistry, Texas Christian University for many helpful discussions and wishes to express his gratitude to Texas Christian University for a University Fellowship, 1967-1968.

(13) R. Mills, Australian National University, personal communication.

(14) J. G. Albright, Texas Christian University, personal communication.

(15) Dr. J. R. Catch, Radiochemical Centre, Amersham, Buckinghamshire, England, personal communication.

## Shereshevsky's Equation and Binary-Solution Surface Tension

by Donald J. Cotton

*Naval Ship Research and Development Center,  
Annapolis, Maryland 21402 (Received May 22, 1968)*

Equation 1, based on thermodynamic considerations and on an assumed model of the surface region of a binary solution, has been derived by Shereshevsky<sup>1</sup>

$$\frac{N_{21}}{\Delta\sigma} = \frac{1}{\Delta\sigma_0} e^{-\Delta F_{12}/RT} + \frac{N_{21}}{\Delta\sigma_0} (1 - e^{-\Delta F_{12}/RT}) \quad (1)$$

where  $\Delta\sigma = \sigma - \sigma_1$ ;  $\Delta\sigma_0 = \sigma_2 - \sigma_1$ ;  $\Delta F_{12} = (\sigma_1 - \sigma_2)A_{2s}/t$ ;  $N_{21}$  is the solute mole fraction;  $\sigma$  is the surface tension of the solution;  $\sigma_1$  is the surface tension of the solvent;  $\sigma_2$  is the surface tension of the solute;  $A_{2s}$  is the molecular surface area of the solute;  $t$  is the thickness of the adsorbed layer;  $T$  is the absolute temperature;  $R$  is the gas constant. Accordingly when  $N_{21}/\Delta\sigma$  is plotted vs.  $N_{21}$  a straight line should result and

(1) J. L. Shereshevsky, *J. Colloid Interfac. Sci.*, **24**, 317 (1967).

**Table I:** Surface Energy and Surface Area Constants for Several Binary Systems of Liquefied Gases

System (solute-solvent)	Temp., °K	$\Delta\sigma_0$ , ergs/cm <sup>2</sup>		$10^{-8}\Delta F_{12}$ , ergs/m	$A_{2s}, \text{Å}^2$		$t$ (layers)
		Calcd	Obsd		Calcd	Density	
N <sub>2</sub> -CO	83.82	1.62	1.60	4.30	4.5	16.2 (78°K)	4
N <sub>2</sub> -CH <sub>4</sub>	90.67	10.91	11.80	10.6	17.4	17.0 (90°K)	1
Ar-CH <sub>4</sub>	90.67	6.14	6.13	5.58	14.4	14.4 (90°K)	1
CO-CH <sub>4</sub>	90.67	10.00	10.13	7.87	16.8	16.8 (90°K)	1
CH <sub>4</sub> -Kr	116.00	4.25	4.24	3.96	15.5	18.1 (133°K)	1

**Table II:** Surface Energy and Surface Area Constants for Molten Mixtures of Tin and Silver at Various Temperatures

Temp., °C	$\Delta\sigma_0$ , ergs/cm <sup>2</sup>		$10^{-10}\Delta F$ , ergs/m	$A_{2s}, \text{Å}^2$			$t$ (layers)	
	Calcd	Obsd		Calcd	Ionic	Covalent	Ionic	Covalent
1000	400.0	399.0	14.93	6.20	6.33	25.1	1.02	4.05
1100	393.0	396.0	15.56	6.56	6.33	25.1	0.96	3.83
1200	383.0	386.0	14.48	6.28	6.33	25.1	1.00	4.00

$$(\text{slope}) = b = \frac{1}{\Delta\sigma_0}(1 - e^{-\Delta F_{12}/RT}) \quad (2)$$

$$(\text{intercept}) = a = \frac{1}{\Delta\sigma_0}e^{-\Delta F_{12}/RT} \quad (3)$$

$$\Delta\sigma_0 = \frac{1}{a + b} \quad (4)$$

$$\Delta F_{12} = RT \ln \left( \frac{b}{a} + 1 \right) = (\sigma_1 - \sigma_2)A_{2s}/t \quad (5)$$

Consequently, if surface tension as a function of concentration is known for a particular binary system,  $\Delta\sigma_0$ ,  $\Delta F_{12}$ , and  $A_{2s}$  can be calculated. This note is to demonstrate the general applicability of the derived equation with surface tension data from a number of widely different types of binary systems.

### Binary Solutions of Liquefied Gases

Surface tension data for cryogenic binary solutions of carbon monoxide, and of methane in nitrogen,<sup>2</sup> and solutions of argon, of carbon monoxide,<sup>2</sup> and of krypton<sup>3</sup> in methane were analyzed. A least-squares fit of mole fraction divided by  $\Delta\sigma$  vs. mole fraction was made for each system, and  $\Delta\sigma_0$ ,  $\Delta F_{12}$ , and  $A_{2s}$  were calculated by applying eq 1-3. Results are summarized in Table I, where  $\Delta\sigma_0$ (calcd) and  $\Delta\sigma_0$ (obsd) were calculated by using eq 4 and the actual data, respectively.  $A_{2s}$ (calcd) was obtained by using eq 5, and  $A_{2s}$ (density) was calculated for the same molecule by Emmett<sup>4</sup> from density data.  $\Delta\sigma_0$ (calcd) corresponds to  $\Delta\sigma_0$ (obsd) to within  $\pm 0.1$  erg/cm<sup>2</sup> for all systems, except N<sub>2</sub>-CH<sub>4</sub>, which was expected inasmuch as their difference is indicative of the degree of orientation of surface molecules.  $A_{2s}$ (calcd) also corresponds closely to an integer multiple of  $A_{2s}$ (density), except for the CH<sub>4</sub>-Kr system for which  $A_{2s}$ (calcd) is approximately 15.0 Å<sup>2</sup>, the molecular area

obtained for solidified-gas density data,<sup>4</sup> and which implies that methane molecules in the surface region are packed as in a pure solid state.

### Binary Mixtures of Molten Metals

Data of the surface tension of molten mixtures of silver and tin at various temperatures measured by Lauermann, Metzger, and Sauerwald<sup>5</sup> were fitted by least squares to the derived equation. Results are summarized in Table II, where  $A_{2s}$ (ionic) and  $A_{2s}$ (covalent) are the molecular surface areas calculated using the Pauling ionic radius of tin,<sup>6</sup> 0.71 Å<sup>2</sup> and the Pauling covalent radius of tin,<sup>7</sup> 1.412 Å, respectively.  $A_{2s}$ (calcd) closely approximates  $A_{2s}$ (ionic), which implies that tin molecules in the surface region are in the ionic state. However, the ratio of  $A_{2s}$ (covalent): $A_{2s}$ (calcd) indicates that the surface region is four layers thick with tin molecules. The latter interpretation is attractive inasmuch as normally covalent metallic bonds are expected to exist in a metal alloy, yet an adsorbed layer four molecules thick is unusually high. In both cases, the results predict that the surface of a liquid metal binary system is rich in the component of lower surface tension. Inasmuch as no large migration of atoms is expected upon solidification, the solid surface of the alloy is also expected to be rich in the same component.

(2) F. B. Sprow and J. M. Prausnitz, *Trans. Faraday Soc.*, **62**, 1105 (1966).

(3) S. Fuks and A. Bellemanns, *Physica*, **32**, 594 (1966).

(4) P. H. Emmett, "Catalysis," Vol. 1, Reinhold Publishing Corp., New York, N. Y., 1954, p 31.

(5) I. Lauermann, L. G. Metzger, and F. Sauerwald, *Z. Phys. Chem. (Leipzig)*, **216**, 42 (1961).

(6) L. Pauling, "The Nature of the Chemical Bond," 2nd ed, Cornell University Press, Ithaca, N. Y., 1940.

(7) L. Pauling, *J. Amer. Chem. Soc.*, **69**, 542 (1947).

**Table III:** Surface Energy and Surface Area Constants for Molten Mixtures of Silver and Alkali Nitrates at 350°

Solute	$\Delta\sigma_0$ , ergs/cm <sup>2</sup>		$10^{-10}\Delta F$ , ergs/m	$A_{2s}$ , Å <sup>2</sup>			$t$ (layers)	
	Calcd	Obsd		Calcd	Density	Ionic	Density	Ionic
LiNO <sub>3</sub>	30.12	29.95	2.53	14.0	16.3	23.2	1.2	1.7
NaNO <sub>3</sub>	24.56	24.00	3.89	26.9	17.7	30.0	0.7	1.1
KNO <sub>3</sub>	29.32	29.15	7.69	43.8	20.2	40.9	0.5	0.9
RbNO <sub>3</sub>	35.42	35.35	8.36	39.3	21.6	46.2	0.5	1.2
CsNO <sub>3</sub>	43.78	44.40	8.36	31.3	23.3	54.6	0.7	1.7

**Table IV:** Surface Energy and Surface Area Constants for Molten Mixtures of Alkali Nitrates at 350°

Solute	Solvent	$\Delta\sigma_0$ , ergs/cm <sup>2</sup>		$10^{-10}\Delta F$ , ergs/m	$A_{2s}$ , Å <sup>2</sup>			$t$ (layers)	
		Calcd	Obsd		Calcd	Density	Ionic	Density	Ionic
KNO <sub>3</sub>	NaNO <sub>3</sub>	5.64	5.18	2.56	75.4	20.2	40.9	0.3	0.5
RbNO <sub>3</sub>	KNO <sub>3</sub>	6.25	6.20	1.76	46.9	21.6	46.2	0.5	1.0
CsNO <sub>3</sub>	KNO <sub>3</sub>	12.94	15.25	4.04	51.8	23.3	54.6	0.4	1.0
RbNO <sub>3</sub>	NaNO <sub>3</sub>	12.53	11.35	3.62	48.0	21.6	46.2	0.5	1.0
CsNO <sub>3</sub>	NaNO <sub>3</sub>	20.47	20.40	5.42	44.0	23.3	54.6	0.5	1.2

**Table V:** Surface Energy and Surface Area Constants for Molten Mixtures of Alkali Chloride and Alkali Sulfate at 1200°

Solute	Solvent	$\Delta\sigma_0$ , ergs/cm <sup>2</sup>		$10^{-10}\Delta F$ , ergs/m	$A_{2s}$ , Å <sup>2</sup>			$t$ (layers)	
		Calcd	Obsd		Calcd	Density	Ionic	Density	Ionic
NaCl	Na <sub>2</sub> SO <sub>4</sub>	83.5	83.4	3.14	6.7	17.0	41.2	2.5	6.1
KCl	K <sub>2</sub> SO <sub>4</sub>	64.0	58.3	6.66	20.4	20.8	41.2	1.0	2.0

### Binary Mixtures of Molten Salts

Surface tension data for various molten mixtures of alkali metal nitrates, alkali metal nitrates and silver nitrate, and alkali metal chlorides and sulfates, obtained by Bertozzi and Sternheim<sup>8</sup> and Bertozzi and Soldani,<sup>9</sup> were analyzed. The results are shown in Tables III-V. In Tables IV and V,  $A_{2s}(\text{calcd})$  and  $A_{2s}(\text{density})$  refer to solute molecules.  $A_{2s}(\text{ionic})$  in Tables III and IV is the sum of the ionic surface areas of the cation and the anion comprising the solute molecule. Pauling ionic radii were used for the cations, and 1.22 Å was used as the radius of the nitrate ion,<sup>10</sup> which was assumed to be symmetrical. In Table V,  $A_{2s}(\text{ionic})$  is the ionic surface area for a monovalent chloride ion. The surface layer thicknesses are labeled according to the molecular surface area employed in their calculation.

In Tables IV and V,  $t(\text{density})$  is fractional, which is physically forbidden. This indicates, as expected for an ionic mixture, that the alkali nitrate molecules are not randomly oriented in the surface region. The surface layer thickness  $t(\text{ionic})$ , however, does closely approximate an integer, except for the KNO<sub>3</sub>-NaNO<sub>3</sub> system.  $A_{2s}(\text{ionic})$ , used to calculate  $t(\text{ionic})$ , is based on a surface structure consisting of a cation lying adjacent to an anion as found in the solid state. Consequently, these results suggest that the surface structure

of the molten mixture is the same as for the solid state.

In Table V,  $t(\text{density})$  for the NaCl-Na<sub>2</sub>SO<sub>4</sub> system, unlike that for the KCl-K<sub>2</sub>SO<sub>4</sub> system, is noninteger.  $t(\text{ionic})$ , however, is approximately an integer for both systems, which indicates that the surface region is comprised of a layer of chloride ions. Since the ionic surface area of a chloride ion is much larger than that of either cation, this result is unsurprising.

### Conclusion

It has been shown how the Shereshevsky equation can be used to obtain knowledge about the surface structure (molecular areas, orientations, and layer thickness) of a wide variety of binary solutions. However, for the results to be physically meaningful, it is necessary that the solutions conform to the assumptions used in the derivation of the equation. Inasmuch as it is impossible to establish independently from surface tension data that the requirements of the equation are satisfied, other confirmation may be desired.

Other equations relating the surface tension of a binary solution to the concentrations and properties of its pure components have appeared in the litera-

(8) G. Bertozzi and G. Sternheim, *J. Phys. Chem.*, **68**, 2908 (1964).

(9) G. Bertozzi and G. Soldani, *ibid.*, **71**, 1536 (1967).

(10) N. Elliott, *J. Amer. Chem. Soc.*, **59**, 1380 (1937).

ture.<sup>11-15</sup> Shereshevsky's equation is similar in form to the latest of these equations, Eberhart's,<sup>15</sup> which Schmidt<sup>16</sup> has shown is a first-order approximation of all the earlier equations and which Ramakrishna and Suri<sup>17</sup> have extensively analyzed. Shereshevsky has utilized the same assumptions and approximations as Eberhart, but his equation generates more detailed information about surface region structure than Eberhart's equation from the same surface tension data.

- (11) B. V. Szykowski, *Z. Phys. Chem. (Leipzig)*, **64**, 385 (1908).
- (12) J. W. Belton and M. G. Evans, *Trans. Faraday Soc.*, **41**, 1 (1945).
- (13) E. A. Guggenheim, "Mixtures," Oxford University Press, London, 1952.
- (14) J. H. Hildebrand and R. L. Scott, "Solubility of Nonelectrolytes," Dover Publications Inc., New York, N. Y., 1964.
- (15) J. G. Eberhart, *J. Phys. Chem.*, **70**, 1183 (1966).
- (16) R. L. Schmidt, *ibid.*, **71**, 1152 (1967).
- (17) V. Ramakrishna and S. K. Suri, *Indian J. Chem.*, **5**, 310 (1967).

### Calculation of the Wavelength Maxima for Some Triphenylmethane Dye Carbonium Ions

by Edward O. Holmes, Jr.

Hughes Research Laboratories, Malibu, California 90265  
(Received June 17, 1968)

In a former publication<sup>1</sup> the author pointed out some interesting relations between the frequencies of the peak values ( $\lambda_{\max}$ ) of the absorption bands of the three triphenylmethane carbonium ions (crystal violet ( $CV^+$ ), malachite green ( $MG^+$ ), and sunset orange ( $SO^+$ )) as related to the structure of these ions. Since then the author has extended the investigation to include several more carbonium ions of this type and has found the ratios to be quite general and consistent, so much so that they are used as a guide in arriving at an empirical equation by which  $\lambda_{\max}$  can be calculated with a fair degree of accuracy for most of the bands. Table I shows the frequency ratios of the ions considered.

The dyes are divided into three groups: (a) symmetrical, those in which all three nitrogens in the *para* position are bonded to hydrogen atoms or the same group: *p*-roseaniline<sup>2</sup> ( $RO^+$ ), crystal violet ( $CV^+$ ), ethyl violet ( $EV^+$ ), and hexahydroxyethyl violet ( $HHEV^+$ ); (b) semisymmetrical, those having one phenyl group containing no amino group: Döbner's violet ( $DV^+$ ), malachite green ( $MG^+$ ), brilliant green ( $BG^+$ ), and bis[*p*-(diphenylamino)phenyl]phenylmethyl carbonium ion ( $2DPP^+$ ); and (c) unsymmetrical, sunset orange<sup>1</sup> ( $SO^+$ ).

All solutions were in absolute ethyl alcohol. The ions were obtained from the leucocarbinols or ether<sup>3</sup> by adding a trace of acid or from the leucocyanides by photolysis with minimum exposure.

**Table I:** Frequency Ratios of the Absorption Maxima for the Carbonium Ion Dyes

Ions	Ratios of $\nu_{\max}$				
	g:x	h:g	n:y	y:x	g:y
$RO^+$	1.89	1.21			
$CV^+$	1.93	1.21			
$EV^+$	1.92	1.21			
$HHEV^+$	1.93	..			
$DV^+$	1.85	..	..	1.41	1.31
$MG^+$	1.93	1.27	1.81	1.45	1.35
$BG^+$	1.96	1.26	1.82	1.45	1.36
$2DPP^+$	2.07	..	..	1.44	1.42
$SO^+$	..	1.31	1.81	..	1.35

A large number of expressions for the calculation of the  $\lambda_{\max}$  of the various bands were tried but none gave results as good as the relatively simple formula stated below which we converted to a form that would yield results in wavelengths (in millimicrons) rather than frequencies.

$$\lambda_{\max} = 1.1^N (\lambda_{\max} \text{ of the } g \text{ band, in } \mu)$$

The g band is chosen for reference as it is common to all ions and can be measured with a fair degree of accuracy on a Cary spectrophotometer.  $N$ , the exponent of 1.1, is designated as the band number. The base 1.1 is used because when raised to the appropriate power it reproduces so many of the band ratios such as 1.21, 1.47, and 1.95, for example. Tables II and III show our results.

### Discussion

The band number  $N$  is assigned the values of 7, 3, 0, -2, and -3 for the bands x, y, g, h, and n, respectively. For the symmetrical ions which have x, g, and h bands only 7, 0, and -2 are used. With one exception the agreement between the measured value and the calculated is fairly good. However, when the band numbers are applied to the semisymmetrical and unsymmetrical ions, the agreement is not as good. (By deviating from the above sequence of band numbers and using 6.5 instead of 7 for the x band of  $DV^+$ , -1 in place of -2 for the h band of  $HHEV^+$ , etc., the agreement is very much closer.) At present we cannot explain the significance of the band numbers chosen.

On calculating the ratios of the frequencies of the y:x bands of six other carbonium ions from the work of Tolbert and others<sup>4</sup> in which the phenyl group was substituted progressively for the methyl groups in malachite green, we find the ratios to be remarkably con-

(1) E. O. Holmes, Jr., *J. Phys. Chem.*, **70**, 1037 (1966).

(2) Highly purified, supplied by Dr. John Vandenberg of the Parke Davis Co.

(3) E. O. Holmes, Jr., *J. Phys. Chem.*, **62**, 884 (1958).

(4) B. M. Tolbert, G. E. K. Branch, and B. E. Berlenback, *J. Amer. Chem. Soc.*, **67**, 890 (1945).

**Table II:** Wavelengths for  $\lambda_{\max}$  for the Bands of the Carbonium Ions Calculated by the Empirical Formula for Symmetrical Ions<sup>a</sup>

Dye ion	Band	$\lambda_{\max}$ (obsd)		N	$\lambda_{\max}$ (calcd)		Difference	
		$m\mu$	eV		$m\mu$	eV	$m\mu$	eV
RO <sup>+</sup>	x	547	2.28	7	566	2.19	19	0.07
	g	290	4.28	0	290	4.28		
	h	240	5.17	-2	238	5.21	2	0.04
CV <sup>+</sup> <sup>b</sup>	x	589	2.10	7	586	2.12	3	0.01
	g	305	4.06	0	305	4.06		
	h	252	4.92	-2	251	4.94	1	0.02
EV <sup>+</sup>	x	592	2.09	7	593	2.09	1	0.00
	g	306	4.05	0	306	4.05		
	h	254	4.88	-2	253	4.90	1	0.02
HHEV <sup>+</sup>	x	590	2.10	7	601	2.06	11	0.04
	g	308	4.03	0	308	4.03		
	h	280	4.43	-2	254	4.88	26	0.45

<sup>a</sup> This group contains no y and n bands. <sup>b</sup> Reference 1.

**Table III:** Calculated Wavelengths for Semisymmetrical and Unsymmetrical Carbonium Ions from Formula

Dye ion	Band	$\lambda_{\max}$ (obsd)		N	$\lambda_{\max}$ (calcd)		Difference	
		$m\mu$	eV		$m\mu$	eV	$m\mu$	eV
DV <sup>+</sup> <sup>a</sup>	x	564	2.20	7	595	2.08	31	0.12
	y	399	3.11	3	405	3.06	6	0.05
	g	305	4.07	0				
	h	?						
	n	?						
MG <sup>+</sup> <sup>b</sup>	x	622	1.99	7	620	2.00	2	0.01
	y	428	2.90	3	423	2.93	5	0.03
	g	318	3.90	0	318	3.90		
	h	257	4.94	-2	262	4.73	11	0.21
	n	236	5.25	-3	239	5.19	3	0.06
BG <sup>+</sup>	x	627	1.98	7	620	2.00	7	0.02
	y	427	2.90	3	422	2.94	5	0.04
	g	317	3.91	0	317	3.91		
	h	252	4.92	-2	262	4.73	10	0.19
	n	235	5.28	-3	238	5.21	3	0.07
2DPP <sup>+</sup> <sup>c</sup>	x	680	1.82	7	644	1.92	36	0.10
	y	470	2.64	3	439	2.83	31	0.19
	g	330	3.76	0	330	3.76		
	h	?						
	n	?						
SO <sup>+</sup> <sup>b</sup>	x	...						
	y	463	2.68	3	459	2.70	4	0.02
	g	345	3.59	0	345	3.59		
	h	264	4.70	-2	287	4.31	23	0.39
	n	255	4.86	-3	259	4.79	4	0.07

<sup>a</sup> R. Meyer and O. Fischer, *Ber. Bunsenges Phys. Chem.*, **46**, 70 (1913). <sup>b</sup> Reference 1. <sup>c</sup> Reference 3.

stant, namely, 1.44 ( $\pm 0.01$ ), and consistent with our values. This ratio is affected very little by the nature of the groups attached to the nitrogen atoms. Unfortunately, Tolbert did not determine the h and n bands for the dye ions. The g:x ratios are the next most constant but tend to increase with some property of the groups attached to the nitrogen atoms.

This extension of the author's earlier work<sup>1</sup> strengthens the previous assignment of the various induced

dipoles to the structure of the ions. Note that the two longest ultraviolet bands of aniline and dimethylaniline are in the ratio 1.21, which corresponds to the h:g frequency ratio in the ions RO<sup>+</sup>, DV<sup>+</sup>, and EV<sup>+</sup>. The corresponding bands ratios of BG<sup>+</sup> and MG<sup>+</sup> are 1.26 and 1.27, respectively, and that in SO<sup>+</sup> is 1.31, undoubtedly due to the fact that these ions contain phenyl groups without a substituted amino group in the *para* position.

## The Sign of the $^{11}\text{B}-^{19}\text{F}$ Coupling Constant in Boron Trifluoride and Related Compounds

by S. A. Fieldhouse and I. R. Peat

Department of Chemistry, University of Toronto,  
Toronto, Ontario, Canada (Received July 18, 1968)

The determination and interpretation of nmr coupling constants,  $J$ , have recently received much attention.<sup>1-5</sup> Furthermore, linear correlations have been found between  $J$  and  $^{19}\text{F}$  chemical shifts,  $\delta(^{19}\text{F})$ , within series of structurally similar fluorine compounds.<sup>6,7</sup>

We find that similar relationships exist for the mixed boron halides<sup>8</sup> and for the  $\text{RBF}_2$  derivatives.<sup>9,10</sup> The appropriate data are collected in Table I, and the results of plotting  $J(^{11}\text{B}-^{19}\text{F})$  vs.  $\delta(^{19}\text{F})$  for each series are shown in Figure 1.

**Table I:** Coupling Constants and  $^{19}\text{F}$  Chemical Shift Data for Boron-Fluorine Compounds

Compd	Ref	$J(^{11}\text{B}-^{19}\text{F})$ , <sup>a</sup> Hz	$\delta(^{19}\text{F})$ , <sup>b</sup> ppm
$\text{BF}_3$	8	+15 ± 2	0
$\text{BF}_2\text{Cl}$	8	-34 ± 1	-51.5 ± 0.2
$\text{BF}_2\text{Br}$	8	-56 ± 1	-68.4 ± 0.3
$\text{BFCl}_2$	8	-74 ± 1	-99.0 ± 0.6
$\text{BFBrCl}$	8	-92 ± 2	-114.8 ± 0.6
$\text{BFBr}_2$	8	-108 ± 2	-130.4 ± 0.7
$\text{CH}_3\text{BF}_2$	9	-77	-51.2
$\text{C}_2\text{H}_5\text{BF}_2$	9	-81	-53.4
$n\text{-C}_3\text{H}_7\text{BF}_2$	9	-82	-54.2
$\text{CH}_2=\text{CHBF}_2$	9	-67	-38.4
$\text{HBF}_2$	10	-84 ± 1 <sup>c</sup>	-60.0

<sup>a</sup> Signs assigned in this paper. <sup>b</sup> Relative to  $\text{BF}_3$  as the internal reference. <sup>c</sup> Sign from E. Whipple, T. H. Brown, T. C. Farrar, and T. D. Coyle, *J. Chem. Phys.*, **43**, 1841 (1965).

It can be seen that an excellent straight-line plot is obtained for the mixed boron halides and a similar, but less well defined, correlation also exists for the  $\text{RBF}_2$  derivatives. Since the  $\delta-J$  plot for the mixed halides intersects the  $\delta(^{19}\text{F})$  axis at -17 ppm, a reversal of the sign of the coupling constant should occur for those compounds whose chemical shift is less than this value. Consequently, the sign of  $J(^{11}\text{B}-^{19}\text{F})$  in boron trifluoride,  $\delta(^{19}\text{F}) = 0$ , is opposite to that of the other members of the series. Experimentally it has been shown that  $J(^{11}\text{B}-^{19}\text{F})$  is negative for difluoroborane,<sup>11</sup> and, since similar trends (see below) are apparent in the  $\text{RBF}_2$  and the mixed halide series, we therefore assign a positive value to the sign of  $J(^{11}\text{B}-^{19}\text{F})$  in boron trifluoride. This is an exception to the prediction<sup>12</sup> that  $J(^{11}\text{B}-^{19}\text{F})$  will always be negative.

In addition some comment on the mechanism of the coupling in the boron halides is possible as in the case of

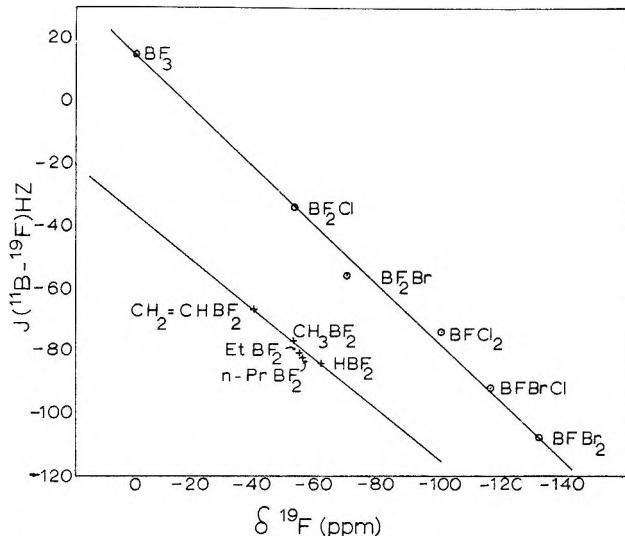


Figure 1. Correlation between  $J(^{11}\text{B}-^{19}\text{F})$  and  $\delta(^{19}\text{F})$ .

organofluorine compounds, where similar relationships were found.<sup>7</sup> These were interpreted as showing that  $\pi$  bonding was the dominant factor in determining the values of  $J(^{13}\text{C}-^{19}\text{F})$ .<sup>7</sup> Since  $\pi$  bonding is important in boron-fluorine chemistry,<sup>13,14</sup> we might expect that the above observations would correlate with this fact. Thus the value of  $J(^{11}\text{B}-^{19}\text{F})$  increases steadily as one or more of the fluorine atoms in boron trifluoride are replaced by less efficient  $\pi$  bonding groups. This corresponds to an increase in the total  $\pi$  bonding per fluorine atom. Thus  $\text{FBBr}_2$  and  $\text{HBF}_2$  have the largest values of  $J(^{11}\text{B}-^{19}\text{F})$  of the mixed halide and  $\text{RBF}_2$  series, respectively. The  $\pi$  bonding to boron, however, will be greater when the attached groups are efficient  $\pi$  bonders and will be at a maximum in boron trifluoride<sup>14</sup> when the  $\pi$  bonding per fluorine is least. Apparently this is sufficient to cause a change in the sign of  $J(^{11}\text{B}-^{19}\text{F})$  for boron trifluoride.

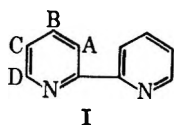
- (1) E. G. Finer and R. K. Harris, *Chem. Commun.*, 58 (1968).
- (2) R. Keiter and S. O. Grim, *ibid.*, 521 (1968), and references cited therein.
- (3) W. McFarlane, *J. Chem. Soc., A*, 1148 (1968).
- (4) R. Ditchfield, M. A. Jensen, and J. N. Morell, *ibid.*, 1674 (1967).
- (5) P. W. Allen, I. T. Muller, and J. C. Tebby, *Tetrahedron Lett.*, 795 (1968).
- (6) H. S. Gutowsky, D. W. McCall, and C. P. Slichter, *J. Chem. Phys.*, **21**, 279 (1953).
- (7) N. Muller and D. T. Carr, *J. Phys. Chem.*, **67**, 112 (1963).
- (8) T. D. Coyle and F. G. A. Stone, *J. Chem. Phys.*, **32**, 1892 (1960).
- (9) T. D. Coyle and F. G. A. Stone, *J. Amer. Chem. Soc.*, **82**, 6223 (1960).
- (10) T. C. Farrar and T. D. Coyle, *J. Chem. Phys.*, **41**, 2612 (1964).
- (11) E. Whipple, T. H. Brown, T. C. Farrar, and T. D. Coyle, *ibid.*, **43**, 1841 (1965).
- (12) A. J. Pople and D. Santry, *Mol. Phys.*, **8**, 1 (1964).
- (13) T. D. Coyle and F. G. A. Stone, *Progr. Boron Chem.*, **1**, 88, 127 (1964).
- (14) L. Pauling, "The Nature of the Chemical Bond," 3rd ed., Cornell University Press, Ithaca, N. Y., 1960, pp 317-320.

**Proton Magnetic Resonance in Octahedral Complexes of Iron(II) and Cobalt(III) with  $\alpha,\alpha'$ -Dipyridyl**

by C. R. Kanekar, C. L. Khetrapal,  
and S. V. Nipankar

Tata Institute of Fundamental Research, Bombay, India  
(Received July 10, 1968)

It is well known that the bidentate ligand  $\alpha,\alpha'$ -dipyridyl (structure I) forms spin-paired diamagnetic



complexes<sup>1</sup> of Fe(II) and Co(III). Proton magnetic resonance has been studied in these complexes with a view to understanding the nature of the metal-ligand bond. The results are reported in the present note.

The complexes were prepared by the method of Burstall and Nyholm.<sup>1</sup> Proton resonance in the cobalt complex was studied in acetone-*d*<sub>6</sub> solution and that of the iron compound in D<sub>2</sub>O using a Varian high-resolution spectrometer at 56.445 Mcps. For comparison, the spectrum of the ligand was also studied in acetone-*d*<sub>6</sub> solution. The chemical shifts of various protons were measured relative to those of the solvent and finally reported relative to tetramethylsilane (TMS) after necessary conversion.

The spectrum of  $\alpha,\alpha'$ -dipyridyl (dipy) has been analyzed by Kramer and West<sup>2</sup> to first order and by Castellano, *et al.*,<sup>3</sup> exactly. The values, estimated by us, of chemical shifts of various protons and the coupling constants between various protons in this molecule are

the D protons. The deshielding is maximum for B protons. The effect is more predominant in the cobalt complex. The coupling constant *J*<sub>CD</sub> markedly increases on complexation. The increase in the *J*<sub>CD</sub> value for the cobalt complex is 1.6 cps, while that for the iron analog is 1.3 cps.

Kanekar, *et al.*,<sup>6</sup> have given the following empirical expression which correlates the chemical shift ( $\Delta\delta_i$ ) of the proton at site *i* in a substituted benzene relative to that for protons in benzene itself and the changes in the  $\pi$ -electron densities at various positions in the ring

$$\Delta\delta_i = K_1\Delta\rho_i + K_2(\Delta\rho_{i-1} + \Delta\rho_{i+1}) + K_3S_i \quad (1)$$

where  $\Delta\rho_i$  is the excess  $\pi$ -electron density at the site *i* over that in benzene,  $\Delta\rho_i - 1$  and  $\Delta\rho_i + 1$  are the excess charge densities at the neighboring carbon atoms, and *S<sub>i</sub>* gives the contribution to the chemical shift arising from the steric effect of the substituent. The constants of proportionality *K*<sub>1</sub> and *K*<sub>2</sub> were found to be 10 and 2.4 ppm/electron, respectively.<sup>6</sup> The last term can be estimated from the changes in the coupling constant<sup>7</sup> and is equal to  $-0.83\Delta J$ , where  $\Delta J$  is the difference in the coupling constant values observed for the unsubstituted compound and the substituted analog.<sup>6</sup> The same equation can be used to explain the chemical shifts at various positions in the  $\alpha,\alpha'$ -dipyridyl complexes of Fe(II) and Co(III).

The chemical shifts of A, B, and C protons can be explained in terms of only the first two terms of eq 1, since the steric-effect contribution is absent at nonadjacent positions. The low-field shifts for these protons can arise from the decrease in the electron charge density of the carbon atoms as a result of N-M linkage, where the positive charge will reside at the metal atom, M. The situation is analogous to the formation of the pyridinium ion. For this ion Smith and Schneider<sup>8</sup>

**Table I:** Proton Chemical Shifts and Spin Coupling in  $\alpha,\alpha'$ -Dipyridyl and Its Complexes with Fe(II) and Co(III)

Compd	Chemical shift relative to TMS, ppm				Coupling constant, cps					
	$\delta_A$	$\delta_B$	$\delta_C$	$\delta_D$	$J_{AB}$	$J_{AC}$	$J_{AD}$	$J_{BC}$	$J_{BD}$	$J_{CD}$
dipy	-8.63	-7.98	-7.47	-8.77	7.6	1.4	0.8	7.6	1.8	4.7
[Fe(dipy) <sub>2</sub> ] <sup>2+</sup>	-8.89	-8.46	-7.78	-7.78	8	~2	...	8	~2	6
[Co(dipy) <sub>3</sub> ] <sup>3+</sup>	-8.73	-8.60	-7.88	-7.63	7.7	~2	...	7.7	~2	6.3

given in Table I; they are in agreement with those reported by earlier workers;<sup>2,3</sup> they also agree with the values reported by Bernstein, *et al.*,<sup>4</sup> and Castellano, *et al.*,<sup>5</sup> for pyridine. The spectra of the complexes and the ligand were similar. The values of the parameters in the complexes could be obtained with a fairly high degree of accuracy even though their solubility is not very high.

It is seen from the chemical shift data that complex formation deshields the protons A, B, and C but shields

- F. H. Burstall and R. S. Nyholm, *J. Chem. Soc.*, 3570 (1952).
- F. A. Kramer and R. West, *J. Phys. Chem.*, **69**, 673 (1965).
- S. Castellano, H. Gunther, and S. Ebersole, *ibid.*, **69**, 4166 (1965).
- H. J. Bernstein, J. A. Pople, and W. G. Schneider, *Can. J. Chem.*, **35**, 1487 (1957).
- S. Castellano, C. Sun, and R. Kostelnik, *J. Chem. Phys.*, **46**, 327 (1967).
- C. R. Kanekar, G. Govil, and C. L. Khetrapal, *Proc. Indian Acad. Sci.*, **65**, 353 (1967).
- S. S. Dharmatti, G. Govil, C. R. Kanekar, C. L. Khetrapal, and Y. P. Virmani, *ibid.*, **63**, 9 (1966).
- I. C. Smith and W. G. Schneider, *Can. J. Chem.*, **39**, 1158 (1961).

postulated that the change in the chemical shift is linearly related to  $\Delta\rho_i$ . Assuming this and neglecting the second term in eq 1, one can estimate the values of  $\Delta\rho_i$  for A, B, and C protons in the two complexes. The values are given in Table II. The corresponding changes in the pyridinium ion are  $-0.128$ ,  $-0.113$ , and  $-0.026$  for the corresponding positions. The ratio  $\Delta\rho_B/\Delta\rho_C$  in the two complexes ( $\sim 1.5$ ) is not much different from that observed in the pyridinium ion ( $\sim 1.2$ ), indicating that (1) the model is applicable and (2) this effect is predominantly responsible for the difference in the shifts of A, B, and C protons with respect to the corresponding protons in the ligand.

Table II

Complex	$\Delta\rho_A$	$\Delta\rho_B$	$\Delta\rho_C$
$[\text{Fe}(\text{dipy})_3]^{2+}$	$-0.026$	$-0.046$	$-0.031$
$[\text{Co}(\text{dipy})_3]^{3+}$	$-0.010$	$-0.062$	$-0.041$

In order to interpret the chemical shift of the D proton in the complexes, it is necessary to take into account the first and the third terms of eq 1.  $\Delta\rho_D$  can be estimated from the corresponding value in pyridinium ion on the assumption that the ratio  $\Delta\rho_D/\Delta\rho_B$  (or  $\Delta\rho_D/\Delta\rho_C$ ) in the complexes is approximately equal to the corresponding ratio in the pyridinium ion. This gives a value of  $\Delta\rho_D$  equal to  $-0.009$  and  $-0.013$  for the iron and the cobalt complex, respectively. It is now evident that the major contribution to the shift of this proton comes from the steric effect between the metal atom (M) and the proton in position D ( $H_D$ ). This effect depends upon the size of the central atom and takes place through the distortion of the  $\text{NCH}_D$  bond angle. When M is charged, the distortion predominantly takes place through an electronic interaction between M and  $H_D$  which can be repulsive or attractive. The increase in the coupling constant upon complex formation indicates that the  $H_D\text{CC}$  angle increases, which means that  $H_D$  is attracted toward the metal ion. The effect is analogous to the metal–nonbonded hydrogen interaction postulated by Miller and Prince<sup>9</sup> for the transition metal complexes of *o*-phenanthroline. Owing to this effect the proton  $H_D$  experiences an increased shielding. This contribution ( $-0.83\Delta J$ ) is  $1.1$  and  $1.3$  ppm for the iron and the cobalt complex, respectively. Adding this to the contribution due to the first term, we get values equal to  $1.0$  and  $1.2$ , respectively, for  $\Delta\delta_D$  for the iron and the cobalt compounds. These values are in quite good agreement with those observed for the two complexes.

The high-field shifts for the corresponding proton in the *o*-phenanthroline complexes of Fe(II) and Co(III) ( $1.3$  and  $1.34$  ppm, respectively) are larger than those observed for the dipyridyl complexes. Busch and Bailar<sup>10</sup> have shown from the absorption spectra of the

ferrous complexes of these ligands that there is a greater donation of 3d electrons in the *o*-phenanthroline complex, indicating a larger double-bond character of the Fe–N bond. This should result in larger electron density at the D proton in *o*-phenanthroline complexes and hence higher shielding. The stability constants of the *o*-phenanthroline complexes of Co(III) and Fe(II) are higher than those of the corresponding dipyridyl complexes,<sup>11</sup> in conformity with greater M–N bond strength in the *o*-phenanthroline compounds.

*Acknowledgment.* It is a great pleasure to thank Dr. G. Govil for extremely helpful suggestions.

(9) J. D. Miller and R. H. Prince, *J. Chem. Soc.*, 3185 (1965).

(10) D. H. Busch and J. C. Bailar, Jr., *J. Amer. Chem. Soc.*, **78**, 1137 (1956).

(11) H. Irving and D. H. Mellor, *J. Chem. Soc.*, 5222 (1962).

## Temperature Dependence of Reactions of the Hydrated Electron

by S. R. Logan

*School of Physical Sciences, New University of Ulster, Coleraine, N. Ireland* (Received July 26, 1968)

The current interest in the Arrhenius parameters of hydrated electron reactions has produced a considerable amount of data by both direct and indirect methods. The discussion of the significance of these results from a collision theory point of view appears in cases to have produced some confusion and in others to have missed the simplest interpretation.

In recent years, some incorrect ideas about the Arrhenius parameters of fast reactions in solution appear to have gained acceptance. Since, from a form of the Smoluchowski equation<sup>1</sup> due to Debye,<sup>2</sup> a reaction occurring on every collision should have an Arrhenius activation energy,  $E_a$ , of  $B + RT$ , where the viscosity coefficient varies with  $T$  as  $\eta = A \exp(B/RT)$ , it has been assumed (i) that in solution the lowest possible Arrhenius activation energy is that of a reaction occurring on every collision, (ii) that this minimum value is equal to  $B$ , and (iii) that where there is a minimum energy requirement or "molecular activation energy" of  $E^*$ , the Arrhenius parameter is then given by  $B + E^*$ . The incorrectness of assumption iii has always been clearly apparent for large values of  $E^*$ . When the average number of collisions made by a reactant molecule with molecules of the other reactant is very much greater than the average number of collisions per en-

(1) M. von Smoluchowski, *Z. Phys. Chem. (Leipzig)*, **92**, 129 (1917).

(2) P. Debye, *Trans. Electrochem. Soc.*, **82**, 265 (1942).

counter,<sup>3</sup> the fact that collisions occur in "sets" is then of little relevance. The situation is akin to that in the gas phase and we again expect a value of  $E^* + \frac{1}{2}RT$ , assuming that  $Z$ , the collision number, in solution is also proportional to  $T^{1/2}$ .

The situation at low values of  $E^*$  has been treated<sup>4</sup> using an expression for the temperature dependence of the rate constant which is valid over the whole range, from very low values of  $p$ , the probability that a collision results in reaction, to  $p = 1$  or reaction on the first collision. This shows that even if the reaction probability is energetic in nature, as when  $p = \exp(-E^*/RT)$ ,  $E_a$  may be less than  $B$  at low values of  $E^*$ , by an amount which is quite sensitive to the average number of collisions per encounter.

In discussing these calculations,<sup>4</sup> it was remarked that the figure then available<sup>5</sup> for the activation energy of the  $e_{aq}^- + H^+$  reaction,  $3.2 \pm 0.3$  kcal mol<sup>-1</sup>, implied that the activation energy for the diffusion of  $e_{aq}^-$  was slightly higher than that for the self-diffusion of water. The more recent data,<sup>6</sup> giving the figure of  $2.6 \pm 0.3$  kcal mol<sup>-1</sup>, suggests that the first may be a little high and that the implication is not correct. (It seems a pity that the conductivity work of Schmidt and Buck<sup>7</sup> was not repeated at other temperatures with a view to estimating the activation energy for the diffusion of the hydrated electron.)

The other result quoted by Cercek and Ebert<sup>6</sup> is, with a little difficulty, compatible with the results of these calculations;<sup>4</sup> when the charge product is positive, the minimum in  $E_a$  as a function of  $E^*$  is lower and a value of about 2 kcal mol<sup>-1</sup> appears acceptable for this reaction. However, the authors of this information<sup>6</sup> deny this possibility.

When the erroneous quotation of the values of these workers<sup>6</sup> is corrected in the table of activation energies derived<sup>8</sup> by competition studies, this selection of reactions, with rate constants ranging from  $6 \times 10^{10}$  to less than  $10^7 M^{-1} sec^{-1}$ , no longer presents quite so uniform a list of Arrhenius activation energies. A larger variation than this was found in values obtained directly<sup>9</sup> by pulse radiolysis. In the case of the very slow reactions, the reasonable conclusion is that although the probability that a collision results in reaction is small chiefly because of a very low temperature-independent factor, there is also a factor of the form  $\exp(-E^*/RT)$ , where  $E^*$  lies in the range of approximately 2–4 kcal mol<sup>-1</sup>. The earlier implication<sup>8</sup> that the value of  $E^*$  was constant seemed very surprising. The only invariants in the reactions listed were the hydrated electron and the aqueous solvent, but the reaction,  $e_{aq}^- + H_2O$ , has been shown<sup>10</sup> to have a significantly higher activation energy of  $6.7 \pm 0.7$  kcal mol<sup>-1</sup>.

Anbar and Hart<sup>9</sup> attributed the small and scarcely significant difference in their activation energies for the reaction  $e_{aq}^- + ClCH_2COO^-$  in  $H_2O$  and  $D_2O$  to what they claim is a very small difference in the  $B$  values for

these two solvents. However, the influence of  $B$  on the activation energy is not important unless the reaction is very fast; from the previous calculations<sup>4</sup> it may be deduced that a variation of 0.4 kcal mol<sup>-1</sup> will not be significant in a reaction whose rate constants are less than about  $3 \times 10^9 M^{-1} sec^{-1}$ .

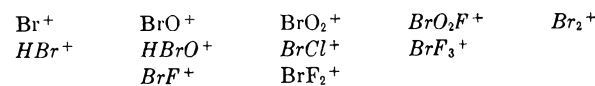
- (3) E. Rabinowitch and W. C. Wood, *Trans. Faraday Soc.*, **32**, 1381 (1936).
- (4) S. R. Logan, *ibid.*, **63**, 1712 (1967).
- (5) J. K. Thomas, S. Gordon, and E. J. Hart, *J. Phys. Chem.*, **68**, 1524 (1964).
- (6) B. Cercek and M. Ebert, *ibid.*, **72**, 766 (1968).
- (7) K. H. Schmidt and W. L. Buck, *Science*, **151**, 70 (1966).
- (8) M. Anbar, Z. B. Alfassi, and H. Bregman-Reisler, *J. Amer. Chem. Soc.*, **89**, 1263 (1967).
- (9) M. Anbar and E. J. Hart, *J. Phys. Chem.*, **71**, 3700 (1967).
- (10) E. M. Fielden and E. J. Hart, *Trans. Faraday Soc.*, **63**, 2975 (1967).

## Mass Spectra of Hydrolyzed Bromine Fluorides<sup>1</sup>

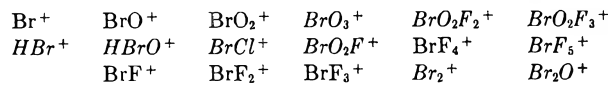
by Eric N. Sloth, Lawrence Stein,  
and Clayton W. Williams

*Chemistry Division, Argonne National Laboratory,  
Argonne, Illinois 60439 (Received August 14, 1968)*

A bromine(VII) oxyfluoride,  $BrO_2F_3$ , has been observed in samples of partially hydrolyzed bromine pentafluoride examined with a modified<sup>2</sup> Bendix Time-of-Flight mass spectrometer. The oxyfluoride is an analog of the recently discovered perbromate compounds.<sup>3,4</sup> A bromine(V) oxyfluoride,  $BrO_2F$ , previously reported by Schmeisser and Pammer,<sup>5</sup> has also been observed in samples of partially hydrolyzed bromine trifluoride. The higher-valent compounds are believed to arise from disproportionation of  $BrF_3$  and  $BrF_5$  during hydrolysis. An unexpected impurity,  $BrCl$ , was found both in the original and product fluorides. In hydrolyzed bromine trifluoride, the observed masses correspond to the ions



In hydrolyzed bromine pentafluoride, the observed masses correspond to the ions



The italicized ions arise from parent species of the

- (1) Based on work performed under the auspices of the U. S. Atomic Energy Commission.
- (2) M. H. Studier, *Rev. Sci. Instr.*, **34**, 1367 (1963).
- (3) E. H. Appleman, *J. Amer. Chem. Soc.*, **90**, 1900 (1968).
- (4) M. H. Studier, *ibid.*, **90**, 1901 (1968).
- (5) M. Schmeisser and E. Pammer, *Angew. Chem.*, **67**, 156 (1955).

same mass formula whereas the others are primarily fragmentation products.

Bromine trifluoride and bromine pentafluoride were obtained from the Matheson Chemical Co. and purified by distillation in the Chemical Engineering Division at Argonne. Infrared spectra revealed only small amounts of  $\text{CF}_4$  and  $\text{C}_2\text{F}_6$  in the pentafluoride; the spectra otherwise agreed with those in the literature.<sup>6,7</sup> Approximately 5-g samples of the fluorides in Kel-F test tubes or nickel containers were frozen with liquid nitrogen. Water was added by vacuum distillations until 0.1 to 0.5 g of ice was present as a separate layer. The samples were allowed to thaw, whereupon vigorous and sometimes violent reactions occurred. Oxygen was liberated both by the hydrolysis and by the partial decomposition of bromine oxide and oxyfluorides. This was pumped off after refreezing the products at  $-196^\circ$ . Vapors were then analyzed as the products warmed slowly to room temperature and distilled into cold traps on a manifold made of  $1/4$ -in. Kel-F tubing, which comprised the inlet to the mass

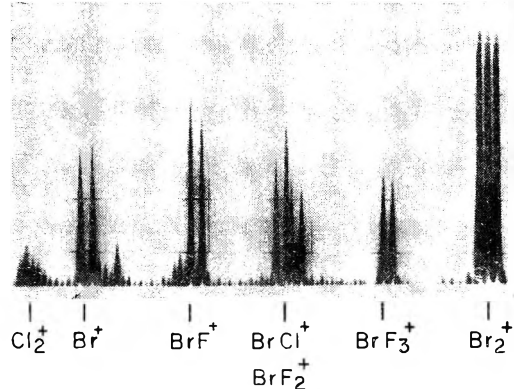


Figure 1. Mass spectrum of bromine trifluoride containing several volatile impurities.

spectrometer. Ions produced by electron impact on the vapors were identified by their masses and characteristic isotope abundance patterns.

In some instances, hydrolyzed samples were distilled at  $-20$  to  $0^\circ$  in a copper and Monel still fitted with cooling coils. The distillate fractions were then stored for periods up to 1 week in Kel-F test tubes cooled with a carbon dioxide-trichloroethylene mixture. Since carbon dioxide and trichloroethylene diffuse through Kel-F plastic, mass spectra of both compounds were observed. The trichloroethylene was eliminated in later experiments to avoid mass spectral interference.

In the hydrolyzed samples, ions arising from water, nitrogen, oxygen, hydrogen fluoride, hydrogen peroxide, carbon monoxide, and carbon dioxide were observed as well as  $\text{CF}_3^+$ ,  $\text{COF}^+$ ,  $\text{CCF}_2^+$ ,  $\text{COBr}^+$ ,  $\text{COFBr}^+$ , and other ions attributable to Kel-F. The most abundant ion was  $\text{O}_2^+$ .

Figure 1 shows the mass spectrum of bromine trifluoride which still contained chlorine, bromine mono-

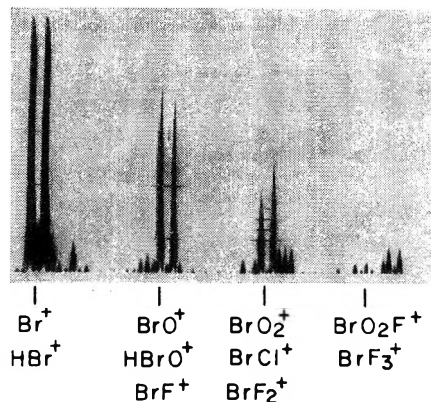


Figure 2. Mass spectra of products from partially hydrolyzed bromine trifluoride ( $\text{Br}_2^+$  peaks not shown).

chloride, and bromine impurities after distillation. Due to the higher volatility of the impurities, their mass peaks appeared sooner and sometimes at higher intensities than the mass peaks of the trifluoride. The doublet of the parent ion  $\text{BrF}_3^+$  was prominent, whereas in spectra of bromine pentafluoride, the doublet of the parent ion  $\text{BrF}_5^+$  appeared with very low intensity.

In partially hydrolyzed bromine trifluoride,  $\text{BrF}$  and  $\text{BrO}_2\text{F}$  were present as independent species (Figure 2). Both were ascribed to the reaction



Diatomeric bromine was also present and contributed to the formation of  $\text{BrF}$  through reaction with bromine trifluoride.

Several bromine oxides and oxyfluorides were observed in partially hydrolyzed bromine pentafluoride (Figures 3-6).  $\text{BrO}_2\text{F}$  was present in most samples and was ascribed to the reaction

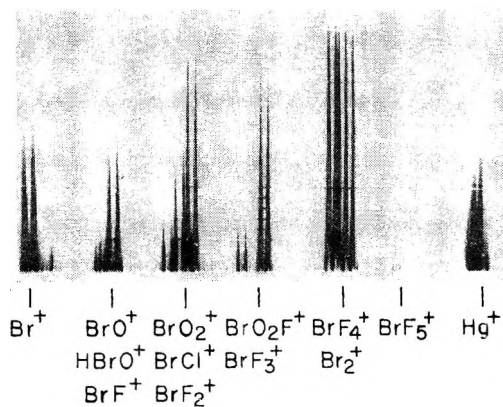
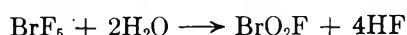


Figure 3. Mass spectra of products from partially hydrolyzed bromine pentafluoride ( $\text{Hg}^+$  peaks due to mercury from diffusion pump).

(6) H. H. Claassen, B. Weinstock, and J. G. Malm, *J. Chem. Phys.*, **28**, 285 (1958).

(7) R. S. McDowell and L. B. Asprey, *ibid.*, **37**, 165 (1962).

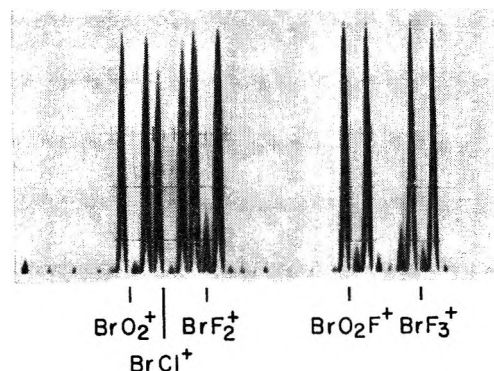


Figure 4. Mass spectra of bromine pentafluoride products on expanded scale;  $\text{BrO}_2\text{F}^+$  prominent,  $\text{BrOF}_2^+$  absent.

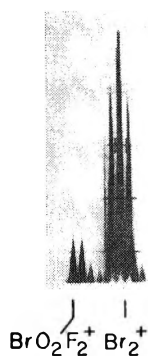


Figure 5. Partial mass spectrum of bromine pentafluoride products showing  $\text{BrO}_2\text{F}_2^+$  and  $\text{Br}_2^+$ .



Figure 6. Partial mass spectrum of bromine pentafluoride products showing  $\text{Br}_2^+$  and  $\text{Br}_2\text{O}^+$ .

$\text{BrO}_2\text{F}_3$  was found in two end fractions of distilled hydrolysate which had been stored for 5 days at  $-78^\circ$ . The first fragment,  $\text{BrO}_2\text{F}_2^+$ , was seen at moderately high intensity, and the parent ion,  $\text{BrO}_2\text{F}_3^+$ , at low intensity. This product was ascribed to the reaction



although bromine trifluoride could not be identified as an independent species due to the interference of bromine pentafluoride.<sup>8</sup>

In earlier mass spectral studies of halogen fluorides, Irsa and Friedman<sup>9</sup> observed bromine oxyfluoride ions in  $\text{BrF}_3$ ,  $\text{BrF}_5$ , and  $\text{BrF}_5\text{O}_2$  mixtures, which were ascribed to the parent  $\text{BrOF}_3$ . In the present study

there was no evidence of this species, as  $\text{BrOF}_2^+$  and  $\text{BrOF}^+$ , the expected fragments from  $\text{BrOF}_3$ , were not observed. Since the two strongest mass peaks of  $\text{BrCl}^+$  coincide with the peaks of  $\text{BrOF}^+$ , bromine monochloride impurity, if present in Irsa and Friedman's samples, may have been ascribed to  $\text{BrOF}^+$ . In almost all of our spectra, bromine monochloride produced peaks at 114, 116, and 118 mass units with intensity ratios of approximately 3:4:1. This pattern can be noted clearly in Figure 4.

In the hydrolyzed bromine pentafluoride samples,  $\text{BrO}^+$ ,  $\text{BrO}_2^+$ ,  $\text{BrO}_3^+$ , and  $\text{Br}_2\text{O}^+$  were also observed. The first two appeared to be fragments from  $\text{BrO}_2\text{F}$ , whereas the last two appeared to be independent species. ( $\text{BrO}_3^+$  might be a fragment from the parent  $\text{BrO}_3\text{F}$ , but no ion corresponding to this formula was observed.) Twin peaks at mass 206 and 208 were seen at low intensity several times and ascribed to the ion  $\text{BrO}_2\text{F}_5^+$ , possibly derived from a complex or a peroxy compound. A compound of this composition,  $\text{O}_2\text{BrF}_6$ , has been reported by Streng.<sup>10</sup> Iodine monobromide was considered to be an unlikely source of the mass 206 and 208 peaks, since  $\text{I}^+$  ion at mass 127 was not detected.

The ability of bromine monochloride to coexist with bromine trifluoride and bromine pentafluoride was confirmed in the following manner. Equal parts of bromine and chlorine were mixed to provide an authentic sample of  $\text{BrCl}$  (Figure 7). One half of the mixture

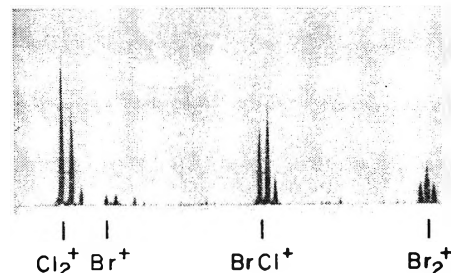


Figure 7. Mass spectrum of bromine monochloride in a bromine-chlorine mixture.

was frozen at  $-196^\circ$  with a fivefold excess of bromine trifluoride and the other half with a fivefold excess of bromine pentafluoride. When the mixtures were warmed to room temperature and examined,  $\text{BrCl}^+$  peaks were found to be still prominent in the spectra.

*Acknowledgment.* We are indebted to Roger L. Jarry of the Chemical Engineering Division for the samples of bromine trifluoride and bromine pentafluoride.

(8) One of the referees has suggested reactions involving hydrogen peroxide as alternates to disproportionation:  $\text{H}_2\text{O}_2 + \text{BrF}_3 \rightarrow \text{BrO}_2\text{F} + 2\text{HF}$  and  $\text{H}_2\text{O}_2 + \text{BrF}_5 \rightarrow \text{BrO}_2\text{F}_3 + 2\text{HF}$ . Several alternate reactions to disproportionation may be postulated using oxygen-containing compounds or oxygen as intermediates.

(9) A. P. Irsa and L. Friedman, *J. Inorg. Nucl. Chem.*, **6**, 77 (1958).

(10) A. G. Streng, *J. Amer. Chem. Soc.*, **85**, 1380 (1963).

## Relaxation Spectra of Nickel(II)- and Cobalt(II)-Picolinic Acid Complexes

by A. Kowalak, K. Kustin, and R. F. Pasternack<sup>1</sup>

*Department of Chemistry, Brandeis University,  
Waltham, Massachusetts 02154 (Received August 19, 1968)*

The complexation rate constants for the formation of the pyridine 2-carboxylate (picolinic acid anion) complexes of nickel(II) and of cobalt(II) have been determined by the temperature-jump method. Experimental procedures and a description of the apparatus have already appeared.<sup>2</sup> In this study Fisher reagent grade nitrate salts of potassium(I), cobalt(II), and nickel(II) were used; picolinic acid was obtained from K & K Fine Chemicals and was used without further purification; the indicator methyl orange was obtained from the Allied Chemical Corp.

### Results and Treatment of Data

The reactions under investigation are of the type

**Table I:** Relaxation Spectra of Metal Ion-Picolinic Acid Solutions<sup>a,b</sup> ( $20^\circ$ ,  $\mu = 0.10 M$ )

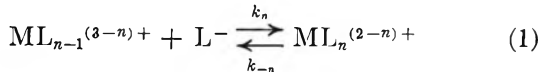
$10^3[Ni^{2+}]_0^c$	$10^3[\text{ligand}]_0^c$	pH	$\tau, \text{ sec}$	
			Exptl	Calcd
2.00	2.00	3.66	0.17	0.23 <sup>d</sup>
2.00	4.00	3.55	0.41	0.31
2.00	6.00	3.68	0.22	0.21
2.00	8.00	3.73	0.12 ( $\tau_+$ ) 0.24 ( $\tau_-$ )	0.10 0.27
2.09	12.0	3.76	0.17	0.19
1.00	2.00	3.70	0.42	0.41
8.01	12.0	3.59	0.11	0.11
$10^3[Co^{2+}]_0^e$	$10^3[\text{ligand}]_0^e$	pH	$\tau, \text{ msec}$	
			Exptl	Calcd
2.02	2.00	4.14	0.95	0.95 <sup>f</sup>
2.02	4.00	4.01	1.3	1.6
2.02	6.00	3.93	0.99	0.90
2.02	8.00	3.93	0.67	0.77
2.02	12.0	3.91	0.61	0.49

<sup>a</sup> All concentrations are molar; the subscript zero refers to the total stoichiometric concentration. <sup>b</sup> Methyl orange indicator was used; the total concentration was  $9.45 \times 10^{-6} M$ , except for the first nickel experiment reported, where it was  $1.89 \times 10^{-5} M$ . For this indicator the acid dissociation constant was  $3.47 \times 10^{-4} M$  (I. M. Kolthoff, *J. Phys. Chem.*, **34**, 1466 (1930)). <sup>c</sup> The step stability constants are:  $\log K_1 = 6.80$ ,  $\log K_2 = 5.78$ ,  $\log K_3 = 4.64$  (see ref 3). <sup>d</sup> The value was calculated using  $k_1$  from J. C. Cassatt and R. G. Wilkins, *J. Amer. Chem. Soc.*, **90**, 6045 (1968). <sup>e</sup> The step stability constants are:  $\log K_1 = 5.74$ ,  $\log K_2 = 4.70$ ,  $\log K_3 = 3.65$  (see ref 3). <sup>f</sup> The value of  $k_1$  estimated from this solution is  $10^7$ . However, none of the cobalt solutions depends significantly on  $k_1$ .

**Table II:** Rate Constants for Reactions of Nickel(II) and Cobalt(II) with Picolinate Anion

Metal	$n$	$k_{n\pm}$ $M^{-1} \text{ sec}^{-1}$	$k_{-n\pm}$ $\text{sec}^{-1}$
$Ni^{2+}$	1	$2.6 \times 10^4$ <sup>a</sup>	...
	2	$1.2 \times 10^6$	0.20
	3	$1.6 \times 10^6$	0.37
$Co^{2+}$	1	$1 \times 10^7$	20
	2	$2.4 \times 10^7$	480
	3	$1.9 \times 10^6$	430

<sup>a</sup> J. C. Cassatt and R. G. Wilkins, *J. Amer. Chem. Soc.*, **90**, 6045 (1968).



where  $n = 1, 2$ , or  $3$  and  $M$  is  $Ni$  or  $Co$ . The symbol  $L^-$  corresponds to the anionic form of the ligand.<sup>3</sup> The reaction conditions and observed relaxation times are shown in Table I. Values of the relaxation times have been calculated from the expression given by Hammes and Steinfield<sup>4</sup> by a trial-and-error fit of the rate constants. The best fit was obtained with the set of rate constants given in Table II.

It was not necessary to include additional hydrogen ion dependent terms to fit the data.<sup>5</sup> We therefore conclude that the rate constant for reaction between metal ion and the neutral form of the ligand is less than 0.01 of that for  $L^-$ , in agreement with the observations of Cassatt and Wilkins.<sup>6</sup>

Moreover, in almost all of the experiments, only reactions in which  $n = 2$  or  $3$  were important. Therefore, the value given for the nickel  $k_1$  is a stopped-flow result,<sup>6</sup> the value of which is more accurate than that of the temperature-jump experiments under these conditions. For cobalt(II), however, no other values of  $k_1$  are available. The value quoted may therefore be regarded only as being an upper limit. All other rate constants have relative errors of  $\pm 20\%$ .

### Discussion

It is well known that complexation reactions of divalent transition metal ions proceed via a sequence of two processes.<sup>7</sup> The more rapid process is ion pair

(1) Department of Chemistry, Ithaca College, Ithaca, N. Y. 14850.  
(2) G. Davies, K. Kustin, and R. F. Pasternack, *Trans. Faraday Soc.*, **64**, 1006 (1968).

(3) "Stability Constants," L. G. Sillén and A. E. Martell, Ed., Special Publication No. 17, The Chemical Society, London, 1964, pp 496-497. At  $20^\circ$   $K_1 = [H^+][HL]/[H_2L^+] = 2.51 \times 10^{-2}$  and  $K_2 = [H^+][L^-]/[HL] = 5.89 \times 10^{-6}$ .

(4) G. G. Hammes and J. I. Steinfield, *J. Amer. Chem. Soc.*, **84**, 4639 (1962).

(5) See ref 3 for an example of competitive attack by two differently protonated forms of a given ligand, in this case cysteine.

(6) J. C. Cassatt and R. G. Wilkins, *J. Amer. Chem. Soc.*, **90**, 6045 (1968).

(7) M. Eigen and R. G. Wilkins in "Mechanisms of Inorganic Reactions," Advances in Chemistry Series, No. 49, American Chemical Society, Washington, D. C., 1965, p 55.

formation, which is (in most cases) in equilibrium with the subsequent slower step or steps. Values of the equilibrium quotient for ion pair formation,  $K_{a_n}$  ( $M^{-1}$ ), depend mainly upon charge type. In normal, nonhindered complexation the slow step in complex formation is the first elimination of a coordinated water molecule, described by the rate constant  $k_{0n}$  ( $\text{sec}^{-1}$ ) for the  $n$ th step.

For normal complexation the observed rate constant is related to the mechanistic constants according to

$$k_n = S_n k_{0n} K_{a_n} \quad (2)$$

where  $S_n$  is a statistical factor depending upon the number of available bonding sites in the coordination shell of the metal ion. When  $n = 1$ ,  $k_{01}$  is approximately  $(1\text{--}3) \times 10^4 \text{ sec}^{-1}$  for nickel(II) and  $(3\text{--}10) \times 10^5 \text{ sec}^{-1}$  for cobalt(II). This value is essentially independent of ligand properties.<sup>7</sup> For the fully aquated dipositive metal ion reacting with a singly negative anion,  $K_{a1} \sim 2 M^{-1}$  and  $S_1 = 1$ . From eq 2 the computed values of  $k_{01}$ , using the results in Table II and the above constants, are: nickel(II),  $k_{01} = 1.3 \times 10^4 \text{ sec}^{-1}$ ; cobalt(II),  $k_{01} < 5 \times 10^6 \text{ sec}^{-1}$ . These figures are consistent with the values cited.<sup>7</sup>

The situation with regard to higher order complexation is less well understood than the corresponding case for reaction of fully aquated metal ions. Nevertheless, it is here that the picolinic acid results are most interesting.

We calculate using  $S_2 = 2/3$ ,  $S_3 = 1/3$ ,  $K_{a2} = 1$ , and  $K_{a3} = 0.3$  the following values of  $k_{02}$  and  $k_{03}$  ( $\text{sec}^{-1}$ ): nickel(II):  $k_{02} = 1.8 \times 10^5$ ,  $k_{03} = 1.6 \times 10^6$ ; cobalt(II):  $k_{02} = 3.6 \times 10^7$ ,  $k_{03} = 1.9 \times 10^7$ . It is therefore concluded that replacement of two or more inner coordination sphere waters by picolinate enhances the rate of water loss.

This effect may arise, in part, from the negatively charged carboxylate ligand. That is, bonding to  $-\text{COO}^-$  should reduce the positive charge density on the central metal ion, thereby loosening the binding to the remaining waters. Studies of  $\alpha$ -amino acids have yielded similar results.<sup>4,8</sup>

Evidence is also available, however, that other factors are involved. Consider, for example, the ligand pyridine-2,6-dicarboxylate (pydic). For the reaction Ni-pydic + pydic<sup>2-</sup>,  $k_2 = 2.4 \times 10^4 M^{-1} \text{ sec}^{-1}$ .<sup>6</sup> With  $S_2 = 1/2$  and  $K_2 = 0.3$ , we obtain  $k_{02} = 1.6 \times 10^5 \text{ sec}^{-1}$  for this ligand, almost equal to the picolinate  $k_{02}$ , despite the presence of an additional  $-\text{COO}^-$  group. Clearly, the formal charge of the bound ligand cannot be a most significant factor in these systems in determining the rate of water loss from the inner coordination sphere of the complexed metal ion. Yet the bound picolinate anion is playing an important role in determining the rate constant for this process, since  $k_{02}/k_{01} = 12$ . Quite likely the enhancement is a result of the interaction of delocalized  $\pi$  orbitals on the ligand with  $T_{2g}$  d orbitals on the metal ion.

The importance of  $\pi$  bonding to kinetics is in its effect on  $\Delta$ , the crystal field stabilization energy. The substitution rate constant  $k_{0n}$  is correlated with the loss of crystal field stabilization energy, being smaller the larger the energy loss in attaining the activated complex structure.<sup>9</sup> Therefore, the enhancement may arise from this effect when  $\Delta$  is decreased by  $\pi$ -orbital interaction. Such is likely the situation for picolinate and terpyridine.<sup>10</sup> It might be mentioned that it is quite possible that in other cases the interaction may be of small consequence, bearing relatively little effect on the enhancement or that the  $\pi$  interaction may even increase the  $\Delta$  value, thus diminishing the rate of water loss. The relative role played by  $\pi$  bonding and back  $\pi$  bonding in the metal chelate will determine the effect on  $\Delta^{11}$  and hence on the rate constants.

*Acknowledgment.* The authors gratefully acknowledge partial support from Public Health Service Research Grant GM-08893-06 from the National Institute of General Medical Sciences, Public Health Service, from the National Science Foundation for College Teacher Research Participation Grant No. GY3796 (A. K.), and from the Petroleum Research Fund for Grant 2982B (R. F. P.).

- (8) (a) K. Kustin, R. F. Pasternack, and E. M. Weinstock, *J. Amer. Chem. Soc.*, **88**, 4610 (1966); (b) A. Kowalak, K. Kustin, R. F. Pasternack, and S. Petrucci, *ibid.*, **89**, 3126 (1967).
- (9) F. Basolo and R. G. Pearson, "Mechanisms in Inorganic Reactions," 2nd ed., John Wiley & Sons, Inc., New York, N. Y., 1967, p 147.
- (10) R. H. Holyer, C. D. Hubbard, S. F. A. Kettle, and R. G. Wilkins, *Inorg. Chem.*, **5**, 622 (1966).
- (11) F. A. Cotton and G. Wilkinson, "Advanced Inorganic Chemistry," 2nd ed., Interscience Publishers, Inc., New York, N. Y., 1966, p 708.

## The Photoxidation of *t*-Butyl Iodide at Low Temperatures

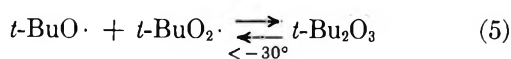
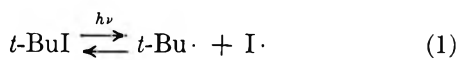
by Theodore Mill and Roger Stringham

Department of Physical Organic Chemistry, Stanford Research Institute, Menlo Park, California 94025 (Received August 23, 1968)

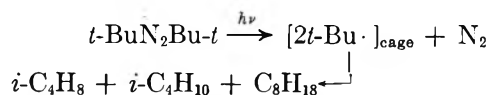
We have examined the photolysis of *t*-butyl iodide in oxygen-saturated  $\text{CFCl}_3$  around  $-100^\circ$  as a possibly efficient source of *t*-butyl peroxy radicals for synthesis of di-*t*-butyl tetroxide and trioxide.<sup>1</sup> At  $25^\circ$  *t*-butyl iodide is reported to give *t*-butyl radicals through photolysis of the C—I bond.<sup>2</sup> Disproportionation of the *t*-butyl radicals gives isobutane and isobutylene, the

- (1) T. Mill and R. Stringham, *J. Amer. Chem. Soc.*, **90**, 1062 (1968).
- (2) C. E. McCawley, W. H. Hamill, and R. R. Williams, *ibid.*, **76**, 6263 (1954).

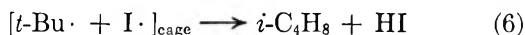
major products of the reaction. The following reaction scheme is expected on the basis of our earlier work with *t*-butyl radicals and oxygen<sup>1</sup>



Using azoisobutane as a photosource of *t*-butyl radicals,<sup>1</sup> we found that the yields of di-*t*-butyl polyoxides were low because of the extensive recombination of caged *t*-butyl radicals



This particular process is not possible in the case of *t*-butyl iodide, although disproportionation in the cage might be significant.



## Experimental Section

**Materials.** *t*-Butyl iodide (K & K Laboratories) was washed with 0.1 N thiosulfate solution, dried, and purified by trap-to-trap distillation at -35 to -65°. It was diluted to 1 M in CFCl<sub>3</sub> and was stored in the dark at 0°. The solution was analyzed periodically by nmr spectroscopy to ensure that no decomposition had taken place.

**Photolyses.** A quartz-to-Pyrex cylindrical cell (15 cm × 4 cm in diameter) with a magnetically driven glass stirrer was used for the irradiation experiments. The stirrer was driven at about 400–500 rpm to ensure adequate diffusion of oxygen into the liquid phase.

Aliquots (1–2 ml) of the 1 M *t*-BuI solution were added to the cell from a tared syringe. The cell was cooled in liquid nitrogen, evacuated to 10<sup>-4</sup> torr, and then refilled with dry oxygen at about 10<sup>3</sup> torr. A coolant bath, usually consisting of 3:1 MeOH:EtOH in a 1200-ml unsilvered quartz dewar, was placed around the cell. The bath temperature was regulated to ±2° by intermittent passage of cold nitrogen gas through a copper heat-exchanger coil in the bath behind the cell. The nitrogen flow was regulated by a controlling pyrometer (West Instrument Corp., Schiller Park, Ill.). The irradiation source was the collimated beam from a 200-W point-source mercury arc (PEK Model 202 lamp with a Model 701 power supply).

**Analyses.** After irradiation, the solutions were degassed by several freeze-thaw cycles. A few were warmed to 25°, then cooled again, and analyzed for evolved oxygen using a gas buret and a Toepler pump.

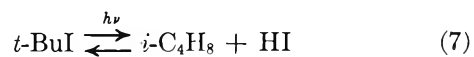
Known amounts of CH<sub>2</sub>Cl<sub>2</sub> and Me<sub>4</sub>Si were added to the reaction mixtures as an internal standard and frequency lock for nmr analyses. The cell was then sealed off from the vacuum line and manually inverted in the dewar, and the contents were directed into an nmr tube sealed to the cell near the top. The nmr tube was then cooled in liquid nitrogen and sealed off from the cell; the contents were analyzed by a Varian 100-MHz nmr spectrometer. This procedure ensured that all components of the reaction mixtures were quantitatively transferred to the nmr tube and that the whole transfer could be effected at some low temperature so that unstable intermediates might be preserved for subsequent analysis by nmr.

Iodine was determined by titration with 0.01 N thiosulfate; HI was determined by titration with 0.01 N sodium hydroxide.

## Results

Several solutions of 0.1–0.15 M *t*-butyl iodide in oxygen-saturated CFCl<sub>3</sub> were photolyzed in a quartz reaction cell at -110 or -100° for 20–30 hr. The light was turned off and residual oxygen was pumped away. Some of the mixtures were then warmed to 25° where any oxygen evolved from reaction 4 could be measured; none was found, indicating an absence of di-*t*-butyl polyoxides.<sup>1</sup> Other mixtures, analyzed by nmr spectroscopy, showed significant amounts of isobutylene and *t*-butyl hydroperoxide but no isobutane. Smaller amounts of *t*-butyl alcohol, *t*-butyl chloride, and what is thought to be *t*-butyl hypoiodite ( $\tau$  8.63) were also detected. Iodine and hydrogen iodide were estimated by titrimetric procedures. Good material balances were obtained and detailed product analyses of two of the experiments are shown in Table I.

Isobutylene and HI were the major products from the photolysis at low temperatures even in the presence of oxygen. The absence of isobutane and the C<sub>8</sub>H<sub>18</sub> dimer, the other recombination products from *t*-butyl radicals, means that isobutylene was formed by disproportionation of the radical pair in the solvent cage (reaction 6) or by an independent molecular elimination



and that all *t*-butyl radicals that escaped from the cage were scavenged by oxygen. The marked increase in the rate of photolysis of *t*-butyl iodide at 25° (run 2) compared with -110° (run 1), under similar conditions of irradiation, is readily accounted for by the competition between escape of the radical pair from the solvent cage with an activation energy of 2–3 kcal/mol and recombination (reaction 1) for which there should be no activation energy. The small decrease in the rate of formation of isobutylene with increasing temperature is consistent with either reaction 6 or 7 or both.

Our principal objective was to learn if *t*-butyl iodide

**Table I:** Photolysis of *t*-Butyl Iodide in Oxygen-Saturated<sup>a</sup>  $\text{CFCl}_3$

	Run			
	1	2	3	4
Temp, °C	-110	25	-100	-100
Time, min	240	240	1800	1440
Reactants				
[ <i>t</i> -BuI], $\mu\text{mol}$	760	580	230	290
[ <i>t</i> -BuI], M	0.13	0.11	0.15	0.15
Products <sup>b</sup> (by nmr), $\mu\text{mol}$				
$\Delta$ [ <i>t</i> -BuI]	130	511	63	45
[ <i>t</i> -C <sub>4</sub> H <sub>8</sub> ]	58	34	39	25
[ <i>t</i> -BuOOH] <sup>c</sup>	66	280	10	5
[ <i>t</i> -BuOH]			4	2.5
[ <i>t</i> -BuCl]			4	0
[ <i>t</i> -BuOI]			5	5
[I <sub>2</sub> ] <sup>c</sup>			19	16
[HI]			20	2
$\Sigma$ [ <i>t</i> -Bu] (in products)	124	451 <sup>d</sup>	62	38
$\Sigma$ [I] (in products)	...	...	63	37

<sup>a</sup> Oxygen at about 10<sup>3</sup> torr. <sup>b</sup> Analyses have an estimated precision of  $\pm 10\%$ . <sup>c</sup> Determined by iodometric titration.

<sup>d</sup> This includes an estimated 137  $\mu\text{mol}$  of unknown *t*-butyl or *t*-butyl peroxy products.

was an efficient source of *t*-butyl peroxy radicals. The results in Table I indicate that 11–50% of the consumed *t*-butyl iodide was converted to products through peroxy

radicals under conditions where only 5–10% efficiency was found for azoisobutane.<sup>1</sup> The total absence of oxygen-evolving polyoxides or di-*t*-butyl peroxide in these solutions must be due to efficient scavenging of the *t*-butyl peroxy radicals by HI, thus preventing their interactions *via* reactions 2–4.



Radical abstractions from HI are known to be exceptionally fast<sup>3</sup> with rate parameters of  $k_8 = 10^{9-2000/R^T}$ . This is comparable with the interaction rate for alkyl peroxy radicals (reaction 3).<sup>4</sup> Since reaction 3 is rapidly reversible even at -100°<sup>5</sup> and reaction 4 has an activation energy of  $\sim 12$  kcal/mol,<sup>1,5</sup> the net effect is a conversion of all the peroxy radicals to hydroperoxide. Thus the photolysis of *t*-butyl iodide is not a useful route to di-*t*-butyl polyoxides unless some other way can be found to remove HI as it is formed.

*Acknowledgment.* We acknowledge support of this work by the National Aeronautics and Space Administration, George C. Marshall Space Flight Center, Huntsville, Ala., through Contract No. NAS8-20220. Mr. William Anderson expertly prepared the nmr spectra.

(3) A. S. Rodgers, D. M. Golden, and S. W. Benson, *J. Amer. Chem Soc.*, **89**, 4578 (1967).

(4) D. G. Hendry, *ibid.*, **90**, 2382 (1968).

(5) P. D. Bartlett and G. Guaraldi, *ibid.*, **89**, 4799 (1967).